Environmental Earth Sciences

Series Editor:
James W. LaMoreaux

For further volumes:
http://www.springer.com/series/8394

Nicolaos Lambrakis
George Stournaras
Konstantina Katsanou
Editors

Advances in the Research of Aquatic Environment

Volume 2

Springer

Editors
Prof. Dr. Nicolaos Lambrakis
University of Patras
Department of Geology
Laboratory of Hydrogeology
Patras
Greece
nlambrakis@upatras.gr

Prof. Dr. George Stournaras
University of Athens
Department of Geology and
Geoenvironment
Athens
Greece
stournaras@geol.uoa.gr

Konstantina Katsanou
University of Patras
Department of Geology
Laboratory of Hydrogeology
Patras
Greece
katsanou@upatras.gr

ISBN 978-3-642-24075-1 e-ISBN 978-3-642-24076-8
DOI 10.1007/978-3-642-24076-8
Springer Heidelberg Dordrecht London New York

Library of Congress Control Number: 2011936434

Cover design: deblik, Berlin

Printed on acid-free paper

Springer is part of Springer Science+Business Media (www.springer.com)

Preface

These two volumes contain the proceedings of the 9th International Congress of Hydrogeology and the 4th MEM Workshop on Fissured Rocks Hydrology, organized by the Hellenic Committee of Hydrogeology in collaboration with the Cyprus Association of Geologists and Mining Engineers.

The number of the manuscripts submitted to the Organizing Committee throughout 15 countries all over the world reflects the rapidly increasing interest that Hydrology gains nowadays worldwide. The papers cover more or less all fields, such as mathematical modeling, statistical, hydro-chemical methods, etc., focusing on the environmental aspect.

Aquatic environment, the main topic of the Congress, as it is shown by the title of the Proceedings "Advances in the research of aquatic environment" is covered by articles mostly dealing with ecological impacts *versus* water requirements, climate change implications on groundwater, anthropogenic impacts on the groundwater quality, groundwater vulnerability, and more.

Both volumes follow the general structure of the Congress topics. Moreover the keynote lectures are also included.

On behalf of the International Scientific Committee I would like to take this opportunity to thank all the authors for their contributions, as well as all participants for their cooperation, which made this Congress possible. Additionally, I would like to express my gratitude to the staff of Springer and especially Christian Witschel and Agata Oelschlaeger for their hard work, patience and support.

Last but not least, I would like to thank my wife Aggeliki and my children Athina and Ioannis for their patience and love.

Prof. Nicolaos Lambrakis
President of the Organizing Committee
University of Patras
Laboratory of Hydrogeology
Rio – Patras, Greece

Address of the Hellenic Committee of Hydrogeology

The Hellenic Chapter of IAH proudly presents the Proceedings of its 9th International Hydrogeological Congress, integrated in the frame, established during the last decade, characterized by internationalization and an opening to adjacent scientific fields. This is the result of continuous and painstaking efforts of all the members of the Hellenic Committee of Hydrogeology and of our foreign colleagues who attended our congresses and contributed by their papers and key notes and chiefly by their presence.

The discussed Congress is characterized by several features and particularities. First of all, it is the first time that our Congress deserts the big cities for the Hellenic periphery cities as it is Kalavrita, the city which entertains our present meeting. Second, the international economic crisis affected both the attendance of delegates and the sponsoring of the event. Despite these difficulties the participants and the sponsors' presence exceeded the expected range. Moreover, the focusing given to our congress' subject matter, the management of the aquatic environment, covers a very important topical and seasonable existing universal problem, especially under the effect of the climatic change. Finally, the association with our new publisher, Springer is something that improves the level of the Congress in the field of the presentation quality and of the international diffusion of the proceedings as well.

The IAH Hellenic National Chapter wishes to express its gratitude to the Organizing Committee and its Chairman, Prof. N. Lambrakis for what they have done, the Sponsors of the event in such a difficult period, the local authorities of the city and the region of Kalavrita, the authors of the papers and key notes, and the participants for their important presence in the congress.

For the Administration Council
The President
Prof. George Stournaras

Acknowledgements

The 9th International Hydrogeological Congress of Greece would not have been possible to be carried out without the active engagement of many persons and the financial support of Institutions and Organizations. I would like to express my gratitude to all of them. Moreover, I would like to thank in particular Mr Dimitris Dalianis for his perfect work in the construction and maintenance of the Congress website. I would also like to acknowledge Mrs Konstantina Katsanou, Panagoula Kriempardi and Katerina Karli, for their valuable contribution during the organization.

Sponsors

BANK OF GREECE

M.E.W.S OF PATRAS

UNIVERSITY OF PATRAS

MARIOLOPOULOS KANAGINIS FOUNDATION

AGRICULTURAL UNIVERSITY OF ATHENS

DR C.J.VAMVACAS LTD HIGH-TECH PRODUCTS-CONSULTANTS

GEOTECHNICAL CHAMBER OF GREECE

KLEOPATRA GOUVA – CHEMICALS PARTNERSHIP LAZARIDIS

Organizing Committee

The 9th International Hydrogeological Congress and the 4th MEM Workshop of Fissured Rocks Hydrology of the Hellenic Committee of Hydrogeology in collaboration with the Geological Society of Greece and the Cyprus Association of Geologists and Mining Engineers, was organized by the Laboratory of Hydrogeology, Department of Geology, University of Patras, with the cooperation of colleagues from several universities and authorities. The Organizing Committee consists by the following members:

President:

Nikolaos Lambrakis, University of Patras, Laboratory of Hydrogeology

Vice President:

Evangelos Nikolaou, IGME Greece

General Secretary:

Anastasia Pyrgaki, Region of Western Greece

Executive Secretary:

Konstantina Katsanou, University of Patras, Laboratory of Hydrogeology

Koumoutsou Eleni Chelmos Vouraikos Geopark

Treasurer:

Eleni Zagana, University of Patras, Laboratory of Hydrogeology

Members:

Christos Petalas, Department of Environmental Engineering, Democritus University of Thrace

Constantinos Constantinou, Geological Survey of Cyprus

Grigorios Krestenitis, Region of Western Greece

Markos Sklivaniotis, M.E.W.S.P of Patras

Georgios Soulios, Aristotle University of Thessaloniki, Department of Geology

Georgios Stamatis, Agricultural University of Athens, Laboratory of Mineralogy-Geology

Georgios Stournaras, Faculty of Geology and Geoenvironment, University of Athens

Leonardos Tiniakos Region of Western Greece

Scientific Committee

Mohamed Aboufirass (N. Africa)
Ian Acworth (Australia)
Apostolos Alexopoulos (Greece)
Bartolome Andreo (Spain)
Athanasios Argyriou (Greece)
Alicia Aureli (Italy)
Giovanni Barrocu (Italy)
Konstantinos Chalikakis (France)
Antonio Chambel (Portugal)
Massimo Civita (Italy)
John Diamantis (Greece)
Alexandros Dimitrakopoulos (Greece)
George Dimopoulos (Greece)
Romeo Eftimi (Albania)
Christophe Emblanch (France)
Dolores Maria Fidelibus (Italy)
Björn Frengstad (Norway)
Michael Fytikas (Greece)
Michael Galabov (Bulgary)
Jacques Ganoulis (Greece)
Panagiotis Giannopoulos (Greece)
Vasileios Kaleris (Greece)
George Kallergis (Greece)
George Koukis (Greece)
John Koumantakis (Greece)
Andre Kranjc (Slovenia)
Jiri Krasny (Czech Republic)
Ioannis Kyrousis (Greece)
Patrik Lachassagne (France)
Nikolaos Lambrakis (Greece)
John Leontiadis (Greece)
Michael Leotsinidis (Greece)
Argyro Livaniou (Greece)
Manuel José Margues (Portugal)
Paulos Marinos (Greece)
Henrik Marszalek (Poland)
Boris Mijatovic (Serbia)
Jacque Mudry (France)
Konstantinos Nikolakopoulos (Greece)
Euagelos Nikolaou (Greece)
Andreas Panagopoulos (Greece)
George Panagopoulos (Greece)
George Papatheodorou (Greece)
Didier Pennequin (France)
Christos Petalas (Greece)
Fotios Pliakas (Greece)
Maurizio Polemio (Italy)
Antonio Pulido Bosch (Spain)
Dimitris Rozos (Greece)
Kim Rudolph-Lund (Norway)
Nikolaos Sambatakakis (Greece)
Allen Shapiro (USA)
George Soulios (Greece)
George Stamatis (Greece)
George Stournaras (Greece)
Luigi Tulipano (Italy)
Peter Udluft (Germany)
Sotirios Varnavas (Greece)
Konstantinos Voudouris (Greece)
Qin Xiaoqun (China)
Eleni Zagana (Greece)
Hans Zojer (Austria)
Nikolaos Zouridakis (Greece)

Contents

Volume 1

Hydrology

Karst Hydrogeology

Volume 2

Fissured rock Hydrogeology

Hydrochemistry

The role of water in constructions projects

Fissured rock Hydrogeology

Hydrogeological properties of fractured rocks (granites, metasediments and volcanites) under the humid tropical climate of West Africa

M. Koïta[1], H. Jourde

Laboratoire HydroSciences Montpellier UMR 5569 Université Montpellier 2
Place E. Bataillon, 34095 Montpellier Cedex 5, France
[1] Now at International Institute for Water and Environmental Engineering (2iE), 1 rue de la Science, 01 BP 594 Ouagadougou 01 Burkina Faso
herve.jourde@univ-montp2.fr

Abstract This study aims to propose a vertical structuring of water production zones for three types of fractured rocks encountered in Ivory Coast, West Africa. In a first step, the methodology consists of the characterization of the weathering profiles based on: i) bedrocks and weathering layers observations at outcrop; ii) interpretation and synthesis of geophysical data and lithologs from different boreholes. In a second step, the evolution with depth of flow rate (air-lift discharge rates) as well as the frequency and the density of water production zones during drilling are statistically analyzed. Then, the distributions of these various properties versus the depth are fitted to probability laws. For each of the geological formations (granites, metasediments and volcanites) the related weathering profile comprises, from top to bottom, four separate layers: *alloterite*, *isalterite*, *fissured layer* and *fractured fresh basement*; these weathering profiles are systematically covered by a soil layer. In granites, the maximal values of flow, frequency and density of the water production zones (WPZ) are situated around 40 m depth systematically within the *fractured fresh granite layer*. In metasediments and volcanites, the maximal values of flow, as well as the maximal frequency and density of WPZ are identified at two distinct depths. The first WPZ, around 40 m depth, is associated to the *fissured layer* for both profiles; the second WPZ, around 80 m depth is associated to the *fractured fresh sandstone layer* for the weathering profile in metasediments and to the *fractured fresh metabasalt layer*, for the weathering profile in volcanites.

1 Introduction

Hard rocks show vertical and horizontal heterogeneities as a result of both the spatial variation of the lithology, as well as the geometric and hydraulic properties of their distinct composite parts. This complexity of the aquifer limits the ability of

N. Lambrakis et al. (Eds.), *Advances in the Research of Aquatic Environment, Vol. 2*
DOI 10.1007/978-3-642-24076-8, © Springer-Verlag Berlin Heidelberg 2011

hydrogeologists to fully understand, describe and predict the hydrodynamic behavior of this type of hydrosystem. The scarcity of available data, their inconsistencies with the potential conceptual processes and mechanisms to be predicted, and their inherent ambiguity do not justify the promotion of models that include all mechanisms in a deterministic manner (Finsterle et al. 2002). Recognizing this limitation, several authors (Geirnaert et al. 1984; Wright 1992; Taylor and Howard 2000; Freyssinet and Farah 2000; Dewandel et al. 2006) developed conceptual models describing simplified lithological sequences above the crystalline basement. Most of these studies concerned granite formation, and few investigations addressed volcanosedimentary formations. Their heterogeneity may be the reason why no conceptual model is proposed for these formations.

This study aims to propose a standard hydrogeological conceptual model for granite and volcanosedimentary rocks describing water production zones as a function of the vertical layering of each geological formation weathering profile under humid tropical climate condition.

2 Geological context of the Dimbokro catchment

Dimbokro catchment (6300 km^2) in which many hydrogeological data are available is chosen as a study case to characterize granites, metasediments and volcanites. This catchment is part of the Nzi River catchment located in the central east of Ivory Coast, West Africa (Fig. 1). The rocks set up is attributed to the "Birimian" tectono-volcanism phase (2000-1880 million years ago (my)) that affect lower proterozoic formations in many part of west Africa (Ivory Coast, Burkina Faso, Ghana, Niger etc.). "Birimian" derives from "Birim" the name of a river in Ghana and refers to volcanites as well as to volcanosedimentary and detritical sediment deposits, set up within numerous furrows or intercratonic basins The geological formations of Dimbokro catchment are roughly divided into two major groups which experienced different tectono-metamorphic changes (Yao et al. 1990, 1995): i) the volcanosedimentary complex and ii) the biotite granites.

Synthesis of the geological history is made by Peltre (1977) and Yao et al. (1995). Set up of the granites domain began at 'Liberian' tectono-volcanism (2900 to 2400 my) and precedes the volcanosedimentary domain. In Lower Proterozoic, the reactivation of deep faults by 'Eburnean' tectono-volcanism phase (about 2200 my) remobilizes 'Liberian' granites and opened in the 'Liberian' platform long and narrow subsidence. At this period, interstratifications of lava and associated sediments flowed out through marginal faults towards an open sea, and formed the volcanosedimentary complex.

The 'Birimian' tectono-volcanism phase (2000 to 1880 my) also called 'main deposit phase' rejuvenated granites rocks and generated thick detrital accumulations made of conglomerates and sandstones, overlaying volcanosedimentary rocks. This accumulation phase supposes the existence of a high relief and strong erosion due to intense tectonic movements. Then the detrital accumulation coming

from erosion processes is folded during this tectonic paroxysm, which transformed this volcanosedimentary complex formation into schists. The metamorphism poorly affected the volcanosedimentary complex formations. These formations show a clayey tendency with grey or green colour passing in yellow green depending on rock weathering degree.

The study site is under the influence of the intertropical convergence with a pluviometric regime characterized by two rainy seasons. The first one is situated between April and June. The second extends between September and November. The average rainfall of the study site is 1200 millimeters.

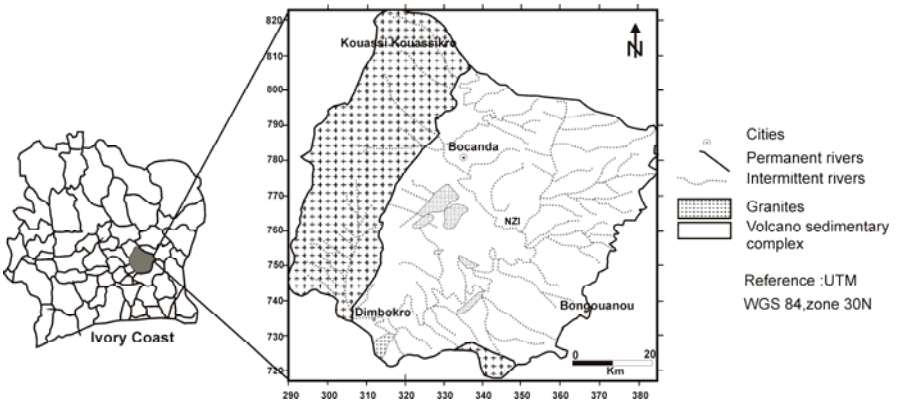

Fig. 1. Geology of the Dimbokro catchment.

3 Vertical structuring of the weathering profiles as a function of the geological units

The interpretation of lithologs (obtained from the cuttings collected each meter, during the drilling phase) and geophysical data (vertical electrical sounding) on the one hand, and the field observation (weathering profiles, as well as granites and volcanosedimentary bedrocks on outcrops) during the field campaign of 2008 and 2009 on the other hand are considered for characterizing the vertical structuring of granites and volcanosedimentary formations.

Observation at outcrop and the analysis of 32 lithologs for granites, 33 lithologs for metasediments and 37 lithologs for volcanites reveal that vertical layering of the weathering profile in each rock type comprises from the top to the bottom the following separated layers (Fig. 2): *alloterite*, *isalterite*, *fissured layer* and *fractured fresh basement*. Each profile is covered by a soil layer.

Though granites, metasediments and volcanites of the Dimbokro catchment experience the same weathering and erosion cycles during the paleoclimatic fluctuations from Eocene to recent quaternary period, they exhibit many differences and

similarities. In granites, the weathering profile is relatively thin due to the absence of iron crust which protects weathering products against dismantling.

In metasediments iron crusts develop better than in granites; in these rocks the alterite (*alloterite* and *isalterite*) is of kaolinitic type and thus more resistant to dismantling. Consequently, metasediments exhibit thicker profiles than granites.

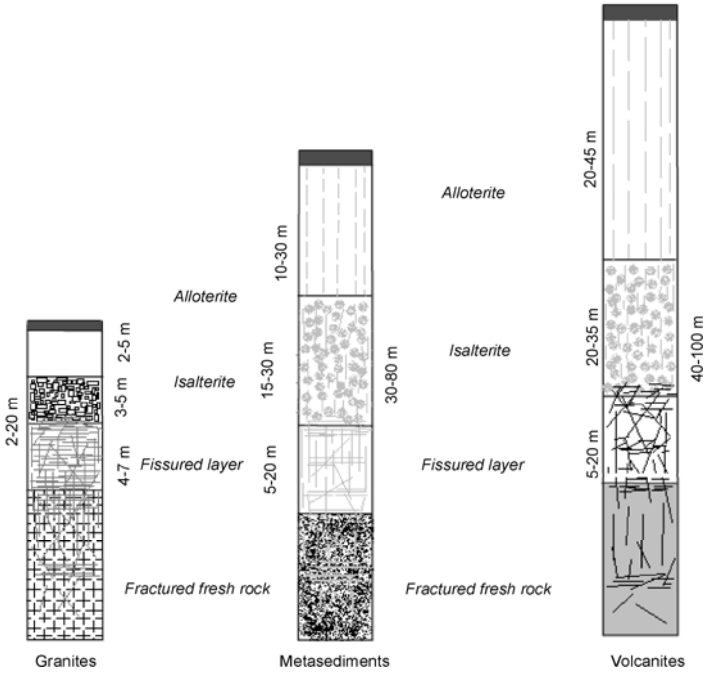

Fig. 2. Vertical layering of the weathering in granite**,** metasediment and volcanites.

In volcanites, the weathering profiles are generally complete and have the largest thickness, which again is related to a well developed iron crust that protect the rocks from dismantling. The high reliefs associated with the rocks show that they have been subjected to less dismantling than metasediments and granites. In each profile, the *fissured* layer is dominated by horizontal fissures (discontinuities in the alteration zone). But the structures of the fresh basement are different:

- In granites, the *fractured fresh basement* comprises a predominance of horizontal fractures (discontinuities in the fresh basement)
- In metasediments and volcanites the *fractured fresh basement* is characterized by vertical fractures intersected by horizontal discontinuity due to quartz veins intrusions.

Regarding the thicknesses it is noted that:

- In granites, alloterite, isalterite and fissured layers have similar thicknesses.

- In metasediments, the thickness of the *fissured* layer is lower than the ones of the *alloterite* and *isalterite* layers that both have similar thicknesses. In volcanites, the thickness of the *fissured* layer is also lower than the one of the *alloterite* and *isalterite* layers.

4 Vertical structuring of water production zones (WPZ) in the different geological units

In order to better understand the hydrodynamic behavior of the weathered mantle and the fractured basement, the WPZ associated with conductive fracture zones are characterized according to the depth from the top of the weathering profile (interface soil/ alloterite). The evolution of flows (air-lift discharge rates) and both the frequency and the density of water production zones during drilling is studied statistically. Then, the distributions of these various parameters versus depth are fitted to probability laws (Fig. 3).

The flow rates of each class of depth in granites, metasediments and volcanites are obtained by using the geometric means of air lift flow rates recording in each class of depth. The choice of geometric means is linked to the fact that it takes into account the disparities (standard deviation) in flow rates between the classes of depth in the same rock on one hand and between in the classes of depth in the three types of rocks on the other hand.

Evolution of flow rates (air lift discharge rates) according to depth shows that the most important flows are recorded in volcanites. Indeed, in volcanites, flow rates grow with depth and reach a maximum of 5 m^3/h between 80 and 100 m (in the *fractured fresh metabasalt layer*) before a drastic decrease. In metasediments, the maximums of flows are observed between 40 and 60 (in *fissured layer*) and between 80 and 100 m (in *fractured fresh sandstone*) with almost identical air lift discharge rates of 2.75 m^3/h. Beyond 100 m this discharge decreases with the depth. Compared to metasediments, granites show lower flows. In granites, flow increases until a maximum of 1.8 m^3/h between 40 and 60 m (in *fractured fresh granites layer*).

In metasediments and volcanites, WPZ are undifferentially localized in *isalterite layer*, *fissured layer* and *fractured fresh basement layer* while in granites, they are only localized in *fissured layer* and *fractured fresh basement*. In each of the profiles, the frequency of WPZ (all layers of the profile having been taken into account) is distributed in a log-normal way. In granites and metasediments, WPZ are observed from 10 m and up to 80 and 100 m below the top of the weathering profile. The maximum of WPZ is observed at about 45 m depth for both the weathering profile in granite (in the *fractured fresh granites layer*) and in metasediments (in the *fissured layer)*. In volcanites, the occurrence of WPZ is deeper; it extends between 30 m and 110 m below the top of the weathering profile.

In granites, evolution of density (number of WPZ per unit length of WPZ) reveals that the highest density of WPZ is localized between 40 m and 60 m depth (in the *fractured fresh granites layer)*, around 40 m depth in metasediments (in the *fissured* layer) and around 60 m depth in volcanites (in the *fissured* layer). Even if the densities are in the same order of magnitude, the highest densities (29 x 10^{-2}) of WPZ are recorded in volcanites and in granites and the lowest (24 x 10^{-2}) in metasediments.

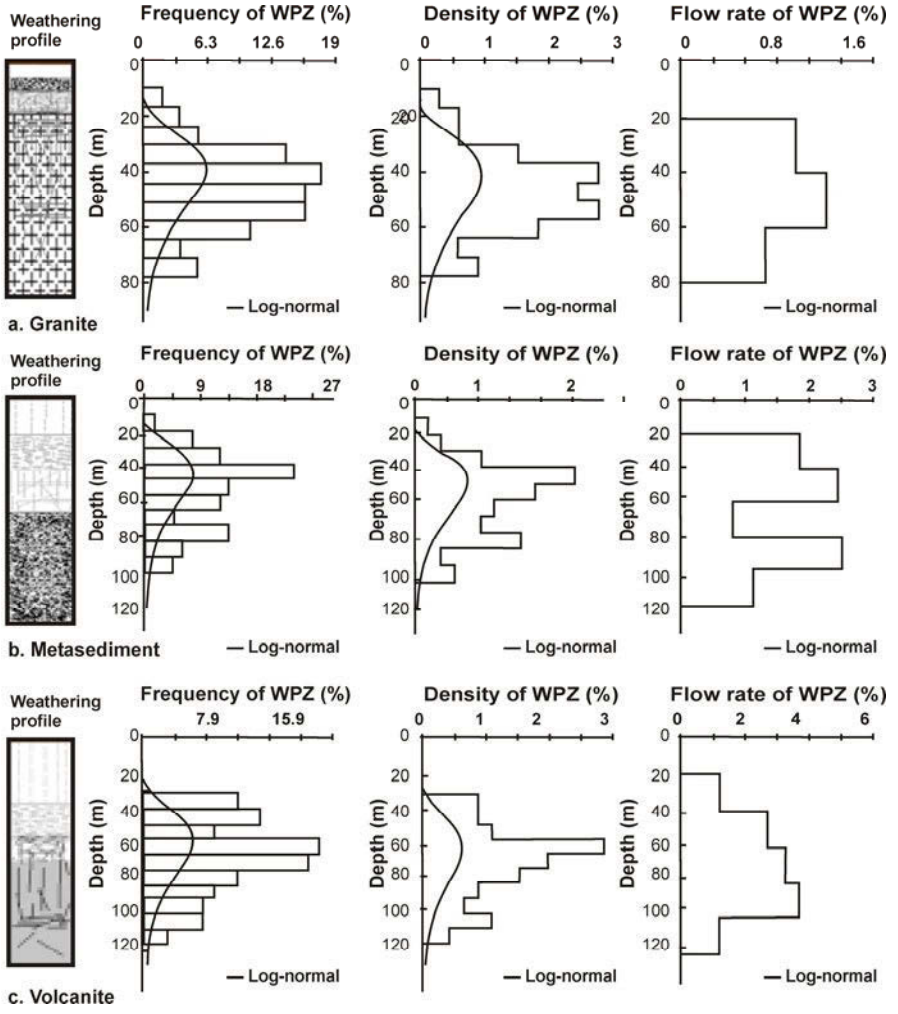

Fig. 3. Evolution of frequency, density and rates of WPZ according to depth. **a**. in granites. **b**. in metasediments. **c**. in volcanites.

Below this highest density level, the density of WPZ decreases with depth for each of the profiles. However, a significant increase of the density of WPZ occurs around 80 m depth in metasediments; this level is associated to *fractured fresh sandstone layer*. The same phenomenon is also observed in granites and volcanites around 75 and 100 m respectively, but in a slightly less significant manner. In hard rocks, this decrease of fracturing density with depth was described by the works of Wyns et al. (1999 and 2002), and Dewandel et al. (2006).

The simultaneous analysis of the evolution of the frequencies, the densities and the flows of WPZ shows that in granites and metasediments, the evolution of the flows of WPZ is coherent with those of the frequencies and densities; while in volcanites, the evolution of flows of WPZ is coherent with those of frequency and densities in the first 60 m depth. Beyond 60 m depth, it is not the case anymore: the class of depth associated with the maximal flows corresponds to the class of depth for which the frequency and the density of WPZ are not high.

In volcanites, deepest wells are the most productive. For these wells, the deep fractures are localized in *fractured fresh métabasalte layer* characterized by low frequency and density of WPZ. High flows supplied by these fractures are probably related to their size (regional fault) or to their interconnection with other systems of fractures.

Many studies defined the optimal depth that a drilling has to achieve to obtain a satisfactory productivity in hard rocks (Taylor and Howard 2000). Most of these studies showed that the productivity decreases with depth, what was interpreted for a long time as being associated with closure of fractures because of the lithostatique pressure (Berger et al. 1980) in depth; the present study and the other works (Wyns et al. 1999; Dewandel et al. 2006; Neves and Morales 2007) show that the decrease of the productivity with the depth would also be related to the decrease of the density of fractures in-depth.

5 Conclusions

Weathering profile characterization in granites, metasediments and volcanites in Dimbokro catchment reveals that each of the three profiles comprises four separate layers overlaid by a soil layer (*alloterite*, *isalterite*, *fissured layer* and *fractured fresh basement*). In granites, the weathering profile is relatively thin. Metasediments exhibit thicker profiles than granites. In volcanites, the weathering profiles are generally complete and have the largest thickness.

As hydrogeological impacts of this geological structuring, occurrence of WPZ is less deep in granites and metasediments than in volcanites. WPZ are localized undifferentially in *isaltérite* layer, *fissured* layer and *fractured fresh basement* in metasediments and volcanites while in granites, they are only localized in *fissured* layer and *fractured fresh basement*.

In the framework of water resource exploitation in granites, metasediments and volcanites localized in West Africa under humid tropical climate, future hydraulic campaigns should constrain the drilling depth limit according to the geological domains and taking into account the classes of depth associated to the highest frequency, density and flow rates of WPZ. This will allow obtaining a good yield in terms of well productivity and hydraulic campaign cost.

References

Berger J, Camerlo J, Fahy J.C, Haubert M (1980) Etude des ressources en eaux souterraines dans une région de socle cristallin: "la Boucle de cacao" en Côte d'Ivoire. Bull. BRGM. Sér. II. Sect. III. 4, 3350-338

Dewandel B., Lachassagne, P., Wyns R., Maréchal J C., Krishnamurthy NS (2006) A generalized 3-D geological and hydrogeological conceptual model of granites aquifers conrolled by single or multiphase weathering, Journal of Hydrology 330, 260-284

Finsterle, S., Fabryka-Martin JT., Wang JSY (2002) Migration of a water pulse through fractured porous media. Journal of contaminant Hydrology 54 (2002) 37-57

Freyssinet P., Farah A S (2000) Geochemical mass balance and weathering rates of ultramafic schists in Amazonia, Chemical Geology 170 (2000), 133-151

Geirnaert W, Groen M, Van Der Sommen J, Leusink A (1984) Isotope studies as a final stage in groundwater investigations on the African shield, challenges in African Hydrology and water resources (Proceeding of the Harare Symposium, July 1984). IAHS publ. 144, 141-153

Neves M A, Morales N (2007) Well productivity controlling factors in crystalline terrains of southeastern Brazil, Hydrogeology Journal 15, 471-482

Peltre P (1977) Le «V» baoulé: Héritage géomorphologique et paléoclimatique dans le tracé du contact forêt-savane, Cahier ORSTOM, 190

Taylor R., Howard K (2000) A tectono-geomorphic model of the hydrogeology of deeply weathered crystalline rock: Evidence from Uganda, Hydrogeology Journal, 8:279-294

Wright E P (1992) The hydrogeology of crystalline basement aquifers in Africa, Geological Society, London, Special Publications, Vol. 66, doi: 10. 1144/GSL.SP.1992.066.01.01, 1-27

Wyns R., Gourry JC., Baltassat JM., Lebert F (1999) Caracterisation multiparametres des horizons de subsurface (0-100 m) en contexte de socle altéré. In: I. BRGM, IRD, UPMC (Eds), 2ème Colloque GEOFCAN, Orléans, France, 105-110

Yao D, Delor C, Gadou G, Kohou P, Okou A, Konaté S, Diaby I (1995) Notice explicative de la carte géologique feuille de Dimbokro, Mémoire SODEMI, Abidjan (Côte d'Ivoire)

Identification of conductible fractures at the upper- and mid- stream of the Jhuoshuei River Watershed (Taiwan)

P.Y. Chou, H.C. Lo, C.T. Wang, C.H. Chao, S.M. Hsu, Y.T. Lin, C.C. Huang

Geotechnical Engineering Research Center, Sinotech Engineering Consultants, Inc., No. 7, Lane 26, Yat-Sen Road, Taipei 110, Taiwan PoYi.Chou@sinotech.org.tw

Abstract The movement and storage of ground water in the mountainous region has a significant impact on the dynamics of surface water flow. An adequate identification of the conductible fracture in the aquifer has thus received growing interest over the past decades. This paper summarizes the major findings from the first year of a hydrogeological investigation program initiated by the Central Geological Survey, Ministry of Economic Affairs (MOEA) of Taiwan since 2010, with a special focus on exploring in detail the fracture permeability. During the on-site investigation, geophysical logging was applied to delineate the lithostratigraphic characteristics of bedrock aquifers. The hydraulic conductivity of 67 observation segments was estimated by the constant head injection method. From the information gathered in this study, the hydraulic conductivities of the identified fractured medium above a depth of 40m are more than one order higher than that of the matrix. The occurrence of ground water in a fracture network, however, is found to be not solely governed by lithological composition, but more possibly by fracture porosity and spacing. A simple linear relationship was found by plotting the hydraulic conductivity against the product of total porosity and cubic aperture ratio (fracture spacing/sealed-off interval between the packers).

1 Introduction

Accompanying with the growing concern on the sustainability of available water resource, to gain more in-depth knowledge on the potential yield of aquifers is a crucial task. The movement of ground water within the mountainous region is either dominated by fracture continua, the porous medium, or even by both. The connectivity of discontinuities and the vector gradient of hydraulic heads are likely the most important factors determining the fracture/matrix permeability. Prior to evaluating whether a specific stratum of geometry is capable of yielding and storing a sufficient amount of ground water by means of any sophisticated numerical models, it is necessary to perform the downhole geophysical investigation to gain more insights into the lithologic composition of stratum unit.

N. Lambrakis et al. (Eds.), *Advances in the Research of Aquatic Environment, Vol. 2*
DOI 10.1007/978-3-642-24076-8,

The identification of conductible fracture in the mountainous-foothill region is often difficult. Within a fractured aquifer network, usually, not all the perceptible fractures will be hydrologically connected. The use of a combination of composite well logs and in-hole tracer tests could provide more than sufficient information regarding to the complex geometries and layering, however, especially when working with limited budget and time, a set of systematic and concise criteria for the quick in-situ identification of conductible fractures is indeed required.

The Central Geological Survey, Ministry of Economic Affairs (MOEA) of Taiwan has initiated a large-scale hydrogeological investigation program since 2010 that aimed at exploring in detail the hydraulic properties of bedrock aquifers in Taiwan mountainous-foothill region. This study presents estimates of hydraulic conductivity obtained by the constant head injection test and, further, to assess the relationship among hydraulic conductivity, fracture porosity and spacing.

2 Geological setting

The study area is located in the Western Foothills of Taiwan within the latitude and longitude of 23° 52' N and 120° 25' E, respectively. It covers the up- and middle-stream basin of the Jhuoshuei River with an area of 1,577 square kilometer. As shown in Fig. 1, the elevation lies between 142 and 1658 meters above sea level (m.a.s.l.). Owing to the collision of tectonic plates (Mouthereau and Lacombe 2006) a series of westward fold-and-thrust belts can be observed. The geological formation in this study area can be roughly separated from East to West into four regions by the orientation of faults. Region I at the most eastern side ranges in age from Eocene to Miocene, where the predominant lithology is massive slate rock accompanied with metasandstones and metasiltstones. Region II extends from Eocene to early Oligocene, the upper part is dominated by hard shale stone and the lower part is coarse quartz sandstone hosted. Region III, bounded by the Shuilikeng, Chelungpu and Tachienshan faults, is underlain by Miocene to Pleistocene sedimentary rocks. A distinct pattern of lithological distribution can be found in this region that closely related to the influence of folding, faulting and metamorphism. Region IV at the most western side is mainly consisted of unconsolidated alluvium and relatively young deposits from late Pliocene to Pleistocene. Topographic slopes in region I, II and III are from 30°-60°, relatively, more gentle topographic slopes (0-30°) are found in the region IV.

A total of 29 vertical fully penetrating boreholes (see Table 1) were drilled to a depth of 100 meters (328ft.) below the land surface. The ground water level (m) from the earth surface was measured on-site during the test in the wet season.

Table 1. Boreholes description.

Topographic region	I			II			III							
Borehole	B11	B12	B13	B02	B10	B21	B04	B05	B06	B08	B09	B16	B17	B18
Geometric height (m.a.s.l.)	391	472	468	431	357	638	409	295	764	633	403	280	227	631
Groundwater level beneath the surface (m)	14.0	77.0	86.1	4.5	9.0	36.5	4.5	11.0	10.0	4.0	16.5	14.3	4.0	23.0

Topographic region	III								IV						
Borehole	B19	B20	B22	B24	B25	B26	B27	B29	B01	B03	B07	B14	B15	B23	B28
Geometric height (m.a.s.l.)	476	1658	943	756	712	1172	191	1201	316	142	345	341	312	749	188
Groundwater level beneath the surface (m)	20.0	53.0	13.0	13.3	15.4	7.0	6.0	18.5	2.0	4.0	4.7	80.0	28.5	9.0	8.8

Rock samples were recovered and allowed for an initial on-site lithostratigraphic identification, as well as various laboratory analyses afterward.

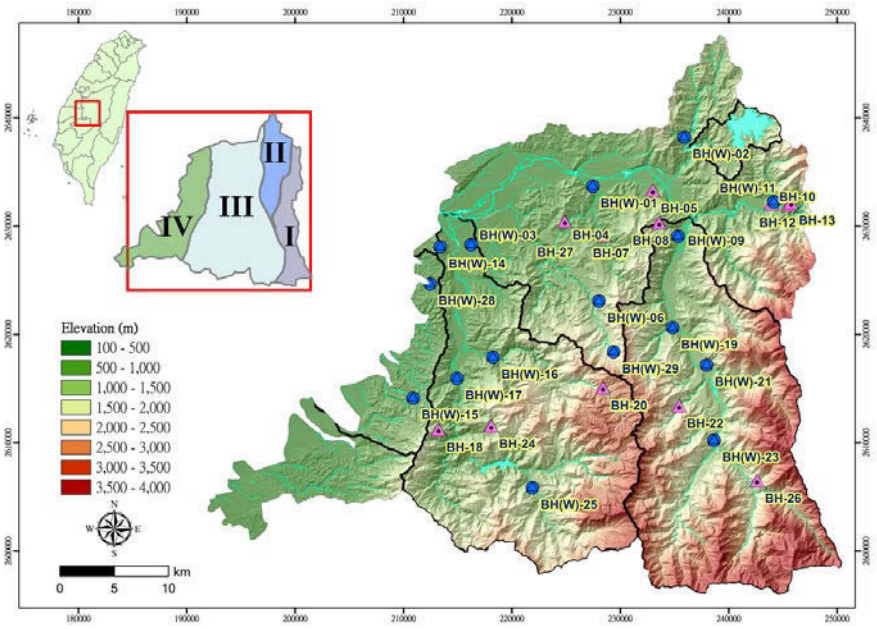

Fig. 1. Geological map of the study area.

3 Methodology

In each borehole a series of borehole loggings were conducted in situ to identify the probable pathways of ground water. The electric log and the full waveform sonic log (from Robertson Geologging Ltd. UK) were adopted. These two sondes have long been used in the field of geosciences, a comprehensive overview has been provided in the study of Timur and Toksoz (1985), and Lau (1998). In this present research, the electric log was used to measure the spontaneous potential, electrical resistivity and natural gamma radiation, while the full waveform sonic log was applied to detect the sonic travel-time at a specific depth within the borehole. By using the acoustic-velocity logging, aquifer porosity can also be determined based on a time-average equation.

Borehole televiewer was performed to un-wrap the oriented circular borehole-wall images, which facilitated the interval of interest can be precisely straddled when performing packer tests. In addition, the fracture related characteristics such as the dip-azimuth, aperture width, and infilling material of fractures can also be quantified by further mapping efforts. The application of borehole televiewer on

fracture identification has been adopted in earlier studies (Hartenbaum and Rawson 1980; Williams and Johnson 2004; Morin 2005; Hubbard et al. 2008). Two types of televiewer were adopted in this project to identify the appearance of fracture zones: the high resolution acoustic televiewer (HiRAT) and the optical televiewer (OPTV) (from Robertson Geologging Ltd. UK). The maximum pressure allowance of both types of televiewer is 20MPa.

Based on the geophysical log and televiewer profiles, four criteria were taken into consideration to identify the conductible fractures: (1) Reduced gamma-ray response; (2) Divergence of the short normal-resistivity log relatively to the long one; (3) Larger acoustic-velocity derived porosity; (4) Appearance of discernible spacing (>0.01m). Since after the conductible fractures in each borehole were identified, the hydraulic conductivity of the selected observation segments was determined by the constant head injection test (CHIT) with double packers system. This technique has been widely employed elsewhere to determine the hydraulic properties of a fractured stratum (e.g. Morin et al. 1988; Howard et al. 1992; Brown and Slater 1999; Niemi et al. 2000; Mejías et al. 2009). The detailed apparatus of the double packer assemblies employed in this study were described by Ku et al. (2009), and the procedures of testing were following the designation of American Society for Testing and Materials method (ASTM D4630-96 2002).

The sealed-off interval was fixed at 1.5m. Water was injected with a constant pressure of 0.2Mpa or at least in excess of the ambient hydrostatic heads. At least two observation segments were specified in each borehole. To diminish the risk of failure due to borehole spalling, the packer testing was carried out from the observation segment located at the lowest position in the borehole and then moving upward to the next. Each test took at least three hours including rig transfer, quick calibration, packer inflation, data recording and pressure recovery. The variation of hydraulic head and injected flow rate within the testing section were recorded per second and stored in a data-logger developed by the Sinotech Inc.

4 Data analysis and interpretation

Sixty seven observation segments, including both fractured and non-fractured media (matrix) in consolidated bedrock, were tested by CHIT. Hydraulic conductivity was derived by the interpretation of injected flow rate with the software AQTESOLV, version 4.5 (HydroSOLVE Inc. Reston, VA). In this study, the generalized radial flow model proposed by Barker (1988) was adopted and written as:

$$S_s \frac{\partial h}{\partial t} = \frac{K}{r^{n-1}} \frac{\partial}{\partial r}\left(r^{n-1} \frac{\partial h}{\partial r} \right)$$

where S_s represents the specific storage of aquifer [L^{-1}]; $h(r, t)$ denotes the change in hydraulic head [L] with time, r represents the radial distance from the borehole [L]; K represents the hydraulic conductivity [LT^{-1}]; n denotes the flow dimension according to the distance from the borehole (1 for linear flow, 2 for cylindrical flow, 3 for spherical flow). The magnitudes of hydraulic conductivity are plotted on a logarithmic scale against the depth in borehole as shown in Fig. 2. The corresponding distribution of the magnitudes with respect to the occurrence of fractures as well as the type of rock is also presented.

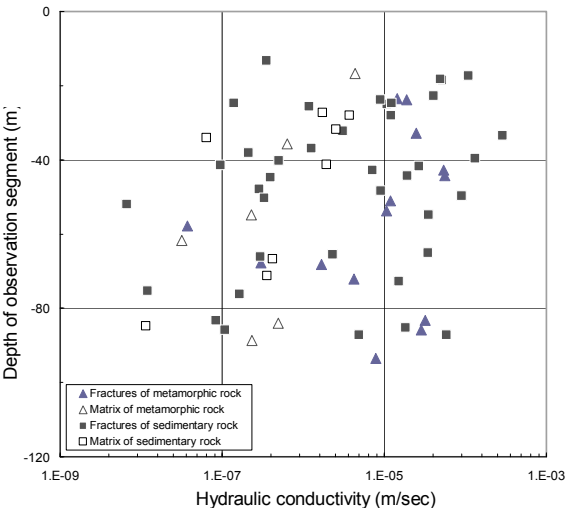

Fig. 2. Plot of the estimated hydraulic conductivity on a logarithmic scale with respect to different types of rock against depth in borehole.

The estimated hydraulic conductivity above a depth of 40m (*i.e.* the upper part of bedrock lying beneath the regolith layer) seems to show a slightly higher magnitude than at the greater depth, however, the overall hydraulic conductivities appear to be no significant depth correlation. With a view to evaluate the water-bearing capacity of fracture and matrix, a further subdivision can be made in terms of the magnitude of hydraulic conductivities as follows: (1) semi conductible medium: $10^{-5} < K < 10^{-3}$ m/s; (2) partial conductible medium: $10^{-7} < K < 10^{-5}$ m/s; (3) non-conductible medium: $K < 10^{-7}$ m/s. It is found that the identified fractures at the upper part of the bedrock possess semi-to-partial conductive capacity, while the fractures at the lower part of the bedrock exhibit a wider range of distribution pattern. Additionally, the occurrence of fractures in this study area shows approximately one order of higher hydraulic conductivity than of the matrix.

Fig. 3 attempts to further reveal the correlation of hydraulic conductivity (K) between total porosity (derived from acoustic velocity), and aperture ratio (fracture spacing/sealed-off interval between the packers, 1.5m). The open fractures with spacing less than 0.01m are not taken into account.

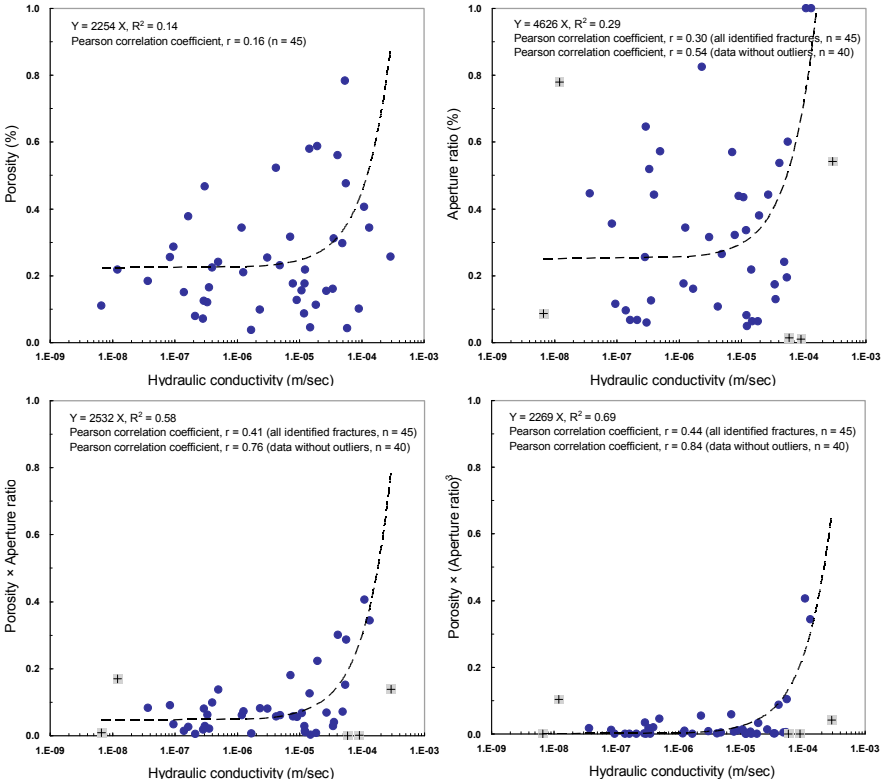

Fig. 3: Hydraulic conductivity in the logarithm scale versus total porosity (up-left), aperture ratio (up-right), product of total porosity and aperture ratio (down-left), and product of total porosity and cubic aperture ratio (down-right).

As shown in Figure 3, when considered individually, there is only a weak positive correlation found between hydraulic conductivity and the total porosity (Pearson's r = 0.16), while a moderate correlation is found with respect to the aperture ratio (Pearson's r = 0.30, all data included; Pearson's r = 0.54, excluding outliers). Interestingly, a slightly stronger correlation (Pearson's r = 0.41, all data included; Pearson's r = 0.76, excluding outliers) is shown when plotting the product of total porosity and aperture ratio versus the hydraulic conductivities. It indicates that the transport of ground water does not controlled by either the intra-aggregate pores, or the inter-aggregate spacing alone, but regulated by both proportionally. After exploring various possible relations, a simple linear relationship (Hydraulic conductivity K = 0.00044[Porosity × (Aperture ratio) ^{3}], coefficient of determination R^2 = 0.69) was identified by plotting the hydraulic conductivity against the product of total porosity and cubic aperture ratio. Note that this relationship has not taken the fracture orientation into account. A further testing of this relation with respect to three-dimensional fracture orientation is recommended.

5 Discussions and recommendations

This paper reports the summary of a just-completed project aiming toward understanding the fracture permeability in mid-Taiwan mountainous-foothill region. It is also the purpose of this study to provide a theoretical and empirical based guideline for quick identification of conductible fractures. On the basis of 29 vertical boreholes at the upper- and mid-stream site of Jhuoshuei River basin, the conjunctive use of geophysical logging and televiewer imaging was carried out and used for determining the lithologic characteristics. Four hypothesized criteria were proposed which are applicable to identify the presence of permeable zone. The hydraulic conductivity at the predetermined depths was estimated by the constant head injection method.

According to the data collected during the first year, it is found that the majority of the identified fractured medium, especially above a depth of 40m, shows more than one order of higher hydraulic conductivity than of the non-fractured medium. However, the transport of ground water in the mountainous region does not independently controlled by either the inter-aggregate spacing, or the intra-aggregate pores alone, but, possibly, regulated by both proportionally. A simple linear relationship was identified by plotting the hydraulic conductivity against the product of total porosity and cubic aperture ratio. This relation could provide as an initial guide in assessing the potential yield of aquifer with the help from a drilling borehole. More systematic research is needed to formulate this relation with respect to fracture orientation.

References

Barker JA (1988) A generalized radial flow model for hydraulic tests in fractured rock. Water Resour Res 24, 1796-1804

Brown D., Slater LD (1999) Focused packer testing using geophysical tomography and CCTV in a fissured aquifer. Q. J. Eng. Geol. Hydrogeol. 32, 173-183

Hartenbaum BA, Rawson G (1980) Subsurface Fracture Mapping from Geothermal Wellbores, U. S. Department of Energy Report DOE/ET/27013-T1

Howard KWF, Hughes M, Charlesworth DL, Ngobi G (1992) Hydrogeologic Evaluation of Fracture Permeability in Crystalline Basement Aquifers of Uganda. Hydrogeol. J. 1, 55-65

Hubbard B, Roberson S, Samyn D, Merton-Lyn D (2008) Instruments and Methods - Digital optical televiewing of ice boreholes. J. Glaciol. 54, 823-830

Ku CY, Hsu SM, Chiou LB. Lin GF (2009) An empirical model for estimating hydraulic conductivity of highly disturbed clastic sedimentary rocks in Taiwan. Eng. Geol. 109, 213-223

Lau KC (1998) A review of downhole geophysical methods for ground investigation. Technical Note No. TN 4/98, Geotechnical Engineering Office, Hong Kong

Mejías M, Renard P, Glenz D (2009) Hydraulic testing of low-permeability formations: A case study in the granite of Cadalso de los Vidrios, Spain. Eng. Geol. 107, 88-97

Morin RH (2005) Hydrologic properties of coal beds in the Powder River Basin, Montana I. Geophysical log analysis. J. Hydrol. 308, 1-4

Morin RH, Hess AE, Paillet FL (1988) Determining the Distribution of Hydraulic Conductivity in a Fractured Limestone Aquifer by Simultaneous Injection and Geophysical Logging. Ground Water. 26, 587-595

Mouthereau F., Lacombe O (2006) Inversion of the Paleogene Chinese continental margin and thick-skinned deformation in the Western Foreland of Taiwan. J. Struct. Geol. 28, 1977-1993

Niemi A, Kontio K, Kuusela-Lahtinen A, Poteri A (2000) Hydraulic characterization and upscaling of fracture networks based on multiple-scale well test data. ater Resour. Res. 36, 3481-3497

Timur A., Toksoz MN (1985) Downhole geophysical logging. Annu. Rev. Earth Planet. Sci. 13, 315-344

Williams JH, Johnson CD (2004) Acoustic and optical borehole-wall imaging for fractured-rock aquifer studies. J. Appl. Geophys. 55, 151-159

Advances in understanding the relation between reservoir properties and facies distribution in the Paleozoic Wajid Sandstone, Saudi Arabia

H. Al Ajmi[1], M. Keller[2,4], M. Hinderer[3], R. Rausch[4]

[1] Ministry of Water and Electricity, Water Resources Development Department, Riyadh, Saudi Arabia, email: hussain.alajmi@yahoo.com

[2] Geozentrum Nordbayern, Abteilung Krustendynamik, Schlossgarten 5, 91054 Erlangen, Germany

[3] Institut für Angewandte Geowissenschaften, TU Darmstadt, Schnittspahnstrasse 9, 64287 Darmstadt, Germany

[4] Gesellschaft für Technische Zusammenarbeit International Services (GTZ-IS), Riyadh, Saudi Arabia

Abstract The Wajid Sandstone is one of the most important groundwater reservoirs in the Kingdom of Saudi Arabia. The knowledge of the dimensions and the distribution of its sedimentary facies are essential for high quality reservoir interpretation. Hitherto, the facies and their dimensions are only roughly known from extrapolation of subcrop data and geophysical surveys.

Sedimentological logging and correlation of the sections led to an interpretation of the depositional processes and a more detailed facies model. Based on systematic lithofacies and architectural element analysis, the so far established and published facies characteristics derived from subcrop information of the depocenter in the West of the Kingdom and also from the outcrop area have to be modified.

These data have important implications on reservoir properties of the Wajid sandstone. The sandy deposits guarantee a high primary porosity and permeability up to 1 D. Bioturbation leads to pronounced anisotropy in some horizons. Of major importance, however, are late diagenetic cementation effects which focus on faults, fractures and horizontal to subhorizontal discontinuities. Most widespread is iron cementation which makes up almost impermeable seals and separates reservoirs horizontally and vertically. The primary control on reservoir quality is due to a gradual facies change from W to E. Fine-grained silty layers are increasingly intercalated towards the E but are almost completely absent in the W. Consequently, in the western area, the Wajid Group forms a combined reservoir but in the subsurface is separated into two layers.

N. Lambrakis et al. (Eds.), *Advances in the Research of Aquatic Environment, Vol. 2*
DOI 10.1007/978-3-642-24076-8,

Introduction

In Saudi Arabia, the Paleozoic Wajid Sandstone is an important groundwater reservoir and in the subsurface, several individual aquifers have been distinguished (GTZ-DCo 2007). The properties of the individual aquifers and their correlation to facies and depositional environment, however, are only poorly known. We present preliminary results of a detailed investigation on facies, lithology, and depositional environment in the Wajid Sandstone (Fig.1). It is subdivided into five formations, the Dibsiyah, Sanamah, Qalibah, Khusayyayn, and Juwayl formations (Kellogg et al. 1986).

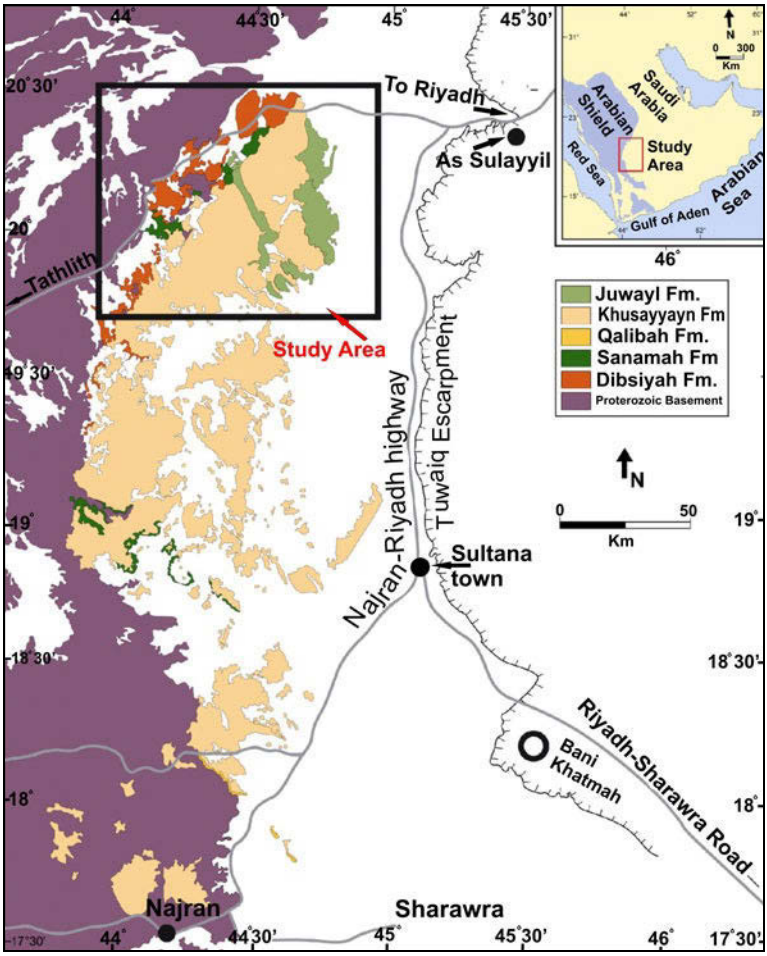

Fig. 1. Outcrops of the Wajid Sandstone and its members (modified from Al Husseini, 2004) in SW Saudi Arabia.

In general, biostratigraphic control on the deposits of the Wajid Sandstone is very poor. It has been dated mainly indirectly through correlation of geophysical data to the subsurface (Evans et al. 1991). Following this correlation, the Dibsiyah is of Cambrian or Ordovician age; the Sanamah corresponds to the latest Ordovician. The Qalibah is interpreted to correspond to the Early Silurian, while the Khusayyayn was deposited during Devonian and Early Carboniferous time. The Juwayl comprises glacigenic deposits and their formation is attributed to the Upper Carboniferous and Lower Permian glaciation.

Dibsiyah Formation

The Dibsiyah is a succession of medium-grained to conglomeratic sandstones with few intercalations of finer siliciclastic horizons. The Dibsiyah is subdivided into a lower and an upper part. The lower unit has a minimum thickness of about 60 m at Jabal Dibsiyah, the upper part a minimum thickness of 130 m.

The lower Dibsiyah consists of a succession of cross-bedded medium to coarse-grained sandstones and fine conglomerates. The dominant color of the sediments is gray, many of the horizons, however, have a red color. Sedimentary structures include lateral accretion complexes and low-angle, 2D-trough cross bedding. In the 3rd dimension, these structures continue in very persistent cross-bedding with near planar lower and upper bounding surfaces. Bioturbation is present from the lowest exposed horizons to the top of the unit. Horizontal burrows have been observed on few bedding planes. Vertical burrows of *Skolithos* sp. are locally abundant in the sandstones of all lithologies, including conglomeratic sandstones. Very scarce *Cruziana sp.* has also been observed.

The upper Dibsiyah is composed of medium to coarse-grained sandstones. Locally, lenses or thin layers of red siltstone to fine-grained sandstone are intercalated. The dominant sedimentary structure is low-angle, 2D-trough cross bedding of the same type observed in the lower unit. They are laterally very persistent and individual units can be traced over several hundred meters. Herringbone cross stratification is present locally and always associated with the large 2D bedforms. Lateral accretion complexes are also present in this upper part of the Dibsiyah; individual complexes may show foresets up to 2 m high and several centimeters thick. They often show a sigmoidal geometry. Many of them are traceable across entire outcrops.

Bioturbation is much more important than in the lower unit. One of the main elements is *Skolithos sp.* that is present widely scattered within individual horizons, somewhat crowded to almost "frame-building" in some horizons. These "pipe rocks", common in many Cambrian and Ordovician siliciclastic successions, are also known as "Tigillites". In the upper Dibsiyah, thickness of *Skolithos* pipe rocks varies between some 10 centimeters to several meters. Simple *Skolithos* burrows are often associated with larger burrows attributed to *"Bergaueria" sp*. The

almost "reef-like" horizons of *Skolithos* and/or *Bergaueria* are up to 13 meters thick. Most of the internal sedimentary structures have been destroyed by burrowing; however, the primary cross-bedding is often faintly visible.

The presence of a variety of burrowing organisms and *Cruziana sp.* in both units testifies to deposition of the entire Dibsiyah in a marine environment. In their majority, the low-angle, 2D through cross-bedded horizons represent tidal channels. The lateral accretion complexes are interpreted as large submarine megaripples or dunes typical of meso- to macrotidal environments (Einsele 2000).

The lower unit received coarser detritus than the upper unit. This might indicate that the rivers delivering the detritus had higher transport capacity than during deposition of the upper unit or that the coast was close by, in turn indicating a relatively low sea level. Towards the upper part of the Dibsiyah, sea-level was relatively rising so that after deposition of large submarine dunes, these dunes or megarippels were burrowed by *Skolithos* and *Bergaueria*. The depth of burrowing (up to 50 cm) indicates that the animals had abundant time during which no additional sediment was supplied that would have forced the organisms to try to evade. This is in agreement with models that suggest that *Skolithos* burrows are dominantly formed during times of transgression or maximum flooding (e.g., Hamon et al. 2005). Depositional environments were shifting rapidly so that there is a repeated succession of burrowed and non-burrowed sediments.

Sanamah Formation / Qusaiba Shale

The Sanamah is a succession of coarse-grained sandstones and conglomerates in its lower part and fine-grained sandstones, siltstones, and some shales in its upper part.

The lower Sanamah rests unconformably on the Dibsiyah and fills an erosional relief up to several 10s of meters deep. In many sections outside the actual channels, and beneath the upper Sanamah, there is just a thin veneer (6 – 10 m) of lower Sanamah preserved. The basal part of the upper unit was deposited across the post-lower Sanamah topography and has a similar distribution as the sediments of the lower unit. The upper part of the succession is only exposed in the Jibal al Qahr. Although genetically related to the Sanamah Formation, these deposits might represent the subsurface Qusaiba Shale of the Qalibah Formation in this part of Saudi Arabia.

In the Jabal Atheer section, the lower Sanamah is 92 m thick. There is no continuous section of the Qusaiba in the study area but in the Jibal al Qahr about 50 m are exposed beneath the unconformity with the Khusayyayn.

The lower Sanamah consists of a succession of conglomerates, conglomeratic sandstones, and medium- to coarse grained sandstones. The conglomerates fill large channels and in most cases are the basal fill of the pre-existing topography. They are composed individual lobes, each several 10 of centimeters thick and

graded, from pebble size at the base to medium or coarse sand in the upper part. Where the basal conglomerate layers had filled up the relief, subsequent layers and channels are locally laterally amalgamating, forming more widespread deposits (on outcrop scale). Conglomerates are not only present as channel fills but also form part of migrating bars. They mainly show an overall fining-upward or show a lateral decrease in grain size. Above this succession there is a package of gray to yellowish medium to coarse-grained sandstones. In many outcrops, these sandstones are massive and lack apparent internal structures. Locally, these massive sandstones eroded into the underlying sediment producing overhanging walls. Outside the main valleys, the thin veneer of lower Sanamah consists of channelized conglomerates and conglomeratic sandstones with well-developed high-angle, 3D trough cross bedding.

Clast- and matrix-supported conglomerates and coarse conglomeratic sandstones represent the basal channel-fill facies association (Keller et al. 2011). They are interpreted as coarse glacial outwash sediment near melt water outlets. A facies association of massive to cross-bedded sandstones, arranged in clinoforms, fills up the upper part of the valleys. These sediments are interpreted as Gilbert-type deltas prograding from sandur plains into the water-filled valleys during glacier retreat. Together with glacial striations, striated clasts, and similar corresponding features, these sediments indicate a glacial origin of this part of the Wajid Sandstone (Keller et al. 2011).

The upper Sanamah starts with an iron-cemented horizon, up to 20 cm which is overlain by some shales and siltstones. Locally sandstones were deposited that indicate large-scale slumping. Up section, white fine- to medium-grained sandstones alternate with shales. In its upper part, the upper Sanamah or Qusaiba consists of a succession of light colored fine sandstones, siltstones, and shales. The sediments are thinly bedded and locally show some burrows. Close to the preserved top of the succession, mud cracks have been observed.

The basal deposits were laid down rather rapidly, so that the sands were subject to slumping. The lateral variability of the sedimentary successions (Stump and Van der Eem 1996) and the mud cracks indicate that they were probably not deposited on an open shelf but either in marginal marine environments (deltas) or in a lake setting.

Khusayyayn Formation

The Khusayyayn Formation (> 52m) is a monotonous succession of medium to coarse-grained sandstones and unconformably rests on older strata. The Khusayyayn consists of a stacked succession of giant cross-bedded sandstones; individual complexes locally are up to 2 meters high. The foresets are several centimeters thick and are often graded. Grain size mainly decreases from coarse sand to medium sand, but locally pebbles have been found in the basal layer of individual

foresets. These thick cross-bedded units are associated with herringbone cross stratification and small low-angle, 2D trough-bedded structures. Discrete packages within the succession were found, which seem to occur in all sections. At Jabal Khusayyayn, the succession starts with mainly coarse-grained, large-scale cross-bedded units. This is followed by small-scale bed forms in which medium to coarse sand dominates. Higher up, a massive sandstone unit was found which shows evidence of slumping and dewatering (flame structures). This unit in turn is followed by some 10 meters of fine to coarse-grained sandstones in small-scale bed forms with abundant channels. The uppermost unit again is dominated by large-scale bed forms and coarse-grained, often pebbly sandstones.

We interpret the Khusayyayn to have been deposited on a high-energy open shelf. This is indicated by the lateral continuity of the large cross-bedded units. They represent submarine megaripples or dunes and testify to strong unidirectional currents of tidal origin. The low-angle-trough cross-bedded units represent tidal channels. A tidal environment is also indicated by herringbone cross stratification repeatedly observed in the sections.

Juwayl Formation

The Juwayl Formation (> 100 m) shows the highest lithologic variability among the Paleozoic sandstones. It was deposited across an erosional surface that deeply cuts into the underlying strata. The Juwayl is present in two outcrop belts trending NW - SE corresponding to two major glacial valleys (Kellogg et al. 1986).

Thick, massively bedded fine to coarse-grained sandstones are a major constituent of the Juwayl. In places, they lack apparent sedimentary structures; in other places, these sandstones consist of stacked channels, often with lateral accretion phenomena. Locally, these sandstones cut vertically into the underlying sandstones and formed positive morphologic forms. Up section, these sandstones are overlain by reddish sandstones with high-angle, 3D through cross bedding and some ripple-drift cross bedding.

Another succession starts with thin conglomeratic sandstones with few pebbles. Up section, finely laminated shales are present. The alternation of mm-thick sandstone and clay laminae indicates a varve origin of these sediments. Large basement boulders and conglomerate clasts are present within these shales.

The varve sediments and the associated boulders and clasts leave little doubt that these sediments were deposited in a proglacial lake. The big boulders represent dropstones indicating the presence of icebergs. Consequently, the accompanying sediments also should be of periglacial origin. The 3D trough cross-bedded sediments were deposited by braided rivers and possibly partly represent braid delta deposits that formed in one the glacial lakes. The massive sandstones without apparent internal structure may represent eskers or drumlins deposited beneath

or in front of the moving ice. The steep walls of the channels indicate that the sediment may have been frozen during erosion.

Implications for aquifer properties

The sedimentary succession of the Wajid Sandstone is dominated by medium- to coarse-grained sandstones. Fine sandstones, pebbly sandstones, and conglomerates are present but of less importance. Siltstones and shales are rare. Almost the entire stratigraphic succession is characterized by very weak cementation and the near total absence of matrix, i.e., of silt and clay in the sediments. This fact has consequences for the reservoir potential of the Wajid Sandstone. In all members, there is a primary visible porosity which has been estimated to vary between 20% and 30% of the rock. This is in agreement with studies by Evans et al. (1991) who report average porosities of 20% for the Dibsiyah, 21% - 25% for the Sanamah, 23% for the Khusayyayn, and locally 30% for the Juwayl. Similarly, Dirner (2007) and Filomena (2007) report porosities between 18% and 31% for the Wajid Sandstone. Together with high effective permeabilities of 1 to 8 darcies, this makes the Wajid Sandstone principally an important reservoir rock.

A recent study (GTZ-DCo 2007) has shown that in the subsurface, the Wajid Sandstone succession represents two individual fractured bedrock aquifers separated by an aquitard. The lower aquifer is represented by the Dibsiyah and the Sanamah, effectively separated from the upper one by the siltstones and shales of the Qusaiba. The upper aquifer comprises the Khusayyayn and the Juwayl.

The distribution of the sedimentary successions of the Wajid Sandstone in the outcrop belt shows a different picture. The Dibsiyah crops extensively in the western part of the study area where it is overlain by the Sanamah. The combined thickness of the Dibsiyah plus the unconformable Sanamah rarely exceeds 200 m. As porosities and permeabilities are on the order of the same magnitude, they should form a homogenous reservoir (equivalent to the lower aquifer in the subsurface). The Khusayyayn is the most widespread unit in the study area and has excellent porosities and permeabilities. The Juwayl is present in two NW - SE trending outcrops that represent the former erosional relief (Kellogg et al. 1986). The petrophysical properties are close to the underlying Khusayyayn, so that these two units together form another combined reservoir (the upper sandstone sequence in the subsurface). The major difference to the subsurface is the absence of an effective aquiclude or aquitard, which in the subsurface is represented by thick shales of the Qusaiba. The lithology and the patchy distribution of the sediments, caused by cut-out of strata beneath the Khusayyayn unconformity; make the Qusaiba an ineffective aquitard. Consequently, as there is no separator between the lower and the upper sandstone sequence, in the Wajid outcrop belt, there is only one major reservoir.

Conclusions

In the study area, the Wajid Sandstone consists of 5 distinct lithologic units: The Dibsiyah, the Sanamah, the Qusaiba, the Khusayyayn, and the Juwayl formations.

The Dibsiyah Formation is a marine succession dominated by tidal deposits which up section grade into open shelf deposits. After deposition of the Dibsiyah, a pronounced relief was developed and filled with glacial sediments of the Sanamah. The Qusaiba is a predominantly fine-grained succession of patchy distribution. The depositional environment may have been a marginal marine setting or even a palustrine environment. It is overlain by the Khusayyayn Formation, which is a very uniform succession and which has the widest distribution of the units. It is composed of an alternation of submarine dunes and tidal sediments. Two large valleys were carved into these deposits prior to the deposition of the glacigenic Juwayl Formation. The latter shows a variety of sedimentary facies; however, the spatial and temporal relations between these deposits are not yet clear.

Except for the Qusaiba, all rocks show well developed porosities and permeabilities between 20% and 30% and 1000 md to 8000 md. In the absence of an effective aquitard, these rocks form one major reservoir.

References

Al-Husseini MI (2004) Pre-Unayzah unconformity, Saudi Arabia. In: Al-Husseini MI (ed) Carboniferous, Permian and Triassic Arabian Stratigraphy. GeoArabia Special Publ. 3, 15-59

Dirner S (2007) The “Upper Wajid Group” south of Wadi Ad Dawasir (KSA), an outcrop analogue study of a Paleozoic aquifer. Dipl. thesis, Univ. Tübingen, 102 pp (unpublished)

Evans DS, Lathon RB, Senalp M, Connally TC (1991): Stratigraphy of the Wajid Sandstone of Southwestern Saudi Arabia. SPE Middle East Oil Show, Bahrain, Paper SPE 21449, 947-960

Filomena CM (2007) Sedimentary Evolution of a Paleozoic Sandstone Aquifer: The Lower Wajid Group in Wadi Ad Dawasir, South Western Saudi Arabia. Dipl.thesis, Univ. Tübingen, 126 pp (unpublished)

GTZ-DCo (2007): Completion report, Wajid water resources studies (unpublished)

Hamon Y, Merzeraud G, Combes PJ (2005) High-frequency relative sea level variation cycles recorded in sedimentary discontinuities. Bull. Soc. Geol. France 176, 57 - 68

Keller M, Hinderer M, Al-Ajmi H, Rausch, R (2011) Palaeozoic glacial depositional environments in SW Saudi Arabia: Process and Product. Geol. Soc. London Spec. Paper

Kellogg, K.S., Janjou, D., Minoux, L. & Fourniget, J. (1986) Explanatory notes to the Geologic Map of the Wadi Tathlith Quadrangle, sheet 20 G. Ministry Petrol. Min. Res

Stump TE, Van Der Eem JG (1996) Overview of the stratigraphy, depositional environments and periods of deformation of the Wajid outcrop belt, south-western Saudi Arabia. In: Al-Husseini MI (ed), Geo '94, the Middle East Petroleum Geosciences Conference, 867-876

Geoelectrical assessment of groundwater potential in the coastal aquifer of Lagos, Nigeria

K.F. Oyedele, S. Oladele

Department of Geosciences, University of Lagos, Lagos, Nigeria

Abstract Rapid urbanization in Lagos has increased the demand for water in recent years. With the aim of delineating the geometry and distribution of fresh water aquifers in the study area, Vertical Electrical Sounding (VES) were carried out at 25 locations; five each on a 100m long traverse and 1-D inversion of the VES data with pseudo 2-D presentation was carried out. The inverted resistivity models were calibrated with borehole data in the vicinity of the survey area. Maximum of four layers geo-electric layers were delineated: Hard peaty clay (15-52 ohm-m), sandy clay (58-119 ohm-m), fine sand (107-258 ohm-m) and medium sand/ coarse sand (260-568 ohm-m). The variety of sands in the area constitutes the aquifers in the study area. Depths to the tops of these aquifers range from 0-100m in both confined and unconfined conditions. This study recommends only the confined aquifers for development as the unconfined ones are prone to contaminations.

1 Introduction

In recent years there has been a growing awareness in the field of groundwater management of the need to accurately assess groundwater resources. To accomplish this, it is essential to have accurate knowledge of aquifer with a view to identify the ones with good potential to furnish portable water in economic quantity. Partly Due to high rate of urbanization, the demand for water has increased globally (UNDP 2006). Lagos particularly is hit more by demand for water due to phenomenal increase in population and urbanization (Longe 2011). The problem is escalated when view against the inability of Water Corporation to provide portable water to the populace. In the light of this, the groundwater is the source to the rescue. Attempts to exploit groundwater resources have made groundwater search an all comer's affairs. This has lead to indiscriminate exploitation of groundwater resources and the attendant poor results. The purpose of electrical surveys is to determine the subsurface resistivity distribution by making measurements on the ground surface as these measurements help to estimate the electrical resistivity of the subsurface. The subsurface electrical resistivity is associated with various geological factors such as the mineral and fluid content, porosity and degree of water saturation in the rock, ionic concentration of the pore fluid and composition of the

N. Lambrakis et al. (Eds.), *Advances in the Research of Aquatic Environment, Vol. 2*
DOI 10.1007/978-3-642-24076-8,

subsurface material (Kelly 1976). The study area is situated at Gbagada, near the coastline of Lagos (Fig 1). Longe (2011) determined transmissivity values of the multi-layered aquifer system of Lagos to range between 345.6 and 2,332 m^2/day while the storage coefficient values range between $2.8x10^{-4}$ and $4.5x10^{-4}$. Adepelumi et al (2008) mapped the intrusion of sea water into coaster aquifer of Lagos using VES technique of Direct Current (DC) resistivity method. Longe et al. (1987) revealed multilayered aquifer system for the metropolis in their study of the hydrogeology of Lagos. The present work is concerned with groundwater exploration through delineation of aquifer geometry using Vertical Electrical Soundings (VES) results to give a tangible solution to the demand for exploitation of water resources for sustainable economic growth in the heavily populated area of Lagos. This study will improve our knowledge of geometry and distribution of aquifer units in the study area, which in turn leads to better decision-making regarding exploitation of groundwater resources.

2 Geological and Hydrogeological Setting

The studied area (Fig. 1) is located within the Nigerian sector of the Dahomey-basin, near the eastern margin of the Basin. Stratigraphy of the eastern Dahomey basin has been discussed by various workers and several classification schemes have been proposed.

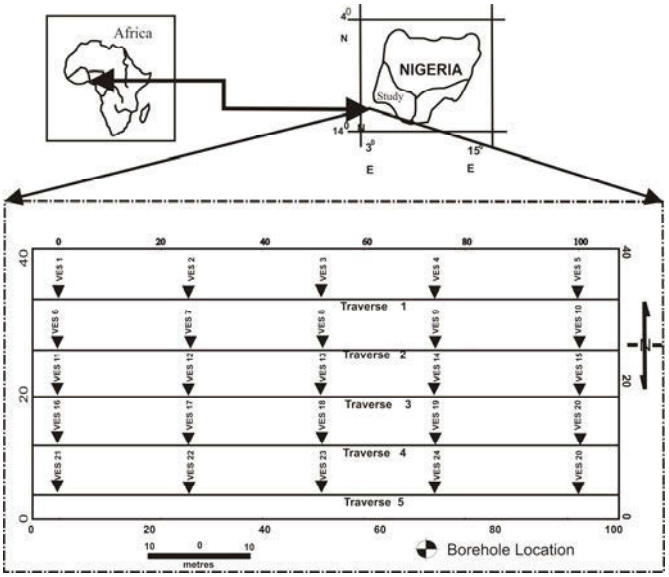

Fig. 1. Study area showing sounding locations.

These notably include those of Jones and Hockey (1964); Omatsola and Adegoke (1981); Coker et al. (1983); Billman (1992), Elueze and Nton (2004). The stratigraphy of Cretaceous to Tertiary sedimentary sequence of the eastern Dahomey basin can be divided into: Abeokuta Group, Imo Group, Ilaro Formation, Coaster plain sands and recent alluvium. The Recent alluvium deposits, the continental Benin sands and the Ilaro Formations were identified as the major aquifers. The aquifers are essentially made of sands, gravels or a mixture of the two [Bureau de Recherches Geologiques et Minieres (1979)].

3 Data acquisition and processing

Geo-electrical methods are the most popular techniques among the geophysical methods for both regional and detailed groundwater explorations because of their wide range of applicability and low cost. For the purpose of this work, 25 VES with a maximum half current electrode separation of 200 m have been carried out along five transects in west-east direction (Fig.1) using PASI Earth Resistivity Meter. Schlumberger configuration was employed for the geoelectrical soundings. The VES stations are 25m apart and profiles separated by distance of 10m in order to image the subsurface at high resolution. VES involves increasing the electrode separations around a mid-point, usually with a logarithmic electrode separation, in order to delineate the layering of strata at increasing depth. In the study area, the VES results show four to five subsurface layers after conventional curve matching and applying the inversion iteration method. Characteristic resistivity sounding curve obtained after inversion are shown in Figure 2.

Table 1. Litholog from existing borehole.

Lithology	Depth (m)
Greyish clay	0 - 1.2m
Peat	1.2 - 4.3m
Sandy clay	4.3 - 9m
Brownish clay	9 - 18.8m
Medium sand	18.8 - 19.4m
Soft greyish clay	19.4 - 27.2m
Medium sand	27.2 - 36m

It should be noted that VES method is suitable only in case of 1-D structure. 1-D inversion is often used to define aquifer geometry that is intrinsically multifaceted. This interpretational practice is erroneous due to unacknowledged multidimensional property. This limitation of 1-D modeling makes 2-D representation indispensable since the aquifers are expected to be more complex than a 1-D model

that VES is able to model. Figure 3 show 2D presentation of interpolated 1D resistivity inversion along traverses 1-5 using WinGLink Software (2007). The geoelectric layers were subsequently calibrated with lithology log from existing borehole in the vicinity of the survey area (Table 1). The spatial distribution of geoelectric materials at different depths of 10m, 25m, 50m and 75m were also generated to overview their occurrence at depths.

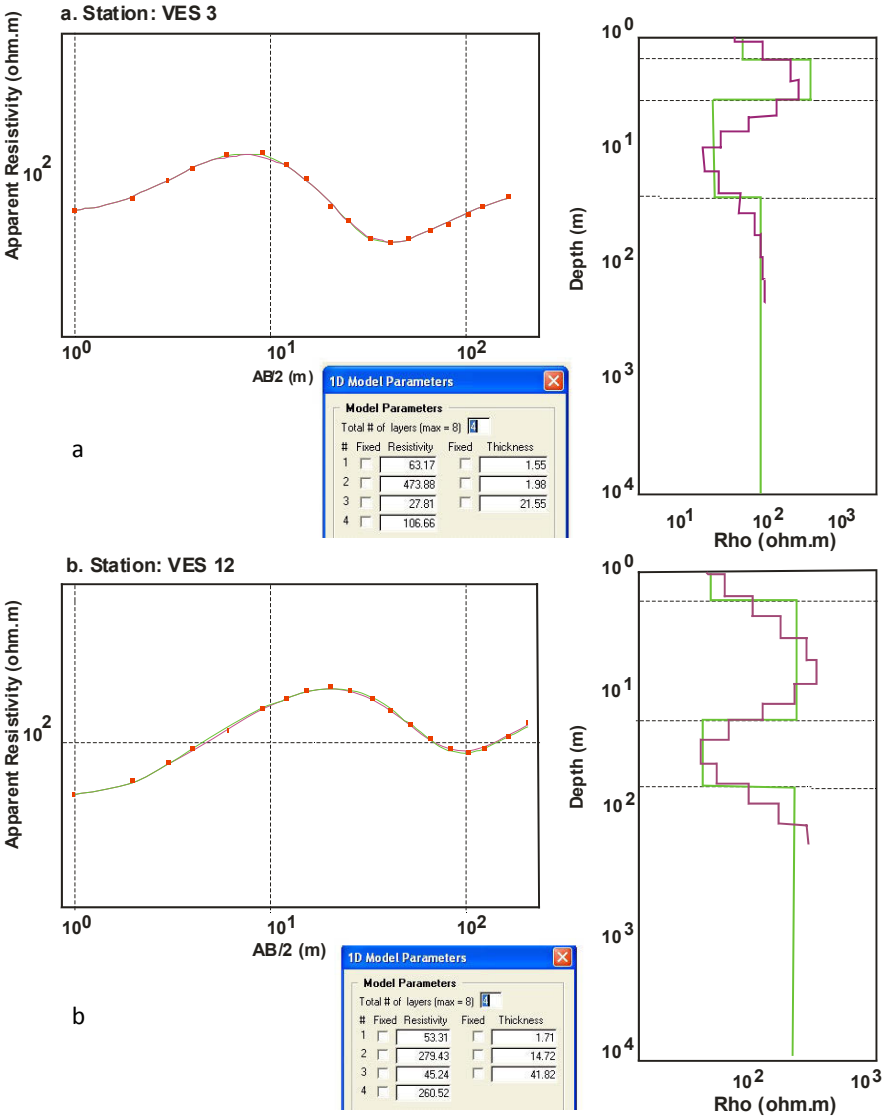

Fig. 2. Typical VES sounding curves showing (a) VES 3 (b) VES 12.

4 Discussions of Results

Interpretation of data was carried out with the aim of delineating geo-electrical parameters of the sequences present in the study area, with a view to identify areas of high groundwater potential. 2-D presentation of interpolated 1D resistivity inversion enabled obtaining a more accurate spatial model of the subsurface than the individual 1-D models. The interpretation shows that the study area contained a maximum of 5 layers and a minimum of 4 layers.

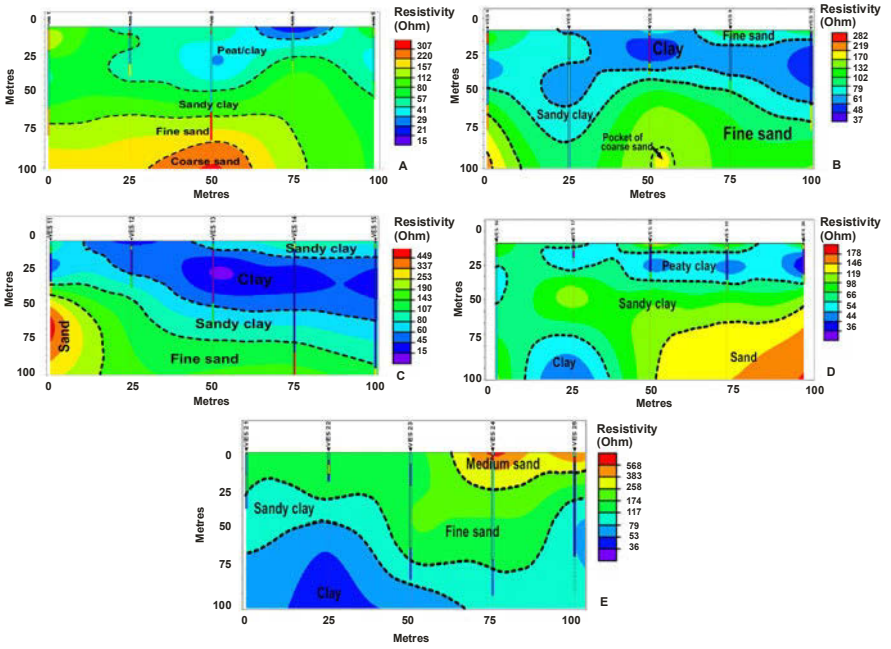

Fig. 3. a. 2-D presentation of interpolated 1-D resistivity inversion along traverse 1, **b.** 2-D presentation of interpolated 1-D resistivity inversion along traverse 2, **c.** 2-D presentation of interpolated 1-D resistivity inversion along traverse 3, **d.** 2-D presentation of interpolated 1-D resistivity inversion along traverse 4 and **e**. 2-D presentation of interpolated 1-D resistivity inversion along traverse 5.

Figure 3a shows the subsurface resistivity model along traverse 1 which indicates that the area is underlined by varying resistivity materials delineated by sharp changes in electrical resistivity values. This model is characterized by four geoelectric layers. The topsoil is essentially hard peaty clay with resistivity ranging from 15-41ohm-metres. The topsoil is observed from the surface to depth ranging from 15 to 35m. Underling this layer is sandy clay having resistivity and thickness ranges from 58-112 ohm-meters and 13-73m respectively. This layer outcrops at the beginning on the traverse to about 20m mark. The third layer is essentially fine sand having resistivity between 115 and 220 ohm-metres and repre-

sents a confined aquifer of about 15-35m thickness. The fourth lithology correspond to coarse sand of resistivity greater than 220ohm-metres observable only at the middle of the transect, occurring probably as pocket within the fine sand. Together they represent good aquifers that can furnish portable water.

The model resistivity section of traverse 2 is shown in Figure 3b. It is shows good lithology geometry semblance with model section of traverse 1. The profile surface shows variation in lithology by alternation of hard clay and fine sand. While the fine sand (79-170 ohm-m) is relatively thin (>10m), the hard clay (35-52 ohm-m) varies in thickness from 10m to 25m at the center of the traverse. A very thin layer (3-9m) of sandy clay (61-79 ohm-m) underlies the clay formation. Fine sand (79-170 ohm-m) with occurrence of pocket of coarse sand (170- 219 ohm-m) is the fourth layer. These sand bodies correspond to the aquiferous zone beneath this traverse, the depth to the top of which varies from 27- 80m along the traverse.

The model resistivity section of traverse 3 shown in Figure 3c illustrates a four layer condition. The surface of this traverse shows occurrence of sandy clay (60-107 ohm-m) at the western and eastern flanks where they attained thicknesses of 32m and 9m respectively and hard clay material sandwiched in between. The clay was hardened due to loss of water in the dry season.

Underlying the surficial sandy clay at depths between 9 -35m is peaty clay (34-50 ohm-m).The clay is in turn underlain by sandy clay (60-107 ohm-m) typically about 12-15m thick at this depth. The fourth layer represents fine sand (107-210 ohm-m). Depth to the top and thickness of the fine sand ranges from 32-75m and 7- > 60 m respectively. Pocket of coarse sand demarcated in the first two traverses is also partly mapped beneath this traverse. The sands together represent the aquifer unit which is important for water supply purposes.

The cross section of traverse 4 (Fig. 3d) shows similar lithologic succession as the previous traverses: peaty clay, sandy clay and sand. The surface of traverse characterize by sandy clay and peaty clay. The topmost thin (<5m) sandy clay (80-119 ohm-m) around the center of the traverse is underlain by peaty clay (44-66 ohm-m) thickness not greater than 15m. Sandy clay (80-119 ohm-m) exists beneath the peaty clay at depth greater than 20m along the length of the profile. However, pocket of clay occurs within the sandy clay at >75m depth beneath VES 17 location. But of groundwater importance is the thick (>25m) sand body at 75m depth and is essentially restricted to the eastern halve of the profile.

The resistivity cross section of traverse 5 (Fig. 3e) shows slightly different succession in that medium sand (>258 ohm-m) is juxtaposed with fine sand (117-258 ohm-m) on the surface. The medium sand and fine sand bodies represent aquiferous units which extend from the surface to about 20m and 55m depths respectively. These aquifers are unconfined and are therefore prone to contamination. Sandy clay (79-117 ohm-m) and clay underlie these aquifers at depths varying from 20-55m and 50-100m respectively.

Figure 4 shows the maps of spatial distribution of geoelectric layers at depths of 10m and 25m. The two maps show similarity and the distribution of geomaterials in space. The southern part is essentially fine to medium sand while the north-

ern and the eastern areas consist of peat/clay and sandy clay respectively. However, dissimilarity exists at the northeastern corners of the two maps. Aquiferous geomedia dominates the northern part of the study area at 50m depth (Fig. 4c) except for a pocket of clay at the northeastern region. The southern area has clay/sandy clay coverage. At depth 75m (Fig. 4d) the northern area is dominated by clay/sandy clay materials except at easternmost part where there is occurrence of relatively high resistivity sand material.

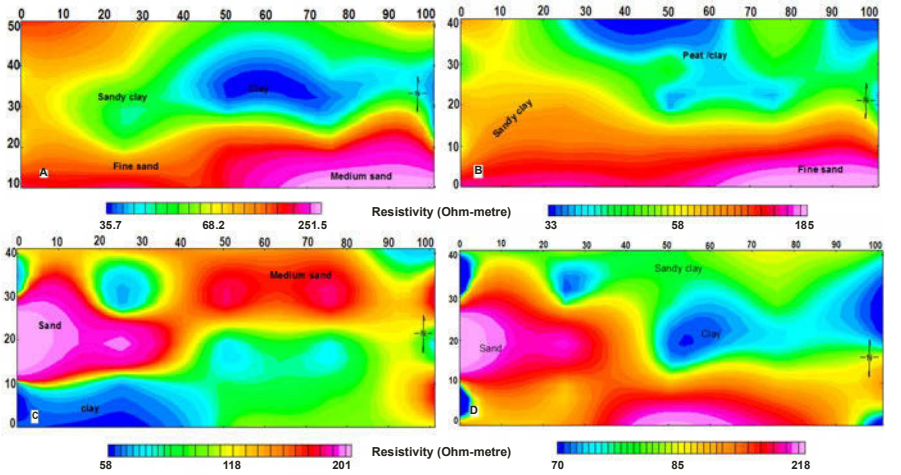

Fig. 4. Spatial distribution of geoelectric layers at (a) 10m (b) 25m depths (c) 50m and (d) 75m depths (the colour code is map specific and should be related to the colour bar).

Conclusion

This study focuses on mapping of geometry and distribution of aquifers in part of Lagos, Nigeria. Four layered electro-stratigraphic earth models were constructed from which peaty clay, sandy clay fine and medium/coarse sands were delineated. The varieties of sand (107-568 ohm-m) are considered the potential water bearing zone and therefore are the targets for productive groundwater exploitation. The depth to the top of these aquifers however, varies from 0-100m. Pockets of clay often interrupt the lateral continuity of the aquifer system, which will negatively impact the yield of the aquifers. Occurrences of aquiferous materials at shallow depths of 10m 25m and 75m are essentially confined to the southern area while sand materials are restricted to the northern half at 50m depth. This study therefore, recommends exploitation of groundwater resources from the confined aquifers and discourages abstraction of water from unconfined aquifers and the localized bodies of sand in that they are prone to contaminations and limited or poor yields respectively.

References

Adeleye, D.R, (1975): Nigeria late Cretaceous Stratigraphy and paleography; AAPG *Bulletin* , volume 59, issue12, pages 2302-2313

Adepelumi A. A., Ako B. D., Afolabi O., Ajayi T. R. and Omotoso E. J. (2008): Delineation of saltwater intrusion into the freshwater aquifer of Lekki Peninsula, Lagos, Nigeria. Environ Geol 00254-008-1194-3

Bureau de Recherches Geologiques et Minieres (1979): Pre-drilling hydrogeological report area 18 and 19 sub-mitted to the Federal Department of Water Resources, Lagos, Nigera, 1-60

Coker, S.J., Ejedawe, J.E. and Oshiorienua (1983). Hydrocarbon source potentials of Cretaceous rocks of Okitipupa Uplift, Nigeria. Journal of Mining and Geology. Vol. 22 pp163-169

Elueze, A.A. and Nton, M.E., (2004). Organic geochemical appraisal of limestones and shales in part of eastern Dahomey basin, southwestern Nigeria. Journal of Mining and Geology, vol. 40, no. 1 pp 29-40

Kelly, W.E. (1976): Geoelectric sounding for delinating groundwater contamination, Ground water V.-14, pp.6-10

Longe, E.O. (2011): Groundwater Resources Potential in the Coastal Plain Sands Aquifers, Lagos, Nigeria *Res*. J. Environ. Earth Sci., 3(1): 1-7

Longe E. O, Malomo S, Olorunniwo MA (1987): Hydrogeology of Lagos Metropolis. Afr J Earth Sci 6(2):163–174

Omatsola, M. E. and Adegoke, O. S. (1981). Tectonic evolution and Cretaceous stratigraphy of the Dahomey basin. Journal of Mining Geology, 18 (1), P.130 -137

UNDP (2006): Country evaluation: assessment of development results of Nigeria, pp 1–80

Winglink (2007): Integrated interpretation software. Version 2.20.01. Geosystem corporation, Milan

Drainage and lineament analysis towards artificial recharge of groundwater

D. Das

Department of Environmental Science,University of Kalyani,India
ddas_kly@rediffmail.com

Abstract Drainage and lineament characteristics of a watershed provide important clues about the hydrogeology of the area. Information about the above characteristics derived from satellite imageries (IRS-IB) aided by field verifications and subsequently analyzed in Geographical Information System (GIS) environment can provide a composite map and which can be used for adopting a suitable strategy for managing watersheds in a better way particularly in relation to the augmentation of the status of groundwater by artificial recharge methods.
On the basis of the above concept, drainage, lineament and hydro geomorphic study of the upper catchment area of Kumari basin, Purulia, eastern India have been performed for demarcating prospective sites for construction of artificial recharge structures. Granitic lithology and uneven topography indicate that the surface run-off is high and infiltration is low and therefore groundwater recharge is inadequate in the area. So, mainly to keep the irrigation practice and drinking water supply alive, groundwater condition has to be improved by artificial recharge method. Integrating different types of thematic layers like drainage density, lineament density, hydro geomorphology in a GIS environment; it has been possible to generate a composite map showing prospective sites for construction of artificial recharge structures.

1 Introduction

Natural replenishment of groundwater is often inadequate and is unable to keep pace with the excessive demand of it. This has resulted in decline of water table and depletion of resources. In order to augment the water table conditions, artificial recharge has become an important and fruitful management strategy through suitable constructions. Natural recharge in India is mainly restricted within three months periods ranging from 10 to 100 days. Artificial recharge methods can provide additional recharge after the monsoon to sustain a groundwater supply for about next couple of months. India receives annually about 4000 billion m^3 water through precipitation both during the south west and northwest monsoon, out of this, about 1280 billion m^3 is lost as evaporation, about 850 billion m^3 seeps into the soil and the remaining 1870 billion m^3 constitutes the average surface water

N. Lambrakis et al. (Eds.), *Advances in the Research of Aquatic Environment, Vol. 2*
DOI 10.1007/978-3-642-24076-8,

flow. Theoretically, this water is sufficient to provide 1.0 m depth on the entire cultivated area in the country. But only about 50 percent of surface water can be put into beneficial use because of topographical and other constraints. Out of the country's utilizable water resource of about 1100 billion m^3, surface water and groundwater account for about 60 percent and 40 percent respectively. Estimates reveal that areas receiving up to 1000 mm annual precipitation hold a potential to add 63 million m^3 water equivalent through runoff (Sharma 2002). According to Veerana (2002) the entire annual water resource planning has to be done by conserving rainfall either by storing in surface or in subsurface reservoir. In fact, any man made system by which the groundwater reservoir is augmented at a rate exceeding to that obtained under natural conditions of replenishment is an artificial recharge system.

2 Review of literature

The necessity of artificial recharge in India was recognized more than four decades ago (Karanth1963). Artificial recharge studies in India have mainly concentrated on the mechanism of recharge but recently a number of studies had focused on site selection process, especially with the help of remote sensing techniques (Anbazhagan and Ramaswamy 2002). Satellite imageries of visible (0.38 μm - 0.72 μm) to near infrared (0.72 μm - 1.3 μm) region of electromagnetic spectrum are very much useful in extracting information on aerial aspects of drainage basin and various hydro geomorphic features (Das1990).Observations from satellite data must be complemented by field checks and existing geologic maps, topographic sheets which are very much useful as supplementary data sources. The identification of lineaments (Kazemi et al. 2009) has immense importance in hard rock hydrogeology as rock fractures localize groundwater (Das 1990). The synergism between remote sensing and GIS techniques is a major advantage in the use of an integrated approach (Saraf et al. 2001).

3 Geologic and Geomorphic setting of the area

The area under present study belongs to Purulia district which is located in the southwestern part of West Bengal state of eastern India. Geologically the area constitutes a part of Chhotanagpur gneissic complex of Precambrian age, lithologically the area is composed mainly of granitic clan of rocks. Geomorphologically the area is an erosional landform with the presence of residual hills. Ajodhya hill, the main upland of the area, is the source of Kumari river and the river ultimately flows in the easterly direction. The upper catchment area of Kumari river, the exact study area has got an undulating micro relief with highs and lows. The maximum elevation is found 660 m (spot height) above msl. The area receives an a.a.r.

of 1180 mm. However, natural recharge is poor due to hard crystalline nature of the country rock and undulated topography.

A small portion is covered by alluvium and latosol and rest of the area is covered by weathered profile of granite gneiss. Hard rock of this region is traversed by network of oriented fractures and also includes pegmatite-dykes. Some where the basement gneiss suffers much weathering and at such places rocks are mantled by soil cover, the thickness of which varies place to place. The rocks of the area are traversed by several sets of joints among which the NNE-SSW master joints are prominent which show steep dip (>50º). The common spacing of joints lies between 1 m-1.5 m. However, the vertical joints are widely spaced. The laterite acts as a protective cover which is resistant to both chemical and mechanical weathering.

4 Objective of the study

With the above backdrop present study involves a new attempt where the approach is based on a watershed. Remote sensing application related to the various pertinent themes of the present investigation like hydro geomorphology, lineaments, aerial aspects of drainage basins ultimately to derive drainage density with the consultation of Survey of India (SOI) topographic sheets has been performed in a particular watershed. The present area under study is the upper catchment area of Kumari basin, Purulia district, West Bengal, eastern India bounded by latitude 22º 55'-23º15' N and longitude 86º08'-86º38'E. The following are the objectives of the present investigation:

- To create a digital data base for the area under study.
- To delineate areas suitable for artificial recharge.

5 Methodology

The information on several pertinent themes mentioned earlier are derived through visual interpretation of IRS-lB, LISS-II, geocoded satellite data (Scale 1:50,000 standard FCC data of February 2001) (Fig. 1) in consultation with SOI toposheets (no.73 I/4,I/12,J/1,J/5,J/9) aided by field verifications. Digital enhancement or classification of surface features is not necessary for the present study. In addition, information has also been obtained about the area of weathered zone and a general idea about recharge and discharge zone (by a well inventory process). Drainage texture analysis has been performed on the basis of 3rd order basins for convenience of the study. Stream ordering has been performed on the basis of Strahler (1952). Lineament number density (isofracture) is derived from 1km×1km grid analysis (Kumanan 2001) and it is classified in to low (poor presence of linea-

ments/grid) and high (considerable presence of lineaments/grid). Digitization of all the themes has been performed by the TNT mips 7.2 version of GIS software package. Subsequent overlay analysis (Burroughs and Mcdonnel 1998) is done to reveal the suitable sites for artificial recharge in the produced maps.

Fig. 1. Satellite data(IRS-1B LISS II).

6 Observations

Visual interpretation of IRS-lB satellite data aided by field observation revels that the Kumari river (Fig. 2) has got a perennial flow. The area comprises mainly agricultural land of single cropping. The undulatory part of the study area shows a thickness of 3 m to 4 m of soil cover, at places the thickness of the soil cover increases up to 6 m. Water divides of the small sub-basins within the major basin under study shows lateritisation. The valley fills have their depth up to several meters, contains relicts of laterites. At places weathered residuum shows a thickness of about 15 m - 20 m. Ground water level reaches almost bottom during dry months (February to June).Here the tributaries in general drain towards SE direction (Fig. 2). The main channel Kumari river (a 5th order stream) shows the effect of structural control in its appearance. Third order sub-basins have been studied in context of their large dimension which facilitate recognition of lithology, structure and nature of sediments in such basins. Right angle bends, a system of parallel tributaries of the same order just opposite to the main channel suggests their entrenchment along lineaments. Number of tributaries align parallel to each other suggest a plane of weakness or a fracture zone. The graded profile of the river in some places has been entrenched into laterite plane.

Morphometrical study of 3rd order drainage basis has been performed with the help of Survey of India (SOl) topographic sheets (scale 1: 50,000), however, updating the information of minor to major streams has been performed with the help of IRS IB Satellite data (scale 1: 50,000) of February 2001. Drainage density theme has got one of the most influential impacts in deriving the result to locate the artificial recharge sites. High to moderate drainage density values are favorable for run-off and do not encourage natural recharge. In the present investigation drainage density values have been classified into two categories, such as within 1.5 km/km² to 3.5Km/Km² is considered as the low drainage density value and above 3.5 Km/Km² is considered as high drainage density value.

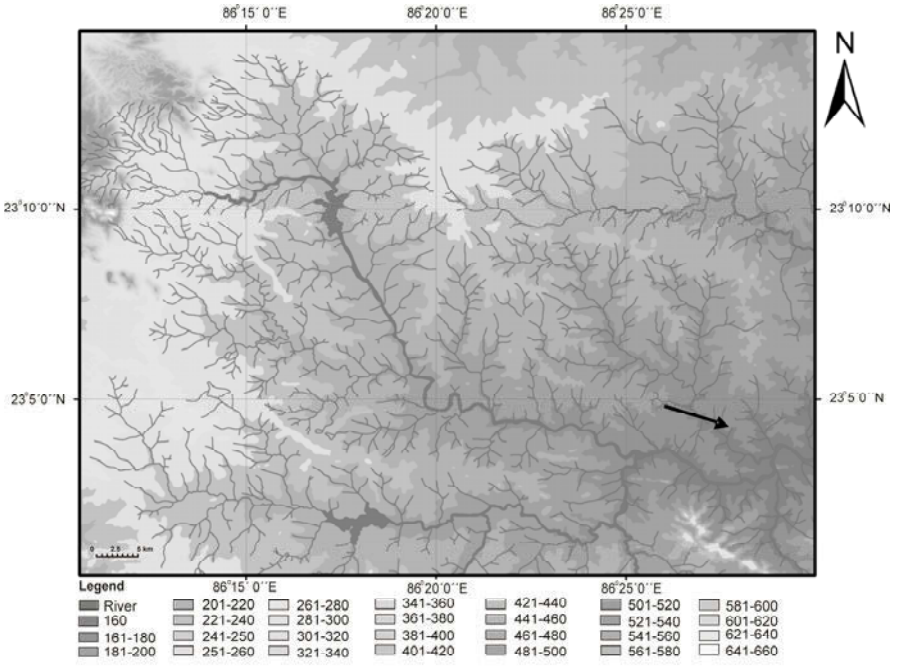

Fig. 2. Drainage map of the area. Arrow mark shows the direction of flow.

7 GIS analysis result

When a wide range of mono-disciplinary resource maps are available, the users must seek ways in which the available information can be combined to give an integrated overview or reclassification or generation as needed (Burrough 1990).

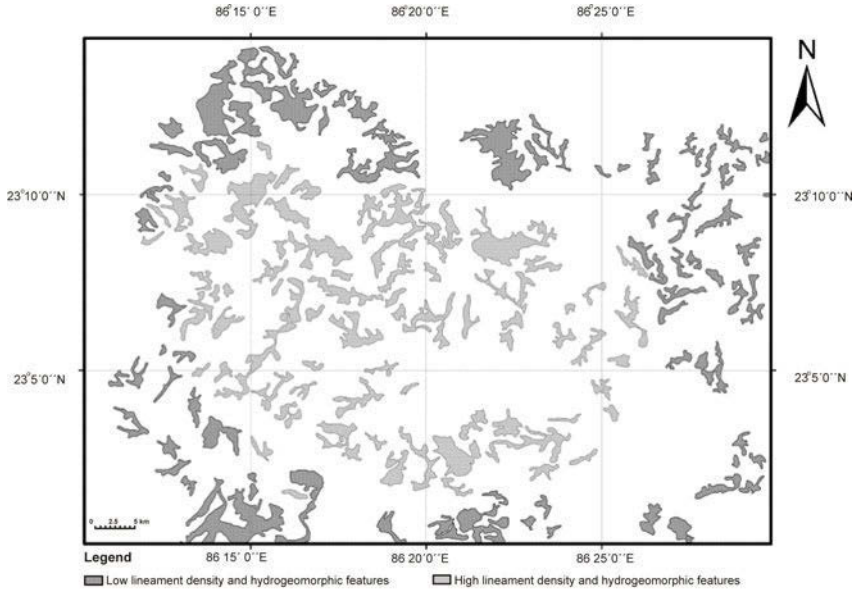

Fig. 3. Sites for artificial recharge (lighter shaded areas).

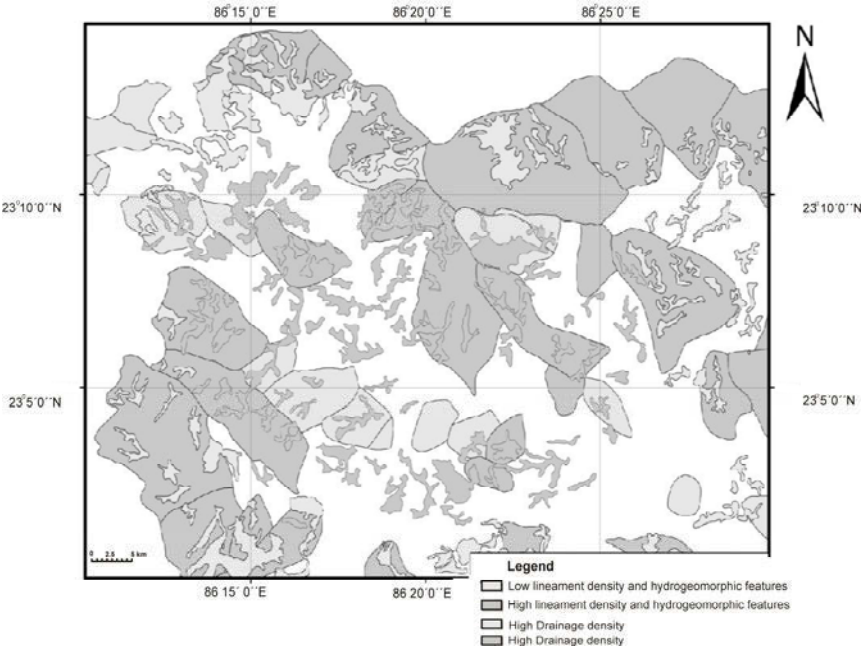

Fig. 4. Sites for artificial recharge (darker small polygons within lighter polygon).

The criteria for analysis are dependent on the objective and on the data sets. In the present investigation, all the thematic vector layers are developed on the basis of hydro geomorphology, lineament and drainage as they are the surface expressions of a potential aquifer. Overlay analysis has been performed between lineament density layer with hydro geomorphology layer and the product (Fig. 3) shows suitable sites for construction of artificial recharge structures and this has been overlaid by drainage density layer and the final out put (Fig. 4) shows sites for artificial recharge.

8 Discussion

Remote Sensing provides unique and unbiased input in various natural resource inventory programs, owing to its multi spectral capability, synoptivity and repetivity in coverage. As a significant step towards the direction of fruitful application of this technology, based on satellite imagery interpretation, in conjunction with existing geological, hydro geological information and topographic sheets, digital data base reveals the sites of artificial recharge of ground water. For this purpose, initially individual layer-wise maps are prepared for hydro geomorphology, drainage, and lineaments. All these maps are separately digitized and overlaid in GIS environment ultimately for generating the site suitability map for artificial recharge of ground water. In the study area, the main hydro geomorphic features are valley fills and weathered residuum of moderate thickness (somewhere it exceeds 15 m of thickness) with reasonable spatial extent. The deep seated interconnecting fractures are potential reservoirs of groundwater though the fractures or the joint systems of compact nature do not hold water. Valley fills are potentially good area for locating artificial recharge structures. Coincidence of valley fills and deep seated lineaments make good reservoir for groundwater accumulation through artificial recharge and which will in turn augment water table in downstream direction. Drainage density and lineament density are highly influential factors in identifying the sites for artificial recharge.

9 Conclusion

Hard - rock hydro geological conditions vary widely and its proper understanding is necessary for ground water development through artificial recharge including the site selection process. The comprehensive information provided by the composite maps has been proved to be highly useful in narrowing down the target zones for selection of artificial recharge sites. Thus the digital data base created for artificial recharge site selection purpose will go a long way for planning, development and management of ground water.

References

Anbazhagan S, Ramaswamy S. M (2002) Remote sensing based artificial recharge studies - a case study from Precambrian terrain, India. In: Dillon, P. (eds) Management of Aquifer Recharge for Sustainability. Proc. of the 4th International Symposium of Artificial Recharge. AA Balkema Publishers: 553-556. Adelaide, Australia

Burrough (1990) PA Principles of GIS for Land Resource Assessment.Oxford science publication,Oxford.

Burroughs P P, McDonnel R A, Oxford university Press (1998)Principles of GIS.Oxford

Das D (1990) Satellite remote sensing in subsurface water targeting. In: Proc. of the ACSM-ASPRS Annual Convention, 99-103.Denver, USA

Karanth K R (1963) Scope of adopting artificial recharge in Babar Formation. In: Proc. of the symposium on groundwater. Geol. Survey of India, Miscellaneous Publication: 206-214. Calcutta, India

Kazemi R, Porchemmat J,Kheirkhah M(2009)Investigation of lineaments related to groundwater occurrence in a Karstic area: A case study in Lar catchment, Iran Res. J. of Environ. Sci. 3(3):367-375, ISSN1819-3412

Kumanan C J (2009) Remote sensing revealed morphotectonic anomalies as a tool to neotectonic mapping-experience south India. http://www.crisp.nus.edu.s/ ~acrs2001/pdf/195kumanan.pdf

Saraf A K, Choudhury P R, Sarma B, Ghosh P (2001) Impacts of reservoirs in groundwater and vegetation: A study based on Remote Sensing and GIS techniques. Int. J. of Remote Sens. Vol 22, No. 13pp 2439- 2448

Sharma, K. D. (2002), Rainwater management in India: Some policy issues. In: Subrahmanyam K (eds) Proc. of the workshop on the Water Crisis - Hope and Action for humanity's future. Hyderabad, India, National Geophysical Research Institute pp 1-8

Strahler, A. N. (1952), Dynamic basis of Geomorphology, Bull.Geol.S oc.America Vol 63 pp 923-938

Veerana, M. (2002), Artificial Recharge Methods of groundwater in hard-rock formations and case studies. In: Subrahmanyam K (eds) Proc. of the Workshop on the Water Crisis - Hope and Action for humanity's future. Hyderabad, India, National Geophysical Research Institute pp 117-125

Fracture pattern description and analysis of the hard rock hydrogeological environment in Naxos Island, Hellas

A.S. Partsinevelou, S. Lozios, G. Stournaras

Department of Dynamic Tectonic & Applied Geology, University of Athens, Panepistimioupolis Ilisia, 15784 Athens, Hellas

Abstract The main parameter that controls the groundwater flow regime in fractured aquifers is the fracture pattern. Its description is crucial for a hydrogeologic/hydraulic or geotechnical study. This paper, aims to describe and analyze the basic characteristics of the fracture pattern in Naxos Island, Greece. The parameters that were analyzed are: a) the frequency and spatial location of the fractures, b) the orientation of fractures, c) the dimensions of fractures, d) the density of fractures and e) the degree of fracture intersection. These parameters were analyzed separately for every dominant lithology of the study area.
The analysis revealed that there are five classes of fracture orientation in the study area, indicating a straight link between faults and fractures. The fragmentation in all lithologies is characterized by high degree of uniformity and very high density and interconnection density of the fractures are observed in areas where the alternations between marbles, schists and amphibolites are very intense.

1 Introduction

Naxos is the largest island of Cyclades and occupies a central position in the Aegean Sea. Its circumnavigation is equal to 44 nautical miles and its area reaches 430 km^2. Naxos is mountainous, having a central mountain range, which crosses the island from the northern to the southern part. The highest altitude is 1001 m, at Zeus peak, located in the central part of the range and it has extremely low precipitation rates (Evelpidou et al. 2005).

Like all the islands of Cyclades, Naxos faces a serious problem of water scarcity. This increasing need of groundwater for water supply, leads to a continuous interest for searching groundwater especially in hard rock hydrogeological environments. The groundwater flow regime in hard rocks depends on several factors, including the dimensions, nature, density, orientation and interconnection of the fractures (Botsialas et al. 2005).

The purpose of this study was the description and analysis of the fracture pattern of Naxos Island, by emphasizing on the frequency, orientation, dimensions,

N. Lambrakis et al. (Eds.), *Advances in the Research of Aquatic Environment, Vol. 2*
DOI 10.1007/978-3-642-24076-8,

density and degree of intersection of the fractures and the initial connection between the discontinuities regime and the groundwater aquifers.

For these purposes, satellite images and air photographs were collected and processed, so the lineaments of the study area could be mapped. An image lineament is a structural expression detected by remote sensing, which is a linear object with geological origin (Scanvic 1997).

2 Geological Setting of Naxos Island

Geologically, the study area belongs to the Attic-Cycladic Massif. This massif has been developed by thrust faulting, ductile thinning and normal faulting and it is mainly built up by metamorphic rocks of several metamorphic facies (Jansen 1977). Naxos Island is described mainly as an elliptic dome with main direction N15^{o}E which is consisted by schists, gneiss and marbles (Evelpidou 2003).
In general, the geology of Naxos can be divided into three main units (Brichau 2004):

- The upper non-metamorphic unit
- The Cycladic blueschist unit
- The granodiorite massif

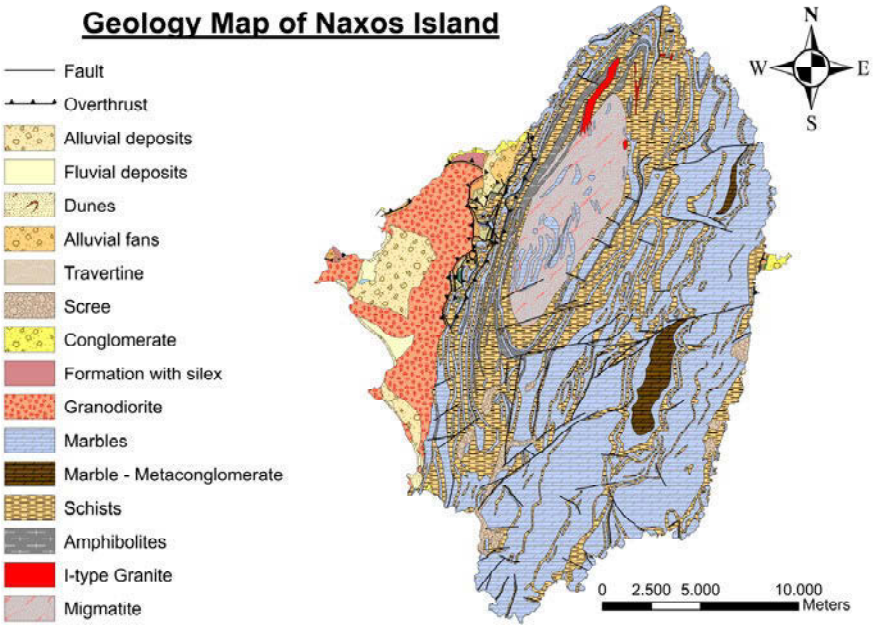

Fig. 1. Simplified geological map of Naxos Island (Jansen 1973, modified).

The upper unit is a very thin and non-metamorphosed nappe which is consisted of Miocene-Pliocene sedimentary rocks and overlies the Cycladic blueschist unit and the granodiorite massif (allochthonous unit). The Cycladic blueschist unit is a metamorphic complex mainly characterized by a migmatite core which is surrounded by a multifolded sequence of marbles, metapelites, schists, amphibolites and gneiss. At the superiorly part of this unit metabauxites and metaconglomerates are appeared. The granodiorite massif appears at the west of the island and it is consisted of an I-type granite which intrudes the Cycladic blueschist unit. Both the Cycladic blueschist and the granodiorite unit constitute the autochonous unit of the island. Also undeformed intrusives, mainly S-Type granites, are found in the northern part of the island (Galanos and Rokkos 1999).

3 Methodology

Lineaments in general are defined as mapable linear surface features, which differ distinctly from the patterns of adjacent features and presumably reflect subsurface phenomena (O'Leary et al. 1976). There are many types of lineaments such as lineaments controlled by geological structures (faults and fractures), lineaments resulted from morphological effects (stream channels) and lineaments caused by human activity (roads). These types of lineaments can exist simultaneously in the same region and it is important to characterize properly each lineament during their mapping (Gülcan 2005).

Lineament mapping and specifically fault and fracture mapping is considered a very important issue for a hydrogeological research especially in hard rock environments. To extract the fracture pattern in the study area, it is necessary to map the area at many different scales. For this purpose, the integration of satellite images and air photographs is necessary.

For this study, one dataset of Landsat 7 – ETM^+ was subset and a combined satellite image of Naxos Island was produced with a resolution of 15m per pixel and 8 available spectral bands to combine. The georeferenced images were orthorectified using a digital elevation model with a cell size of 10m and finally projected on the Hellenic Geodetic Reference System (GGRS'87). Also, a set of aerial photographs (1/30.000 scale) was orthorectified at the same projection and an orthophoto mosaic was produced reaching a high resolution of 5 meters per pixel. The high and the low resolution images were merged resulted in an image which has the same spectral characteristics of Landsat 7, but better resolution. The new image was used for lineaments extraction and interpretation and a furthermore study was made for the orientation, length, density, frequency and degree of intersection of the fractures.

4 Fracture Description and Analysis

The lineaments map of the island, as shown in Figure 2, demonstrates 887 features which have been extracted from satellite images and aerial photographs and correspond to fractures that exist in the study area. These fractures are the result of post-alpine movements.

For the description and analysis of the fractures, six subareas were determined based on the lithology that dominates in each area of the island. Each of these six subareas refer correspondingly to marbles, schists and gneisses, migmatitic dome, S-type granite, I-type granite (granodiorite), post-alpine sediments and meta-conglomerates. The parameters that were analyzed in each subarea are: a) the frequency and spatial location of the fractures, b) the orientation of the fractures, c) the dimensions of the fractures, d) the density of the fractures and e) the degree of fractures intersection.

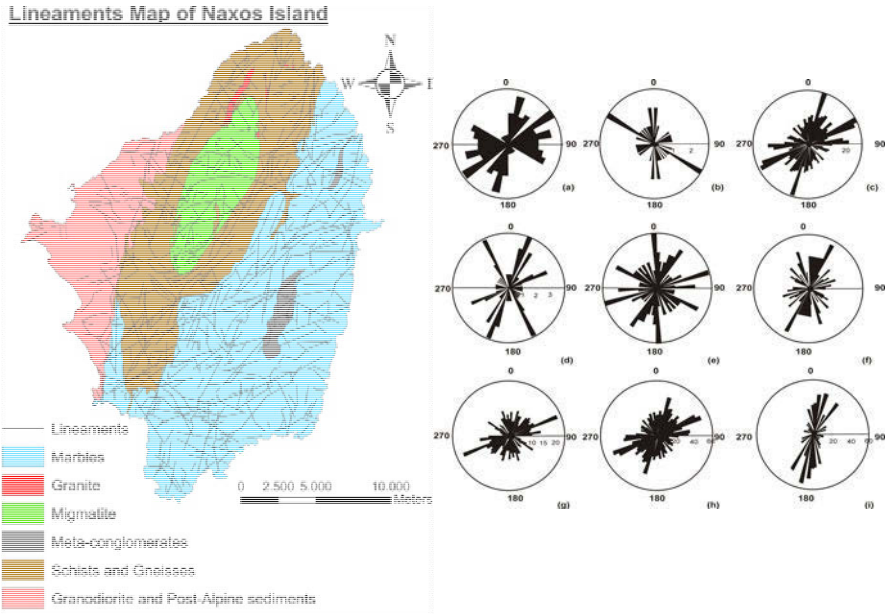

Fig. 2. Lineaments map of Naxos Island in which are shown the six subareas based on the dominant lithology and the primary and secondary orientations of fractures and lineaments in Naxos Island. a) Faults rose plot (Galanos 1999), b) Lineaments rose plot in granite, c) Lineaments rose plot in marbles, d) Lineaments rose plot in meta-conglomerates, e) Lineaments rose plot in post-alpine sediments, f) Lineaments rose plot in the migmatite dome, g) Lineaments rose plot in schists, h) Total lineaments of the study area rose plot, i) Fractures rose plot of measures taken during field work.

Frequency and spatial location of the fractures

The lineament map (Fig. 2) shows that the fracture distribution is hardly homogeneous. The frequency of the lineaments is high in the biggest part of the study area with an exception in the west of the study area, where the frequency of the fractures is very low to zero. The majority of the fractures are located on lithologies that correspond to the term "hard rocks", which generally refers to igneous and metamorphic rocks (Krasny 1996, 2002). Therefore, the discussed character represents a initial indication for the unified tectonic and hydrogeologic behavior of the hard rock environment. The minority of the fractures is located on the granodiorite massif and post-alpine sediments.

Orientation of the fractures

The orientation of the lineaments is analyzed by constructing rose diagrams (Fig. 2). Even though these diagrams are not length-weighted, they can indicate in each occasion the most dominant directions of the fractures. This analysis is very critical for the study of groundwater flow, as in most cases the orientation of the fractures is identical with the orientation of the preferential flow path.

The faults rose plot indicates two sets of orientation classes. The three main classes have NNE-SSW, NE-SW and ENE-WSW strike, while the secondary ones have E-W and N-S strike. Important is that the lineaments rose plot indicates the same main orientation classes as the faults rose plot, a fact that suggests the link between faults and lineaments. The relationship between faults and lineaments can be found also from the rose plots of each subarea and measurements taken during field work, as they indicate also that the main and secondary orientations are the same. Also it should be noted that in the case of the granites, the metaconglomerates and the post-alpine sediments, the main orientation classes are different with the N-S, NE-SW and NW-SE directions to be dominant. These differences should not be taken into account, as the number of the lineaments in these lithologies is very small. Despite the differential tectonic reaction of the lithologic units, the uniformity of the fractures orientation becomes an additional indication for the tectonic and hydrogeologic regime.

Size of the fractures

Fracture dimensions (aperture and apparent aperture), are very difficult to be defined and the depth of the apertures makes the measurements even more complicated. Nevertheless, length measurements are relatively easy to be done and they are significant too, as a greater length of fractures affects the groundwater flow in

a more dominant way, than those of smaller length. A first statistical approach on the length of the fractures revealed that lengths between 600m and 1200m have the biggest frequency in the study area. Calculating the total length of fractures and the length of fractures per unit area in each lithology (Table 1) showed that these dimensions are reversely proportional. Also it is noted a high uniformity of the fragmentation in all lithologies, as the length of fractures per unit area does not differ very much in each subarea.

Table 1. Total length of fractures in each subarea.

Lithology	Length of fractures (km)	Area (km^2)	Length of fractures per unit of area (km)
Marbles	552.361	207.200	2.660
Schists and Gneisses	362.748	117.300	3.090
Migmatite	120.815	35.700	3.380
Granodiorite and Post-Alpine sediments	112.120	60.200	1.860
Meta-conglomerate	55.830	7.200	7.750
Granite	27.469	3.700	7.420

Density of the fractures

The purpose of the fracture density analysis is to calculate frequency of the fractures per unit area. With this analysis a map has been produced showing concentrations of the lineaments over the study area (Fig. 3a).

The map in Figure 3 showed that very high density is observed in areas where the alternations between marbles, schists and amphibolites are very intense, citing the high degree of hydraulic interconnection between the above lithologic units as surface water circulates through these discontinuities. This is verified in the next consideration (degree of fractures intersection). On the other hand, very low density is observed in granodiorites, post-alpine sediments and in areas where one lithology dominates. This verifies that these lithologies are not much affected by tectonic activity.

Degree of fractures intersection

The density of lineaments along with degree of lineaments intersection determine the degree of anisotropy of groundwater flow in the fracture network, as in environments with high degree of interconnection, groundwater flow is smoother and more uniformly.

Fracture intersection density is a map showing the frequency of intersections that occur in a unit cell. The purpose of using intersection density map is to estimate the areas of diverse fracture orientations. If the fractures do not intersect in an area, the resultant map will be represented by a plain map with almost no density contours and the fractures are almost parallel or sub-parallel in an area.

The lineaments intersection map of the study area (Fig. 3b) indicates high and very high intersection density in the same areas where there are observed very high density of lineaments.

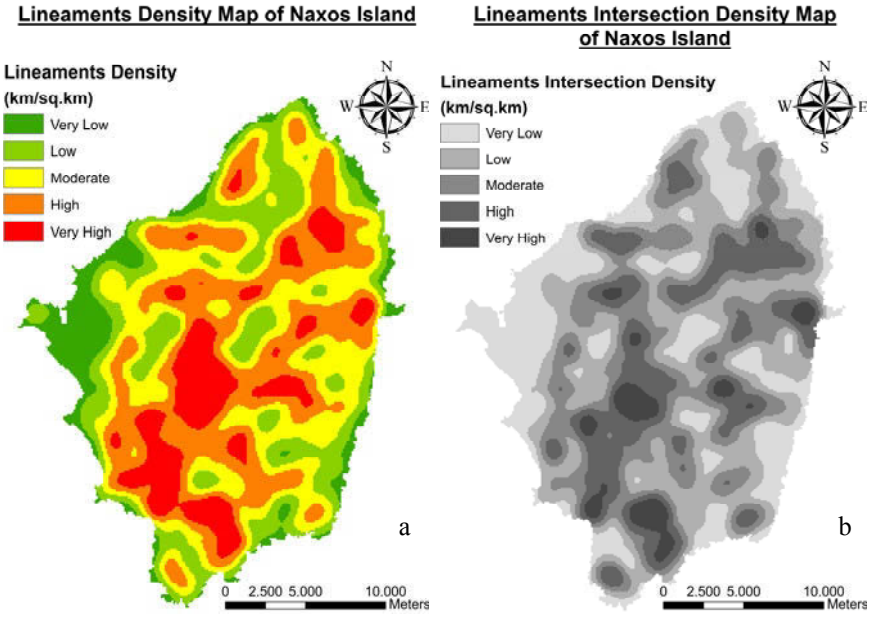

Fig. 3. Lineaments (a) density and (b) intersection density maps of Naxos island.

5 Conclusions

The fracture pattern of an area is straightly connected with the hydrogeological conditions in a hard rock environment. A thorough study is practical for the right exploitation of groundwater supplies in regions with water scarcity problems. The analysis of the fractures in Naxos Island revealed that:

- The combination of Remote Sensing, GIS and field work, leads to a reliable description of the fracture pattern in hard rock environments.
- Five orientation classes of fractures are located in the study area. The three main classes have NNE-SSW, NE-SW and ENE-WSW strike, while the two secondary classes have E-W and N-S strike.

- Fractures have the same main orientation classes with faults, a fact which indicates the straight link between them.
- The biggest total length of fractures and the smallest length of fractures per unit area are observed in marbles. Measuring these dimensions in all lithologies it reveals that they are reversely proportional. Also it is noted a high homogeneity of the fragmentation in all lithologies.
- Very high density and interconnection density of the fractures are observed in areas where the alternations between marbles, schists and amphibolites are very intense.

References

Botsialas K, Vassilakis E, Stournaras G (2005) Fracture pattern description and analysis of the hard rock hydrogeological environment, in a selected study area in Tinos island, Hellas. 7th Hellenic Hydrogeological Conference - Athens 2005, Volume II, pp. 91-100

Brichau St (2004) Constraining the tectonic evolution of extensional fault systems in the Cyclades (Greece) using low-temperature thermochronology. PhD Thesis, Mainz University

Evelpidou N (2003) Geomorphological and geographical observations on Naxos Island, using Remote Sensing and G.I.S. methods, PhD Thesis, N.K.U.A., Greece

Evelpidou N, Leonidopoulou D, Vassilopoulos A, Stournaras G (2005) Procedures concluded to erosion geomorphological characteristics of Naxos, Mykonos, Tinos islands (Aegean Sea). 7th Hellenic Hydrogeological Conference - Athens 2005, Volume II, pp. 117-125

Galanos I, Rokkos D (1999) Exploring the possibility of lithological and structural mapping using principal component analysis on Landsat TM images of Naxos island. Tech. Chron. Sci. J. TCG, I, No 3, pp. 89-91

Gülcan S (2005) Lineament analysis from satellite images, north-west of Ankara, MSc Thesis, Middle East Technical University

Jansen J., 1977.The geology of Naxos. Institute of Geological and Mining Research, Greece

Krasny J., 1996. Hydrogeological Environment in Hard Rocks: An attempt at its schematizing and terminological consideration. Acta Univesitatis Carolinae Geologica, 40, 115-122

Krasny J (2002) Hard Rock Hydrogeology. 1st Workshop on Fissured Rocks Hydrogeology Proceedings, Athens, pp. 11-18

O'Leary DW, Friedman JD, Pohn HA (1976) Lineament, linear, lineation: Some proposed new standards for old terms. Geological Society America Bulletin, 87, 1463-1469.

Scanvic JY (1997) Aerospatial remote sensing in geology. Rotterdam, Balkema, 239 p

Stournaras G, Alexiadou Ch, Leonidopoulou D (2003) Correlation of hydrogeologic and tectonic characteristics of the hard rock aquifers in Tinos Island (Aegean Sea, Hellas). International Conference on Groundwater in Fractured Rocks, Prague

Quantitative investigation of water supply conditions in Thassos, N. Greece

Th. Tzevelekis, I. Gkiougkis, Chr. Katimada, I. Diamantis

Democritus University of Thrace, Department of Civil Engineering, Geotechnical Section, Laboratory of Engineering Geology, Xanthi, 67100, Greece.

Abstract Lack of available water resources is a typical problem for the water supply of Greek islands which is difficult to be confronted with the use of groundwater resources (groundwater wells and springs). However, it is proved that the availability of water resources in Thassos island (N. Greece) is rather satisfactory due to the geological settings of the island itself. Although no water supply problems are observed during the winter months for the local population, the problem becomes quite distinct during the summer period due to the sudden increase in population attributed to the touristic development of the island. The interpretation of the water supply balance (water consumption vs. available water resources) leads to the conclusion that this balance is positive during winter in all municipal districts and negative during summer in 60% of the municipal districts.

1 Introduction

Thassos island is located at the most northern part of the Thracean Sea (N. Greece), being at a distance of 7 to 8 miles from the coast of Eastern Macedonia (very close to Keramoti Bay) and south of Nestos river delta. The water supply of all settlements of the island is satisfied by the use of groundwater wells, springs or in some cases by combination of both. The springs are located mainly at the mountainous zone of the island, while the groundwater wells are mainly installed at places of topographical depression (Fig. 1) (Diamantis et al. 1994).

The availability of water supply mainly depends on the seasonal fluctuation of the island population (permanent/local and touristic population), the condition of the water supply distribution system (hence water losses) and finally on the amount of annual precipitation (Leontiadis et al. 1996; Karavitis and Kerkides 2002). Additionally, it is observed that general household uses of water (e.g. irrigation of small house gardens) also affect the availability of water supply of the island. The evaluation of the balance between water consumption and water resources availability (with respect to water supply) indicates the water supply quantitative problems in different settlements at different seasons throughout the

N. Lambrakis et al. (Eds.), *Advances in the Research of Aquatic Environment, Vol. 2*
DOI 10.1007/978-3-642-24076-8, © Springer-Verlag Berlin Heidelberg 2011

hydrological year and therefore rational recommendations can be proposed in order overcome such water supply problems.

2 Geomorphological, geological and hydrogeological setting

Thassos island regards three unique geomorphological settings: (a) the coastal setting, (b) the hilly and semi-hilly setting and (c) the mountainous setting. Most of the island area is covered by small torrents of radial order (with the eastern and north-eastern part being the centre) while the estuaries of these torrentsare are composed of small alluvial fans which are formed.

From a geological point of view, Thassos island is a part of Rhodope massif, consisting mainly of metamorphic rocks (marbles, gneisses, shales) being developed within successive stratigraphic horizons (Zahos 1977). A small area of extent is covered by tertiary formations mainly composed of conglomerates, while the quaternary formations (sands, gravels, pebbles and breccias) are present at the areas covered by alluvial fans close to the coast (Fig. 1).

The hydrogeological unities of the island are mainly classified into the following formations: (a) metamorphic rocks (except marbles), (b) marbles and (c) sedimentary rocks (at the hilly and semi-hilly parts of the coastal parts). Groundwater potential of the metamorphic rocks (apart from marbles) is rather limited; with the majority of the groundwater wells which are installed at these areas having a discharge of 8–18 m^3/h. The discharge of the mountainous springs is most of the cases approximately 2 m^3/h, with annual fluctuations which respond to the annual precipitation (Diamantis and Tzevelekis 1992). The main aquifer unities of the island are the marbles –at parts which are karstified- providing with water of excellent quality and enough quantity for the supply of the local population (through groundwater wells and springs).

3 Quantitative analysis of the water availability

Springs located at the parts of the mountainous zone are the main source of water supply of Thassos; while during the summer period -when their discharge is limited due to limited precipitation- the water supply needs (mainly of the coastal settlements which are highly touristic) are supported by the installed groundwater wells.

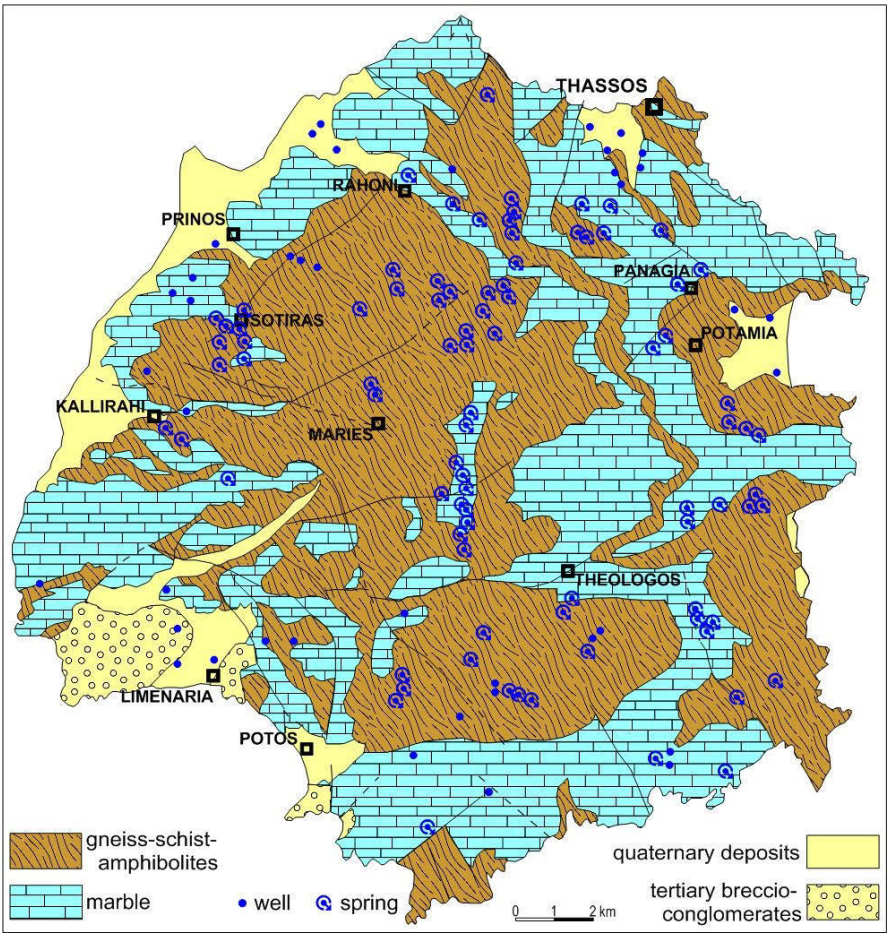

Fig. 1. Geological map of Thassos Island and positions of wells and springs (from IGME Geological map 1:200,000, modified).

Tables 1 and 2, provide an overview of the water supply balance (consumption vs. available water resources) based on measurements and data of the Municipal Enterprise for Water Supply and Sewerage of Thassos (Katimada 2010). Table 1 shows the results from the interpretation of data for the period October – June, which mainly regards the local (permanent) population, while Table 2 shows the results referring to August (period of touristic peak) where the population is six times higher than the permanent.

Columns (1) and (2) of Table 1 show the mean discharge of the springs and groundwater wells during the winter period as they were recorded by the local authorities (Papacharalambos 2007).

The calculations for mean monthly consumption shown in column (3) are based on the census 2001 data and daily consumption of 0.22 m^3/person /day. The daily consumption in column (4) considers also an amount of 18% of water losses (due to water supply network failures) based on relative assessment of the Municipal Enterprise for Water Supply and Sewerage of Thassos. The mean daily discharge in column (5) for both groundwater wells and springs considered 18hrs/day pumping operation of the groundwater wells and 24hrs/day water abstraction of the springs. The interpretation of the data presented in Table 1, shows that for the period October – June, a significant excess of water supply is observed, and this observation regards all the settlements of the island. A significant excess of available water resources is observed at the Municipal District of Potamia where karst springs are present.

Table 2, columns (1) and (2) show the discharge from springs and groundwater wells for August, as they are recorded by the Municipal Enterprise for Water Supply and Sewerage of Thassos, which appears in much lower rates. The calculations for the monthly consumption of August - column (3) - was based on the peak population (touristic peak) and daily consumption of 0.22 m^3/person /day for both natives (permanent) as well as tourists. The daily demand in column (4) refers only to the weekends of August, considering an additional amount of water supply network loses of 18% (based on data of the Municipal Enterprise for Water Supply and Sewerage of Thassos). At this point it has to be noted that the total population of the island; during the weekends of August reaches an amount of approximately 77,000 people (against 13,765 habitats during the remaining period of the year) -including both tourists and locals- and therefore the calculations of column (4) regards the maximum possible water supply demands. The daily discharge in column (5) was calculated after considering a 24hrs/day abstraction of the karst springs and 18hrs/day pumping operation of the groundwater wells. The interpretation of the results of Table 2 shows that during August, 6 Municipal Districts show a shortage in water supply availability.

The comparison of Table 1 and 2 reveals that the mean discharge of the springs is significantly lowered during the summer period, especially in August, while on the contrary, the mean discharge of the groundwater wells appears almost for the entire summer period (June – September; with the exception of August). With respect to August, 7 Municipal Districts show a decrease of 10-20% while in the rest 3 the decrease ranges between 70-75%.

Table 1. Water supply balance (consumption vs. water availability) for the island of Thassos during the period October – June.

Municipal District	Spring discharge (m^3/d) October – June during winter	Maximum abstraction rate from groundwater wells (m^3/d)	Monthly consumption (m^3) during October – June (census 2001)	Mean daily consumption (m^3/d) during October – June (18% network water losses)	Daily water supply rates (m^3/d) (24hrs daily water abstraction from springs and 18hrs daily pumping operation of groundwater wells)	Difference (m^3/d)
	(1)	(2)	(3)	(4)	(5)	(6)
Limenas	960	3,960	20,724	815	3,930	3,115
Panagia	2,520	-	5,603	220	2,520	2,300
Potamia	63,120	1,920	8,329	328	64,560	64,232
Theologos	5,088	4,200	11,537	455	8,238	7,783
Limenaria	1,152	2,208	16,183	637	2,808	2,171
Maries	1,440	960	3,690	145	2,160	2,015
Kallirahi	1,080	1,248	8,461	333	2,016	1,683
Prinos	3,240	1,200	8,982	353	4,140	3,787
Sotiras	288	960	2,587	102	1,008	906
Rahoni	2,688	2,880	4,752	187	4,848	4,661
TOTAL	81,576	19,536	90,848	3,574	96,228	92,654

Table 2. Water supply balance (consumption vs. water availability) for the island of Thassos during August.

Municipal Disctrict	Total discharge (springs (2) and groundwater wells (3)) (m^3/d)		Monthly consumption (m^3)	Consumption during week-ends (m^3/d) (18% network water losses)	Daily water supply rates (m^3/d) (24hrs/day water abstraction from springs and 18hrs/day pumping operation of groundwater wells)	Percentage of daily water supply with respect to the remaining period	Difference (m^3/d)
	(1)	(2)	(3)	(4)	(5)	(6)	(7)
Limenas	960	3,840	99,112	4,169	3,840	2.3%	-329
Panagia	1,680	-	29,568	1,244	1,680	33.3%	436
Potamia	3,600	1,680	37,204	1,565	4,860	92.5%	3,295
Theologos	4,320	3,360	69,927	2,942	6,840	17%	3,898
Limenaria	960	1,800	79,609	3,349	2,310	17.7%	-1,039
Maries	600	240	22,737	952	780	63.9%	-172
Kallirahi	192	1,248	45,652	1,921	1,128	44%	-793
Prinos	960	1,200	46,378	1,951	1,860	55.1%	-91
Sotiras	240	240	14,586	614	420	58.3%	-194
Rahoni	720	960	25,087	1,055	1,440	70.3%	385
TOTAL	14,232	14,568	469,860	19,762	25,158		

4 Conclusions

The water supply availability in the island of Thassos mainly depends on the population fluctuation between summer and winter period, the condition of the water supply network (percentage of water losses) as well as on the amount of annual precipitation (Katimada 2010). The availability in water resources is found to be satisfactory mainly in winter, in contrast to the majority of the Greek islands in the Aegean Sea, with the need of making proper interventions during the summer period to provide water to the local and the touristic population.

During the winter period, there is an over-excess of available water resources for all the settlements of the island, with a daily supply rate of 96,228 m^3. The excess in available water is estimated up to 92,654 m^3/daily, with the exception of the Municipal District of Potamia which amounts up to 64,232 m^3/day (67%) due to the presence of the karst springs at the area. The majority of the water supply needs are covered by the springs of the island, whereas the groundwater wells are mostly used for supporting purposes.

During the summer period the total (both springs and groundwater wells) water supply amounts 25,158 m^3/day (74% less than the water supply in winter). There is a significant difference in water resources availability between the winter and summer period mainly due to the following reasons: (a) extreme population during the summer period (b) decrease in water discharge in springs and some groundwater wells. Specifically in August, a month of touristic peak, only 4 out of 10 Municipal Districts, show water surplus. The water discharge from the springs is significantly limited during the summer, especially when the precipitation during the winter period is limited. During these conditions, there is a need for the exploitation of the groundwater wells of the coastal sedimentary aquifer and this practice results to the encroachment of seawater and hence to groundwater salinization. Due the fact above, the availability of water supply is not enough to fully cover the needs for the daily water consumption; problem which is more pronounced during August. Additionally some settlements show water shortage during some summer months mainly due to the decrease in spring discharge.

The confrontation of the water supply problems in many Municipal Districts of Thassos, during the summer period can be achieved with the following measures:

- Development of specific water works for the improvement of the water exploitation of the springs
- Exploitation of new springs selecting from the existing springs that are not yet exploited (numbering in 81 springs), after studying their hydrogeological potential.
- Increase of the volume of available water by constructing special water tanks capable to store appropriate amounts
- Replacement of older parts of water pipelines of the water supply network in order to minimize further losses.
- Construction of small surface water works (water tanks, small dams)

– Joint management of water resources between different municipal districts (re-distribution of the water from springs and groundwater wells from places with water surplus to places of water shortage.

References

Diamantis I, Tzevelekis Th, Georgiadis P (1994) Hydrogeological behavior of formations in Thassos Island. Problems with the exploitation of the water resources potential. Proceedings of the 4th Conference of the Geological Society of Greece, Volume XXIII/4, 173-182, (in Greek)

Zahos S (1977) Report for the geological mapping of Thassos Island, (in Greek).

IGME, Institute of Geological and Mineral Exploration. Part of geological map (scale 1:200,000), (in Greek)

Diamantis I, Tzevelekis Th (1992) Hydrogeological and hydrochemical conditions in the coastal alluvial fans of Thasos island. Proceedings of the 2nd Hellenic Hydrogeological Conference. Bulletin of Cyprus Association of Geologists and Mining Engineers (6) 131-148, (in Greek)

Karavitis C A, Kerkides P (2002) Estimation of the Water Resources Potential in the Island System of the Aegean Archipelago, Greece, Water International, Volume 27, Issue 2, pages 243 - 254

Katimada Chr (2010) Water resources management of Thassos island in terms of origin, quality and quantity. Diploma Thesis. Department of Civil Engineering, Democritus University of Thrace, Xanthi, Greece, (in Greek)

Leontiadis I L, Vergis S and Christodoulou Th (1996) Isotope hydrology study of areas in Eastern Macedonia and Thrace, Northern Greece, Journal of Hydrology, Volume 182, Issues 1-4, pp. 1-17

Papacharalampos Chr (2007) Assessment of the water supply needs of Thassos Island. Assessment for the Municipal Enterprise for Water Supply and Sewerage of Thassos (in Greek)

Hydrological properties of Yesilcay (Agva) Stream Basin (NW Turkey)

H. Keskin Citiroglu[1], I.F. Barut[2], A. Zuran[3]

[1] Zonguldak Karaelmas University, Engineering Faculty Department of Geological Engineering, 67100 Zonguldak, Turkey (keskinhc@yahoo.com)
[2] Istanbul University, Institute of Marine Sciences and Management, 34116 Vefa- Istanbul, Turkey (barutif@istanbul.edu.tr)
[3] State Hydraulic Works 14th. Regional Directorate, 34696, K. Camlıca-Istanbul, TURKEY (aynurzuran@dsi.gov.tr)

Abstract This study seeks to determine the hydrological and hydrogeological properties of the basin of Yesilcay (Agva) Stream which runs 19.2 km through the settlement of Agva and flows into the Black Sea (Turkey). To this end, the precipitation and evaporation characteristics of the study area were calculated by means of the Thornthwaite (1948) and Schendel (1968) methods on the basis of the meteorological data for the last 45 years (1966-2010). It was deduced that the Schendel method yielded results very close to values of pan evaporation measured in the area. Therefore, this method is more suitable to use for the study area. The calculations performed reveal that precipitation occurring in the study area will not be sufficient to have access to the amount of water that can be used safely. Therefore, it is of great significance to utilize as water source the karstic limestones present in the study area, and Yesilcay and Goksu Streams flowing into the Black Sea.

1 Introduction

Agva is a recreation and tourism centre on the Anatolian side of Istanbul close to the province of Izmit (Kocaeli, Turkey). It is a township of Sile and lies 40 km to the north. Construction activities in Agva, which lies on the Black Sea, are concentrated in a delta situated between Goksu Stream and Agva Stream. Its climate has characterized by climates of the Black Sea region, the Balkans and Anatolia. Agva referred to as Yesilcay in official records is a Latin word meaning a village situated between two streams. It has a natural beach 50 m wide and 3 km long. Agva lies within the area where feasibility study is carried out for Isakoy, Sungurlu and Kabakoz Dams to be built in the framework of the Yesilcay Project. The present study is aimed at determining the hydrological and hydrogeological properties of the Yesilcay (Agva) Stream Basin.

N. Lambrakis et al. (Eds.), *Advances in the Research of Aquatic Environment, Vol. 2*
DOI 10.1007/978-3-642-24076-8,

2 Geological setting

Upper Cretaceous sedimentary rocks occurring to the north of Istanbul comprise conglomerate with an intercalation of sandstone, siltstone, marl, claystone and limestone, and displays the properties of flysch (Yeniyol and Ercan 1989/1990). Marly elements of Upper Cretaceous age are encountered around Dudubayir Hill and extend to the west running along the coast. Marls crop out along the highway running between Isakoy and Agva (Ertek 1995). The Eocene limestones with layers of medium thickness are composed of limestone and marls. Marls present in the study area and limestones overlying them harmoniously lie along the Black Sea coast and run from the east to the west. The stratigraphic formation contains clayey limestone, sandy limestone, sandstone and limestone. Quaternary sediments made up of alluvium and beach sand cover a wide area around the township of Agva (Yesilcay) and Agva (Yesilcay) Stream. The sand is uncemented and has low clay content (Fig. 1).

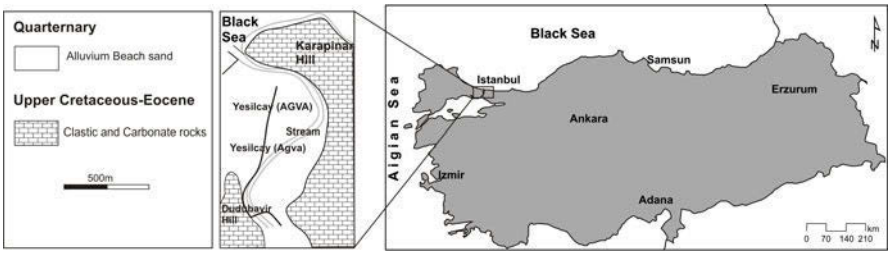

Fig. 1. Location and geological map of the study area (GDMR 2002).

3 Hydrology and hydrogeology of the study area

Extensive meteorological studies were carried out in order to provide insight into the hydrological and hydrogeological properties of the study area. The arithmetic average was taken of meteorological data obtained from the records of The State Meteorological Station covering the last 45 years (TSMS 2010) and the precipitation and evaporation characteristics of the study area were determined. The maximum amount of water lost due to evaporation and transpiration depending on the climatic conditions yields potential evapotranspiration (Etp). Potential evapotranspiration (Etp) and real evapotranspiration (Etr) occurring in the study area were calculated by means of the Thornthwaite (1948) and Schendel (1968) methods on the basis of the data relating to average monthly temperature and relative humidity measured by The State Meteorological Station (Equations 1 and 2 respectively) (Thornthwaite 1948, Schendel 1968).

$$Etp = 16 \times \left(\frac{10 \times t}{I} \right)^{a} \times p, \qquad i = \left(\frac{t}{5} \right)^{1.514}, \qquad I = \sum i \tag{1}$$

$$a = 6.75 \times 10^{-7} \times I^{3} - 7.71 \times 10^{-5} \times I^{2} + 1.79 \times 10^{-2} \times I + 0.49239$$

$$Etp = \frac{t}{h} \times 480 \tag{2}$$

where Etp is potential evapotranspiration (mm), t average monthly temperature (ºC), i monthly temperature index, I total annual temperature index, p latitude correction coefficient and h relative humidity (%).

3.1 Precipitation and temperature

It is evident from the average of meteorological data for the last 45 years that precipitation increases starting from October and continues to fall heavily until February. The total precipitation height for the study area in the last 45 years (1966-2010) was found to be 812.1 mm. The area receives less precipitation in the months of May, June and July compared to the other months, and the most precipitation falls in winter. 34.7% of total annual precipitation occurs in winter, 18.6% in spring, 13.7% in summer and 33% in autumn (Fig. 2a). Average annual temperature that is experienced in the area is 14.1 ºC, with the highest average annual temperature of 23.4 ºC occurring in August and the lowest in February with 5.6 ºC (Fig. 2b). The decrease in temperature occurring in November gives way to an increase starting from April.

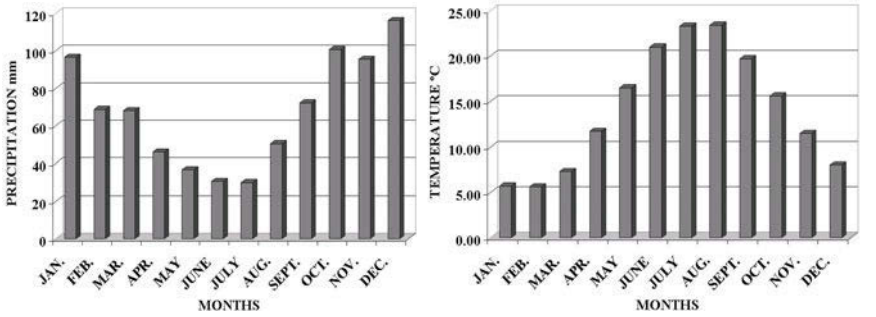

Fig. 2 a. Average precipitation and**, b.** temperature for the last 45 years (1966-2010).

3.2 Evaporation

The amounts of evaporation calculated using the Schendel method (1968) and the water balance values are given in Table 1, and the graph depicting annual variations in precipitation-potential evaporation in Figure 3a. The calculations performed reveal that October experiences the highest real evapotranspiration (Etr) (99.7 mm) and July the lowest (30 mm).

Table 1. Water balance for the study area calculated using the Schendel (1968) method (period of 1966-2010).

Features	Jan.	Feb.	Mar.	Apr.	May	June	July	Aug.	Sept.	Oct.	Nov.	Dec.	Total
Precipitation P	96.6	68.7	68.1	46.0	36.9	30.7	30.0	50.5	72.2	100.8	95.5	116.2	812.1
Temperature t	5.7	5.6	7.3	11.7	16.5	21	23.3	23.4	19.7	15.6	11.5	8.0	169.3
Relative humidity h	75.6	73.5	72.4	69.2	69.2	66.1	67.6	69.7	70.7	75.1	74.9	74.7	858.7
Etp	36.2	36.6	48.4	81.2	114.5	152.5	165.4	161.2	133.8	99.7	73.7	51.4	1154.6
P-Etp	60.4	32.1	19.7	-35.2	-77.6	-121.8	-135.4	-110.7	-61.6	1.1	21.8	64.8	-342.4
Reserve water	100	100	100	64.8	00	00	00	00	00	1.1	22.9	87.7	-
Etr	36.2	36.6	48.4	81.2	101.7	30.7	30.0	50.5	72.2	99.7	73.7	51.4	712.3
Water shortage	00	00	00	00	-12.8	-121.8	-135.4	-110.7	-61.6	00	00	00	-442.3
Water surplus	60.4	32.1	19.7	00	00	00	00	00	00	00	00	00	112.2
Runoff	30.2	31.2	25.4	12.7	6.4	3.2	1.6	0.8	0.4	0.2	0.1	0.05	112.2
Humidity rate %	1.7	0.9	0.4	-0.4	-0.7	-0.8	-0.8	-0.7	-0.5	0.01	0.3	1.3	-

Table 2. Water balance (period of 1966-2010) calculated using the Thornthwaite (1948) method.

Features	Jan.	Feb.	Mar.	Apr.	May	June	July	Aug.	Sept.	Oct.	Nov.	Dec.	Total
Precipitation P	96.6	68.7	68.1	46.0	36.9	30.7	30.0	50.5	72.2	100.8	95.5	116.2	812.1
Temperature t	5.7	5.6	7.3	11.7	16.5	21	23.3	23.4	19.7	15.6	11.5	8.0	169.3
M. temp. index i	1.22	1.19	1.77	3.62	6.10	8.78	10.28	10.35	7.97	5.60	3.53	2.04	62.45
Lat. correction p	0.83	0.83	1.03	1.11	1.25	1.26	1.27	1.19	1.04	0.96	0.82	0.80	-
Etp	11.61	11.31	20.75	44.81	83.75	120.45	141.51	133.43	90.48	59.22	32.27	18.44	768.03
P-Etp	84.99	57.39	47.35	1.19	-46.85	-89.75	-111.51	-82.93	-18.28	41.58	63.23	97.76	44.17
Reserve water	100	100	100	100	53.15	00	00	00	00	41.58	100	100	-
Etr	11.61	11.31	20.75	44.81	83.75	83.45	30.0	50.5	72.2	59.22	32.27	18.44	518.31
Water shortage	00	00	00	00	00	-37.0	-111.51	-82.93	-18.28	00	00	00	-249.72
Water surplus	84.99	57.39	47.35	1.19	00	00	00	00	00	00	63.23	97.76	351.91
Runoff	42.5	50	48.6	24.9	12.5	6.2	3.1	1.6	0.8	0.4	31.8	64.8	287.2
Humidity rate %	7.3	5.1	2.3	0.0	-0.6	-0.8	-0.8	-0.6	-0.2	0.7	2.0	5.3	-

In addition, total annual real evapotranspiration (Etp) occurring in the area has a value of 712.3 mm. As to potential evapotranspiration (Etp), it is the highest in July (165.4 mm) and the lowest in January (36.2 mm). The area has 1154.6 mm of total annual potential evapotranspiration (Etp). Starting October until April, the amount of precipitation occurring in the study area is greater than that of potential evapotranspiration. The reserves of soil moisture are depleted from late April to mid-May. The shortage of water that is experienced from mid-May until late September amounts to 442.3 mm. During this period cultivated land requires irrigation. A portion of 712.3 mm that is about 87.7%, of the total annual precipitation of 812.1 mm falling in the area is released back into the atmosphere through evapotranspiration. Water surplus accounts for about 13.8% of total precipitation.

The values of evaporation amounts and water balance calculated by means of the Thornthwaite (1948) method are illustrated in Table 2 and the graph depicting monthly variations in rainfall-potential evaporation in Figure 3b.

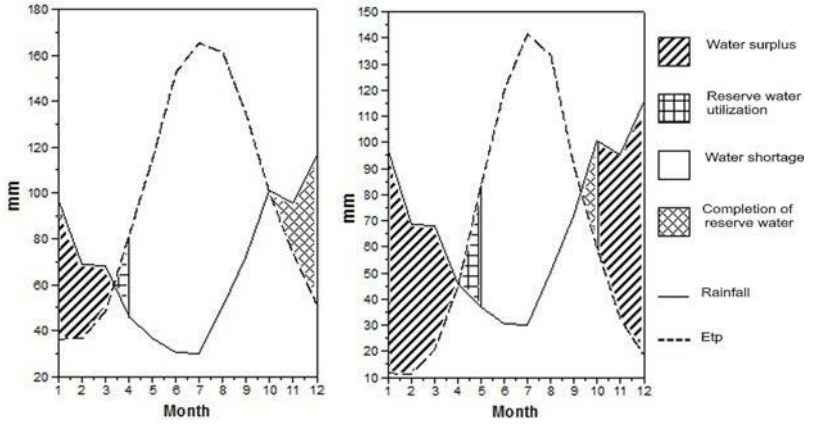

Fig. 3. Graphs illustrating variations in precipitation and evapotranspiration in months according to **a.** the Schendel method **b.** the Thornthwaite method (period of 1966-2010).

It is clear from the calculations performed that the highest real evapotranspiration (Etr) (83.75 mm) occurs in May and the lowest (11.31 mm) is experienced in February. Also, the area has 518.31 mm of total annual evapotranspiration (Etr). The highest potential evapotranspiration (Etp) (141.51 mm) was observed in July and the lowest (11.31 mm) in February. Total annual potential evapotranspiration (Etp) the area experiences is 768.03 mm. Potential evaporation taking place in the period from October to May is higher than transpiration. The soil moisture reserves are used up by mid-May. The water shortage occurring from mid-May to late September 249.72 mm, making it necessary for the cultivated land in the area to be irrigated during this period. 518.31 mm, that is to say 63.8%, of a total annual precipitation of 812.1 mm falling in the area is sent back into the atmosphere by means of evapotranspiration. The water surplus is 43.3% of total precipitation.

A comparison of the results from the two methods employed reveals that the Schendel method yields maximum values and the Thornthwaite method minimum ones except water surplus (Table 3). Considering the humidity rates and the amounts of water shortage, the months when water is in short supply cover the period from April to October on the basis of the Schendel method and the period from May to September on the basis of the Thornthwaite method.

Table 3. Evaporation parameters obtained by means of different methods (period of 1966-2010).

Evaporation Members (mm)	Precipitation P	Etp	Etr	Water shortage	Water surplus
Schendel (1968) method	812.1	1154.6	712.3	-442.3	112.2
Thornthwaite (1948) method	812.1	768.03	518.31	-249.72	351.91

3.3 Runoff

Water surplus calculated using the Schendel (1968) method was determined to be 112.2 mm and 13.8% of precipitation. In view of total annual runoff calculated to be 112.2 mm, the portion of precipitation comprising 13.8% runs over the land surface (Table 1). Water surplus calculated by means of the Thornthwaite method was found to be 351.91 mm. Water surplus which makes up 43.3% of precipitation. Considering total annual runoff established to be 287.2 mm, 35.4% of precipitation joins surface runoff. After that part of water surplus that joins surface runoff is subtracted from the total, the remaining 64.71 mm comprising 8% of total annual precipitation is infiltrated into the soil (Table 2). The period when water surplus and surface runoff occur covers the months from January to March on the basis of the Schendel (1968) method and the months from November to April on the basis of the Thornthwaite (1948) method.

3.4 Water balance

The water source that feeds the 395 km² study area is precipitation. The area has 812.1 mm of total average precipitation. For the study area of 395 km², the amount of precipitation that falls in the water catchment area equals 320.78×10^6 m³/year. The amount of annual real evaporation in the area calculated is to be 712.3 mm on the basis of the Schendel method is 281.36×10^6 m³/year of water for a catchment area of 395 km². In this case, the difference between gain and loss is 39.42×10^6 m³/year. The amount of annual real evaporation is calculated to be 518.31 mm using the Thornthwaite method, which equals to 204.7×10^6 m³/year for the same precipitation area. The difference between gain and loss is 116.1×10^6 m³/year (Table 4).

Table 4. Water balance for the study area (period of 1966-2010).

Methods	Gain	(m^3/year)	Loss	(m^3/year)	Difference between gain and loss
Schendel (1968)	Precipitation	$320.78x10^6$	Evaporation	$281.36\ 10^6$	$39.42x10^6$
Thornthwaite (1948)	Precipitation	$320.78x10^6$	Evaporation	$204.7x10^6$	$116.1x10^6$

3.5 Yesilcay (Agva) stream

Agva (Yesilcay) Stream, which has a very curving course from Agva to the west, runs from Dudubayir Hill (84 m) to the north east extending to the slope made up of Upper Cretaceous limestones. Agva Stream called Yesilcay in this region follows a course along the west side of Karapinar Hill which is composed of limestone and flows into the Black Sea (Fig. 4a). The stream is 19.2 km in length.

3.6 An approach to properties of the lithological units

The geological units present in the study area are classified as permeable and semipermeable depending on their hydrogeological properties. The permeable units, that are the uncemented medium, are made up of alluvium, beach sand and backfill. The permeable units consist of sediments carried away from Yesilcay (Agva) Stream, material in the size range of uncemented sand, gravel and blocks, and alluvium. The uncemented sand extends along the shoreline as a strip. The semipermeable units are composed of Upper Cretaceous sedimentary rocks and Eocene limestones (Fig. 4b).

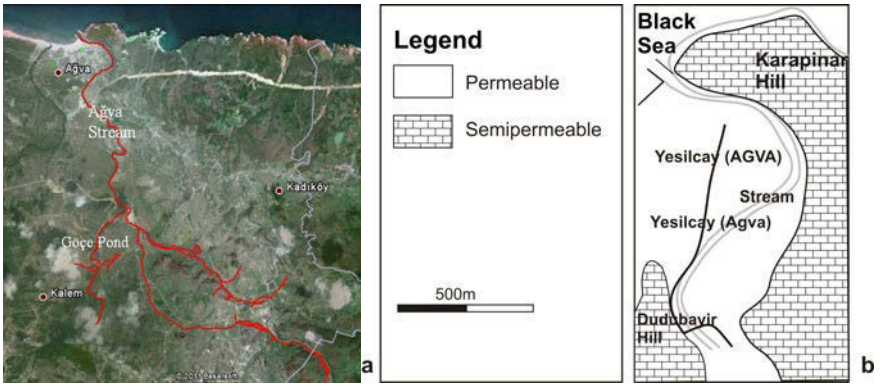

Fig. 4. a. Satellite image (Google Earth 2011) and **b**. hydrogeological map of the study area.

These units characterized by flysh properties, which are made up of conglomerate and an intercalation of sandstone, siltstone, marl, claystone and limestone, are overlain by limestone and marls. Limestones that have melting spaces and fractures may contain a considerable amount of ground water. Eocene limestones that have karstification feature constitute the permeable medium. However, claystone, siltstone, firmly cemented sandstone occurring in the lower layers reduce the property of permeability. Eocene limestones may display the properties of karstic aquifers, but, as they are intercalated with impermeable units, they make up the semipermeable units.

4 Discussion

Potential evapotranspiration (Etp) and real evapotranspiration (Etr) experienced in the study area were calculated using the Thornthwaite (1948) and Schendel (1968) methods and it was established that the Schendel method yielded maximum values and the Thornthwaite method minimum ones. When the real evaporation values obtained through the Thornthwaite and Schendel methods were compared with those of pan evaporation for the area, the Schendel method was determined to deliver results that are very close to values of pan evaporation occurring in the area (TSMS 2010). Therefore, it is obvious that real evaporation values calculated on the basis of the Schendel method are more suitable to use.

5 Conclusions

The stratigraphic formation existing in the study area contains marl, clayey limestone, sandy limestone, sandstone and limestone of Upper Cretaceous-Eocene ages, and Quaternary alluvium and beach sand. Yesilcay (Agva) Stream sediments, uncemented sand, gravel, block-sized materials and alluvium constitute the hydrogeologically permeable units. The intercalations composed of Upper Cretaceous sedimentary rocks and Eocene limestones make up the semipermeable rock medium. Based on water balance and evaporation calculated by means of the two different methods for the period 1966-2010, it can be stated that values obtained using the Schendel (1968) method is more suitable to use for the study area. The period when the area is short of water encompasses the months from April to September. Water shortage experienced from mid-May to late September is 442.3 mm, which necessitates irrigation of cultivated land during this period. During the period from January to March, when water surplus and runoff occur, 13.8% of precipitation joins surface runoff. The amount of precipitation falling in the water catchment area is 320.78×10^6 m³/year. The 712.3 mm annual real evaporation (Etr) occurring in the study area adds up to 281.36×10^6 m³/year for the water

catchment area of 395 km². In this case, the difference between gain and loss amounts to 39.42×10^6 m³/year. This means that, considering this amount, precipitation experienced by the study area will not be sufficient enough for the amount of water that can be used safely. Therefore, it is of utmost importance to utilize karst limestones that occur in the study area and Yesilcay and Goksu Streams flowing into the Black Sea as a water source.

References

Ertek A (1995) Geomorphology of north-eastern part of Kocaeli Peninsula. Çantay Bookstore. Istanbul (in Turkish)

GDMR (2002) Geological Maps of Turkey, scale 1: 500 000, No:1 Istanbul Section. General Directorate of Mineral Research, Ankara

Google Earth (2011) http://www.google.com.tr/earth/index.html

Schendel U (1968) Messungen mit grundwasser lysimeter über den wasserverbrauch aus oberflachennahem grunwasser. *Z.* Grundwasser. Kulturtechnik Flurbereich. Berlin/Hamburg. 9, 314-326

Thornthwaite CW (1948) An approach a rational classification of climate, The Geographical Review. New York 38, 55-94

TSMS (2010) Meteorological data of Yesilcay Meteorological Station No:1071 and Kocaeli Meteorological Station No:17066. Turkish State Meteorological Service, Ankara

Yeniyol M, Ercan T (1989/1990) Geology of North, petrochemical properties of Upper Cretaceous volcanism and regional dispersion in pontides. IU İstanbul Earth Sciences Review 7 (1-2), 125-147 (in Turkish)

Application of the SWAT model for the investigation of reservoirs creation

K. Kalogeropoulos[1], C. Chalkias[1], E. Pissias[2], S. Karalis[2]

[1]Department of Geography, Harokopio University, El. Venizelou Str., Kalithea, 17671 Athens, Greece
[b]Department of Surveying Engineering, Technological Educational Institute of Athens, Ag. Spyridonos Str., 12210 Aigaleo, Athens, Greece

Abstract Efficient Water Management is an important factor for regional development and requires a set of actions in order to manage water resources in a sustainable way. This paper describes a methodology of water resources exploitation, with the potential of creating small mountainous and upland reservoirs. This can be done with the integration of Geographic Information Systems (GIS), while using the SWAT hydrological modeling and Reservoir Simulation software. Andros Island was chosen as the study area. This project involves the hydrologic analysis and the assessment of runoff (using SWAT model for a 100 years simulation in the Afrouses basin). In two different selected sites, the feasibility of constructing a dam with the simultaneous creation of a reservoir based on annual failure rates of deliverability of certain volume of water is investigated.

1 Introduction

The sustainable management of the environment, even if it has global characteristics, it is a tool for decision making in any area. Water resources management is a crucial action in this direction and could not be treated apart from this overall framework. Andros is a "*gifted*" island in terms of water potential in relation to other Cycladian islands. However, as many islands in Cyclades, Andros is periodically deficient in water balance. This lack is either high or low depending on many reasons. Small reservoirs, instead big reservoirs (over 150.000m^3), is based on a logic that takes into account economic criteria, social necessities and environmental commitments (Forzieri et al. 2008) such as economic and sustainable growth of small regions, ecological flow, conservation of landscape regime etc.

The purpose of this study is to investigate the possibility of creating small reservoir with the construction of a small dam. This investigation is possible by applying the hydrological model SWAT and exploitive the given results in terms of surface runoff (Schuol et al. 2008). The rainfall-runoff modeling approach is used in order to investigate if the total runoff is adequate to justify the creation of a res-

N. Lambrakis et al. (Eds.), *Advances in the Research of Aquatic Environment, Vol. 2*
DOI 10.1007/978-3-642-24076-8, © Springer-Verlag Berlin Heidelberg 2011

ervoir in the selected sites, based on total annual discharge, rock formation permeability, appropriate topography, protection of lowland settlements etc. This study is actually an attempt in order to find the annual discharge in a place (Andros) with great uncertainty in terms of hydrological data due to lack of meteorological stations on it.

2 Study area

Andros is the northernmost island of Cyclades with an area of 374km^2 and a perimeter of 176km. The entire island has a mountainous topography with a central mountainous area (highest peak is 997m). In order to develop the proposed methodology Afrouses basin was chosen. This basin has an area of 12.9km^2, a perimeter of 28.70km and an average altitude of about 510m.

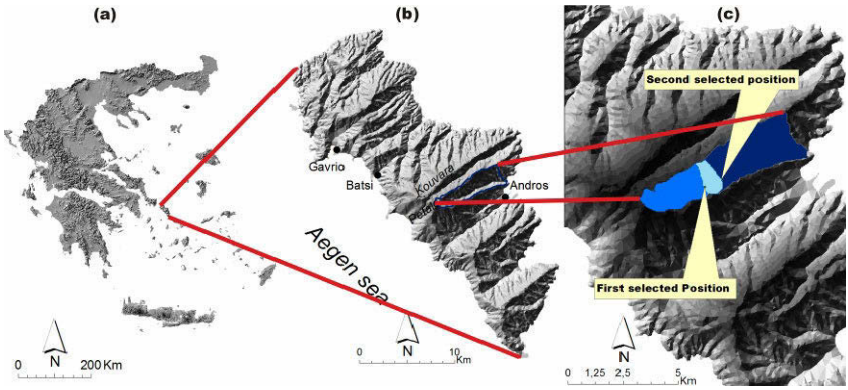

Fig. 1. The study area, a. Greece, b. Andros Island, c. Afrouses basin.

3 Development of the methodological process

3.1 General

The methodology followed in this study involves the application of the hydrological model SWAT (Neitsch et al. 2004) in Afrouses basin (in Andros), for the calculation of monthly runoff at two selected sites of the basin. Those sites are suitable due to their topography (steep small gorges), position (almost in the center of Andros) and rock formations permeability (low or very low permeability). The simulated runoff is used as an entry data in the Reservoir Simulation software and

the monthly failure is examined in order to qualify the optimal positioning of the dam, the height of the dam and the annual volume of water release based on failure rate of extraction of the required water volume.

3.2 The hydrological model SWAT

The introduction of GIS technology led researchers to develop data processing automations and to produce reliable simulation models. The hydrological model used in this work is SWAT (SWAT2009 version), acronym for Soil and Water Assessment Tool. The simulation of the hydrologic cycle in SWAT involves a large number of meteorological and spatial data (Zheng et al. 2010). SWAT uses the standard equations of hydrology to simulate the parameters of the hydrological cycle. The general equation which describes the hydrologic cycle is:

$$SW_t = SW + \sum_{i=1}^{t}(R_i - Q_i - ET_i - P_i - QR_i)$$

Where SW_t is the content of the soil water (soil moisture), t is time in days, R is the daily precipitation, Q is the surface runoff, ET is the evapotranspiration, P is the infiltration and QR is the underground flow (Neitsch et al. 2004). The model also uses the curve number method to calculate runoff. The curve number method of SCS (Soil Conservation Service) is an empirical method widely used in the U.S. Curve number provides a method of manufacturing unit hydrograph through which water concentration times can be assessed/measured. Furthermore, one of the main characteristics of SWAT is the possibility of sub-division of a watershed or sub-watershed into smaller areas known as Hydrologic Response Units (HRUs). An HRU is a smaller entity within the catchment basin, which has the same characteristics of hydrologic soil type (same permeability), land use and slope. Input data are divided into two main categories: i) the spatial data and ii) the meteorological data.

Spatial data

a) Digital Elevation Model (DEM). The DEM of the study area was created within ArcGIS environment from digitized topographical data (Andros, Gavrion and Piso Meria map sheets, source: Hellenic Military Geographical Service -HMGS- scale of 1:50000). This type of DEM is suitable for hydrological analysis (Chaplot 2005).

b) Land cover map. In this study a map of the ILOTING Project by the Ministry of Agriculture is used. The correlation between ILOTING land cover and SWAT land cover database was implemented in order to import the land cover data of Andros to SWAT model.
c) Soil map. An attempt was established in order to link the hydrological characteristics of the different geological formations of the standard 1:50000 geological maps of IGME (Institute of Geological and Mineral Exploration) to the SWAT database. The correlation was made by using the permeability of geological formations (maps of IGME in relation to Master Management Plan by the Ministry of Development) with the corresponding permeability of model database soils. A table with the hydrologic / hydraulic characteristics of the geological formations of Andros Island is given below.

Table 1. Hydrologic/Hydraulic characteristics of Andros rocks (source: Master Management Plan, Ministry Of Development and IGME, modified).

Hydrogeololgy type	Permeabity		Description
Alluvial	3	C	Low-moderate
Marble, limestone, dolomite	4	D	Moderate-high
Coarse torrential deposits, marine terraces	4	D	Moderate-high
Slates, amphibolites, quartzites	1	A	Low-very low

The selected map has a 25m x 25m raster analysis. This analysis is critical for the simulation within SWAT, since the model provides better results according to the accuracy of the map (Geza and McCray 2008).

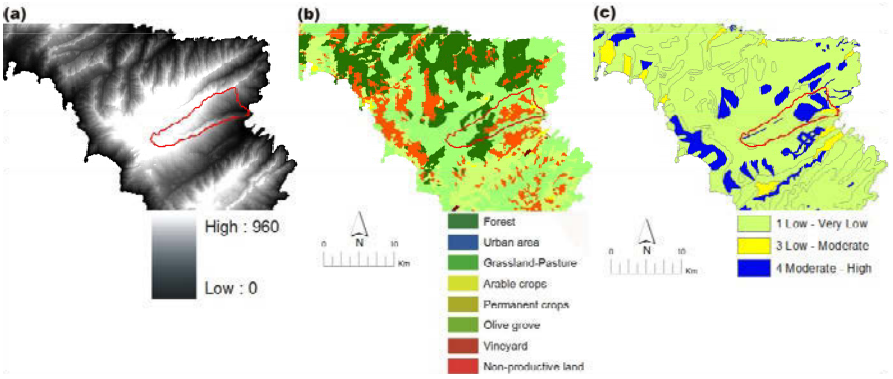

Fig. 2. Spatial data, a. Andros DEM, b. Land Cover Map (source: Ministry of Agriculture, modified), c. Rocks formations permeability (source: Master Management Plan, Ministry of Development and IGME, modified).

Meteorological data

SWAT provides the opportunity either to enter historical data of rainfall, temperature, wind speed and solar radiation or to create a statistical weather station, in the absence of previous data. Andros Island has an unjustifiable lack of reliable primary meteorological data (raw data). Therefore, the creation of a synthetic statistical weather station was the only option. The rainfall data of this weather station was derived from the "Study of Small reservoirs in Northern Cyclades Islands" by the Ministry of Agriculture. Rainfall data (of Karystos: P_K and Naxos: P_N) are correlated across Karystos-Naxos axis and Andros is treated as a part of this axis so that the necessary hydrological information can be attached. Based on the correlations of the rainfall data given by the Hellenic National Meteorological Service (HNMS), the average monthly rainfall for Andros (P_A) is determined as $P_A = 0.7* P_K + 0.3* P_N$. Based on correlations of temperature data given by HNMS (for islands with available data) the average monthly temperature for Andros (T_A) is determined as a combination of mean monthly temperature of Syros (T_S) and Karystos (T_K) $T_A = 0.5* T_S + 0.5* T_K$. For the solar radiation a weather station from the SWAT database was used with the same latitude of Andros. The wind speed data was provided from the nearest weather station and specifically from Syros Island (source: HNMS).

Simulation

The next step was dedicated to the implementation of the simulation scenario. Simulation was carried out for two selected dam sites (the choice of two candidate sites for dam construction was based on the low permeability of the specific sites, the strength of the ground in a barrier $\leq$ 15m, and the total water demand around the area) and for Afrouses basin, in total. The simulation period was 100 years.

The simulation was carried out for Afrouses basin in total and showed an average annual rainfall of 565.2mm (the average annual rainfall imported into the model is 569.4mm- almost identical to that calculated by SWAT for a hundred years simulation) and surface runoff of about 291.1mm. This means that the mean annual percentage of drainage for Afrouses basin is 0.52. The basin water capacity is 23mm/km^2. This figure is almost in line with the numbers referring to the Master Management Plan (due to Framework Directive 2000/60) by the Ministry of Development, where the average annual rainfall is 661mm and the surface runoff is 293mm. In this plan the mean annual percentage of drainage for Afrouses basin is slightly reduced (0.44) by using a Thornwaite rainfall-runoff model, but the basin water capacity is 23mm/km^2, same as the result of this study.

3.3 Reservoir Simulation

Reservoir Simulation software (version 7.0) simulates the reservoir operation of single or multiple feasibility and also can treat, practically, unlimited points that describe the change of reservoir volume in terms of pairs of level-area points.
The input data required for the execution of Reservoir Simulation software are: a) Level- area Curve, b) Hydrologic Data (precipitation, temperature, input per day-carried out by SWAT), c) Latitude of the area under investigation, d) Annual extraction volume, e) Monthly outflow rates, f) Volumes function (m^3) based on lower and upper levels operation (overflow and lack of energy) and g) Deviation.

For each of the two selected sites the level-area curve is calculated at a topographic chart (scale 1:5,000) of HMGS.

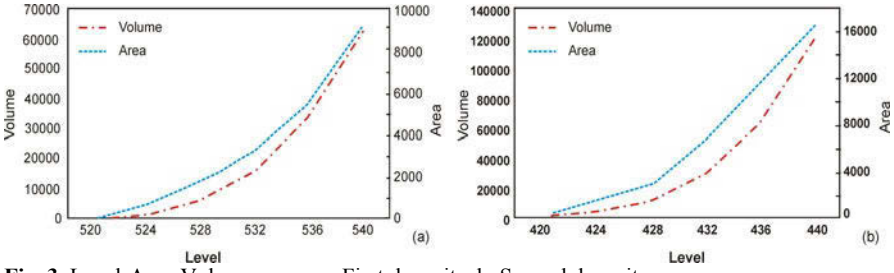

Fig. 3. Level-Area-Volume curve, a. First dam site, b. Second dam site.

The level-area curves for the two selected dam sites are presented in the previous chart. As already mentioned, this study examines the possibility of creation of a reservoir based on the failure rates of deliverability of a certain water volume annually at the selected sites. The number of failures in months (where the offer does not meet the demand) is taken into account in order to calculate this. For example:

Number of failures (in months) = 223 within Total months = 1200

The failure that arises is: 223/1200 = 0.18583 ≈ 18.6%.

For this study four scenarios of annual volume of water extraction (50, 100, 150 and 200.000m^3 per year) were considered for each of the two dam sites and for eight different dam heights (8, 9, 10, 11, 12, 13, 14 and 15m). A certain scenario is adopted in terms of monthly outflow rates. These coefficients are smaller during months with low consumption (period without large demands for water for domestic use and irrigation), such as the period from October to March (coefficients varies from 4 to 6% of the total usable volume) and increase during summer period (when in August a peak seasonal population, due to the tourists, is observed and the monthly outflow rate is up to 18%). The above mentioned coefficients are shown in the next Figure 4.

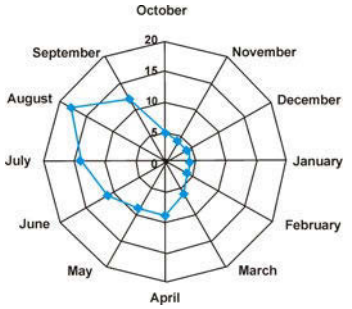

Fig. 4. Monthly outflow rates.

Table 2 shows the failure rate, as discussed previously. It is obvious that the rate of failure increases as the requested water volume increases for every dam height and decreases as the dam height increases for each volume of extraction, as it is expected. The corresponding table of the failure rate for the second selected dam position is presented below. Similarly, for the second selected dam position the rate of failure increases as the requested water volume increases for every dam height and decreases as the dam height increases for each volume of (water) extraction.

Table 2. Failure rates (%) for a variety of annual volume of water extraction and dam heights (first dam site).

Annual volume of extraction (m^3)	Dam height (m)							
	8	9	10	11	12	13	14	15
50,000	14.3	9.9	4.9	2.8	0.7	0.3	0.2	0.0
100,000	24.9	23.1	19.2	17.4	9.0	8.9	5.8	3.2
150,000	29.4	28.3	26.9	24.8	21.7	20.1	17.3	12.2
200,000	32.4	31.4	29.8	28.3	27.8	25.3	22.8	20.8

Table 3. Failure rates (%) for a variety of annual volume of water extraction and dam heights (second dam site).

Annual volume of extraction (m^3)	Dam height (m)							
	8	9	10	11	12	13	14	15
50,000	6.9	3.1	0.8	0.3	0.0	0.0	0.0	0.0
100,000	20.4	16.7	12.9	6.7	3.7	0.9	0.3	0.1
150,000	25.8	24.1	19.8	17.5	12.3	7.8	4.1	1.5
200,000	29.3	27.3	26.0	22.3	20.2	16.8	11.0	6.9

4 Results - Discussion

The methodology described above is only a part (although significant) of the total decision making policy and the simulation results are satisfactory, based on the assumptions made and the data which is used (Bouraoui et al. 2005). Taking this into account, the conclusions from the reservoir simulation are:

1. For small volumes up to 50.000m^3, the creation of a reservoir in the first selected site is possible. For dam height of 8m the failure is 14.3% and for dam height 9m the failure falls below 10% (9.9%), which is the limit of acceptable failure.
2. It is obvious that the first site is inappropriate for the creation of a reservoir, in order to meet the demand for large volumes of water extraction (from the reservoir). For this site the failure is about 20%, even for a dam height of 15m and a volume of 200,000m^3, which is quite high percentage and not acceptable to meet the demand (based on the results, failure mainly occurs during the summer season). Thus the first site is insufficient to meet water needs.
3. The second dam site is selected as the most reliable solution for large usable volume of about 200.000m^3. A dam height up to 15m is satisfactory in order to meet water needs for this amount of water extraction from the reservoir (acceptable failure rate of 7%).

These findings are not panacea in order to take a decision towards the construction of a dam and the simultaneous creation of a reservoir. It is necessary to take into account and prioritize some additional functions, such as the control curves (Adeloye et al. 2003).

Acknowledgments The authors gratefully acknowledge Assistant Professor Andreas Tsatsaris (Director of the GeoInformatics Laboratory, Department of Surveying Engineering of the Technological Educational Institute of Athens) for his assistance and provision of data. This paper is an application of the methodology developed within the research project "Exploitation of the surface runoff on the Island of Andros in the creation of mountain water reservoirs" (2009-2011) undertaking by Water Resources Management Laboratory of the Department of Surveying Engineering of the Technological Educational Institute of Athens. Thus, the authors acknowledge everyone who helped during this project. This project continues with the installation of a meteorological station and with continuous water metering in the stream of Afrouses in order to improve the results of SWAT.

References

Adeloye A, Psarogiannis A, Montaseri M (2003) Improved heuristic reservoir operation using control curves incorporating the vulnerability norm, Water Resources Systems-Hydrological Risk, Management and Development (Proceedings of symposium HS02b held during IUGG2003 at Sapporo, July 2003), IAHS Publ. 281, 192-199

Bouraoui F, Benabdallah S, Jrad A, Bidoglio G (2005) Application of the SWAT model on the MedJerda river basin (Tunisia), Physics and Chemistry of the Earth, 30, 497-507

Chaplot V (2005) Impact of DEM size and soil map on SWAT runoff, sediment, and NO3-N loads predictions, Journal of Hydrology 312, 207-222
Forzieri G, Gardenti M, Caparrini F, Castelli F, (2008) A methodology for the pre-selection of suitable sites for surface and underground small dams in arid areas: A case study in the region of Kidal, Mali, Physics and Chemistry of the Earth, 33, 74-85
Geza M, McCray J (2008) Effects of soil data resolution on SWAT model stream flow and water quality predictions, Journal of Environmental Management, 88, 393-406
Ministry of Development (2003) Master Management Plan, Andros
Neitsch SL, Arnold JG, Kiniry JR, Srinivasan R, Williams JR (2004) Soil and Water Assessment Tool Input/Output File Documentation Version 2005, Grassland, Soil and Water Research Laboratory, USDA-ARS
Schuol J, Abbaspour K, Shrinivasan R, Hong Y (2008) Estimation of freshwater availability in the West African sub-continent using the SWAT hydrologic model, Journal of Hydrology, 352, 30-49
Vlastou A, Kloni A (2010) Study of Positioning of Mountain Reservoir in Andros, undergraduate dissertation, Department of Surveying Engineering, Technological Educational Institute of Athens (Greek language)
Zheng J, Li G, Han Z, Meng G (2010) Hydrological cycle simulation of an irrigation district based on a SWAT model, Mathematical and Computer Modelling, 51, 1312-1318

Evaluation of geological parameters for describing fissured rocks; a case study of Mantoudi - Central Euboea Island (Hellas)

G. Yoxas, G. Stournaras

Faculty of Geology and Geoenvironment, Department of Tectonic Dynamic and Applied Geology, University of Athens, Panepistimioupolis Zografou, GR 15784, Athens, Greece, yoxas@geol.uoa.gr

Abstract The present paper is dealing with the analysis and characteristics of the discontinuous media, represented by the ophiolite nappe in central Euboea (Mantoudi). It is aiming at the conception, the development and the subsequent validation of an integrated methodology for the description of fissured rocks, in the frame of intrinsic vulnerability assessment and mapping. The vulnerability is not being considered as a characteristic of a particular element at risk, but as a peculiarity of a complex territorial system, in which the different elements are reciprocally linked in a functional way. In order to estimate and to define both the quality and quantity, a group of parameters are being considered. The estimation and definition of those parameters are based on the geoenvironmental conditions of an area that may be vulnerable to contamination, in order to distinguish the geological, geomorphologic and hydrogeological criteria that affect the environmental impact of hard rock aquifers. These criteria are being calibrated in GIS so as to be able to support a correct territorial planning and a suitable management of the water resources protecting its quality which is essential to increase efficient use of existing water supplies. Furthermore, a sensitivity analysis has been performed to evaluate the influence of single parameters on aquifer vulnerability assessment.

1 Introduction

The increasing need of groundwater for water supply during the last decades, led to a continuous interest for groundwater in hard rocks. This interest was focused on a better knowledge about the hydrogeological environment of hard rocks and the recharge, flow and composition of groundwater as well (Krasny 1996). The hydraulic conditions of fissured rocks depend on climate conditions and on several factors, such as geomorphology, hydrolithology but mainly they are controlled by soil cover and the tectonic regime (Stournaras 2008).

N. Lambrakis et al. (Eds.), *Advances in the Research of Aquatic Environment, Vol. 2*
DOI 10.1007/978-3-642-24076-8, © Springer-Verlag Berlin Heidelberg 2011

The study area is located in Central Euboea Island (Mantoudi), 60 km far from the city of Chalkida. It covers an area of 71.4 km^2. The area of Mantoudi belongs to the Pelagonian Zone (Katsikatsos et al. 1986), the Pre-Upper Cretaceous tectonic nappe. Each geotectonic unit in Hellas, based on its lithological and tectonic structure develops certain type of aquifers and displays its own hydrogeological characteristics, so that the directions of the groundwater flow are related to the fracture pattern.

2 Geomorphological setting

According to drainage network analysis, the R_h factor is 5.25, the hydrographic density RD is 3.05 km/km^2 and the hydrographic frequency R_F is 6.53 per km^2.

Horton's Laws (Horton 1945) were also applied, in order to study the development stage of the drainage basin. The 1st order class are long with wide catchment areas. On the contrary 2nd order class and 3rd order class have a short length with narrow catchment areas. The hydrographic texture shows the interaction between the activities of deepening and surface resistance, while it influences the ability of surface flow in a region at the duration of intense floods (Knighton 1998). Two main factors are affecting the hydrographic texture; the factors that check the quantity and quality of water that remains in the surface and the factors that check its later distribution and its corrosion respectively. The first team relates itself with the climate, whilst the second one relates itself with the lithological structure, the vegetation, the ground characters and the topography.

According to slope analysis, 86% of the total area represents a flat to semi-flat region. Taking into consideration the low values of hydrographic texture and low values of morphological slope, it is obvious that surface water is limited. Thus the intrinsic vulnerability is being affected as there is low possibility for infiltration of water, due to low permeability.

3 Geological setting

The encountered geologic formations belong to Sub-Pelagonian Zone (Fig.1). It is characterized by the intense lithological transformations within its whole extent. The stratigraphy of the zone is the following (Katsikatsos et al. 1986):

- Neo-Paleozoic formations which are composed of sandstones, phyllites and schists,
- Formations of Lower – Middle Triassic which are composed of i) sandstones, ii) basic volcanic rocks and iii) intercalations of limestones.
- Neritic limestones of Middle Triassic - Upper Jurassic. Locally, the neritic sedimentation passes to pelagic with radiolarites, pellites, clay, schists, etc.

- Clastic formations of Upper Jurassic - Lower Cretaceous which are composed of radiolites, conglomerates, sandstones and shales with olistostromes of ophiolites.
- A tectonic nappe of pre – upper Cretaceous age, which is divided in two tectonic units. A lower unit which is composed of volcano – sedimentary formations, and an upper one, which is composed by ophiolites.
- Formations of Upper Cretaceous composed of limestones, which are laying trangressively over the previous formation. Finally flysch of Paleocene occurs.

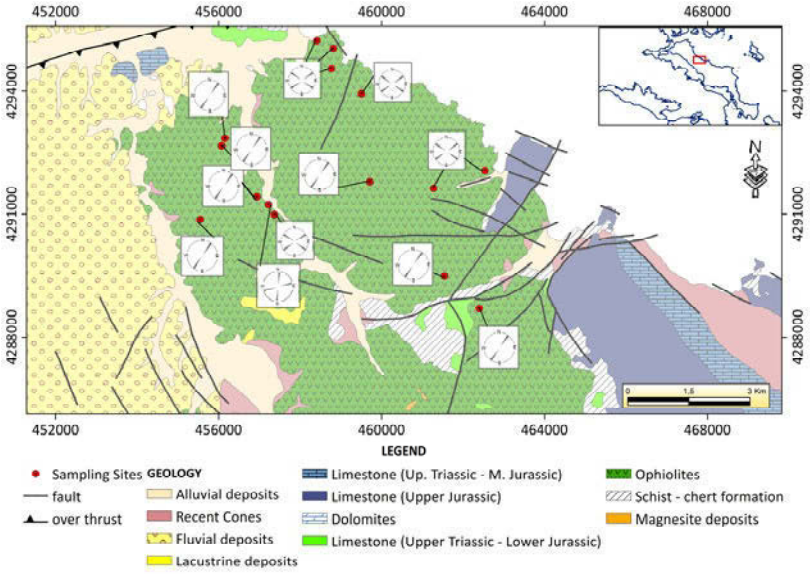

Fig. 1. Geological map of the study area with rose diagrams of specific sites (by Katsikatsos et al. 1986; Yoxas 2009; with modifications).

The Euboea artificial Island, especially the central part, corresponds to the typical Sub - Pelagonian zone and is consisted by Paleozoic basement, covered by non metamorphic Mesozoic formations, which present tectonic intercalations of ophiolites (Migiros 1983b). Among the different lithostratigraphic phases, the potential and existing fractured rocks aquifers on the Central part of Euboea mainly belong to the following sequences.

The crystalline basement presents a thickness over 800 m of gneiss and gneissic schist. The upper part is composed by mica and amphibolitic schist, while the carbonate rocks are entirely absent. The Neopaleozoic sequence is consisted by sandstones, sandstones-schists, arkoses, graywackes and clay schists. The Lower-Middle Triassic sequence presents clayey-sandstone phases, basic volcanic rocks and tuffs. The ophiolitic tectonic nappe, is composed by volcano-sedimentary formations, ultra basic bodies (serpentinized peridotites), gabbros, amphibolites,

and basalts. Figure 2 depicts the lineaments in the ophiolitic cover as they were derived by a Landsat – 7 ETM+ image, whereas three main categories of orientation were being recognized, showing a NE-SW preferential orientation.

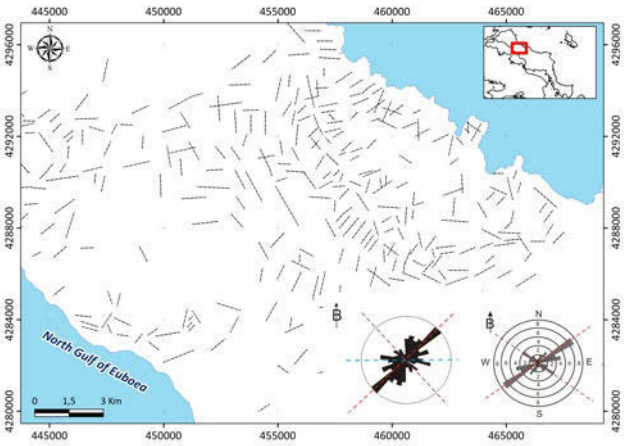

Fig. 2. Lineament map of ophiolitic cover with rose diagrams. **a.** frequency of fault direction (left), **b.** frequency of fractures/linears direction (right).

Most of the discontinuities were easily identified in the field either as fractures/lineaments (57%), or meso-scale faults (41%) and large scale fractures (2%).

4 Hydrogeological conditions

The main fracture aquifer seems to be the ophiolitic cover, presenting an intense differentiation related to the lithology, the geological structure and the tectonic regime. The hydrogeological conditions of the study area show that the distribution of the springs is related to the tectonical setting. Specifically there are three main teams with a NE – SW, NW – SE and E – W orientation (Fig. 3c). This fact leads to the conclusion that the orientation of the springs is identical with the orientation of the fractures. In this frame, a correlation between the ruptures and the faults and plies has been attended. In the frame of the hydrogeological behaviour, the hydraulic characters of the simple porosity, double porosity, and multiple porosity fractured media are examined and evaluated. In the field of the remote sensing, used in the tectonic approach, atmospheric and geometric correction, mosaic synthesis, and data integration led from the fault's density map (Fig. 3a) and lineament/fracture density map of several groups (Fig. 3b), to the statistical analysis of the discontinuities (Fig. 3d). Since fracture density is an important parameter for the delineation of the groundwater flow in hard rocks, density maps which were also constructed in a GIS environment represent the total length of linea-

ments/fractures per square kilometre of the area. The comparison of these two maps leads to the conclusion that the density pattern of lineaments/fractures and faults in the study area is almost identical. The comparison of lineaments/fracture and fault density distribution led to the spatial density map of discontinuities, where these sub areas show a fine correlation with the three main fold axes, striking from NW to SE and from NNE to SSW respectively (Fig. 3d).

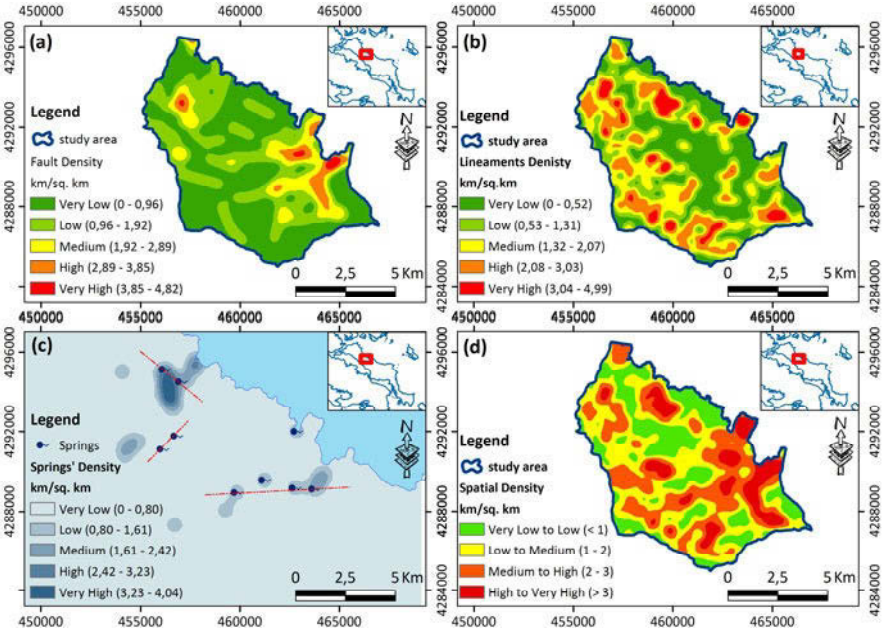

Fig. 3. a. Fault density map. **b.** Lineaments/ photolines density map. **c.** Springs'density map. **d.** Spatial density map.

5 Procedure of estimating geological parameters

In order to estimate and to define, qualitatively and quantitatively, a group of parameters are being considered. The estimation and definition of those parameters is based on the geoenvironmental conditions of an area that is vulnerable to contamination, in order to distinguish the geological, geomorphologic and hydrogeological criteria that affect the environmental impact of hard rocks. These criteria are being calibrated in GIS with respect to AHP analysis (Saaty 1977) so as to be able to support a correct territorial planning and a suitable management of water resources protecting its quality which is essential to increase efficient use of existing water supplies, which is the main problem in the study area.

In order to depict the degree of fractures interconnection, intersection of points between two or more discontinuities were digitized. Consequently the density map of intersection points was produced, in which the frequency of intersection points per square kilometre is illustrated. The higher the density the higher is the degree of interconnection. The interconnection density map (Fig. 4) shows a medium (central part of study area) to a very high density (south-western part) in which the urbanised part of the study area is mainly represented. This could be explained by the fact that firstly the most of the fractures, which are mostly open, controlling the groundwater flow, are in that area, and secondly the horizon of soil cover is shallow. On the contrary in the southern part fractures seem to be close due to existence of serpentinite (product of olivine alteration), which fills the fractures (Yoxas 2009).

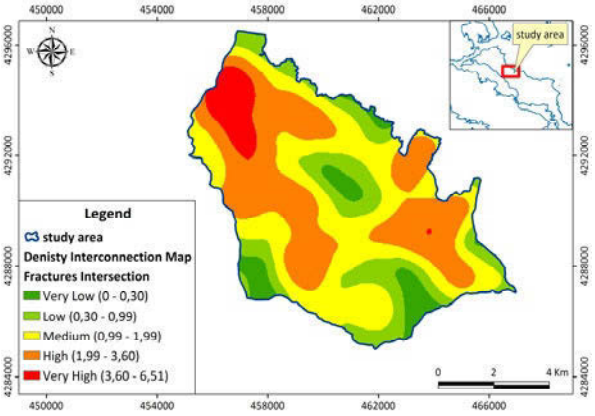

Fig. 4. Distribution of Density Interconnection of discontinuities in study area.

6 Nitrate concentrations correlated with density interconnection

Nitrate contamination has been suggested as an indicator of overall groundwater quality (2006/118/EC). Because drinking water with high nitrate concentrations is a potential health risk, European Union (2006) has set a minimum standard for nitrate in drinking water of 50 mg/L. Identifying areas in the study area where ground water has been impacted by anthropogenic activities (nitrate concentrations at or above 3 mg/L) can help water resource managers protect the water supply by targeting land-use planning and monitoring programs to these vulnerable areas. In order to estimate the correlation of hydrochemical conditions, a water sample collection (springs, boreholes, wells and surface water) was made.

According to the Piper diagram (Fig. 5b), the hydrochemical type of the hard rock aquifers is Mg-HCO_3. The underground water is classified as cold with T_w values ranging between 15.3°C and 17.6°C respectively, while T_{air} values range

between 16.2 and 25.2°C respectively. According to electrical conductivity measurements, and to Na/Cl ratio, it is obvious that there is no sea water intrusion as EC values range ranging between 307μS/cm and 822μS/cm. The concentration of NO_3^- ions range between 4.84 mg/L and 62.92 mg/L respectively.

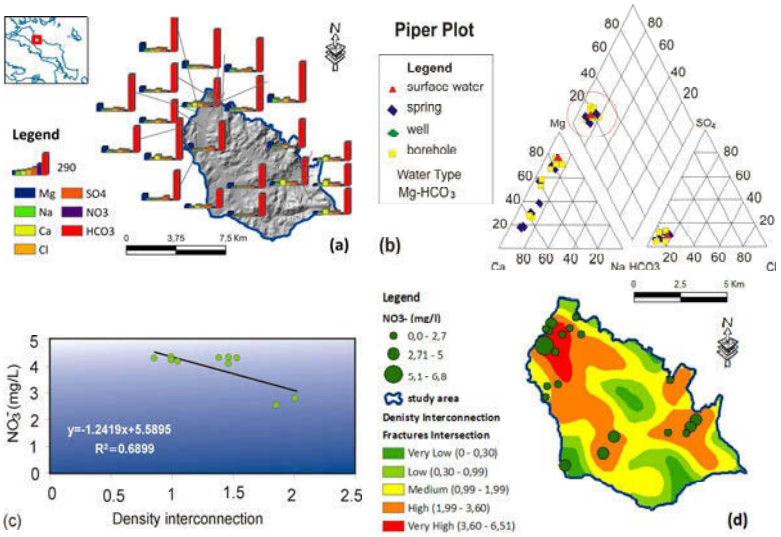

Fig. 5. a. Statistical hydrochemical characteristics of groundwater. **b.** Piper diagram. **c.** Cross - plot diagram of nitrate concentration vs density interconnection. **d.** Density Interconnection map vs NO_3^- concentration.

According to statistical analysis of hydrochemical characteristics for the main water points, the beginning of springs' depletion is combined with an increase of the TDS concentration. This happens due to the mix of fresh waters with permanent waters which are chemical enriched by the long-lasting storage into the aquifer. However in the expiry of springs' depletion, certain samples present decreased TDS. This phenomenon is due to the fact that these kinds of springs are characterized by a depletion that lasts till November mostly, where the wet period starts and their chemical affect is not intensive.

Additionally, electrical conductivity shows a similar behavior with TDS, where there is a gradually decrease during depletion till the expiry of spring's depletion where electrical conductivity is stabilized.

In order to estimate the affection of density interconnection of discontinuities (DI) a correlation between nitrate ions and DI factor was made. According to fig. 5d regions with high values of nitrate ions were established mainly due to human activities which are intensive in those areas. By the comparison of territorial distribution results of concentration of nitrate ions with the results of territorial distribution of density, an interconnection was observed and the correlation factor of cross-plot of these parameters is ordered 70% (Fig. 5c).

7 Conclusions

The basic factors which affect and form the hydrological and hydrogeological character of the study area are the discontinuous media character (secondary porosity), due to the tectonic and microtectonic activity on the geologic formations and the degree of weathering of the given formations. The fissured rock medium can be accessed with different methodologies of work. Among these methodologies hydrogeological and hydrochemical evaluations are included but the detailed study of structural pattern of the rock proved efficient to contribute in a better way in evaluating the hydrogeological conditions. According to the degree of fracture intersection regions showing similar plastic deformity and lithological characteristics present the same density of discontinuities. However, fractures, mostly open, are localized in areas (northern part) characterized by shallow soil cover. On the contrary in the southern part fractures seem to be close due to existence of serpentinite (product of olivine alteration).

The comparison of nitrate ions with density interconnection of discontinuities shows a clear correlation. Areas with medium to high values of nitrate ions are presented by medium to high density interconnection. That should be expected, as long as the high mark of connection affects extensively water's infiltration, while tectonics structures, such as folds and fractures, take charge of the underground water's selective movement to the points of normal discharge of aquifer.

References

European Union (2006) Water Framework Directive 2006/118/EC of the European Parliament and of the Council, Official Journal of the European Union

Horton RE (1945) Erosional development of streams and their drainage basins: hydrophysical approach to quantitative morphology. Bulletin of the Geological Society of America, Vol. 56, 275 – 370

Katsikatsos G, Migiros G, Triantaphyllis M, Mettos A (1986) Geological structure of internal Hellenides. Geol. Geoph. Res., Special Issue, 191 – 212

Knighton D (1998) Fluvial forms and processes, Arnold, London, 383

Krasny J (1996) Hydrogeological Environment in Hard Rocks: An attempt at its schematizing and terminological consideration. Acta Universitatis Carolinae Geologica 40, 115 – 122

Migiros G (1983b) The Geology and Geochemistry of ophiolithic rocks in the Area of East Thessaly (Greece). Ophioliti 8, 46

Saaty TL (1977) A scaling method for priorities in hierarchical structures, Journal of Mathematical Psychology 15, 231 – 281

Stournaras G (2008) Hydrogeology and vulnerability conditions of limited extension fissured rocks islands. The case of Tinos Island (Aegean Sea, Hellas), Intern. Conference, Ecohydrological Processes and Sustainable Floodplain Management, Lotz, Poland

Yoxas G (2009) Hydraulic study of fractured rocks and groundwater vulnerability assessment in the region of Mantoudi – Central Euboea, Master Thesis, National and Kapodistrian University of Athens (in Greek)

First outcomes from groundwater recharge estimation in evaporate aquifer in Greece with the use of APLIS method

E. Zagana, P. Tserolas, G. Floros, K. Katsanou, B. Andreo[1]

Laboratory of Hydrogeology, Department of Geology, University of Patras, 26500 Rion Patras, Greece
[1]Department of Geology and Centre of Hydrogeology, Faculty of Sciences, University of Malaga, 29071 Malaga, Spain

Abstract Groundwater recharge in karstic aquifers has to be determined taking into consideration the hydrogeological particularities of these aquifers. The APLIS method has been used to estimate the mean annual recharge in carbonate aquifers in southern Spain, expressed as a percentage of precipitation based on the variables altitude, slope, lithology, infiltration landform and soil type. The method developed for Mediterranean conditions, has been applied to a karstified evaporate aquifer in West Greece. In this paper, maps of the above variables have been drawn for the study area using a geographic information system. The autogenic groundwater recharge and the spatial distribution of the mean annual values by means of the APLIS method have been obtained. Because of the absence of previous studies about groundwater recharge estimations in the study area and detailed discharge values, it was impossible to corroborate the validity of the method in this phase of the research. In the frame of a research project taken place in the study area, discharge values are measured at the springs draining the system; thus the validation of the method will be done in the next step of this study.

1 Introduction

Knowledge of groundwater recharge is very important because it permits us to identify the water inputs entering the aquifer, which is very essential for appropriate water resources management and hydrologic planning. Different methods for groundwater recharge estimation have been developed in the last 20 years. These methods (direct measurement, water balance methods, Darcian approaches, tracer techniques, hydrochemical or isotopic models) and many of the problems encountered with each have been described by Gee and Hillel (1988), Sharma (1989), Lerner et al. (1990), Allison et al. (1994), Simmers (1997), Scanlon et al. (2002) among others. Recent advances on distributed methods of groundwater recharge calculations have been done by Udluft and Kuells (2000), Udluft et al. (2003),

N. Lambrakis et al. (Eds.), *Advances in the Research of Aquatic Environment, Vol. 2*
DOI 10.1007/978-3-642-24076-8, © Springer-Verlag Berlin Heidelberg 2011

Heathcote et al. (2004), Hughes et al. (2006), Brito et al. (2006) and Zagana et al (2007). Most of the above mentioned methods have been developed in porous aquifers and are then used in carbonate aquifers. However, in karst aquifers, recharge computing is more complex, due to the specific characteristics of these aquifers and the duality of the recharge. In this sense the concentrate and the diffuse type of recharge are defined; these types have been also as allogenic and autogenic differentiated.

In Europe, carbonate terrains cover 35% of the land-surface and karst groundwater makes an important contribution to the total drinking water supply (European Commision, 1995). In Greece carbonate rocks cover more than 35% of the surface (European Commision, 1995). However, studies about groundwater recharge estimations in carbonate aquifers are not known. Generally studies about groundwater recharge estimations in any type of aquifer and/or in catchment area scale are very limited in Greece (Lambrakis and Kallergis 2001, Zagana et al. 2007).

In this paper the mean rate of the annual autogenic groundwater recharge as a percentage of precipitation has been estimated in the study area with the use of the APLIS method (Andreo et al. 2008), which has been developed from the studies carried out in carbonate aquifers in Andalusia (S Spain). Recently the APLIS method has been modified in order to improve the results (Marin 2009) and has been used for recharge estimations in tropical climatic conditions (Farfan et al. 2010). However, it is necessary to note that in the frame of this paper the recharge rate values obtained by this method have not been compared with recharge calculations by other methods or their corresponding discharge rates. The validation of the method is the next step and will be done in the immediate future.

2 Characteristics of the study area

The study area is located in the West Greece (Aitoloakarnania Province) with a surface of 146.3 km^2. It is a karstified system, which presents general lack of permanent streams, existent of shallow holes, small caves and occurrence of large springs at the southern part of the area. This front of springs (Lambra -Agios Dimitrios) drains the karstic system and presents discharge rates approximately $8m^3/s$ (Nikolaou 1993). The springs cover the drinking water needs of many villages in the broad area. The relief of the area is gentle, with the maximum altitude 520 m and the lowest altitude around 10 m above sea level (Fig. 1a). In the eastern part the karstic system comes in contact with Acheloos River and Ozeros Lake (Fig. 1a). According to previous studies (Marinos and Fragopoulos 1972, Marinos 1993) river water seeps through the karstified rocks and feeds the springs.

The area is characterized by mean annual precipitation of 914 mm, estimating using the data of four rain stations located in the broad area for a time period of

twenty years (1981-2001). From the geological standpoint the study area belongs to the Ionian geotectonic Zone of the External Hellenides. It is part of the karstified mountainous chain system of Akarnanika Mountains which is developed at the Western part of Greece. Triassic breccias dominate in the study area (Fig. 1b).

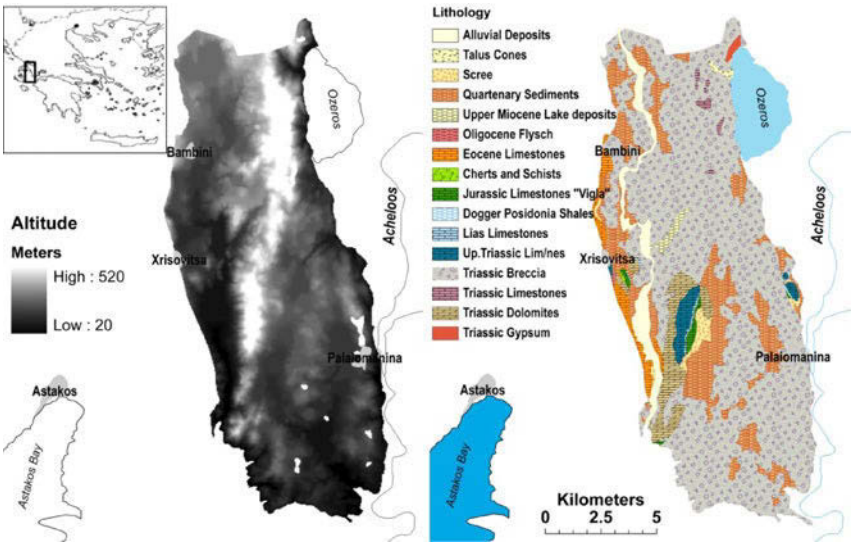

Fig. 1. a: Location and topographic map of the study area, **b:** Geological map of the study area.

They are typically un-bedded rocks including masses of dark-grey, brown or black fragments of limestones and dolomites, as well as gypsum. Similar dark colored Triassic limestones occur as individual masses in the northeastern part of the area, west of Ozeros Lake, while the Triassic dolomites outcrop in the southwestern part of the area, with a thickness approx. 200m. Several bodies of gypsum occur also west of Ozeros Lake. Bornovas (1960) mentioned that gypsum is relatively old and had been brought to the surface by diapisism phenomena, assisted by faulting. The Triassic breccias were derived from the fragmentation of the Triassic limestones and dolomites through the diapirism of the evaporate series. These structures play a significant role in the karstification of the breccias presented in the study area. Jurassic - Eocene limestones and Quaternary deposits, which consist of red clays and sandy material, with dispersed carbonate and siliceous pebbles occur also in the study area. In the western margins of the area Oligocene flysch appears in small parts. Fault tectonics has also contributed in the formation of the karstic structure of the area. A big thrust known as Makhalas thrust combined with strong normal faulting extend along the belt of the Triassic breccias. The intensively karstified breccias host significant aquifers, which are delimited by evaporite masses functioning as hydro-

geological barriers. The soils above the Triassic breccias outcrops in the area are poorly developed and belong to leptosol type. The soils above carbonate rocks (Triassic - Eocene limestones) are less permeable and belong to calcareous lithosols, while above alluvial deposits the soils are fluvisols. The soil map of the area is presented in Figure 2a.

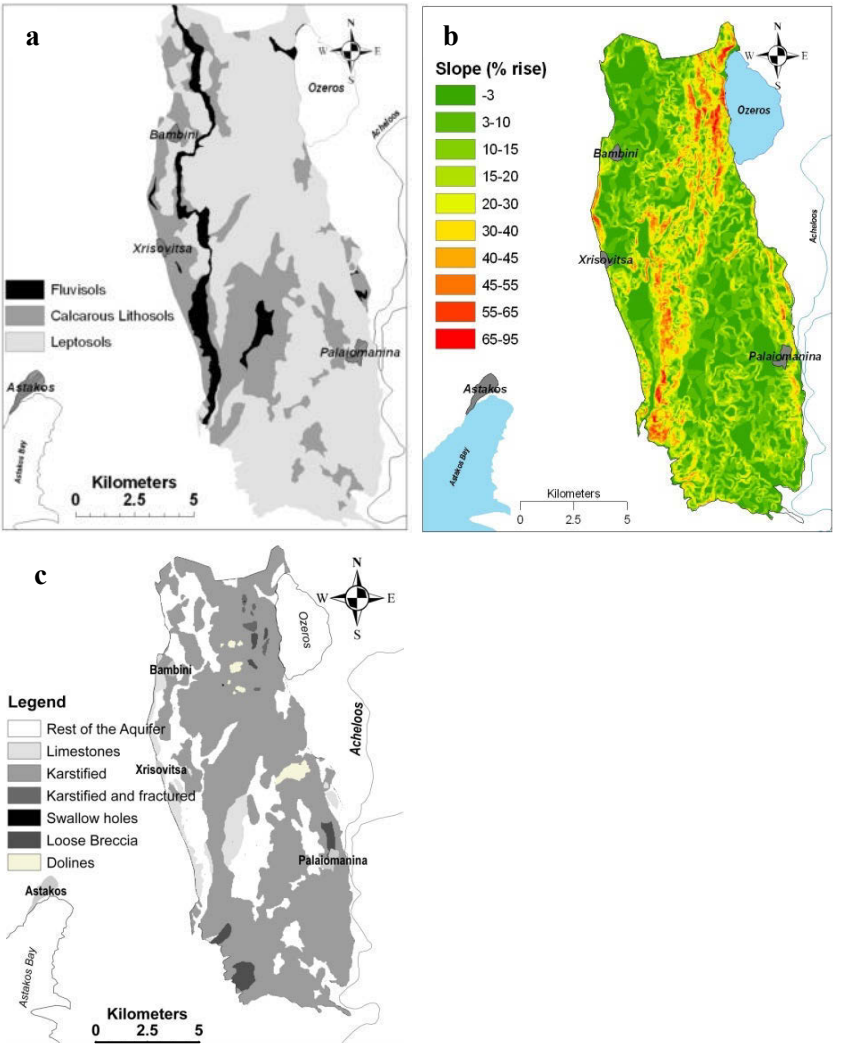

Fig. 2. a: Soil map of the study area**, b:** The map of slopes of the study area, **c:** Areas of preferential infiltration.

3 Methodology

APLIS is a parametric methodology, which enables us to estimate the mean rate of annual autogenic recharge in carbonate aquifers, expressed as a percentage of precipitation and based on the variables that influenced the recharge (Andreo et al. 2008). The method uses 5 variables, the initials of which (in Spanish) comprise its acronym and a correction factor. These variables are: Altitude (A), Slope (P), Lithology (L), Preferential Infiltration layers (I), Soils (S) and a correction factor (F_h), the last one depends on the hydrogeologic characteristics of the material outcropping on the surface. Maps for the above mentioned variables have been drawn for the study area using ArcGIS 9.3. The altitude map (Fig. 1a) and the map of slopes (Fig. 2b) have been derived from the digital elevation model (DEM) produced by digitizing the 1:50.000 contour lines map of the area. Soil maps are available only for some areas in Greece. The soil map of the study area was derived from field word (soil mapping) using also as basis a land resource map 1:50.000 of the Ministry of Agriculture. Finally the areas of preferential infiltration (Fig. 2c) were mapped over aerial photographs. For each variable, categories or intervals were established, and for each of these a rating value between 1 and 10 were assigned. A value of 1 indicates a minimal incidence of the values of this variable on aquifer recharge, while a value of 10 means maximum influence on recharge (Andreo et al. 2008). As the method has been developed for karstified limestones and dolostones, a slight modification related to the lithology has been necessary. For the karstified Triassic breccias has given the score 9 considering them as karstified limestones. In the Table 1 the values of all variables are presented.

Table 1. Rating values in APLIS for altitude, slope soil, lithology and preferential infiltration areas.

Altitude (m)	Rating (A)
0-300	1
300-600	2
Slope (%)	Rating (S)
<3	10
3-5	9
5-10	8
10-15	7
15-20	6
20-30	5
30-45	4
45-65	3
65-100	2

Soil	Rating (S)
Fluvisols	6
Calcareous Lithosols	6
Leptosols	10
Lithology	Rating (L)
Alluvial	4
Quaternary	1
Scree	3
Flysch	1
Non karstified Limestones	2
Triassic Dolomites	7
Triassic Limestones	9
Triassic Breccia	9
Triassic Evaporates	2

Infiltration areas	Rating (I)
Rest of the aquifer	1
Non karstified limestones	1
Karstified limestones, breccias	5
Swallow holes	10
Dolines	10

Then the layers of information corresponding to the variables that influence recharge have been introduced into a GIS. The rate of the recharge and its spatial distribution was finally estimated. The final recharge map is computed be the expression (Andreo et al. 2008):

$$R = ((A + P + 3 * L + 2 * I + S) / 0.9) / Fh$$

where R means Recharge (expressed in percentage of precipitation); A: Altitude; P: Slope; L: Lithology; I: Infiltration areas; S: Soil and Fh factor derived from the lithology map.

4 Results

With the APLIS method the recharge rate has been calculated and the map of recharge spatial distribution has been obtained in a GIS (Fig. 3a).

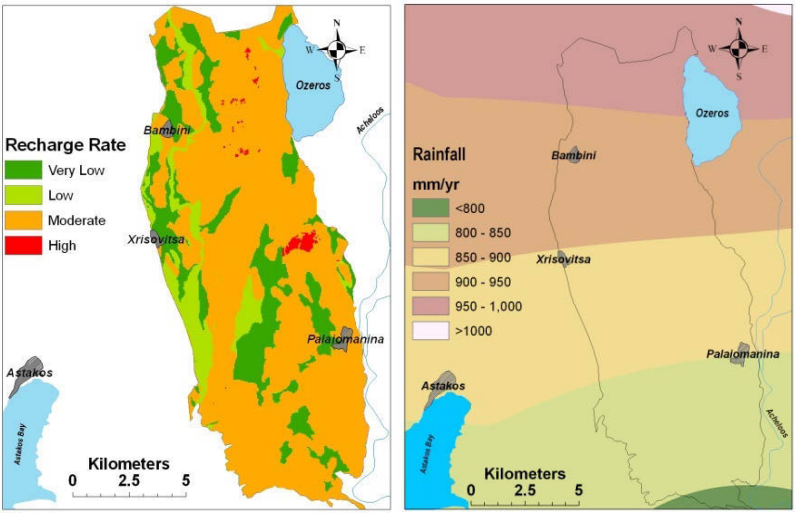

Fig. 3. a: Recharge map in the study area, **b:** Precipitation map of study area.

In the study area moderate recharges (40-60% of precipitation) are the most represented. They are associated with karstified breccias and limestones. These results are acceptable, taking into account the study of Marinos and Fragopoulos (1972) presenting that the infiltration rate in the karstified formations is 50% of precipitation. The areas with non karstified rocks and quaternary deposits present very low recharge rates, 20% of the mean annual precipitation as is shown in Table 2, while the alluvial deposits show low recharge rates. High recharge areas are

associated with the presence of shallow holes and dolines. In these areas the recharge raters represent 60 - 80% of mean annual precipitation (Table 2). The average value of the autogenic recharge rate for the study area deduced from APLIS method is 53% of precipitation, while the average value of the infiltration coefficient according to Marinos and Fragopoulos (1972) is 52.5% of the precipitation. Using the recharge map by means of the APLIS method (Fig. 3a) and the distribution map of precipitation (Fig. 3b) the recharge rates as mm/y of precipitation were derived (Table 2). As it is shown in table 2 in the areas with moderate recharge rates, the recharge rate varies from 170mm/y to 550 mm/y dependent of the spatial distribution of the precipitation.

Table 2. Recharge rate as (%) and mm/y of mean annual precipitation.

Recharge rate	(%) of Mean annual precipitation	mm/y of precipitation
Very Low	20	13-60
Low	20-40	60-170
Moderate	40-60	170-550
High	60-80	550-600

5 Conclusions

In this study, the APLIS method is applied to estimate the mean annual autogenic recharge expressed as a percentage of precipitation in a study area in Greece, which consists mainly of karstified evaporite and carbonate breccias. The application shows that autogenic recharges remain prevalent in the area; the major part of the area presents moderate recharges. Thus, in the major part of the study area the recharge rate is 40-60% of the mean annual precipitation. The average value of the autogenic recharge rate deduced from APLIS method is 53% of precipitation. These results are acceptable, taking into account that the average value of the infiltration coefficient according to an older study is 52.5% of precipitation.

References

Allison GB, Gee GW, Tyler SW (1994) Vadose –zone techniques for estimating groundwater recharge in arid and semiarid regions. Soil Sci. Soc. Am. J 58, 6-1

Andreo B, Vias J, Duran JJ,Jimenez P, Lopez-Geta JA, Carrasco F (2008) Methodology for groundwater recharge assessment in carbonate aquifers:application to pilot sites in southern Spain. Hydrogeology J. 16,911-925

Bornovas J (1960) Observations nouvelles sur la geologie des zones preapulienne et ionienne (Grece occidentale). Bull Soc geol Fr (7) 2, 410-414

Brito MG, Costa CN, Almedia JA, Vendas D, Verdial PH (2006) Characterization of maximum infiltration areas using GIS tools. Eng Geol 85(1-2), 14-18

European Commission (1995) Hydrogeological aspects of groundwater protection in karstic areas. EUR 16547 ENG Final rep. COST Action 6, 446

Farfan H, Corvea JL, Bustamante Ide (2010) Sensitivity Analysis of ALPIS Method to Compute Spatial Variability of Karst Aquifers Recharge at the national Park of Vinales (Cuba). Advances in Research in Karst Media, 19-24

Gee GW, Hillel D (1988) Groundwater recharge in arid regions: review and critique of estimation methods. Hydrol Process 2, 255-266

Heathcote JA, Lewis RT, Soley RWN (2004) Rainfall routing to runoff and recharge for regional groundwater resources models. Q J Eng Geol Hydrogeol 37(2), 113-130

Hughes AG, Mansour MM, Robins NS, Reach DW (2006) Numerical modelling of runoff recharge in a catchment in the West bank. In MODFLOW and More: Managing Ground-Water Systems, Conference Proceedings, vol 1, Colorado Scholl of Mines, Golden, CO, 385-389

Lambrakis N, Kallergis G (2001) Reaction of subsurface coastal aquifers to climate and land use changes in Greece: modelling of groundwater refreshening patterns under natural recharge conditions. J Hydrol (Amst) 245:19-31

Lerner DN, Issar AS, Simmers I (1990) Groundwater recharge. A quid to understanding and estimating natural recharge, IAH Int Contrib Hydrogeol 8, Hannover. Heinz Heise

Marin A.I. (2009) Los Sistemas de Informacion Geografica aplicados a la evaluacion de recursos hidricos y a la vulnerabilidad a la contaminacion de acuiferos carbonatados. Caso de la Alta Cadena (Provincia de Malaga). Tesis de Licenciatura, Universidad de Malaga. 131 pp

Marinos P (1993) The hydrogeological conditions in the detla area of Achelooos River. IGME, Athens

Marinos P, Fragopoulos JA (1972) Systeme des sources karstiques de lambra (Akarnanie – Greece pccidentale). IGME, Athens

Nikolaou E (1993) The hydrogeological conditions in Delta of Acheloos River, IGME, Athens

Scanlon BR, Healy RW, Cook PG (2002) Choosing appropriate techniques for quantifying recharge. Hydrogeol J 10, 18-39

Sharma ML (ed) (1989) Groundwater Recharge. AA Balkema

Simmers I. (ed) (1997) Recharge of preatic aquifers in (semi-) arid areas. IAH Int. Contrib. Hydrogeology 19, Rotterdam. AA Balkema

Udluft P, Kuells Ch (2000) Mapping the availability and dynamics of groundwater recharge – I Modelling techniques. Proceedings of the Third Congress on Regional Geological Cartography and Information Systems, Munich, 337-340

Udluft P, Dünkeloh A, Mederer J, Kuells Ch, Schaller J (2003) Water balances for catchments and the whole island. GRC-Project Report T 6/7, Geological Survey Department of Cyprus, Nicosia

Zagana E, Kuells Ch, Udluft P, Constantinou C (2007) Methods of groundwater recharge estimation in eastern Mediterranean: a water balance model application in Greece, Cyprus and Jordan. Hydrol Process 21 (18), 2405-2414

Multiple criteria analysis for selecting suitable sites for construction of sanitary landfill based on hydrogeological data; Case study of Kea Island (Aegean Sea, Hellas)

G. Yoxas, T. Samara, L. Sargologou, G. Stournaras

Department of Geology and Geoenvironment, University of Athens, Panepistimioupolis Zografou, GR 157 84, Athens. yoxas@geol.uoa.gr

Abstract The scope of this paper is to define the appropriate geoenvironmental parameters that directly affect the identification of the most suitable sites for sanitary landfill construction subject to hydrogeological data. The methodology developed in this research, includes four distinct stages of research, data collection, analysis, definition of the geological parameters, calibration and standardization of the criteria in a GIS environment and evaluation of suitability index corresponding to the most suitable sites for landfill construction. The preparation of the final map was the result of the combination between the thematic maps with respect to Analytical Hierarchy Process (AHP). The resulting land suitability is reported on a grading scale of low to high, which is, respectively, from least to most suitable areas.

1 Introduction

The determination of the most appropriate sites for sanitary landfill construction is more or less complicated because it requires thorough knowledge and understanding of the social, environmental and technical parameters (Chalkias and Stournaras 1997). Taking into consideration that the Hellenic territory is characterized by the presence of a different geomorphological character or cultural features as well as the fact that during the summer period there is a considerable population growth, a rank – ordered list of candidate sites for secure landfill construction must be prepared. Geographical Information Systems (GIS) is a form of technology capable of storing, retrieving, transforming and displaying all the involved environmental data. GIS make the results transparent and understandable to the public (Dörhöfer and Siebert 1997; Kontos et al. 2005). The above investigations constitute an accepted methodology for assessing the environmental impact of a landfill construction. The selected criteria from environmental point of view take into consideration all important aspects of the search process and help to select the

N. Lambrakis et al. (Eds.), *Advances in the Research of Aquatic Environment, Vol. 2*
DOI 10.1007/978-3-642-24076-8,

site which has the highest ranking. The objective is to recognize potential conflicts and problem areas as early as possible, so as to minimize regrettable and expensive environmental deterioration. The paper is intended to make the reader aware of certain aspects that frequently seem to be underestimated and to alert owners to potential problems as well as possible courses of action to avert problems. Additionally, the present procedure aims to highlight preferable sites for sanitary landfill construction based on hydrogeological data. The points outlined in the paper will also assist owners in evaluating the qualifications of potential contractors who may propose on landfill construction projects.

The evaluation criteria are determined based on international practice in landfill sitting and National and European Union (EU) legislation (Stournaras and Eleftheriou 2000). Based on the relevant literature review, the innovation of the evaluation criteria used is obvious.

2 Methodology of Research

In order to obtain a complete description of Kea Island from environmental point of view all necessary information from field work and remote sensing techniques were gathered and processed (the data were obtained from the literature;). Then, the thematic layers were constructed, at which criterion they correspond. The synthesis of these layers has led to the creation of the final thematic map, where areas over permeable formations, large morphological slope, distance less than 500 m from water sources and 300 m from riverbeds respectively, areas with high values of fractures density and degree of interconnection (predominance of flow concentration which leads to deviation of unsaturated zone) and protected areas both Natura and archeological sites, were isolated.

The parameters taken into account and their criteria for calibration and subsequent separation of categories are described respectively, as shown in Table 1.

Table 1. Geological Parameters.

Parameter	Criteria
Geomorphology	Slope /slope direction
	Distance from the hydrographic network
Hydrogeology	Soil's Imperviousness
	Water Source
	Density Interconnection of Fractures
Geoenvironmental Protection	Protected Areas
	Archeological sites

3 Geographical, Geological and Tectonic Settings

Kea Island belongs to the Cyclades complex and is located 60 km SE from Athens. Its climate is arid and its terrain is hilly. Kea is 19 km long from north to south and 9 km wide from west to east. Kea Island presents an area of about 131.7 km² while its highest point presents an elevation of 560 m.

Kea Island is part of the called Attic-Cycladic Unit (Lepsius 1983) and consists almost exclusively of metamorphic rocks. There are mainly schist and marble remains, which overlie the shale or from layers within the schist (Fig. 1). The rocks are multifolded and have identified three places of tectonic fold at least. They are characterized by greenschist metamorphic phase (LT/HP).

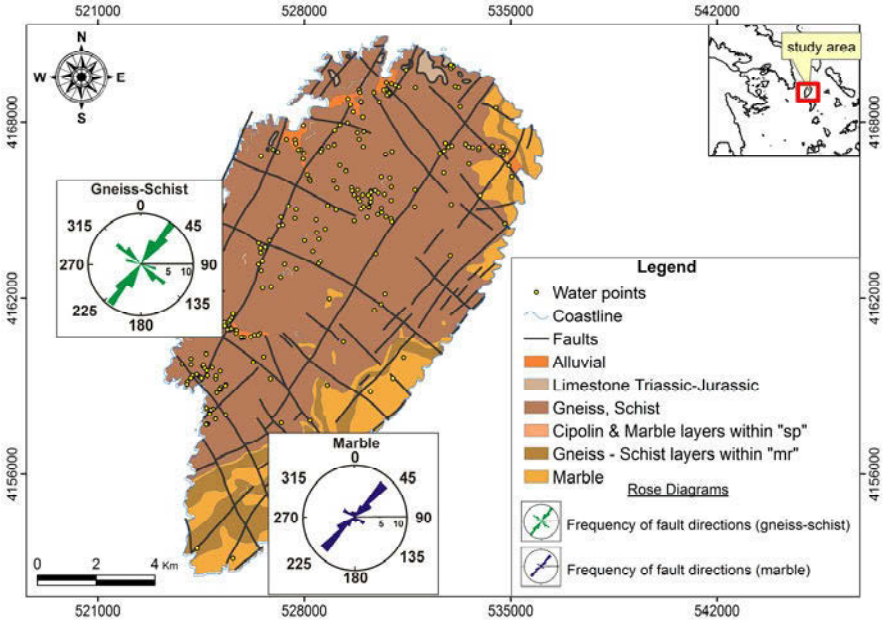

Fig. 1: Geological-Tectonic-Water source Map of Kea Island (Lepsius 1983; with modifications).

The rocks of Kea have been lifted with vertical faults, which occur in two groups of fault almost perpendicular to each other. The first system has an orientation of NE-SW and NW-SE respectively, following the general direction of the island and seems to be the oldest (it breaks up the continuity of the hydrographic network). The other system is an ENE-WSW and NNW-SSE one until E-W and N-S is the latest (development of alluvial valleys along). The tectonic activity on the island lasted until the Upper Miocene. Finally the folded tectonic of Kea Island includes aspects in two main axial directions. The prevailing direction is NE-SW, while the secondary is ENE-WSW. The latest one breaks the continuity of the morphological structures of the previous direction.

4 Geomorphological Conditions

Kea is an island with mountainous and diverse terrain, characterized by solid growth mountains. The slopes of the relief is substantial, with 30.6% of the total area of the island is being characterized by slopes over 40°. These large slopes intimate rift origins of mountain sides. However, a significant rate of the area (37.1%) formed areas with mild relief (< 15°) to complete flattening (Samara and Sargologou 2010).

Kea's hydrographic network is developed lateral of the base ridge that crosses the island from the southern part to the northern part. The hydrographic network shows a parallel and angular form and expands parallel to the mountain ridges with same directions.

The most important geomorphological criterias, which are considered to be selected in a location for sanitary landfill construction are i) morphological slope and, ii) distance from the hydrographic network, in accordance with legislation (JMD 29407/3508/2002).

In the proposed methodology, land morphology was evaluated by the slope gradation, which was expressed in degrees whilst the distance from the hydrographic network was expressed by buffer zones.

5 Hydrogeological Conditions

Kea Island is composed primarily of hard rocks whereas infiltration and movement of underground water are possible, due to severe fragmentation of the mass. The discontinuities are highly active hydrogeologically and particularly those of large scale faults. The underground water movement becomes easier along preferential fractured pathways such as the horizons of marble and the horizons of the fractured gneiss. Due to discontinuous media most of the springs are located across the main faults with an orientation of NE – SW respectively. The vast majority of the springs are located within the gneiss – schists, whereas a few others with highest discharge rates are contact springs. These contact springs occur near the boundaries with the overlying marbles, which host the highest quantities of water. More specifically, the alluvial formations are characterized by a low permeability (porous media), due to their lithological structure, which consists by products of weathering gneiss-schist. The carbonate formations (marble - limestone) are characterized by high values of hydraulic conductivity (karstic media). Gneiss and schist are characterized by middle values of hydraulic conductivity (discontinuous media).

From hydrochemical point of view springs' water shows good quality with low electrical conductivity values, which confirms the limited path of groundwater through the fracrtured geological formation. Water, is percolating into deeper depths, moves by gravity to lower levels of reference, and sea level is the major (Yannatos 2002).

6 Calibration of criteria in GIS environment

The geoenvironmental criteria and their calibration are shown in Table 2.

Table 2: Calibration of Criteria.

Criteria	Calibration			
	3	2	1	0
Distance from Water Points		> 500 m	< 500 m	
Distance from Hydrographic Network		> 300 m	< 300 m	
Morphological Slope (degrees)	< 5	5 - 10	10 - 20	> 20
Soil's Imperviousness	Low	Low to Middle	Middle to High	High
Density Interconnection		Low	High	
Protected Areas		No	Yes	
Distance form road network		> 300 m	< 300 m	

The selection's criteria for the localization of sanitary landfill construction used in the present application are the following:

Criterion 1: Distance from Water Points (springs, wells, boreholes). Landfill site must not be adjacent to any groundwater source, such as springs or groundwater wells. According to European Union Law three zones of perimeter protection for each water supply were determined, where the third one is the most suitable due to the fact that this zone is referred to the time of 50 – 60 days (time of most pathogenic micro-organism's life). Although there are not sufficient data for the above protection zone, international practice states that a minimum distance of 500 m from any water source is required for a landfill site (Chalkias and Stournaras 1997). Figure 2a shows the calibration of this criterion where four buffer zones were created with values ranging from 0 to 3 respectively.

Criterion 2: Distance from Hydrographic Network. According to Greek legislation the proper sites are considered those been at least at a distance of 300 m from the hydrographic network (Fig. 2b).

Criterion 3: Morphological Slope. Land morphology was evaluated by the slope gradation, which was expressed in degrees. The grading was based on the premise that the flatter area is, the greater its suitability for landfill construction. Areas with values of slope over 20° were assigned a grade of 0, areas with values of slope between 10° and 20° were assigned a grade of 1. The most suitable areas were considered to be the inclined planes (5° - 10°) with a grading value of 2 and finally the flat areas (< 5°) with a grading value of 3. The spatial representation of land morphology is shown in Figure 2c.

Criterion 4: Soil's Imperviousness: In order to avoid the eventual pollution of the ground water table by the leakages of the waste disposal, the possible areas should be consisted by impermeable soil formations. This is also demanded from the Greek Legislation (FEK 63/14-020-1964, art 5, par. 1.2) (Fig. 2d).

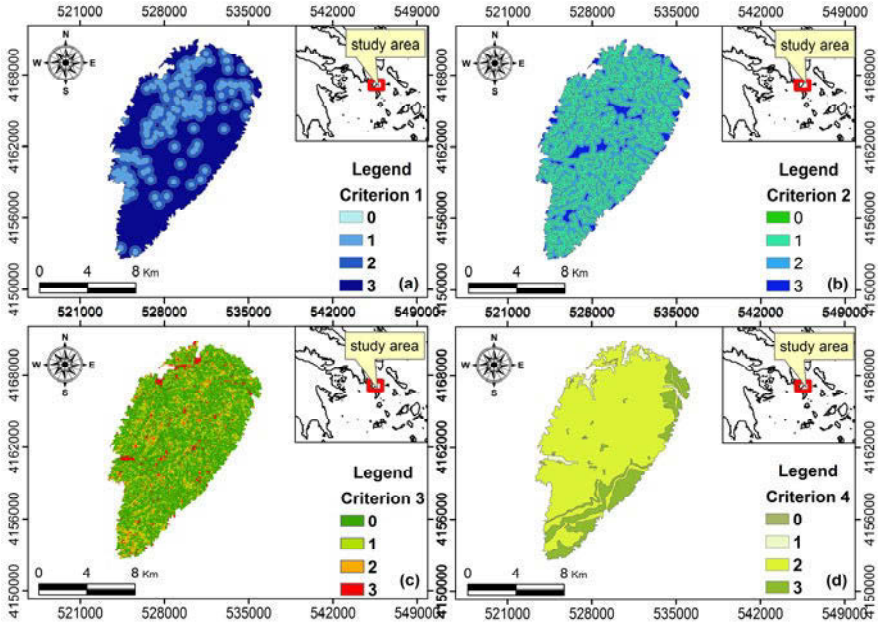

Fig. 2: a. Distance from Water Points, **b**. Distance from Hydrographic Network, **c.** Morphological Slope, **d**. Soil's Imperviousness (according to calibration values of Table 2).

Criterion 5: Density Interconnection (fracture density, degree of fracture intersection). It refers to the deviation of unsaturated zone in which the given problem is dealing with both superficial and ground aquatic systems. Nevertheless, between these categories, some differences occur, concerning the pollution conditions, the mechanisms of the pollutants transport and the mechanisms of the pollutants confrontation. The higher the density interconnection the higher is the possibility of selecting sites that will maximize hazards to the public health as well as to the environment by the leakages of the waste disposal (Fig. 3 a, b).

Criterion 6: Protected Areas (Natura areas, archeological sites). Likewise, the sites are considered those not been both into protected areas, such as Natura and into places with special interest such as archeological sites. Additionally, possible sites are considered those not been visible from cities and villages (minimum distance 500m) (Fig. 3c).

Criterion 7: Distance from road network. The sites should be at a same distance from hydrographic network, which is 300m (Fig. 3d).

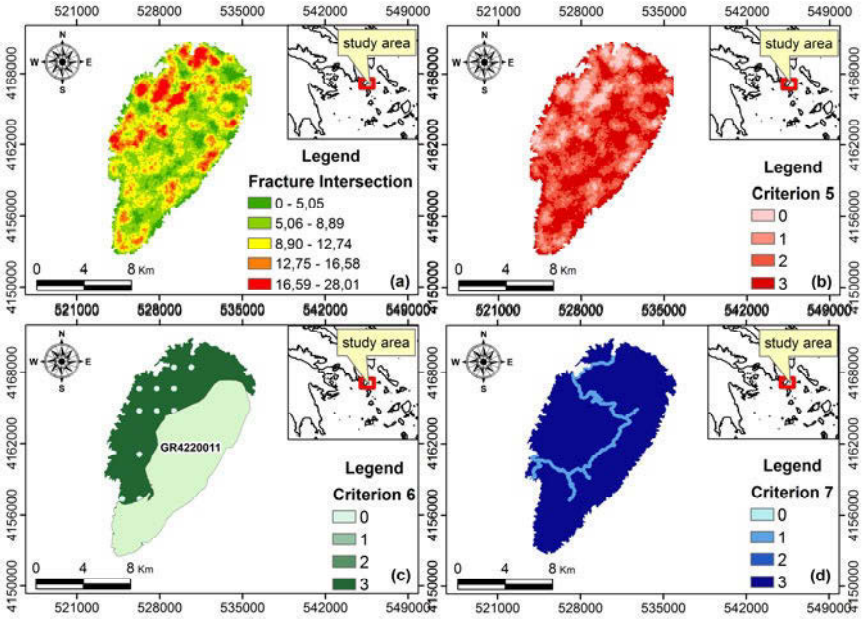

Fig. 3. a. Fracture intersection map, **b.** Density Interconnection, **c.** Protected Areas, **d.** Distance from road network.

7 Results - Discussion

The preparation of the final map was the result of the combination among the thematic maps with respect to Analytical Hierarchy Process (Saaty 1977). The AHP parameters are shown in Table 3, indicating the priority vectors of all criteria.

From the combination of the above thematic maps, using the tool Spatial Analyst of ArcGIS, revealed the final map identifying areas of potential Landfill site, on a scale grading from low to high values respectively.

The land suitability of Kea Island for landfill sitting, as calculated by the suitability index, is shown in Figure 4. In order to calculate the suitability index, the evaluation criteria shown in Figures 2, 3 were used with their respective weight value. According to AHP analysis criterion 5 takes the highest weighted value. The role of groundwater due to its importance in selecting sites for landfill construction leads to the conclusion that areas characterized by hard rocks terrains should be taken under serious consideration. The method of simple additive weighting was selected as the proper way to dissolve the multiple criteria problem of the landfill sitting. As shown in Figure 4, land suitability increases as the suitability index increases. The evaluation criteria were developed according to Greek and EU legislation. However, the GIS-aided sitting methodology presented is flexible as far as the criteria determination is concerned. Thus, it is quite easy to

expand the methodology by taking into account even more parameters, such as wind orientation, sensitive ecosystems and required surface.

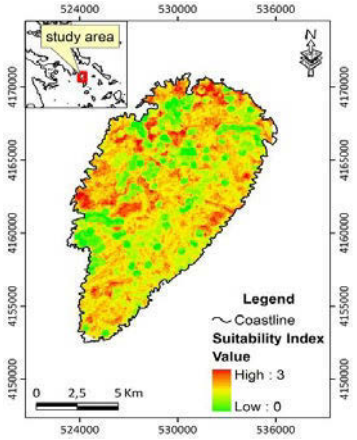

Fig. 4: Final Map of combined criteria for sitting sanitary landfill construction

Table 3. Application of AHP analysis including relative importance weights of the evaluation criteria.

Criteria	1	2	3	4	5	6	7	priority
1	1	3/2	2	5/2	3/4	1	1	0.178
2	2/3	1	3/2	2	2/3	1	1	0.141
3	1/2	2/3	1	1/2	1/3	2	3/2	0.104
4	2/5	1/2	2	1	1/2	3	2	0.147
5	4/3	3/2	3	2	1	2	3	0.236
6	1	1	1/2	1/3	1/2	1	1	0.097
7	1	1	2/3	1/2	1/3	1	1	0.098

Consistency Ratio (CR)=0.0659<0.1

References

Chalkias Ch, Stournaras G (1997) G.I.S. application for the selection of sanitary waste disposal landfills and quarries sites in major Sparti area, Greece

Dörhöfer G, Siebert H (1997) The search for landfill sites - requirements and implementation in Lower Saxony, Germany. Environ. Geol. 35, 55 - 65

Kontos T, Komilis D, Chalvadakis C (2005) Siting MSW landfills with a spatial multiple criteria analysis methodology. Waste Management 25, 818 - 832

Lepsius R (1983) Geologie von Attika. Berlin

Saaty TL (1977) A scaling method for priorities in hierarchical structures, Journal of Mathematical Psychology 15, 231 - 281

Samara T, Sargologou L (2010) Research of construction sanitary landfill in Kea Island using GIS applications, Dissertation, University of Athens (in Greek)

Stournaras G, Eleftheriou M (2000) Domestic Waste Management in Hellas. Report of Int. Assoc. of Engineering Geology, Committee No 14 “Waste Disposal”, Hannover

Yannatos G (2002) Ground Water flow controlled by the discontinuities in fissured rocks - Two cases histories In: Stournaras G. (eds.) Proc. of the 1st Workshop on Fissured Rocks Hydrogeology pp. 147-156. Tinos Island, Hellas

Adumbration of Amvrakia's spring water pathways, based on detailed geophysical data (Kastraki - Meteora)

J.D. Alexopoulos, S. Dilalos, E. Vassilakis

Faculty of Geology and Geoenvironment, National and Kapodistrian University of Athens, Panepistimiopolis, GR 157 84, Greece. jalexopoulos@geol.uoa.gr

Abstract The Amvrakia spring is located at the bottom of Meteora pillars and more specifically near the village of Kastraki (Kalambaka municipality). It is a seasonal spring since it functions only during the wet period. The Meteora conglomerates which dominate the area are characterized by large discontinuities creating a network of groundwater pathways above the impermeable strata of the underlying marls. The research targets was to define these water pathways in order to understand the mechanism of Amvrakia spring, by mapping the exposed discontinuity network and define their underground extension with the contribution of geophysical techniques. Electrical Resistivity Tomography (ERT) and Very Low Frequency (VLF) methodologies were applied. The VLF method is indicated for the detection of water-bearing fracture zones, but before the application of their filters they had to be processed for topographic corrections, as the area had not smooth relief. Five (5) VLF profiles were conducted with different directions around the spring's area, in order to detect possible conductive zones in the conglomerates surrounding the study area. Moreover, two (2) ERT sections of a total length of 140m were carried out, parallel to existent VLF sections, for cross-checking the geophysical information. Both techniques revealed important conductive zones (<200 Ohm.m) from the south-eastern Meteora conglomerate pillars, possibly interpreted as discontinuities filled with water feeding the spring.

1 Introduction

The Amvrakia spring is located at the Meteora pillars area and more specifically SE of the Kastraki village. The local cultural association was planning to take advantage of the spring and use the water by drilling it. Due to the fact that during the summer the spring suspends its function, they wanted to define its water capacity and mechanism. The study area is surrounded by vertical bluffs consisted of the Meteora conglomerates (Fig. 1) and several difficulties had to be overcome for applying geophysical techniques. The dense vegetation, the increased arduous ac-

N. Lambrakis et al. (Eds.), *Advances in the Research of Aquatic Environment, Vol. 2*
DOI 10.1007/978-3-642-24076-8, © Springer-Verlag Berlin Heidelberg 2011

cessibility and the relatively intense relief were the most significant problems that needed to be solved at the fieldwork. Taking into account that the spring's supplying mechanism would be probably through the discontinuities of the conglomerates, we had to define the orientation of these water pathways and the geophysical investigation had to be focused on the detection of conductive zones. Geoelectrical and VLF electromagnetic methods are the most indicative geophysical techniques for such environments (Sharma and Baranwal 2005; Papadopoulos et al. 2008, 2010).

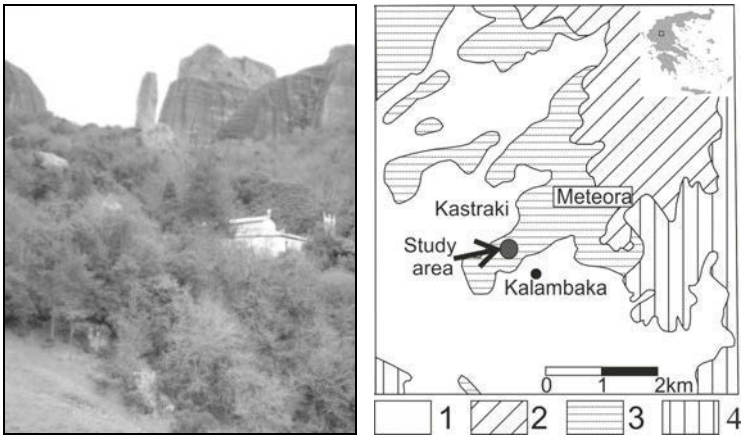

Fig. 1. Schematic geological map of the study area (modified by J.Ferriere et al 2004). 1: Quaternary and recent deposits, 2: Upper Conglomerates (Tsotyli formation), 3: Lower Meteora conglomerates (Pentalofos formation), 4: Oligocene conglomerates, sandstones and marls (Eptachorion formation).

2 Geological and hydrogeological setting

Meteora bluffs belong to the southern part of the Meso-Hellenic molassic basin, of Oligo-Miocene age, consisting mainly of the Meteora conglomerates (Ori and Roveri 1987). The same authors mention that the Meso-Hellenic basin is consisted of Gilbert-type delta deposits and deep channel fills, describing in detail the geometry of the sedimentary bodies of Meteora conglomerate, built by transferred pebbles probably due to the erosion of the Pentalofos unit (Brunn 1956; Ferriere et al. 2004).

More thoroughly, in the area of Meteora bluffs, three of the five units of the Meso-Hellenic molassic basin can be identified (Brunn 1956, Ferriere et al. 2004), while the stratigraphy of the study area is comprised of 3 different formations.

- The deepest formation is part of the transgressive succession of Eptachorion unit consisting of impermeable grey-blue marls of Upper Oligocene age (600 m. thickness).
- Above these marls, massive conglomerate (700 m. thickness) appears normally overlying (Brunn 1956, Papanikolaou et al. 1988), consisting of pebbles up to 20cm in diameter and originated from ophiolithes, marbles, limestones and metamorphic rocks in a sandy matrix. These massive crossed layered conglomerates have been deposited during Aquitaine (Brunn 1956) and are considered to be the southern extension of Pentalofos unit (which can be found north of the study area). It is the material that the impressive pillars are comprised of and, is known as the Meteora conglomerate strata dipping gently westwards (Ori and Roveri 1987). The uppermost part of the formation consists of well-bedded sandstones (Ori and Roveri 1987).
- The upper formation of the area consists of disorganized conglomerates (100 m. thickness) and covers through an angular unconformity the Meteora conglomerate. It is quite often found at the tops of the pillars and seems to be part of Tsotyli unit with Burdigalian age, known as the Upper Conglomerate of Meteora area (Ori and Roveri 1987).

The observed discontinuities (Brunn 1956; Savoyat et al. 1972; Ferriere et al. 2004, this study) in the area have been created after several episodes of the paleogeographic Meso-Hellenic molassic basin evolution, during Upper Eocene-Lower Miocene and their hydrogeological significance is that they usually allow the water flow. The general trending orientation of these almost vertical and open discontinuities is between N040E and N080E. The underlying marls of Eptachorion unit restrict the water flow within the discontinuities of the overlying conglomerates because of their impermeable character.

3 Electromagnetic Survey (VLF)

VLF measurements are proved to be ideal for detecting possible vertical to subvertical conductive zones or karstic structures for hydrogeological investigations (Monteiro Santos 2006; Papadopoulos et al. 2008; Sharma and Baranwal 2005; Dilalos 2009). Based on that and taking into account the tectonic analysis and orientation of the exposed fractures, five (5) profiles were conducted (Fig. 2) with several directions around the spring's area, in order to detect the conductive zones in the conglomerates surrounding the study area. The spacing of the measurement stations was 2 meters, as a more detailed investigation needed to be carried out.

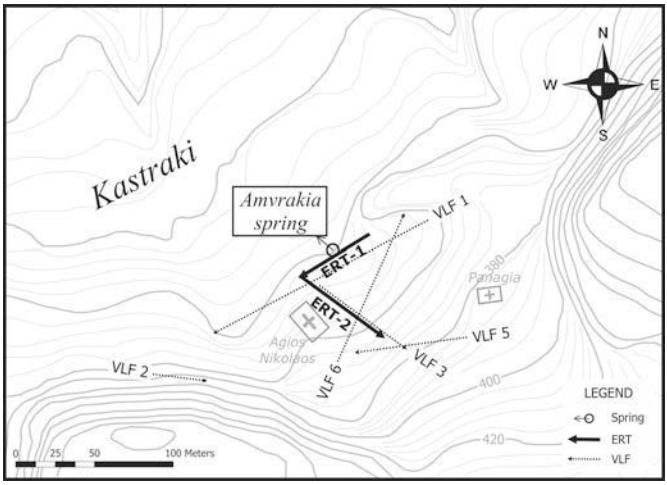

Fig. 2. Topographic sketch map with the ERT and the VLF geophysical sections.

A main VLF source frequency of 23.4 KHz was used, due to the good signal and alignment, towards the direction of the expected anomalies (westwards inclination). The processing of the VLF profiles included smoothing of the raw data and topographic corrections, according to Baker and Myers (1980) and Eberle (1981).

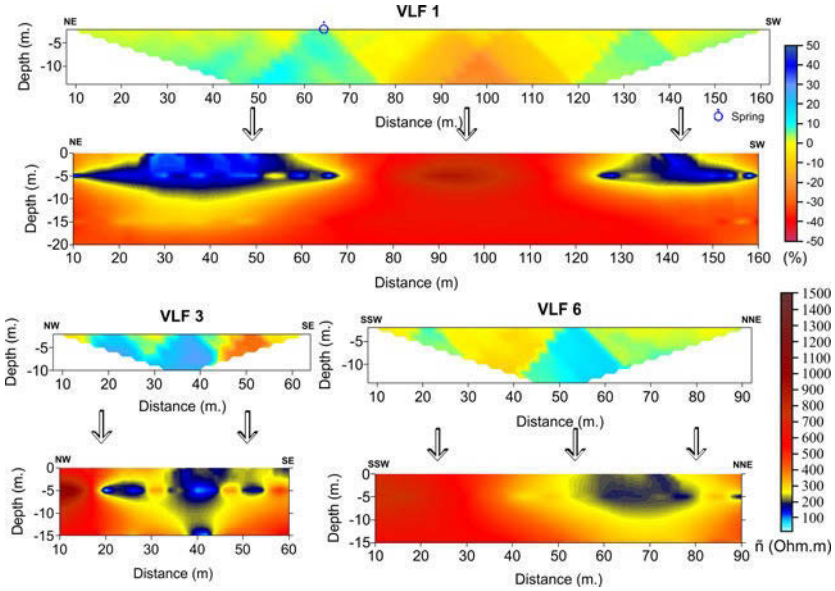

Fig. 3. VLF processing results. The Karous-Hjelt pseudo-sections of profiles VLF 1, VLF 3 and VLF 6 are illustrated. The respective resistivity section derived from inversion with Inv2DVLF software is also included (Initial resistivity 500 Ohm.m with 20 iterations. $RMS_{VLF\ 1}$ =1.16%, $RMS_{VLF\ 3}$=1.82%, $RMS_{VLF\ 6}$=0.95%). Frequency: 23.4 KHz.

Afterwards, we applied the Fraser (1969) and Karous-Hjelt (1979, 1983) filters, which both spotlight the anomalies. Karous-Hjelt filter is providing information of relative current's density distribution with depth, producing the pseudo-sections of Figure 3 (semi-quantity interpretation). In VLF 1 pseudo-section, a main conductive zone is located between 30-75m, after the starting point, probably due to the spring (located at 65m) and a smaller one at 125-140m. VLF 3 pseudo-section indicates a conductive zone at 25-55m, while VLF 6 pseudo-section indicates a main conductive zone between 40-70m and a smaller one at 15-30m.

Additionally, the VLF measurements were processed with *Inv2DVLF* inversion software presented by Monteiro Santos (2006, 2007). The software is basically an algorithm inverting regularized VLF data with the method of smoothed least-squares, based on the scalar tipper originated from the relation of vertical and horizontal component of the magnetic field. The result of this procedure is the subsurface distribution of the resistivity and has been proved to give reliable results similar with those of detailed geoelectrical measurements (Monteiro Santos 2006a and 2006b, Dilalos 2009). The resistivity profiles originating from this procedure, are illustrated in Figure 3 below each Karous-Hjelt pseudo-section, illustrating almost the same conductive (<200 Ohm.m) zones, highlighted due to the color scale. The initial resistivity chosen for the inversion (20 iterations according to the software's author) was 500 Ohm.m, based on the dominant resistivity of the conglomerates (Alexopoulos et al. 2005).

4 Electrical Resistivity Tomography

The ERT technique had been performed in order to validate the conductive zones, detected from VLF measurements in high detail. With this procedure, we investigated the lateral and vertical resistivity distribution.

In the study area, two (2) ERT sections with crossed directions were carried out (Fig. 2), with a total length of 140m. These were both parallel to previously performed VLF sections (VLF 1 and VLF 3), in order to combine results of both geophysical methods. A 41-electrode system providing Wenner array (190 measurement points of apparent resistivity) with electrode spacing up to 2m was applied, along with topographic leveling measurements. The ERT measurements were processed with the *RES2DINV* software of *GeoTomo*. Except for the raw resistivity data, topographic measurements of each section were provided into the software due to the relatively intense relief of the study area. The inverse 2D model resistivity sections, derived from this interpretation are illustrated in Figure 4.

The processing results are quite impressive and detailed. In ERT-1, a conductive (<200 Ohm.m) curvy area has been revealed in the center of the section (15-35m), underneath the spring (overflow mechanism). Another conductive zone (smaller) seems to have been investigated at the distance of 45m. In ERT-2, two parallel conductive zones (<200 Ohm.m) have been investigated, with a clear tilt

to NW, towards the spring. These could be interpreted as water-bearing discontinuities of the conglomerates.

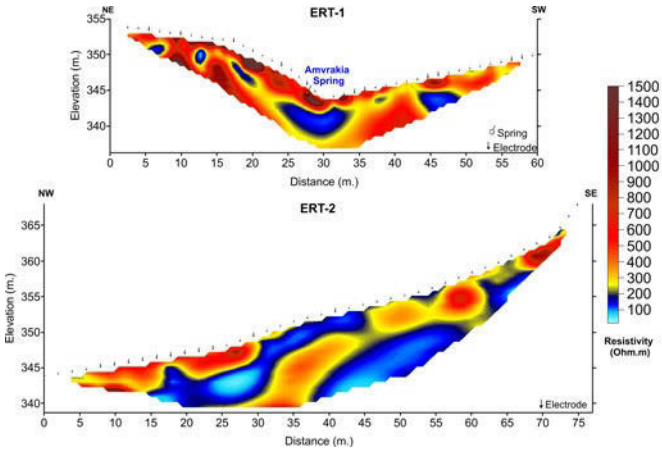

Fig. 4. Electrical Resistivity Tomographies, including topographic relief (ERT-1: 10th iteration, RMS: 2.38%, ERT-2: 11th iteration, RMS: 2.74%).

5 Discussion

Both the geophysical techniques applied in the study area, indicated conductive zones, which was the target of this study. In the two places where we had ERT and VLF sections together, we can also see that the detection of the conductive zones is identical, confirming the results.

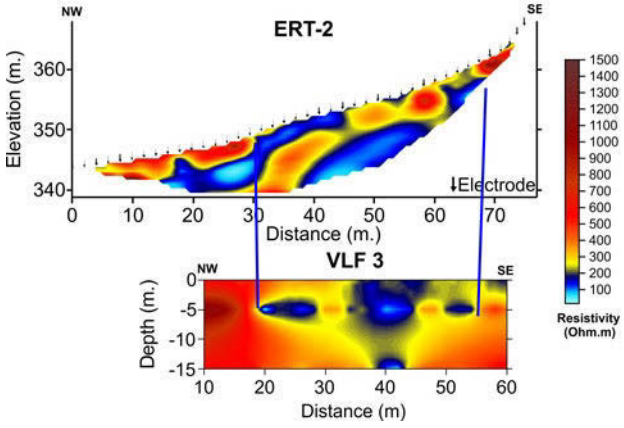

Fig. 5. Comparison of resistivity sections originated from the inversion of the ERT-2 data (up) and from the VLF-3 data inversion with Inv2DVLF (down).

Figure 5 illustrates the resistivity section originated from the inversion of the ERT-2 data (upper Fig. 4), compared with the resistivity section originated from the VLF-3 data inversion with *Inv2DVLF* (down Fig. 4). The ERT section, obviously illustrates the conductive zones in more detail than the VLF measurements.

6 Conclusions

Considering the geology of the area and that the massive conglomerates of the area are resistant (>500 Ohm.m) formations (Alexopoulos et al. 2005), we were able to identify these conductive zones as the most probable water-bearing discontinuities, trending towards the Amvrakia spring. ERT-2 indicates a tilt of these underground pathways to NW (better shown on ERT section), where the spring is located, while the section of ERT-1 indicates a local concavity, which is in agreement with the mechanism of an overflow spring.

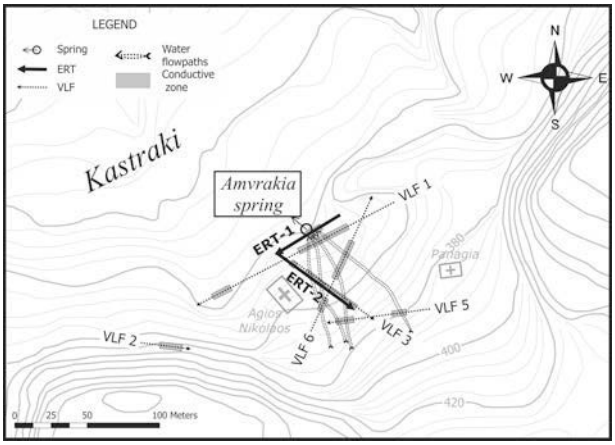

Fig. 6. The investigated conductive zones are being illustrated together with the feeding pathways of the Amvrakia spring.

In Figure 6, all the conductive zones are illustrated along with the delineated water pathways leading towards the spring, corresponding to the discontinuities of the south-eastern Meteora conglomerate pillars arising impressively above the survey area. We have to point out that the spring's water should not be potable, since these adumbrated water pathways run nearby the small cemetery of the neighboring abandoned Agios Nikolaos church.

Acknowledgments The authors would like to thank Prof. A. Kelepertzis for his advices and Mr. A. Chormovas, president of the Kastraki Cultural Association for his support and hospitality. Moreover, we would like to thank Professor Fernardo Monteiro Santos for the kind provision of the *Inv2DVLF* software.

References

Alexopoulos JD, Papadopoulos T, Mastroyannis A (2005) Investigation of hydrogeological factors affecting the potable water wells of Kalampaka urban by using geophysical techniques. Proc. of the 7th Hellenic hydrogeological conference, 19-30

Baker HA, Myers JO (1980) A topographic correction for the VLF-EM profiles based on model studies Geoexploration 18, 135-144

Brunn JH (1956) Etude geologique du Pinde septentrional de la Macedoine occidentale Ann. Geol. Pays. Hellen. 7, 1-358

Dilalos S (2009) Exploration of hydrogeological and environmental conditions with geophysical techniques, at selected sites in Chios island (Greece) M.Sc Thesis. National and Kapodistrian University of Athens, Faculty of Geology and Geoenvironment. Athens

Eberle D (1981) A method of reducing terrain relief effects from VLF-EM data Geoexploration 19, 103-114

Ferriere J, Reynaud J, Pavlopoulos A, Bonneau M, Migiros G, Chanier F, Proust J and Gradin S (2004) Bull. Soc. Geol. Fr. 175/4, 361-381

Fraser D.C. (1969) Contouring of VLF-EM data Geophysics 34/6, 958-967

Karous M (1979) Effect of relief in EM methods with very distant source Geoexploration 17, 33-42

Karous M, Hjelt SE (1983) Linear filtering of VLF dip-angle measurements Geophysical Prospecting 31, 782-794

Monteiro Santos FA (2006) Instructions for running PrepVLF and Inv2DVLF; 2-D inversion of VLF-EM single frequency programs Version 1.0. Lisboa

Monteiro Santos FA (2007) New features PrepVLF and Inv2DVLF, Version 1.1. Lisboa

Monteiro Santos FA, Almeida EP, Gomes M, Pina A (2006) Hydrogeological investigation in Santiago Island (Cabo Verde) using magnetotellurics and VLF methods Journal of African Earth Sciences 45, 421-430

Monteiro Santos FA, Mateus A, Figueiras J, Concalves MA (2006) Mapping groundwater contamination around a landfill facility using the VLF-EM method - A case study Journal of Applied Geophysics 60, 115-125

Ori GG, Roveri M (1987) Geometries of Gilbert-type deltas and large channels in the Meteora Conglomerate, Meso-Hellenic basin (Oligo-Miocene), central Greece. Sedimentology 34, 845-859

Papadopoulos TD, Alexopoulos JD, Dilalos S, Pippidis MJ (2008) Resistivity and VLF measurements for spring mechanism determination at NE Chios Isl. Proc. of the 8th International hydrogeological congress of Greece, 337-346

Papadopoulos TD, Stournaras G, Alexopoulos JD (2010) Geophysical investigations for aquifer detection in fissured rocks of volcanic origin. A case history. Journal of the Balkan Geophysical Society 13/2, 1-8

Papanikolaou DJ, Lekkas EL, Mariolakos ID, Mirkou RM (1988) Contribution to the geodynamic evolution of the Mesohellenic basin (in Greek) Bull. Geol. Soc. Greece 20, 17-36

Sharma SP, Baranwal VC (2005) Delineation of groundwater-bearing fracture zones in a hard rock area integrating very low frequency electromagnetic and resistivity data. Journal of Applied Geophysics 57, 155-166

Savoyat E, Lalechos N, Philippakis N, Bizon G (1972) Geological map of Greece, scale 1:50.000, Kalambaka Sheet. Inst Geol and Miner. Explor., Athens

Fracture pattern analysis of hardrock hydrogeological environment, Kea Island, Greece

V. Iliopoulos, S. Lozios, E. Vassilakis, G. Stournaras

[1] Faculty of Geology and Geoenvironment, National & Kapodistrian University of Athens, Department of Dynamic Tectonics and Applied Geology, Panepistimioupolis Zografou,15784 Athens - Greece, viliopoulos@geol.uoa.gr

Abstract The geological and hydrogeological regime of Kea Island is presented, focusing on the fracture pattern analysis of the crystalline-schist mass outcrops the island. The combined use of field mapping and geological data digital analysis extracting lineament density maps and fracture intersection density maps reveals a high relationship between the fracture pattern and the groundwater occurrence. In order to obtain a complete description of the fracture network, the study area is mapped at various scales with the aid of GIS and remote sensing techniques were integrated along with the data gathered from field work. Remarkable correlations between the hydrochemical data of the main springs (located along the SE and NW part of the island), and the results of lineament analysis and the hydrolithological regime of Kea Island, contribute to extract an integrated conception for the relation of the groundwater potential with the structure of fissured rocks.

1 Geology and Tectonic setting

Kea Island belongs to the Attic-Cycladic Belt which is characterized by a complicated deformational and metamorphic development from Late Cretaceous up to present times (Fig. 1). This tectono-metamorphic history involves a Late Cretaceous –Eocene high pressure/low temperature metamorphism followed by a Late Oligocene–Miocene greenschist to amphibolites facies overprint, coeval with the Aegean (post-) orogenic extension (Durr et al. 1978; McKenzie 1978; Altherr et al. 1982). The mid- to late Miocene magmatic activity in the Attic-Cycladic core complex is also closely related to the large-scale extension of the Aegean Arc during this period (Liati et al. 2009).

N. Lambrakis et al. (Eds.), *Advances in the Research of Aquatic Environment, Vol. 2*
DOI 10.1007/978-3-642-24076-8,

The island of Kea represents the northernmost island of the Western Cyclades island. According to Iglseder et al. (2008), two tectonostratigraphic units have been identified, separated by a low-angle normal fault-zone (shear zone): i) the lower unit, which occupies almost the whole island and corresponds to the foot-wall block and ii) the upper unit, in the form of sparse relics at the northern part of the island, which corresponds to the detachment itself.

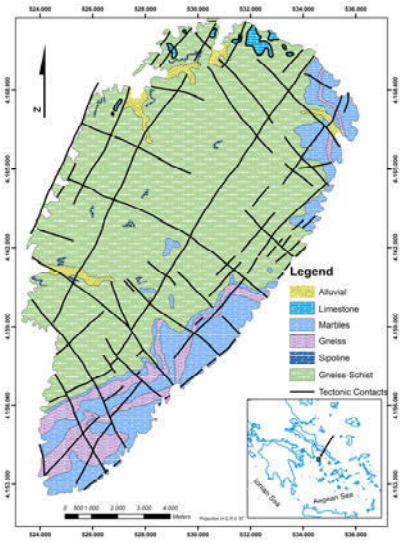

Fig. 1. Geological map of Kea Island (Davis 1982).

The footwall, which has a structural thickness of 380>m, predominantly comprises of chloritic schists with lithologically lensoid variations in quartz, carbonate, epidote, actinolite, biotite and talc. Near the detachment zone, talc is locally more common and is associated with small serpentine bodies, dolomite and magnetite-garnet glaucophane schists. All these lithological types are equivalent to the gneiss-schist formation of the previously published geological map (IGME, Davis 1982). Along the SE part of the island, the chloritic schists are interbedded with blue-grey calcite marbles and thin quartz layers Iglseder et al. (2008) and corresponds to the marbles with gneiss-schist intercalations. The upper unit is mainly represented by a 100 m thick zone of tectonic related rocks and is preserved in sparse small klippen up to approximately one square kilometer in size. Calcite ultramylonit and protoclastic dolomite (locally strongly ankeritised) near the fault zone are overlay by weakly deformed dolomite and limestone with occasional ultramylonitic calcitic shear zones (Muller 2009). This upper unit is equivalent with the Triassic-Jurassic carbonate formation. In general, from the hydrogeological point of view, the crystalline complex of Kea Island can be separated in two main groups: i) gneiss-schist group and ii) alternations of marbles and gneiss-schist.

The tectonic structure of Kea Island is dominated by an antiformally domed low-angle normal fault system within a high strain shear zone, cropping out across the whole island and formed during green-schist facies metamorphic conditions (Müller et al. 2007). Isoclinal refolded sheath-type folds and a strongly expressed NNE-SSW stretching lineation, represent the ductile deformation structures during these conditions, showing a top-to-SSW sense of shear. This event followed by at least two phases of brittle deformation, dominated by high-angle normal faults and a population of fractures and joints. Field observations show that the varying orientations of faults and other fractures and the cross-cut relations between different sets, indicate different generations and multiple reactivation periods. Some of them are open, some are bearing angular breccias of the host rock and some others are infilled by ore-rich fluids, quartz, calcite etc. The length, the number and the density of the fractures varies from place to place and in some cases highly fractured zones are cutting the crystalline mass, representing the cataclastic domain of a probable fault-rock zone. The detailed analysis of results of the brittle deformation and the related structures is very important for understanding the hydrogeologigal environment of Kea Island, comprising a work in progress.

2 Hydrogeological setting

The metamorphic rocks of Kea Island (mainly schists and gneisses with some intercalations of marbles at the SE part) are in general permeable due to the fragmentation that characterizes them. The groundwater flow seem to follow selective paths associated with the fragmentation and the intercalation of carbonate horizons. Furthermore the hydrolithological conditions for the carbonate rocks are characterized by high degree of karstification. The particularities of fissured rocks affect the vulnerability assessment and the risk mapping, as well their role in the framework of an ecohydrological consideration (Stournaras 2008). The alimentation of these formations depends only on the infiltration from the rain precipitation and the discharge is manifested by the springs. Although rocks like gneiss and schist typically are characterized of compact structure, the brittle deformation produce fractured, fissured and cataclastic formations that allow the groundwater flow and infiltration, along the discontinuities.

3 Hydrochemical setting

The groundwater generally flows in a limited depth in Keas' crystalline complex and this water comes out through springs (Fig. 2a). At northern Kea, the overdrilling during decades combined with the low precipitation led to the sea intrusion and the high salinity of the deeper aquifer of crystalline complex. According

Schoeller's diagram the spring water samples (Yannatos 2003) are characterized of high concentrations in Cl, HCO_3 and Ca (Fig. 2b).

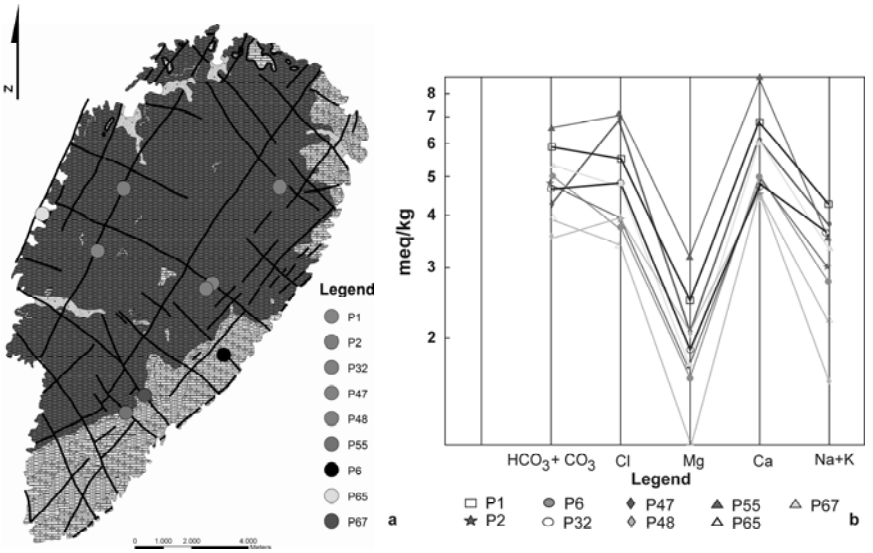

Fig. 2. a. Location of the main springs along the SE and SW part of the island. **b.** Schoeller diagram for the spring water analysis.

The groundwater hydrochemical analysis results are categorized according to the Chebotarev (1955) hydrochemical facies system. The estimated percentages of each parameter represented into the Chebotaref system for the determination of the each spring water type.

Table 1. The water types determined according to the Chebotaref system (1955).

Type of water	Clase of water	Springs	Na+K (%)	Ca (%)	Mg (%)	Cl (%)	SO_4 (%)	HCO_3+CO_3 (%)	TDS
Chloride-Bicarbonate	II	P1	27.55	14.38	3.15	20.6	4.43	45.16	945.39
Bicarbonate	I	P2	10.37	14.50	3.06	2.07	2.74	47.43	675.26
Bicarbonate-Chloride	II	P6	9.87	15.3	2.97	20.36	2.89	48.56	653.13
Bicarbonate-Chloride	II	P32	12.61	13.6	3.19	24.15	3.97	42.42	704.49
Chloride	V	P47	11.38	15.6	3.2	31.47	4.49	33.73	777.45
Bicarbonate-Chloride	II	P48	6.96	16.7	4.62	25.99	4.96	40.74	538.91
Chloride Sulfate	IV	P55	7.99	16.8	3.7	24.2	7.05	40.17	1032.49
Bicarbonate	I	P65	9.49	16.9	2.43	21.9	4.79	44.4	549.52
Bicarbonate-Chloride	II	P67	10.16	15.87	2.73	22.2	4.57	44.3	756.08

The springs P2 and P65 belong to I Clase of water (higher hydrochemical zone), which is characterized of HCO_3-CO_3 water, low TDS and high flow. Spring P65 displays high scores in Chloride, apparently due to its location near the coastal zone where the sea-intrusion is possible. Springs P6, P32, P48, P67 and P47 belong to II Clase of water (lower hydrochemical zone), which is characterized of low flow with Chloride character, as a result of the sea intrusion. Spring P55 belong to the intermediate hydrochemical zone which is characterized by the high degree of TDS, and moderate groundwater flow. Spring P55 belongs into the intermediate hydrochemical zone with high degree of SO_4 and HCO_3. It is positioned on marble intercalations nearby the coastal area. Spring P1 belongs to the intermediate hydrochemical zone with a high degree of TDS and HCO_3-CO_3 character.

4 Fracture Pattern extraction

Lineament orientation and lineament density distribution can play an important role in groundwater exploration or productivity analysis. One of the most convenient methods of understanding and analyzing the fracture pattern of a selected area is the interpretation of remote sensing data. Several techniques of data fusion with various spectral and spatial characteristics have been applied to Kea island aiming to the generation of different scale lineament maps.

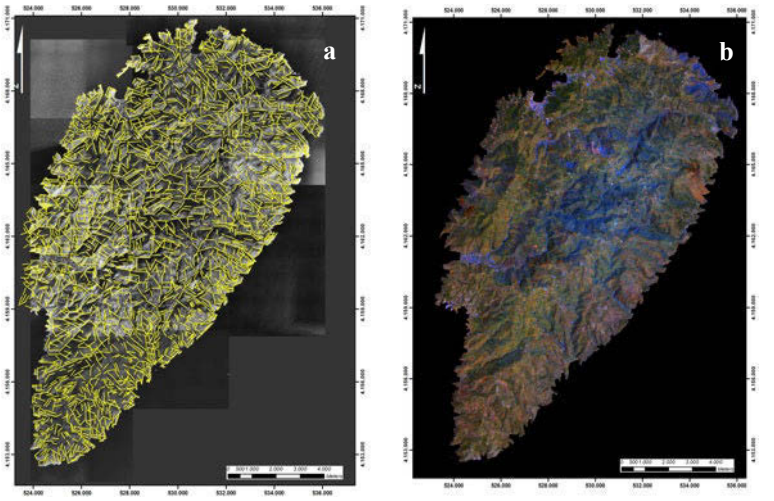

Fig. 3. a. Lineament map over the ortho-mosaic of aerial photos. **b**. An example of a pseudo-color (7,5,4/R,G,B), spatial enhanced (12) image of Kea Island, which was used -among others- for the lineament map generation.

A 25 meter resolution DEM (produced by the 20 m contours of 1:50,000 topographic maps) was used for the ortho-rectification of a Landsat-7 ETM+ scene (182/34, 30-6-2000) on a high resolution mosaic of panchromatic ortho-air-photographs, with the aid of Erdas Imagine 2010 software (Vassilakis 2006).
Several color composite high resolution images where interpreted, with different band combinations and a set of lineament maps has been generated, comprising a lineament distribution map, a lineament density map and a lineament cross-point intersection density map (Botsialas et al. 2005) (Fig. 3).

5 Orientation of fractures

The study of the fracture orientation is fundamental, for the study of ground water flow (Stournaras et. al. 2007). As it can be seen from the rose diagrams of Figure 4, a great number of orientations characterize the lineaments pattern, mainly reflecting the complex combination and interaction between the different scale tectonic structures. Four equivalent major orientations prevail in the hydrogeological group of marbles with intercalation of gneiss-schist (NNE-SSW, NE-SW, E-W and NW-SE), whereas in gneiss-schist group one major N-S trending set and three subsidiary NE-SW, E-W and NW-SE trending sets can be observed.

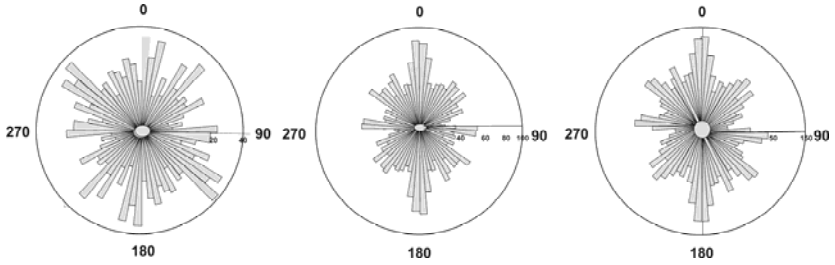

Fig. 4. Lineament rose diagrams for the two main hydrogeological groups (marble, gneiss-schist) and the whole island.

Since the most of the lineaments could be mainly correspond to conjugate sets of faults and fractures, we can correlate them with the dominant NE-SW dome like structure of the island and the NE-SW ductile structures (i.e. stretching lineation) that accompanied the main, green-schist facies, metamorphic event. The analysis of the whole island lineaments rose diagram show that the four major sets are oriented parallel, normal and in $\pm 45^0$, angle to the NE-SW dominant syn-metamorphic structure direction.

6 Dimension of fractures

Fractures dimensions such as aperture and apparent aperture, are very difficult to be defined in terms of spatial analysis. Additionally, the effect of depth on the aperture makes its measurement even more complicated. The groundwater flow is being affected in a high degree by the length of the lineaments (Fig. 5).

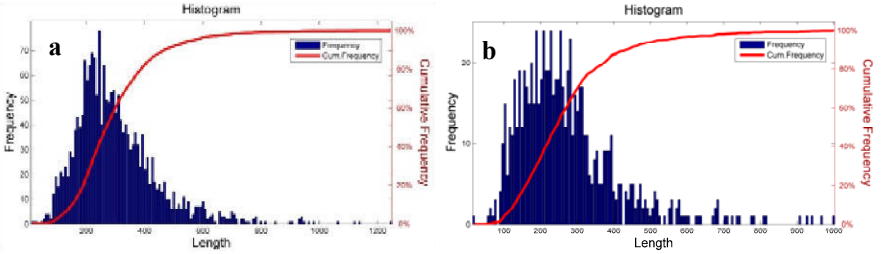

Fig. 5. Lineaments Length Size histograms, of gneiss-schist **(a),** and marble (**b**) dominated areas.

The length variations depend on the trends that exerted on the formations and moreover the magnitude of the erosion. The fracture map reveals lengths of surface traces between 15m and 1km at the marble dominated area. On the other hand the lineament length in gneiss-schist group varies between 9 m and 1.25 km.

7 Fracture Frequency and Fracture Intersection Density

Density maps represent the total number of lineaments per square kilometer area (Fig. 6a). The density varies from high to very high in the eastern side of the island, where marbles are cropping out. At the western side of the island, where gneiss-schist formation is the dominating lithology, the density varies from moderate to very high. Consequently the density map of lineament intersection points was derived, in which the frequency of intersection points per square kilometer, is illustrated (Fig. 6b).

Both, marbles and gneiss-schist mass, show a wide variety of the degree of interconnection. It is clear that the higher the density, the higher is the degree of interconnection. It is also easily observed, from the Fractures Interconnection Map, that there are two zones of high density, one in the eastern side of the island and another in the western, that represent the most internal areas of the detachment footwall with more systematic expression of the brittle tectonism.

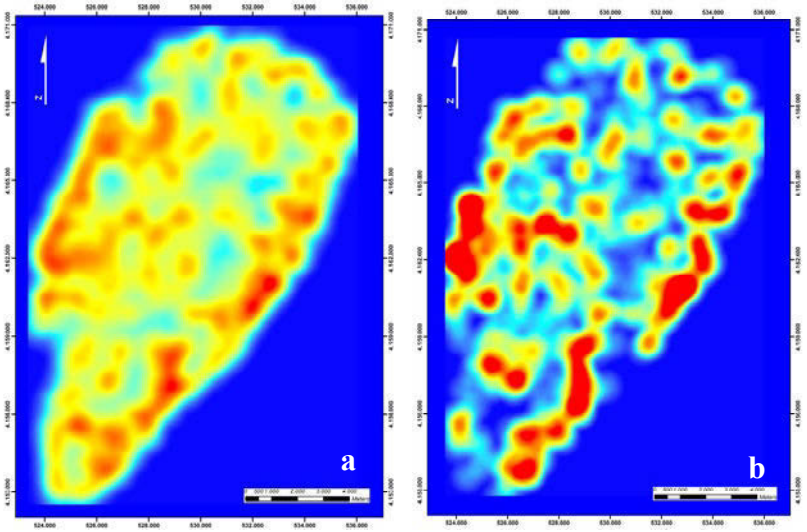

Fig. 6. a. Lineament Density Map. **b**. Fracture Intersection Density map.

Conclusions

The main lineament orientations, extracted from the pattern analysis of remote sensing data, coincide with five major sets in the marble dominated hydrogeological group (trending NNE-SSW, NE-SW, E-W and NW-SE). Besides a major N-S trending set and three minor, NE-SW, E-W and NW-SE trending sets characterize the gneiss-schist group.

The groundwater flow occurs in various levels into the crystalline complex of Kea Island. There is a very close relation between the origin of these levels and the tectono-stratigraphic and deformational structure of the island. This structure is characterized by the alternation of higher compact and low-fragmentation petrographic masses with highly fractured and cataclastic deformed zones. The deeper level of aquifer development is expected to be the sea level. The groundwater which flows at low depth into the crystalline-schist mass of the island characterized by a high quality and low conductivity HCO_3-CaMg water type. Most springs belong into the lower hydrochemical zone in which the flow is very low with high Bicarbonate-Chloride character. The groundwater is not only karstic because during the flow path it crosses gneiss-schist horizons and as a result of that these enrich the groundwater and degrade the water quality. The search is still being processed and the results of the satellite images lineament pattern analysis is correlated with the detail field work and the study of the brittle deformation of the island. This approach is necessary for understating and interpreting the relation between the hydrochemical and hydrolithological conditions and the way that the fracture pattern of fissured rocks affects the groundwater storage and flow.

References

Altherr R, Kreuzer RH, Wendt I, Lenz H, Wagner GA, Keller J, Harre W, Hohndorf A (1982) A Late Oligocene/Early Miocene high temperature belt in the Attic-Cycladic crystalline complex (SE Pelagonian, Greece). Geol. Jah. E23, 97-164

Botsialas K, Vassilakis E, Stournaras G (2005) Fracture pattern description and analysis of the hardrock hydrogeological environment, in a selected study area in Tinos Island, Hellas. Proc. of 7th Hell. Hydrogeol. Conf., Athens, 91-100

Chebotarev IJ (1955) Metamorphism of natural waters in the crust of weathering. Geoch. and Cosmoch. Acta, Vol. 88, 22-48

Davis E. N (1982) Geological Map of Greece, scale 1:50.000, Kea Island Sheet. Inst Geol and Miner. Explor., Athens

Durr S, Altherr R, Keller J, Okrusch, M, Seidel, E (1978) The median Aegean crystalline belt: stratigraphy, structure, metamorphism, magmatism. In: Cloos, H., Roeder, D. and Schmidt, K. (eds). Alps, Apennines, Hellenides, 455-477, Schweitzerbart, Stuttgart

Iglseder C, Grasemann B, Schneider DA, Lenauer I, Rice AHN, Nikolakopoulos KG, Tsombos PI, Müller M, Voit, K (2009) Characteristics of low-angle normal fault formation on Kea (Western Cyclades, Greece). Trabajos de Geologia, Univ. de Oviedo, 29, 372-374

Liati A, Skarpelis N, Pe-Piper G (2007) Late Miocene magmatic activity in the Attic-Cycladic Belt of the Aegean (Lavrion, SE Attica, Greece): implications for the geodynamic evolution and timing of ore deposition. Geol. Mag., Sept. 2009, 146, 5, 732-742

McKenzie D (1978) Active tectonics of the Alpine-Himalayan belt: the Aegean Sea and surrounding regions. Geophys. J. R. Astron. Soc., 55, 217-54

Müller M (2009) Structural Investigations/Observations along a Low-angle Normal Fault and their Implication for the Geology on Northwest Kea – Examining a Major Shear Zone. Diblomarteit, Universitat of Wien

Stournaras G (2008) Hydrogeology and vulnerability of limited extension fissured rocks islands. Ecohydrology & Hydrobiology Vol. 8, No 2-4, 391-399

Stournaras G, Alexiadou MCh, Leonidopoulou D (2003) Correlation of hydrogeological and tectonic characteristics of the hardrock aquifers in Tinos Island (Aegean Sea, Hellas). Intern. Conf. on Groundwater in Fract. Rocks, Prague, Abstracts, p. 103

Stournaras G, Migiros G, Stamatis G, Evelpidou N, Botsialas K, Antoniou B, Vassilakis E (2007) The fractured rocks in Hellas. In: Krasny J., Sharp J. (eds.), GROUNDWATER IN FRACTURED ROCKS, Volume 9, Taylor & Francis, p. 133-149

Vassilakis E., (2006) Study of the tectonic structure of Messara basin, central Crete, with the aid of remote sensing techniques and G.I.S., PhD thesis, pp.546, Athens, National and Kapodistrian University of Athens

Yannatos G. (2003) Groundwater flow controlled by the discontinuities in fissured rocks. Two case histories. (Preliminary Announcement), 1st Workshop on Fissured Rocks, Hydrogeology proceedings, Tinos Greece

Hydrochemistry

Geochemical and isotopic controls of carbon and sulphur in calcium-sulphate waters of the western Meso-Cenozoic Portuguese border (natural mineral waters of Curia and Monte Real)

M. Morais, C. Recio

Centre for Geophysics of the University of Coimbra, Coimbra, Portugal.

manuelmorais@engenheiros.pt

Abstract The groundwater chemistry and stable isotopic composition of aqueous C- and S-bearing species were determined for mineral waters from Monte Real and Curia Spas. The results support dedolomitization -dolomite dissolution occurs as the gypsum dissolves and calcite precipitates- as a principal geochemical process controlling Ca - SO_4 facies of these waters. Soil CO_2 of atmospheric origin and carbonate weathering are the primary sources of dissolved inorganic carbon (DIC). However, dissolution / precipitation of carbonates, through incongruent dissolution of dolomite, is the controlling factor for the evolution of the C isotopic composition of DIC, as shown by $\delta^{13}C$ values of -11.8‰ (Monte Real) and -9.4‰ (Curia). When present, the dissolved sulphide species ($\delta^{34}S_{H2S}$= -36.1‰ for Monte Real) appears to be derived from biogenic reduction of dissolved sulphate ($\delta^{34}S_{SO4}$ = +16.1‰ for Monte Real and +14.8‰ at Curia), itself derived from dissolution of Hettangian evaporites gypsum ($\delta^{34}S_{Gy}$ = +14.4‰).

1 Introduction

Monte Real and Curia Spas are located in Central West Portugal (Fig. 1), benefiting from a Mediterranean climate with Atlantic influence. Those Spas use mineral waters that emerge at a temperature around 20°C, showing, therefore, a small thermal disequilibrium with the mean air temperature, which is 15°C for both locations. With a long balneotherapic tradition, they contribute to the preservation of the Spa culture, a heritage which is deeply rooted in the country.

N. Lambrakis et al. (Eds.), *Advances in the Research of Aquatic Environment, Vol. 2*
DOI 10.1007/978-3-642-24076-8,

The hydromineral circuits of the waters cropping out at Monte Real and Curia spas crosscut Mesozoic carbonate formations with associated Hettangian evaporitic rocks. The ubiquitous presence of carbonates (calcite and dolomite), sulphates (gypsum/anhydrite) and halides (halite) in both hydromineral systems point towards those minerals as responsible for the chemical composition of the waters studied. This paper deals with the geochemical interpretation of major elements and stable isotopes of carbon and sulphur for those mineral waters.

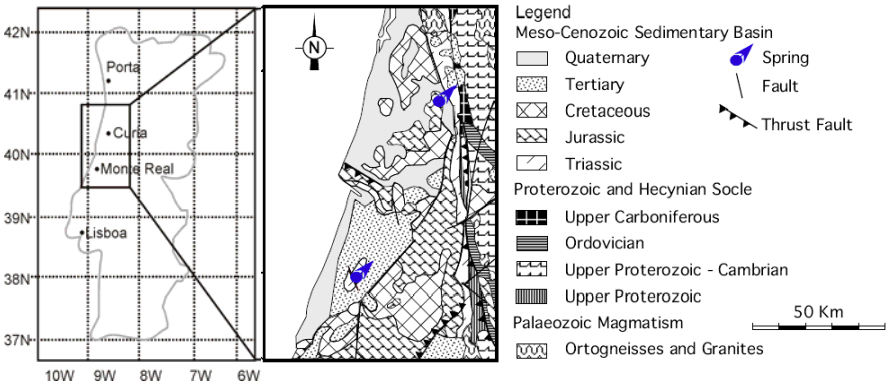

Fig. 1. Geographical location and generalized geological setting for the mineral springs Monte Real and Curia. Adapted from Carta Geológica de Portugal, 1/500000 (IGM 1992).

2 Geological and hydrogeological setting

The springs occur in the Western Meso-Cenozoic Portuguese border and emerge from Lower Jurassic formations (Teixeira and Gonçalves 1980; Neiva 1982; IGM 1992) in a hydrogeological context particularly influenced by Hettangian evaporites (Fig. 1).

Sediments of the Western Sedimentary Border lie on top of the ante-Mesozoic Massif. The "Grés de Silves", an Upper Triassic detrital complex largely formed by sandstones and conglomerates, is overlain by the "Margas da Dagorda", a unit of Hettangian age with clays, marls, masses of halite, and gypsum/anhydrite with lime-dolomite intercalations. These occurrences crop out in a more or less continuous band with North-South orientation. To the West, the Hettangian materials reappear in a patchy way in the middle of younger formations mostly associated with diapiric structures. Particularly in Monte Real, the migration of the evaporitic deposits to a diapiric anticline has reunited thick bodies of gypsum and halite, reaching great depths, as shown by the results of deep drilling for mineral exploration (Manuppella et al. 1978). The "Margas da Dagorda" is overlain by a Lower Jurassic carbonate unit made of dolomitic limestones, more or less argillaceous limestones, and marls.

At a local scale the natural emergences at Curia seem to be associated to fractures with a general NNE-SSW orientation which are visible in the outcrops of a karstified limestone. One of the wells exploring mineral water is 207 m deep and has intersected only Liassic formations e.g. limestone, dolomitic limestones, gypsum and marls (probably Sinemurian and Hettangian lithologies). The productive levels were some dolomitic formations found at 75 m depth (INAG 2001), providing the well ACP2 with a specific capacity of 28 L/s m. At Monte Real the mineral springs are also linked to a Lower Jurassic carbonate unit overlying the "Margas da Dagorda". Those springs are associated to the intersection of N-S to NNE-SSW faults limiting two diapiric structures (Neiva 1982). At the time of this study exploitation of the mineral aquifer was made by an 80 m deep artesian well.

3 Results and discussion

3.1 Facies and hydrochemical evolution

These waters belong to the calcium-sulphate hydrochemical facies, with sulphate and calcium contents representing more than 80% of the total mineralization. However, they present different anionic and cationic sequences:

- Monte Real: $rSO_4^{=} >> rCl^- > rHCO_3^-$ and $rCa^{2+} >> rNa^+ > rMg^{2+}$
- Curia: $rSO_4^{=} >> rHCO_3^- > rCl^-$ and $rCa^{2+} >> rMg^{2+} > rNa^+$

with r meaning concentration in meq/L.

The greater abundance of hipersaline evaporite minerals -particularly halite- in the diapiric region of Monte Real is directly reflected by the sodium and chloride contents of that water. This raises the solution's ionic strength, which in turn favours the continued dissolution of minerals as an effect of the decreasing ion activity coefficients, leading to a global increase of the salinity of the mineral water. The total dissolved solids (TDS) of Monte Real water (2.8 g/L) is about one and a half times that of Curia (1.9 gr/L) (Table 1).

Unity Na/Cl molal ratios for both waters reflects stoichiometric halite dissolution ($NaCl \rightarrow Na^+ + Cl^-$). Similarly, a Ca/SO_4 ratio of one would be expected if gypsum or anhydrite dissolution controlled calcium and sulphate (e.g. anhydrite: $CaSO_4 \rightarrow Ca^{2+} + SO_4^{2-}$). That is, indeed, the case for Curia ($Ca/SO_4 = 1.0$), but not for Monte Real waters, which have $Ca/SO_4 = 0.84$. This ratio, however, becomes very close to 1 when considering calcium plus magnesium relative to sulphate ($Ca+Mg/SO_4 = 0.93$). This could indicate that the magnesium added to solution by incongruent dissolution of dolomite tends to equal calcium removed by calcite precipitation (Sacks and Tihansky 1996; Sacks et al. 1995). This process could potentially be induced by the common-ion effect caused by dissolution of gypsum by calcite-saturated water.

Table 1. Chemical and isotopic data and saturation indices of Monte Real and Curia waters.

	Monte Real	Curia
Date	1996/09	1996/04
Sampling Point	Well	Well ACP2
Field Parameters		
Temperature, ^{o}C	19.0	20.6
Conductivity, µS cm^{-1}	2600	1975
pH	7.40	7.10
Eh, mV	-111	+230
Constituents, mg/L		
Na^{+}	97.0	21.2
K^{+}	3.6	2.0
Ca^{2+}	628	445
Mg^{2+}	48.9	52.0
Fe^{2+}	<0.03	0.22
Cl^{-}	160	29.5
HCO_3^{-}	124	238
SO_4^{2-}	1759	1100
HS^{-}	4.1	n.d.

	Monte Real	Curia
Date	1996/09	1996/04
Sampling Point	Well	Well ACP2
Calculated Parameters*		
Eh, mV	-218	n.c.
pCO2, log atm	-2.44	-1.81
DIC, mmol/L	2.08	4.48
Total dissolved solids, mg/L	2840	1897
Isotopes		
δ13C(DIC), ‰ vs PDB	-11.8	-9.4
δ34S(SO4), ‰ vs CDT	+16.1	+14.8
δ34S(H2S), ‰ vs CDT	-36.1	n.m.
Saturation Indices*		
Calcite	0.34	0.29
Dolomite	-0.19	-0.07
Gypsum	0.02	-0.22
Anhydrite	-0.22	-0.45

n.d: not detected; n.c: not calculated; n.m: not measured

*Computed with Wateq4F, version 2.63 (2004) (Ball and Nordstrom, 1991)

Plotting those waters on a modified Langelier-Ludwig diagram (Pastorelli et al. 1998) illustrates the hydrochemical characteristics, and the geochemical processes resulting from groundwater circulation through carbonate- evaporite rocks. In this graph (Fig. 2a) percentages of equivalent units for the main ionic solutes (*i.e.*, Ca^{2+}, Mg^{2+}, HCO_3^{-} and $SO_4^{=}$) are plotted in adjusted scale in a way that the coordinate values of three vertices fits the theoretical composition of calcite, dolomite and anhydrite.

The studied waters plot close to the anhydrite vertex, and near the anhydrite-dolomite tie-line, reflecting the determinant role of these minerals in the structural chemistry of the waters. On the other hand, water composition shifts away from the calcite vertex, which may be caused by calcite precipitation. This analysis is consistent with the geochemical indices presented and the saturation state of the waters with respect to the minerals considered, according to data in Table 1 and Figure 2b.

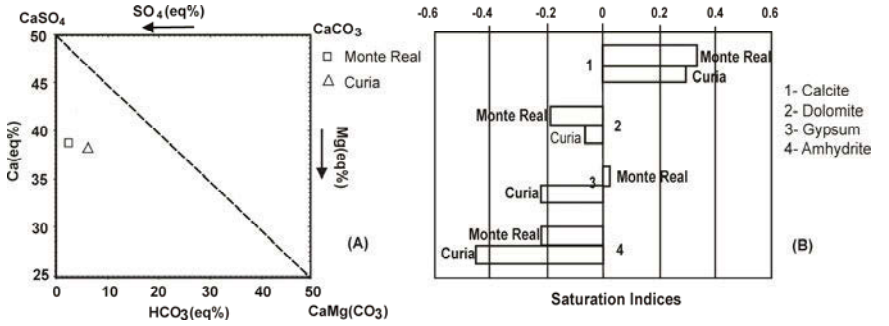

Fig. 2. a. Modified Langelier-Ludwig diagram for the studied waters **b.** Saturation states of the waters with respect to selected mineral phases.

Both waters are supersaturated with respect to calcite; in equilibrium (Curia) or slightly under-saturated (Monte Real) relative to the less soluble dolomite; in equilibrium (Monte Real) or under-saturated (Curia) in gypsum, and both of them are under-saturated in anhydrite. From thermodynamic and isotopic considerations it is reasonable to admit that dedolomitization is one of the major mechanisms controlling the chemical character and the isotopic evolution of C on those mineral waters (see next section). Dedolomitization is the process by which incongruent dolomite dissolution occurs as gypsum dissolves and calcite precipitates (Deines et al. 1974; Hanshaw and Back 1979; Appelo and Postma 1994; Sacks et al. 1995). The Ca^{2+} common-ion effect, induced by gypsum dissolution, can cause supersaturation of calcite, and consequently its removal from the solution. That will promote incongruent dissolution of dolomite, and as a result, an increase in calcium, magnesium and sulphate of the solution.

3.2 Stable carbon isotopic geochemistry of dissolved inorganic carbon

The dissolved inorganic carbon (DIC= $mH_2CO_3 + mHCO_3^- + mCO_3^{-2}$) exists almost entirely as HCO_3^-, as indicated by the near neutral pH values of the mineral waters. HCO_3^- is the second most abundant anion in Curia water, where it is more abundant than at Monte Real, indicating that more calcite has been dissolved. Identical magnesium contents for both waters imply sub-equal quantities of dolomite dissolved, if that mineral was the only source of magnesium in solution.

This interpretation is coherent with calculated P_{CO2} values (Table 1), that are higher at Curia ($10^{-1.8}$ atmospheres) than at Monte Real ($10^{-2.4}$ atm). Both values are within the range typical for soil P_{CO2} in recharge environments with vegetal cover ($10^{-1.5}$ - $10^{-2.5}$; Freeze and Cherry 1979; Appelo and Postma 1994). Therefore, carbonate dissolution has occurred in a system partially open to soil CO_2. However, a lower DIC and higher pH for the Monte Real water indicate faster in-

filtration to the saturated zone, isolating the water from the gaseous phase and/or encountering sulphate minerals in an initial stage of its hydrochemical evolution, thus very soon attaining calcite supersaturation and preventing the dissolution of the most soluble carbonates.

There is a strong difference in solubility among the carbonate minerals presumably in contact with water since its infiltration. Even admitting simultaneous calcite and dolomite dissolution, it is generally agreed that dissolution of magnesium carbonates (dolomite, but also magnesian calcite) only takes place significantly within the saturated zone, under closed-system conditions (Freeze and Cherry 1979; Appelo and Postma 1994; Clark and Fritz 1997). In those circumstances, if calcite equilibrium was attained, dolomite dissolution could only occur incongruently, as represented by the reaction (Clark and Fritz 1997):

$$Ca^{2+}+HCO_3^-+CaMg(CO_3)_2+H_2O \rightarrow Ca^{2+}+Mg^{2+}+2HCO_3^-+CaCO_3+OH^- \quad \text{(Eq. 1)}$$

The loss of carbon from solution, concomitant with calcite precipitation, removes some of the isotopically heavy carbon (enrichment factor $\varepsilon^{13}C_{CaCO3\,-\,HCO3}$ = +2.0‰ at 25ºC; Deines et al. 1974), causing a reduction in $\delta^{13}C_{DIC}$. However, that effect is largely compensated by addition of carbon enriched in ^{13}C from dissolution of dolomite ($\delta^{13}C_{Dol}$ frequently near 0‰), which in a global balance determines a ^{13}C enrichment of the initial DIC.

Models concerning the isotopic evolution of dissolved carbon in waters are widespread (as an example, Wigley et al. 1978; Clark and Fritz 1997). These use as premises the isotopic evolution of carbon in water at equilibrium with soil CO_2 ($\delta^{13}C_{CO2}$= -23 ‰ at our latitudes) and then dissolving marine carbonates ($\delta^{13}C \approx 0$ ‰) in open or closed system conditions for various P_{CO2} pressures. (see, for example, Clark and Fritz 1997; their Figure 5-6).

None of those models can explain de isotopic composition of dissolved carbon shown by the waters studied ($\delta^{13}C_{DIC}$= -11.8‰ for Monte Real and -9.4‰ for Curia) (Table 1). In a first approach, expected values for $\delta^{13}C_{DIC}$ (Clark and Fritz 1997) would be around -15‰ (at 25°C) to -14‰ (at the mean annual temperature of 15°C in the region). Therefore, measured values must result from additional reactions occurring in the saturated zone.

Incongruent dolomite dissolution is an important mechanism of carbon transfer between reservoirs, which results in a significant ^{13}C enrichment of DIC. Dedolomitization, and the associated carbon isotopic evolution, is discussed by Wigley et al. (1978). Carbon isotope data reported in this study are compatible with such a process, favouring the thesis of incongruent dissolution in the aquifer.

DIC species derive from soil CO_2 and from interaction of water with carbonates. However, an additional source, derived from biological sulphate reduction, contributed to Monte Real water.

According to the stoichiometry of sulphate reduction (Equation 3) and considering the total sulphide measured on the water, a HCO_3^- contribution of 0.248 mmol/L can be estimated, which would represent about 12% of the actual DIC of

Monte Real water. Given its organic carbon origin, this secondary addition of a carbonate species causes a decrease of the heavy stable carbon isotope and contributes to water saturation with respect to calcite. The role of this carbon source in the DIC isotopic evolution can be modelled using the following mass balance equation:

$$\delta^{13}C_{Final}.mDIC_{Final} = \delta^{13}C_{Initial}\, mDIC_{Initial} + \delta^{13}C_{Organic}.\ 2mHS^{-}) \qquad \text{(Eq. 2)}$$

For an approximate $\delta^{13}C_{Organic}$ value of -25‰, and knowing the final isotopic composition of carbon ($\delta^{13}C_{Final}$), the above equation can be resolved in order to determine de isotopic composition of DIC prior to sulphate reduction ($\delta^{13}C_{Initial}$). The calculated value of -10‰ indicates that the DIC could be enriched by about 2 ‰ in $\delta^{13}C$, had biogenic sulphate reduction not occurred.

3.3 Stable sulphur isotopic geochemistry of dissolved sulphate and sulphide

The reducing character of Monte Real water is manifested by the presence of reduced sulphur species (mainly HS^-, but also H_2S) co-existing with species of a higher oxidation state, such as sulphate.

Measured redox potential is -111 mV, while the value calculated by the redox couple sulphate/sulphide is -218 mV (Table 1). Measurement errors associated to analytical difficulties and/or absence of equilibrium between aqueous redox couples (Appelo and Postma 1994; Stumm and Morgan 1996) may lie behind the differences between calculated and measured values. Nevertheless, both values agree qualitatively, indicating reducing conditions at Monte Real water, in contrast with the oxidizing character of Curia water (field measured value of Eh= +230 mV, emphasizing the absence of reduced sulphur forms from its chemical composition).

Aqueous sulphate at Monte Real has $\delta^{34}S$ = +16.1‰ and that at Curia is +14.8‰ (Table 1). Those values are close to $\delta^{34}S$ = +14.4‰ measured on a sample of Hettangian gypsum, which in turn is within the range of admissible values for sulphates of that age (Triassic - Jurassic transition; Claypool et al. 1980; Clark and Fritz 1997). Gypsum dissolution is essentially a non-fractionating process (Everdingen et al. 1982; Clark and Fritz 1997; Hoefs 2004); therefore sulphate content of spring water is unequivocally derived from evaporite gypsum (or anhydrite), contributions of other sources being negligible.

In the absence of oxygen, some bacteria, such as *Desulphovibrio desulfuricans*, can metabolize organic matter using aqueous sulphate as electron acceptor, giving bicarbonate and sulphide as by-products (Freeze and Cherry 1979; Hoefs 2004):

$$2CH_2O + SO_4^{2-} \rightarrow 2HCO_3^- + H_2S \qquad \text{(Eq. 3)}$$

Since the light isotope forms weaker bonds, $^{32}SO_4^{2-}$ is preferentially used, resulting in isotopically light sulphide, and, by mass balance, a residual sulphate with higher $\delta^{34}S$. Kinetic fractionation factors of up to about 50‰ are known from laboratory experiments and field studies (Krouse 1980; Everdingen et al. 1982; Hoefs 2004).

$\delta^{34}S_{HS^-}$ measured at Monte Real was -36.1‰, resulting in an apparent fractionation between $SO_4^=$ and HS^- of 52.2‰. This value is similar to those frequently attributed to bacterial sulphate reduction.

From the actual contents of sulphate and sulphide of Monte Real waters, about 1% reduction of sulphate would suffice to account for the sulphide observed. Considering a closed system, and applying the isotopic mass balance equation:

$$\delta^{34}S_T = (\delta^{34}S_{SO4}{}^{=} mSO_4^{=} + \delta^{34}S_{HS} \text{-} mHS^-)/mSO_4^{=} + mHS^- \qquad \text{(Eq. 4)}$$

would result in $\delta^{34}S_T$ = 15.7‰ for total sulphate before reduction. This value is closer to that measured at Curia, where no reduction is evidenced, or to that of the outcrop gypsum sample.

4 Conclusions

The hydrothermal circuits of the waters cropping out at Monte Real and Curia spas crosscut Mesozoic carbonate formations with associated Hettangian evaporite rocks.

Molar ratios $Ca^{2+}/SO_4^=$, $(Ca^{2+} + Mg^{2+})/SO_4^=$, Na^+/Cl^- and thermodynamic equilibrium calculations show that dissolution of evaporitic rocks and interaction with carbonate formations controls the structural chemistry of those waters.

$\delta^{13}C$ evolution of the DIC is accounted for by the contributions of C in the soil gas phase together with that of carbonate minerals of marine origin, modified by subsurface precipitation of secondary calcite due to the incongruent dissolution of gypsum and dolomite.

Both waters present $\delta^{34}S$ values of dissolved sulphate which are comparable to those of Hettangian gypsum. The presence of reduced sulphur species (H_2S and HS^-) in Monte Real water records oxidation-reduction reactions.

References

Appelo CAJ, Postma D (1994) Geochemistry, Groundwater and Pollution, A.A.N. Balkema, Rotterdam

Ball JW, Nordstrom DK (1991) User's manual for WATEQ4F, with revised thermodynamic data base and test cases for calculating speciation of major, trace, and redox elements in natural waters. U.S.G.S. Open-File Report, 91-183

Clark ID, Fritz P (1997) Environmental Isotopes in Hydrogeology.Lewis Publishers, New York
Claypool GE, Holser WT, Kaplan IR, Sakai H, Zak I (1980) The age curves of sulphur and oxygen isotopes in marine sulphate and their mutual interpretation. Chemical Geology, 27, 199-260
Deines P, Langmuir D, Harmon RS (1974) Stable Carbon isotope ratios and the existence of a gas phase in the evolution of carbonate ground waters. Geochim. Cosmochim. Acta, 38, 1147-1164
Everdingen R O, Shakur A, Krouse H R (1982) Isotope geochemistry of dissolved, precipitated, airborne, and fallout sulphur species associated with springs near Paige Mountain, Norman Range. Can. J. Earth Sci., 19, 1395-1407
Freeze RA, Cherry JA (1979) Groundwater. Englewood Cliffs, New Jersey
Hanshaw BB, Back W (1979) Major geochemical processes in the evolution of carbonate aquifer systems. Journal of Hydrology, 43, 287- 312
Hoefs J (2004) Stable Isotope Geochemistry. Springer-Verlag, Berlin
IGM (1992) Carta Geológica Portugal: 1:500.000. Instituto Geológico Mineiro, Lisboa
INAG (2001) Plano de bacia hidrográfica do Rio Vouga, Anexo 4: Recursos hídricos subterrâneos, Lisboa
Krouse HR (1980) Sulphur isotopes in our environment. In: Fritz P, Fontes JCh. (Eds.), Handbook of Environmental Isotope Geochemistry, vol. 1, Elsevier, pp. 435-472 (Chapter 11)
Manuppella G, Zbyszewski G, Ferreira OV (1978) Notícia explicativa da Folha 23-A (Pombal) da Carta Geológica de Portugal, escala 1/50000. S. G. P., Lisboa
Neiva JMC (1982) Geologia e águas mineromedicinais de Portugal. Publ. Inst. Clim. Hidr. da Univ. Coimbra, 25, 65-76
Pastorelli S, Marini L, Hunziker JC (1998) Water chemistry and isotope composition of the Acquarossa thermal system, Ticino, Switzerland. Geothermics, 28, 75-93
Sacks LA, Tihansky AB (1996) Geochemical and Isotopic Composition of Ground Water, with Emphasis on Sources of Sulfate, in the Upper Floridan Aquifer and Intermediate Aquifer System in Southwest Florida. U.S. G. S. Water-Resources Investigations Report, 96-4146
Sacks LA, Herman JS, Kauffman SJ (1995) Controls on high sulphate concentrations in the Upper Floridan aquifer in southwest Florida. Water Resources Research, 31, 2541-2551
Stumm W, Morgan JJ (1996) Aquatic Chemistry: chemical equilibria and rates in natural waters. John Wiley, New York
Teixeira C, Gonçalves F (1980) Introdução à geologia de Portugal. INIC, Lisboa
Wigley TML, Plummer LN, Pearson FJJr (1978) Mass transfer and carbon isotope evolution in natural water systems. Geochimica Cosmochimica Acta, 42, 1117-1139

The impact on water quality of the high carbon dioxide contents of the groundwater in the area of Florina (N. Greece)

W. D'Alessandro[1], S. Bellomo[1], L. Brusca[1], S. Karakazanis[2], K. Kyriakopoulos[3], M. Liotta[1]

[1] Istituto Nazionale di Geofisica e Vulcanologia – Sezione di Palermo, Via U. La Malfa 153, 90146 Palermo, Italy, w.dalessandro@pa.ingv.it

[2] MSc Geologist, karasty@gmail.com

[3] National and Kapodistrian University of Athens, Dept. of Geology and Geoenvironment, Panepistimioupolis, 157 84 Ano Ilissia, Greece, ckiriako@geol.uoa.gr

Abstract Gas and water samples were collected at CO_2-rich wells in the plain of Florina (N. Greece). Chemical and isotopic composition of the analysed gases reveals their main crustal origin even if a small but significant contribution of mantle derived gases can be recognized. As a consequence of CO_2 dissolution, HCO_3^- is always the main dissolved anion while cationic composition allows us to distinguish at least two main groups characterized by Na or Ca as dominant dissolved cations. The water-rock interaction is strongly enhanced by the dissolution of CO_2 and the consequent lowering of pH. Such a process increases the mobility of some trace elements whose concentrations very often exceed UE drinking water limits. This study confirms that the Florina basin represents a good natural analogue of carbon storage systems and underscores the fact that possible deterioration of water quality due to CO_2 leaks of the reservoirs must be carefully taken in account.

1 Introduction

Carbon capture and storage (CCS) aims to reduce the climate impact of burning fossil fuels by capturing carbon dioxide (CO_2) from power station smokestacks and disposing of it underground. Geological reservoirs with sufficient capacity, such as depleted oil and gas reservoirs, deep saline aquifers and unminable coal beds are good candidates for storing captured CO_2 (Bachu 2000). In all cases, it is critical to ensure that the long-term integrity of the storage reservoir is not compromised. The understanding of gas migration mechanisms from depth to ground surface is fundamental to choose the best locations for CO_2 geological storage sites, to engineer them so that they do not leak, and to select the most appropriate monitoring strategy and tools to guarantee public safety. Natural analogues provide the best oppor-

N. Lambrakis et al. (Eds.), *Advances in the Research of Aquatic Environment, Vol. 2*
DOI 10.1007/978-3-642-24076-8, © Springer-Verlag Berlin Heidelberg 2011

tunity to study migration mechanisms, as they incorporate such issues as scale, long-time system evolution, and interacting variables that cannot be adequately addressed with laboratory studies or computer models (Beaubien et al. 2005).

The Florina basin, being the main commercial source of CO_2 in Greece, represents a good natural analogue for the study of the impact of carbon storage. Its importance is further increased by the fact that it belongs to a wider NNW-SSE oriented graben, which extends for about 150 km. This graben filled with a thick sedimentary succession represents with its lignite deposits the main autochthonous source of fossil combustible of Greece, with about 50% of national stationary CO_2 emissions coming from this area (Koukouzas et al. 2009). Due to the fact that during exercise of CCS systems one of the main costs derive from CO_2 transport, the Florina-Ptolemais-Servia basin, being the site of many CO_2 point source, has been recently considered in a preliminary nationwide assessment of geological storage opportunities (Koukouzas et al. 2009). The importance of the Florina basin is further highlighted by its inclusion in the European research project (NASCENT) on natural analogues (Pearce 2004).

This study presents new chemical and isotopic data on gas and water samples collected in the Florina area. Groundwater samples were collected throughout the Florina plain to give insight on the areal distribution of the analysed chemical and physico-chemical parameters. Particular attention was given to the impact of the high CO_2 concentrations on water quality.

2 Study area

The studied area is part of the Florina-Amynteon sedimentary basin. It is located in North-West Macedonia (Greece), between the coordinates 40º 42'-40º 54' latitude and 21º 20'-21º 35' longitude, and it belongs to Pelagonian geotectonic Zone (Pavlidis and Mountrakis 1987) (Fig. 1). The basement is characterized by the metamorphic rocks of Varnounta and Voras and Carbonate rocks at the eastern margins of the basin (Kilias 1980).

Metamorphic rocks deposited during the Upper Carboniferous period constitute two complexes, Voras and Vernon respectively (Pavlidis and Mountrakis 1987). The Voras complex is composed of orthogneiss with relative homogeneous mass of biotitic gneiss, granular banded muscovitic gneiss, and a layer that is composed of mica and amphibolitic schist and phyllites. The Vernon complex has been subdivided in Vitsi-Nemfeon, Kleisouras, Kastorias, Siderochoriou and Aposkepou zones with decreasing metamorphic grade. Volcanic activity characterised the area of Voras during Quaternary (Kolios et al. 1980).

The Florina basin has been filled up by Neogene and Quaternary sediments (Pavlidis and Mountrakis 1987). According to Karakatsanis et al. (2007) the basin fill is characterised by 41 sedimentary cycles with a total thickness up to 560 m. The lower part is the Base formation up to 297 m thick, whereas middle part, Vevi

formation is up to 127 m thick and the upper part that corresponds to Lophon formation is up to 124 m thick. The beginning of sedimentation in the basin, with alternated sand, clay and conglomeratic beds, with presence of xylite, at the lowermost part of Base formation, indicates a weak tectonic activity and low sedimentation rate. Tectonic activity increased and alluvial fans were formed in the rest part of Base formation. Depositional environment changed in the Vevi formation from terrestrial to lacustrine, where lacustrine and fluvio-lacustrine deposits were accumulated. Finally, the basin filled up with terrestrial deposits in the Lophon formation.

Tectonic activity of the area was characterized in Late Miocene by NE-SW extension (Pavlidis and Mountrakis 1987) whereas a subsequent Pleistocene episode of NW-SE extension resulted in the fragmentation of the initial basin into several sub-basins, i.e., the sub-basins of Florina, Ptolemais and Servia (Pavlidis and Mountrakis 1987; Steenbrink et al. 2006).

3 Sampling and analytical methods

In the period March 2007 – September 2010, 12 gas and 44 groundwater samples were collected. Almost all samples were collected from drilled wells. Some of them come from the wells that the company Air Liquide (AL) drilled in the main gas reservoir close to the village of Mesochori for CO_2 production. Three gas and water samples were collected from the gas-water separation device at the wellhead. The remaining samples were collected from wells drilled at variable depth (60-130 m) for irrigation and drinking purposes. At some of these sites bubbling gases were collected with an inverted funnel. All analyses were made at INGV-Pa.

Gases were collected in pyrex bottles with two stopcocks and analyzed by gas-chromatography. Helium isotopic ratio in gas samples was analyzed directly from the sampling bottles, after purification in the high-vacuum inlet line of the mass spectrometer. Helium isotope measurements were made with a VG 3000 mass spectrometer. $^3He/^4He$ ratios, determined against an air standard, are referred to the atmospheric ratio ($R_a = 1.386 \times 10^{-6}$) as R/R_a. Carbon isotope analyses were performed with a Finnigan MAT Delta S mass spectrometer, after purification of CO_2 under vacuum. $^{13}C/^{12}C$ ratios are reported as $\delta^{13}C$ units (±0.1 ‰) with respect to V-PDB standard. Analytical results are shown in Table 1.

Water samples were stored in HDPE bottles. An aliquot for metal analysis was filtered in the field (0.45 μm MF Millipore filters) and acidified with HNO_3. The temperature, pH and conductivity of waters were measured upon sampling and their alkalinity determined by titration with HCl 0.1N. Water chemistry was analysed in the laboratory by standard methods: major anions (F, Cl, Br, NO_3 and SO_4) and major cations (Na, K, Mg, Ca) by IC, minor and trace elements with ICP-OES and ICP-MS. Saturation indexes and theoretical PCO_2 were calculated from measured pH, T and chemical composition with the computer program

PHREEQC. Analytical results are shown in Table 2. Total dissolved solids (TDS) are calculated summing up all major anions and cations and dissolved silica.

4 Results and discussion

4.1 Gases

All gas samples display a CO_2-dominated composition with CO_2 concentrations (corrected for air contamination) of at least 90%. The rest is composed of O_2 (from < 100 ppm up to 6.7%), N_2 (from 600 ppm to 28.5%) and CH_4 (from 22 ppm to 1.3%), while He displays very low concentrations (0.3-66 ppm) and H_2 was detected only in the AL wells (29-60 ppm).

Table 1. Chemical and isotopic composition of the Florina gas samples.

sample	date	He	H_2	O_2	N_2	CH_4	CO_2	$\delta^{13}C$	R/Ra	He/Ne
		ppm	ppm	ppm	ppm	ppm	ppm	‰		
Air Liquide	3-03-2007	3.3	34	600	4000	524	989900	-1.6	0.61	2.7
Air Liquide	1-06-2008	1.7	60	130	3100	353	992400	-1.5	0.66	5.9
Air Liquide	28-04-2010	< 5	29	2500	5900	85	989900	-1.6	n.d.	n.d.
Itea	4-03-2007	31	< 5	1400	41100	576	949400	-0.3	0.28	41.2
Giatsovo	4-03-2007	22	< 5	24700	111800	4117	842800	0.3	0.27	9.8
Marina	4-03-2007	25	< 5	4600	35400	1657	949400	-0.3	0.24	31.1
Papagiannis	1-06-2008	< 5	< 5	67100	285000	106	636900	-1.7	n.d.	n.d.
Kampos	1-06-2008	0.4	< 5	130	600	22	993300	-1.7	0.46	3.1
Sarri	27-04-2010	0.6	< 5	4000	15800	44	970500	-2.3	0.55	1.3
Sarri	21-09-2010	0.3	< 5	143	729	38	997900	n.d.	0.82	3.4
Tropeouchos	28-04-2010	66	< 5	100	64800	12900	900000	-0.4	0.44	2.1
Tropeouchos	21-09-2010	65	< 5	100	59200	13400	921700	n.d.	0.32	11.7

Although He, N_2 (corrected for air contamination) and CH_4 concentrations span over nearly three orders of magnitude their relative ratios are relatively constant. On the contrary He/CO_2, N_2/CO_2 and CH_4/CO_2 ratios are highly variable. Such a pattern indicates that processes that enrich or deplete CO_2 in the gas mixtures mainly regulate the overall composition of the gases. Helium, N_2 and CH_4 have similar solubilities in water, which are much lower than that of CO_2. Due to the fact that during their travel to the surface these gases interact with many aquifers the differences in solubility between CO_2 and the other gases could be responsible for the compositional variability of the sampled gases.

CO_2-C isotopic composition ranges from –2.3 to 0.3 ‰ (vs. V-PDB), while He isotopic composition ranges from 0.24 to 0.82 R/R_a (Fig. 1). Both C and He isotopic composition point to a prevailing crustal origin of the gases with a small but significant mantle contribution (~10%). Such mantle contribution can be ascribed to the nearby Quaternary volcanic activity in Voras mountains.

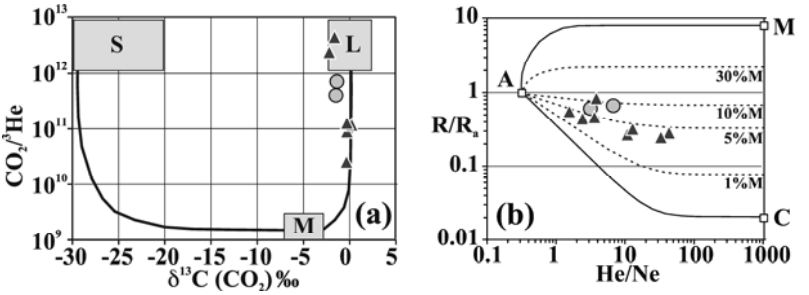

Fig. 1. a. $CO_2/^3He$ vs. $\delta^{13}C$ (CO_2) plot of the gas samples (circles = Air Liquide wells; triangles = other wells). The endmember compositions for sediments (S), MORB-like mantle (M) and limestones (L) are $\delta^{13}C$ (CO_2) = –30‰, –5‰ and 0‰; and $CO_2/^3He$ = 1×10^{13}, 2×10^9 and 1×10^{13}, respectively (Sano and Marty 1995) **b.** R/R_a vs. He/Ne plot of the gas samples. A, M and C represent three possible end-members: atmospheric air, crust and MORB-like mantle. Continuous lines show the mixing between A and the end-members C and M while dashed lines the mixing between A and different mixtures of C and M.

4.2 Groundwaters

The analysed groundwater samples can be subdivided in two groups, those collected from the Air Liquide wells, belonging to an about 300 m deep artesian aquifer, and those collected from the shallower (< 130 m) wells. The first group displays pH values in the range from 6.10 to 6.48 and moderate saline contents (TDS = 6.6 – 10.6 g/L) and has a uniform Na-HCO_3 composition. The other group has a wide range of pH values (5.20 – 7.40), lower saline contents (mostly < 1 g/L) and nearly all samples have a Ca-HCO_3 composition (Fig. 2).

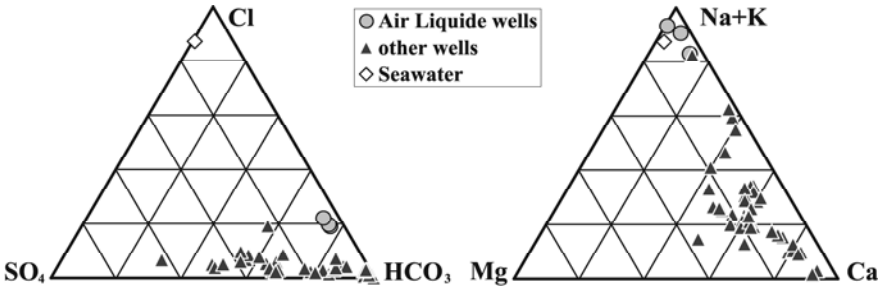

Fig. 2. Main anion and cation triangular plots of the Florina groundwater samples (in mg/L).

The importance of geogenic CO_2 dissolution in the aquifers of the plain of Florina is underscored by the, sometimes very high, calculated theoretical CO_2 partial pressures (Fig. 3a; range 0.013-1.92, median 0.48 atm), always exceeding those characteristic of the atmosphere (0.00038 atm) and soil gases (0.01-0.001 atm). Values calculated for the AL wells (pCO_2 1.0-2.2 atm) are not representative of the conditions at depth because waters were sampled after the water/gas separation device. Data from the Air Liquide Company indicate that the pressure within the reservoir is > 20 atm so that the pCO_2 could be close to this value.

The large quantity of CO_2 that dissolves in the Florina aquifers, further highlighted by the fact that HCO_3^- represents sometimes up to 75% of the TDS (Fig. 3b), lowers the pH of groundwater enhancing its aggressiveness with respect to the aquifer rocks. The consequent weathering processes are evidenced by the positive correlation between alkalinity and the major cations. Fig. 3c shows for example the correlation between Ca and HCO_3^-. Samples from AL wells deviate significantly from the shallow aquifer trend. This is due to the fact that the water, loosing CO_2 on the way up to the surface, becomes oversaturated in and precipitates carbonate minerals. Due to the fact that HCO_3^- is in excess with respect to Ca, the latter is scavenged by the precipitating solid phases. Scaling limits the productive lifetime of the CO_2 extraction wells to about one year. To continue CO_2 extraction new wells have to be drilled, therefore our samples have been collected from different wells.

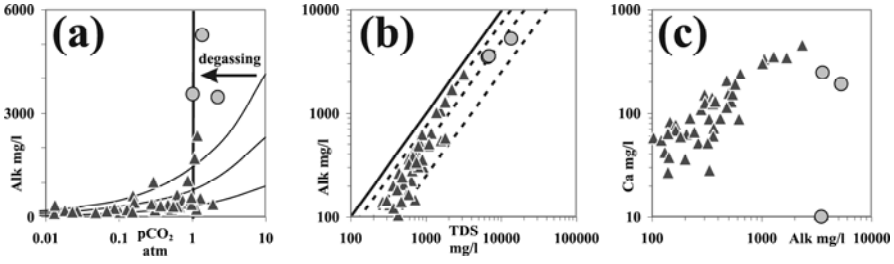

Fig. 3. a. Relationship between calculated pCO_2 and Alkalinity, curves represent equilibrium values at temperatures between 25 and 100 °C, **b.** Alkalinity-TDS binary plot, bold line represents the 1/1 ratio, while dashed lines are the 0.75, 0.5 and 0.25 TDS fractions, **c.** Alkalinity-Calcium binary plot.

4.3 Water quality issues

The weathering processes within the Florina aquifers, enhanced by the abundant dissolved CO_2, affect also the analysed trace elements some of which reach very high concentrations (e.g. Al up to 1.3 mg/L, B up to 4.5 mg/L, Fe up to 226 mg/L; Mn up to 4 mg/L). For many of these elements the very low pH values reached within the aquifer sharply increase their solubility.

The extremely high Fe values probably derive from the dissolution of amorphous and/or crystalline oxy-hydroxide phases that precipitated in the terrestrial sedimentary environment which make up most of the shallower aquifer rocks. The good positive correlation between Fe and HCO_3^- supports the CO_2 driven dissolution of the Fe-bearing phases (Fig. 4a). On the contrary oxidation and dissolution of Fe-sulphides, which are sometimes responsible of very high Fe concentrations, could be excluded by the inverse correlation between Fe and SO_4^{2-} (Fig. 4b). Possibly only the AL samples and a few other deriving from much deeper horizons, whose aquifer rocks were deposited in limnic (probably reducing) environment, could derive Fe and SO_4^{2-} from Fe-sulphide dissolution. A clear inverse relationship can also be seen in the Fe – NO_3^- plot (Fig. 4c). This can be related both to their different origin (the former from aquifer rock dissolution and the latter from irrigation backflow waters) and their opposite redox behaviour.

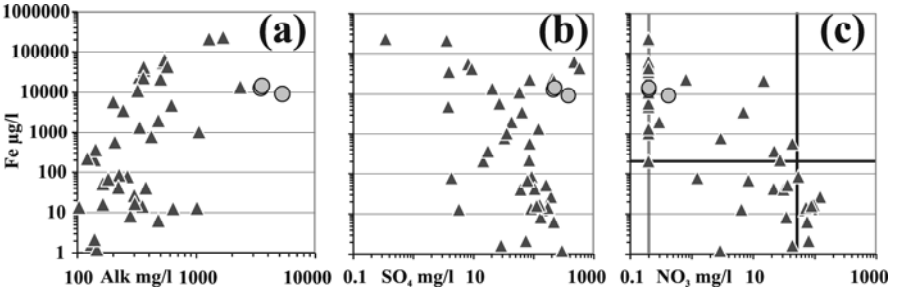

Fig. 4. a. Binary Fe – HCO_3^- diagram showing a positive correlation, **b.** Binary Fe – SO_4^{2-} diagram showing an inverse correlation, **c.** Binary Fe – NO_3^- diagram showing an inverse correlation, bold grey line is the limit of detection for NO_3^- (0.2 mg/L) and the black lines are the EU drinking water limits for Fe (200 µg/L) and NO_3^- (50 mg/L).

The same plot highlights the fact that many water samples exceed EU drinking water limits for one or both parameters. Considering all analysed species (Table 2) we could note that water sample exceed drinking water limits also for other parameters (e.g. Na^+, SO_4^{2-}, F^-, Al, B, Ba, Mn and Ni) and that only 4 samples comply with those limits. If we exclude NO_3^-, most of the exceeding values can be attributed to the high dissolved CO_2 values. But the while most of the elements derive from the dissolution of the aquifers rocks, some of them probably derive from the alteration of the well-case and tubes. Such a process could easily explain the high concentrations of Ni and Zn and to some extent also of Fe. Finally mixing with AL-type groundwater is probably responsible of the sometimes-high contents of Na and B.

Table 2. Chemical composition of the Florina groundwater samples. AL=Air Liquide wells, O=other wells, DWL=drinking water limit (EU), n. exc.= number of samples exceeding DWL.

		T °C	pH	TDS	Na	K	Mg	Ca	Cl	NO_3	SO_4	Alk	F	Al	As	B	Ba
				mg/L	mg/L	mg/L	mg/L	mg/L	mg/L	mg/L	mg/L	mg/L	mg/L	µg/L	µg/L	µg/L	µg/L
AL	min	22.4	6.10	6570	1570	76	87	10	877	<0.2	211	3470	0.1	7.0	1.2	54600	49
	max	28.3	6.48	10600	2780	132	119	246	1620	0.4	374	5270	0.2	18	7.7	92400	156
O	min	8.8	5.20	267	5.1	0.6	8.0	27	3.8	<0.2	0.3	104	0.1	<0.1	0.1	9.0	4.5
	max	28.5	7.40	3200	288	59	159	452	77	123	583	2350	4.9	1260	9.3	4500	796
	median	14.2	6.04	687	24	4.1	20	89	13	6.5	80	332	0.4	6.6	0.7	62	72
	DWL		6.50		200				250	50	250		1.5	200	10	1000	300
	n. exc.		31		1				0	9	3		5	4	0	4	2
		Cd	Co	Cr	Cu	Fe	Li	Mn	Mo	Ni	Pb	Rb	Se	Sr	U	V	Zn
		µg/L	µg/L	µg/L	µg/L	µg/L	µg/L	µg/L	µg/L	µg/L	µg/L	µg/L	µg/L	µg/L	µg/L	µg/L	µg/L
AL	min	<0.05	0.9	<0.05	<0.1	9200	5390	56	<0.1	4.1	<0.01	565	<0.05	3220	0.51	0.9	7.3
	max	<0.05	1.7	0.38	1.1	14400	9120	522	0.9	6.6	<0.01	718	0.13	3700	0.77	2.1	100
O	min	<0.05	0.1	<0.05	<0.1	1.2	1.4	0.4	<0.1	0.2	<0.01	0.1	<0.05	179	<0.05	<0.1	0.7
	max	0.36	22	5.79	36	227000	716	3970	13	53	1.30	55	4.93	4650	7.41	4.3	915
	median	0.14	1.4	0.36	0.8	359	13	423	0.4	3.9	0.07	4.6	0.48	373	0.71	0.8	14
	DWL	5		50	2000	200		50		20	10		10		1400		3000
	n. exc.	0		0	0	23		27		8	0		0		0		0

5 Conclusions

The area of Florina is characterized by the upflow of great quantities of geogenic CO_2 probably associated to Quaternary volcanic activity. The gas originates mainly from crustal sources but has also a minor (~10%) mantle contribution. This strong upflow of nearly pure CO_2 can be recognized in industrially exploitable gas reservoirs, high pCO_2 groundwaters and surface gas manifestations. But the increased CO_2 contents have a deleterious impact on groundwater quality. Due to the increased aggressiveness of the low-pH CO_2-charged waters with respect to the aquifer rocks, EU drinking water limits are exceed for many parameters (e.g. pH, Na^+, SO_4^{2-}, F^-, Al, B, Ba, Fe, Mn and Ni). Considering the additional impact of widespread agricultural activities, which is recognizable in elevated NO_3^- contents, only few of the sampled waters could be used for potable purposes.

Future developments of CCS programs in the sedimentary basin of Florina-Ptolemais-Servia have to carefully take in account the possible deterioration of the groundwater due to CO_2 leaks of the storage reservoirs.

References

Bachu S (2000) Sequestration of CO_2 in geological media: criteria and approach for site selection in response to climate change. Energy Conversion and Management 41, 953-970

Beaubien SE, Lombardi S, Ciotoli G, Annunziatellis A, Hatziyannis G, Metaxas A, Pearce JM (2005) Potential hazards of CO_2 leakage in storage systems-learning from natural systems. In: Rubin ES, Keith DW, Gilboy CF (Eds.), Proc. 7th International Conference on Greenhouse Gas Control Technologies, vol. 1. Elsevier, Oxford, UK, pp. 551-560

Karakatsanis S, Koukouzas N, Pagonas M, Zelilidis A (2007) Preliminary sedimentological results indicate a new detailed stratigraphy for the Florina sedimentary basin and relate them with CO_2 presence. Bull. Geol. Soc. Greece 40, Proc. 11th Internat. Congr., Athens, May 2007

Kilias A (1980) Geological and tectonic study of eastern Varnountas area (NW Macedonia). PhD Thesis, University of Thessaloniki

Kolios N, Innocenti F, Manetti P, Peccerillo A, Giuliani O (1980) The Pliocene volcanism of the Voras Mts (Central Macedonia, Greece). Bull. Volcanol. 43, 553-568

Koukouzas N, Ziogou F, Gemeni V (2009) Preliminary assessment of CO_2 geological storage opportunities in Greece. Int. J. Greenhouse Gas Control 3, 502-513

Pavlidis SB and Mountrakis DM (1987) Extensional tectonics of northwestern Macedonia, Greece, since the late Miocene. J. Struct. Geol. 9, 385-392

Pearce JM (Ed.) (2004) Natural analogues for the geological storage of CO_2. Final report of the Nascent project. British Geological Survey Technical Report, 122 pp

Sano Y and Marty B (1995) Origin of carbon in fumarolic gas from island arcs. Chem. Geol. 119, 265-274

Steenbrink J, Hilgen FJ, Krijgsman W, Wijbrans JR, Meulenkamp JE (2006) Late Miocene to Early Pliocene depositional history of the intramontane Florina-Prolemais-Servia Basin, NW Greece: Interplay between orbital forcing&tectonics. Palaeog. Palaeo. Palaeoec.238, 151-178

Pore Water - Indicator of Geological Environment Condition

O. Abramova, L. Abukova, G. Isaeva

Oil and Gas Research Institute. Russian Academy of Sciences (OGRI RAS). Moscow.
abramova_olga@bk.ru

Abstract The data on experimental works on the analysis of the chemical composition and the organic matter of the pore water extracted from bottom sediments of water bodies and shale rocks of aquifers are given here. It is shown that pore water can be a source of the secondary pollution of water bodies and underground water under the influence of natural and anthropogenic loads.

1 Introduction

Development of hydrocarbon resources (development of oil and gas fields, recycling of industrial effluents, etc.) impacts negatively the environmental condition. Any failure in normal operation of the oil field facilities causes pollution of surface water and underground hydrosphere. Waste water from oil and gas fields frequently contains considerable amounts of oil products, salts of heavy metals, radionuclides; the physicochemical equilibrium of the medium is disturbed with their ingress into water bodies and the composition of natural water changes. On entering open water basins numerous pollutants are absorbed by the pellite fraction of bottom sediments and eventually are partially removed from the bulk water. In a calm geodynamical situation the bottom sediments can act as accumulators of pollutants for a long time.

However, activation of geodynamic regime (in particular, seismic effect) results in desorption of a number of heavy metals - toxic substances from the bottom shale deposits into pore osmotic water. Consequently, pore water becomes a source of the secondary pollution of free water in open water bodies. Particularly often such a mechanism of mass transfer of environmentally harmful substances shows itself on the coastal shelf areas where geodynamic and vibroacoustic tensions are associated with operation of oil and gas field and other industrial facilities (Simonenko et al. 2002). Apparently, a similar pollution mechanism is possible for aquifers of domestic and drinking purpose. Development of hydrocarbon deposits, underground gas storage, and operation of oil and gas pipelines generate anthropogenic geodynamic processes. They induce enhanced production from shale deposits of various trace elements adsorbed earlier during

N. Lambrakis et al. (Eds.), *Advances in the Research of Aquatic Environment, Vol. 2*
DOI 10.1007/978-3-642-24076-8,

injection of produced or waste water to maintain reservoir pressure. It is also possible that the shale thicknesses, as natural mineral and organic accumulators, in stressful temperature and pressure and geodynamic situations can be a source of high (up to hazardous) concentrations of heavy metals, radioactive elements and organic substances. Squeezed out pore water penetrating reservoirs via fractures and voids increases the concentration of heavy metals and organic compounds harmful to human health in aquifers of domestic and drinking purpose. This mechanism will show itself specifically in water-saturated thicknesses with alternation of shale micro-particles with coarse-grained terrigenous and carbonate varieties.

2 Materials and methods for experimental work

Experimental simulation allowed detailed studying of the processes of desorption of trace elements and organic substances from fine-grained silt sediments and argillaceous confining beds (clays, mudstones) as well as their dissolution in pore water under baric alternating loads combined with vibroacoustic effect. This formulation of the research is determined by the fact that in the areas with high hydrocarbon production abrupt drops in pressure are recorded and vibroacoustic activity of the medium is high (Orlov ets al. 1989). For example, even weak seismic events can disturb the equilibrium in the subsurface hydrosphere and bring on generation of hydrodynamic and hydrochemical anomalies. Depending on the strength of earthquakes and the depth of seismic sources such anomalies extend to quite considerable areas (Nikolaev 1993).

The silt sediments from the northern water area of the Caspian Sea and Lower Miocene shales of the West-Kuban trough were used to carry out the experiments. The methods of experimental work included a series of sequential steps allowing making the simulation closer to real environmental conditions. Extraction of pore water was carried out using a special unit in a high-pressure chamber fitted with devices for generation and adjustment of temperature and vibroacoustic impact, with sensors recording radiation frequency of resonant oscillations (λ) from 6 to 60 kHz and temperature measurements.

The selected range of the radiation frequency of resonance oscillations corresponds both to natural microseismic amplitude and frequency parameters (20 to 5000 Hz) and technical vibration loads on ecosystems. It is known, for instance, that the integrated noise of acoustic fields at compressor stations and linear parts of pipelines is within the range of frequencies from 20 Hz to 20 kHz.

Pore water was squeezed out using 2 modes. Mode I provided for simulation of conditions of gradual plunge and compaction of plastic rocks: slow load on the sample in the range of 0 - 10 - 20 MPa. Mode II ensured conditions for activation of natural seismicity and anthropogenic impact: creation of alternating baric loads in the range of 0 - 10 - 20 MPa, with vibroacoustic oscillations varying

from 6 to 20 kHz with power capacity of 1 kW. The experiments were carried out under the same time (110 hours) and isothermal conditions at the temperature of ~25º C).

The experiments on studying pollution of open water ecosystems were carried out using the models of artificial basins with capacity of 20000-30000 cm^3. ¼ of the basin volume was filled with fine-grained silt sediment and ¾ - with water, the chemical composition of which is close to that of sea water with added salts of heavy metals (V, Ni, Co, Fe, Pb, Cu, Zn) and oil products (simulation of wastewater discharge). After 72 hours of settling the "polluted seawater" was discharged, and the basin was refilled twice with "sea" water without polluting additives. Repeated volumes of water were successively decanted after 72 hours of settling and the silt bottom sediments were subjected to squeezing out of pore water both under Mode I and Mode II conditions with subsequent determination of trace elements and organic carbon content in it. The results obtained allowed evaluating the possibility of influence of the pore water from bottom sediments on the secondary water pollution of water basins with toxic elements under natural and anthropogenic loads.

3 Discussion

The chemical analysis of the free water in the basin showed that the content of most elements in the primarily polluted volume after a double refilling with clean water has decreased nearly to the maximum allowable values. However, in the pore water extracted from the bottom sediments, even under loads simulating gradual compaction in Mode I, noticeably higher concentrations of metals and organic compounds were identified. On creating of alternating baric and vibroacoustic impacts in Mode II the content of all components in the pore water of the bottom sediments became higher: Cd, Fe, Ni, Pb, Zn - 3 - 4 times; Co, Cu, V - 6 -7 times, Mo - 11 times. Along with release of heavy metals the content of water-soluble organic substances was increased. A shift in the dynamic equilibrium between the bottom sediments and pore water is accompanied by an enhanced “release” of a number of toxic elements. In natural conditions this process will occur in places where in the zones of geochemical anomalies of benthic ecosystems seismic activity is high and there are traces of recent geodynamic activation. Under their influence pore water, passing from the bound state into the free one, becomes highly aggressive and is capable of dissolving considerable amounts of mineral and organic components. A layer of relatively high concentrations of heavy metals is formed directly near the mineral surface of the bottom sediments, and the presence of oil products (being real within oil and gas offshore areas) may cause appearance of even more hazardous complex organometallic compounds. In the zones of geochemical anomalies of benthic ecosystems the content of chemical elements in pore water is much higher than in

the main water column. Dispersion of elements-toxicants in the bulk water volume of the basin occurs gradually; therefore it has no immediate impact on changing of regional hydrochemical indicators of the water body. However, in the conditions where the natural processes of compaction and anthropogenic impact contribute (especially in stressful situations) to pulsed release of hazardous elements their content in pore water is much higher than the maximum allowable concentrations. It should also be noted that even after multiple repeated water refilling in the basin the pore water of the bottom sediments retains sufficiently high concentrations for a long time.

The second part of the experiments dealt with the assessment of pore water impact on contamination of aquifers. The analysis of the chemical composition of argillaceous deposits (shales and clays) studied "before" and "after" squeezing of pore water out of them showed that compaction of rocks under load (in simulation close to natural and anthropogenic ones) contributes to destruction of the aluminosilicate matrix, intensive production of oxides of rock-forming elements and salts of heavy metals and organic substances (Fig. 1).

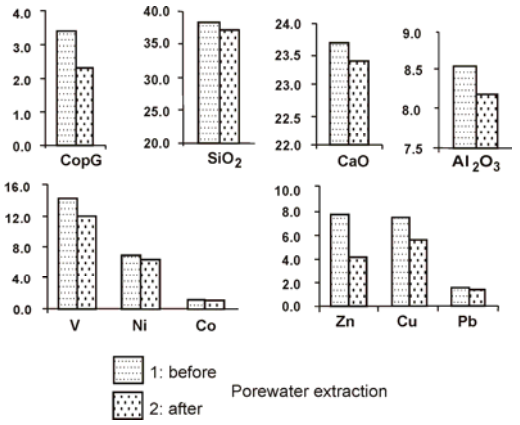

Fig. 1. Changes of the content of mineral components and organic carbon in shale 1) "before" and 2) "after" pore water extraction.

Loss of mineral and organic compounds is accompanied by formation of numerous aggressive products - CO_2, H_2S, H_2, etc. causing deformation changes within the beds. Desulfation, decarbonation, dolomitization and loss of organic matter cause development of fracturing, fragmentation, formation of weak zones (Yusupova et al. 2007) which can further serve as drainage systems for migration of pore fluids. These processes are of both local and large-scale areal character. Geochemical transformations of rocks are enhanced under the influence of seismic factors. Figure 1 shows the reduction of the content of mineral elements and organic carbon in argillaceous rocks after pore water extraction.

Migration of solutions potentially hazardous for environment enhances with increasing of seismic activity, activation of natural acoustic vibrations, imposed anthropogenic impacts and other factors.

There is a possibility of pore water penetration in the aquifers lying above and, as a consequence, the content of heavy metals, organic substances and many other toxic components is increasing in them. Table 1 provides the characteristics of pore fluids extracted from shales.

Table 1. Content of Mineral and Organic Substances in Pore Water Extracted from Shale Rocks (the table provides the average values of experiment results).

Elements	Maximum allowable concentration in drinking water	Pore water extracted from shales in different modes of experiments (the number of experiments are given in brackets)	
		I (24)	II (24)
Al	0.05	0.05	0.1
Cd	0.001	0.001	0.010
Cu	1.0	0.86	1.2
Fe	0.3	0.26	1.3
Mn	0.1	0.25	0.39
Ni	0.1	0.24	0.89
Co	0.1	0.073	0.18
Pb	0.03	0.029	0.036
Si	10.0	14.9	16.0
V	0.1	0.1	0.19
Zn	5.0	5.28	7.44
Ti	0.1	0.016	0.046
Org.car.	10.0	67.0 (12)	204.0 (12)

It is evident that production of mineral and organic substances from shales is accompanied by growth of their concentrations in pore water, and while simulating gradual loads (Mode I) the content of certain components remained nearly equal to or even lower than the maximum allowable concentrations (MAC) in drinking water (for example, Al, Cu, Fe, Co, V). However, during compaction of shale rocks with impact of seismic and vibroacoustic loads (Mode II) the content of all components increases dramatically in the extracted pore water. This is related to showing of anomalous solvent properties of pore water during extraction from fine-grained systems when cohesion to the basal mineral surface is overcome. It is known that in severe temperature and pressure conditions pore water can dissolve hardly soluble compounds such as UO_2, Al_2O_3, SnO, NiO, Fe_2O_3, etc., authigenic minerals, and even earth silicon.

Conclusions

The comparative characteristics of the chemical composition of the pore water extracted from the shale rocks in Mode II indicates that the content of most elements and organic carbon is ten times as high as MAC for drinking water.

The experimental simulation of pollution processes for aquatic ecosystems allows pointing out the following:

- pore water of contaminated bottom sediments is a source of prolonged processes of ingress of toxic elements in water bodies; under various loads (natural and anthropogenic) even after multiple refilling of the water basin with clean (flow) water they can be a source of the secondary pollution of water bodies and create a threat of poisoning first of all for benthic organisms and for the local fish communities in general.
- influenced by active seismic processes (natural and anthropogenic) pore water acts as a transfer agent of various trace elements including toxic ones and organic substances from rocks to free reservoir water; due to this a slow and steady contamination of aquifers of domestic and drinking purpose takes place.
- Thus, the recommended set of actions on monitoring of aquatic ecosystems for timely detection and mapping of geochemical anomalies may include conducting of monitoring observations of any change in the chemical composition of the pore water of: a) the bottom sediments of water basins, b) the clayey impermeable beds of aquifers. To prevent adverse environmental situations it is essential that such studies are performed in the areas of active oil field development.

Reference

Nikolayev AV (1993) Impact of Seismic Effects on Oil Reservoir and Groundwater / Seismic Impact on Oil Reservoir. pp. 7-24

Orlov VS, Maksimov VP, Pavlov VI. (1989) The Study of the Physical Fields of Pipelines in the Ground Underwater Passages to Develop Environmental Activities. Ecology of Oil and Gas Industry. CH.2. pp. 44-52

Simonenko VF, Abukova LA, Lashkevich VS, Zhilnina TI (2002) Trace Pore Water as Possible Indicator of Productivity and Environmental Situation in Offshore Oil and Gas Areas. New Ideas in Geology and Geochemistry of Oil and Gas. M. GEOS. Book 2. pp. 171-175

Yusupova IF, Abukova LA, Abramova OP (2007) Loss of Concentrated Organic Matter in Rocks during Their Immersion as Factor in Destabilization of Geodynamics. DAN. t. 414, No. 1. pp. 74-77

Nitrogen sources and denitrification potential of Cyprus aquifers, through isotopic investigation on nitrates

Ch. Christophi, C.A. Constantinou

Geological Survey Department, 1415 Nicosia, Cyprus, cchristophi@gsd.moa.gov.cy

Abstract Nitrates is one of the most common groundwater pollutants. Being able to identify the source(s) as well as evaluating the denitrification capacity of aquifers can help shape appropriate remedial action. This paper aims to investigate the isotopic composition of nitrates in groundwater samples in order to identify primary and secondary nitrate sources as well as to evaluate denitrification potential of aquifers in Cyprus. A total of 135 groundwater samples from 12 different Ground Water Bodies (GWB) were analyzed for $^{15}N/^{14}N$ and $^{18}O/^{16}O$. It was concluded that the dominant primary source of nitrate in rural Cyprus is fertilizers. For many samples a secondary nitrate source with an isotopic signature of organic source is contributing. This organic source is, in most cases, assumed to be manure. In 16% of the groundwater samples, manure was identified as the primary nitrate source. Finally, the potential of denitrification is seen in 21% of the samples from 7 different GWBs.

1 Introduction

There are two stable isotopes of nitrogen, ^{15}N and ^{14}N and they are both active in the nitrogen cycle participating in various nitrogen compounds. The ratio at which these two isotopes are incorporated in compounds depends on the processes and reactions that produce such compounds. Therefore, $\delta^{15}N$ in nitrates can be used in isotope hydrogeology because of such fractionation between the various nitrogen compounds, enabling tracing of nitrogen sources, sinks and fate. For example, nitrates derived from synthetic fertilizer can be distinguished from animal manure through $\delta^{15}N$ values (Hoefs 1997, Clark and Fritz 1997). The use of isotopes in hydrogeology to trace nitrogen fate gained reliability and further attention when it became possible, through advance analytical processes, to analyze $\delta^{18}O$ in nitrates. Nitrogen molecules of different origin have large oxygen isotopic difference between them. Therefore, $\delta^{18}O$ can distinguish between nitrates that originate from the atmosphere, fertilizers or manure/effluent. The combination of the isotopic composition of $\delta^{18}O$ ‰ VSMOW and $\delta^{15}N$ ‰AIR can be used not only in distinguishing nitrate sources more reliably but most importantly in,

N. Lambrakis et al. (Eds.), *Advances in the Research of Aquatic Environment, Vol. 2*
DOI 10.1007/978-3-642-24076-8,

among other applications, recognizing denitrification processes (Amberger and Schmidt 1987, Bottcher et al. 1990, Durka et al. 1994). More specifically, ammonium and nitrate synthetic fertilizers have an isotopic signature of $\delta^{15}N$ ranging from -1 to 5‰ and $\delta^{18}O$ from 17 to 22‰. Nitrate originating from litter, soil and sewage/manure have similar with each other $\delta^{18}O$ values that are very close to 0‰, but their $\delta^{15}N$ vary significantly (Clark and Fritz 1997; Mook 2000; Lorence et al. 2010). Ammonia evaporation causes enrichment of $\delta^{15}N$ whereas the process of denitrification causes a simultaneous increase of both $\delta^{15}N$ and $\delta^{18}O$ values. This work aimed to use nitrate isotopes in order to investigate nitrate sources in GWB as well as denitrification potential, in order to help shape the necessary action plans within the nitrate vulnerable zones, in accordance to the European Directive 91/676/EEC. Nitrate isotopic investigations in Cyprus have been carried out earlier by a number of researches, but on a smaller scale (Constantinou 2004; Udluft et al. 2006).

2 Sampling

The sampling was carried out in two phases; groundwater samples were collected in September 2009 and September of 2010. In the 2009 campaign, 98 samples were collected from all 12 different GWBs whereas in 2010, 37 samples from the Western Mesaoria GWB; 16 of these samples were common with that of the 2009 campaign. Sampling was restricted to the area that the Republic of Cyprus exercises effective control. Sample volume varied from one to five liters, depending on the nitrate concentration. Upon sampling, field pH, conductivity, dissolved oxygen and water level were measured and recorded. One liter of sample was collected in the cases of nitrate concentration equal or above 20 mg/L, whereas in lower concentrations, up to five liters were collected. Polyethylene bottles were used and ten drops of chloroform were added upon collecting the samples. Samples were stored in a cool place until they were shipped for analysis to the lab Hydroisotop, in Germany. In addition, a second one liter sample was also collected and used in analyzing SO_4^{-2} and Cl^- with ion chromatography.

3 Nitrate Isotope Analysis and Methodology

The dissolved nitrate was separated using cation exchange and neutralization with KOH. After elimination of sulfate and phosphate by precipitation with $BaCl_2$ the water samples were evaporated to dryness. The samples were heated to 570 °C together with graphite under vacuum and conversed to N_2 and CO_2. After cryogenic separation these two gases were analyzed in an isotope ratio mass spectrometer. The isotope ratio analysis was done using mass spectrometer “MAT-251” with

double inlet system. The mass spectrometer was daily calibrated with international standards (N-3, SDGS 34, USGS 35) (Lorence et al. 2009, Lorence et al. 2010). The analyzed isotope ratios are reported in delta notations ($\delta^{18}ONO_3$, $\delta^{15}NNO_3$ in ‰) relative to standard mean ocean water or to air nitrogen as the standards as defined bellow:

$$\delta^{15}NNO_3 = (Rs/Rst - 1)*1000 \text{ and } \delta^{18}ONO_3 = (Rs/Rst - 1)*1000$$

Where Rs and Rst is the $^{15}NNO_3/^{14}NNO_3$ and $^{18}ONO_3/^{16}ONO_3$ ratio(s) of the sample and standard.

4 Results and Interpretation

A total of 135 samples from 12 Aquifers (Table 1) were analyzed for conductivity, chlorites, sulfates, dissolved oxygen, $\delta^{18}ONO_3$ and $\delta^{15}NNO_3$. Figure 1 shows the samples' spatial distribution as well as nitrate concentration. Nitrate concentration ranges from 1.7 to 408 mg/L with mean and median values being 64 and 29 mg/L, respectively. Nitrate concentrations are rather inhomogeneous even within the same GWBs and it is related to a number of factors such as the complexity of certain GWBs and the variations of land use within a single aquifer area.

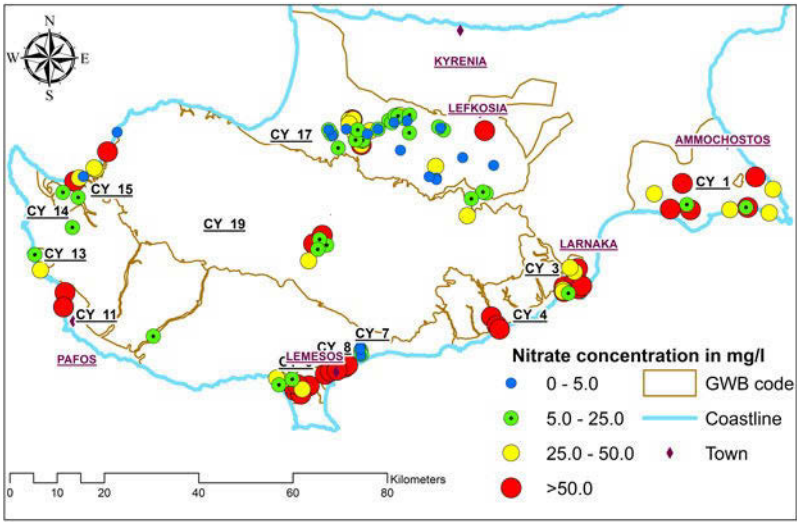

Fig. 1. Sample distribution and nitrate concentration in groundwater samples.

Table 1. Primary nitrate source and denitrification potential as number of samples per GWB.

GWB CODE	Ground Water Body (GWB) Name and Type	Samples/ GWB	Significant denitrification	Primary source of nitrates			
				Fertilizer	Organic	Industr.	Mixing
CY1	Kokkinochoria (Clastic, unconfined / confined)	11	4	11	-	-	5
CY3	Kiti-Perivolia & Tremithios Riverbed (Alluvial, unconfined)	13	3	12	1	-	3
CY4	Softades-Vasilikos coastal plain & riverbeds (Alluvial, unconfined)	3	-	3	-	-	1
CY7	Germasogia Riverbed (Alluvial, unconfined)	5	4	4	1	-	-
CY8	Lemesos (Alluvial, unconfined)	9	3	1	8	-	8
CY9	Arkotiri (Alluvial, unconfined)	10	-	9	1	-	4
CY11	Pafos Coastal Plain & riverbeds (Alluvial, unconfined)	3	1	3	-	-	2
CY13	Pegeia limestones (Semiconfined)	2	-	2	-	-	1
CY14	Androlikou limestones (Semiconfined)	2	-	2	-	-	-
CY15	Chrysochou-Gialia coastal plain & riverbeds (Alluvial, unconfined)	8	1	7	1	-	2
CY17	Central-Western Mesaoria (Clastic, unconfined – confined)	62	13	53	8	1	19
CY19	Troodos area (Ophiolites –fractured)	7	-	5	2		4
Total		135	29	112	22	1	49

There is no strong correlation between conductivity and nitrate concentration that would suggest evaporative nitrate enrichment. Nonetheless, in the cases of the GWBs of Southeastern Mesaoria (CY 1), Kiti-Pervolia (CY 3), Lemesos (CY 8) and Akrotiri (CY 9), such a correlation seems to exist. The isotopic composition of nitrates in all of the samples is presented in Figure 2. Primary and secondary sources are attributed to all samples based on nitrate isotopic composition and consequently their position within the graph. Based on the primary isotope signature, denitrification paths can be calculated and the enrichment paths modeled. Such paths, using published fractionation ratios, are sketched in Figure 2 (Lorenz 2010; Amberger and Schmidt 1987; Bottcher et al. 1990).

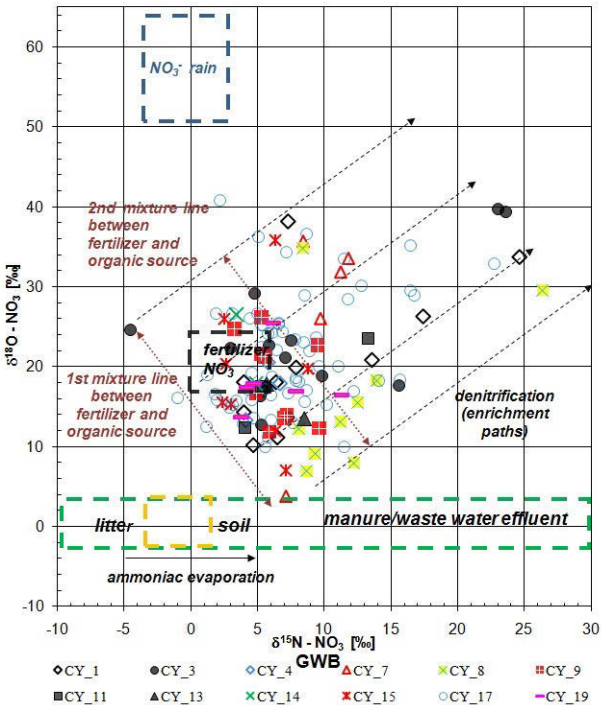

Fig. 2. Isotopic composition of NO_3 in all groundwater samples.

Samples that have isotopic signatures to the right of the first mixing line are already going through some degree of denitrification. However, in this paper, a more conservative approach is adapted and only the samples positioned far to the right of the second mixing line were considered as having significant denitrification potential. The majority of the samples, 112 samples (83%), from all aquifers, show nitrate isotopic composition very similar to that of mineral fertilizers. This indicates that the dominant, primary contributing source of nitrates in groundwater, for these samples is mineral fertilizers. Twenty-nine of these samples (21%) fall along the mixing lines of mineral fertilizers and manure/waste water effluent.

This is interpreted as having an additional, less significant, secondary, organic source that is also contributing to the concentration of nitrates in these groundwater samples. The organic source of mixing can be either manure that is used as fertilizer in the fields or direct infiltrates from animal manure and/or animal waste water. The isotopic composition of animal waste water does not differ from that of the urban waste water therefore in theory the organic source could also be urban waste water. A total of 22 samples from 7 different GWB (16%) show organic as the primary nitrate source; 20 of them indicate mineral fertilizers as a secondary contributing source. Most of these samples however come mainly from Central-Western Mesaoria (CY 17) and Lemesos (CY 8) GWBs. It is also clear that 29 samples from 7 different GWBs (21%) show significant denitrification potential. Most of these samples come from Central–Western Mesaoria (CY 17) GWB, suggesting a significant denitrification potential of this aquifer. It should also be noted that, the majority of the denitrifying samples tend to have lower nitrate concentrations than those with insignificant denitrification thus supporting the scenario of denitrification. The spatial distribution of the samples, their denitrification potential and primary source are presented in Figure 3 and tabulated in Table 1. For presentation purposes, only the two end sources are presented as primary source and the rest of the samples are presented as mixing samples. No further classification is made for the mixing samples, in terms of which of the two sources is the prevailing one.

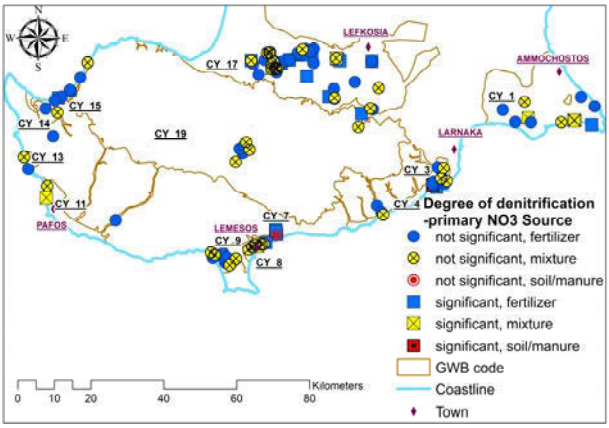

Fig. 3. Sample spatial distribution, denitrification potential and primary nitrate source.

A more detail presentation of the results pertaining to the GWBs of Germasogia river bed (CY 7), Lemesos (CY 8) and Akrotiri (CY 9) is undertaken bellow. Germasogia, Lemesos and Akrotiri are alluvial GWBs that develop along the south central coast of the island. The Germasogia GWB (CY 7) is a river alluvial aquifer that develops along its channel. In 1969, Germasogia dam was constructed and since then recharge is done by systematic, controlled water releases. A total of five samples were collected from this GWB and nitrate concentration was below 7 mg/L.

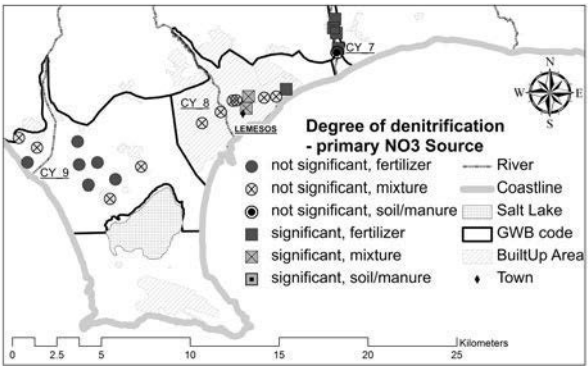

Fig. 4. Sample distribution, denitrification capacity and primary source in GWBs 7, 8 and 9.

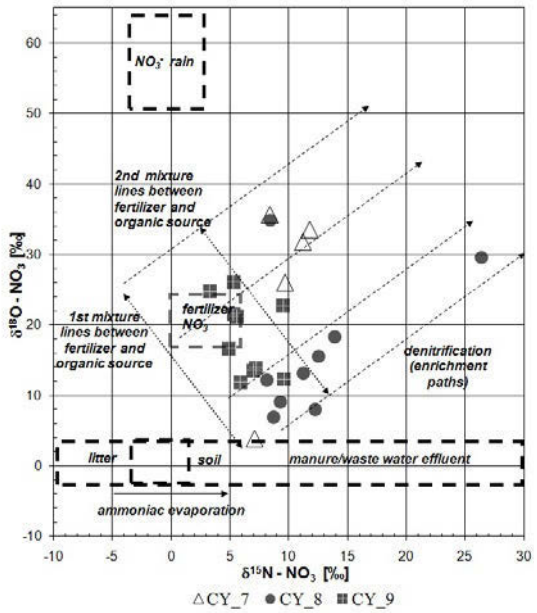

Fig. 5. Isotopic composition of nitrates in groundwater samples from GWBs 7, 8 and 9.

Nitrate isotopic signatures from the collected samples is distinguished from the other two GWBs and suggest that the dominant nitrate source in CY7 groundwater is mineral fertilizers. Denitrification capacity of this aquifer appears to be high since four out of five samples show significant denitrification (Table 1 and Fig. 4 - 5). Lemesos (CY 8) and Akrotiri (CY 9) are adjacent, coastal, alluvium GWBs. The Lemesos GWB develops within the city of Lemesos and it is recharged by the Garilles River.

The area is heavily urbanized and up to 1995 sewage effluent absorption wells were used in all buildings. In 1965 the Polemidia dam in the Garilly River channel

was constructed thus reducing recharge of this part of the aquifer which depends heavily on river flow. A total of 11 samples were collected and analyzed from the Lemesos GWB. Samples show nitrate values above 50mg/L and conductivity values above 1200μS/cm. The primary source of nitrates in groundwater is organic with minor mixing with chemical fertilizer. Samples from Lemesos GWB exhibit the heaviest influence of an organic source on the isotopic signature of the nitrates to such an extent, that they are distinguishable from all other samples. It appears that urbanization and the use of sewage effluent absorption wells in the past, remains the dominant nitrate source. In addition, a weak correlation between nitrate concentration and conductivity exists. This may suggest partial nitrate enrichment through evaporation brought about by reduced recharge. The samples that show denitrification potential tend to have lower nitrate concentration than those with insignificant denitrification. Denitrification appears to reduce nitrate concentration from about 100 - 140mg/L to about 60mg/L.

The Akrotiri GWB is adjacent to the Lemesos GWB. The major land use in this case is predominantly agriculture with a number of smaller in extent builtup areas. The Kouris River that runs from north to south intersects and recharges this part of the aquifer. It discharges to the sea to the southwest part of the aquifer. In 1987, Kouris, the biggest dam of Cyprus, was constructed on this river and changed the recharge regime of the GWB. Recharge is now limited to direct infiltration from rain, return irrigation and to the rare, controlled releases from the dam. The aquifer is pumped mostly for irrigation water and its water balance is negative. As a result, seawater intruded primarily from the west. A total of 8 samples have been collected from Akrotiri GWB. Nitrate concentration ranges from 19 to 279mg/L. The isotopic signature of the samples confirms that mineral fertilizer is the main source of nitrates in groundwater. Organic contribution is only seen near and downstream from Episkopi, Trahoni and Asomatos Villages. None of the samples shows significant denitrification capacity. This might be attributed to the relatively thin unsaturated zone, high hydraulic conductivity and most importantly to the much lower clay content in the Akrotiri GWB in comparison to that of the Lemesos GWB (U.N.D.P. 1970). Nitrate isotopic composition from the collected samples from the above three aquifers shows distinct differences between them that reflect the different status of each GWB.

5 Conclusions

From the nitrate isotopic investigation of the groundwater samples collected from 12 aquifers in Cyprus the following can be summarized:

- Nitrate sources in groundwater can be assigned through investigation of the isotopic signature of nitrates.
- The dominant primary source of nitrates in rural Cyprus is fertilizers.

- For 21% of the samples, a secondary nitrate source with an isotopic signature of organic source is contributing. This organic source is in most cases assumed to be manure.
- 16% of the samples show organic as the dominant nitrate source. The majority of these samples are from GWBs CY 17 and CY 8. Samples from CY 8 exhibit the heaviest influence of an organic source. It is thought that the organic source in this area is old sewage effluent.
- The potential of denitrification is seen in 21% of the samples in 7 different GWBs. Denitrification potential seems to be higher in GWBs CY 17 and CY 7.
- The low denitrification potential of CY 9 might be due to the low clay content and high permeability of the GWB.

References

Bottcher J, Strebel O, Voerkelius S, Schmidt HL (1990) Using Isotope Fractionation of nitrate-nitrogen and nitrate-oxygen for evaluation of microbial denitrification in a sandy aquifer. J.Hydrol. 114, 413-424

Clark I, Fritz P (1997) Environmental Isotopes in Hydrogeology New York

Constantinou C A (2004) Hydrogeological conditions of the area Larnaca-Vasilikos, Cyprus Unpublished PhD thesis, Patra University, Greece (In Greek)

Durka W. Schulze E-D., Gebauer G., Voerkelius S(1994) Effects of forest decline on uptake and leaching of deposited nitrate determined from ^{15}N and ^{18}O measurements. Nature 372: 765-767

Hoefs J (1997) Stable isotope geochemistry. Berlin and New York

LÉTOLLE R (1980) Nitrogen-15 in the natural environment. In: Handbook of Environmental Isotope Geochemistry Vol.1. FRITZ P. FONTES J C (eds.) Elsevier, Amsterdam

Lorenz G, Voropaev A, Voerkelius S (2009) Isotope investigation in groundwater samples from Cyprus, Geological Survey Department (Unpublished report), Lefkosia

Lorenz G, Voropaev A, Voerkelius S (2010) Isotope investigation in groundwater samples from Cyprus, Geological Survey Department (Unpublished report), Lefkosia

U.N.D.P. (1970) Survey of groundwater and mineral resources-Cyprus. United Nations Development Program. United Nation. New York

Water Development Department (2002) Re- assessment of water resources and demand of the island of Cyprus (Unpublished report), Lefkosia

Udluft P, Dünkeloh A, Mederer J, Külls C, Schaller J (2006) Re-evaluation of the groundwater resources of Cyprus, Lefkosia

The behaviour of REE in Agios Nikolaos karstic aquifer, NE Crete, Greece

E. Pitikakis, K. Katsanou, N. Lambrakis

Department of Geology, University of Patras, Rio-Patras, GR 26 504, Greece.
manolispitikakis@gmail.com

Abstract Water and rock samples were collected from the karstic aquifer hosted in the Mirambello region, NW of Lasithi. In both rock and groundwater samples REE were determined. The rare earth elements' concentrations increase according to the groundwater flow. The origin of REE in groundwater along the recharge area of the aquifer is due to the dissolution of the mineral matter of the aquifer skeleton. Afterwards, they move conservatively showing a similar character with that of the REE of the hosting rocks. The REE concentrations in the water during their transportation within the aquifer are straightly connected to the physico-chemical conditions that prevail. The variations of REEs that have been observed in the brackish and in the freshwater coastal zone of the aquifer show that their behavior alters and they adopt similar character to those of the salt water rare earths. These variations show that the brackish zone and the penetration depth of sea water can be divided into a coastal karstic aquifer among the standardized diagrams of brackish and freshwater samples of the aquifer.

Introduction

The rare earth elements (REE) constitute a special group of elements due to similar chemical properties, and they show a gradual reduction of the ionic radius La 1.03 A (57) in 0.861 A for Lu (71) (lanthanide contrast) (Taylor and McLennan, 1988, Piper, 1974) which results in the preferential reception of the heavier rare earth elements from certain minerals. All the elements of this group are trivalent apart from Ce which, in oxidizing conditions, oxidizes into a tetravalent as well as Eu, which in reducing conditions, is reduced into a divalent which results in a different behavior compared to the other elements of the group (Piper 1974, Sholkovitz et al. 1992).

Due to the above mentioned properties, the REE have been widely used in mineralogical and petrographic comparative research (McLennan et al. 1980, Whitney et Olmested 1998), and in geochemical and oceanographic research (Shields and Webb 2004). Recently the REE have been used in hydrochemical research, for the tracing of the groundwater flow from different aquifers (Johannes-

N. Lambrakis et al. (Eds.), *Advances in the Research of Aquatic Environment, Vol. 2*
DOI 10.1007/978-3-642-24076-8,

son et al. 1997), the mixing of fresh and salt water (Nozaki et al, 2000, Duncan and Shaw 2003) as well as the ion exchange between the groundwater and the aquifer (Johannesson et al. 1999, Dia et al. 2000, Gruau et al. 2004).

The aim of this study is to present the evolution of the REE during the groundwater flow in the karstic aquifer of the Tripolis zone. Additionally, in order to test their variation and/or association with their equivalent within the aquifer rocks, the standardized diagrams of the water samples were compared to those of the rock samples from the same or neighboring areas (as have been identified from the chemical composition of the main elements of the water samples). Finally, the brackish water from the Almyros spring was also compared to the sea water sample and the corresponding rock samples from the Almyros region.

Geology-Hydrogeology

The geological setting of the research area consists of two different tectonic unities of metamorphic and non-metamorphic rocks (Fig. 1).

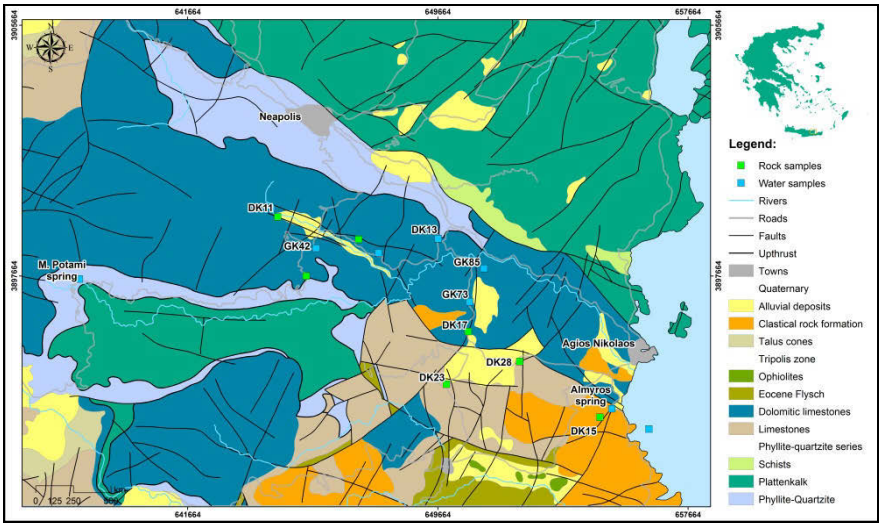

Fig. 1. Geological map of research area with the site of sampling.

The metamorphic rocks include the plattenkalk and the phyllite-quartzite unit, while the non-metamorphic include the limestones of the Tripolis zone. Plattenkalks comprise the lower geotectonic unit of the area and can be observed in the form of crystalline marbles and limestone. Between the marble layers there are flint layers and bulbs. The phyllite -quartzite unit is tectonically sandwiched between the plattenkalk and the carbonate rocks of the Tripolis zone. The Tripolis

zone consists of limestone, dolomitic limestone and dolomites of the Upper Triassic which end up in the Eocene flysch. The flysch of the Tripolis zone consists of alternations of shale limestone and sandstone. The thickness of the Tripolis zone is calculated to reach up to 600m.

The formations of the study area, according to their hydraulic characteristics (thickness, length, transmission and storage ability) can be classified into three groups (Fig. 3). The first group includes porous, non-cohesive soils; these are breccias, conglomerates, alluvial deposits, talus cones and river sediments. The second group consists of cohesive rocks with secondary porosity. This category further includes the limestone, dolomitic limestone and the dolomites of the Tripolis zone as well as the plattenkalk. Their porosity is due both to their fragmentation from the intense tectonic activity and the karst development. The third group comprises of the impermeable rocks and includes the phyllite-quartzite unit, the flysch of Tripolis zone, the schists, and the ophiolithes.

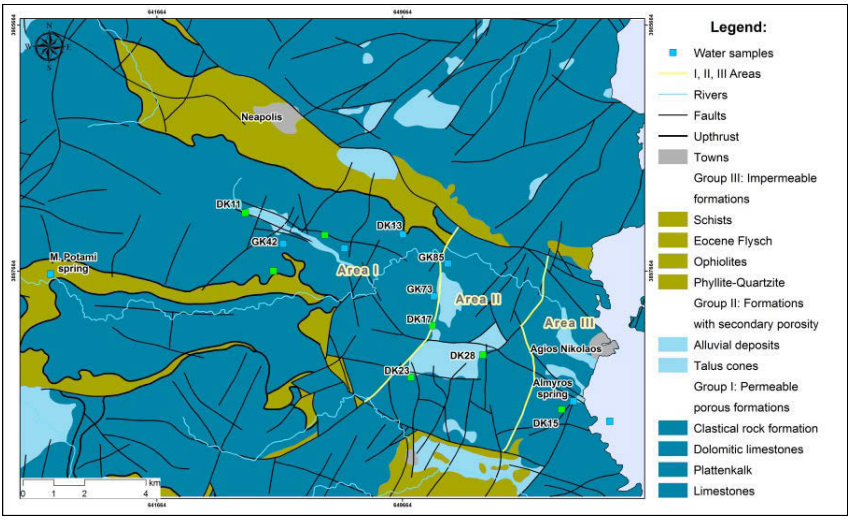

Fig. 2. Hydrolithologic map of the study area.

Hydrochemistry

In the frames of this study both groundwater and rock sources samples were collected from the corresponding aquifers of the water samples. Moreover, sea water sample was also collected. During the collection of the water samples the unstable physicochemical parameters were measured (Tw, Ec, pH, Eh, O_2 and alkalinity). Anion (NO_3^-, NO_2^-, PO_4^{3-}, SO_4^{2-}, and F^-), SiO_2 and NH_4^+ concentrations were measured in a Hach® DR 4000 spectrophotometer except from Cl^- concentration, which was measured using titration. Major cation (Ca^{2+}, K^+, Mg^{2+}, Na^+) concen-

trations were determined in a GBC® Avanta flame atomic absorption spectrophotometer. REE concentrations were measured using inductively coupled plasma-mass spectrometry (ICP-MS) in an ELAN 6100 Perkin-Elmer.

After they were pulverized, the rock samples were digested with acid mixtures in a MLS-1200 MEGA microwave oven. The weight of the samples which had been selected for the digestion, ranged from 0.1 to 0.5gr. The acid mixture and its volume depended on the sample weight and its mineralogical composition. After the digestion of the samples, the concentrations of the rare earth elements in the digested solution and in the overall solid rock were determined.

The analytical error, as far as the water samples are concerned, did not exceed 4%. The results of the chemical analysis of the physicochemical parameters and the main elements of the water samples are shown in Table 1.

Table 1. Physicochemical parameters and ion concentrations (ppm) in the water samples.

Sample	S. Almyros	M. Potami	GK85	GK73	GK42
T (^{o}C)	14.4	9.9		19	15.9
pH	7.59	7.13	7.98	7.4	7.4
E.C. (μS/cm)	8930	328	1797	1640	455
Eh (mV)	158	179		162	167
Ca^{2+}	91	76.4	73.6	125.6	54.4
Mg^{2+}	210	5	39.2	41.4	24.8
Na^{+}	1786	13.5	210.9	133.2	14.2
K^{+}	93	0.4	6.6	3.6	0.6
NH_4^{+}	0	0	0.078	0.035	0.03
Cl^{-}	3320	16	415	353	23.8
SO_4^{2-}	533	34.4	82.8	68.1	0.3
NO_3^{-}	1.69	3.9	3.96	7.19	3.58
NO_2^{-}	0.0132	0.0132	0.0132	0.0132	0.0099
HCO_3^{-}	152.5	195	179.3	285.5	257.4

According to the chemical composition of the water samples, three different water types can be identified, in the area occupied by the aquifers, which develop in the geological zone of Tripolis and correspond to three separate regions. The first region is of Ca^{2+}-HCO_3^{-} and Ca^{2+}-Mg^{2+}-HCO_3^{-} water type that are originated from the dissolution of the aquifer rocks. Region A includes the recharge area of the karstic aquifer and consists of the regions of the Lasithi Plateau, Drasi and Selena.

Region B (called Lakonia) is of Ca-Na-HCO_3-Cl^{-} up to Na-Ca-Cl-HCO_3 water type. The karstic aquifer of this region is affected by the seawater intrusion; while in region C, which is of Na-Cl water type, the seawater is involved to a greater extent compared to region B. Region C (brackish water) includes the area of Agios Nikolaos and Almyros.

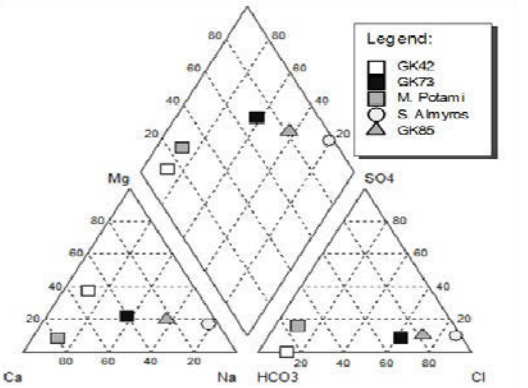

Fig. 3. Piper diagram.

The concentrations of REE measured both in water and rock samples (Table 2) were normalized according to the concentrations of the standard European slates (Sholkovitz, 1988), into three variation areas of the chemical composition of the main elements of the karstic aquifer (I, II, III). The rock samples DK-11 and DK13 belong to region I, the samples DK-23 and DK-28 belong to the region II, the samples DK-15 and DK-17 to the region III, while concerning the water samples, the sample from the spring of M.

Table 2 Rare earth element concentrations in rock samples (ppb) and in the water samples (ppt).

	DK11	DK13	DK23	DK28	DK15	DK17	M.POT	GK42	GK73	GK85	ALM	SEA
La	15.2	21.8	11.7	20.9	27.1	0	223	792.4	6519	1375	4653	10946
Ce	14	3.1	14.4	32.1	7.5	3	329	405.5	291.8	276.6	306	352
Pr	24.1	15.1	30.4	37.3	19.4	13.6	36.8	39.3	35.9	30.1	43.2	66.4
Nd	12.4	2.8	16.7	42.4	9.1	3	126.1	99.11	72.6	66.7	105	266
Sm	8.2	2.3	16.2	52.1	8	2.8	7.7	11.1	25	26.2	23.1	96.3
Eu	7.7	1.9	18	70.2	8.6	3.4	3.6	4.5	16.7	16.6	13.8	24.2
Gd	12.3	3.5	21.5	62.6	11.2	4.4	18.4	18.6	10.9	7.9	17.6	29.2
Tb	5.9	0.6	13.9	46	6.4	2.8	1.83	1.9	0.7	0.6	2.2	9.8
Dy	8.1	2.3	17	60.6	9.9	3.6	6.7	6.8	2	0.5	6.2	56.5
Ho	5.2	1.3	13.4	42.8	7.1	4.3	1.4	1	0.4	0.1	4.9	20.7
Er	5.9	1.7	13.3	42	7.7	3.2	3.4	3.5	1.5	0.5	10	36
Tm	2.4	0	10.6	32.5	3.9	3.5	0.2	0.5	0.2	0	1.1	11.6
Yb	5.1	1.5	12.1	38	6.8	3.1	1.3	1.7	0.3	0	5.1	29.2
Lu	2.9	0	10.4	29.1	5.4	3.3	0.025	0.3	0	0	4.7	9.8

Potami and GK-42 belong to region I, the GK-73 and GK-85 samples to region II while the sample from the Almyros spring (region III). For presentation purposes, the seawater sample from Ammoudara area is included to the last group of water samples. Finally, normalized concentrations are presented on the basis of the serial number of each REE in Figure 4.

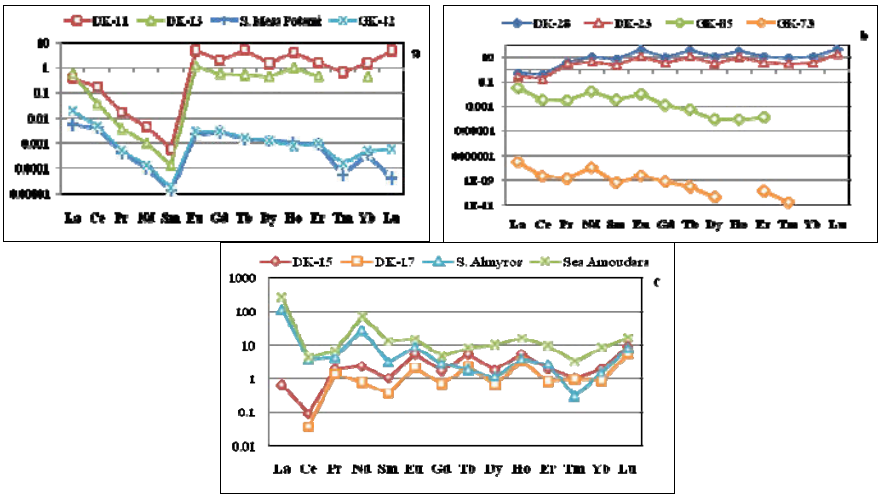

Fig. 4. Normalized concentrations of the REE for the ground and water in region **a.** Area I. **b.** Area II. **c.** Area III.

Discussion

Almyros springs' recharge area is situated in the area of Drasi and Selena. The REE in the groundwater samples are due to the carbonate dissolution of the rocks of that area, as is clearly shown in Figure 4.a, b and c.

The trend which develops in the curves of REE is similar to those of the rocks. The REE show a conservative behavior in a neutral Ph environment and in redox conditions (McCarthy et al. 1996; Zhang and Nozaki 1996; Johannesson and Lyons 1994; Johannesson et al. 1994) due to their ability to be absorbed and form strong negative complexes with the carbonate ions of the solution, which predominate over the other ions and especially the HREE (Johannesson et al. 1997) so as not to be able to resist, to some extent, to the tendency to be absorbed by the solid surfaces of the aquifer material. In this case, the groundwater develops a diagram similar to the one of the materials through which it has flowed (Smedley, 1991; Johannesson et al, 1997). Area II (Fig. 4b) is characterized by the same physicochemical conditions of the aquifer with those in Area I (Fig. 4a), but in contrast to Area I, three variation can be observed in the diagram of the rare elements, especially for the HREE (Er-Lu) where there is a downward trend with reference

to the one of the rock rare earth elements. This can be either because the REE cease to constitute a complex with carbonate ions, therefore, the free ions of HREE tend to constitute complexes in the solid surfaces of the aquifer skeleton, or due to the fact that the water of the limestone aquifer is mingled with fresh water of a similar chemical composition from the carbonate conglomerates of the area. Furthermore, due to the existence of a neutral pH no anomaly in the Eu is developed, and despite the slightly oxidizing environment of the aquifer, the Ce still remains within the solution as trivalent and does not precipitates, as Ce_2O_4 oxide.

In the discharge area of the aquifer the REE concentrations change dramatically both as far as the water and rock samples are concerned and resemble to that found in the seawater (Elderfield and Greaves, 1982). Thus, a negative anomaly of Ce can be observed, as a result of the domination of the oxidizing conditions in the water and its separation from the brackish water in the form of Ce_2O_4 and as a result of the adsoption of a similar behavior from the rock, as appears in carbonate rocks (Johannesson et al, 1997). Figure 4c shows the effect of the sea water intrusion into the aquifer, to the extent that it affects the REE's concentrations and behavior, a case which was not observed in the two previous areas.

Conclusions

The research conducted for the REE in the karstic aquifer of the carbonate rocks hosted in the Tripolis Zone have shown that the REE in the aquifer have originated from the dissolution of the crystal structure of the aquifer of the Area I.

The concentrations of REE in groundwater depends on the reactions of the cation exchanges processes that take place between the aquifer and the water and the coagulations of the elements into pellets or oxides, due to the physicochemical conditions dominating within the aquifer.

The REE act conservatively in the neutral pH conditions of the karstic aquifer, so that they are presented with almost identical diagrams compared to the diagrams of the rocks through which they have flowed.

The effect of seawater intrusion area in the concentration of REE is important and this is reflected in the diagrams variations. There can be a separation of brackish water from fresh water based on REE and the brackish zone of a coastal karstic aquifer can be determined by means of the diagrams of the REE.

References

Bizon G, Thiebault, F, (1974) Donnew nouvelles sur l' age des marbles et quartzies du Taygete (peloponnese meridional, Greece). C. R. Acad Sci Paris 278, 9-12

Calmbach L, (1997) Aquachem, Version 3.7. Aqueous Geochemical Dara Analysis and Plotting, Waterloo, Hydrogeologic, Ontario, Canada

Dia, A, Gruau, G, Olivie-Lauquet, G, Riou, C, Molenat, J, and Curmi, P, (2000) The distribution of rare earth elements in graondwaters: Assessing the role of source-rock composition, redox changes and colloidal particles, Geochim. et Cosmochim. Acta, 64:24, 4131-4151

Doutsos T., Piper, G., Boronkay, K., Koukouvelas, I., (1993) Kinematics of the Central Hellenides. Tectonics 12, 936-953

Duncan, T, and Shaw, T, (2003) The mobility of Rare Earth Elements and Redox Sensitive Elements in the Groundwater/Seawater Mixing Zone of a Shallow Coastal Aquifer, Aquatic geochemistry, 9, 233-255

Elderfield, H, and Greaves, MJ, (1982) The rare earth elements in sea water. Nature 296, 214-219

Gruau, G, Dia, A, Olivie lauquet, G, Davranche, M, and Pinay, G, (2004) Controls on the distribution of rare earth elements in sahllow groundwaters, Water Reseasch, 38, 3576-3586

Johannesson, KH, Lyons, WB, (1994) The rare earth element geochemistry of Mono Lake water and the importance of carbonate complexing, Limnol. Oceanogr. Vol 39, 00 1141-1154

Johannesson, KH, Stetzembach, KJ, Hodge, VF, Kreamer, DK, and Zhou, X (1997) Delineation of Ground-Water Flow Systems in the Southern Great Basin Using Aqueous Rare Earth Element Distributions, Ground Water, 35:5, 807-819

Johannesson, Stetzenbach, KJ, Hodge, VH (1997) Rare earth elements as geochemical tracers of regional groundwater mixing, Cosmochim. Acta, 61:17, 3605-3618

Johannesson, KH, Farnham, IM, Guo, C, and Stetzenbach, KJ (1999) Rare earth element fractionation and concentration variations along a groundwater flow path within a shallow, basin-fill aquifer, southern Nevada, USA, Geochim. Et Cosmochim. Acta, 63:18, 2697-2708

McCarthy, JF, Stafford, Pl, and Toran, LE, 1996, Colloid-facillitated field-scale transport of lanthanides and actinides in fractured saprolita. EOS 77, F212

McLennan, S M, Nance, W B, and Taylor, SR (1980) Rare earth element-thorium correlations in sedimentary rocks, and the composition of the continental crust. Geochim. Cosmochim. Acta, 44, 1833-1839

Nozaki, Y, Lerche, D, Alibo, DS, and Snidvongs, A (2000) The estuarine geochemistry of rare earth elements and indium in the Chao Phraya River, Thailand, Geochim. Et Cosmochim. Acta, 64, 3983-3994

Piper Z, (1974) Rare earth elements in the sedimentary cycle: A summary, Chemic. Geol., 14, 285-304

Shields, GA, and Webb, GE (2004) Has the REE composition of seawater changed over geological time? Chem. Geol, 204, 103-107

Sholkovitz, ER, (1988) Rare earth elements in the sediments of the North Atlantic Ocean, Amazon Delta, and East China Sea: Reinterpratation of terrigenous input patterns to the Oceans. Amer. J Of Science, 288, 236-281

Sholkovitz, ER, Shaw, TJ, and Schneider, Dl (1992) The response of rare earth elements to seasonal anoxia in the water column and pore waters of Chesapeake Bay, Geochem et Cosmochem Acta 56, 3389-3402

Smedley, PL, (1991) The geochemistry of rare earth elements in groundwater from the Carnmenellis area, southwest England. Geochim Cosmochim. Acta, 55, 2767-2779

Taylor SR and McLennan SM (1988) The significance of the rare earths in geochemistry and cosmochemistry. In Handbook on the Physics and Chemistry of the Rare Earths. Vol. 11 (ed. KA Gschneidner, Jr, and L Eyring), pp. 485-497. Elsevier

Whitney, P H, and Olmsted J M (1998) Rare earth element metasomatism in hydrothermal systems: The Willsboro-lewis wollastonite ores, New York, USA, Geochem. et Cosmochem. Acta, No 17, pp 2965-2977

Zhang, J, and Nozaki, Y (1996) Rare earth elements and yttrium in seawater: ICP-MS determinations in the East Caroline, Coral Sea, and South Fiji basins of the western South Pacific Ocean, Geochim et Cossmochim Acta 60, 4631-4644

Hydrochemical study of metals in the groundwater of the wider area of Koropi

K. Pavlopoulos[1], I. Chrisanthaki[1], M. Economou – Eliopoulos[2], S. Lekkas[2]

[1]Harokopio University, Geography Department

[2]University of Athens, Department of Geology and Geoenvironment

Abstract Groundwater samples collected twice, during March-April 2009 (wet period) and in November 2009 (dry period), from two aquifer systems, the karstic and granule type, covering the wider area of Koropi, and springs were analyzed for the elements As, Cd, Cr, Li, Se, B, Fe, Tl, U, Zn, K, Na, Ca, Mg, Si, S by ICP-MS. The analytical data presented showed a small temporal variability and a significant variation in the Na, Ca, B, As, Li and Se concentrations in both aquifers. The range of B (1-4300 μg/L), As (0.5 - 68 μg/L, Se (0.13 - 230 μg/L) concentrations exceed often the recommended limits for drinking water (10 μg/L). A salient feature is that the Na-enrichment is accompanied by As, Se, Li and Cl and the very good positive correlation between the former and the latter elements. The recorded salinization (sea-water contribution to the aquifers) is attributed to their over exploitation. In general, the evaluation of the chemical characteristics of both aquifers and the lack of any correlation with Cr and Mg point to water contamination by anthropogenic activities rather than of natural sources. Therefore, industries should follow regulate for the restriction of heavy metal releases into the environment, and citizens should be informed about the potential risk for diseases connected with the use of water from drilling wells and the Loumparda springs.

1 Introduction

The encumbering of the Attica aquifer with toxic metals has been studied by many researchers (Economou-Eliopoulos et al. 2011; Ihyane and Lekkas 2008; Vasilatos et al. 2010; Vasilatos et al. 2008; Chrisanthaki 2010). The problem of high toxic concentration in the ground-water due to the Industrial activity at the area of Koropi is dated since March 2004 and it is extended into a wide region. Groundwater samples were collected from 29 domestic and irrigation wells covering the wider area of Koropi. The objective of the present study was the assessment of the groundwater contamination by heavy metals. The presented data concerning samples collected during March-April 2009 (wet period) and in November 2009 (dry period); aim to define a probable temporal variability.

N. Lambrakis et al. (Eds.), *Advances in the Research of Aquatic Environment, Vol. 2*
DOI 10.1007/978-3-642-24076-8,

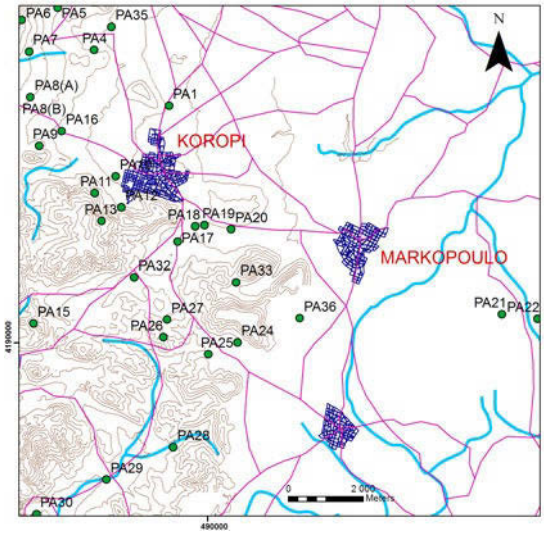

Fig. 1. Map Plaka – Koropi area with groundwater drillings.

2 Hydrogeologic characteristcs of the basin and sampling

Two systems can be distinguished at the area of Koropi: a. the post-alpine formation and b. the limestone system (Lekkas 2003). The granular aquifer extending into the wider area of Koropi-Markopoulo-Paiania-Spata (Giannoulopoulos 2006) is developed within Quaternary and Neogene deposits reaching a depth more than 60m (Lekkas 1993). The supply of the granular aquifers is considered to be directly related with the rainfall water.

The karstic-type aquifer is located within the lower Ymittos unit, consisting of marbles and dolomites, and the Vari-Kiros unit, flowing into the coastal and underwater springs (Loumparda springs at the NW of the Aghia Marina). The karstification continues into a depth exceeding 130 m, while the ground-water capacity is found to vary from 80-150 m, depending on the altitude (Lekkas 1993). The capacity of the drilling works is clearly higher than that of the overlying granular formations. The drillings wells of that type are labeled as PA4, PA7, PA8 (A), PA9, PA19, PA20, PA25, PA27, PA28, PA29, PA35 and PA36. The drillings wells concerning the karst type are coming from the area west, south and east of the city of Koropi area and are labeled as PA1, PA5, PA6, PA8(B), PA10, PA11, PA12, PA13, PA15, PA17, PA18, PA21, PA22, PA24, PA26, PA30, PA32 and PA33.

Table 1. The concentrations of major and trace elements in ground water in the wider area of Koropi (sample collection April 2009).

	As*	Cd*	Cr*	Li*	Se*	Zn*	Fe*	B*	Tl*	U*	Ca**	Na**	K**	Mg**	Si**	S**	Cl**[1]
PA1	11	<.5	16	23	11	<.5	25	180	<1	2	140	340	8	70	11	50	340
PA4	4	<.5	11	5	3	<.5	<10	90	<1	1	130	90	3	40	8	30	170
PA5	2	<.5	8	2	2	<.5	<10	70	<1	<1	130	60	2	15	5	20	130
PA6	2	<.5	9	2	3	<.5	10	50	<1	<1	110	90	3	26	4	10	280
PA7	2	<.5	15	2	2	15	<10	30	<1	1	2	200	<1	6	6	20	120
PA8-A	1	<.5	9	1	<5	5	<10	<.5	<1	<1	50	10	1	6	2	10	90
PA8-B	2	<.5	10	3	2	404	<10	1.5	<1	1	90	20	1	40	6	10	120
PA9	6	<.5	8	11	10	<.5	53	121	<1	1	130	320	11	70	6	40	410
PA10	3	<.5	11	7	2	20	27	3	<1	<1	110	60	1	27	3	20	110
PA11	6	<.5	11	6	8	220	11	100	<1	<1	130	260	9	40	5	20	680
PA12	7	<.5	11	5	8	1080	38	210	<1	<1	180	270	9	40	7	30	670
PA13	3	<.5	8	3	4	5	51	40	<1	<1	160	90	2	20	8	20	190
PA15	9	<.5	10	2	11	<.5	11	110	2.4	1	110	330	8	80	9	30	320
PA16	2	<.5	8	2	2	<.5	18	60	<1	1	130	60	5	40	3	30	100
PA17	13	<.5	17	5	6	<.5	<10	110	<1	1	120	200	6	50	8	30	
PA18	5	<.5	14	9	6	1	83	210	<1	<1	180	180	3	80	5	50	1080
PA19	17	<.5	10	18	16	4	21	130	<1	<1	70	430	6	110	9	20	470
PA20	4	<.5	10	16	7	<.5	47	400	<1	<1	190	180	3	60	3	50	190
PA21	3	<.5	9	3	3	<.5	12	40	<1	<1	160	80	2	20	8	20	190
PA22	8	<.5	9	3	2	<.5	26	40	<1	1	140	60	1	20	5	20	280
PA24	7	<.5	7	4	5	1	<10	40	<1	1	110	100	3	30	9	20	790
PA25	9	<.5	9	8	15	<.5	94	130	<1	3	120	410	14	70	5	40	990
PA26	9	<.5	10	10	16	5	43	140	<1	<1	120	430	20	80	5	40	110
PA27	1	<.5	10	4	2	5	25	70	<1	<1	110	7	1	30	4	20	
PA28	23	<.5	27	14	29	5	100	250	<1	<1	170	810	30	110	7	80	1850
PA29	22	<.5	19	17	30	5	184	264	<1	<1	1830	830	30	110	6	90	710
PA32	10	<.5	13	11	11	5	<10	720	<1	<1	140	290	10	60	5	20	130
PA33	2	<.5	11	3	3	540	14	190	<1	<1	120	60	2	30	6	10	3500
PA30	54	<.5	21	40	88	5	128	9	<1	<1	240	280	83	280	5	210	260
PA35	7	<.5	23	5	4	<.5	<10	100	<1	<1	150	130	4	30	6	30	140
PA36	6	0.11	12	2	3	395	39	30	<1	<1	140	50	3	20	6	20	
KYA Y2	10	5	50		10												250

* units: μg/L, ** units: mg/L

[1] Chloride after Repapis et al. (2010)

Table 2. The concentrations of major and trace elements in ground water in the wider area of Koropi (sample collection November 2009).

	As*	Cd*	Cr*	Li*	Se*	Zn*	Fe*	B*	Tl*	U*	Ca**	Na**	K**	Mg**	Si**	S**
PA1	11	<.5	19	39	9	2000	<10	210	<.1	3	140	390	10	80	13	70
PA4	2	<.5	10	7	3	4000	46	90	<.1	1	130	100	4	50	9	30
PA5	1	<.5	11	5	3	2000	<10	120	<.1	1	140	120	5	30	7	30
PA6	1	<.5	10	5	3	1000	<10	70	<.1	<.1	110	110	4	30	5	20
PA8-A	1	<.5	5	2	1	14	<10	20	<.1	<.1	50	6	.9	7	2	10
PA8-B	2	<.5	8	3	2	1000	23	30	<.1	1	90	30	1	40	7	20
PA10	1	<.5	10	12	1	1000	<10	140	<.1	1	10	60	1	30	11	20
PA11	5	<.5	26	12	7	1000	<10	190	<.1	<.1	120	310	11	50	6	50
PA12	5	<.5	16	10	7	2000	<10	270	<.1	<.1	220	300	11	50	7	60
PA13	5	<.5	18	22	14	1000	<10	310	<.1	1	150	580	24	70	4	80
PA15	5	<.5	21	22	7	374	<10	160	6	11	90	300	12	80	10	50
PA16	1	<.5	6	2	1	1.2	<10	70	<.1	1	80	30	5	30	8	30
PA17	7	<.5	21	10	1	14	<10	170	<.1	1	90	200	6	60	10	50
PA18	5	<.5	37	16	1	<.5	<10	320	<.1	2	150	180	4	90	12	80
PA19	8	<.5	15	24	12	<.5	<10	330	<.1	2	120	530	18	110	8	80
PA20	5	<.5	16	27	1	2000	<10	500	<.1	1	180	186	4	60	10	70
PA21	2	<.5	7	3	1	1000	<10	40	<.1	<.1	150	40	1	10	5	30
PA22	6	<.5	7	5	2	<.5	<10	50	<.1	1	70	60	1	20	7	20
PA24	8	<.5	5	6	4	<.5	<10	60	<.1	2	80	110	3	30	7	20
PA27	1	0.5	9	6	1.2	3000	<10	100	<.1	1	120	70	.9	30	9	20
PA29	13	<.5	26	35	23	12	<10	520	<.1	2	160	100	40	10	8	150
PA30	68	<.5	58	204	213	<.5	<10	4300	<.1	3	430	860	327	10	4	1300
PA32	9	<.5	24	20	9	<.5	<10	310	<.1	1	120	350	13	70	9	90
PA33	4	<.5	7	4	2	<.5	<10	50	<.1	2	70	70	3	30	8	20
PA36	6	<.5	7	3	3	1000	<10	50	<.1	1	160	80	3	20	9	30
KYA Y2	10	5	50		10		2000						500	17	5	
ACME Std	43	148	382	22	25	464	403	19	20	56	21	9.29	0.95	5.8	0.36	8

* Units: μg/L, ** units: mg/L

3 Method of the water analysis

The water samples were analyzed for As, Cd, Cr, Li, Se, B, Fe, Tl, U, Zn, K, Na, Ca, Mg, Si, S using Inductively Coupled Plasma Mass Spectroscopy (ICP-MS) at Analytical Laboratories Ltd in Canada. The re-testing of measurements for several samples (all elements) was found highly satisfactory and in accordance to international standard.

4 Geochemical results

The analytical data presented exhibit a significant variation in several elements. More specifically, the Na concentration exhibits a wide variation in both aquifers, granular and karstic-type of the area of Koropi, as is exemplified on the triangular diagram Na-Ca-Mg (Fig. 2), in contrast to the typical karst-type aquifer of Mavrosouvala (Vasilatos et al al. 2008).

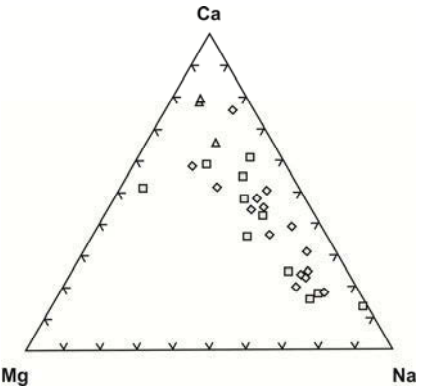

Fig. 2. Triangular diagram Ca-Mg-Na. The diamonds represent the karst aquifer and the squares the granular aquifers of Koropi. The triangles represent the Mavrosouvala wells (after Vasilatos et al. 2010).

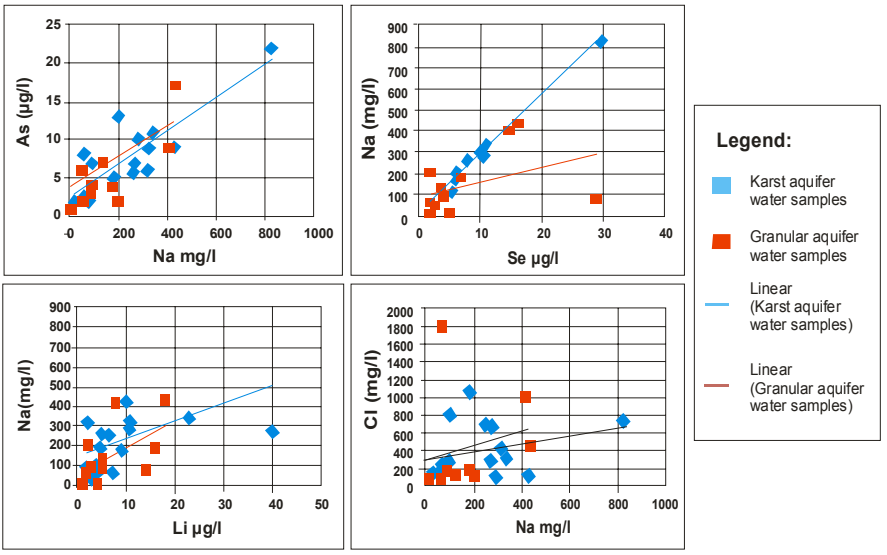

Fig. 3. Plots of As vs Na, Li vs Na, Cl vs Na and Se vs Na (samples collection April 2009).

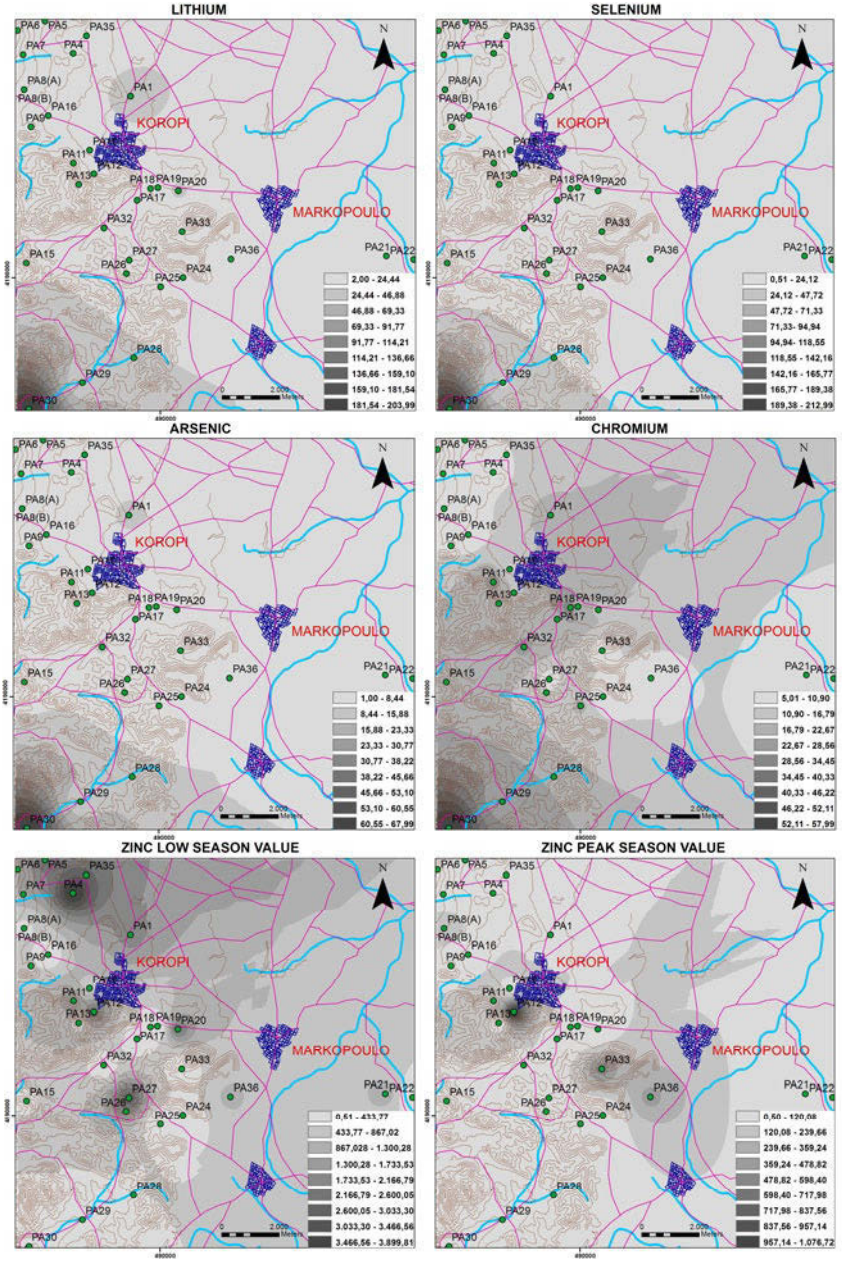

Fig. 4. Distribution of heavy metal in groundwater from the wider Koropi region.

The concentration of arsenic ranges from 0.5 to 68 μg/L, although average (7.1 μg/L during low season, and 8.4 μg/L, during peak season) are below the permeable limit for potable water (10 μg/L). The concentration of selenium ranges from

0.13 to 230 μg/L (average 13 μg/L, low season) and 10 μg/L, peak season) exceeding the recommended limit for drinking water (10 μg/L). A salient feature is that the Na-enrichment is accompanied by As, Se, Li and Cl and the very good positive correlation between the former and the latter elements (Fig. 3).

The concentration of total chromium (Cr), varies from 5 to 58 μg/L, with average value 16 μg/L (low season). Although higher values than the permeable limit for total Cr in drinking water (50 μg/L) were determined, they are lower than those determined by Giannoulopoulos (2006) during 2005-2006 in drilling wells west of Koropi (Fig. 4) reaching values up to 110 μg/L. The Zn concentration varies from 0.5 to 3900 μg/L with average value 960 μg/L (low season) and lower than detection limit to 1080 μg/L with average value 90 μg/L (peak season). Zinc is characterized by a negative correlation with other elements, while any significant correlation between Zn and Cl in both aquifers was not recorded. The spatial distribution of zinc (Fig. 4) indicated that the elevated values in both aquifers were recorded at the area around the city of Koropi. Uranium and thallium concentrations are low. However, in certain well (drilling PA15) at the north-northwest part of the area of Koropi there is a significant increase, in particular during low season (Tables 1, 2; Fig. 4).

5 Conclusive remarks

Assuming that the chemical composition of the water is affected by the interaction between water and rocks and the sea water contribution into the groundwater aquifer, the presented analytical data for the period of the sample collection (Tables 1 and 2), the inter-element correlations (Fig. 3) and their distribution (Fig. 4) provide evidence for the assessment of the heavy metal contamination, their source and the degree of the water salinization (contribution of sea-water). Since the concentrations of Na, Cl, as, Se, Li and B are elevated in the sea-water (Rose et al., 1979) the relatively high concentrations in several drilling wells from the area of Koropi may indicate a major contribution of sea-water to both aquifers, due probably to their over exploitation. Although the occurrence of ophiolite rocks are components of the geological formations in wider area of Koropi and their interaction with water could be a source for Cr in water, the chemical characteristics of both aquifers (Tables 1, 2) and the lack of any correlation with Cr and Mg point to the water contamination by anthropogenic activities rather than a naturals source.
Furthermore research is required at the area of Koropi, including monitoring of ground water, a systematic study of the soil-plants composition, as a part of the food-chain in order to evaluate the potential risk for diseases connected with the use of water from drilling wells and Loumparda springs, and the food. It is necessary, the citizens to be informed that the drilling water should not be used, and the industries should follow regulate for the restriction of heavy metal releases into the environment.

References

Chrisanthaki I (2010) Hydrogeological and Hydrochemical Study of the Toxic Metals Behavior in the Wider Area of Koropi MSc thesis – Harokopio University

Giannolopoulos P (2006) Hydrogeological – hydrochemical research of qualitative burdening of underground waters of wider region of Koropi, Inst Geol and Miner. Explor., Athens

Economou-Eliopoulos M, Megremi I, Vasilatos Ch (2011) Factors controlling the heterogeneous distribution of Cr (VI)in soil, plants and groundwater: Evidence from the Assopos basin, Greece Chemie der Erde 71, 39-52

Ihyane B, Lekkas S (2008) Degradation anthropogene de la nappe karstique de la region de Mesogeia (Attique, Grece), 8th International Hydrogeological Congress of Greece, pp. 22-27

Lekkas, S (1993) Hydrogeological observations in the area of Mesogia, deltio EGE XXVIII/3, 309-322

Repapis, E, Repapis N, Skourlis G, (2010) Hydrochemical observations in underground water in the surrounding area of Koropi. Diplomatic paper, University of Athens

Rose, W, Hawkes, E, Webb, S., (1979) Geochemistry in Mineral Exploration, 2nd ed. Academic Press

Vasilatos Ch, Megremi I, Economou- Eliopoulos M, and Mitsis I, (2008) Hexavalent chromium and other toxic elements in natural waters in the Thiva – Tanagra – Malakasa Basin, Greece, Hellenic Journal of Geosciences 43, 57-66

Vasilatos Ch., Megremi I. and Economou-Eliopoulos M., (2010). "Geochemical characteristics of natural waters contaminated by hexavalent chromium, in Eastern Sterea Hellas, Greece", XIX Congress of the Carpathian Balkan Geological Association, Thessaloniki, Greece, vol. 99, p. 347-353

Factors controlling major ion and trace element content in surface water at Asprolakkas hydrological basin, NE Chalkidiki: Implications for elemental transport mechanisms

E. Kelepertzis[1], A. Argyraki, E. Daftsis

[1] Corresponding author: Section of Economic Geology and Geochemistry, Faculty of Geology and Geoenvironment, National and Kapodistrian University of Athens, Panepistimiopolis, Zographou 157 84, e-mail: kelepert@geol.uoa.gr

Abstract Chemical characteristics of stream water at Asprolakkas hydrological basin were determined in February 2009 in order to examine the main factors controlling the hydrogeochemistry of the drainage system. A total of 20 surface water samples were collected and analyzed for the major ions K, Na, Ca, Mg, HCO_3, SO_4 and the trace elements Fe, Pb, Zn, Mn, Cu, Ni, As, Sb, Mo and Ba. The application of R-mode factor analysis revealed that the polymetallic carbonate replacement type sulfide deposits, together with the porphyritic intrusions and the associated porphyry copper style mineralization, occurring in the studied area, impose fundamental control on the water chemistry. A third influencing factor includes the parameters As and HCO_3 and is attributed to the competitive behavior of As and bicarbonate ions, for filling in available absorption space on Fe(III) oxides. SEM-EDS methods, performed on retained filters from the filtration of representative water samples, showed that Pb is mainly transported by fine particulate matter. The chemical elements Mn, Zn, Mo and Sb are predominantly present as dissolved free ions, and correlate strongly with the electrical conductivity of the water samples.

1 Introduction

Mineral deposit regional geology and geochemical processes are fundamental controls on the surface water quality (Kelley and Taylor 1997). Apart from the very mobile and bioavailable dissolved forms of trace metals, suspended particulate matter and colloids are significant metal carrier phases. Colloids are particles that have at least one dimension in the size range of 1-1000 nm, and due to their small size they have a large specific surface area. These physical properties make colloids to have a significant impact on the transport of trace metals through sorption

N. Lambrakis et al. (Eds.), *Advances in the Research of Aquatic Environment, Vol. 2*
DOI 10.1007/978-3-642-24076-8,

mechanisms (Kretzscmar and Schäfer 2005). They are also believed to be as reactive as suspended particulates and as mobile as dissolved solutes.

The present study aims to investigate the main factors that govern the hydrogeochemistry of running streams located at the mineralized wider area of Stratoni in NE Chalkidiki peninsula. Some general surface water quality characteristics and transport mechanisms of potentially toxic elements are also discussed.

2 Description of the study area

Geologically the study area consists of the metamorphic rocks of Vertiskos and Kerdylian geotectonic units, separated by the NW-SE trending Stratoni-Varvara fault (Fig. 1).

The main lithological types are represented by gneiss and amphibolites while Kerdylian sequence also comprises several marble horizons (Kockel et al. 1977), outcropping at the northern part of the area. The lower part is underlain by alluvial and Pleistocene deposits. The rocks have been intruded by Tertiary magmatic calc-alkaline granitoids, represented by the Stratoni granodiorite and the porphyritic intrusions of Skouries and Fisoka. Various ore deposits in the area are strongly related to the Tertiary intrusive bodies, including the Pb-Zn-Ag carbonate hosted replacement ore bodies of Madem Lakkos and Mavres Petres, the Piavitsa mixed sulfide and manganese ore deposits and the porphyry Cu-Au deposits at Skouries and Fisoka areas (Kalogeropoulos et al. 1989, Eliopoulos and Economou-Eliopoulos 1991).

The region is characterized by semi mountainous relief, typically around 300 m ASL, and by a well developed dendritic style drainage network. The average pluviometry in the catchment area is 650 mm and the flow rates of the streams present strong variations. From a hydrological point of view, the studied streams are flowing within the sub-basins of Piavitsa, Kerasia and Kokkinolakkas (Fig. 1). They all discharge (their waters) in Asprolakkas stream which has an E-W direction flowing towards the north part of Ierissos Gulf.

The current mining activity carried out in the Kassandra metallogenic province is represented by the exploitation of the Mavres Petres sulphide ore deposit whereas one of the future mine development plans is the Skouries project.

3 Sampling and analytical procedure

Water sampling was carried out in February 2009 under high flow conditions. A total of 20 samples were collected, preferably near stream confluences (Fig. 1).

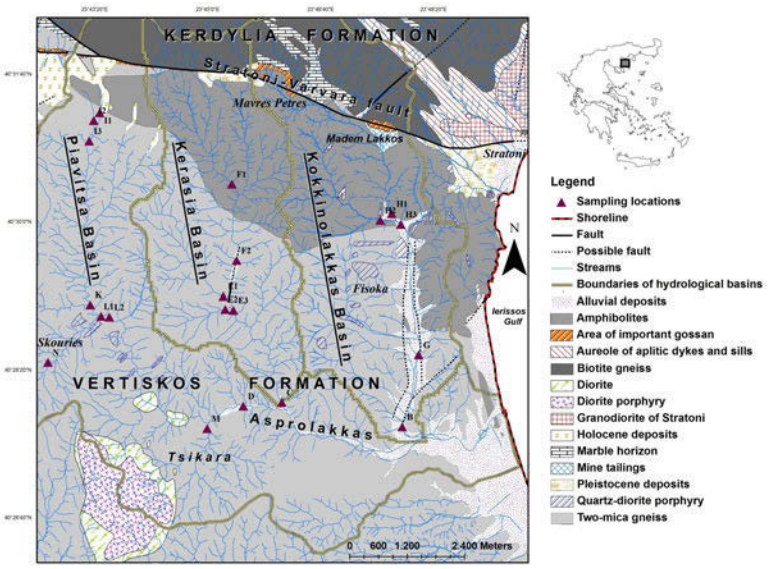

Fig. 1. Geological map of the study area showing sampling locations and hydrological catchments (after Kockel et al. 1977).

Special care was taken in order to ensure that the majority of streams that contribute to Asprolakkas hydrogeochemistry was sampled. Sample N represents water discharged by the old exploration adit of Skouries deposit.

Major physicochemical parameters such as pH and electrical conductivity were determined in the field. Samples were filtered with 0.45 μm membrane filter for the analysis of anions (HCO_3^-, SO_4^{2-}). Moreover, samples for major cations (K^+, Na^+, Ca^{2+}, Mg^{2+}) and metals (Fe, Pb, Zn, Mn, Cu, Ni, As, Sb, Mo, Ba) were filtered immediately in the field through 0.45 μm Millipore filters and acidified down to pH<2. Potassium, Na, Ca and Mg concentrations were determined by Inductively Coupled Plasma Emission Spectroscopy (ICP/AES) and SO_4 was measured gravimetrically as $BaSO_4$ (Laboratory of Quality Control of "Hellas Gold SA" at Stratoni). Heavy metals and metalloids were measured by Atomic Absorption Spectroscopy and Inductively Coupled Plasma Mass Spectroscopy (ICP/MS) at the Laboratory of Economic Geology and Geochemistry (Faculty of Geology and Geoenvironment, University of Athens) and the ACME Analytical Laboratories Ltd of Kanada. Quality control was performed by analysis of certified reference materials for trace element content verifying the good accuracy of the analytical results.

In order to identify metal bearing phases that are transported with the water flow as suspended particulate matter and colloidal particles with size greater than 0.45 μm, the filters retained by the filtration of 3 representative samples were examined by scanning electron microscope (SEM), equipped with an energy dispersive X-Ray spectrometer for microanalysis (EDS, Oxford LINK ISIS 300).

4 Results and Discussion

4.1 General water quality characteristics

A summary of the basic statistics of the chemical characteristics for the collected waters is shown in Table 1. The pH values remain constant for all the streams, displaying neutral to slightly alkaline conditions. Potassium and Na are found in low concentrations, deriving from the dissolution of biotite/muscovite and albite respectively, abundant in the geological formations of the study area. Chemical parameters such as Ca, Mg, HCO_3, SO_4, Fe, Pb, Zn, Mn, Ni, As and Sb present great variability among the examined samples.

Table 1. Basic descriptive statistics of the measured parameters for the collected waters from Asprolakkas watershed (February 2009).

	Number of samples	Mean	Median	Standard deviation	Min	Max
pH	20	8.1	8.1	0.2	7.6	8.5
EC (μS/cm)	20	602	463	314	328	1416
K (mg/L)	20	3	3	2	1	8
Na (mg/L)	20	13	13	4	7	20
Ca (mg/L)	20	79	64	44	40	191
Mg (mg/L)	20	25	17	17	11	68
HCO_3 (mg/L)	20	169	172	40	79	230
SO_4 (mg/L)	20	165	82	207	28	705
Fe (μg/L)	11	80	13	159	10	681
Pb (μg/L)	20	13	9	12	3	57
Zn (μg/L)	20	200	14	386	4	1150
Mn (μg/L)	20	1151	35	2443	3	7899
Cu (μg/L)	20	2	2	1	1	5
Ni (μg/L)	12	17	7	18	0.5	50
As (μg/L)	20	28	19	28	4	130
Ba (μg/L)	20	13	15	8	2	30
Mo (μg/L)	20	4	0.6	5	0.5	14
Sb (μg/L)	20	4.1	2.5	5	0.5	16

Kelepertzis et al. 2010 studied surface water quality within the Asprolakkas watershed during one hydrologic year and reported that each one of the studied basins displays its own hydrogeochemistry and dissolved contaminant concentrations. Samples H1, H3, G and B from Kokkinolakkas were plotted in the region of

Ca-SO_4 water type on a Piper diagram, reflecting the influence of the polymetallic sulfide deposits exploited at Mavres Petres and Madem Lakkos areas.

On the contrary, stream waters from Kerasia and Piavitsa fall within the Ca-HCO_3 type and present significantly lower Ca, Mg, SO_4, Zn, Mn, Ni and Sb values. Sample M drains the geological formations comprising the diorites and diorite porphyries southwards of Asprolakkas stream, and as a result it displays a Ca-SO_4 water type (Kelepertzis et al. 2010). Both of Piavitsa and Kerasia water samples are characterized by Pb and As values higher than the European Union limits (EU Council Directive 98/83/EEC). The geochemical behavior of those elements is discussed later.

Iron concentrations for a noticeable number of samples are below the detection limit of the analytical technique (10 μg/L), whereas the measured concentrations in all the collected waters are considered low. This is expected bearing in mind the slightly alkaline pH conditions prevailing in the studied drainage system. A few isolated elevated Fe values (samples H1, H3 and F2) are possibly explained by the presence of Fe rich colloids that passed through the used 0.45 μm pore-size membranes filters (Kimball et al. 1995).

4.2 Application of R-mode factor analysis

With the aim of determining the main factors that control the chemistry of the stream waters, factor analysis was applied to the data (Table 2). Factor analysis characterizes different groups of chemical elements with approximately similar geological and geochemical patterns. The three factor model explaining 86% of the data variability was deemed appropriate for the obtained data. Iron and Ni were excluded from the application since a remarkable number of samples is characterized by concentrations below the detection limit of the analytical technique.

The most significant Factor, accounting for 51% of the total variance, reflects the signature of the massive sulfide carbonate replacement type mineralization of the area. This factor includes elements such as Ca and Mg that originate from the dissolution of the gangue minerals (calcite, dolomite), whereas SO_4 and metals derive from the sulfide minerals of the mineral deposits, and their oxidation products. Additionally, the participation of electrical conductivity with high factor loadings denotes that potentially toxic elements like Zn, Mn, Mo and Sb are primarily present as dissolved free ions. Surprisingly, Pb is not involved in this factor, despite its strong association with the sulfide deposits. Various authors have demonstrated that Pb is scavenged by iron oxide colloids and transported on their mineral surfaces in many water systems (e.g Hassellöv and Kammer 2008). These particles can be of such low diameter that they can be easily pass through conventional 0.45 μm membrane filters, mainly comprising ferrihydrite and schwertmannite at high and low pH conditions respectively. Thus, the low positive factor loadings of Pb in Factor 1, which consists of dissolved form of metals.

Table 2. Varimax component loadings of three factors, communality and percentage of variance explained for the analyzed parameters.

Variable	Factor 1	Factor 2	Factor 3	Communality
EC	0.94	-0.28	-0.05	0.97
K	0.06	-0.92	-0.13	0.87
Na	0.76	-0.20	0.15	0.64
Ca	0.95	-0.22	-0.04	0.95
Mg	0.88	-0.32	0.02	0.87
SO_4	0.94	-0.22	-0.18	0.96
HCO_3	-0.39	0.03	0.80	0.79
Pb	0.32	-0.76	0.30	0.76
Zn	0.96	-0.08	0.02	0.91
Mn	0.96	-0.15	-0.11	0.96
Cu	0.30	-0.79	0.07	0.71
As	0.36	0.09	0.88	0.92
Sb	0.88	0.00	0.31	0.86
Ba	0.07	-0.87	-0.42	0.94
Mo	0.69	-0.59	-0.04	0.83
% Variance	50.6	23.3	12.4	86.4

The second factor, explaining 23% of the total variability, contains negative factor loadings for K, Cu, Ba, Pb and Mo, and indicates the influence of the porphyritic intrusions of Skouries and Fisoka areas on the chemistry of the examined streams. Intense potassic alteration halo, characteristic of the high-grade ore, and porphyry Cu mineralization are strongly associated to the Tertiary intrusive bodies, whereas the Skouries stock also exhibits unusual high Ba concentrations (Eliopoulos and Economou-Eliopoulos 1991). Galena representing the primary source of Pb, is found in the peripheral parts of the alteration haloes within the country rock basement, mainly in the propylitic zone. Molybdenum is a typical metalloid that accompanies many porphyry copper deposits around the world.

Finally, the third factor, accounting for 12% of the total variance, is controlled by HCO_3 and As, and signifies that the elevated concentrations of As in the studied water samples can be attributed to its desorption/release from the Fe(III)-hydroxides, due to the competitive behaviour of bicarbonate ions. Adsorption and desorption reactions between arsenic and ferric oxide mineral surfaces are considered the most important factors controlling the concentrations of dissolved As (Cheng et al. 2009). Bicarbonate ions adsorb onto hydrous ferric oxide particles, reducing in that way arsenic removal by adsorption phenomena onto the previously mentioned oxides.

4.3 Membrane filter SEM observations

The examination of filters retained by the filtration of water samples H1,B and C revealed that particulate material is characterized by grains of Fe and S, enriched in Pb, As and Zn. It has been suggested that Pb can be removed in sulfidic environments by surface adsorption onto FeS particles and that sulfides compete with hydrous iron oxides to scavenge Pb (Taillefert et al. 2000). Additionally, filters from Kokkinolakkas stream are dominated by Pb oxidized particles (size< 3 μm), containing traces of Zn, Cu, As and Sb, and by sulfate oxidized phases of Pb and Zn (size 1-2 μm), comprising As and Sb. Fragments of probably pyrite and arsenopyrite (size> 10 μm) deriving from the mineral deposits, located upstream of the sampling locations, were routinely identified.

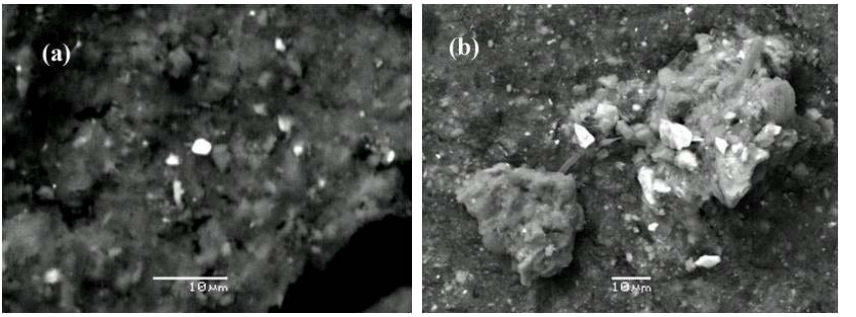

Fig. 2. Back-scattered microphotographs from the retained filters: a) Pb-Fe-S particle containing traces of Cu and Zn, Pb: 60%, S:10%, Fe:6%, Cu:2%, Zn:1% (sample H1), b) Grains of Fe and S, enriched in Pb and As, Fe: 38%, S: 42%, Pb:3%, As: 2% (sample B).

Figure 2 presents representative photographs from the retained filters, together the semi-quantitative chemical analyses of the corresponding spots. It should be mentioned that particles/phases with size smaller than 1.5 - 2 μm cannot be analysed and identified through SEM-EDS methods.

It becomes obvious that Pb is mainly transported in the particulate phase for Kokkinolakkas stream, a fact that is strengthened remarking the results of chemical analyses for filtered and unfiltered samples (Pb dissolved and Pb total respectively), provided by the Laboratory of Quality Control of Hellas Gold SA (Table 3).

Table 3. Dissolved and total concentrations of Pb in Kokkinolakkas water samples (April 2008).

Sample	Pb Dissolved (μg/L)	Pb Total (μg/L)
H1	5	116
H3	11	148
G	9	48
B	6	83

5 Conclusions

Results of this research clearly demonstrate that the chemistry of stream waters in the studied watershed is mainly governed by the regional geological and mineralogical characteristics. Geochemical processes also play an important role in controlling the environmental behavior of potentially toxic elements, such as Fe, Pb, Zn, Mn, As and Sb. Regarding Konninolakkas stream water, colloids and suspended matter represent a significant transportation pathway for Pb, and to a lesser extent for other metals like As, Cu, Zn and Sb. On the contrary, Mn, Mo, as well as Zn and Sb are mainly transported as free ions, presenting a high affinity for the electrical conductivity of the studied water samples.

References

Cheng H, Hu Y, Luo J, Xu B, Zhao J (2009) Geochemical processes controlling fate and transport of arsenic in acid mine drainage (AMD) and natural systems. Journal of hazardous materials. 165, 13-26

Eliopoulos DG, Economou-Eliopoulos M (1991) Platinum-group element and gold contents in the Skouries porphyry copper deposit, Chalkidiki peninsula, northern Greece. Economic Geology. 86, 74-749

European Union Council (1998) Council Directive on the quality of water intended for human consumption, 98/83/EC. Official Journal of the European Communities. 330, 32-54

Hassellöv M, Kammer FV (2008) Iron oxides as geochemical nanovectors for metal transport in soil-river systems. Elements. 4, 401-406

Kalogeropoulos SI, Kilias SP, Bitzios DD, Nicolaou M, Both RA (1989) Genesis of the Olympia carbonate-hosted Pb-Zn (Au, Ag) sulfide ore deposit, Eastern Chalkidiki peninsula, Northern Greece. Economic Geology. 84, 1210-1234

Kelepertzis E, Argyraki A, Daftsis E, Ballas D (2010) Quality characteristics of surface waters at Asprolakkas river basin, N.E. Chalkidiki, Greece. Bulletin of the Geological Society of Greece. Proceedings of the 12th International Congress, Patra, 1737-1746

Kelley KD, Taylor CD (1997) Environmental geochemistry of shale-hosted Ag-Pb-Zn massive sulfide deposits in northwest Alaska: natural background concentrations of metals in water from mineralized areas. Appl.Geochem. 12, 397-409

Kimball BA, Callender E, Axtmann EV (1995) Effects of colloids on metal transport in river receiving acid mine drainage, upper Arkansas River, Colorado, U.S.A. Applied Geochemistry. 10, 285-306

Kockel F, Mollat H, Walther HW (1977) Erlauterungen zur geologischen Karte der Chalkidiki und angrenzender Gebiete 1:100000 (Nord-Griechenland). Hannover, Bundesanstalt Geowiss, Rohstofee, 119

Kretzschmar R, Schäfer T (2005) Metal retention and transport on colloidal particles in the environment. Elements. 1, 205-210

Taillefert M, Lienemann C-P, Gaillard J-F, Perret D (2000) Speciation, reactivity, and cycling of Fe and Pb in a meromictic lake. Geochimica et Cosmochimica Acta. 64, 169-183

Trace and ultra-trace element hydrochemistry of Lesvos thermal springs

E. Tziritis, A. Kelepertzis

National & Kapodistrian University of Athens, Faculty of Geology & Geoenvironment
e-mail: evtziritis@geol.uoa.gr, Ilissia 157 84, Athens

Abstract The present study examines the hydrochemical characteristics that rise from trace and ultra-trace elements of Lesvos thermal springs. Six main thermal springs were sampled and analyzed extensively for a large set of parameters. The detected concentrations of REE (La, Ce, Nd, Gd, Er, and U) are attributed to specific geochemical processes and environmental conditions, such as complexation, acidic environment and elevated temperatures. The presence of As is related with epithermal sulphide gold mineralization, as well as the presence of Pb, Sb, Cu, Zn and Fe. Germanium is correlated with the existence of Si-rich acid volcanic formations and possibly with Cu-rich sulphide minerals. Thallium is enriched in thermal waters of Lesvos, compared with other geothermal fields, and consists a significant environmental threat for human environment, due to its presence at the majority of the sampled springs which are used for blaneotherapy purposes.

1 Introduction

Lesvos is one of the largest Greek Islands, located in the NE Aegean Sea. Its geological evolution is strongly influenced by the geotectonic setting of the Aegean Sea. The consequent outcome of the primary collision and subduction processes, was the secondary development of intense magmatic activity, which influenced the entire regions of Aegean and Anatolia from Oligocene and onwards (Le Pichon and Angelier 1981). Due to the elevated geothermal gradient of Lesvos with a mean value of 87.1 mW/m^2 (Jongsma 1974), several geothermal researches have been conducted since the late 60's (i.e. Papastamataki and Katsikatsos 1969; Fytikas et al. 1989; Michelot et al. 1993; Bencini et al. 2004). This unique geological environment contributed to the formation of 6 main thermal springs (Argenos, Eftalou, Polychnitos, Lisvori, Therma Geras and Loutra Thermis) (Fig. 1). Most of them have been well known since ancient times due to their healing properties. Regarding the structural geological setting, Lesvos Island is a part of the Pelagonian zone of Inner Hellinides (Katsikatsos et al. 1986).

N. Lambrakis et al. (Eds.), *Advances in the Research of Aquatic Environment, Vol. 2*
DOI 10.1007/978-3-642-24076-8, © Springer-Verlag Berlin Heidelberg 2011

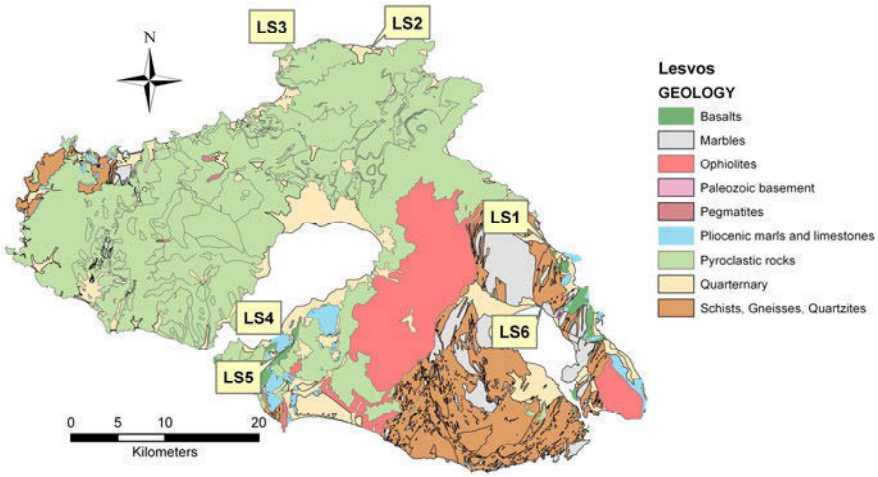

Fig. 1. Simplified geological map of Lesvos (modified by IGME) and thermal springs.

In general, Lesvos is dominated by Miocenic volcanic formations of great thickness which overlie a Paleozoic metamorphic substrate. The autochthonous unit which covers the SE part of the Island is characterized by the presence of an ophiolite-bearing phyllitic basement with embedded marble lenses of low grade metamorphism (Bencini et al. 2004). Several parts of the Island are characterized by the presence of a metamorphic basement which compiles the allocthonous unit, covered by calc-alkaline or shoshonitic volkanics (Pe-Piper 1980) of Miocene age. In the NW part of the Island the dominant geology is consisted of acid pyroclastic rocks, with well preserved forest fossils. Scattered in the island there are outcrops of marine and continental sediments, mainly affected by the extensive tectonics during Miocene (Bencini et al. 2004). Despite the numerous geothermal researches for the hot springs of Lesvos Island, very few of them (Lambrakis and Stamatis 2007) have dealt with trace and ultra-trace element hydrochemistry. Under this scope, the present study aims to contribute to this lack of information by focusing on the hydrochemical conditions that affect thermal springs, regarding their trace and ultra-trace concentrations, as well as the their geochemical signatures.

2 Sampling and analysis

Sampling was carried out during October 2010. Groundwater was taken from the 6 main thermal springs of Lesvos Island (Fig. 1). Samples were filtered on site using Millipore syringe capsules containing 0.45 mm cellulose acetate filters, and afterwards they were preserved with 0.4% ultra pure HNO_3 to acidify the sample pH to 2.0. A duplicate sample was also collected out of 3 of the sampled springs, in

order to evaluate the analytical accuracy. The physicochemical parameters of water temperature and pH were measured in situ. All samples were sealed with crew caps and stored in coolers at 4°C. Water samples were finally air-shipped to ACME Analytical Laboratories (Canada) for trace and ultra-trace element analysis by direct inductively coupled plasma–mass spectrometry (ICP–MS). Analytical precision was determined by duplicates and standardized reference samples. The results are shown on Table 1.

3 Results and Discussion

Interpreting the analytical values of Table 1, Al seems to be enriched in samples LS1 (349μg/L), LS3 (304μg/L) and LS5 (362μg/L), probably due to the weathering of clay minerals such as kaolinite and alunite, which exist at the alteration zones of the Island (Kelepertsis 1993; Vamvoukakis 2009). Boron concentrations are typical for geothermal systems ranging from 1204 μg/L (LS6) to 6000 μg/L (LS3), and exists in aqueous solutions in the forms of $B(OH)^{4-}$ and undissociated boric acid H_3BO_3 (Mather and Porteous 2001). The elements of Ba, Fe, Cu, Pb, Sb, and Zn are associated with the occurrence of sulphide mineralization, and probably their concentrations, apart from the geological source, are controlled by the acidity of thermal waters and the reducing environment (Lambrakis and Stamatis 2007). In general, the higher values for the majority of heavy metals and metalloids appear to be mainly at LS1 (Loutra Thermis) and LS3 (Eftalou), and secondary for some parameters at LS2 (Argenos) and LS5 (Polychnitos). Although samples were analyzed after being filtered, which means that their concentrations are less than at the unfiltered samples (Biddau et al. 2009), they appear to have measurable amounts of trace and ultra-trace elements in μg/L or ng/L quantities. The concentrations for the majority of these elements are higher compared to those of fresh water samples deriving from aquifers with similar geological substrate with the study area (Biddau et al. 2009). Thus, the fluctuation of their concentrations reflects the favourable hydrochemical conditions, in respect to their mobility and solubility. In more details, ultra-trace elements and especially REE are often present in geothermal environments, indicating specific hydrochemical characteristics. Under acidic conditions, REE become mobilized (Neal 2005) while at alkaline environments their absence is significant probably due to their coprecipitation with iron oxyhydroxides.

More specifically regarding LREE the measured elements included La, Ce and Nd. Their concentrations ranged from practically non detectables (below detection limit), up to 5000 ng/L for La at LS2 (Argenos), up to 2000 ng/L for Ce at LS5 (Polychnitos), and up to 2000 ng/L for Nd at LS5 (Polychnitos). The only measured HREE were Gd and Er, with concentrations up to 1000 ng/L at LS1 (Loutra Thermis) and LS2 (Argenos) for Gd, and up to 1000 ng/L at LS1 (Loutra Thermis) for Er.

Table 1. Analytical results of the detected trace and ultra trace elements of Lesvos Thermal Springs, with the addition of pH and temperature values (bdl: below detection limit).

Trace		L.Thermis (LS1)	Argenos (LS2)	Eftalou (LS3)	Lisvori (LS4)	Pol/tos (LS5)	Geras (LS6)
Al	μg/L	349	159	304	212	362	76
As	μg/L	74	56	331	21	67	6
B	μg/L	3996	4252	6000	2665	4474	1204
Ba	μg/L	337	105	358	80.5	340	85.2
Cs	μg/L	775	2354	1358	389	847	10
Cu	μg/L	24	19	20	6	16	2
Fe	μg/L	bdl	1341	1262	bdl	bdl	bdl
Mn	μg/L	116	1116	1336	334	160	4
Ni	μg/L	30	bdl	bdl	bdl	bdl	bdl
Pb	μg/L	27	bdl	15	2	bdl	bdl
U	μg/L	bdl	bdl	bdl	0.3	bdl	2
V	μg/L	bdl	43	23	9	28	bdl
W	μg/L	bdl	bdl	36	17.4	2	bdl
Zn	μg/L	268	bdl	51	78	69	18
Sb	μg/L	27	10	25	2.2	8	bdl
Se	μg/L	0	183	68	22	0	0
Sn	μg/L	bdl	18	bdl	bdl	bdl	bdl
Ge	μg/L	7	5	13	8	7	bdl
Tl	μg/L	26	66	15	2.1	10	1
Gd	ng/L	1000	1000	bdl	100	bdl	bdl
Nd	ng/L	bdl	bdl	bdl	bdl	2000	100
La	ng/L	2000	5000	1000	500	2000	200
Er	ng/L	1000	bdl	bdl	100	bdl	bdl
Gd	ng/L	100	1000	bdl	100	bdl	bdl
Ce	ng/L	bdl	bdl	bdl	100	2000	200
Er	ng/L	1000	bdl	bdl	100	bdl	bdl
Y	ng/L	bdl	bdl	bdl	200	bdl	bdl
pH		6.7	6.4	6.7	6.2	6.4	7.2
T	^{o}C	47	90	45	70	85	40

From the above concentrations can be conducted that LREE seem to prevail at Polychnitos spring, HREE at Loutra Thermis, while Argenos (LS2) contains both. The extent of their mobilization and subsequent fate depends upon a number of factors. These factors include the kinetics of mineral dissolution, surface sorption-desorption mechanisms (e.g. onto iron oxide / hydroxide minerals), ion complexation (e.g. with organic matter) and the degree of acidification and colloidal transport (Johannesson and Zhou, 1999; Gammons et al. 2005). According to Mayano-

vic et al. (2007) the transport of REE ions in hydrothermal fluids is affected by formation of complexes with ligands such as H_2O, Cl^-, CO_3^{2-}, SO_4^{2-} and elevated temperatures of hydrothermal fluids. The elevated temperatures as well as the abundant presence of especially Cl^- and SO_4^{2-}, are similar conditions with those present in Lesvos thermal springs (Bencini et al. 2004), and possible highlight complexation combined with low pH and high temperatures as a major processes for their mobilization.

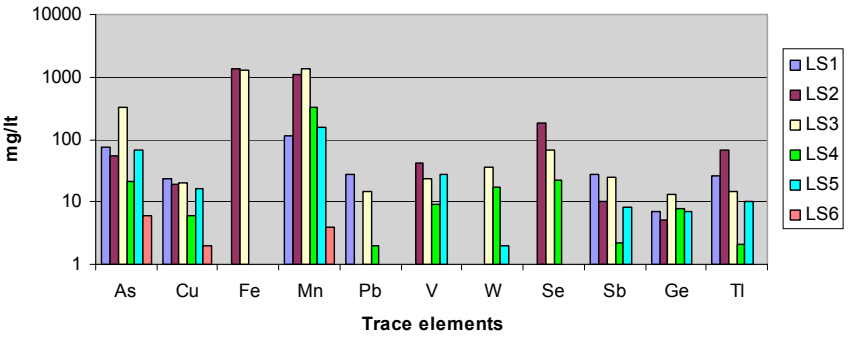

Fig. 2. Comparative diagram of trace element concentrations of Lesvos thermal springs.

Regarding other trace elements, arsenic appears to be less abundant than expected in thermal waters, where in other geothermal systems concentrations reach 500 μg/L (Birkle et al. 2010) and rarely sometimes increase even higher in an order of magnitude to mg/L (Welch and Stollenwerk 2003). Apart from Eftalou spring which has the higher content of As with 331 μg/L, all the others range below 100 μg/L. Nevertheless, compared with other thermal waters across Greece, arsenic concentrations of Lesvos are much higher than those reported for Santorini, which reach the maximum concentration of 16 μg/L (Varnavas and Cronan 1988), and similar to those of Edipsos thermal springs, which range from 44 to 84 μg/L (Kelepertsis et al. 2009). The differences at the concentrations of arsenic may be attributed at two main factors. Firstly, due to bedrock geology as northern Lesvos is characterized by epithermal gold deposits which are accompanied by elevated concentrations of As (Kelepertsis 1993). Secondly, quite important are the differential redox environments, as arsenic is readily mobilized in anaerobic conditions with increased H_2S content (Smedley and Kinniburgh 2002). A further interesting note for arsenic is its positive correlation (see Table 3) with Tl (r^2 = + 0.78). The latter is abundant in Lesvos thermal waters, compared to other geothermal fields (Valentino and Stanzione 2003). This correlation and subsequently the Tl enrichment is frequently observed at arsenic gold deposits (Percival and Radtke 1993), similar to this of study area, and in general may be attributed to weathering of Tl-As sulphide minerals, such as lonardite ($TlAsS_2$) (Xiao et al. 2004).

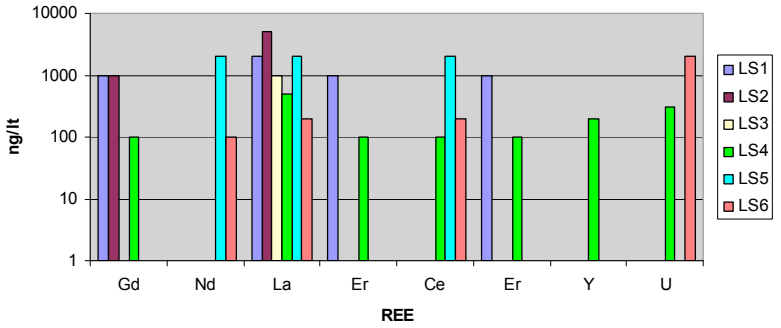

Fig. 3. Comparative diagram of REE concentrations of Lesvos thermal springs.

According to Valentino and Stanzione (2003), thallium's mean concentration at geothermal systems is about 10 μg/L. Taken into account that three of the samples (LS1, LS2, LS3) appear to have concentrations greater than the mean value; Tl is enriched at Lesvos springs. Its presence is normally associated with sulphide minerals and is often found in mineralized areas interspersed with sulphide deposits (Zitko 1975), similar of Lesvos. Thallium generally exists in natural waters as the species Tl^{+} and Tl^{3+}, but the Tl^{+} species is dominant in the aqueous environment (Vink 1993). What is of special concern about Thallium is the fact of being more acutely toxic than Hg, Cd, Pb, Zn and Cu in mammals (Cheam 2001). Thallium intake by humans, apart from drinking water, could be made through skin absorption and mucous membranes, which is widely distributed throughout the body and accumulates in bones, renal medulla and, eventually, in the central nervous system (Peter and Viraraghavan 2003). The latter detail is crucial considering the blaneotherapy activities of Lesvos thermal springs. In more details, all of the sampled springs except from LS2 (Argenos) are used for spa purposes, and the significant Tl values in some of them (LS1, LS3 and LS5) consist possibly a major threat for human environment, under long term exposure conditions. Finally, germanium is detectable in all samples apart from LS6 (Geras), with a maximum measured concentration (13 μg/L) at LS3 (Eftalou). The above values as well as the rest of them, fall into the range of Ge mean concentrations (1-15 μg/L) for geothermal systems (Arnorsson 1984). Germanium presence in thermal waters is correlated with sulphide deposits, and its presence in geothermal aqueous systems is mainly with the form of germanic acid, which is both expressed as H_2GeO_3 and H_4GeO_4 (Arnorsson 1984). More specifically, germanium occurs in hydrothermal systems along with rare copper sulphide minerals, in the forms of renierite $(Cu,Zn)_{11}(Ge,As)_2Fe_4S_{16}$ or germanite $(Cu_{26}Fe_4Ge_4S_{32})$ (Kalenov et al. 1962) or secondary hosted in other metal sulphide minerals, such as chalcopyrite ($CuFeS_2$) (Mortlock et al. 1993). Although the existence of such minerals was not validated by mineralogical analysis (SEM), it has to be pointed out that Ge shows a strong affinity (r^2= + 0.86) with Cu in the sampled springs. The initial presence of Ge in the geological substrate should be attributed to acid rock volkanics (Arnorsson

1984). Such formations, mainly as ignimbrites or rhyolitic domes, are developed at Polychnitos area, at the NE part of the Island, and as an underlying unit near Argenos (Vamvoukakis 2009).

4 Conclusions

The thermal springs of Lesvos Island were studied regarding their concentrations to trace and ultra trace elements. The main factors that control hydrochemistry seem to be the geological substrate and the existing epithermal mineralization. Compared to other springs, Therma and Eftalou are the most enriched in trace and ultra trace elements. The detected concentrations of REE (La, Ce, Nd, Gd, Er, and U) are attributed to specific geochemical processes and environmental conditions, such as complexation and acidic environment. Arsenic, Pb, Sb, Cu, Zn and Fe are related with epithermal gold mineralization, while the presence of germanium is correlated with Si-rich volcanic formations and possibly with Cu-rich sulphide minerals. Thallium which is also enriched at the majority of the sampled springs which are used for blaneotherapy purposes, impose a significant environmental threat for human environment, due to its toxicity through skin absorption.

5 References

Arnorsson S (1984) Germanium in Icelandic geothermal systems. Geoch. Cosm. A. 48, 2489-2502

Bencini A, Duchi V, Casatello A, Kolios N, Fytikas M, Sbaragli L (2004) Geochemical study of fluids on Lesbos Island, Greece. Geothermics. 33, 637-654

Biddau R, Bensimon M, Cidu R, Parriaux A (2009) Rare earth elements in groundwater from different alpine aquifers. Chemie der Erde. 69, 327-339

Birkle P, Bundschuch J, Sracek O (2010) Mechanisms of arsenic enrichment in geothermal and petroleum reservoirs fluids in Mexico. Water Research. 44, 5605-5617

Cheam V (2001) Thallium contamination of water in Canada. Wat. Q. Res. J. Can. 36(4), 851-877

Fytikas M, Kavouridis T, Leonis C, Marini L (1989) Geochemical exploration of the three most significant geothermal areas of Lesbos Island, Greece. Geothermics. No3. 18, 465-475

Gammons C, Wood S, Pedrozo F, Varekamp J, Nelson B, Shope C, Baffico G (2005) Hydrogeochemistry and rare earth element behaviour in a volcanically acidified watershed in Patagonia, Argentina. Chem. Geol. 222, 249-267

Johannesson KH, Zhou X (1999) Origin of middle RE element enrichments in acid waters of a Canadian high Arctic lake. Geochim. Cosmochim. Acta. 63, 153-165

Jongsma D (1974) Heat flow in the Aegean Sea. Geophys. J. R. astr. Soc.37, 337-346

Kalenov AD, Anikeyeva VI, Maslenkov SB (1962) Germanium minerals in chalcopyrite ores. Dokl.Akad.149, 675-676

Katsikatsos G, Migiros G, Triantafyllis M, Mettos A (1986) Geological structure of Internal Hellinides. IGME/Geol. Geoph. Res. Special Issue, 191-212

Kelepertsis A (1993) Hydrothermal alteration of basic island-arc volcanic rocks north and south of Mytilini Town, Lesvos Island, Greece. Terra Nova.5, 52-60
Kelepertsis A, Tziritis E, Kelepertsis E, Leontakianakos G, Pallas K (2009) Hydrogeochemical characteristics and genetic implications of Edipsos thermal springs, north Euboea, Greece. Centr. Eur. J. Geosc. 1(3), 241-250
Lambrakis N, Stamatis G (2007) Contribution to the study of thermal waters in Greece: chemical patterns and origin of thermal water in the thermal springs of Lesvos. Hydrol. Process 22, 171-180
Le Pichon X, Angelier T (1981) The Aegean Sea. Philos. Trans. R. Soc. Lond. A300, 357-372
Mather D, Porteous N (2001) The geochemistry of Boron and its isotopes in groundwater from marine and none marine sandstone aquifers. Appl. Geochem. 16, 821-834
Mayanovic R, Anderson A, Bassett W, Chou IM (2007) On the formation and structure of rare earth element complexes in aqueous solutions under hydrothermal conditions with new data on gadolinium aqua and chloro complexes. Chem. Geol. 239, 266-283
Michelot JL, Dotsika F, Fytikas M (1993) A hydrochemical and isotopic study of thermal waters of Lesbos Island (Greece). Geothermics. 22, 91-99
Mortlock R, Froelich P, Feely R, Massoth G, Butterfiled D, Lupton J (1993) Silica and germanium in Pacific Ocean hydrothermal vents and plumes. Earth. Plan. Scien. Letters. 119, 365-378
Neal C (2005) La, Ce, Pr and Y in waters in an upland acidic and acid sensitive environment, mid-Wales. Hydr. Earth. S. Sc. 9, 645-656
Papastamataki A, Katsikatsos G (1969) The thermal springs of Polichnitos-Lesbos. Unpublished IGME report (in Greek)
Pe-Piper G (1980) Geochemistry of Miocene Shoshonites, Lesbos, Greece. Contrib. Min. Petrol. 72, 387-396
Percival TJ, Radtke AS (1994) Sedimentary rock-hosted gold mineralization in the Alsar district, Skopje. Can. Mineral. 32,649-665
Peter J, Viraraghavan T (2005) Thallium: A review of public health and environment concerns. Env. Int. 31, 493-591
Smedley PL, Kinniburgh DG (2002) A review of the source, behaviour and distribution of arsenic in natural waters. Appl. Geochem. 17, 517-568
Valentino GM, Stanzione D (2003) Source processes of the thermal waters from the Phlegrean Fields (Naples, Italy) by means of the study of selected minor and trace elements distribution. Chem. Geol. 194,245-274
Vamvoukakis K (2009) Epithermal mineralization Au-Ag at Lesvos Island. PhD Thesis. p418
Varnavas SP, Cronan DS (1988) Arsenic, Antimony and Bismuth in sediments and waters from the Santorini hydrothermal field, Greece. Chem. Geol. 67, 295-305
Vink BW (1993) The behaviour of thallium in the (sub) surface environment in terms of pH and Eh. Chem. Geol. 109, 119-123
Welch AH, Stollenwerk KG (2003) Arsenic in Ground Water: Geochemistry and Occurrence: Boston. Kluwer Academic Publishers, 475 p
Xiao T, Guha J, Boyle D, Liu CQ, Zheng B, Wilson G, Rouleau A, Chen J (2004) Naturally occurring thallium: A hidden geoenvironmental health hazard. Envir. Internat. 30, 501-507
Zitko V (1975) Toxicity and pollution potential of thallium. Sci. Total. Environ. 4,185-192

Stable isotope study of a karstic aquifer in Central Greece. Composition, variations and controlling factors

E. Tziritis

National & Kapodistrian University of Athens, Faculty of Geology & Geoenvironment

e-mail: evtziritis@geol.uoa.gr, Ilissia 157 84, Athens

Abstract The present study examines the isotopic composition of a karstic groundwater system in Boeotia (Greece) and the factors that control its variations. For this purpose 42 samples were analyzed for oxygen and hydrogen stable isotopes, and their ratios defined the local groundwater isotope line (LGIL). The results showed a shift of the LGIL in comparison to LMWL, which is expressed by an enrichment of heavier isotopes and lower d-excess values. Apart from the ambient conditions that affect the initial isotopic signature, the secondary processes seem to be a major factor too. These processes are related to the specific geological and hydrogeological setting of the area and include the evaporation of soil water, mixing with paleowaters, hydraulic connection with groundwater systems of different isotope characteristics, and finally water-rock reactions with the karstic aquifer.

1 Introduction

The environmental stable isotopes of hydrogen and oxygen (H/D and $^{16}O/^{18}O$) have been used extensively in a large variety of hydrological applications over the last decades as they provide vital assessments regarding water management and water cycle in nature. The fundamental process is the "isotopic fractionation", which according to Faure (1977) can be achieved through: a) redistribution of an element's isotopes through isotopic exchange reactions, b) bidirectional reactions in which kinetics are related to isotope composition of both reactants and products, and finally c) natural processes such as evaporation, condensation, adsorption etc. The isotopic composition of precipitation depends on local conditions and various environmental factors such as longitude and latitude, altitude, temperature and distance from sea (Drever 1997; Schwartz and Zhang 2003; Argiriou and Lykoudis 2006). After precipitation, isotope composition may be changed again due to secondary processes either prior or after the infiltration of groundwater, like (Hoefs 1980; Allison et al. 1984; Drever 1997): a) evaporation of soil water, b)

N. Lambrakis et al. (Eds.), *Advances in the Research of Aquatic Environment, Vol. 2*
DOI 10.1007/978-3-642-24076-8,

differential movement of water due to soil or groundwater anisotropy, c) interaction with geological formations due to isotope exchange, and d) mixing with non-meteoric water or enrichment from surface hydrological reservoirs.

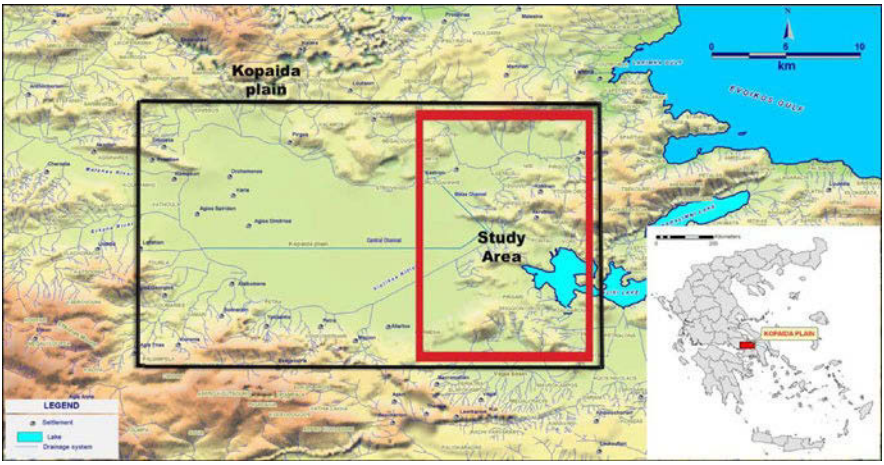

Fig. 1. Geographical setting of the study area.

The study area (Fig. 1) is located in the Eastern part of Central Greece. The geological substrate consists of dolostones, a tectono-volcanic formation (composed of schists and ophiolites) and karstified limestones, while the post-Alpine formations include mainly a thick series of recent fluvial Quaternary deposits. The hydrological system of Kopaida plain is the latter part of the great system of Viotikos Kifisos River. It is hydraulically connected with the median route of Viotikos Kifisos basin (from W) and with mountain Elikonas (from S), which are the main sources of groundwater recharge. In the study area there are developed three individual aquifers which are practically interconnected and may be considered as a unified heterogeneous karstic system with piezometric levels ranging from 20m to 160 m (Tziritis 2008).

2 Sampling and Analyses

Totally 42 groundwater samples (Fig. 3) were collected from all available boreholes of the karstic aquifer. Stable isotope analyses were performed in the laboratory of Research Institute of Materials, Akita University, Japan. Water was converted to hydrogen gas through reaction with zinc metal at 415^{o}C. The D/H ratio was measured with the use of a mass spectrometer (MAT 250), while oxygen isotopic ratio was determined using the H_20-CO_2 equilibrium technique. Isotope concentrations δD and δ^{18}O are expressed as the difference between the measured ra-

tios of the sample and reference divided by the measured ratio of the reference, which is expressed as the VSMOW values. Results are shown on Table 1.

Table 1. Results of stable isotopes in ‰ with reference to VSMOW for the groundwater samples.

Sample	$\delta^{18}O$	δD	Sample	$\delta^{18}O$	δD	Sample	$\delta^{18}O$	δD
S3	-6.6	-42.8	S64	-8.2	-51.8	S83	-4.3	-31.8
S31	-6.9	-43.9	S66	-7.1	-50.6	S84	-3.3	-26.2
S35	-7.2	-45.8	S67	-7.1	-46.5	S85	-6.5	-41.6
S36	-6.8	-45.4	S69	-7.5	-52.6	S86	-5.6	-37.9
S38	-6.2	-41.8	S70	-7.9	-51.6	S87	-4.1	-29.7
S41	-6.4	-43.4	S73	-7.9	-50.4	S88	-5.4	-36.8
S44	-7.1	-46.3	S75	-7.0	-45.8	S89	-6.8	-44.0
S46	-6.3	-42.5	S76	-7.8	-49.8	S90	-7.0	-46.4
S47	-5.3	-37.1	S77	-6.7	-43.0	S91	-7.3	-46.1
S49	-7.5	-48.5	S78	-7.2	-46.9	S92	-6.8	-44.2
S55	-7.0	-45.8	S79	-7.2	-46.4	S93	-6.0	-40.2
S57	-6.0	-41.1	S80	-6.9	-45.6	S94	-6.2	-41.4
S59	-5.1	-36.4	S81	-6.7	-44.4	S95	-6.4	-42.2
S61	-5.7	-39.8	S82	-5.8	-39.8	S97	-5.5	-38.0

3 Results and Discussion

Despite the fact that several groundwater isotopic studies have been published for Greece (i.e. Kallergis and Leontiadis 1983; Leontiadis et al. 1996; Leontiadis et al. 2006), very few of them regarded precipitation and thus defined local meteoric water lines. In the present study, the assessments were made considering as LMWL the meteoric water line for Central Greece ($\delta D=5.56\delta^{18}O-1.2$) as defined by Dotsika et al. (2010a). Based on Table 1, the isotopic ratio of Deuterium (δD) in the study area ranges between -26.2‰ and -52.6‰ with a mean value of -43.31‰±0.85. This value is lower than the mean value obtained from spring waters of Central Greece which is -45.4‰ (Dotsika et al. 2010a). Likewise, the isotopic ratio of Oxygen-18 ($\delta^{18}O$) which ranges between -3.3‰ and -8.2‰ and has a mean value of -6.52‰±0.16, is lower than the relative obtained mean value for spring waters of Central Greece (-7.44‰) defined by the same researchers. Thus, the isotope signature of groundwater for the study area appears to be enriched in heavier isotopes.

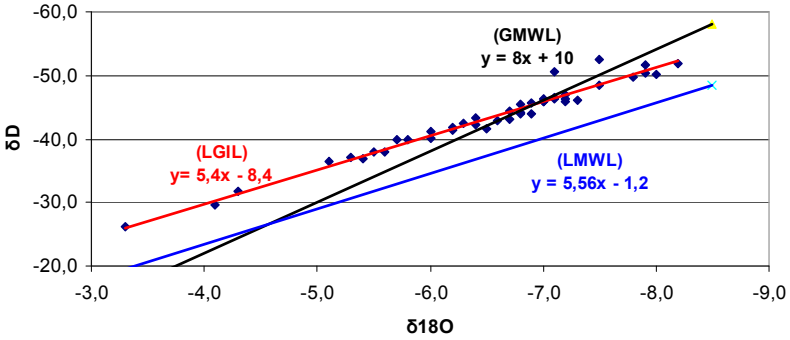

Fig. 2. Plot of δD vs. δ^{18}O values of the groundwater samples with the addition of regression line (LGIL) along with GMWL (Craig 1961) and LMWL (Dotsika et al. 2010a).

The projection of δD and δ^{18}O ratios to a common plot (Fig. 2) defines the Local Groundwater Isotope regression Line (LGIL), which is based on the analytical values of stable isotopes (Table 1) for the study area. The function that express LGIL is y = 5.4x – 8.4 (δD = 5.4 δ^{18}O – 8.4) with R^2 = 0.96. Compared to LMWL (Dotsika et al. 2010a) the projection of LGIL is parallel, as their slopes are nearly equal (5.4 and 5.56), but there is a significant shift of LGIL due to different values of the d-excess parameter. Deuterium excess is usually considered as a more or less conservative property in the part of the atmospheric water cycle beginning with water vapour formation by evaporation to rainfall just below cloud level (Ciais and Jouzel 1994). Deuterium excess in rainfall of Mediterranean origin generally has a relatively high value. This is due to a strong kinetic isotopic effect during evaporation in the summer above the Mediterranean Sea, because of the low relative humidity of the atmosphere. According to Dotsika et al. (2010b), differences in d-excess arise as a consequence of varying temperature, relative humidity and wind speed at the sea surface, where global atmospheric moisture mainly originates, as well as from admixture of recycled continental vapour. Negrel et al. (2011) reports that 'd-excess' values of less than 5 suggest significant evaporation of rainwater, leaving the residual groundwater with lower 'd-excess' values and depleted δ^{18}O. Thus, the low d-excess values (-8.4) for the study area, should have the same origin and may be attributed to ambient conditions. As already mentioned, the majority of the samples are enriched in heavier isotopes compared to other spring waters of Central Greece (Dotsika et al. 2010a). Regarding the observed shift between LGIL and LMWL there is a significant enrichment of δ^{18}O which is accompanied by lower values of δD. Similar conditions occur when secondary processes take place due to the impact of geological substrate, water recharge and water-rock interactions (Fontes 1981; Mathieu and Bariac 1996; Drever 1997; Gat 2010). With the aid of Figure 3 which presents the interpolated δ^{18}O values, we can assume that the higher values (isotope enrichment) are recorded at the central part of the study area (Districts A, E and D), as well

to a NE-SW oriented axe which includes the fringes of Ptoon mountain and a part of Kastro basin. All other areas appear less isotopic enrichment or sometimes depletion, compared to the aforementioned.

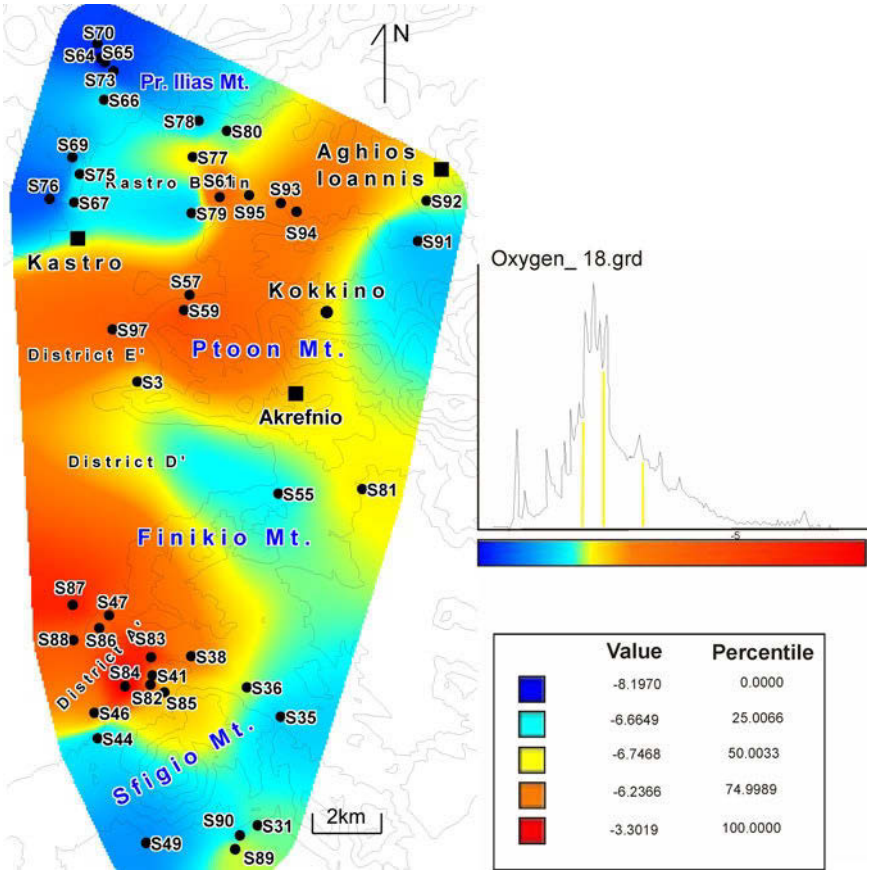

Fig. 3. Sampling points and simulation of $\delta^{18}O$ values with the use of spatial interpolation.

Taken into account Figure 3 and Table 1, we can distinguish 3 major groups of samples, which are characterized by different isotopic signatures either due to the impact of secondary processes or to different recharge conditions. The first group (A) is consisted of 18 samples (S3, S38, S41, S46, S47, S57, S59, S61, S82, S83, S84, S86, S87, S88, S93, S94, S95 and S97) and embraces the samples with isotopic enrichment, the second group (B) is consisted of 16 samples (S31, S44, S49, S64, S65, S66, S67, S69, S70, S73, S75, S76, S78, S79, S89 and S90) and embraces the samples with isotopic depletion, and the third group (C) includes the rest 8 samples (S35, S36, S55, S77, S80, S81, S91 and S92) and expresses intermediate enrichment conditions. Assuming that precipitation in the study area is not diversified, due to the small area size and the relatively homogeneous terrain,

the isotopic variations reflect the effects of subsequent secondary processes. Based on geology, the central part of the study area (Districts A, D, E) and Kastro Basin which appear the higher $\delta^{18}O$ values, are consisted of high thickness Quaternary deposits, which are characterized by low hydraulic conductivity and diminished surface water percolation. Thus, infiltration is achieved through extremely low velocities. These conditions are favourable for the evaporation of precipitates during the percolation through soils (Kendall and McDonnell 1998). Similar conditions of elevated subsoil evaporation may also be the case at other areas with occurrence of low permeability formations. Such a case may potentially cause the isotopic variation in the fringes of Ptoon Mountain, where either the flysch or the tectonic-volcanic complex occurs. The above assessments may be confirmed by the obtained slope of LGIL (a=5.4) which is close to the theoretical slope as defined by Allison et al. (1984) and describes the effects of evaporation at unsaturated soils. All the other locations of the study area are dominated by the karstic substrate which ensures direct infiltration with high velocities and therefore similar isotopic ratio to those of precipitates (e.g. samples S49, S64, S66, S73, S76 a.o.). The above assessment is in accordance with the studies of Mathieu and Bariac (1996), who report that fast and direct infiltration through conducting fissured zones (such as the karstic terrain of the area), generates $\delta^{18}O$ values close to the mean rainfall input, while slow infiltration through soil generated enriched $\delta^{18}O$ values.

Additionally to the above, we should also consider the scenario of hydraulic connection with the adjacent areas of high water recharge, which could possible be the case for the samples of group B. For example, the northern and the southern part of the study area (Fig. 3) which appears isotopic depletion should be affected by the hydraulically connected areas of mountain Elikonas at the south or Pr. Ilias Mountain at the north. The elevated water recharge of those areas may alter the isotopic signature, causing isotopic depletion and similar ratios with those of precipitation. On the contrary, the aquifer beneath the central part of the study area (District A, D and E) which is characterized by non-direct infiltration, is recharged by the upward hydrogeological systems of Viotikos Kifisos River, and characterized by greater transient times which lead to the enrichment of heavier isotopes. This scenario of admixing may be verified by the observed shift of the LGIL compared to LMWL, accompanied by significant low d-excess values, as described in similar cases by Gat (2010). According to Tziritis (2008), the wider area of District A is characterized by complicated hydrogeological conditions of strongly anoxic reducing waters. The lack of oxygen features limited water recharge, thus these waters may be considered as practically stagnant or under circumstances as paleowaters. Paleowaters are defined (Fontes 1981) as waters originating from water cycles under environmental conditions which are different from the present ones. Obviously, one expects to encounter such waters in systems with a very long residence or transit time, especially when these became stagnant due to the curtailment of recharge at present. The stable isotope composition of these paleowaters differs from the sparse modern precipitation; usually showing both more de-

pleted $\delta^{18}O$ and also aligned along a LMWL with a smaller d-excess value (Gat 2010), just like in the study area. Thus, the climate changes of Kopaida plain during Pleistocene and Quaternary (Griffiths et al. 2002) along with the specific local hydrogeological setting, may have resulted in significant variations of isotopic signature. Finally, unlike the chemical nature of the groundwater which can be continuously modified by geochemical interactions with the aquifer material, the isotopic composition of groundwater is practically invariant with respect to interaction with the aquifer material during the passage through the aquifer as long as the temperature is less than 60°C (Gat 2010). Consequently, in view of the temperatures generally encountered in the subsurface, the stable isotopes of water can be considered as conservative and not affected by exchanges with soil or rock. According to Drever (1997), δD is generally unaffected by reaction with aquifer materials at low temperatures just like $\delta^{18}O$ which is generally unaffected by reaction with silicates at low temperatures for short periods of time (less than 1m years or so). On the contrary, exchange with $CaCO_3$ in limestone aquifers may cause significant shift towards heavier $\delta^{18}O$ values (Drever 1997). Thus, if groundwater has the nearly same δD values as local precipitation but slightly heavier $\delta^{18}O$, the water is probably meteoric, but affected by exchange with calcite (Drever 1997). The above hypothesis can be verified for the study area, if we take into account the dominant geology and Fig.2, where for δD groundwater values similar to those of precipitation, the $\delta^{18}O$ values are significant lower (^{18}O enrichment).

4 Conclusions

The isotopic ratios of oxygen ($^{18}O/^{16}O$) and hydrogen (H/D) were defined by analysing 42 samples of the karstic aquifer. The outcome assessed the functional relation of $\delta D = f(\delta^{18}O)$ which defined Local Groundwater Isotope Line (LGIL). The measured isotope values and the comparison of LGIL with LMWL, revealed that the initial isotopic signature is affected, showing an enrichment of heavier isotopes and low d-excess values. The main factors that control these isotopic variations may be attributed to the ambient conditions, differences in water recharge and secondary processes. Ambient conditions include strong kinetic isotopic effects during evaporation, significant evaporation of rainwater before infiltration and climate variances (temperature, humidity, and wind seed). On the other hand, secondary processes depend on the geological and hydrogeological setting. More precisely, isotope values are affected by the evaporation of soil water due to low infiltration velocities on the central part of the study area, as well as by the possible occurrence of paleowaters in deeper parts of the aquifer. Long transient times of groundwater should also be considered a controlling factor, especially for the central part of the area. Finally, isotope composition is affected by the water-rock interactions with the karstic aquifer through exchange reactions with $CaCO_3$.

References

Allison G, Barner C, Hughes M, Leaney F (1984) Effect of climate and vegetation on δ18O and δD profiles in soils. Proceedings of IAEA Symp.Vienna, 105-123

Argiriou A, Lykoudis S (2006) Isotopic composition of precipitation in Greece. J.Hydr.327, 486-495

Ciais P, Jouzel J (1994) Deuterium and oxygen 18 in precipitation: isotopic model, including mixed cloud process. J.Geoph.Research. 99, 16793-16803

Craig H (1961) Isotopic variations in meteoric waters. Science.133, 1702-1803

Dansgaard W (1964) Stable isotopes in precipitation. Tellus.16, 436-438

Dotsika E, Lykoudis S, Poutoukis D (2010a) Spatial distribution of the isotopic compostition of precipitation and spring water in Greece. Glob.Plan.Change.71, 141-149

Dotsika E, Poutoukis D, Raco B, Psomiadis D (2010b) Stable isotope composition of Hellenic bottled waters. J.Geoch.Explor. 107, 288-304

Drever J (1997) The geochemistry of natural waters: Surface and groundwater environments. Prentice-Hall. 3rd ed., p.436

Faure (1977) Isotope Geochemistry. Springer, p.564

Fontes J (1981) Paleowaters. In: Stable isotope hydrology: Deuterium and Oxygen-18 in the water cycle. Technical report series.No210, 273-302

Gat J (2010) Isotope hydrology: A study of the water cycle. Series on environmental science and management. 6, p.197

Griffiths S, Street-Perrott F, Homes J, Leng M, Tzedakis C (2002) Chemical and isotopic composition of modern water bodies in the Lake Kopais Basin, central Greece: analogues for the interpretation of the lacustrine sedimentary sequence. Sedimentary Geology.14, 79-103

Hoefs J (1980) Stable isotope geochemistry. Springer-Verlag, 2nd ed. Heidelberg, p.327

Kallergis G, Leontiadis I (1983) Isotope hydrology study of the Kalamos Attikis and Assopos river plain areas in Greece, J.Hydr.60, 209-225

Kendall C, McDonnell J (1998) Isotope tracers in watershed hydrology. Elsevier, p.839

Leontiadis I. Nikolaou E, Dotsika E (2006) Environmental isotopes in determining groundwater flow systems, Epirus, Greece. Bull. Geol. Soc. Gre.14(2), 47-70 (in Greek with English abstract)

Mathieu R, Bariac T (1996) An isotopic study (^{2}H and ^{18}O) of water movements in clayey soils under a semiarid climate. Wat.Res.Resear.32, 779-789

Negrel P, Pauwels H, Dewandel B, Gandolfi J, Mascre C, Ahmed S (2011) Understanding groundwater systems and their functioning through the study of stable water isotopes in a hard rock aquifer. J.Hydr.397, 55-70

Schwartz F, Zhang H (2003) Fundamentals of groundwater. John Wiley and Sons Inc., p.583

Tziritis E (2008) Hydrogeochemical - Environmental study of east Kopaida – Yliki karstic system and assessment of vulnerability with the use of Geoinformatics. PhD thesis, University of Athens, p.512

Evaluation of the geochemical conditions in the deep aquifer system in Vounargo area (SW Greece) based on hydrochemical data

E. Karapanos, K. Katsanou, A. Karli, N. Lambrakis

Department of Geology, University of Patras, Rio-Patras, GR 26 504, Greece
heliaskarapanos@hotmail.com, katsanou@upatras.gr, nlambrakis@upatras.gr

Abstract This article investigates the origin and chemical composition of the aquifer hosted in the coastal part near Pyrgos town as well as any possible connection with the tectonic structures of the area. The bedrock in the study area consists of Paleocene limestones of the Ionian zone and evaporites. The post-alpidic sediments consist mainly of clay, marl, siltstone and sandstone. Three major fault trends develop a complex fault system in the wider Pyrgos area. The tectonics and seismicity of the study area are active to date and have played a prominent role in the structure of post-alpidic sediments, the shaping of today's relief, the development of the drainage network and the local hydrogeological characteristics. Groundwater samples can be classified into two groups based on their water type. The first group corresponds to fresh groundwater of Ca-Mg-HCO_3-(SO_4) type and the second to alkaline waters of Na-(Ca, Mg)-HCO_3-SO_4 type. A number of samples classified into the second group are considered to be modified by rock-water interaction processes. Trace elements exhibit generally low concentrations, while boron concentrations suggest discrimination between the above two water groups. The correlations between different elements and their distribution maps suggest that the main fault of Vounargo provides a preferential path for deep circulation, transmission and mixing of deep and shallow groundwater.

1 Introduction

The chemical composition of surface water and shallow groundwater reflects the geochemistry of local geological formations and results from the interactions of water (rainwater and groundwater) with crystalline and amorphous minerals in the rocks. The suite of solutes at any point along a flow path is dependent upon (1) initial composition of the recharge water, (2) composition and relative solubility of the rock through which the water passed and (3) residence time of the water. Thus, rock-water interactions give groundwater its essential mineral type (Edmunds and Smedley 1996). In contrast to shallow aquifers where groundwater's chemical composition mirrors the surface geology, deeper groundwater can undergo signifi-

N. Lambrakis et al. (Eds.), *Advances in the Research of Aquatic Environment, Vol. 2*
DOI 10.1007/978-3-642-24076-8, © Springer-Verlag Berlin Heidelberg 2011

cant changes in its chemistry caused by increasing residence time (Edmunds and Smedley 2000). It is therefore necessary to consider the possible variations or sequential changes taking place both between areas with different geology and within an aquifer.

The study area is part of the Grape graben which is located in the western part of Peloponnese (SW Greece), 3 km north of Pyrgos town in Ilia prefecture. The geomorphology of the area is characterized by steep hills at the margins of the graben formed by the Vounargo fault zone, while a smooth relief prevails in the lowland part of the graben, with a mean altitude of 20 m a.s.l. The intense tectonic activity during the post alpine period has played a defining role in the shaping of today's relief, as well as the development of the drainage network and the formation of the local hydrogeological characteristics.

Etiope et al. (2006) reported that in the nearby town of Katakolo, methane and hydrogen sulfide gases migrating from deep carbonatic reservoirs seep to the surface in high concentrations. The aim of this study is to investigate the hydrogeochemical conditions that prevail within the aquifer in order to examine the possible rise of deep water via the active faults of the area.

2 Geological and hydrogeological setting

The study area is part of Pyrgos sedimentary basin (Hageman 1976; Koukouvelas et al. 1996) and consists of two sedimentary systems overlying the Paleocene limestone basement of the Ionian zone (Kamberis 1987). The lower system consists of the marine-lacustrine Vounargo formation (Fm) (Fig. 1b) up to 1000 m thick, which is the major lithological unit in Pyrgos basin, consisting mainly of sand with alternations of clay and marl (Kamberis 1987). The upper sedimentary system consists of three formations. At the bottom, the 200 m thick Pliocene Olympia Fm is a coarsening-up fluvio-lacustrine succession overlain by the 400 m thick Erymanthos conglomerates. On top of this system the 80 m thick Middle Pleistocene-Holocene Alfios Fm is exposed in the low-land area of Pyrgos basin (Fig.1a, b).

The structure of Grape graben (Fig. 1a), which is part of Pyrgos sedimentary basin, was determined by Pliocene faults and newly formed faults. The ENE-trending Grape graben, of dimensions 3 km by 10 km, was reactivated by ruptures at depth during the Pyrgos earthquake in 1993 (Koukouvelas et al. 1996). It is defined to the north by the Vounargo fault (Fig.1a), which has a total maximum throw of 1060 m, and to the south by the Prasino-Abelon fault (Fig.1a) which has a total maximum throw of 620 m and a slip rate of 0.18 mm/yr. A continuous temporal decrease of the slip rate from 0.35 mm/yr during the Pliocene to 0.14 mm/yr during the Quaternary is calculated on the Vounargo fault (Koukouvelas et al. 1996).

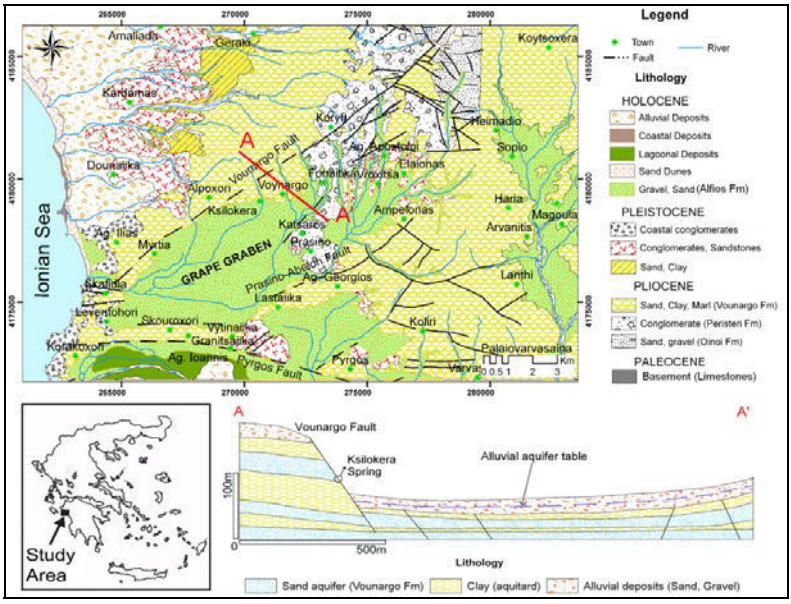

Fig. 1. 1a, b, c: Geological map, stratigraphy and cross section of the study area (Streif 1980).

According to Thornthwaite and Mather (1955) method, the hydrological balance was estimated to be 58% evapotraspiration, 20% infiltration and 22% surface runoff of the mean annual precipitation (748mm) (Karapanos 2009). The most significant aquifer of the area develops in the sands of Vounargo Fm in depths between 60-120 m (Karapanos 2009). It consists of successive sand layers with diverse permeability that alternate with clay lenses. This formation is fractured by normal faults in the graben, possibly connecting shallow and deep aquifers. This assumption is also derived from the fact that adjacent wells developed within the same aquifer and abstracting of the same depth, seem to have different groundwater levels (Karapanos 2009).

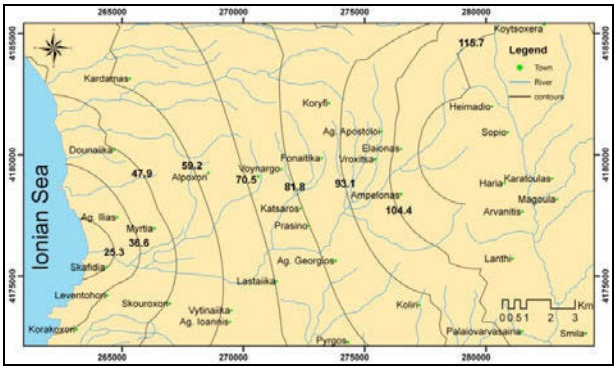

Fig. 2. Potentiometric surface of the confined aquifer of the study area (17/04/2006).

The aquifer is mainly recharged by direct infiltration from precipitation in the NE part of the area where Vounargo sands outcrop. The general direction of groundwater flow is from higher altitude areas in the ENE part, moving towards the sea in the west part of the basin (Fig. 2). Groundwater level fluctuations vary between 0.1 to 2m, while the hydraulic gradient varies between 8‰ in the centre of the basin to 18‰ in higher altitudes (Karapanos 2009).

3 Groundwater chemistry - Results and Discussion

In order to define the hydrochemical composition of the aquifer hosted in the study area, a total number of 82 samples were collected in the period between October 2005 and September 2008, according to US EPA (1976) procedures. In addition, seawater and rain water samples were also collected. Unstable hydrochemical parameters including pH, water temperature (T_w), electric conductivity (E.C.) and redox potential (Eh) were measured in-situ using portable Consort® equipment. Alkalinity was also measured in-situ using the titration method. Major anions (SO_4^{-2}, NO_3^-, NO_2^- and $PO4^{-3}$) and NH_4^+ were determined using ultraviolet spectrophotometer and Cl^- were measured by titration method. Major cations (Ca^{2+}, K^+, Mg^{2+}, Na^+) concentrations were determined in a GBC® Avanta flame atomic absorption spectrophotometer. Trace element concentrations were measured using Inductively Coupled Plasma-Mass Spectrometry (ICP-MS) in an ELAN 6100 Perkin Elmer.

Field measurements show that water samples are mostly characterised by negative redox values (Fig. 4b) thus indicating strong reductive conditions related to high amounts of NH_4^+, low concentrations of NO_3^- and the presence of H_2S, with the majority of them having high T.D.S concentrations as shown by E.C. values (Fig. 4c). The pH values range between 6.72 and 8.52.

Groundwater samples can be classified into two main groups according to the Piper diagram (Fig. 3a), with the following chemical composition: Ca-(Mg)-HCO_3-(SO_4), Na-(Ca, Mg)-HCO_3-(SO_4). The first group, where the dominant cation is calcium, represents groundwater samples that have better recharge and correspond to the fresh water of the area. Water samples of this group are plotted in the edges of Vounargo fault zone (Fig. 4a, green signs). They have low water temperature ranging between 11.4 and 20.9°C and pH values range between 6.86 and 7.71. The second group represents water samples that exhibit high Na^+ concentrations. Water temperature ranges between 17.0 and 24.5°C and pH values range between 6.93 and 8.52. Redox potential displays negative values for all samples throughout the three year period, indicating reductive conditions (Fig. 4b). This group is also characterized by low concentrations in Ca^{2+} and contrary to the first group, by a slight shift in F^-, B and Li concentrations. In some cases, samples of this group have high Mg^{2+} concentrations and show enrichment in Ca^{2+}.

Water samples of both groups were plotted in scatter plots (Fig. 3b, c, d, e, f, g, h, i) and in distribution maps (Fig. 4b, c, d, e, f). As shown in Fig. 3b, samples of the first group are almost ordered along the solid line which is the concentration-dilution characteristic line for seawater indicating that they have the same Cl/Na ionic ratio. On the contrary, samples of the second group are plotted above the solid line, showing their excess in Na^+. The excess of sodium can be attributed to hydrochemical processes such as the dissolution of minerals rich in sodium (e.g. Albite) or ion exchange processes.

As shown in Fig. 4a, samples of the second group are plotted along the Vounargo fault zone (Fig. 4a, red signs) suggesting that water of deep origin rises to the surface through fractures and faults in Vounargo Fm and mixes with aquifer water hosted in this area. Figure 3c confirms that samples of this group show excess in B, with the higher concentrations distributed along the fault zone (Fig. 4d).

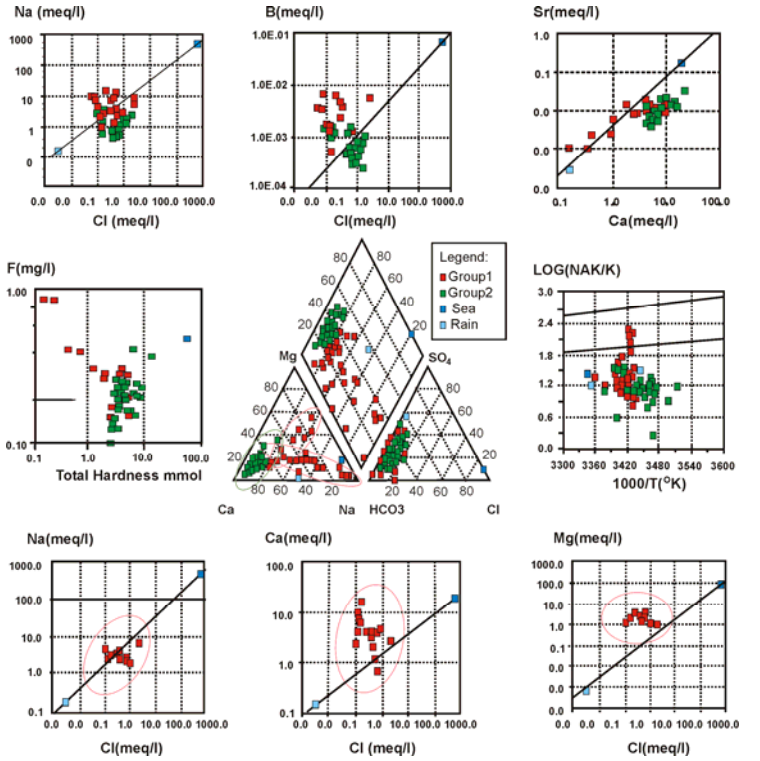

Fig. 3. a. Piper diagram, Scatter plots **b.** Cl-Na, **c.** Cl-B, **d.** Ca-Sr, **e.** Total hardness vs. F, **f.** Na/K geothermometer (Fournier, 1973) for both water types and **g.** Cl-Na, **h.** Cl-Ca, **i.** Cl-Mg for part of the second group that is shown with the doted area.

Boron is one of the most mobile elements during hot fluid-rock interactions (Ellis and Mahon 1967). It exhibits high concentrations in seawaters, in thermal waters and in wastewaters due to the detergents and consequently all the above

may contribute to the chemical composition of an aquatic system. In Vounargo area where groundwater is unaffected from seawater intrusion and wastewater, Boron concentration varies. Pennisi et al. (2000) reported that alkaline and relatively cold groundwater from turbidite deposits that filled the basement depressions of the western and south western flank of Mt. Etna have a Boron concentration ranging from 0.5 to 1.45 mg/L.The contribution of deep waters originating from the bedrock (Paleocene limestones) of the study area is also confirmed by Fig. 3d, where it is clear that there is a common origin of both Sr and Ca^{+2} in the samples of group II. It is worth mentioning that samples of this group also show a shift in Ba concentrations (Group II: 16.7-367.7 mg/L, Group I: 0-113.7 mg/L). According to Edmunds et al. (2002), Sr and Ca^{+2} elements are related with calcareous minerals. As mentioned earlier these minerals constitute the bedrock of the study area and therefore it can be concluded that their dissolution leads to enrichment of the above mentioned elements.

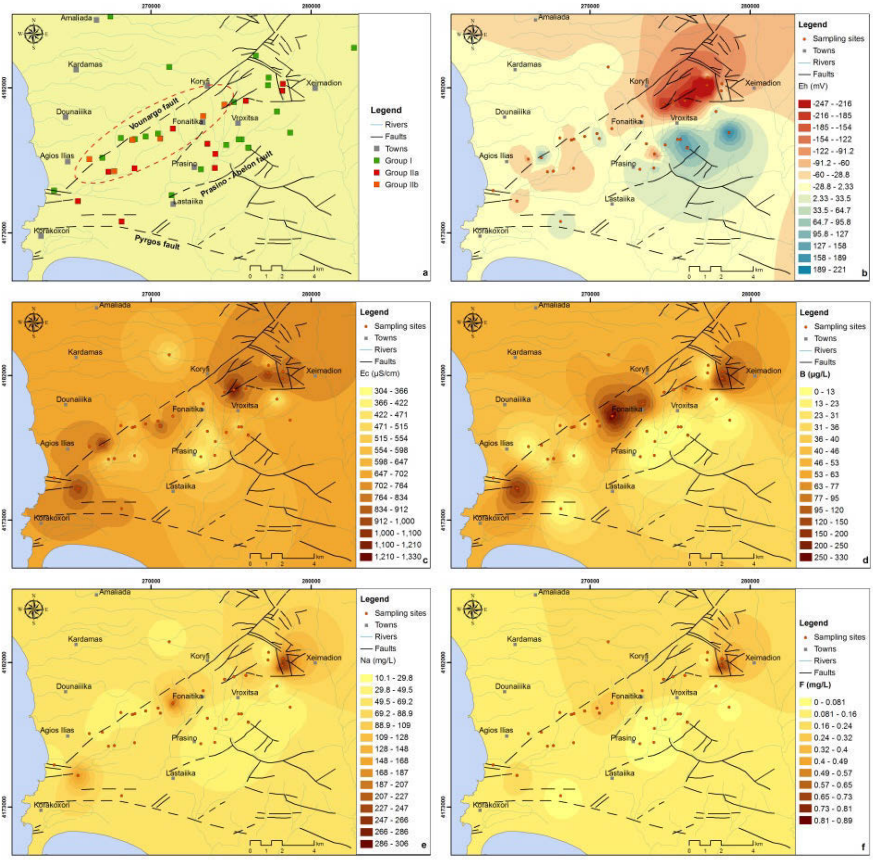

Fig. 4. Distribution of **a.** groundwater types, **b.** Eh, **c.** E.C., **d.** B, **e.** Na^{+}, **f.** F^{-} (Karapanos 2009).

The second group, which results from the contribution of deep water, proved to be rich in F^- (0.20-0.89 mg/L). Sodium may exhibit a positive correlation with fluoride in many types of groundwater, especially those having low concentrations of calcium (waters undergoing base exchange). This correlation is clear as Na^+ and F^- display similarities in their distribution maps (Fig. 4e, f, respectively) and has also been observed in other aquifers in Greece belonging to Na-Ca-HCO_3 type (Katsanou 2007).

Total hardness was calculated for all samples and the results were plotted versus fluoride concentrations (Fig. 3e). As shown, all samples are of quite the same total hardness (90 mg/L, on average). According to Boyle (1992), "hard" groundwater with low Na^+ content displays F^- concentrations that are generally in the range of 0.02-3.0 mg/L. As shown in Fig. 3e, samples most affected by deep water mixing processes are of Na-HCO_3 type and exhibit a much lower total hardness and high F^- concentrations due to the precipitation of Ca^{+2} under common ion effects. The equation below, results in the continuous removal of calcium that leads to solutions under calcite saturation.

$$CaCO_{3(s)} + H^+ + 2F^- \leftrightarrow CaF_{2(s)} + HCO_3^-$$

There is also positive correlation between fluorine and bicarbonate, which appears to be increased in the second group (416 mg/L). This can be explained by the mass law equation for calcite and fluorite when both are in contact with water (Handa1975; Kundu et al. 2001). Alkalinity of the circulating water depleted in calcium is mainly responsible for the high concentration of F^-. Samples with low hardness appear to also have higher T_w values that range between 18.1 and 24.5 ^oC which strengthens the assumption of their deep origin as well. A number of samples in group II seem to be affected by ion exchange processes causing a masking effect (Fig. 4a, orange signs). All samples that appear to have mixed/unclear water types were plotted separately (Fig. 3g, h, i). In these plots it is clear that these samples are depleted in Na^+ but in the same time they show an excess in Ca^{+2} and Mg^{+2}. Cation exchange processes are described by the equations below, where X denotes the aquifer matrix (Andrews et al. 1994):

$$CaX_2 + 2Na^+ \leftrightarrow 2NaX + Ca^{+2}$$

$$MgX_2 + 2Na^+ \rightarrow 2NaX + Mg^{+2}$$

5 Conclusions

Groundwater samples in the wider Vounargo area can be classified in two major groups based on their chemical composition. The first group hosts samples that represent waters with better recharge and are plotted in the edges of the active

Vounargo fault zone. Group II resumes samples that exhibit high concentrations of sodium along with an excess in F^-, B and Li and constitute the Na-HCO_3 water type. Deep water mixing with fresh groundwater along the Vounargo fault zone is suggested by various correlations between major and trace elements that are also confirmed by plots and scatter hydrochemical diagrams. A number of samples belonging to group II, show a masking effect in their chemical composition which is attributed to possible ion exchange phenomena. The presence of Sr, Ba and Ca^{+2} in high concentrations confirms the assumption that deep water hosted in the underlying limestones of the Ionian zone rises through the Vounargo fault zone causing mixing effects in the aquifer water.

References

Andrews N, Fontes JC, Aranyossy JF, Dodo A, Edmunds WM, Joseph A, Travi Y (1994) The evolution of alkaline groundwaters in the continental intercalaire aquifer of the Irhazer Plain, Niger. Water Resources Research 30 (1), 45-61

Apambire WB, Boyle DR, Michel FA (1997) Geochemistry, genesis and health implications of fluoriferous groundwater in the upper regions of Ghana. Environmental Geology, 33: 13-24

Boyle DR (1976) The geochemistry of fluorine and its application in mineral exploration. PhD Thesis. University of London, Imperial College Science and Technology

Boyle DR (1992) Effects of base exchange softening on fluoride uptake in groundwaters of the Moncton Sub-basin, New Brunkswick, Canada. In: Kharaka, Y.K., Matest A.S. (eds.) Water-rock interaction, pp. 771-774. Proc. 7th Int. Symp Water-rock interaction. A.A. Balkema, Rotterdam

Edmunds WM and Smedley PL (1996) Groundwater geochemistry and health: An overview in: Appleton, J.D., Fuge, R and MaCall, G. JH (Eds.) Environmental geochemistry and Health, BGS, Special Publ., 113

Edmunds WM and Smedley PL (2000) Residence time indicators in groundwater: the East Midlands Triassic sandstone aquifer. Appl. Geochem. 15, 737-752

Edmunds WM, Carrillo-Rivera JJ, Cardona, A (2002) Geochemical evolution of groundwater beneath Mexico City. Journ. Hydrol. 258, 1-24

Ellis AJ, Mahon WAJ (1967) Natural hydrothermal systems and experimental hot water/rock interactions (Part II). Geochim. Cosmochim. Acta 31, 519-531

Etiope G, Papatheodorou G, Christodoulou D, Ferentinos G, Sokos E, Favali P (2006) Methane and hydrogen sulfide seepage in the northwest Peloponnesus petroliferous basin (Greece): Origin and geohazard. AAPG Bulletin, v. 90, no. 5: pp. 701–713

Fournier RO, Truesdell AH (1973) An empirical Na-K-Ca geothermometer for natural waters. Geochim. Cosmochim. Acta 37, 1255-1275

Hageman J (1976) Stratigraphy and sedimentary history of the Upper Cenozoic of the Pyrgos area (Western Peloponnesus), Greece. Ann.Geol. Pays. Helleniques, 28, 299-333

Handa BK (1975) Geochemistry and genesis of fluoride-contamination ground waters in India. Ground Water 13 (3), p: 275-281

Kamberis E (1987) Geological and oil study of NW Peloponnese. PhD thesis. Polytechnic School. Section of Geological Sciences. Athens (in Greek)

Karapanos E (2009) Hydrogeological – hydrochemical parameters of the drained Mouria Lake (Prefecture of Ilia), controlling the rehabilitation and the sustainable management of the wetlands. PhD thesis. Department of Geology, University of Patras. 310 pp. (in Greek)

Katsanou K (2007) Environmental and hydrogeological study of the hydrological basins in the broader area of Aigion region by the use of hydrochemical methods. Master Dissertation. University of Patras. 171 pp (in Greek)

Koukouvelas I, Mpresiakas A, Sokos E & Doutsos T (1996) The tectonic setting and earthquake ground hazards of the 1993 Pyrgos earthquake, Peloponnese, Greece. Journal of the Geological Society, London, Vol. 153, pp 39-49

Kundu N, Panigrahi MK, Tripathy S, Munshi S, Powell MA, Hart BR, (2001) Geochemical appraisal of fluoride contamination of groundwater in Nayagargh District, Orissa, India using geochemical and resistivity studies. Environmental Geology 41 (3-4): 451-460

Palmer MR (1991) Boron-isotope evidence of Helmahera arc (Indonesia) lavas: Evidence for involvement of the subducted stab. Geology 19, 215-217

Pennisi M, Leeman PW, Tonarini S, Nabelek P (2000) Boron, Sr, O, and H isotope geochemistry of groundwaters from Mt. Etna (Sicily) – hydrologic implications. Geochim. Cosmochim. Acta 64 (6), 961-974

Streif H (1980) Geological map of Greece, Pyrgos sheet, 1:50000. Institute of Geological and Mining Research. Athens (in Greek)

Thornthwaite CW, Mather JR (1955) The water balance. Climatology 8, 1-37

U.S. Environmental Protection Agency (1976) Quality criteria for water. Washington, DC, 501p

Voroshelov YI (1966) Geochemical behaviour of fluorine in the groundwaters of the Moscow region. Geochem. Int. 2: 261

Phenanthrene Sorption onto Heterogeneous Sediments Containing Carbonaceous Materials in Fresh Water and in Marine Environments: Implications for Organic Pollutant Behavior During Water Mixing

K. Fotopoulou[1], G. Siavalas[2], H.K. Karapanagioti[1,3], K. Christanis[1,2]

[1] School of Natural Sciences, University of Patras, Rio-Patras, GR 26504, Greece, fotopoulou@upatras.gr

[2] Department of Geology, University of Patras, Rio-Patras, GR 26504, Greece

[3] Department of Chemistry, University of Patras, Rio-Patras, GR 26500, Greece

Abstract Phenanthrene is used as a model hydrophobic organic compound to study the sorption properties of the Gulf of Aliveri (Greece) marine sediments. Sorption of hydrophobic organic compounds is mainly related to the organic matter present in the sediments. The presence of particles due to anthropogenic activity in the sediments can highly influence their sorption behavior. Sediments from the Gulf of Aliveri contain different proportions of such particles i.e., lignite, coal, and char. The hypothesis of the present study is that salinity can affect the fate of this pollutant by affecting the degree of sorption nonlinearity and sorption capacity. Since the sorption nonlinearity is a function of heterogeneity, different materials are used to compare their sorption behavior in solutions with and without salinity. Results expected from this study include a) the surface properties of the different sediments and the materials tested and b) sorption capacities in i) fresh and ii) salt water for phenanthrene. In general, it is observed that for carbonaceous particles and sediments containing such particles at lower phenanthrene concentrations, sorption in saltwater solutions is lower than in fresh water solutions.

1 Introduction

The sorption into marine sediments, and thus the fate of a hydrophobic organic compound in aquatic systems is directly related to the organic matter present in the sediments (Yasser et al. 2003). Sorption of organic pollutants into carbonaceous materials tends to be strong and nonlinear (Yang and Sheng 2003, Cornelissen and Gustafsson 2005), whereas adsorption and/or pore-filling are the dominant processes. Recognizing the effects of the nature of the organic matter

N. Lambrakis et al. (Eds.), *Advances in the Research of Aquatic Environment, Vol. 2*
DOI 10.1007/978-3-642-24076-8,

on the sorption properties was a significant step in studying these important processes (Kleineidam et al. 1999; Karapanagioti et al. 2000). Small amounts of carbonaceous materials may significantly change the sorption behavior of sediments for organic contaminants. High sorption capacity and non-linearity have been attributed to small amounts of these materials (Chiou et al. 1995, 1998). Organic particles demonstrate different surface properties than the conventionally termed soil organic matter and various sorption mechanisms (Karapanagioti et al. 2000).

In a sorbent water system hydrophobic organic compounds dislike water and prefer to interact with the organic carbon included in the sorbent. In marine systems salinity increases the tendency of non polar organic compounds to leave the aqueous phase, thus salinity increases the sorption of hydrophobic compounds to organic carbon (Schwarzenbach et al. 2003). However, in our previous studies where activated carbon was used as a sorbent, salinity was found to affect negatively sorption capacity and also to affect nonlinearity. Sorption was less efficient in salt water than in fresh water solutions where phenanthrene was present at relatively low concentrations (Karapanagioti 2006). The objective of this study is to compare fresh water and salt water equilibrium sorption behavior of marine sediments and carbonaceous materials.

2 Materials and Methods

In this study, phenanthrene is used as a model chemical. Phenanthrene, (C_6H_{10}), is a 3-ring PAH found in fossil fuels demonstrating low solubility in water (1.29 mg/L at 25 ^oC), low volatily (Henry's law constant: 2.6 10^{-5} atm m^3/mol), and moderate hydrophobicity (log K_{ow}: 4.6). Marine sediments with heterogeneous organic matter composition were sampled from the Gulf of Aliveri. The sediments are silty sands containing low amounts of organic carbon (1.2 and 0.7 wt. %). The dominant components of the organic matter are coal particles from the local lignite deposit and of higher rank imported coal, as well as carbonized particles originating from the power plant, which is installed in the Gulf of Aliveri. A xylite rich sample from the Aliveri lignite deposit and a higher rank (bituminous) coal sample from Brazil, both resembling the major components of the organic matter in the sediments were also used.

Solutions used in batch studies were prepared in synthetic fresh water (FW) that was prepared by adding 44 mg/L $CaCl_2.2H_2O$, 14 mg/L $CaSO_4$, 17 mg/L $NaHCO_3$ and 200 mg/L NaN_3 to distilled water and synthetic sea water (SW 36‰) that was prepared by adding 31 g/L NaCl, 19 g/L $MgSO_4.7H_2O$, 40 mg/L $NaHCO_3$ and 200 mg/L NaN_3 to distilled water. All sorption equilibrium experiments were conducted in triplicates in 40 or 120 mL glass vials with Teflon coated septa. The initial aqueous sorbate concentration in the solutions was known. The solutions were mixed with a known sorbent mass. At certain sampling

times, the aqueous sorbate concentration was measured and the loss was assumed to be due to sorption. Phenanthrene in the aqueous phase was measured with a Perkin Elmer LS - 50B fluorescence detector using a quartz cuvette at excitation wavelength 252 nm and emission wavelength 347 nm. Blank samples with solution only and without the sorbents were also prepared to determine the initial concentrations. The amount sorbed was determined through a mass balance. The surface properties such as surface area, porosity, and pore average size were determined using BET methods, Micrometrics Tristar Analyzer.

3 Data Analysis

Non linear isotherms can be described by the Freundlich equation. The Freundlich equation relates the mass of phenanthrene sorbed per unit mass of solid (q_e) to the equilibrium phenanthrene concentration (C_e) through the following equation:

$$q_e = K_{fr} * C_e^{\ N}$$

where K_{fr} is the Freundlich constant and N is the Freundlich exponent. K_d is the sorption distribution coefficient and is defined as the ratio of q_e over C_e. The sorption distribution coefficient is defined as:

$$K_d = q_e / C_e$$

For non linear isotherms K_d is concentration dependent and can be estimated as:

$$K_d = K_{fr} * C_e^{\ N-1}$$

The organic content normalized distribution coefficient is described by:

$$K_{oc} = K_d * f_{oc}^{\ -1}$$

where f_{oc} is the organic content of the sorbent.

4 Results and Discussion

Isotherm constants derived from equilibrium experiments are presented in Table 1. The sorption isotherms for the sorbents in FW and SW are presented in Figure 1 - 4. The isotherms for all the samples have a Freundlich curvilinear shape

suggesting more than partitioning of phenanthrene into the organic matter. BET surface area, pore volume, and pore size as well as the organic carbon content are presented in Table 2.

Table 1. Kfr is the Freundlich constant and N is the Freundlich exponent.

Sorbents	Water	K_{fr}	Standard Error K_{fr}	N	Standard Error N	R^2
Bituminous coal	Fresh	4.0 E+06	± 4.7 E+05	2.0 E-01	± 3.0 E-02	8.0 E-01
	Salt	3.7 E+04	± 1.5 E+04	1.1 E+00	± 9.8 E-02	7.9 E-01
Xylite	Fresh	3.0 E+05	± 5.6 E+04	5.8 E-01	± 4.5 E-02	9.3 E-01
	Salt	2.6 E+03	± 1.2 E+03	1.4 E+00	± 1.0 E-01	9.5 E-01
Aiveri Marine sediment 7	Fresh	8.3 E+03	± 1.2 E+03	5.6 E-01	± 3.6 E-02	9.7 E-01
	Salt	3.2 E+03	± 7.0 E+02	7.9 E-01	± 6.3 E-02	9.5 E-01
Aliveri Marine sediment 10	Fresh	1.8 E+04	± 3.2 E+03	3.6 E-01	± 4.3 E-02	8.9 E-01
	Salt	4.0 E+03	± 5.2 E+02	6.1 E-01	± 3.3 E-02	9.7 E-01

Figure 1 presents the sorption isotherms for phenanthrene and bituminous coal in FW and SW. Both isotherms are nonlinear and are fitted well with the Freundlich model. In FW, a highly nonlinear isotherm is obtained. In SW, the isotherm is almost linear. At most of phenanthrene concentration range, in FW more phenanthrene sorption is observed compared to that in SW. Thus, salinity seems to decrease sorption capacity especially at low phenanthrene concentrations. Figure 2 presents the sorption isotherms for phenanthrene and xylite in FW and SW. Xylite demonstrates lower sorption capacity compared to the bituminous coal. However, the results related to the effects of salinity to the sorption behavior are similar to those of the bituminous coal

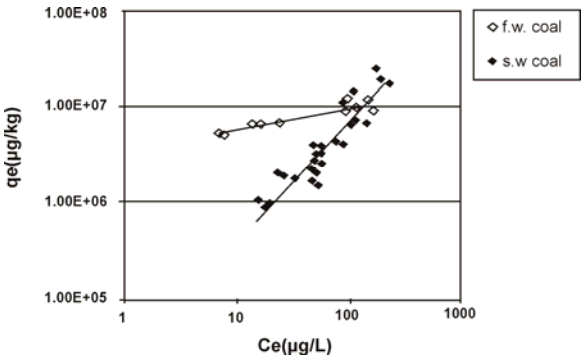

Fig. 1. Sorption isotherms for bituminous coal in FW and SW.

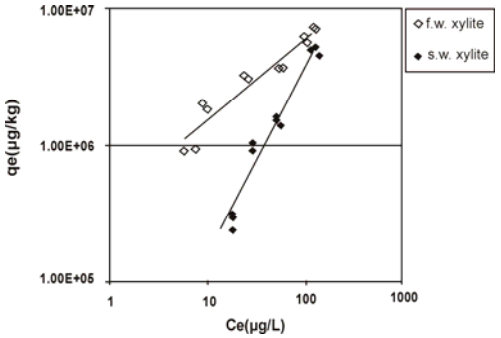

Fig. 2. Sorption isotherms for xylite in FW and SW.

Figure 3 presents the sorption isotherms for phenanthrene and Aliveri marine sediment 7 in FW and SW.

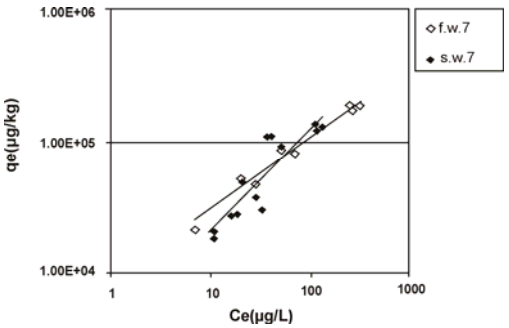

Fig. 3. Sorption isotherms for Aliveri marine sediment 7 in FW and SW.

As expected based on the f_{oc} of the sample (Table 2) the sorption capacity of this sediment is lower than for the carbonaceous materials. No significant difference in the sorption capacity or the isotherm linearity is observed for this sediment due to the presence of salinity.

Table 2. BET surface area (S.A.), pore size (P.S.), pore volume (P.V.) and organic carbon content (f_{oc}).

Sorbent	S.A.(m^2/g)	P.S (Å)	P.V. (cm^3/g)	f_{oc}
Bituminous Coal	31	56	0.043	0.64
Xylite	1.0	60	0.0014	0.54
Aliveri marine sediment 7	8.0	130	0.030	0.012
Aliveri marine sediment 10	6.0	160	0.020	0.0070

Figure 4 presents the sorption isotherms for phenanthrene and Aliveri marine sediment 10 in FW and SW. For this sediment, the f_{oc} of the sample (Table 2) is lower and the effect of salinity on sorption is similar. At lower phenanthrene concentrations, sorption in SW solutions is lower than in FW.

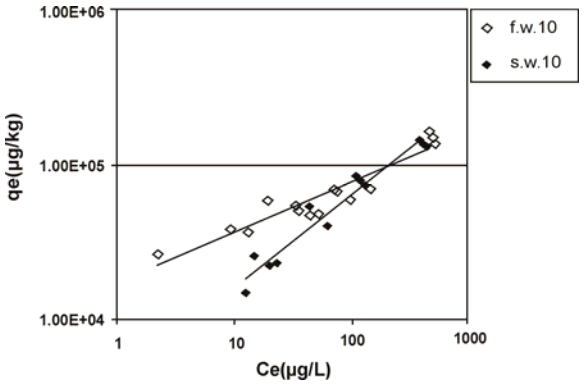

Fig. 4. Sorption isotherms for Aliveri marine sediment 10 in FW and SW.

A more detailed study is needed at lower phenanthrene concentrations to be able to significantly differentiate the two behaviors in the two solutions (FW and SW). More characterization techniques will be utilized in order to better understand the effect of salinity on the characteristics of the various sorbent materials and thus, to their sorptive properties. Additionally, it is suggested that the effect of the inherent salinity of the sediments should be taken into consideration in order to better interpret the obtained isotherm curves.

5 Conclusions

The most important conclusions of this study, utilizing marine sediments and carbonaceous materials in phenanthrene FW and SW solutions are as follows:

- At high phenanthrene concentrations, salt water does not have a significant effect on the sorption capacity of a sorbent.
- At low phenanthrene concentrations, sorption capacity is lower in salt water than in fresh water for the two carbonaceous materials used in the present study.

These results could be utilized in shallow marine and estuary systems or coastal aquifers, where mixing processes between fresh and saltwater take place. At such systems pollutants arrive sorbed onto suspended particles traveling through river water flow and deposited in the saline environments or precipitate through the infiltration of rain and surface water. The addition of amendments such as

carbonaceous materials into soils and sediments demonstrates increasing popularity as a remediation method. Using this method in both fresh water and salt water systems, as well as in areas where mixing takes place requires detailed knowledge of its performance and effectiveness in different geochemical conditions. Understanding microscale phenomena such as sorption mechanisms into different particles improves the current understanding of organic pollutants fate in aquatic systems and assists in remediation method development and optimization.

Acknowledgments This study is funded by the program "K. Karatheodori 2009" of the University of Patras Research Committee.

References

Cornelissen G, Gustafsson O, (2005) Importance of unburned coal carbon, black carbon, and amorphous organic carbon to phenanthrene sorption in sediments. Environmental Science & Technolology 39, 764-769

Chiou CT, (1995) Comments on "thermodynamics of organic chemical partition in soils". Environmental Science & Technology 29, 1421-1422

Chiou CT, Kile DE, (1998) Deviation from sorption linearity on soils of polar and non polar organic compounds at low relative concentrations. Environmental Science & Technology 32, 338-343

Karapanagioti HK, Sabatini DA, (2000) Impacts of heterogeneous organic matter on phenanthrene sorption: different aquifer depths. Environmental Science & Technology 34, 2453-2460

Karapanagioti HK, Kleineidam S, Ligouis B, Sabatini DA, Grathwohl P, (2000) Impacts of Heterogeneous Organic Matter on Phenanthrene Sorption: Equilibrium and Kinetic Studies with Aquifer Material. Environmental Science & Technology 34, 406-414

Karapanagioti HK, (2006) Removal of phenanthrene from saltwater solutions using activated carbon. Desalination 210, 274-280

Schwarzenbach RP, Gschwend PM, Imboden DM, (2003) Environmental Organic Chemistry, second edition, Wiley Interscience

Kleineidan S, Rugner H, Ligouis B, Grathwphl P, (1999). Organic matter facies and equilibrium sorption of phenanthrene. Environmental Science & Technology 33, 1637- 1644

Yang Y, Sheng G, (2003) Enhanced pesticide sorption by soils containing particulate matter from crop residue burns. Environmental Science &Technology 37, 3635-3639

Yasser Z, El-Nahhal, Jamal M S, (2003) Adsorption of phenanthrene on organoclays from distilled and saline water. Journal of Colloid and Interface Science 269, 265 - 273

Hydrochemical investigation of water at Loussi Polje, N Peloponnesus, Hellas

R. Koutsi[2], **G. Stournaras**[1]

[1]Professor of Hydrogeology and Engineering Geology, Department of Geology and Geoenvironment, National and Kapodistrian University of Athens, GR 157 84, Panepistimioupolis Zografou, Athens, Greece, stournaras@geol.uoa.gr
[2]Dr Geologist, Athens, reginakoutsi@yahoo.gr

Abstract Loussi Polje, situated in the west of Helmos Mountain, N Peloponnesus, Greece, drains carbonate aquifers through several small karst springs. In the area, which is scarcely populated, few boreholes can be found, mostly used for irrigation purposes. In the framework of an integrated study of karst aquifer vulnerability, the physical and chemical characteristics of the water from these springs and boreholes were studied for two years. This paper deals with the hydrochemical analysis and results, in order to better understand the main factors that control the groundwater composition and its seasonal variations and to reveal the existence of any possible source of contamination.

1 Introduction

Loussi Polje is situated 12 km SW of Kalavryta, in N Peloponnesus (Fig. 1a). It covers approximately 20 km^2 and the altitude ranges from 940 to 1100 m. The polje's main axis addresses SSE – NNW, whereas in the north changes to WNW – ESE. It is drained by the Manna River into two pair of sinkholes at an altitude of 967 m. Karst carbonate formations cover about 35 % of the polje's area. Several small karstic springs and few boreholes are located around the polje, at the roots of the limestone volumes. The water from the boreholes and some springs is used primary for irrigation purposes and less for domestic use. Groundwater sampling in the study area was aimed at (a) providing an overview of the chemical signatures of groundwater, (b) monitoring their variation during wet and dry seasons and (c) identifying areas susceptible to pollution.

In all, 32 samples from springs and boreholes were collected for two dry and two wet periods during September 2002 - May 2004. Sampling localities are shown in Fig. 1b. Samples were collected in 1000 ml polyethylene bottles. Onsite measurements for physicochemical parameters (pH, EC, water and air temperature) were carried out on a monthly basis for two years. Major and some minor ion chemistry were measured in the laboratory of Geochemistry and Economic Geology, Faculty of Geology and Geoenvironment, NKUA.

N. Lambrakis et al. (Eds.), *Advances in the Research of Aquatic Environment, Vol. 2*
DOI 10.1007/978-3-642-24076-8, © Springer-Verlag Berlin Heidelberg 2011

2 Geology

The geology of Loussi polje is characterized by the presence of two geotectonic zones, the Olonos - Pindos which is overthrusted above the zone of Tripolis. The geological formations in the study area from youngest to oldest are: (1) recent alluvium and talus cones, which form the totality of the polje's surface sediments, and emanate mainly from Pindos formations (2) flysch of Eocene, (3) stratified limestones of Upper - Cretaceous, (4) radiolarites of Upper - Jurassic, (5) Upper - Triassic limestones. The Cretaceous stratified limestones of the Pindos zone present the greater extent of all other karstic formations. Upper - Cretaceous thick-bedded limestones of Tripolis zone appear in the NE part of the polje. The characteristic intense tectonism in Pindos zone results in the folding of the strata and the formation of faults. Smaller and bigger faults have a general NNW-SSE direction and they are connected with faults of NW - SE and E - W direction. A big distinctive regular fault of SE - NW direction in the E part of region, brings in contact the two geotectonic zones of Pindos and Tripolis. The fault is visible at the sinkholes area and is directed towards the Cave of the Lakes.

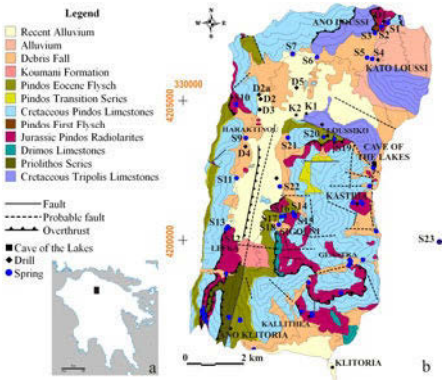

Fig. 1. a. Schematic map, **b.** geological map and sampling points in the study area.

3 Hydrogeology

Pindos and Tripolis limestones as well as the alluviums of the polje are the main aquifers in the region. The Pindos limestones, characteristic of their small thickness and folds, are found in alternations with the relatively impervious strata of flysch and radiolarites of the same zone. This results in the appearance of several springs at the contact of limestones with the impermeable formations at a relatively high altitude. Tripolis limestones do not present folds or thrusts and their thickness is up to 1000 m. The degree of karstification is much higher, with chan-

nels of bigger size and a deeper drainage. Their springs have a significantly greater mean volume and they usually appear at lower altitudes than those of Pindos limestones.

4 Physicochemical Parameters

Water's physicochemical parameters were monthly monitored for two consecutive years. It became therefore feasible to depict their variations throughout the year and to end up with more specific conclusions for each sampling point. Descriptive statistics and correlation analysis appeared to be an indispensible tool.

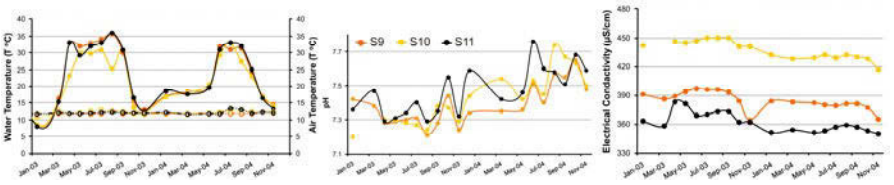

Fig. 2. (a) Temperature (°C) (● air temperature, ○ water temperature), **(b)** pH and **(c)** electrical conductivity (μS/cm) variation for typical springs S9, S10 and S11.

Table 1. Mean, median, minimum and maximum values of water temperature (°C), pH and Electrical Conductivity (μS/cm) for all sampling points during the four sampling periods.

	September 2002			March 2003			October 2003			May 2004		
	T °C	pH	EC	T °C	pH	EC	T °C	pH	EC	T °C	pH	EC
Mean	12.9	7.48	414	11.4	7.53	397	12.2	7.55	418	12.0	7.50	400
Median	13.0	7.42	401	11.8	7.51	382	12.5	7.55	397	12.0	7.50	380
Minimum	10.2	7.20	292	7.6	7.11	268	9.7	7.27	281	9.1	7.14	284
Maximum	16.3	7.99	573	13.2	7.77	564	15.1	7.98	609	14.5	7.84	638

Water's temperature is low during wet periods and obtains maximum values (16.3 and 15.1 °C) during dry periods. There is a direct effect from air temperature and rainfalls. This leads to the conclusion of a groundwater circulation through a surface karst system (Shuster and White 1971, Karanjac and Altug 1980).

The pH in the study area is normal and in acceptable levels. It characterizes a slightly alkaline groundwater during summer months with increased values. During wet periods the values decrease, which most likely indicates the direct influence of rainfalls (Shuster and White 1971, Andreo and Carrasco 1999). The decrease of pH values in all water samples during the wet season of 2003 is very characteristic. In general, the mean values remain constant.

Electrical conductivity of water is a parameter giving comprehensive information on water chemistry. EC values remain low and typical for groundwater in karst formations. The highest values occur at the end of dry periods, while lower values were measured at the end of the wet seasons. A slight increase in electrical conductivity is generally observed during dry periods due to the relatively large residence time of water in the subsoil (Shuster and White 1971, Andreo and Carrasco 1999). There is a general trend in 2003, during which values are decreased compared to those of 2004. According to Zojer et al. (1986), springs that drain Olonos – Pindos aquifers whose catchment areas are local and where the water comes directly from the melting of snow, show quite low values of EC (about 200 μS/cm). S6, S7, S15 and S18 showed values very close to this limit and therefore these characteristics should be taken into account. Higher EC values show waters which run along faults or fault zones (Andreo and Carrasco 1999). S1, S2, S19, S21, S23 and D1 showed such values which probably witness a primary water movement along discontinuities or faults. Higher values of electrical conductivity up to 600 mS/cm are due to water infiltration through loose sediments, resulting increasing grain dissolution in water. Probably this is the reason why S3, S4, S5, S13, S14, S16, S20, D5 showed increased values of EC. Finally, a small change in conductivity during the year indicates a poorly developed karst system (Andreo and Carrasco 1999). Samples from S8, S9, S10, S11, S12, S14, S15, S18, S19 and S21 showed values of EC almost constant, which leads to the conclusion of a poor developed karst system drained from the specific sampling points.

5 Hydrochemical Analysis and Data

All chemical analyses were carried out at Department of Economic Geology and Geochemistry of the University of Athens. The limited extend of this paper did not allowed to list all the results from the hydrochemical analyses during the four sampling periods. For this purpose the average values of physicochemical and hydrochemical data were calculated and depicted on Table 2.

The values of Ca^{2+} are considerably higher than those of Mg^{2+}, which suggests a groundwater's movement mainly within limestones and calcareous formations. The low concentrations of Ca^{2+} and Mg^{2+}, indicates waters of relatively low hardness. Na^{+} and K^{+} are low and show a remarkable stability. HCO_3^{-} shows higher values relative to other ions, which confirms that Loussi Polje drains mainly carbonate aquifers. SO_4^{2-} generally doesn't show high values and most concentrations are negligible. Some very high values observed, were probably due to the presence of Na_2SO_4.The values of NO_3^{-} are low. The values of NO_2 are negligible, demonstrating the absence of pollution of groundwater by nitrate fertilizers.

Table 2. Average values of hydrochemical (ppm) and physicochemical data (T °C, pH, EC μS/cm) for each point during all sampling periods.

	EC	pH	T	Na^{+}	K^{+}	Mg^{+2}	Ca^{+2}	Cl^{-}	NO_3^{-}	$PO4^{-3}$	$SO_4^{=}$	HCO_3^{-}	NO_2^{-}	NH_4^{+}
S1	372	7.55	12.0	3.1	0.4	5.1	70.4	3.9	6.0	0.04	1	217	0.005	0.00
S2	366	7.59	12.7	3.2	0.5	2.2	65.1	4.4	6.7	0.03	2	187	0.009	0.25
S3	563	7.48	12.9	9.0	9.9	6.2	83.2	10.5	18.2	0.53	17	260	0.010	0.05
S5	468	7.44	12.4	5.5	8.4	3.1	73.3	8.5	20.0	0.21	8	230	0.007	0.12
S6	454	7.49	12.4	4.3	3.7	2.8	74.0	3.3	11.4	0.51	4	223	0.013	0.02
S7	344	7.71	10.6	3.7	0.7	3.1	60.5	4.0	6.7	0.03	2	192	0.010	0.07
S9	338	7.72	12.5	4.4	0.6	3.7	53.8	3.4	6.5	0.10	1	169	0.012	0.08
S10	330	7.59	12.3	4.4	0.4	2.7	58.8	4.3	4.4	0.10	2	179	0.012	0.04
S11	419	7.43	12.5	3.9	1.1	2.5	76.9	4.8	13.3	0.20	5	215	0.010	0.05
S12	453	7.40	11.6	6.4	5.8	3.0	76.3	9.6	10.2	0.34	12	209	0.009	0.06
S13	349	7.71	10.9	4.3	1.5	2.2	59.4	4.6	11.7	0.06	4	163	0.009	0.04
S14	434	7.54	12.6	6.4	3.1	2.3	74.8	9.4	31.2	0.05	13	178	0.009	0.04
S16	370	7.61	11.7	4.4	0.7	2.4	65.4	4.9	13.9	0.01	5	179	0.008	0.02
S17	408	7.50	12.5	4.1	0.9	2.7	77.3	5.6	11.6	0.07	5	212	0.011	0.06
S18	481	7.35	12.6	5.9	2.8	4.7	85.3	8.7	16.5	0.18	3	231	0.013	0.06
S19	366	7.59	11.9	3.0	0.6	1.8	46.8	3.9	6.4	0.06	1	183	0.007	0.02
S20	373	7.46	12.0	3.4	0.7	2.0	65.1	4.6	9.2	0.05	2	200	0.016	0.02
S21	427	7.43	12.1	3.2	0.9	6.2	72.4	3.6	6.2	0.03	2	222	0.009	0.06
S23	404	7.68	10.8	2.8	0.4	10.3	54.3	4.2	13.3	0.05	29	179	0.009	0.12
C1	365	8.13	13.8	5.0	0.6	9.58	46.8	7.65	8.36	0.1	17	178	0.019	0.58
D1	472	7.43	13.6	5.4	0.7	5.7	73.4	6.2	7.3	0.08	1	248	0.010	0.11

D4	464	7.44	13.2	9.4	1.2	4.2	73.6	10.9	25.7	0.08	8	208	0.007	0.18
D7	397	7.51	14.1	5.3	0.8	4.2	68.5	5.0	10.6	0.14	1	215	0.010	0.07
D8	418	7.50	13.4	4.4	0.6	3.3	67.0	5.2	14.2	0.03	2	196	0.005	0.05
D9	420	7.50	13.1	4.3	0.7	3.9	70.7	5.2	12.2	0.04	2	189	0.011	0.03
D12	383	7.54	12.7	3.6	1.3	2.2	65.2	4.9	6.9	0.04	2	193	0.010	0.03
D17	410	7.45	13.0	7.6	1.2	3.2	67.0	7.4	9.5	0.22	4	210	0.010	0.20

Table 3. Mean, median, minimum and maximum values of the hydrochemical data from all points during each sampling period.

	September 2002				March 2003				October 2003				May 2004			
	Mean	Med	Min	Max	Mean	Med	Min	Max	Mean	Med	Min	Max	Mean	Med	Min	Max
Mg^{+2}	3.99	2.7	1.3	11	3.73	3	1	11	3.46	2.8	1.2	8.9	3.57	2.75	1.1	12.4
Ca^{+2}	74.17	76	7.35	105.9	64.36	65	43	97	64.23	63.7	39.0	105.4	67.91	65.5	44	109
Na^{+}	4.78	4.1	2.6	12.3	4.66	4.1	2.8	10.8	4.85	4.3	2.9	11.9	4.66	3.95	2.5	10.6
K^{+}	1.53	0.6	0.3	9.2	1.61	0.6	0.3	9.5	1.77	0.6	0.3	10.3	1.791	0.7	0.4	10.4
Cl^{-}	9.05	7.1	3.1	20.4	4.45	4	1.4	10.8	5.85	4.8	2.7	16.5	4.52	3.95	2.2	16.5
NO_3^{-}	10.6	7.92	2.64	35.2	9.11	7.48	3.96	24.64	16.67	12.54	1.72	74.36	12.33	9.24	3.96	55.44
$SO_4^{=}$	4.72	3	0	17	5.76	1	0	37	3.77	2	0	16	5.41	1	0	43
HCO_3^{-}	201.7	201	148	269	207	202	156	275	172.5	173	124	229	214.3	217	152	291
NO_2^{-}	0.02	0.01	0	0.24	0.01	0.01	0.00	0.02	0.018	0.008	0	0.24	0.01	0.009	0.006	0.019
NH_4^{+}	0.10	0.06	0	0.59	0.07	0.04	0.00	0.54	0.11	0.07	0.02	0.59	0.07	0.035	0	0.6
PO_4^{-3}	0.11	0.05	0.01	0.53	0.11	0.06	0.00	0.56	0.135	0.07	0	0.6	0.098	0.045	0	0.52

Cl^- also shows low values, which are indicative of water in karstic rocks and range well below the indicative levels. Finally, the values of NH_4^+, PO_4^{3-} and CO_3^{2-} are negligible and therefore not suitable for evaluation.

6 Statistical Analysis and Piper Diagrams

In order to obtain a better overview of the main trend and variability of the region's hydrochemical data, descriptive statistics and correlation analysis were used (Table 3) and led to the following conclusions.

Ca^{2+} and Mg^{2+} values – apart from September 2002 – remain roughly the same and show the same variability as their medians. Na^+ mean values show a small increase during dry sampling periods whereas the median values stay approximately constant. K^+ mean values increase slightly from 1.53 mg/L in September 2002 to 1.79 mg/L in May 2004. Median values stay almost constant at 0.6 mg/L. HCO_3^- values and medians show a small decrease during dry periods. SO_4^{2-} shows a significant increase in the maximum values during wet seasons which affects in the same way the mean values. The medians show very small changes instead. NO_3^- maximum values remarkably increase during dry periods and overall show a significant increase during the third and fourth sampling period. The medians are constant, tend to increase during dry periods and show the same trend as the mean values for the last two periods. NO_2^- shows intense increased maximum values during dry periods, whereas the medians stay constant. Cl^- shows almost double mean median and maximum values during the first sampling period in September 2002. The median values tend to increase during dry periods. Consistency characterizes NH_4^+ values whose medians slightly increase during wet periods. PO_4^{3-} gets very small values whose variation and medians are almost constant. CO_3^{2-} values are zero.

Based on the decreasing values of anions and cations it was found that the dominant water type is carbonate, according to which: HCO_3^->SO_4^{2-}>Cl^- and Ca^{2+}>Mg^{2+}>Na^+ (in Kallergis 2000). The majority of the springs and boreholes in the region are characterized by a Ca-HCO_3 water type. According to the hydrochemical facies, the samples belong to Chebotarev's upper hydrochemical zone (Chebotarev 1955). Samples from the Cave of the Lakes (C1) showed a Ca - Mg - HCO_3 water type. The presence of Mg^{2+} witnesses a dolomitic limestone effect on water from the carbonate series of Tripolis. Samples from Planitero spring (S23) confirm a Ca - Mg - HCO_3 - SO_4 groundwater type, which indicates the Tripolis carbonate aquifers' drainage from the specific spring. The presence of SO_4^{2-} is due to its increasing concentration during the water's movement in the aquifer towards the spring (in Kallergis 2000).

According to Piper diagrams (Piper 1944) (Fig. 3), there is an almost uniform distribution for all sampling points. Due to the dissolution of $CaCO_3$ from water, samples are allocated entirely to the left outer corner with small deviations mainly parallel to the Ca + Mg side, up to a maximum of 20% for Mg.

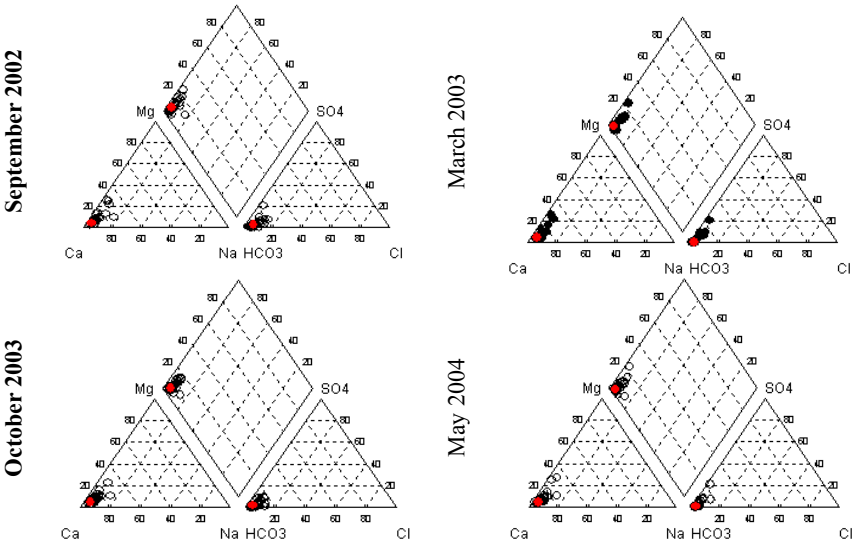

Fig. 3. Piper diagram for typical spring S9 (red color) and all the other samples (black color) for the four sampling periods. Similar diagrams have been carried out for all sampling points.

Therefore almost all water samples belong to a Ca - HCO_3 type. In three sampling points (C1, S23 and D5), a slight deviation from the dominant distribution was observed. For C1, the distribution of all sampling periods apart from October 2003, shows anions values slightly increased towards SO_4, and Mg values slightly increased on the cations side. This may be due both to the movement of water through the carbonate series of Tripolis and to the droppings of bats, which live inside the cave, leading to water pollution in the Lakes. The PIPER diagram for Planitero spring, S23, shows a transfer over 20% on the side of cations, parallel to Ca–Mg axis. The distribution is influenced by the fact that the spring drains water from carbonate aquifers of Tripolis.

7 Conclusions

Groundwater shows small variations in the concentration of major ions and meets with the requirements for irrigation and drinking water (according to EU Directive 80/778 EEC). It also belongs to the hydrochemical Ca-HCO_3 type indicating its origin from Pindos limestones. Instead, the Cave of the Lakes (C1) and the Planitero spring (S23) show a Ca - Mg - HCO_3 and a Ca - Mg - HCO_3 - SO_4 water type respectively. Temperature and pH values are influenced by rainfalls which is an indication of a surface circulation of water. Three categories of sampling points could be grouped according to their EC: (i) < 200 μS/cm, (ii) those with constant

moderate values and (iii) ≤600 μS/cm. Both hydrochemical (major and minor ions) and physicochemical data (T °C, pH, EC) remain within normal limits for carbonate formations. The fact that in many cases EC shows a fairly constant value during wet and dry periods probably indicates a water circulation in a poorly developed surface karst system. At present, groundwater in the study area does not face an immediate risk of pollution due to the existence of only small and controlled pressures. Two major karstic features and touristic attractions in the area are hydrogeologicaly connected with Loussi polje. The Cave of the Lakes is recharged by water that infiltrates through the Tripolis carbonate volume above it, at the south-west limits of Loussi polje (Stournaras et al. 1991) and the important Planitero spring is partly recharged by water that is drained through Loussi sinkholes (Koutsi and Stournaras 2005). Therefore, it should be a priority to maintain the good quality of the groundwater in the region for two more important reasons.

Acknowledgments The authors would like to thank Prof. A. Kelepertsis for his permission to use the laboratories of the Department of Economic Geology and Geochemistry in Athens, and especially Dr. D. Alexakis for his kind and helpful scientific guidance in conducting the analyses of the samples. The research was co-funded by the European Social Fund and National Resources in the framework of "HERACLEITOS" project.

References

Andreo B, Carrasco F (1999) Application of the geochemistry and the radioactivity in the hydrogeological investigation of carbonate aquifers (Sierras Blanca and Mijas, southern Spain). Appl. Geochem .14, 283-299

Chebotarev IJ, (1955) Metamorphism of natural water in the crust of weathering. Geochem. Cosmochim. Acta 8, 22-212

Kallergis, G (2000) Applied Environmental Hydrogeology, TCG, Athens

Karanjac J, Altug A (1980) Karstic spring recession hydrograph and water temperature analysis: Oymapinar Dam Project, Turkey. J. Hydrol. 45, 203-217

Koutsi R (2007) The role of epikarst in assessment and mapping of the karstic formations vulnerability, using the under establishment new relevant European method, PhD Thesis, NKUA

Koutsi R, Stournaras G (2005) Tracer test at Loussi polje karst system (Kalavryta – North Peloponnesus, Hellas), 7th Hellenic Hydrogeological Conference and 2nd MEM Workshop on fissured Rocks Hydrology, Conference proceedings, 2, 241-248

Piper AM (1944) A graphical procedure in the geochemical interpretation of water analyses. Trans. Amer. Geophys. Union 25, pp. 914-923

Shuster ET, White WB (1971) Seasonal Fluctuations in the Chemistry of Limestone Springs: A Possible Means for Characterizing Carbonate Aquifers. Journal of Hydrology, 14, 93-128

Stournaras G, Panagopoulos A, Sotiropoulou K, Alexiadou Ch (1991) Aspects hydrogéologiques des bassins fermés karstiques. La grotte de Limnes Kastrion (Peloponnèse, Grèce) 116e Congrès des Sociétés Savantes, Chambéry, 5ème Colloque d' Hydrologie en pays calcaire, Neuchâtel, 1992

Zojer et al. (1986) Karst Hydrogeology of the Central and Eastern Peloponnesus (Greece), 5th International Symposium on underground water tracing. In Kommission Springer- Verlag Wien

Chemistry of Submarine Groundwater Discharge in Kalogria Bay, Messinia-Greece

A. Pavlidou, I. Hatzianestis, Ch. Zeri, E. Rouselaki

Institute of Oceanography, Hellenic Centre for Marine Research (HCMR) 46.7 Km Athens-Sounio Av., Anavyssos, 19013, Greece, aleka@ath.hcmr.gr

Abstract Concentrations of inorganic nutrients (nitrate, nitrite, phosphate, silicate and ammonium), trace metals (Cd, Cu, Ni, Fe, Pb), Total Organic Carbon (TOC), Dissolved Oxygen (DO) and organic pollutants (pesticides and insecticides, organochlorines, hydrocarbons, etc) were determined in samples taken from Kalogria Bay submarine spring and the adjacent marine environment (SW Aegean Sea), in order to present, for the first time, the chemical characteristics of Submarine Groundwater Discharge (SGD) in Kalogria Bay and to study the effect of the SGD on the marine ecosystem. We also used estimations of the mean monthly spring discharge, in order to quantify the release of chemical constituents via the submarine discharge system to the marine environment. The results show that the loads of chemical constituents released by the SGD in the marine environment of Kalogria Bay do not impact the functioning of the marine ecosystem. All the chemical constituents measured, were well below the criteria set by the Directive 98/83/EC of 3rd of November 1998 on the quality of water intended for human consumption.

1 Introduction

Submarine Groundwater Discharge (SGD) into the sea is an integral part of the global hydrological cycle. The chemical load associated with SGD has been recognized to have a significant impact on coastal marine ecosystems. It is noteworthy that even a small net flux of submarine groundwater can deliver a comparatively large flux of nutrients to the sea (Beck et al 2007; Stieglitz 2005; Johannes 1985). Consequently, SGD can potentially contribute to pollution of the marine environment as it is enriched in nutrients, metals and organic pollutants, depending on the anthropogenic activities that impact on the groundwater and play important role as a pathway for the cycling of chemical constituents (Pavlidou 2003; Boehm et al 2006; Gallardo and Marui 2006; Moore 2006).

In most parts of the world the economic development of coastal regions is leading to a series of problems that highlight the urgent need of using the water of submarine springs in order to provide fresh water for human needs.

In Kalogria Bay, in SW Aegean Sea, Greece, four single point submarine springs of varying discharge rates have been observed. The only permanent SGD emanates at 25-26 m depth. It is noteworthy that the outflowing water creates at

N. Lambrakis et al. (Eds.), *Advances in the Research of Aquatic Environment, Vol. 2*
DOI 10.1007/978-3-642-24076-8,

the sea- surface a gyre with variable diameter, from 25 to 60 m, visible from long distance. The potential use of the SGD water for drinking purposes motivated a multi-disciplinary study of the spring, from July 2009 to May 2010. The main goals of this study are:

- to present the chemical data for the Kalogria Bay SGD, in SW Aegean Sea,
- to study the effect of the SGD to the marine ecosystem close to the SGD discharge and
- to make preliminary estimates of the chemical loads via the submarine discharge system in order to quantify, the release of chemical groundwater substances to the marine environment of Kalogria Bay in SW Aegean Sea.

2 Materials and methods

Samples were taken during 8 surveys (July, September, October, November and December 2009 and January, February, March and May 2010), at the site of the selected SGD, at water depth of 25 m, 20 m and 10 m and at the sea surface. Samples were also taken at different sites in the marine environment, located at different distances from the SGD (ST01:790 m; ST02: 580 m; ST03:1180 m; ST04: 330 m; ST05: 1490 m; and M2: 2500 m from the SGD) (Fig. 1). Station M2 was used as reference station as it is monitored since 2006, in the framework of a monitoring program of HCMR. Measurements of trace metals (Cd, Cu, Ni, Fe, Pb), inorganic nutrients (nitrate, nitrite, phosphate, silicate and ammonium), TOC, Dissolved Oxygen (DO) and organic pollutants (insecticides, organochlorines, hydrocarbons, phthalates) were performed. DO measurements were performed immediately after the sampling using the Winkler method modified by Carpenter (Carpenter 1965). Nutrient analysis was performed at the certified by ISO 17025 biogeochemical laboratories of HCMR using standard methods. Ammonium was measured with a UV-VIS Perkin-Elmer 25 Lamda spectrophotometer (Korroleff 1970). Nitrate, nitrite, silicate and phosphate concentrations were measured with a BRAN+LUEBBE III nutrient autoanalyzer using standard methods (Murphy and Rilley 1962; Mullin and Rilley 1955; Strickland and Parsons 1977). TOC analysis was carried out following the method described by Cauwet (1994), using an automatic analyzer (Shimadzu TOC-5000). Dissolved trace metals were determined following the method described by Riley and Taylor (1968) as modified by Kingston et al (1978) by graphite furnace AAS, using a Perkin-Elmer 4100, HGA 700. Organic pollutants were determined by gas chromatography – mass spectrometry and gas chromatography – ECD after extraction of the water samples collected in clean glass bottles with n-hexane.

In order to quantify the SGD-derived flux of chemical constituents from land to the marine environment, we used measurements of dissolved constituents at the outflow of the spring and calculation of SGD mass flux based on radionuclides as tracers (Tsabaris et al 2011, in this book).

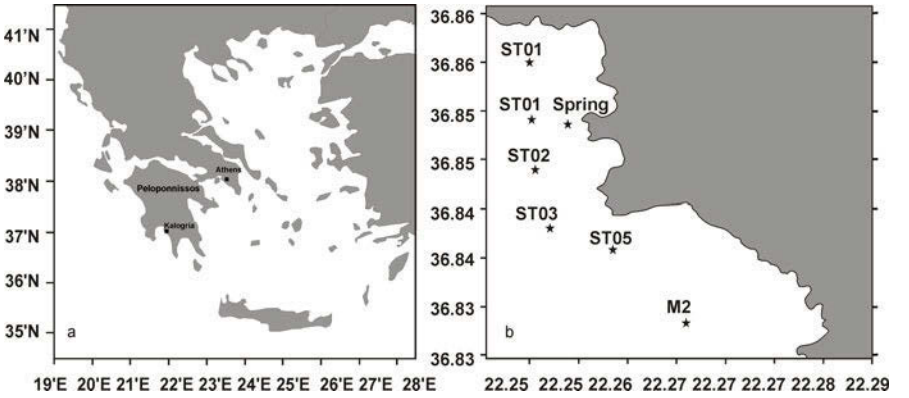

Fig. 1. Study area location (a) and sampling stations in Kalogria Bay (b).

3 Results and Discussion

3.1 Dissolved Oxygen and Nutrients

Salinity values measured in all the samples taken from the submarine discharge (25m depth) for chemical analyses, varied from 14 to 24, indicating that the emanated groundwater is strongly influenced by seawater. Only in November 2009 the samples taken from the SGD had salinity 36, indicating that in this case seawater was rather sampled instead of freshwater. During this survey, the divers could hardly reach the SGD without the danger of abrupt ascending, because of the high discharge of the spring. Figure 2a-f shows the monthly concentrations of DO and nutrients in the SGD at 25 m, at 20 m and 10 m under sea surface and at the sea surface. Temporal variation is related to the flow rate variation of the SGD. Most nitrate and silicate concentrations in SGD are higher than those measured at the sea surface and in the adjacent marine area. Relatively low nutrient concentrations were recorded at the SGD during November 2009, coinciding with the high salinity of the samples. The brackish SGD collected at 25 m depth contained relatively high concentrations of silicate during all the surveys (20.05±11.05 μmol/L; maximum silicate value: 34.3 μmol/L in May 2010), low values of soluble reactive phosphate (0.10±0.02 μmol/L) and relatively high dissolved inorganic nitrogen (DIN) (7.08 ± 4.30 μmol/L; maximum nitrate concentration: 13.8 in October 2009); on average, in the samples taken at 25 m during all the surveys, nitrate comprised 95% of the nitrogen. The nitrate concentrations in SGD may be associated with large pools of nitrate and high rates of remineralization in upland soils. Human activities also alter N concentrations in groundwater, mainly ammonium and nitrite concentrations. In this region (near Stoupa), the nitrates found in groundwater could originate from fertilizers and manure from agricultural and

farming uses. Low phosphate concentrations (<0.14 μmol/L) were recorded at all depths in the SGD, as at the sea surface, indicating underground absorption mechanisms of phosphorus. During the sampling period the mean water discharge of the spring was 319 ± 165 l/s (Tsabaris et al 2011, in this book).

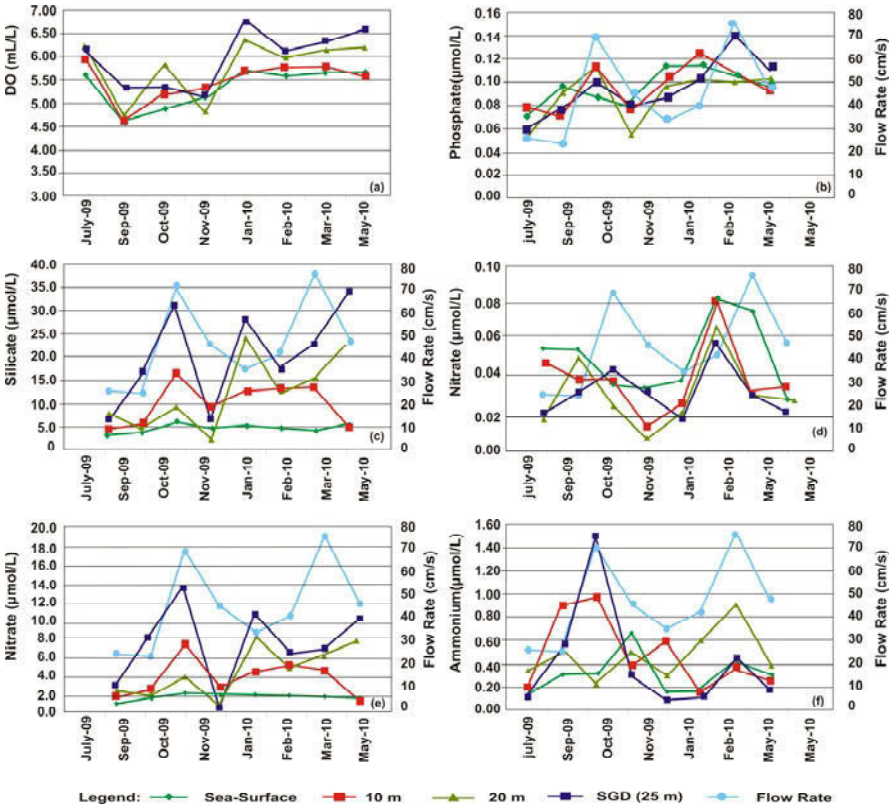

Fig. 2. (a-f) Concentrations of DO and nutrients together with SGD flow rate at the depth of the SGD (25m), 10m, 20m, and sea surface, for the sampling period July 2009 – May 2010 in Kalogria Bay (SW Aegean Sea).

The calculations of nutrient fluxes showed that the submarine spring releases to the marine environment 21890 ± 15090 mol/month of silicates, 7830 ± 5804 mol/month of nitrates, 456 ± 773 mol/month of ammonium and 94.8 ± 64.6 mol/month of phosphates. The variation of nutrient fluxes during the surveys is shown in Figure 3. Mean integrated nutrient concentrations of the water column in the marine ecosystem of Kalogria Bay; correspond to an oligotrophic environment, even close to the SGD. At the stations ST04 and ST01 nitrate and silicate concentrations were an order of magnitude lower than those measured in the close SGD, indicating that the delivery of nutrients during submarine groundwater discharge does not impact the functioning of the marine ecosystem. N: P ratio at the

SGD was higher than the theoretical values for phytoplankton growth, whereas in the adjacent marine area was lower, indicating the nitrogen as the limiting factor for phytoplankton growth.

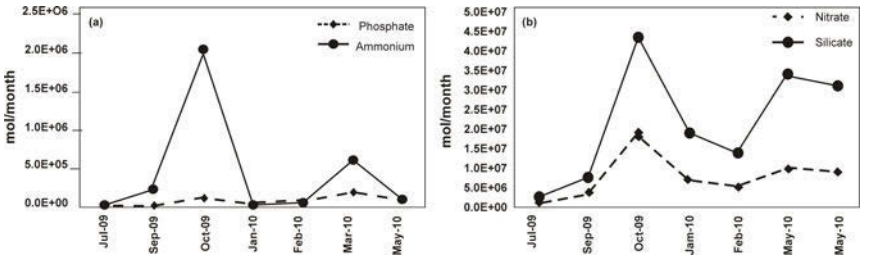

Fig. 3. Variation of nutrient fluxes at 25 m of SGD for the sampling period July 2009 - May 2010 in Kalogria Bay (SW Aegean Sea).

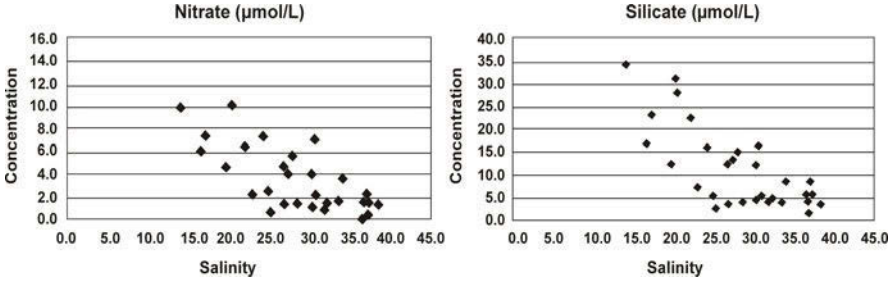

Fig. 4. Silicate and Nitrate relationship with salinity at the SGD (25m, 20, 10, and sea-surface) during all the samplings.

Nutrient and salinity correlation diagrams showed good negative correlation for nitrate and silicate (Fig. 4) but no significant correlation for ammonium, nitrate and phosphate. This picture implies that the groundwater discharge carry some amounts of nitrates and silicates, but these are rapidly mixed with the oligotrophic Mediterranean waters without posing any problems in the adjacent marine ecosystem (about 7-8 times decrease of nitrate and silicate concentrations at seawater salinities). Nitrate, ammonium and phosphate concentrations measured at the SGD were well below the limits set by the Directive 98/83/EC of 3rd of November 1998 on the quality of water intended for human consumption.

3.2 Trace Metals

The mean average values of dissolved Cd, Cu, Ni, Fe and Pb at the brackish SGD collected at 25m depth of the seawater column for all the samplings were: Cd: 0.004 ± 0.001 µg/L; Cu: 0.445 ± 0.325 µg/L; Ni: 0.219 ± 0.107 µg/L; Pb: 0.191 ±

0.146 ± 0.146 μg/L; Zn: 3.90 ± 1.21 μg/L. Fe was measured only during October 2009 and found 1.10 μg/L. Our calculations of metal fluxes via SGD to the marine ecosystem resulted the following amounts for each metal: 4.3 ± 3.8 g Cd /month, 310.2 ± 129 g Cu /month, 2242 ± 1501 g Ni /month, 4163 ± 2764 g Zn /month and 131.9 ± 26.31 g Pb/month. The monthly variations of the concentrations of Cd, Cu, Ni and Pb in the SGD at 25m under sea, at 20m, 10m and finally at the sea surface are shown in Fig. 5.

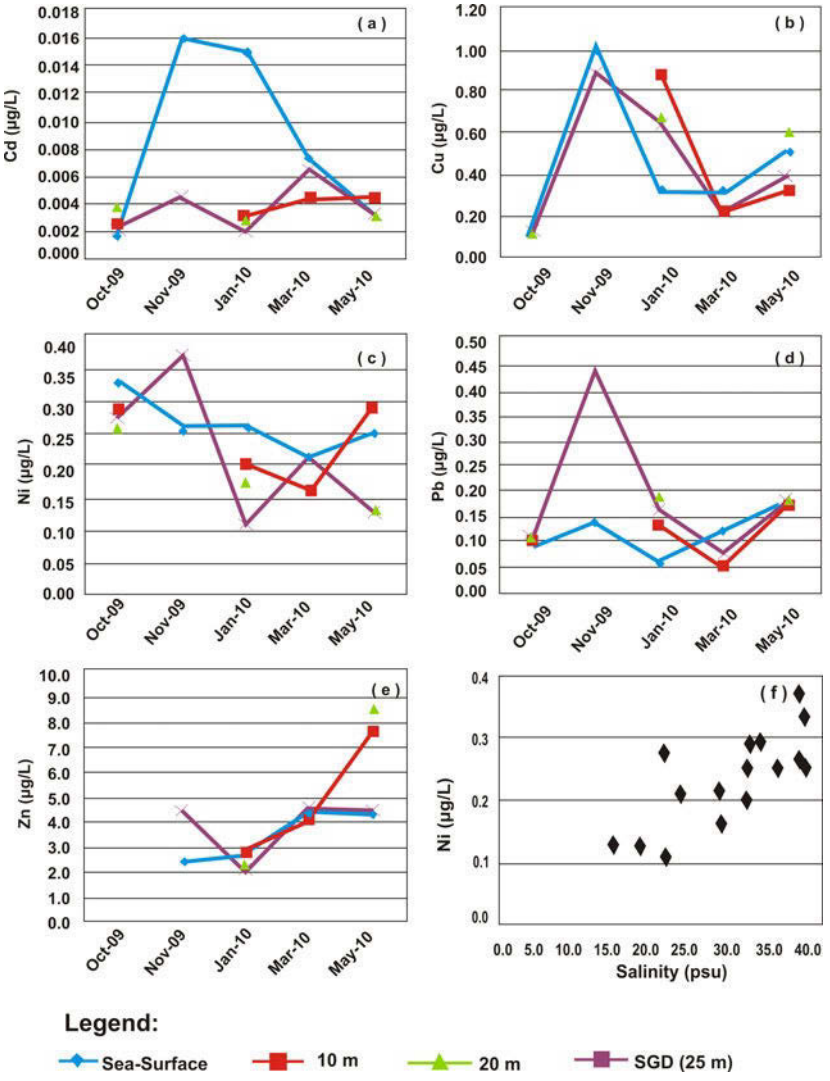

Fig. 5. (a-e) Trace metal concentrations at the depth of the SGD (25m), 10m, 20, and sea surface, for the sampling period October 2009 – May 2010. (f) Ni relationship with salinity.

Most metal concentrations in SGD are lower than those measured at the sea surface and the adjacent marine area. Cd, Cu, and Pb did not show trends relative to salinity indicating that the SGD is not a source of these metals for the marine environment of Kalogria Bay. Only Ni showed significant positive correlation with salinity (R^2: 0.51) which further indicates that there is no enrichment in metals from the SGD. It seems that biogeochemical processes along the groundwater flowpath may impact metal concentrations at the SGD.

Mean metal concentrations of the water column at the reference station M2, during the sampling periods were at the same levels as at SGD (0.005± 0.325 μg/L for Cd; 0.477± 0.293 μg/L for Cu; 0.254± 0.071 μg/L for Ni; 0.148± 0.079 μg/L for Pb and 4.14± 1.45 μg/L for Zn), indicating again that SGD is not a source of metals for the area.

3.3 Organic Carbon

TOC concentrations in the marine stations adjacent to SGD (ST1, ST2, ST3, ST4, ST5 and M2) ranged from 58 to 136 μmol/L. These values are considered typical for an oligotrophic coastal marine environment and indicate the absence of anthropogenic organic carbon sources. At the SGD station, the TOC values were lower than those in the rest of the area and varied between 34 and 87 μmol/L. Figure 6a presents the monthly variations of TOC concentrations at the SGD station. It is noteworthy, that in most cases the lowest values were recorded close to the bottom (25 m) indicating that the groundwater organic carbon load was very low. This is further confirmed by the good positive correlation (R^2: 0.60) observed between TOC values and salinity (Fig. 6b).

Based to the estimated monthly water discharge (Tsabaris et al. 2011, in this book), the spring releases to the marine environment are 58815 ± 5804 mol TOC/month. It is clear that the quality of the discharged groundwater regarding the organic carbon content is very good.

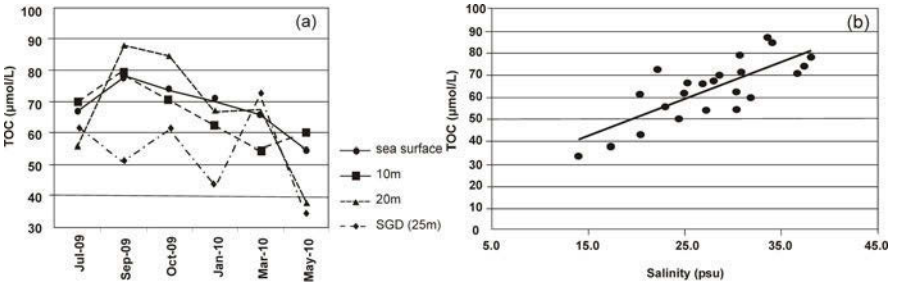

Fig. 6. (a) TOC concentrations at the 25, 20 and 10 m of the SGD and at the sea surface and **(b)** correlation between TOC and salinity values for the SGD waters (July 2009 – May 2010).

3.4 Organic Pollutants

Pesticides and insecticides: The concentrations of these compounds were below the detection limit (0.02 μg/L) in all analyzed samples

Organochlorine compounds: Polychorinated biphenyls (PCBs) were detected in all samples but in very low concentrations (0.8-3.2 pg/L). DDTs concentrations were also very low (1.5-4.9 pg/L) while lindane and hexachlorobenzene were undetectable (<0.1 pg/L). These values are characteristic of unpolluted marine areas. There was no differentiation between the SGD site and the other stations and no correlation between PCBs or DDTs concentrations and salinity was observed.

It was calculated that 978.1± 502.6 μg of PCBs /month and 1837 ± 984 μg of DDTs/month were released to the marine environment via the SGD.

Hydrocarbons: The only hydrocarbons detected were n-alkanes and some low molecular weight PAHs (especially naphthalene and phenanthrene). Their concentrations were very low and similar to those found in unpolluted aquatic ecosystems. No correlation was observed between hydrocarbons and salinity. The lowest values were recorded at water depth of 20 and 25m of SGD site where the lowest values of TOC and salinity were also recorded.

Other organic pollutants: Phthalates were detected in all samples in low concentrations. These compounds are commonly used as plasticizers and are widespread in all aquatic environments. It is noteworthy that their concentrations around the SGD, although very low, were slightly elevated compared to the reference station M2. This might be an indication that the groundwater contains trace amounts of phthalates.

The concentrations of all the organic pollutants detected were well below any drinking water criteria values, suggesting the good quality of the groundwater for any human use.

4 Conclusions

Measurements of Dissolved Oxygen, inorganic nutrients (nitrate, nitrite, phosphate, silicate and ammonium), trace metals (Cd, Cu, Ni, Fe, Pb), TOC and organic pollutants at Kalogria SGD and estimation of their fluxes released in the marine environment per month, showed that SGD does not impact the functioning of the marine ecosystem of Kalogia Bay. According to our results, all the chemical constituents measured were well below the criteria set by the Directive 98/83/EC on the quality of water intended for human consumption.

References

Beck AJ, Tsukamoto Y, Sanchez AT, Huerta-Diaz M,, Bokuniewicz HJ, Sanudo-Wilhelmy SA (2007) Importance of geochemical transformations in determining submarine groundwater discharge-derived trace metal and nutrient fluxes. Applied Geochemistry 22, 477–490

Boehm AB, Shellenbarger AG, Davis KA (2006) Composition and flux of groundwater from a California beach aquifer: Implications for nutrient supply to the surf zone. Continental Shelf Research 26, 269–282

Carpenter JH (1965) The accuracy of the Winkler method for the dissolved oxygen analysis. Limnology and Oceanography, 10, 135-140.

Cauwet G (1994) HTCO method for dissolved organic carbon analysis in seawater: influence of catalyst on blank estimation. Marine Chemistry 47, 55–64

Johannes RE, Hearn CJ (1985) The effect of Submarine Groundwater Discharge on nutrient and salinity regimes in a coastal lagoon off Perth , Western Australia. Estuarine, Coastal and Shelf Science 21, 789–800

Kingston HM, Barnes IL, Brady TJ, Rains TC, Champ MA (1978) Separation of eight transition elements from alkali and alkaline earth elements in estuarine and seawater with chelating resin and their determination by graphite furnace atomic absorption spectrometry. Analytical Chemistry 50 (14), 2065–2070

Koroleff F (1970) Revised version of "direct determination of ammonia in natural waters as indophenol blue I.C.E.S., C.M. 1970/C: 9. ICES information on Techniques and Methods for the sea water analysis. Interlab. Rep. No. 3, 19-22

Moore WS (2006) The role of submarine groundwater discharge in coastal biogeochemistry. Journal of Geochemical Exploration 88, 389–393

Mullin J B, Riley J. P (1955) The colorimetric determination of silicate with special reference to sea and natural waters. Analytica Chimica Acta, 12, 162-176

Murphy J, Riley JP (1962) A modified solution method for determination of phosphate in natural waters. Analytica Chimica Acta, 27, 31-36

Pavlidou, A (2003) Monitoring of the groundwaters, Lake Koumoundourou and the adjacent marine area in relation to the landfill of Western Attica. Technical report, pp. 248, Hellenic Centre for Marine Research, in Greek

Riley JP, Taylor D (1968) Chelated resins for the concentration of trace elements from seawater and their analytical use in conjunction with atomic absorption spectrometry. Analytica Chimica Acta 40, 479–485

Strickland JD, Parsons TR (1977) A practical handbook of sea water analysis. Fisheries Research Board of Canada, 167, 310p

Tsabaris C, Patiris D, Karageorgis A, Eleftheriou E, Georgopoulos D, Papadopoulos V, Papathanassiou E (2011) Application of an in-situ system for continuous monitoring of radionuclides in submarine groundwater sources. Submitted in 9th International Hydrogeological Congress, Kalavrita 3-8 October 2011 (pages number must be added after the final editing)

Chemical characterization of the thermal springs along the South Aegean volcanic arc and Ikaria island

S. Karakatsanis[1], W. D'Alessandro[2], K. Kyriakopoulos[3], K. Voudouris[4]

[1] MSc Geologist, karastyl@gmail.com

[2] Istituto Nazionale di Geofisica e Vulcanologia – Sezione di Palermo, Via U. La Malfa 153, 90146 Palermo, Italy, w.dalessandro@pa.ingv.it

[3] National and Kapodistrian University of Athens, Dept. of Geology and Geoenvironment, Panepistimioupolis, 157 84 Ano Ilissia, Greece, ckiriako@geol.uoa.gr

[4] Aristotle University of Thessaloniki, Laboratory of Engineering, Geology and Hydrogeology kvoudour@geo.auth.gr

Abstract The south Aegean volcanic arc and Ikaria island are characterised by the presence of many thermal springs. Hydrochemical data from 46 springs were used to get insight on their water quality. Highest temperatures were recorded in Ikaria (58.3 °C), Santorini (50 °C) and Milos (43.7 °C). There is a wide range of major ions' concentration but the predominant water type is Na-Cl. The composition of waters is mainly influenced by seawater intrusion and secondly by mixing with deep hydrothermal and shallow meteoric waters. The trace elements' concentration is mainly controlled by high temperature dissolution of primary volcanic minerals and precipitation of secondary solid phases. Factor analysis explains 90% of the total compositional variance with a five factor model.

1 Introduction

The geothermal fields in Greece are often associated with the volcanic activity, as well as with the presence of a shallow magma, especially along the South Aegean volcanic arc (Megalovasilis 2005). This arc extends from Sousaki-Loutraki to Nisyros island and the presence of geothermal fields of low, medium and high temperature are the expression of post-volcanic activity. The region of the south Aegean volcanic arc is characterized by abnormal heat flow, originated from recent intense volcanic activity (Fytikas 1977).

The volcanic activity is strongly related to fault systems that favors deep groundwater circulation and the development of thermal springs. In a large area behind the volcanic arc, normal faults of E-W direction are recorded. In the islands of the volcanic arc many thermal springs are discharged. Numerous investi-

N. Lambrakis et al. (Eds.), *Advances in the Research of Aquatic Environment, Vol. 2*
DOI 10.1007/978-3-642-24076-8, © Springer-Verlag Berlin Heidelberg 2011

gations have been carried out during the last 30 years in order to study the origin and composition of their waters. Lambrakis and Kallergis (2005) reviewed the hydrogeological and hydrochemical characteristics and origin of thermal waters of the whole Greece. This paper investigates the spring-water composition from the islands of the south volcanic arc and Ikaria island using conventional hydrochemical techniques and statistical analysis (R-mode factor analysis).

2 Geological and hydrogeological setting

The Aegean region represents an active convergent zone, where continental micro-plates exhibit a complex interaction under the influence of the overall N-S convergence between the African and the Eurasian plates (McKenzie 1972). From a geotectonic point of view, the study area is part of the Attic-Cycladic massif and is composed of metamorphic rocks such as shists, phyllites and marbles and granite. Neogene and Quaternary deposits overlay the aforementioned rocks. The volcanoes of the South Aegean volcanic arc were especially active in the Late Pleistocene-Holocene as well as were active in historical times. The composition of magmatic rocks in various volcanic fields of Attico-Cycladic massif range from basalts - andesites and trachyandesites to rhyolites showing a calc-alkaline chemical character (Fytikas et al. 1976, Kyriakopoulos 1998).

The hydrogeological regime of the study area is directly related to the lithological composition of the geological formations and the intense tectonics. Aquifer systems of low transmissivity are developed in faulting zones, where the rocks show secondary porosity, as well as in weathered subsurface zones. The result was emerging of numerous springs in these zones. Recharge to these aquifer systems is commonly derived from local precipitation which infiltrates slowly. Deep aquifers are developed locally, which are exploited in the island of Milos and Nisyros by 5 and 2 boreholes, respectively. Average annual rainfall is 400 mm and the actual evapotranspiration is 75-82 % of the annual rainfall.

3 Sampling and analytical methods

Forty-six (46) water samples were collected from springs during the years 2005-2007. The samples were collected from the following islands: Ikaria (15), Methana peninsula (12), Kos (6), Milos (5), Santorini (3) and Nisyros (2), as well as from Loutraki-Sousaki region (3). Water sampling locations are shown in Figure 1. The temperature (T), the electrical conductivity (EC), pH, and redox potential (Eh) of water samples were measured in situ by portable instruments. The samples were filtered in situ, with 0.45 μm filters (Millipore) and were stored in HDPE bottles. The aliquots for major and trace metal analyses were preserved by acidification with HNO_3.

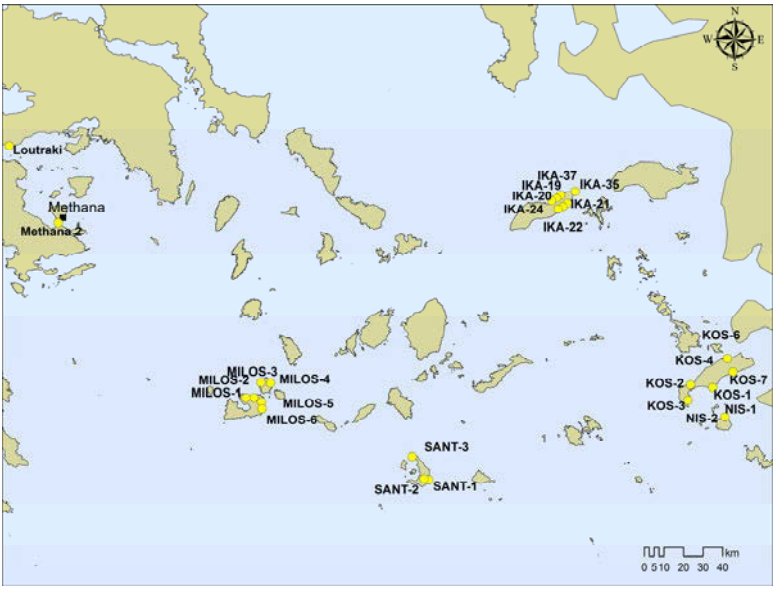

Fig. 1. Map showing the location of thermal springs along the south Aegean volcanic arc.

All chemical analyses were performed at INGV-Pa (Istituto Nazionale di Geofisica e Vulcanologia – Sezione di Palermo Italy). The following chemical parameters were determined: Na^+, K^+, Mg^{2+}, Ca^{2+}, F^-, Cl^-, NO_3^-, SO_4^{2-} via ionic chromatography, Li, Be, B, Al, Mn, Co, Ni, Cu, Zn, Rb, Sr, Ag, Cd, Sb, Ba, Hg, Tl, Pb, Bi, U, V, Cr, As, Fe, Se, Mo, Cs and SiO_2 by using inductively coupled plasma techniques (ICP-MS or ICP-OES) while HCO_3^- was determined by titration (HCl 0.1N). The overall precision of the analyses is within ±5%, as indicated by ionic balance. Summary statistics e.g. mean value, standard deviation, minimum-maximum values and coefficient of variation of the chemical parameters are listed in Table 1.

4 Results

4.1 Hydrochemical water types

Based on the diagrams of Piper (Fig. 2), the following hydrochemical types of waters can be identified.

Ikaria island: Percentage of 53.3% of water samples belongs to Na-Cl or Na-Ca-Cl hydrochemical types and are classified in primary geothermal fluids (Nicholson 1993). The temperature ranges between 28.1 and 58.3 °C. The pH mean value is less than 7 indicating the slightly acid character of waters with maximum value 7.23. Electrical conductivity (EC) varies between 22030-50600 μS/cm and

this is indicative of solutions close to marine composition. The second dominant type Na-Ca-Cl-HCO_3 (33.3% of the water samples) represents cold waters with high concentrations of Ca and HCO_3, indicating mixing processes with water of phreatic origin. Their temperature values are moderate ranging between 18 and 21 °C, pH values are greater than 7, indicating the slightly alkaline character of waters. These waters are characterized by low EC (232-438 μS/cm) and TDS (182-360 mg/L) values, respectively. Other dominant hydrochemical water type is Na-Ca-Mg-Cl-HCO_3, which is probably related to local petrology of the island.

Kos island: The predominant water type is classified as sodium type in the triangle cations, and as chloride type in the anions triangle (Na-Cl, 33.3% of samples), similar to the predominant type in Ikaria island. The maximum temperature value is 42 °C, EC ranges between 674-51100 μS/cm, pH values range between 6.00-7.30 and TDS between 492.6-40736 mg/L. Other hydrochemical types are: Na-Ca-Mg-Cl-HCO_3, Ca-Na-Mg-HCO_3-SO_4-Cl, Ca-Mg- HCO_3 and Ca-Mg-Na-Cl-HCO_3. These types correspond to relatively cold waters with temperature ranging between 14.7 and 19.8 °C. The EC varies between 571-1373 μS/cm, pH values between 7.30-7.42 and TDS between 257-1161 mg/L.

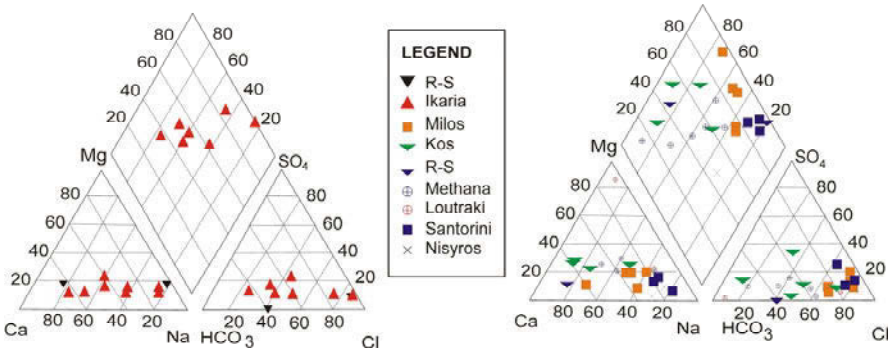

Fig. 2. Piper diagram samples of Ikaria on the left and other areas on the right.

Methana peninsula: All of samples, except one, are thermal waters. Percentage of 50% of the samples corresponds to Na-Cl hydrochemical water type. The temperatures range from 30.5 to 37.5 °C and pH values range between 5.82- 6.32, indicating the acidic behaviour of waters. Total Dissolved Solids vary from 8517 to 39717 mg/L and EC from 15700 to 58000 μS/cm. Other hydrochemical types are: Na-Mg-Cl-HCO_3, Na-Ca-HCO_3-Cl, Ca-Na-Mg-HCO_3, Na-Ca-Mg-Cl-HCO_3, Na-Ca-Mg-HCO_3-Cl and Na-Mg-Cl. These types represent relative cold water with temperature values ranging between 16.5 and 26 °C. EC varies between 734-10,200 μS/cm, pH values between 5.95-7.35, while TDS between 618-3674 mg/L (D'Alessandro et al. 2008).

Milos: Based on results of chemical analyses it is concluded that the dominant type of water is Na-Ca-Cl. The temperature varies from 15.8 to 22.2 °C and EC ranges between 3300-3850 μS/cm. pH values are greater than 7 and TDS values

range between 2210-2558 mg/L. Other water types representing mixed waters (meteoric water and sea water) are: Na-Ca-Cl-HCO_3, Na-Cl-HCO_3 and Ca-Na-Cl-SO_4. The composition of these waters should be attributed to local petrology and their physical and chemical characteristics are: temperature values ranging between 23.2 and 43.7 °C (thermal waters), pH values less than 7, EC 2370-3910 μS/cm and TDS values 2750-6906 mg/L. It is pointed out that, hot springs with high temperatures (40°-75°) were recorded in Milos island (Fytikas 1977).

Loutraki-Sousaki: Two of the three water samples belong to Na-Mg-Cl hydrochemical type. Temperature values range between 17.8 and 31.3 °C, pH values are greater than 7, EC ranges between 592-2950 μS/cm and TDS values range between 560-1868 mg/L. Thermal water of this area is the result of volcanic activity. The third sample belongs to the Mg-HCO_3 type, indicating fresh water. The high concentration of Mg (70 mg/L) can be attributed to dissolution of ultramafic rock minerals.

Santorini: The samples can be classified into the two types: 1) Na-Cl with low temperatures (21.2 -23 °C) and pH values greater than 7 (7.90-8.02), EC values range between 2680-4890 μS/cm and TDS between 1643-3286 mg/L, 2) Na-Cl-SO_4 hydrochemical type with high temperature (50 °C) which is related to geothermal water of this island, pH is 6.96, EC 4890 μS/cm and TDS 3558 mg/L.

Nisyros: One sample belongs to Na-Cl water type with temperature 27.5 °C, pH 7.07, high EC 38600 μS/cm and TDS 28650 mg/L. The second one belongs to Na-Ca-HCO_3-Cl hydrochemical type with low temperature 20.5 °C, pH 8.72 and low EC (941 μS/cm) and TDS 741 mg/L. This type is considered mixing type and is affected by meteoric water of the area.

4.2 Major elements composition

The data of Table 1 show a wide dispersion for the majority of parameters (coefficient of variation generally greater than 100%). A significant relationship is observed between the major ions Na-Cl, Ca-Na, Ca-SO_4, K-Cl, Ca-Mg.

The highest values of Na and Cl concentrations were observed in spring-water of Ikaria island, affected by seawater intrusion. However it has to be pointed out that, the salinity of rainfall in Cyclades Archipelago is high, due to airborne sea spray and this has a strong effect on the chemical composition of the groundwater of the islands even without direct seawater intrusion (Dazy et al. 1997).

High Ca concentrations are recorded at Kos island, indicating their origin from Mesozoic marbles and dolomite breccia. Sulphur is widely distributed in a reduced form in both igneous and sedimentary rocks, as metallic sulphides. The high sulphate concentrations in water could be attributed to the dissolution and oxidation of the mineral pyrite (FeS_2). Sulphur in reduced or oxidized form may be volatilized and released in large amounts in volcanic regions and can be present in geothermal water as well (Hem 1985). Hydrogen sulphide (H_2S) results from the reduction of SO_4 (Methana) under reducing hydrothermal conditions.

The maximum value of SiO_2 is observed in Milos island and can be associated with the high temperature dissolution of igneous rocks. The deep aquifer in marbles has low SiO_2 content and the shallow aquifer in gneiss shows high SiO_2 content. The maximum value of K concentration recorded in Nisyros island is related to K-feldspar dissolution.

Table 1. Statistical summary of the chemical parameters of the water samples.

Parameter	Min	Max	Mean value*	Standard deviation	Coefficient of Variation(%)	Number of samples
Na	1.0	12350	3377.7	4675.3	138	46
Ca	3.8	1578	452.0	524.3	116	46
Mg	0.5	1456	329.6	426.2	129	46
Cl	4.0	22360	6184.5	8527.8	138	46
SO_4	0.1	3555	867.0	1134.7	131	46
pH	5.82	8.76	6.55	6.4	98	46
T	14.7	58.3	28.0	11.5	41	46
E.C.	31.1	67480	15709.7	20608.2	131	46
Sr	0.06	14.93	3.363	3.9	116	45
Mn	0.0	2.796	0.311	0.6	193	44
Fe	0.0	0.758	0.089	0.2	225	43
F	0.022	1.269	0.38	0.4	105	30
SiO_2	11.0	219	58.0	47.9	83	46
As	0.0	0.312	0.023	0.05	217	45
B	0.0	11.47	2.146	2.8	130	46
K	0.0	622	141.4	183.0	129	46
Li	0.0	1.728	0.274	0.43	157	46
Ba	0.005	0.627	0.081	0.1	123	45
Zn	0.0	0.492	0.038	0.09	237	38
Cu	0.0	0.203	0.012	0.036	300	34
Ni	0.0	0.154	0.007	0.024	343	39

* Concentrations in mg/L, electrical conductivity in μS/cm.

4.3 Trace elements composition

High concentration of Sr observed in the majority of samples (Ikaria, Nisyros and Kos island) is related to carbonate minerals. The highest As concentration is recorded in Nisyros island and can be associated to high enthalpy geothermal fluids. The presence of Li can be associated with the increased temperatures of the geothermal fluids. It is well known that high temperatures increase its mobility and release into waters (Apello and Postma 1994, D'Amore and Panichi 1987).

The iron (Fe) concentration deriving either from mafic mineral dissolution or from sulphide minerals oxidation is locally high. Elevated manganese (Mn) concentrations are related to granite of Ikaria (Ikaritis), rich in Mn (Mitropoulos and Tarney 1992). The high boron (B) concentration (mean value 2.1 mg/L) is attributed to geothermal fluids. In the peninsula of Methana high concentrations of Li, Cu and Al are recorded. High concentrations of elements Ba, Zn and Ni occur in Milos and can be associated with the presence of metamorphic graywacke and crystalline basement of schists (Kyriakopoulos 1998).

4.4 Factor analysis

In order to examine the relationships between the hydrochemical parameters R-mode factor analysis was applied (Voudouris et al. 1997). Using factor analysis, the parameter distribution in the samples is explained in terms of five (5) factors. The selected factors explain approximately 90% of the total variance of the data set (Table 2).

Table 2. Loadings for the 5-factors model.

	Factors				
	I	II	III	IV	V
SO_4	.975	.160	-.026	-.067	-.079
Cl	.975	.126	.015	-.167	-.027
Na	.972	.110	.010	-.175	-.023
K	.952	.240	.084	-.125	-.020
Mg	.942	.211	.155	-.173	-.021
Ca	.935	.148	-.013	.047	-.098
Sr	.866	.286	.182	-.108	.099
B	.718	.538	.368	-.053	.045
Mn	.182	.859	.331	.122	-.056
Rn	.410	.801	.334	.110	.017
Li	.457	.773	.348	.080	-.060
Fe	.121	.733	-.225	-.271	.012
As	.099	.430	-.135	-.035	.728
HCO_3	-.001	.288	.888	.066	.179
Al	.484	-.047	.667	-.253	-.106
NO_3	-.183	-.098	-.156	.838	.098
SiO_2	-.246	.215	.517	.660	.075
Ba	-.114	-.105	.159	.149	.911

Factor I: It accounts for 51.5% of total variance with high loadings in the parameters Cl (0.97), Na (0.97), SO_4 (0.975), K (0.95), Mg (0.94), Ca (0.93), Sr (0.87) and B (0.72). This factor can be associated with the intrusion of seawater into aquifers, which increases the concentration of the previous parameters.

Factor II: The second factor represents 17.3% of the total variation and has positive loading in the parameters Mn (0.86), Rb (0.80), Li (0.77), Fe (0.73) and B (0.54). The high loading of Mn and Fe is related to reduced environment and presence of igneous rocks. The high loading of parameters should be attributed to granite dissolution, named Ikaritis, which is rich in these elements.

Factor III: This factor is dominated by HCO_3 (0.89), Al (0.67) and SiO_2 (0.52), and accounts for 8.35% of the total variation. HCO_3 ions are the dominant ions in fresh water and are related to soil CO_2 dissolution and dissociation of the unstable form of carbonic acid (Stamatis et al. 2001). The high loadings of the Al and SiO_2 can be associated with the dissolution of silicate minerals.

Factor IV: It accounts for 6.8% of the total variation and exhibits high loadings with respect to NO_3 (0.84) and SiO_2 (0.66). Nitrate is the most abundant nutrient in water and can be attributed to different sources, the most important of which are the excessive application of fertilizers and the use of septic tanks in conjunction with the disposal of untreated domestic effluent into abandoned wells that are currently used as septic tanks. The high positive loading of SiO_2 reflects the dissolution of silica minerals and high temperatures.

Factor V: This factor accounts for 5.6% of the total variance and shows high loadings on Ba (0.91) and As (0.73). The presence of these elements is related to hydrothermical solutions.

5 Conclusions

The aim of this study is to determine the spring-water quality in the islands of south Aegean volcanic arc. These springs occur in the post-orogenic part of the Aegean arc, which is characterized by the presence of geothermal fields.

The majority of aquifers, which discharge through springs, is firstly associated with the seawater intrusion and secondly with the mixing of meteoric waters and deep thermal water. There is wide range of values of major ions in water. High temperature values were recorded in Ikaria (58.3 °C), Santorini (50 °C) and Milos (43.7 °C), indicating important geothermal anomaly. The predominant water type is Na-Cl. The presence of trace elements is attributed to dissolution of minerals and hydrothermical solutions of the volcanic arc formations.

References

Appelo C, Postma D (1994) Geochemistry, groundwater and pollution. Balkema

D´Amore F, Panichi, C (1987) Geochemistry in geothermal exploration. In: Economides M and Ungemach P (eds). Applied geothermics, Wiley & Sons, New York

D' Alessandro W, Brusca L, Kyriakopoulos K, Michas G, Papadakis G (2008) Methana, the westernmost active volcanic system of the south Aegean arc (Greece): Insight from fluids geochemistry. Journal of Volcanology and Geothermal Research, DOI:10.1016/jjvolgeores. 2008.09.014 , Vol. 178, 818-828

Dazy J, Drogue C, Charmanidis Ph, Darlet Ch (1997) The influence of marine inflows on the chemical composition of groundwater in small islands: the example of the Kyclades (Greece). Environmental Geology 31 (3/4), 133-141

Fytikas M, Giuliani O, Innocenti F, Marinelli G, Mazzuoli R, (1976) Geochronological data on recent magmatism of the Aegean Sea. Tectonophysics, 31, T29-T34

Fytikas M (1977) Geological and geothermal investigation of Milos. PhD thesis, Dept. of Geology, Aristotle University of Thessaloniki

Hem JD (1985) Study and interpretation chemical characteristics of natural water. U.S. Geol. Survey. Water Supply, Paper No 2254

Kyriakopoulos GK (1998) K-Ar & Rb-Sr isotopic data of white micas from Milos island geothermal boreholes field. Anal. Geol. Pays Hell. 38, 37-48

Lambrakis N, Kallergis G (2005) Contribution to the study of Greek thermal springs: hydrogeological and hydrochemical characteristics and origin of thermal waters. Hydrogeology Journal 13, 506-521

McKenzie D, (1972) Active tectonics of the Mediterranean region. Geoph. J. R. Astr. Soc., 30, 55-71

Megalovasilis P (2005) Geochemical investigation of sediments of bottom and regions of Aegean volcanic arc. PhD thesis, University of Athens

Mitropoulos P, Tarney J (1992) Significance of mineral composition variations in the Aegean islands arc. J Volcanol. Geotherm. Res. 15, 283-303

Nicholson K (1993) Geothermal fluids-Chemistry and exploration techniques. Springer Verlag. Berlin

Stamatis G, Voudouris K, Karefilakis Th (2001) Groundwater pollution by heavy metals in historical and mineral area of Lavrio (Attica). Water, Air and Soil Pollution 128, 61-83

Voudouris K, Lambrakis N, Papatheodorou G, Daskalaki P (1997) An application of factor analysis for the study of the Hydrogeological conditions in Plio-Pleistocene aquifers of NW Achaia (NW Peloponnesus, Greece). Mathematical Geology, Vol. 29, No 1, 43-59

Application of an in-situ system for continuous monitoring of radionuclides in submarine groundwater sources

C. Tsabaris†, D.L. Patiris, A. Karageorgis, G. Eleftheriou, D. Georgopoulos, V. Papadopoulos, A. Prospathopoulos, E. Papathanassiou

Institute of Oceanography, Hellenic Centre for Marine Research GR 19 013, Greece

Abstract The application of an in-situ gamma-ray spectrometer for long-term measurements of natural radionuclides into groundwater emanating from submarine groundwater discharge (SGD) sources is described. The system (named KATERINA) has been developed for aquatic applications by Hellenic Centre for Marine Research and as a preliminary study it was deployed at three pilot SGD sites in Greece. After the initial deployment into the lake Tsivlou where background spectrum was obtained, the system was deployed for several hours in Hellenic coastal submarine groundwater sources at Chalkida, Stoupa and Korfos. The radon progenies activity concentration at Chalkida measured in a range from 1.2 to 1.3 Bq/L while at Stoupa from 2.4 to 2.6 Bq/L. Also, the concentration of the radon progenies in the region of Korfos varied from 1.4 to 2.3 Bq/L and an inversely linear dependency with salinity values was observed. The system monitoring radon progeny variations may contribute to hydrological studies concerning the transport, the emanation and the quantification of the groundwater using radiotracing techniques.

1 Introduction

Groundwater contains enhanced radon concentrations, in comparison with surface or sea water, due to radium presence and decay in aquifers soil and rocks. There are four isotopes of radium in subsoil as partners of the primordial natural radioactive series of uranium and thorium but the most abundant is radium ^{226}Ra. Radon ^{222}Rn is the first decay product of ^{226}Ra and is an inert gas. It is transported into groundwater by diffusion through the aquifer soil contains ^{226}Ra or by the decay of diluted ^{226}Ra inside the groundwater mass. Despite the potential hazard for the public health which follows the use of enhanced radon groundwater, radon may be served as a radio-tracer in multiple hydrology studies. As noble gas does not react chemically with aquifer solids or other substances into the water, it is entirely dis-

N. Lambrakis et al. (Eds.), *Advances in the Research of Aquatic Environment, Vol. 2*
DOI 10.1007/978-3-642-24076-8, © Springer-Verlag Berlin Heidelberg 2011

solved, it has a short half life (3.8days) and can be measured directly (Porcelli 2008).

Radon has been already utilized as tracer in many studies around the world concerning mainly the subsurface discharge of groundwater from coastal aquifers into the sea, usually called SGD (Charette et al. 2008). In general, this discharge contains meteoric water from land drainage and possibly seawater which may enter from coastal aquifers. A more detailed definition of SGD has been reported (Burnett et al., 2003) while many studies consider the phenomenon as an important pathway of dissolved matter transport to the ocean (Burnett and Dulaiova 2003; Burnett et al. 2006; Moore 1999). The flux of SGD to the oceans has been estimated globally as a percent fraction of 6 % of the river water flux (Taniguchi et al. 2002). If only the Atlantic ocean is considered this fraction increases up to 80-160% of the river flux (Moore et al. 2008). There are three main sources for SGD: i) coastal freshwater aquifers where SGD is driven by the hydraulic gradient between land and sea; ii) re-circulated seawater in which tides and or internal waves cause a circulation of seawater though coastal sediments; and iii) a mixture of both i) and ii)

The detection and quantification of such sources is realized by direct measurements with e.g. seepage flux meter (measurement of the flow of water out of a known discharge) or by tracer techniques. The later are based on measurements of geochemical species which are naturally enriched in SGD relative to seawater. As groundwater is reached of radon, many studies use this noble radioactive gas to quantify the emanating water as well as, to investigate the temporal and spatial distribution of SGD (Burnett et al. 2006, Burnett and Dulaiova 2006; Burnett et al. 2008). The measurement of radon is based on the detection of alpha particles emitted during its transmutation and/or by the detection of rays (beta- and gamma-rays) emitted as result of the transmutation of its progenies. Measurements of radon are conducted by laboratory based methods like, e.g., liquid scintillation (Purkl and Eisenhauer 2004), by stripping of radon from a water sample (Mathieu et al. 1988) and consecutive measurement in the laboratory and by in-situ methods. In-situ methods prevail in advantages as the detection systems are immersed exactly on the point of interest. So, they provide concentration of radon as time series allowing the investigation of the SGD temporal and spatial variation. However such applications are scarce due to the instrumentation which needed for detection purposes. They require special, fully-integrated detection systems able to withstand many hardships (e.g. enhanced pressure and mechanical stress, chemical corrosion fatigue etc.) due to “unfriendly” acquiring conditions. The Hellenic Centre for Marine Research (HCMR) has developed and maintains from 2007 an autonomous underwater gamma-ray spectrometer named “KATERINA” (Tsabaris et al. 2008). This article describes the deployments of the system into a lake (Tsivlou) and three pilot SGD point sources in Greece (Chalkida, Stoupa and Korfos) which were contributed to the preparation of the system for long-term monitoring of radionuclides into SGD sites.

2 Study areas

The underwater gamma-ray spectrometer was initially deployed into the lake Tsivlou (Achaia prefecture, Peloponnesus) in order to obtain background data. Afrer this deployment three pilot sites of SGD were selected located at Chalkida (Evvoia prefecture, Central Greece), Korfos (Korinthos prefecture, Peloponnesus) and Stoupa (Messinia prefecture, Peloponnesus). The SGD sites in these regions are well known, visible as gyres at the sea surface and are considered point sources emanating groundwater (see Fig. 1).

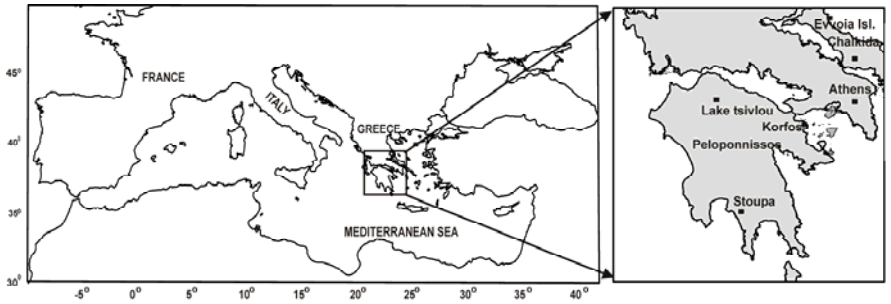

Fig. 1. Study area locations, lake Tsivlou (background level) and three SGD sites at Chalkida, Korfos and Stoupa.

Lake Tsivlou

The lake Tsivlou is one of the recently formed lakes in Europe, located in the prefecture of Achaia (38° 4' 33.3588" N, 22° 13' 58.2672" E) at an altitude of 800m surrounded by the slopes of Mount Helmos. It was created in 1913 as a result of a massive landslide which blocked the Krathes river bed. The lake is extended over an area of 200 m^2 and it has a maximum depth of 80m. As radon and potassium activity concentrations are considered negligible in the fresh water of the lake, the system was deployed to obtain a first background level of their concentrations.

Chalkida

The SGD source at Chalkida is located in the coast a few kilometers southern of the city of Chalkida in Evvoia Island. The rocks formations in the adjacent area are permeable limestones and loose alluvial deposits. The main source consists of 4-5 SGDs locations visible as gyres at the water surface. The water depth at the deployment site was 4-5 m.

Korfos

Korfos is a small coastal village located in Corinth prefecture in NE Peloponnissos. The geological formations of the area are dominated by more than 1000 m thick, karstified limestones and dolomites (Triassic-Jurassic). Faults show a general orientation E-W to NE-SW, and sea water intrusion into coastal aquifers have been identified. The SGD source is associated with karst aquifers outcropping in a submarine cave which is connected to the sea. The submarine cave has elliptical shape with axes of 65m and 42m, respectively. All SGD study was performed inside the submarine cave.

Stoupa

The SGD site at Stoupa, named after the small town of Stoupa in SW Peloponnissos, is located ~500 m off the coast. Limestones and dolomites, and to a lesser extent metamorphic rocks characterize the geological made-up of the coastal zone. The carbonate rocks are heavily karstified and almost completely permeable. The submarine springs have been first recorded in 1975, though local inhabitants are well-aware of their existence and claim that the springs have never stopped emanating water for at least the past 60 years. Although, the main spring discharges water from significant depth (~26 m), the strength of the outflow generates a gyre at the surface, which is clearly visible, particularly under calm weather conditions.

Preliminary observations by scuba divers revealed a system of four locations of SGDs, two strong (in terms of discharge) ones and two smaller ones all within a distance of less than 100 meters. The two strongest SGDs emanate directly from rocks, with very strong currents especially during winter.

3 Materials and methods

The Hellenic Centre for Marine Research (HCMR) has developed and maintains two autonomous underwater gamma spectrometers named “KATERINA” for underwater spectrometric applications (Tsabaris et al. 2008). The system consists of a detector unit and a number of electronics shielded by an aluminum and polyester pressure tube (Fig. 2). The detector unit is a 3”x 3” NaI(Tl) scintillation crystal with built in with a photomultiplier tube, a preamplifier, an analog-digital converter, a high voltage controller and electronic modules for autonomous data acquisition and data storage. In order to keep the size of the housing as small as possible (84 x 550 mm), high density electronics modules are fitted. The power units filter and distribute input voltage (12 - 15 V DC) to independent modules (preamplifier, amplifier, high voltage and multichannel analyzer).The small size and

relatively low power consumption allow the integration of KATERINA into autonomous submersible vehicles (remote operating vehicle (ROV)), a feature which provides significant operational advantages.

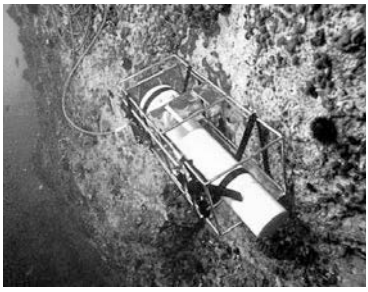

Fig. 2. The gamma-ray spectrometer named KATERINA.

The underwater system has already been energy calibrated and tested for its stability with respect to temperature variations and energy resolution. Measurements of the marine efficiency (the efficiency of the system in the aquatic environment) have also been performed by experimental and simulation studies (Tsabaris et al. 2008; Bagatelas 2008). For this purpose a calibration tank of 5.5 m^3 volume, filled with freshwater water has been used. The system was immersed in the middle of the tank, mounted onto a dedicated small platform. In this way it was surrounded by one meter of water, which is enough to simulate the real aquatic environment, due to the high attenuation of gamma rays in water. At the bottom of the tank, an electric pump was placed for circulation purposes, mixing the water with known concentration of appropriate radionuclides (^{137}Cs, ^{40}K and ^{99m}Tc) insuring homogeneity. From this experiment the marine efficiency coefficient was experimentally measured. Also, Monte Carlo calculations were performed for the estimation of the marine efficiency of the system using the GEANT4 code. The results of the simulations were found in good agreement (2-3%) with the results of the tank experiment. So the underwater system may provide quantitative data about the activity concentration of several natural and artificial radionuclides in any aquatic ecosystem.

4 Deployments and Results

4.1 Initial deployment in lake Tsivlou

The underwater gamma-ray spectrometer was initially deployed into the freshwater of lake Tsivlou attached on a special platform for autonomous operation. All

acquisition parameters were pre-programmed and an underwater battery pack supplied the system. The aim of the deployment was to obtain the background level of radon daughters (^{214}Pb and ^{214}Bi) and potassium (^{40}K) in terms of a gamma-ray spectrum. These natural radionuclides are considered important for several studies related with groundwater and submarine springs. The system acquired the spectrum at a depth of 3m (where the interaction with atmospheric radionuclides are strongly reduced) and 1.2m above from the bed of the lake. The background spectrum is presented in Figure 3 together with a typical spectrum acquired at the SGD spring of Stoupa. At the background spectrum the absence of radon daughters (^{214}Pb and ^{214}Bi) is clearly observed together with a significant lower peak corresponding to potassium ^{40}K.

4.2 On line monitoring at Chalkida

At the SGD spring of Chalkida the system was installed in a frame and it was connected to a shore-based portable computer using a special data transmission cable. Also, the power supply was provided from a shore-based external battery via another 20m power cable. In this way the system operates on-line and it is fully controlled via the computer. The user directly supervised the acquisition adjusting any potential parameter. The deployment lasted 6 hours and two 3-hours spectra were obtained. Their analyses realized during the acquisition and radon daughters activity concentration measured in a range from 1.2 to 1.3 Bq/L.

4.3 Autonomous monitoring at Korfos

At the SGD spring of Korfos the system was installed together with a temperature and salinity data logger on a special frame which was moored into the submarine cave. The acquisition lasted for 4 h and four one-hour spectra were obtained. The measured values of activity concentration of radon daughters were found from 1.4 to 2.3 Bq/L. Comparing those data with the salinity records, an inversely linear dependency of radon daughters' activity concentration with salinity was found.

4.4 Operating mounted on a remote operating vehicle at Stoupa

At the SGD spring of Stoupa the system was mounted on the HCMR's remote operating vehicle (ROV) Super Achille. The vehicle carried and powered the system which operated autonomously at a water depth of 26m directly into the spring.

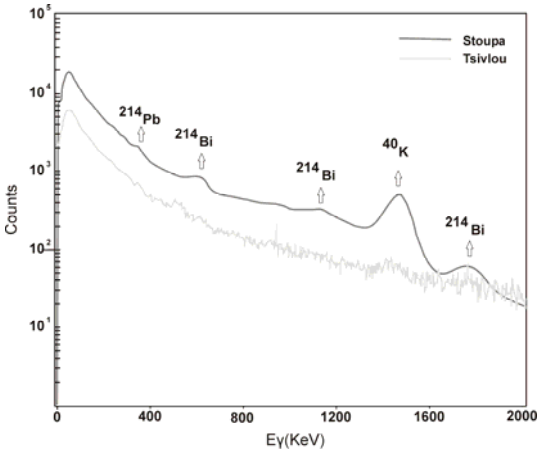

Fig. 3. Typical gamma-ray spectra obtained by the underwater spectrometer KATERINA. The spectrum from the lake Tsivlou (background level) is depicted by the light gray line while a typical spectrum from a SGD site (Stoupa) is depicted by the dark gray line. In the latter, several gamma-rays peaks due to radon daughters (^{214}Pb and ^{214}Bi) and potassium (^{40}K) are observed.

The acquisition period was 2 h and the gamma-ray spectrum obtained is showed in Figure 3. The activity concentration of radon daughters were measured from 2.4 to 2.6 Bq/L.

5 Conclusions and future plans

In this article the first deployments during the development of a new innovative in-situ sensor is described. The underwater gamma-ray spectrometer of HCMR has been calibrated for quantitative measurements of important radionuclides in hydrological studies and it has been deployed in several SGD sites by various ways (autonomously, on-line, mounted on a remote operated vehicle). The results may be obtained as time-series providing information about the temporal and spatial variation of the emanation of groundwater from submarine springs. Parameters like the flow velocity, the salinity and the intensity of the mixing process between fresh and brackish/seawater can be investigated by just one sensor using radiotracing methods. At the same time, the levels of activity concentration in groundwater of several natural (radon progenies) and artificial (cesium, iodine) radionuclides can be monitored for long periods for radioprotection and radioecology purposes. Future applications of KATERINA are planning as the mounting of the detector on platforms for continuous monitoring of radionuclides combined with other sensors like salinity/temperature data loggers and flow meters. Such configuration of the system has already been applied for one year in the region of Stoupa and the analysis is under progress. The system is also planned to be used as

an early warning system for radioactivity levels on river estuaries, on coastal agricultural regions where phosphate fertilizers are used, near coastal industrial zones and ports. Finally it is under process the upgrade of the system for mapping of radionuclides concentration in the sediment of coastal regions and lake beds.

Acknowledgments Dr. Patiris was supported by a scholarship for post doctoral research in Greece in the field of Soil and Water Sources Science from the State Scholarship Foundation of Greece (IKY).

References

Bagatelas C, Tsabaris C, Kokkoris M, Papadopoulos C T, Vlastou R (2010) Determination of marine gamma activity and study of the minimum detectable activity (MDA) in 4pi geometry based on Monte Carlo simulation. Environ. Monit. Assess. 165, 159-168

Burnett WC, Bokuniewicz H, Huettel M, Moore WS, Taniguchi M (2003) Groundwater and pore water inputs to the coastal zone. Biogeochem. 66, 3-33

Burnett WC, Dulaiova H (2003) Estimating the dynamics of groundwater input into the coastal zone via continuous radon-222 measurements. J Environ. Radioactiv. 69, 21-35

Burnett WC, Aggarwal PK, Aureli A, Bokuniewicz H, Cable JE, Charette MA, Kontar E, Krupa S, Kulkarni KM, Loveless A, Moore WS, Oberdorfer JA, Oliveira J, Ozyurt N, Povinec P., Privitera AMG, Rajar R, Ramessur RT, Scholten J, Stieglitz T, Taniguchi M, Turner JV (2006) Quantifying submarine groundwater discharge in the coastal zone via multiple methods. Sci. Total Environ. 367, 498–543

Burnett WC, Dulaiova H (2006) Radon as a tracer of submarine groundwater discharge into a boat basin in Donnalucata Sicily. Cont. Shelf Res. 26, 862-873

Burnett WC, Peterson R, Moore WS, de Oliveira J (2008) Radon and radium isotopes as tracers of submarine groundwater discharge - Results from the Ubatuba, Brazil SGD assessment inter-comparison. Estuar. Coast. Shelf S. 76, 501-511

Charette MA, Moore WS, Burnett WC (2008) Uranium and Thorium series nuclides as tracers of submarine groundwater discharge. Radioactiv. Environm. 13, 155-191

Mathieu GG, Biscaye PE, Lupton RA, Hammond DE (1988) System for measurement of ^{222}Rn at low levels in natural waters. Health Phys. 55, 989-992

Moore WS (1999) The subterranean estuary: A reaction zone of ground water and sea water. Mar. Chem. 65, 111-125

Moore WS, Sarmiento JL, Key RM (2008) Submarine groundwater discharge revealed by ^{228}Ra distribution in the upper Atlantic Ocean. Nat. Geosci. 1, 309-311

Porcelli D (2008) Investigating groundwater processes using U- and Th-series nuclides. Radioactiv. Environm. 13, 105-153

Purkl S, Eisenhauer A (2004) Determination of radium isotopes and ^{222}Rn in a groundwater affected coastal area of the Baltic Sea and the underlying sub-sea floor aquifer. Mar. Chem. 87, 137-149

Taniguchi M, Burnett WC, Cable JE, Turner JV (2002) Investigation of submarine groundwater discharge. Hydrol. Process. 16, 2115-2129

Tsabaris C, Bagatelas C, Dakladas Th, Papadopoulos CT, Vlastou R, Chronis GT (2008) An autonomous in situ detection system for radioactivity measurements in the marine environment. Appl. Radiat. Isot. 66, 1419 - 1426

Conceptual Model and Hydrochemical Characteristics of an Intensively Exploited Mediterranean Aquifer

V. Pisinaras, C. Petalas, V.A. Tsihrintzis

Laboratory of Ecological Engineering and Technology, Department of Environmental Engineering, Democritus University of Thrace, Xanthi, GR 67 100, Greece
xpetalas@civil.duth.gr

Abstract The conceptual model and the hydrochemical characteristics of the aquifer system of Vistonis plain in Northeastern Greece are presented. The study area is a rural region whose irrigation needs are met by the semi-confined aquifer system. Studies were undertaken in years 2003-2005 which utilized geological data, pumping test data and groundwater level measurements, in order to investigate the hydrogeological conditions of the semi-confined aquifer system of the study area. Based on this data a FLOWPATH II simulation was developed. The hydrochemical characteristics of the aquifer system of the study area were analyzed using basic statistics, Principal Component Analysis (PCA) and the expanded Durov diagram. The hydrogeological characteristics of the aquifer system vary significantly across the study area and are largely the result of contrasts in depositional environments. FLOWPATH II showed a clear tendency for groundwater to flow from a NW to a SE or E direction. The groundwater chemical analyses results showed that, the aquifer is locally affected by a geothermal field. PCA rendered seven significant PCs (eigenvalue > 1), explaining 76.8% of the total variance of the dataset. PCA revealed factors influenced by anthropogenic activities, such as fertilizer application and waste disposal, and also naturally induced hydrochemical processes.

1 Introduction

The continuous increase in crop production in Greece during the last 30–40 years was possible only with intensive irrigation of cropland and application of significant quantities of fertilizers and pesticides. Therefore, with the expansion of developing activities in Greece, it is essential to develop a groundwater management strategy to avoid any environmental impacts on the aquifer system due to the extensive future abstraction of groundwater. Integrated groundwater management can be defined as the efficient and effective use of the groundwater resource available by minimizing pollution and improving groundwater quality alongside main-

N. Lambrakis et al. (Eds.), *Advances in the Research of Aquatic Environment, Vol. 2*
DOI 10.1007/978-3-642-24076-8,

taining a sustainable economic development. With a proper groundwater management plan one could minimize the effect of over extraction and aquifer deterioration. Two important steps in planning an appropriate groundwater assessment and management study are: 1) the conceptual groundwater flow model and 2) the hydrochemical regime of the studied area.

2 Materials and methods

The study area is a flat region of about 85 km^2, extending from the city of Xanthi to Vistonis Lagoon, and crossed by Kosynthos River (Fig. 1). Common crops in the area are corn and cotton. The climate of the area is Mediterranean, with hot and dry summers. The mean annual precipitation ranges from 368 mm to 1,307 mm for the period of record 1956-2001.

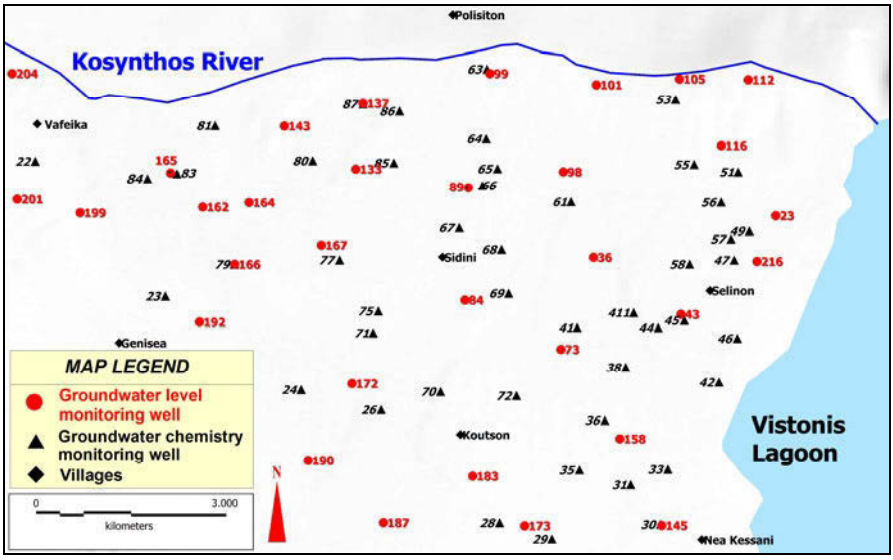

Fig. 1. Groundwater monitoring networks of the study area.

More than 500 irrigation wells, densely distributed are widely used for irrigation of about 75 km^2 of agricultural land. Groundwater quality is locally impaired because of various reasons: 1) the river water, recharging the aquifer through its alluvial cone, is occasionally polluted; 2) Ilicit waste effluent discharge is practiced in sewage lagoons and 3) diffuse pollution from agricultural activities takes place.

Studies were undertaken in years 2003-2005 which utilized geological data, geophysical techniques and hydrochemistry to investigate the hydrogeological

conditions of the semi-confined aquifer system west of Vistonis Lagoon (Fig. 1). Data from 32 wells, uniformly distributed, were used to characterize the potentiometric surface of the aquifer system (Fig. 1). Groundwater level data was used in order to apply FLOWPATH II model. FLOWPATH II (Waterloo Hydrogeologic 1998) is a two-dimensional, numerical, groundwater flow model, capable of simulating confined, unconfined, and leaky aquifers. The purpose of conducting the FLOWPATH II simulation was to investigate the flow pattern in the study area, to highlight areas where recharge to or discharge from the aquifer occurs, to demonstrate some of the physical characteristics of the site, and overall to examine the validity of the regional hydrogeological conceptual model.

To establish groundwater quality characteristics, a regional hydrochemical survey was performed in July 2004, during the pumping period, when considerable groundwater quantities were extracted. Water samples for chemical analyses were obtained from 47 carefully selected sampling points to cover the entire study area (Fig. 1). In order to distinguish and group the groundwater of the study area into several chemical groundwater types, the expanded Durov diagram (Lloyd and Heathcote 1985) was used, which facilitates interpretation of the evolutionary trends and hydrochemical processes occurring in the groundwater system. Principal Component Analysis and factor analysis in general, are useful tools and have been widely used for groundwater quality exploration (Lambrakis et al. 2004, Petalas et al. 2005). Here, PCA was performed with a view to assess the compositional differences among different water samples, spatial variations in water quality and influence of anthropogenic activities.

3 Hydrogeologic Conditions and Conceptual Model

The aquifer system is bound by the diverted reach of Kosynthos River to the north, Vistonis Lagoon to the east and south, and by the national road Xanthi - Porto Lagos - Komotini to the west (Fig. 1). The aquifer system extends upstream, along a narrow zone, to the alluvial cone of the river near the city of Xanthi. The hydrogeological characteristics of the aquifer system vary significantly across the study area and are largely the result of contrasts in depositional environments. The straightening and shortening of channels, man-made cutoffs, and bank stabilization has significantly altered the floodplain environment. The aquifer thickness increases from the NW to the SE direction. The minimum aquifer thickness (about 40 m) is near Kosynthos river, while the maximum aquifer thickness is near the southeastern part of the study area (about 90 m). Pumping tests results revealed high heterogeneity of the aquifer materials, with transmissivity and storage coefficient values varying from 45 to 2,930 m^2/d and from 2.4×10^{-4} to 1.4×10^{-2}, respectively. The horizontal hydraulic conductivity values range from 1.9 to 138 m/d. Groundwater levels show a seasonal pattern of fluctuation. This results from influences, such as rainfall and irrigation, which follow well-defined seasonal cycles.

Thirteen water level measurements were conducted in a network of 32 selected wells in the study area from December 2003 to November 2005. Groundwater level declines significantly through the irrigation period, which is from June to August. It has to be mentioned that December 2003 to November 2005 was a period with significant rainfall even during summer. Thus, groundwater abstractions for irrigation purposes were considerably reduced in comparison to that of of a typical hydrologically year.

4 Two- Dimensional Groundwater Flow Model Results

The boundary conditions were specified based on the piezometric information as well as the data obtained from the productive wells of the study area. The northern boundary was not simulated by river flow cells as it would be expected. The main course of Kosynthos river used to follow a way south of Vafeika village (Fig. 1) and discharge directly to the sea. The river course, downstream of Vafeika was diverted to a west-south direction in 1958. The presence of an extensive clay material layer under the diverted river course, in combination with the fact that there are only a few productive wells installed near Kosynthos, indicates that there is no direct hydraulic connection between Kosynthos river and the underlying aquifer. Some lateral groundwater inflows occur from the northern boundary (Pliakas et al. 2005) (Fig. 2). The eastern boundary of the aquifer is a no flow boundary, as there is no hydraulic connection between the aquifer body and Vistonis lagoon (Diamantis 1985) (Fig. 2). This is also proved by the hydrochemical characteristics of the aquifer waters, which are significantly different from those of Vistonis lagoon, indicating thus that no water mixing occurs. The western and southern boundaries are determined as specified flux boundaries. The volume of water entering laterally the aquifer through these boundaries was initially estimated using the hydraulic gradient along those specified locations. Thereafter, those fluxes were subject to calibration in order to achieve a best fit with the observed piezometric level.

Recharge was estimated based on previous studies for the wider study area (Diamantis 1985, Pliakas et al. 2005, Pisinaras et al. 2007) and corresponds to about $8x10^6$ m^3. Data from the National Statistical Service of Greece shows that corn dominates the study area, as it covers about 60% of the cultivated land, cotton follows with 22.45% and beets with 10.27%. The total volume of extracted groundwater from pumping wells was estimated to about $26x10^6$ m^3 for the whole irrigation period.

During model calibration, the match between simulated and measured water levels satisfied several criteria used in groundwater modeling (Pisinaras et al. 2007). The Mean Error was -0.192 m, indicating that on the average the simulated water levels were slightly lower than the corresponding observed water levels. The Mean Absolute Error was 0.630 m, being again very close to 0. The Root Mean

Square Error was 0.532 m. The Normalized Objective Function value, which was 0.052, is much lower than 1.0 and very close to 0, indicating an excellent calibration. The γ value, which is 0.9849 is very close to 1.0, indicating again an excellent calibration and that the model only slightly under-estimated the water level of Vistonis plain aquifer. The R^2 was 0.9918 and approached satisfactorily 1.0. For values within these limits groundwater model performance can be considered very satisfactory (Boonstra and De Ridder 1981).

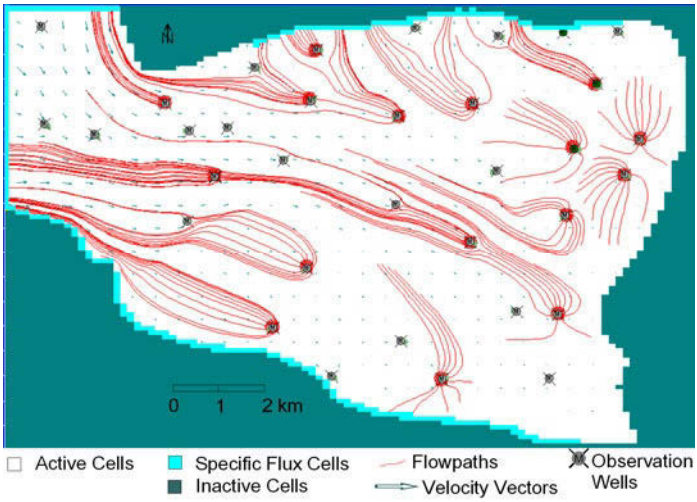

Fig. 2. Conceptual 2D model, vector map and flowpaths for the study area.

FLOWPATH II results indicates the clear tendency for groundwater to flow from a NW to a SE or E direction and, as shown in Fig. 2, the highest velocities occur in the NW inflow boundary, whereas velocities are minimized in the central and eastern part, where the aquifer thickness is maximum. This tendency is continuous all year round. The calibrated model indicates that the greatest inflows occurred from the north-western boundary of the study area. The western and southern boundary indicated inflows to the aquifer of about $15x10^6$ m^3, while the north lateral groundwater inflows were simulated at about $3x10^6$ m^3.

The 2D groundwater flow model, through the delineation of 1000 day capture zones, also highlights the aquifer areas where particular attention should be paid in order to prevent pollution. Most attention should be paid in the west and north part of the study area, because possible pollution in these areas will probably affect the rest of the aquifer. The groundwater model indicates that the major inflows occurred from the alluvial fan of Kosynthos river through the western boundary of the study area, which points out that Kosynthos river water quality should be carefully protected.

5 Hydrochemical investigation results

Table 1 presents a statistical overview of the hydrochemical data of the study area based on the 47 groundwater samples. The pH values of groundwater vary from 6.67 to 7.81, indicating a predominance of the dissolved carbonates in the form of HCO_3^-.

Table 1. Univariate statistical overview of the dataset.

	Mean	Median	Min	Max		Mean	Median	Min	Max
pH	7.25	7.24	6.67	7.81	Cd^{**}	0.12	0.09	0.03	0.77
T (^oC)	18.12	17.70	12.00	25.20	Cr^{**}	6.88	2.40	0.25	201.82
EC (μS/cm)	1008.6	702.0	408.0	5230.0	Cu^{**}	3.42	1.82	0.35	20.81
Na^{+*}	95.1	31.95	13.68	931.7	Fe^{**}	41.19	18.00	4.00	410.00
K^{+*}	3.3	2.00	0.50	19.0	Ga^{**}	2.81	2.51	0.91	6.24
Mg^{2+*}	23.0	18.20	6.00	68.5	Li^{**}	4.89	1.48	0.44	49.91
Ca^{2+*}	129.3	118.50	36.50	269.8	Mn^{**}	141.62	3.25	0.52	3626.1
Cl^{-*}	135.1	34.49	14.50	1437.6	Ni^{**}	1.83	0.94	0.05	23.90
HCO_3^{-*}	168.8	161.0	107.4	429.8	Pb^{**}	0.09	0.05	0.00	0.77
SO_4^{2+*}	276.9	225.9	51.5	835.7	Rb^{**}	0.36	0.25	0.07	1.45
NO_3^{-*}	12.4	11.51	2.20	67.5	Se^{**}	8.06	5.17	1.35	34.65
NO_2^{-*}	0.01	0.01	0.00	0.23	Sr^{**}	582.2	501.2	236.4	2255.4
NH_4^{+*}	0.34	0.10	0.01	2.57	U^{**}	10.38	8.97	2.05	66.91
PO_4^{3-*}	0.06	0.03	0.01	1.06	Zn^{**}	54.79	50.07	19.21	160.61
As^{**}	2.46	0.86	0.26	33.7	V^{**}	5.73	4.66	0.57	20.87
Ba^{**}	69.9	69.0	19.7	179.5	B^{**}	53.60	22.12	11.23	436.19
Co^{**}	0.24	0.17	0.04	0.96	Mo^{**}	7.68	4.38	0.71	64.93
Be^{**}	0.05	0.03	0.01	0.91					

*units: mg/L, **units: μg/L

A geothermal field exists near the south part of the study area at Nea Kessani (Fig. 1) (Kolios et al. 2005). Groundwater from six wells located in the part of the study area mentioned above, display high temperature values (>20^{o}C, up to 25.2 ^{o}C). Also, these samples display high EC and SO_4^{2-} values, while their As and Mn concentrations exceed the EEC/80/778 and WHO safe drinking water standards. High Na^+ and Cl^- content samples from the area of Nea Kessani reflects local mixing with saline geothermal water (Kolios et al. 2005).

NH_4^+ concentrations greater than 0.5 mg/L and NO_3^- concentrations greater than 50 mg/L characterize several samples taken from wells located in the south part of the study area. Agricultural practices, i.e., use of fertilizers containing nitrogen, cattle feeding activities and sewage from septic tank systems are the important sources for this kind of contamination.

High Mn concentrations have been locally recorded in four wells. Mn values down to 0.5 mg/L have an adverse effect on the potability of water. These values can be attributed to the mixing of fresh groundwater with thermal groundwater. Groundwater with high U content was measured in well "22". Uranium in groundwater originates in uranyl compounds or other uranium species present in the aquifer or in the unsaturated zone. High concentrations of Fe and Cr were observed in well "63". High chromium content is mainly found in groundwaters polluted by human activities, while high iron content can be associated with the oxidation of reduced iron mineral as iron sulphide in the boundary zone between reducing and oxidizing environments.

As it appears in the expanded Durov diagram (Lloyd and Heathcote 1985) (Fig. 3), most of the samples of the study area present complex water types. The order of cation dominance is generally Ca^{2+}>Mg^{2+}, although sodium (Na^{+}) is the dominant cation in 9 out of 47 water samples. The majority of the water samples present the following order of anion dominance SO_4^{2-}>HCO_3^{-}>Cl^{-}. Certain characteristic chemical types are shown in Table 3. The dominant water type is Ca-SO_4-HCO_3, while the second most frequent water type is Ca-Mg-SO_4-HCO_3.

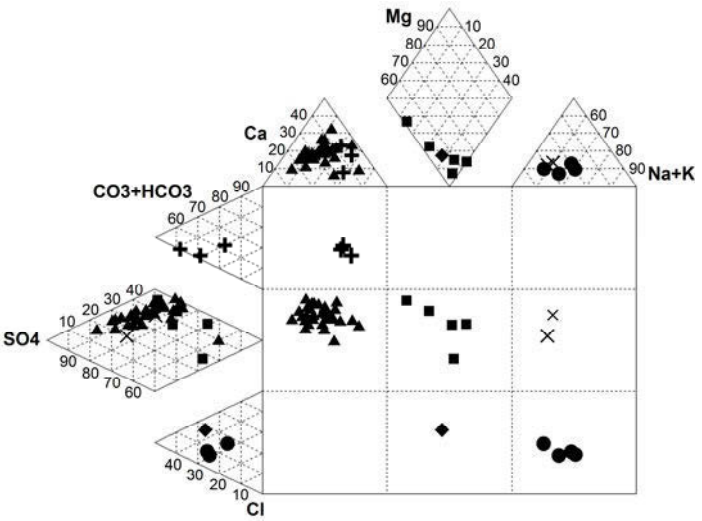

Fig. 3. Expanded Durov diagram for the groundwater samples of the study area.

6 PCA application results

The Bartlett's sphericity test carried out on the correlation matrix of variables show that significance is equal to zero, thus indicating that PCA can achieve a significant reduction of the dimensionality of the original dataset.

PCA rendered seven significant PCs (eigenvalue > 1) explaining 76.80% of the total variance of the dataset. Comparing with other studies, the percentage explained by the seven PCs is adequate. PC1 explains 24.98% of the variance and is contributed mainly by EC, Cl^-, Na^+, K^+, Mg^{2+}, Sr, Li and B. Thus, PC1 contains hydro-geochemical variables (Cl^-, SO_4^{2-}, Na^+ and Mg^{2+}) originating from mineralization of the geological components of soils. The contribution of Na^+ and Mg^{2+} to this factor can be a result of cation exchange processes at the soil–water interface. This is the most common factor revealed by PCA for groundwater systems.

PC2, explaining 15.60% of the variance, is characterized by positive loadings of NO_2^-, PO_4^{3-}, Cr, Fe, Ni and Zn. Their contribution in this factor shows anthropogenic influence. Stock farms and the application of phosphatic fertilizers are sources of NO_2^- and PO_4^{3-} in the north part of the study area, while small industries discharge wastes which load the local aquifer with Cr, Ni, and Zn. PC3, explaining 9.9% of the variance, exhibited moderate to high loadings on Ba, Ga, Ca, U. PC4 (9.60%) is mainly contributed by NO_3^- and As, and reflects contributions from applications of nitrogenous agro-chemicals and natural sources of As, respectively. PC5 (6.10%) displays the high loading of Mn, which is another significant hydro-geochemical variable, and Co whose concentrations are insignificant. Mn occurrence could be related to anthropogenic activities (e.g., gravel mining adjacent to stream channels) or natural sources (important constituent of some alkaline volcanic rocks). PC6 (5.35%) illustrates the factor that represents the major anions for the study area, which are HCO_3^- and SO_4^{2-}. PC7 (5.28%) displays high positive loadings to Cu and Zn, showing anthropogenic influence.

References

Boonstra J, Deridder NA (1981) Numerical Modelling of Groundwater Basins. ILRI, The Netherlands. 226 pp

Diamantis I (1985) Hydrogeological research of Vistonis basin, aquifers study in a strong field of heterogeneity. PhD Thesis. Democritus University of Thrace, Department of Civil Engineering, Xanthi, Greece (in Greek)

Kolios N, Koutsinos S, Arvanitis A, Karydakis G (2005) Geothermal situation in Northeastern Greece. Proceedings of World Geothermal Congress, Antalya, Turkey, 24-29 April

Lambrakis N, Antonakos A, Panagopoulos G (2004) The use of multicomponent statistical analysis in hydrogeological environmental research. Water Research 38, 1862-1872

Lloyd JW, Heathcote JA (1985) Natural inorganic hydrochemistry in relation to groundwater. Clarendon Press – Oxford. 294 pp

Petalas C, Lambrakis N, Zaggana E (2005) Hydrochemistry of volcanic rocks: The case of the volcanosendimentary rocks of Thrace, Greece. Water, Air and Soil Pollution 169, 375-394

Pliakas F, Petalas C, Diamantis I, Kallioras A (2005) Modeling of Groundwater Artificial Recharge by Reactivating an Old Stream Bed. Water Resources Management 19, 279-294

Pisinaras V, Petalas C, Tsihrintzis VA, Zagana E (2007) A groundwater flow model for water resources management in the Ismarida plain, North Greece. Environmental Modeling and Assessment 12(2), 75-89

Waterloo Hydrogeologic Inc. (1998) FLOWPATH II: User's manual. 128 pp

Hydrogeological conditions of the Kotyli springs (N. Greece) based on geological and hydrogeochemical data

C. Angelopoulos, E. Moutsiakis

Envicon, Anaximandrou 10, Thessaloniki, GR 54 250, Greece. envicon@otenet.gr

Abstract The Kotyli springs are located in northern Greece on the NW part of Rhodope Mountains, which is the oldest mountain range of the country. The climate is semi-humid with water excess and deficiency during winter and summer, respectively. The area belongs to the Rhodope isopic zone, specifically in Sidironero unit, consisting of a Paleozoic sequence of neritic-sea metamorphosed sediments and plutonic intrusions successed by tertiary plutonic, volcanic and coastal deposits. The fractured granodiorites in valley depression areas gives rise to most of the springs, the discharge values and the overall hydrogeological data being consistent with this scenario. Hydrogeochemical analyses performed on samples showed that the springs are classified to the Na-Ca-Cl-HCO_3 type, except for two of the springs in Pacni area classified to the Na-K-Ca-Cl-HCO_3 type and the Aimonio spring which is classified to the Ca-Cl-HCO_3 type. The low values of the dissolved minerals, expressed in TDS and electric conductivity values indicate a function mechanism, which involves the existence of a shallow aquifer in fractured rock with restricted size and the development of the springs at their current site due to the presence of depressions in the small valleys of the area. However, the function mechanism of the Aimonio spring involves the existence of a shallow aquifer in slightly carstified marbles and the development of the spring at its current site due to the presence of a depression in the small valley of the area.

1 Introduction

The Kotyli springs are the essential source of drinking water for the settlements of the area. They are located, on the NW Thraki, on the mountainous part of Xanthi Prefecture (Fig. 1, 2). The springs are located in the area of the settlements Kotyli, Aimonio, Pachni and Dimario, all being part of the Municipality of Kotyli, in altitudes over 800 m.

In the studied area a dentritic pattern hydrographic network prevails, of a medium density, which is characteristic of a development of streams on hard crystalline rocks (Fig. 1). The springs are located along secondary valleys, some of them

N. Lambrakis et al. (Eds.), *Advances in the Research of Aquatic Environment, Vol. 2*
DOI 10.1007/978-3-642-24076-8, © Springer-Verlag Berlin Heidelberg 2011

of a probable tectonic origin. Along those valleys and at a distance of their axe, rocks are fractured and altered, at a certain depth, subsequently presenting a secondary porosity, which assists the development of an aquifer (Stournaras 2007).

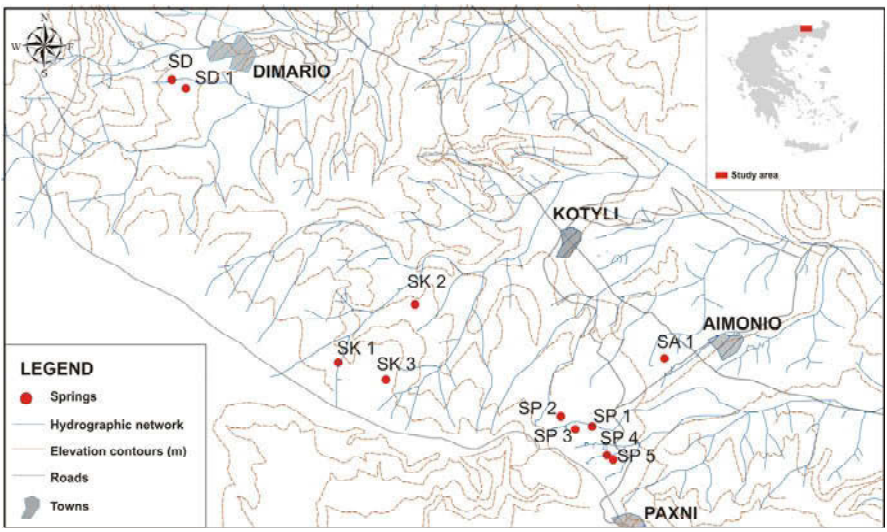

Fig. 1. Map of the hydrographic network of the Kotyli spring area.

The mean annual precipitation in the area, in the period 1970-2005 (Ministry of Agriculture, 2007), is 1076 mm, the climate being semi-humid with water excess and deficiency during winter and summer, respectively. The hydrological balance of the same period in the area was estimated according to the method of Turc (Kallergis 1999). It is calculated that approximately 63% of the mean annual precipitation in the area returns to the atmosphere through evaporo-transpiration, 34% supplies surface runoff and 3% infiltrates in groundwater. The infiltration coefficient is high enough to recharge the existing low potential groundwater aquifers, but on the other hand is low and explains the low discharge rates of the springs.

The present study took place during the study for the collection of the water of 11 of these springs (July 2008-October 2009), aiming to evaluate the hydrochemical characteristics of the water of the springs, as well as to investigate their hydrogeological conditions with respect to local geology.

2 Geological and hydrogeological setting

Geologically, the area belongs to the Rhodope isopic zone, specifically to the Sidironero unit (Mountrakis 1985, 1994). The lower part of the unit is composed of rocks of medium grade metamorphism, that is gneisses and augen gneisses with

intercalations of marbles, while the upper part is composed of rocks of low grade metamorphism (green schist metamorphism), that is gneisses, mica schists, amphibolites and marbles. In the upper part, intrusions of plutonic rocks are observed (granitic intrusions); aging 35 million years or older, but locally even volcanic rocks dating 30 millions years are observed (Mountrakis 1985; Kokkinakis 1980; Kronberg et al. 1970, Kronberg and Eltgen 1973).

These neritic-sea metamorphosed sediments and plutonic intrusions are overlaid by tertiary deposits, consisting of coastal deposits, volcanic deposits and more recent plutonic intrusions.

The studied area is composed of tertiary deposits dating in Oligocene, consisting of volcanic rocks (rhyolites and ignimbrites), coastal deposits (conglomerates and sandstones) and magmatic intrusions (granodiorites and old granodiorites), as well as Paleozoic metamorphic rocks, that is the upper amphibolitic sequence, represented in the studied area by the lower marble – amphibolite series (marbles, amphibolites, schists and gneisses) and the gneiss - augen gneiss - migmatite series. No major faults have been located in the studied area; however the crystalline rocks present two main discontinuity systems (minor faults and joints), dipping 243/32 and 307/87 (Angelopoulos 2009).

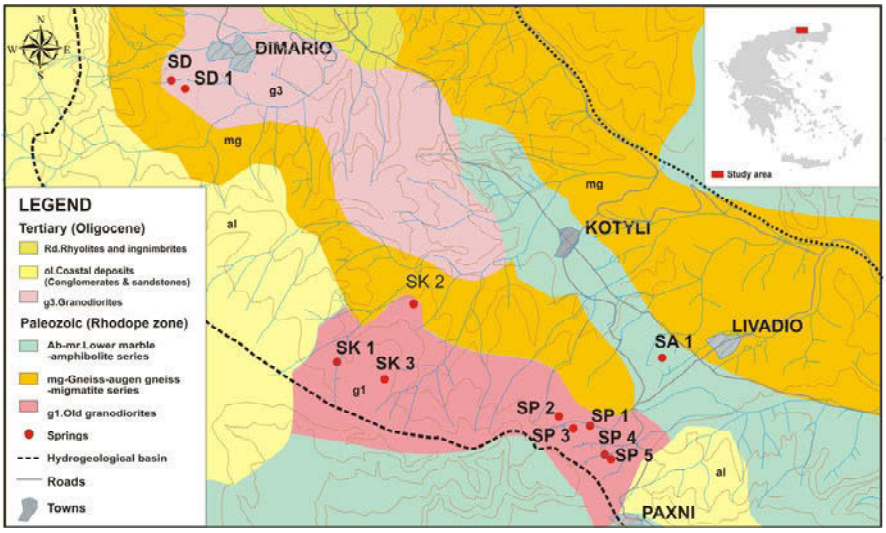

Fig. 2. Geological map of the Kotyli spring area (after IGME (1982), modified).

The springs in Kotyli area (SK) and in Pachni area (SP) discharge through discontinuities present in the old granodiorites, while those in Dimario (SD) area through discontinuities in the rhyolites and that in Aimonio (SA) area through carstic discontinuities in marbles of the lower marble – amphibolite series (Angelopoulos 2009) (Fig. 2).

The springs discharge was monitored in June 2008 and, using older data (Community of Kotyli, 2008) as well, is considered to be generally low, consistent with the low infiltration rates of the area as mentioned above (Table 1).

Table 1. Discharge of Kotyli springs.

Springs	Number of springs	Monitored (mean) discharge (m^3/h)	Minimum estimated discharge (m^3/h)	Maximum estimated discharge (m^3/h)
Kotyli springs	3	10.0	7.5	12.0
Aimonio spring	1	3.0	2.0	4.0
Pachni springs	5	4.0	2.5	5.0
Dimario springs	2	10.5	7.5	12.0

The spring discharge values of the Table 1 concern the total of every group of springs, measurements being possible only in the cistern of every settlement.

The hydrogeological basin of the springs is included between the watershed of the main valley (Small River Valley) and the course of the river, and is estimated to be about 30 km^2 (Fig. 2).

3 Hydrogeochemical characteristics and classification

Water samples were collected in October 2009 for chemical analyses. According to the Piper diagram, the hydrochemical type of the springs is Na-Ca-Cl-HCO_3, with the exception of the springs SP4 and SP5 in Pachni area displaying Na-K-Ca-Cl-HCO_3 type and the Aimonio spring, which displays Ca-Cl-HCO_3 type (Fig. 3). It is evident that the Aimonio spring samples display a different type to the others being consistent with its different origin.

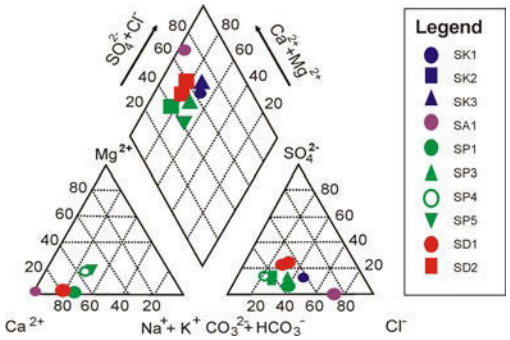

Fig. 3. Piper diagram.

According to Schoeller diagram all the springs present the same chemical pattern, except for Aimonio spring which presents higher concentration of Ca, lower of Mg and lack of SO_4, while the Pachni springs SP4 and SP5 presents higher concentration of Ca, Na and K (Fig. 4).

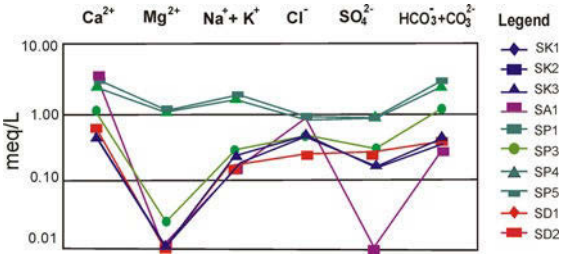

Fig. 4. Schoeller diagram.

The pH values range between 7.0 and 8.0, while the electric conductivity values (ρ_α) range between 49 and 590 μS/cm, the springs SA1, SP4 and SP5 presenting the higher values. The TDS value range between 75 and 431 mg/L, the same as aforementioned springs presenting the higher values.

The concentration of all ions, as represented of the values of electric conductivity (ρ_α), in the water of the springs is very low and very close to that of rain water. Only the two springs in Pachni area and that of Aimonio, to a lesser extent, present concentrations close to the values of that of the Komotini - Xanthi Plain groundwater (Angelopoulos 2010) (Fig. 5).

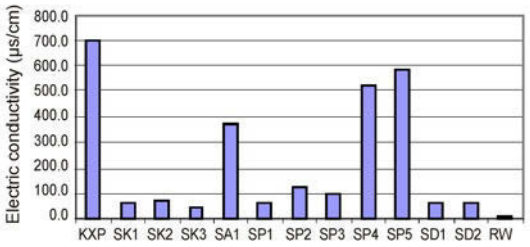

Fig. 5. The values of electric conductivity of the springs comparatively to that of rainwater (RW) and the Komotini-Xanthi Plain groundwater (KXP).

4 Discussion

According the way the springs discharge through rocks suggests that the springs can be considered as fracture springs, while the Aimonio spring can be considered as carstic spring (Kallergis 2000, Todd and Mays 2005).

The geochemical characteristics of spring water and especially the very low TDS and ρ_α values indicate that rain water infiltrates through rock fractures and having a high flow rate discharge through joints at small valley depressions. Is it possible that the low values of TDS and ρ_α, combined to the reduced solubility of the formations and the fact that they are under conditions of lack of extended ruptures, the limited depth of the discontinuities do not permit a groundwater extended circulation.

According to hydrodynamic conditions described above, the springs can be considered as contact springs (Stournaras, 2007), inasmuch the whole of the water of the aquifers is located in altitudes higher than those of the springs, as all available data suggest (Fig. 6).

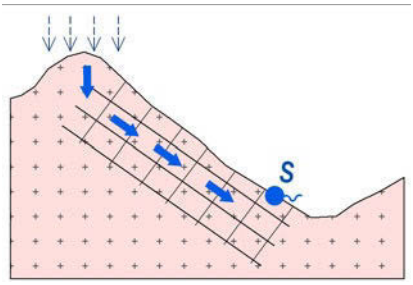

Fig. 6. Schematic representation of the fracture springs function mechanism.

Although the case of the springs to be of the overflow springs type, the water of the aquifers being located in altitudes higher and lower than those of the springs, cannot be excluded, due to the lack of spring hydrographs and geophysical data, but the concentrations of dissolved minerals is rather low, hence the model of contact springs being the most probable.

The same pattern applies for the Aimonio spring, the only difference being geochemical characteristics, which indicate infiltration and rapid flow in carstic cavities, being considered as carstic spring.

The very low TDS and, consequently, ρ_α values are justified from the very shallow extent of the fractures, perhaps less than 50 m and the high flow rate in them, so as the time for the water to be in contact with the fractured media and dissolve minerals is extremely short.

In the case of the two springs in Pachni area with higher values of TDS and ρ_α it is supposed that the time for the water to be in contact with the fractured media is prolonged, permitting in this way the water to dissolve a significant amount of minerals and indicating a possibly deeper extend of the fractures

As far as the Aimonio spring is concerned, the fact that marbles are intercalated in amphibolites restricts the circulation in carstic cavities and thus limiting the necessary time for the water to be in contact with the fractured media in order to dissolve a significant amount of minerals.

5 Conclusions

The Kotyli springs are hosted in the tertiary volcanic and plutonic rocks of the West Rhodope zone, being considered as fracture springs. Exception to this is the Aimonio spring which is hosted in the Paleozoic upper amphibolites sequence, in the marbles intercalating amphibolites, considered as carstic spring. All springs however are considered, as far as hydrodynamic behaviour is concerned, as contact springs.

The Aimonio spring displays a different chemical composition than the rest of the springs in the area, justified from the different host rock. The relatively high concentration of SiO_2, almost identical with that of the other springs varying between 9.0 and 14.8 mg/L, indicates the contribution of amphiboles in its chemical composition.

The hydrogeochemical data suggest a shallow, very limited in size aquifer in fractured rock, which flows rapidly, having low dissolution of various elements, and discharges, at very low discharge rates, at valley depressions, while concerning the Aimonio spring the same function model applies, with the difference of a carstic aquifer present instead of one in fractured rock.

References

Angelopoulos C (2009) Hydrogeological study of the Kotyli, Aimonio, Pachni and Dimario springs area, Community of Kotyli (in Greek), Thessaloniki

Angelopoulos C (2010) Data from groundwater wells in the Komotini – Xanthi Plain area (in Greek), Unpublished personal data

Bornovas I, Rondoyianni-Tsiabaou Th (1983) Geological Map of Greece, scale 1:500.000, Inst Geol and Miner. Explor., Athens

Community of Kotyli (2008) Discharge rate data of the Kotyli springs (in Greek), Unpublished data

Kallergis G (1999) Applied Hydrogeology, Vol. A (in Greek). Athens

Kallergis G (2000) Applied Hydrogeology, Vol. B (in Greek). Athens

Kokkinakis A (1980) Alterbeziehungen zwischen Metamorphosen, mechanischen Deformationen und Intrusionen am Sudrand des Rhodope-massiv, Makedonien, Griechenland. Geol. Rdsch. 69: 726-744, Stuttgardt

Kronberg P, Meyer W, Pilger A (1970) Geologie der Rilla-Rhodope Masse zwischen Strimon und Nestos, Beith. Geol. jb 88, 133-180

Kronberg P, Eltgen H (1971) Geological Map of Greece, scale 1:50.000, Xanthi Sheet, Inst Geol and Miner. Explor., Athens

Ministry of Agriculture (2007) Temperature and precipitation data from the Echinos Meteorological Station, in the Xanthi area (in Greek), Unpublished data

Mountrakis D (1985) Geology of Greece (in Greek). Thessaloniki

Mountrakis D (1994) Introduction to geology of Macedonia and Thrace. Suggestions over the geotectonic evolution of the Greek inland and internal Hellenides (in Greek).Hell. Geol. Soc. Bull., XXX, 31–46

Stournaras G (2007) Water: Environmental dissociation and course (in Greek), Athens

Todd D, Mays L (2005) Groundwater Hydrology, Wiley, New Jersey

Water quality and agriculture

Subsurface contamination with petroleum products is a threat to groundwater quality

N. Ognianik, N. Paramonova, O. Shpak

The Institute of Geological Sciences of the NAS of Ukraine 55-b, O. Gonchara-st., Kiev, 01054, Ukraine

gwp_ign@gwp.org.ua, shpak_lena@yahoo.com

Abstract Subsurface contamination with oil poses a threat to groundwater quality on the whole territory of Ukraine. The methods of search and prospecting of contaminated plums were analyzed. Oil behaviour in the subsurface and the methods of remediation were studied. The effectiveness of aviation kerosene removal was examined in a sandy column. Nonhazardous distances from a contamination source to water-supply wells for different hydrogeological conditions were determined by mathematical modelling. The case of drinking groundwater contamination with oil in Kherson City is examined.

1 Introduction

Subsurface contamination with petroleum products (oil) has become one of the most important environmental problems on the whole territory of Ukraine. Taking into consideration wide distribution of petrol stations, fuel storehouses, pipelines, etc., subsurface contamination with oil is supposed to spread to large areas. Groundwater contamination with oil is the most threatening because groundwater is the main source of drinking water supply. Maximum contaminant levels are accepted to be extremely low for oil (0.001-0.1 mg/L) and in one or two orders of magnitude less than solubility so even small oil concentrations render water unfit for domestic use and hazardous to health. At present, groundwater is contaminated in a number of cities and towns in Ukraine such as Kherson, Lugansk, Poltava, Lutsk, Uzin, and others. More than 120 large water-supply-well systems are located within contaminated sites.

There is an environmental risk on the whole territory of Ukraine (see Fig. 1). This situation is considered to be critical with grave consequences in the nearest future. In order to recover from the crisis, it is necessary to liquidate or control current contamination cases and prevent potential ones.

N. Lambrakis et al. (Eds.), *Advances in the Research of Aquatic Environment, Vol. 2*
DOI 10.1007/978-3-642-24076-8,

Fig. 1. The scheme of complex regional environmental risk of Ukraine [Ognianik, Paramonova et al.].

2 Goals and tasks

The primary tasks are search and prospecting of contaminated plums to estimate a size, a volume and a stage of contamination, oil distribution in the subsurface and an effect on surrounding wells, ponds, rivers, etc. The complex estimation of subsurface contamination at the territories of oil-products objects must be the first stage of remediation.

Searching includes detection of contaminated plumes within large areas exposed to oil contamination. A direct method of studying contamination cases (well drilling and sampling) is rather expensive and can promote oil spreading in the subsurface. The attempt to use a geophysical surface method based on measurements of electromagnetic conductivity failed to provide correct results. Contaminated plumes revealed by this method within Uzin military airbase in Kiev region did not correspond to the map made by well drilling and sampling (Ognianik et al. 2003). However, we concluded that mapping and monitoring can be sped up measuring hydrocarbon concentrations in samples near a well in situ. For this a portable chromatograph (less 5 kg) can be used to measure hydrocarbon contents in water, soil and air for one minute. Such an apparatus developed on basis of a flame-ionization detector was tested.

3 Oil behaviour in the subsurface and methods of remediation

Light oil with a density less than 1 g/cm^3 enters in the unsaturated zone and moves down due to gravitation. At this, light oil undergoes the influence of physical and chemical properties such as dissolution, evaporation, sorption and biodegradation. A three-fluid "water-oil-air" system is formed in the unsaturated zone where water and oil are retained due to capillary forces depending on dispersivity, soil moisture and fluid interfacial tension. An oil lens is formed on a low permeable layer or a groundwater table (see Fig. 2). The core of the lens contents mobile oil that can move due to hydraulic gradient and flow into a well. Upper the core the unsaturated oil capillary fringe is formed due to the interfacial air-oil tension while under the core the saturated capillary fringe is formed due to the interfacial oil–water tension. Upper the lens a film-drop zone remains after gravitational oil draining while under the lens a retained oil zone is formed due to oil spreading or water table rise. In the aquifer the lens is surrounded with dissolved oil (Baehr and Corapcioglu 1987).

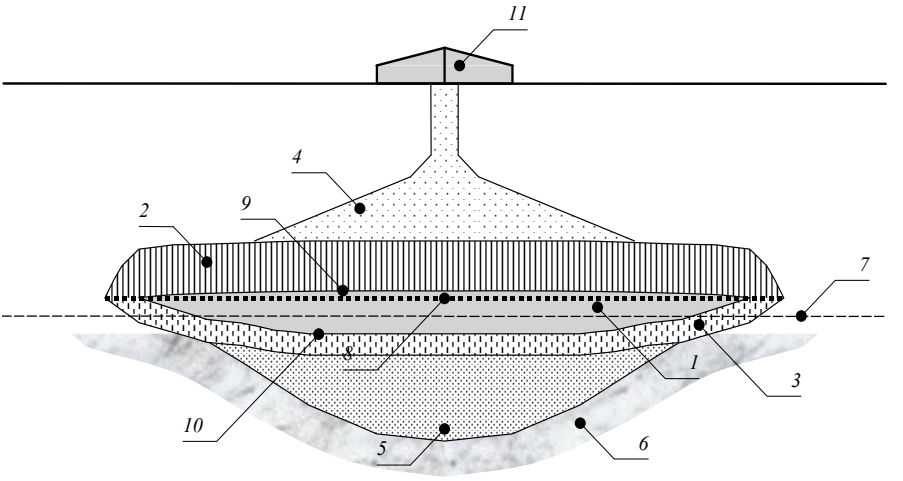

Fig. 2. An oil lens in homogeneous isotropic sediments (1 – mobile oil; 2 – the air-oil capillary zone; 3 – the oil-water capillary zone; 4 – residual oil as films or drops; 5 – retained oil in the saturated zone; 6 – dissolved oil; 7 – a water table; 8 – a buoyancy table; 9 – an air-oil level; 10 – an oil-water level; 11 – a contamination source).

It is necessary to define oil distribution and volume in each zone because oil behaviour and methods of oil recovery are different in them (Farr et al. 1990).

In the film-drop zone oil is retained by soil and can migrate as a water solution or an emulsion. In the unsaturated capillary fringe oil can be thrown down into the saturated zone due to the weight of an oil column only or together with a water column accumulated on top if the weight exceeds capillary forces.

In the saturated zone mobile oil can spread on a water table and flow into surrounding wells, ponds, rivers, etc. Such cases were observed in wells near Uzin and Lutsk airbases (Bricks et al. 2002), and in the Ros River near Bila Tserkva airbase (Shpak et al. 2003) located from hundred metres to one kilometre away from contamination sources. Mobile oil can be recovered by pumping and open or closed drainage. However, no more than forty percent of mobile oil is recovered by these methods (Ognianik, Paramonova et al.). Thus, 14 514 tones of kerosene remained in soil after pumping at Uzin airbase and 5 917 tones of kerosene remained after pumping at Priluky airbase (Ognianik et al.). After drainage of mobile oil the most part of this zone passes into the capillary oil-water zone and then into the oil-entrapped-in-water zone. This oil cannot be recovered mechanically. It is necessary to reduce surface tension due to pumping of surfactant species that can also contaminate groundwater. Therefore, remediation based on microbial biodegradation is an optimal method for contamination removal. Aerobic biodegradation is applied in near-surface layers and anaerobic biodegradation is applied in deep layers.

4 Physical modelling of remediation

The effectiveness of aviation kerosene removal was examined by all these methods using physical modelling at the laboratory. A column filled with fine sand imitated the porous subsurface containing a kerosene lens in which 220.34 cm^3 of kerosene were in the saturated zone and 80.36 cm^3 of kerosene were in the unsaturated zone. First of all, kerosene was removed from the saturated zone due to gravitational drainage, which corresponded to pumping with a gradient 1. 49 cm^3 of kerosene (22% of all the kerosene in the saturated zone) flew out and after that 251.7 cm^3 of kerosene retained by capillary forces remained in the sandy column. Then, there was an attempt to remove the rest of kerosene by vacuuming (-7.2 m of water column). At this, 91 cm^3 (36.15%) of kerosene were removed.

We tried to wash out kerosene remained in soil imitating water input in the unsaturated contaminated zone and water output from the aquifer. The water input of 980 cm^3, which is six times greater than the kerosene amount, with the velocity of 1.64 cm/hour resulted in the kerosene output of 35 cm^3. 125.7 cm^3 of kerosene remained in pores less than 3 μm. The output of hot water (80°C), which must have reduced kerosene surface tension, resulted in the kerosene output of 10 cm^3 only. During filtration water temperature sharply decreased.

Biopreparation “Simbinal” developed by the Institute of Botany of the National Ukrainian Academy of Sciences (www.biorosinfo.ru/papers-society/Strategy_Bioindustry.pdf) was used to remove kerosene from pores less than 3 μm. “Simbinal” input resulted in the value of saturation 0.7. After eleven days the amount of kerosene decreased in 19.35% and after 25 days – in 7%. Then, a new portion of kerosene was added into the column. After 30 days the amount of kero-

sene decreased in 6.79% only and 12.9% of kerosene remained in sand. The results of the experiment showed that as the content of kerosene decreased the velocity of biodegradation decreased too. Therefore, all the kerosene was not removed from sand for two months. Table 1 demonstrates the results of the physical modelling.

Table 1. The results of physical modelling of aviation kerosene recovery.

Method of recovery	% recovery	rest, %	Annotation
Gravitational draining	22.2/16.3	77.8/83.7	Of the volume in the saturated zone / of all volume
Vacuumization	36.15	63.85	Of the retained volume
Washing-out by cold water	13.9	49.95	— // —
Washing-out by hot water	4.0	45.95	— // —
Biodegradation: «Simbinal»:			
I portion: after 11 days	19.35	26.6	— // —
I portion: after 25 days	7.0	19.6	— // —
II portion after 15 days	6.7	12.9	— // —

5 Mathematical modelling of dissolved oil spreading

In case of long-term contamination sources a zone of dissolved light oil around a lens can spread in an aquifer at large distances especially when large water-supply well systems increase hydraulic gradient accelerating a contaminated water flow. Nonhazardous distances from a contamination source at which water-supply wells remain uncontaminated for 27 years (the term of well exploitation) were calculated using mathematical modelling (Table 2). A number of profile tasks were solved for typical hydrogeological conditions using PMWIN program complex. Water flow and oil mass transport in aquifers were modelled. Stationary problem was solved. Tabular hydrogeological parameter values were used. Distances from a source at which contamination does not reach wells were determined for 5, 10 and 27 years. The results of modelling provide to predict groundwater contamination, plan monitoring and remediation.

A significant contamination case of a large water-supply well system in a confined aquifer overlain with a discontinuous low-permeable layer occurred in Kherson City where water-supply wells are located four kilometres away from a refinery (Shpak 2006). Dissolved oil transport in a high-permeable limestone aquifer was imitated using PMWIN program complex. Modelling results showed that aquifer contamination occurred due to “gaps” in an overlying layer and oil reached water-supply wells in two and half years.

Table 2. Calculated nonhazardous distances from a contamination source to water-supply wells.

Hydrogeological conditions	Parameters*	Nonhazardous distance, m
III. Unconfined aquifer		
Ia. High permeable sediments (sand, shingle)	1. k = 5.0; n_a = 0.15	2,000
	2. k = 30.0; n_a = 0.20	3,500
	3. k = 100.0; n_a = 0.25	6,700
Ib. Low permeable sediments	1. k = 1.0; n_a = 0.10	550
	2. k = 0.10; n_a = 0.05	300
Ic. Two-layer sediments	1. k = 0.10; n_a = 0.05 (upper)	2,800
	1. k = 10.0; n_a = 0.15 (lower)	3,500
	2. k = 25.0; n_a = 0.20	
II. Interstratal unconfined aquifer		
II. Overlying low-permeable layer	$k/m < 3 \times 10^{-6}$	
II. Aquifer	k > 30.0	2,000**
III. Confined aquifer		
IIIa. Overlain with a continuous low-permeable layer	1. $k/m < 1 \times 10^{-6}$; k ≥ 70.0	2,500
	2. $k/m = 1 \times 10^{-5}$-1×10^{-6}; k ≥ 70.0	2,500-7,000
IIIb. Overlain with a discontinuous low-permeable layer	k = 30.0-70.0	5,000-20,000***

* k - a hydraulic conductivity, m/day; n_a – active porosity; k/m - leakance, 1/day;
** if k/m increases and k decreases, a nonhazardous distance reaches the values in the unconfined aquifer;
*** a nonhazardous distance depends on the location of "gaps" in a low-permeable layer.

6 Conclusions and recommendations.

There is an environmental risk from oil-products objects on the whole territory of Ukraine. It is necessary to liquidate or control current contamination cases and prevent potential cases.

The complex estimation of subsurface contamination at the territories of oil-products objects must be the first stage of remediation.

Under a long-term contamination source a mobile oil lens is formed on a water table and can flow into surrounding wells, ponds, rivers, etc. No more than forty percent of mobile oil is recovered by pumping. The rest of oil is retained in soil and it cannot practically be removed.

In aquifers dissolved oil can spread at large distances from contamination sources, which poses a sufficient threat for drinking water-supply well systems.

Monitoring of groundwater quality must be carried out at drinking water-supply well systems. In case of groundwater contamination with oil it is necessary to reveal the cause of contamination and carry out remediation. Designing new water-supply well systems, the impact of oil-products objects should be taken into consideration.

References

Baehr A.L. and M.Y. Corapcioglu. (1987) A compositional multiphase model for groundwater contamination by petroleum products. Water resources research. Vol. 23. 191-200

Bricks A., Negoda Y., Shpak O. (2002) Using computer modelling for predictions of groundwater contamination with petroleum products in the area of Lutsk aerodrome and development of actions to localize contamination. Proceedings of "IAP 2002", Hungary. 99

Farr A.M., Houghtalen R.J., McWhorter D.B. (1990) Volume estimation of light non aqueous phase liquids in porous media. Ground Water. No1. 48-56

Ognianik N, Shpak O., Golub G., Negoda Y., Nasedkina O. (2003) The estimation of subsurface contamination with oil within the airbase (in Russian). Proceedings of "Sergeevskie chtenia", Moscow. 342-348

Ognianik N.S., Paramonova N.K., Bricks A.L., Pashkovskiy I.S., Konnov D.V. (2006) The fundamentals of studying of subsurface contamination with light petroleum products (in Russian). Kiev. 278 p

Shpak O. (2006) Groundwater contamination with oil within large water-supply well systems (in Ukrainian). Proceedings "Modern areas of geology in Ukraine", Kiev. 159-167

Shpak O., Ognianik N., Negoda Y., Golub G. (2003) Assessment of military airbase impact on the environment. Proceedings of CERECO'2003, Hungary. 366-369

www.biorosinfo.ru/papers-society/Strategy _Bioindustry.pdf

Assessment of specific vulnerability to nitrates using LOS indices in the Ferrara Province, Italy

E. Salemi[1], N. Colombani[1], V. Aschonitis[2], M. Mastrocicco[1]

[1]University of Ferrara, Department of Earth Sciences, Ferrara, Italy

clo@unife.it

[2]Aristotle University of Thessaloniki, School of Agriculture, Thessaloniki, Greece

Abstract A set of indices (LOS), based on a deterministic approach and regression analysis were used to assess intrinsic and specific vulnerability to nitrates in Ferrara Province, in northern Italy. To calibrate the LOS indices, using multiple regression analysis, the simulation results of GLEAMS model for combinations of different soil properties, topography and climatic conditions of a reference field-crop were used as "observed values". Results of model were introduced in a GIS environment to obtain the vulnerability maps. Maps of water and nitrogen losses under the root zone (LOSW-P and LOSN-PN respectively) were used to obtain the map of relative concentration of percolated water (RCPW). Data on individual crops were used to calculate specific crop evapotranspiration rates (ETc) from potential evapotranspiration (PE). ETc values replaced PE values in the indices, to obtain both specific vulnerability map for water and nitrogen losses under the root zone (LOSW-P mod; LOSN-PN mod) and for relative nitrogen concentration of percolated water (RCPW mod). The RCPW mod map shows that concentration of nitrogen losses under the root zone is under water drinking limit of 50 mg/L (WFD; 2006/118/EC) all over the territory with highest concentrations along small areas of the coastal zone, where sandy textured soil are present (coastal dunes) and lowest concentrations where ETc is higher.

1 Introduction

Nitrogen losses from non point agricultural sources have been recognized as one of the most serious threats in agricultural-dominated system, where agrochemicals are widely used and are the principal cause of groundwater nitrate contamination (Almasri 2008). This issue has recently become a priority within the European

N. Lambrakis et al. (Eds.), *Advances in the Research of Aquatic Environment, Vol. 2*
DOI 10.1007/978-3-642-24076-8,

Community Framework Directive for water protection (WFD 2000/60 CE), which has established a list of measures and limitations to be applied in areas declared "vulnerable to nitrate from agricultural sources". An example is the Ferrara Province (Northern Italy), an intensively cultivated area affected by serious nitrate pollution since decades, principally deriving from nitrogen fertilizers used in agriculture, that often cause nitrate leaching towards shallow groundwater. The most used method to determine water and agrochemicals losses from agricultural land is the use of process-based mathematical models, describing water movement and the transport and transformations of dissolved species through the soil profile (Simunek et al. 2008). More simple models like classification indices (vulnerability or risk indices) use fewer and more accessible data such as climatic data, topography and general soil physical properties (Gogu and Dassargue 2000) and can be employed easily in large scale application using GIS tools. The most popular vulnerability indices, using weights and ratings, that describe the intrinsic vulnerability of the groundwater to contamination are the DRASTIC index (Aller et al. 1985), the SINTACS index (Civita and De Maio 1997) and the MERLIN (Aveline et al. 2010). Petelte-Giraude et al. 2000), COP (Zwahlen 2003) and MERLIN (Aveline et al. 2010).

When intrinsic vulnerability of the groundwater is studied, errors are introduced by the uncertainties related to field measurements used for the calibration procedure. It's been demonstrated that field measurements are affected from land uses (especially from human induced processes) and from the hydraulic gradients in the saturated zone (either due to the aquifer's nature or to groundwater abstraction) (Barnes and Raymond 2010). In general, these factors lead to a misinterpretation of the intrinsic groundwater vulnerability to pollution. To avoid the subjectivity of the indices using weights and ratings, the LOS method has been developed (Aschonitis et al. under review). In this method the loss of water and nitrogen indices are calibrated, by regression analysis, via Gleams v3.0 model. The GLEAMS V3.0 model is a software used to simulate water quality events on agricultural fields. GLEAMS has been used internationally and especially in the U.S.A. to evaluate the hydrologic and water quality response of many different scenarios considering different cropping systems, wetland conditions, subsurface drained fields, agricultural and municipal waste application, nutrient and pesticide applications and different tillage systems. In order to simulate the many events occurring on the field, GLEAMS model is divided into three separate submodels: hydrology, erosion/sediment yield and chemical transport/transformation (i.e. nutrients and pesticides) (Leonard et al. 1987; Knisel and Davis 2000). Regarding nitrogen, the chemical transport/transformation submodel of GLEAMS, is adjusted to different soil and climate environments using reaction coefficients for nitrification, denitrification, ammonia volatilization, mineralization, immobilization, which are self-calibrated functions of soil moisture, soil temperature and other soil physicochemical characteristics. The results of calibration are used as observed values. Consequently the ranking of LOS indices has a physical meaning, using units of measurement for the amounts and concentrations of water and nitrogen

losses. Thus, LOS indices results are very easy to introduce into GIS software to obtain vulnerability maps of agricultural lands to nitrogen percolation. The aim of this study was to apply the LOS indices to the Ferrara Province cropping system to create a specific vulnerability map of nitrogen in the percolated water based on real crops and to compare it with the vulnerability map based on hypothetical turf grass.

2 Study area

The Ferrara Province is located in the north-eastern part of Emilia-Romagna region, Italy (Fig. 1) covering an area of 2636 km². This area is completely flat and most of the sediments that outcrop on the surface are recent (Holocene, <10.000 years). The predominant soil textures in Ferrara Province are silt loam and silty clay (68% of the territory), while sandy and peaty soils are less common (9% and 23% of the territory respectively). The altitude varies from -11 to 38 m above mean sea level (a.m.s.l.). An accurate description of geological and geomorphological settings, land use, soil and climate description is given in Mastroccicco et al. (2010).

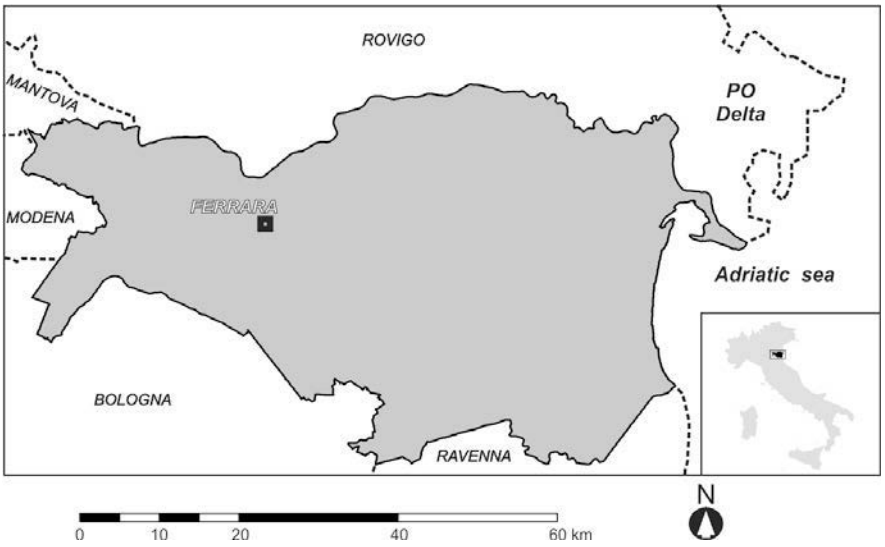

Fig. 1. Location map of study area.

3 Application of LOS indices

The general form of LOS indices for water and nitrogen losses, are the following:

$$LOSW-P=\left\{\begin{matrix}0.0941\sqrt{Ks}-0.761\sqrt{S}+0.4185\sqrt{PCP}\\-0.0487\sqrt{PE}+0.0903\sqrt{IR}\end{matrix}\right\}^{2}$$

$$LOSN-PN=\left\{\begin{matrix}-0.1536\sqrt{OM}+2.6981\sqrt{T}+0.0439\sqrt{Ks}\\-0.2046\sqrt{S}+0.0471\sqrt{PCP}-0.2515\sqrt{PE}\\-0.0116\sqrt{IR}\end{matrix}\right\}^{2}$$

$$RCPW=100\frac{(LOSN-PN)}{(LOSW-P)}$$

where *LOSW-P* is the water losses (mm year^{-1}), *LOSN-PN* is the nitrogen losses (kg ha^{-1} year^{-1}), K_s is hydraulic conductivity (mm day^{-1}), *S* is the surface slope (%), *PCP* is the precipitation (mm year^{-1}), *PE* is the potential evapotranspiration (mm year^{-1}), *IR* is the irrigation applied by the model (mm year^{-1}), *OM* is the organic matter (%), *T* is the mean annual temperature (^{o}C), RCPW is the nitrogen relative concentration of the percolated water under the root zone (mg/L).

The application of the indices is based on elaboration of surface model for each independent variable via spatial geostatistical interpolation. To accomplish this task, 3D Analyst and Spatial Analyst tools of ESRI ArcMap 9.3 were used. Grid maps were the results of the spatial interpolations, as below explained for each variable. The slope model was obtained by processing digital elevation models (DEM) from NASA SRTM (NASA Shuttle Radar Topographic Mission - 90x90m pixel resolution). The minimum, maximum and mean slopes for the Ferrara Province are 0.0, 13.6 and 0.8 % respectively. Meteorological data for temperature and rainfall were obtained by twelve meteorological stations property of the Regional Agency for Environmental Protection (ARPA Emilia Romagna), homogenously distributed in the whole Ferrara Province area The resulting mean annual temperature is 13.1°C and the mean annual rainfall is 651 mm. Potential evapotranspiration (PE) surface model was obtained using the Thornthwaite method (1957). The minimum, maximum and mean values of PE are 750.9, 804.8 and 781.4 mm respectively. Crop evapotranspiration (ETc) surface model was obtained using the equation: ETc = Kc * PE, where Kc is the crop factor. Land use of the study area was identified using CORINE Land Cover 2000, while crop distribution was obtained by the reports of the Regional Administrative Units (Statistical Office - Agricultural and Economical Development Sector of Ferrara Province). The crop distribution in the agricultural area is shown in Table 1.

Table 1. Main features of each crop present in the Ferrara Province.

Crop Class	CODES	Water needs (mm)	Type	Crop factor	Coverage (%)
Fruit-trees	Apricot, Cherry, Plum Tree, Walnut, Peach, Nectarines, Apple, Pear	600-700	perennial	0.81	8.03%
Vineyard	Screw	550-650	perennial	0.73	0.41%
Winter cereals	Farr and other cereals, Rye, Wheat, Durum Wheat, Oats, Barley	350-400	winter	0.75	32.11%
Maize (sillage/grain)	Maize grain	350-450/ 550-650	summer	0.75/0.78	22.63%
Rice	Rice	1200-1500	summer	1.15	4.23%
Beet	Beet	600-700	summer	0.88	4.29%
Energy plants	Rape, Sunflower, Sorghum, Soy	600-700	summer	0.87	10.04%
Tomato	Tomato	550-650	summer	0.92	4.17%
Grain legumes	Peas, Pea Protein, Fresh Beans	350-450	winter	0.78	1.93%
Annual forage crops	Fodder, alfa alfa	400-500	perennial	0.63	7.74%
Gardening fruits	Melon, Watermelon	400-600	summer	0.8	0.82%
Other	Garlic, Asparagus, Hemp, Carrot, Onion, Vegetable and Flowers in greenhouse, Potato ecc				3.60%

Soil profile analyses and soil map development have been conducted by the Geological, Seismic and Soil Service of Emilia-Romagna Region (SGSS 2006) according to the USDA classification (Soil Survey Staff 1996).

Surface integration of hydraulic conductivity (*Ks*) was carried out using the values determined for each soil textural class according to USDA soil taxonomy based on the Green-Ampt equation approach (Greppi 2009); surface integration of organic matter was based on a wide number of field measurements that cover the entire region (SGSS 2006). Once RCPW vulnerability map was obtained, ETc surface model was used to develop specific vulnerability map (RCPW mod).

4 Results and discussion

RCPW vulnerability map (Fig. 2) shows that relative nitrogen concentration (mg/L) ranges between 4 and 49 mg/L all over the territory. The highest class is

very poorly represented, while medium values, ranging between 16 and 20 mg/L, are concentrated along the coastal zones. Coastal zones are characterized from fine and medium textured soil pertaining to the sand dunes, and in minor part along river banks and paleo-channels of the Po and the Reno rivers (Aschonitis et al. under review).

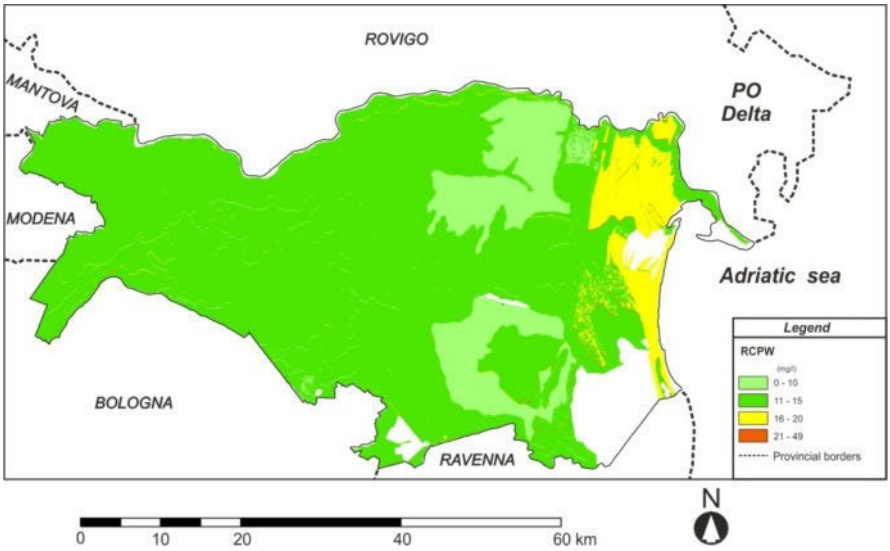

Fig. 2. Vulnerability map (RCPW) of the relative nitrogen concentration in percolated water under the root zone.

The lowest nitrogen concentration are predominant in coincidence with rice cultivated land (central upper part of the territory), where moderately acid peaty soils with high organic matter content are present. Low concentrations occur in the south-eastern part of the Ferrara Province as well where peaty soils with elevated organic matter content are present. In RCPW mod map, nitrogen concentration values range between 6 and 26 mg/L, with a different class distribution with respect to the RCPW map. Highest values are present along the coastal zones and in a very small area in the southern part of the Ferrara Province, along the Reno River. The most representative class is that ranging from 16 to 20 mg/L widespread all over the territory, where silty loam and silty clay loam are present. The lowest values are only present in the northern part, where rice is cultivated, in agreement with RCPW map, while the concentration values in the south-eastern part of the Ferrara Province are slightly higher, probably due to the type of crop, which is characterized by a low value of the crop factor (0.78), that causes a reduction of the amount of infiltration water towards the shallow aquifer.

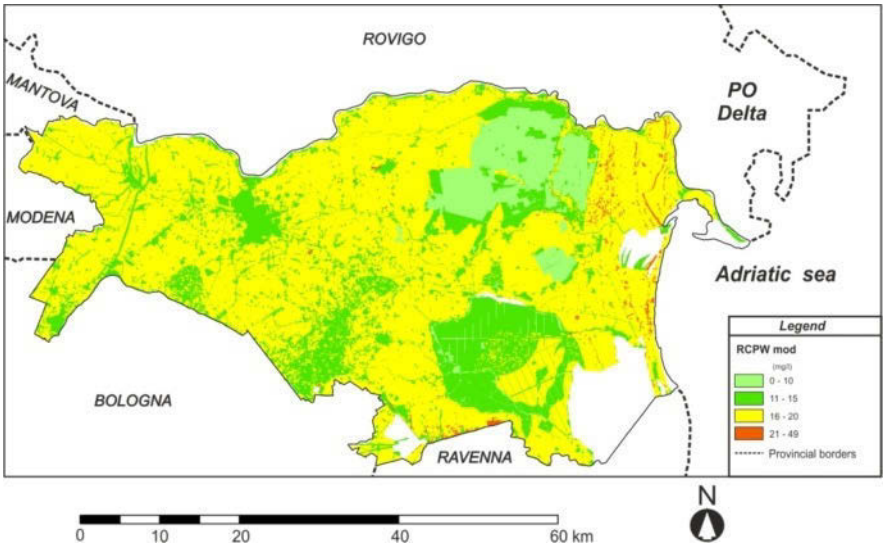

Fig. 3. Specific vulnerability map (RCPW mod) of the relative nitrogen concentration in percolated water under the root zone.

5 Conclusions

The application of the LOS indices to a lowland subject to intensive agricultural practices, as the Ferrara Province territory, showed the potentialities of this method, providing an integrated description of the specific vulnerability of agricultural lands to water and nitrogen losses and the possibility to compare the results with other regions. The rankings used have a physical meaning and can be easily introduced in a GIS environment. The RCPW map was used as a basis to obtain specific vulnerability map (RCPW mod, Fig. 3), based on the crop evapotranspiration (Etc), calculated from crop coefficients. The authors believe that, although the method gives already a reliable assessment of nitrogen groundwater risk, it can be improved by adding other input parameters such as the hydraulic gradient of the groundwater and other man induced inputs, such as the use of N fertilizers.

Acknowledgments The work presented in this paper was financially supported by the European Union, within EU.WATER project "Transnational integrated management of water resources in agriculture for the European WATER emergency control", of the South-East Europe Program" (contract n. SEE/A/165/2.1/X).

References

Aller L., Bennett T., Lehr J.H. and Petty R.J. (1985) Drastic: A standardized system for evaluating groundwater pollution potential using hydrogeologic settings. EPA/600/2-85/018 U.S. Environmental Protection Agency, Robert S. Kerr Environmental Research Laboratory, Office of Research and Development

Almasri M., N., Kaluarachchi J. J. (2007) Modeling nitrate contamination of groundwater in agricultural watersheds. J. of Hydrol. 343, 211-229

Aschonitis V.G., Mastrocicco M., Colombani N., Salemi E., Kazakis N., Voudouris K., Castaldelli G. (submitted) Assessment of the intrinsic vulnerability of agricultural land to water and nitrogen losses, via deterministic approach and regression analysis. Part I: methodology development, Water Air Soil Poll. (under review)

Aschonitis V.G., Mastrocicco M., Colombani N., Salemi E., Kazakis N., Voudouris K., Castaldelli G. (submitted) Assessment of the intrinsic vulnerability of agricultural land to water and nitrogen losses, via deterministic approach and regression analysis. Part II: Case study in Italy and Greece, Water Air Soil Poll. under review

Aveline A., Rousseau M.L., Guichard L., Laurent M., Bockstaller C. (2009) Evaluating an environmental indicator: Case study of MERLIN, a method for assessing the risk of nitrate leaching. Agr. Syst. 100, 22-30

Barnes R. T. and Raymond P. A. (2010) Land-use controls on sources and processing of nitrate in small watersheds: insights from dual isotopic analysis. Ecol. Appl. 20(7), 1961-1978

Civita M. and De Maio M. (2000) Valutazione e cartografi a automatica della vulnerabilità degli acquiferi all'inquinamento con il sistema parametrico SINTACS R5. Pitagora Ed.: 240 pp

Directive 2000/60/EC of the European Parliament and of the Council of 23 October 2000 establishing a framework for Community action in the field of water policy; *OJ L 327, 22.12.2000,* p. 1-73

Knisel W.G. and Davis F.M. (2000) GLEAMS, Groundwater Loading Effects from Agricultural Management Systems V3.0. Publ. No. SEWRL-WGK/FMD-050199, U.S.D.A., Tifton, Georgia

Leonard R.A., Knisel W.G., Still D.A. (1987) GLEAMS: groundwater loading effects of agricultural management systems. Trans. Am. Soc. Agr. Eng. 30, 1403-1418

Mastrocicco M., Colombani N., Salemi E., Castaldelli G. (2010) Numerical assessment of effective evapotranspiration from maize plots to estimate groundwater recharge in lowlands. Agr Water Manage. 97(9), 1389-1398

Gogu R.C. and Dassargues A. (2000) Current trends and future challenges in groundwater vulnerability assessment using overlay and index methods. Environ Geol 39(6), 549-559

Greppi M., 2009. Idrologia. HOEPLI Editions, Milano, pp.371. (in Italian)

SGSS (2006) http://www.regione.emilia-romagna.it/wcm/geologia/index.htm

Šimunek J., Šejna M., Saito H., Sakai M., Van Genuchten M.Th. (2008) The HYDRUS-1D Software Package for Simulating the Movement of Water, Heat, and Multiple Solutes in Variably Saturated Media, V. 4.0, HYDRUS Software Series 3, Dep of Environ Scie, University of California Riverside, Riverside, California, USA, p. 315

Soil Survey Staff (1996) Soil survey laboratory methods manual. Soil Survey Investigations Rep. 42, Version 3.0. USDA-NRCS, Lincoln, NE

Thornthwaite C.W. and Mather J.R. (1957) Instructions and tables for computing potential evapotranspiration and the water balance. Climatol. 10(3), Centerton , N.J. Drexel Inst

Groundwater nitrogen speciation in intensively cultivated lowland areas

N. Colombani[1], E. Salemi[1], M. Mastrocicco[1], G. Castaldelli[2]

[1]University of Ferrara, Department of Earth Sciences, Ferrara, Italy

[2]University of Ferrara, Department of Biology and Evolution, Ferrara, Italy

clo@unife.it

Abstract The study was conducted in Ferrara Province (Italy), a lowland area covering 2636 km^2, located in the southern part of the Po River Delta. It is an intensively cultivated area, with more than 50% of land cultivated with winter cereals (32.11%) and maize (22.63%). The main nitrogen fertilizer used in this area is synthetic urea which is suspected to cause nitrate leaching towards shallow groundwater. A network of 56 piezometers, homogeneously distributed throughout the whole area, was installed in order to monitor both water table fluctuations and nitrogen species distributions in the shallow aquifer, over time. Data collected at the end of November 2010 were used to obtain maps of water table, urea ($CO(NH_2)_2$), ammonium (NH_4^+), nitrate (NO_3^-) and nitrite (NO_2^-) distributions. Maps show an accumulation of NH_4^+ overlapping a stagnant zone, where drained peaty soils are present. The peaty soils are characterized by a pH ranging between moderately acid and slightly acid, and by high values of organic matter content. Along the drainage line induced by peaty soils dewatering, the flow velocity is very low or almost motionless, determining anaerobic conditions. Instead, the largest accumulation NO_3^- is observed in the Eastern part of the province, where the groundwater head gradient is higher and soils are characterized by values of pH that range between 8.1 and 8.3, providing the best conditions for nitrification processes.

1 Introduction

Nitrate (NO_3^-) is a widespread inorganic pollutant in shallow groundwater aquifers due to the use of nitrogen fertilizers in intensive agriculture (Galloway et al. 2008; Rivett et al. 2008) and to industrial and municipal point sources (Wakida and Lerner 2005). In shallow aquifers, NO_3^- concentrations are often found spatially and temporally variable (Böhlke et al. 2002; Wriedt and Rode 2006; Thayalaku-

N. Lambrakis et al. (Eds.), *Advances in the Research of Aquatic Environment, Vol. 2*
DOI 10.1007/978-3-642-24076-8, © Springer-Verlag Berlin Heidelberg 2011

maran et al. 2008) and this is usually related to variations in groundwater flow and NO_3^- attenuation rate (Tesoriero et al. 2000; Almasri and Kaluarachchi 2007). This is particularly true in lowland areas where the flat topography minimize surface run off and where nitrogen leaching from non point agricultural sources to the aquifer has been recognized as one of the most serious threat. In the last decades the use of urea ($CO(NH_2)_2$) has increased worldwide from 5% of world nitrogen fertilizer budget up to >50% and supposed to reach 70% by 2020 (FAO 2001; Glibert et al. 2006). $CO(NH_2)_2$ hydrolysis is rapid and occurs in a few days (Yadav et al. 1987; Sankhayan and Shukla 1976) and afterwards several processes regulate nitrogen fate. Released ammonia (NH_3) may adsorb onto soil particles, be assimilated by crops, volatilized to the atmosphere or nitrified to NO_3^-, which in turn may be assimilated by crops, lost in runoff water, leached to the water table and partly denitrified to nitrous oxide (N_2O) or to nitrogen gas (N_2).

In Italy, the Po River valley is the largest and more intensively farmed alluvial plain, and is heavily impacted by NO_3^- groundwater contamination (Mastrocicco et al. 2010a; Onorati et al. 2006; Cinnirella et al. 2005) and surface water eutrophication (Palmieri et al. 2005). The Province of Ferrara, chosen as study site, is located in the lowest terminal portion of the Po Basin. In this area, cattle farming and the use of manure as fertilizer ceased about 40 years ago, replaced by the synthetic fertilizers such as ammonium-nitrate (NH_4NO_3) and $CO(NH_2)_2$. The purpose of this research is to investigate the importance of soil organic matter (SOM) content and pH on nitrogen speciation, in shallow groundwater aquifers located in lowland areas. Specifically, this study investigates the relative abundance of nitrogen species, like NH_4^+ and NO_3^-, in soils fertilized with $CO(NH_2)_2$ and with a variable content of SOM.

2 Study area

The Ferrara Province is located in the north-eastern part of Emilia-Romagna Region, Italy (Fig. 1) covering an area of 2636 km². The study area is flat with an altitude varying from -11 to 38 m above sea level (a.s.l.) and most of the sediments that outcrop on the surface are recent (Holocene, <10,000 years) and characterized by an elevated spatial heterogeneity due to the presence of paleo-channels interconnected with crevasses splay and marsh lagoon environments.

According to the World Reference Base for Soil Resources classification (2006), the dominant soils in the Ferrara Province are: medium and medium-fine textured soils (68% of the territory), medium-fine sands (9% of the territory) and peaty soils (23% of the territory). The peaty soils present high SOM (25-28.3%) except for the Mottalunga-Burano sub-unit (6.8%) because of the modest thickness of the intercalated turf layer; pH values are low and soils can be classified as moderately to slightly acid, according to the Natural Resources Conservation Service classification (1999). The remaining soils outcropping in the study area, pre-

sent a low SOM (1.2-2%) and are slightly alkaline with pH values ranging between 7.9 and 8.3 (Table 1). An accurate description of geological and geomorphological settings, land use, soil and climate description is given in Mastroccicco et al. (2010b).

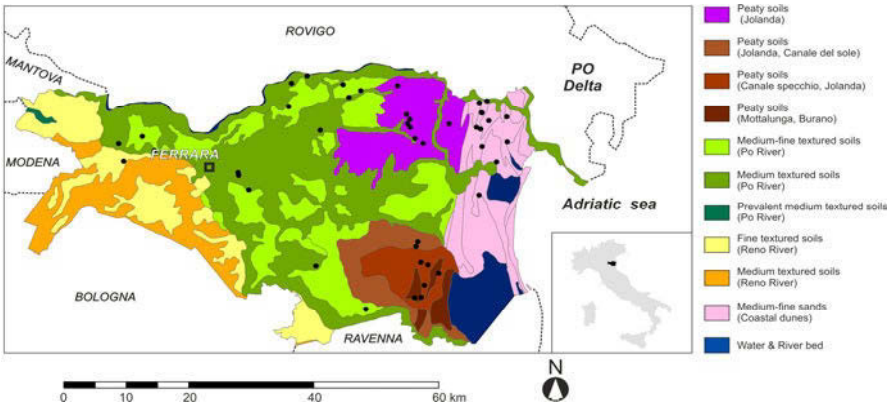

Fig. 1. Soil classification map of the Ferrara Province; black dots represent piezometers.

Table 1. Soil classification based on World Reference Base for Soil Resources (2006).

Soil	Soil group	Sub-unit	SOM (%)	pH
Medium-fine textured soils (Po River)	1B	/	2	8.2
Medium textured soils (Po River)	1c	/	1.3	8.3
Prevalent medium textured soils (Po River)	3B	/	1.2	8.2
Fine textured soils (Reno River)	2A	/	1.6	8.3
Medium textured soils (Reno River)	3A	/	1.2	8.1
Medium-fine sands (Coastal dunes)	1D	/	1.4	7.9
		Jolanda	28.3	5.4
		Jolanda, Canale del sole	25	8.2
		Canale specchio, Jolanda	25.5	6.1
Peaty soil	1A	Mottalunga, Burano	6.8	6.2

3 Materials and Methods

A distributed network of 56 piezometers was installed to monitor water table fluctuations and to take water samples. Standard PVC piezometers (2.5 cm inner diameter) were drilled manually with an Ejielkamp Agrisearch auger equipment. Depending on the water table depth, piezometers were installed at depths between 1.1 and 6 m below ground level (b.g.l.). They were located in agricultural fields, in which crop type, preceding crop, irrigation amount, type and amount of fertilizers applied are known. The piezometers location was also selected on the base of the soil characteristic (Fig. 1) to cover the different soil types present in the Ferrara Province. Groundwater were sampled via a low flow purging technique (using inertial pumps) stored in vials with no head space, kept refrigerated and analyzed within two days. Groundwater concentration of NO_3^- and NO_2^- were determined by an isocratic dual pump ion chromatography ICS-1000 Dionex, equipped with an AS9-HC 4 x 250 mm high capacity column and an ASRS-ULTRA 4mm self-suppressor. An AS-40 Dionex auto-sampler was employed to run the analyses. Groundwater concentration of $CO(NH_2)_2$ and NH_4^+ were determined according to Price and Harrison (1987) and Bower and Holm Hansen (1980) using a double beam Jasco V-550 UV/VIS spectrophotometer. Groundwater organic carbon concentration was determined with a Carbon Analyzer Shimadzu TOC-V-CSM after acidification with one drop of 2 M HCl to remove dissolved carbonate. SOM and organic nitrogen content were determined with an Elemental Analyser, Carlo Erba Strumentazione.

4 Results and discussion

The unconfined aquifer thickness ranges between 2 and 7 m, but can even be more than 45 m where the principal Po paleo-channels are in erosional contact with sediments pertaining to the underlying confined aquifer (Mastrocicco et al. 2010c). The water table elevation ranges between 0.5 and 5.5 m b.g.l. (Fig. 2). The analysis of the water table elevation highlights three different zones moving from West to East. In the western portion of the Ferrara Province the water table elevations range between 2.3 and -1 m a.s.l. and the groundwater flow direction is toward the sea, locally influenced by canals. In the central part of the Ferrara Province the water table elevation is below the sea level at all locations, with values ranging between -1 and -7.3 m a.s.l. It represents a North-South drainage axis induced by dewatering pumping stations used to reclaim swap areas, characterized by a flat central stagnant zone and steep slopes on both right and left sides (from 0.6% to 1%). In the Eastern part of the Ferrara Province a flat water table is present with elevations below sea level and a weak head gradient toward inland (from 0% to 0.06%).

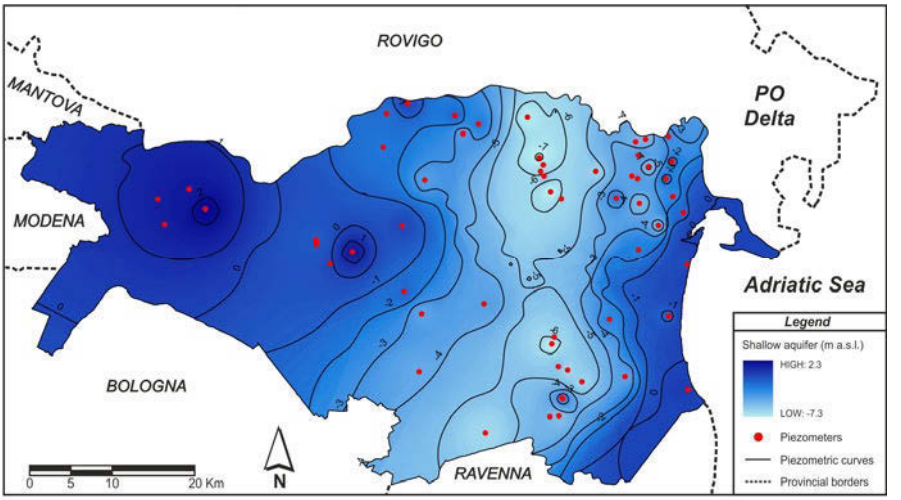

Fig. 2. Map of the shallow aquifer water table elevation in the Ferrara Province.

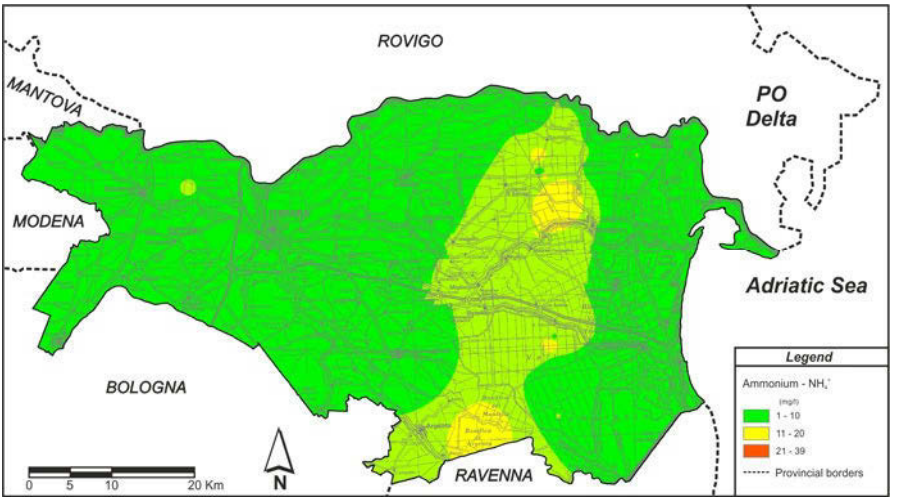

Fig. 3. Map of NH_4^+ concentration in Ferrara province.

The map of NH_4^+ concentration (Fig. 3) shows values ranging between 0 and 30.9 mg/L with a mean value of 7.1 mg/L. The greater concentrations are found in the stagnant zone of the central part of the map, along the North-South drainage axis, with values higher than 11 mg/L and mean concentration of 14.5 mg/L. The map of NO_3^- concentration (Fig. 4) shows values ranging between 0 and 109.7 mg/L, with a mean value of 6.7 mg/L. Concentration rise in the Western part of the Ferrara Province, and in the far North-Eastern part of the Ferrara Province, close to the shore line, where a peak of concentration with values that reach 67

mg/L is found. The central portion of the Ferrara Province displays very low NO_3^- concentration. Finally, $CO(NH_2)_2$ is always found at very low concentration, with average concentration of 0.3 mg/L, variance of 0.2 mg/L and maximum concentration of 1.3 mg/L.

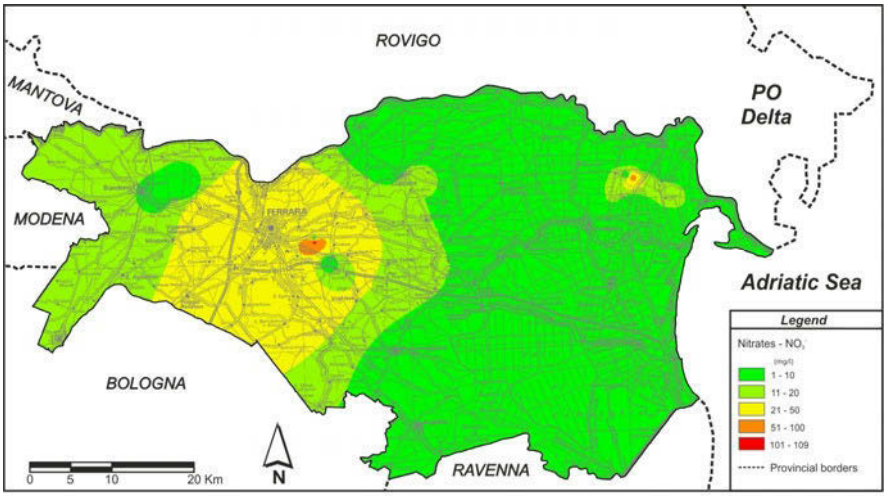

Fig. 4. Map of NO_3^- concentration in Ferrara province.

This indicates that, in the upper soil horizons, $CO(NH_2)_2$ is readily transformed into NH_4^+ and subsequently nitrified to NO_3^- in soils where the pH is not inhibiting this reaction. While, in anaerobic peaty soils with low pH values NH_4^+ is the stable form of nitrogen. NO_2^- concentration is also found very low with average concentration of 0.3 mg/L, variance of 0.4 mg/L and maximum concentration of 2.3 mg/L. Since NO_2^- is an intermediate species of most of the nitrogen transformation reactions (Appelo and Postma 2005), the low NO_2^- concentration found in groundwater suggests that microbial processes are fast compared with groundwater fluxes.

5 Conclusions

This study shows that in the Ferrara Province, nitrogen speciation in shallow groundwater is closely linked to groundwater flow velocity. In fact, maps show an accumulation of NH_4^+ overlapping the stagnant zone where drained peaty soils are present. The peaty soils are characterized by moderately and slightly acid pH and by elevated values of organic matter content. Along a drainage line induced by dewatering pumps the flow velocity is very low or almost motionless, determining anaerobic conditions where NH_4^+ is the dominant species in groundwater. Instead,

NO_3^- is the prevalent species in the Eastern part of the Ferrara Province, where the groundwater head gradient is higher and soils are characterized by alkaline pH and low organic matter content.

Acknowledgments The work presented was made possible and financially supported by PARCAGRI (Delib. CIPE n 202) and by the Provincial Administration of Ferrara within the EU-Water Project "Transnational integrated management of water resources in agriculture for the EUropean WATER emergency control, of the South-East Europe Program" (contract n. SEE/A/165/2.1/X). A special thank goes to Dr. Umberto Tessari and Dr. Fabio Vincenzi for their technical and scientific support.

References

Almasri MN, Kaluarachchi JJ (2007) Modeling nitrate contamination of groundwater in agricultural watersheds. J. of Hydrol. 343, 211-229

Appelo CAJ, Postma D (2005) Geochemistry, groundwater and pollution, 2nd Edition, Balkema, Rotterdam, The Netherlands

Böhlke JK, Wanty R, Tuttle M, Delin G, Landon M (2002) Denitrification in the recharge area and discharge area of a transient agricultural nitrate plume in a glacial outwash sand aquifer, Minnesota. Wat. Resour. Res. 38(7), 10.1-10.26

Bower CF & Holm-Hansen T (1980) A salicylate-hypoclorite method for determining ammonia in seawater. Canadian J. of Aquatic Sci. 37: 794-798

Cinnirella S, Buttafuoco G, Pirronea N (2005) Stochastic analysis to assess the spatial distribution of groundwater NO3- concentrations in the Po catchment (Italy). Environ. Poll. 133, 569–580

FAO, IFA (2001) Global estimates of gaseous emissions of NH_3 NO and N_2O from agricultural land. FAO, IFA Rome 106. Available from http://www.fertilizer.org/ifa

Galloway JN, Townsend AR, Erisman JW, Bekunda M, Cai Z, Freney JR, Martinelli LA, Seitzinger SP, Sutton MA (2008) Transformation of the nitrogen cycle: recent trends, questions, and potential solutions. Science 320, 889-892

Glibert PM, Harrison J, Heil CA, Seitzinger S (2006) Escalating worldwide use of urea - a global change contributing to coastal eutrophication. Biogeochemistry 77, 441-463

IUSS Working Group WRB (2006) World reference base for soil resources 2006. World Soil Resources Reports No. 103. FAO, Rome

Mastrocicco M, Colombani N, Castaldelli G, Jovanovic N (2010a). Monitoring and modeling nitrate persistence in a shallow aquifer. Water Air and Soil Pollution 217(1-4), 83-93

Mastrocicco M, Colombani N, Salemi E, Castaldelli G (2010b) Numerical assessment of effective evapotranspiration from maize plots to estimate groundwater recharge in lowlands. Agricult. Wat. Manag. 97(9), 1389-1398

Mastrocicco M, Colombani N, Palpacelli S, Castaldelli G (2010c) Large tank experiment on nitrate fate and transport: the role of permeability distribution. Environ. Earth Sci. DOI: 10.1007/s12665-010-0759-0

Onorati G, Di Meo T, Bussettini M, Fabiani C, Farrace MG, Fava A, Ferronato A, Mion F, Marchetti G, Martinelli A and Mazzoni M (2006) Groundwater quality monitoring in Italy for the implementation of the EU water framework directive. Phys. and Chem. of the Earth 31, 1004-1014

Palmieri L, Bendoricchio G and Artioli Y (2005) Modelling nutrient emissions from river systems and loads to the coastal zone: Po River case study, Italy. Ecolog. Model. 184, 37-53

Price NM, Harrison PJ (1987) Comparison of methods for the analysis of dissolved urea in seawater. Mar. Biol. 94, 307-317

Rivett MO, Buss SR, Morgan P, Smith JWN, Bemment CD (2008) Nitrate attenuation in groundwater: A review of biogeochemical controlling processes. Wat. Res. 42, 421-4232

Sankhayan SD and Shukla UC (1976) Rates of urea hydrolysis in five soils of India. Geoderma 16:171-178

Soil Survey Staff (1999) Soil taxonomy: A basic system of soil classification for making and interpreting soil surveys. 2nd ed. Natural Resources Conservation Service. United States Department of Agriculture Handbook 436

Tesoriero AJ, Liebscher H, Cox SE (2000) Mechanism and rate of denitrification in an agricultural watershed: Electron and mass balance along groundwater flow paths. Wat. Resour. Res. 36 (6), 1545-1559

Thayalakumaran T, Bristow K L, Charlesworth PB, Fass T (2008) Geochemical conditions in groundwater systems: Implications for the attenuation of agricultural nitrate. Agricult. Wat. Manag. 95, 103-115

Wakida FT, Lerner DN (2005) Non-agricultural sources of groundwater nitrate: A review and case study. Wat. Res. 39 (1), 3-16

Wriedt G, Rode M (2006) Modelling nitrate transport and turnover in a lowland catchment system. J. of Hydrol. 328, 157-176

Yadav DS, Kumar V, Signh M and Relan PS (1987) Effects of temperature and moisture on kinetics of urea hydrolysis and nitrification. Aust. J. Soil Res. 25: 185-191

Hydrogeological and hydrochemical characteristics of North Peloponnesus major ground water bodies

K. Nikas[1], A. Antonakos[2]

[1] IGME, Spyrou Loui 1. Olympic Village. 136 77Acharnai nikask@igme.gr

[2] General Secretariat for Civil Protection, Evagelistrias 2, 105 33 Athens. aantonakos@yahoo.gr

Abstract During the period 2004-2008 a hydrogeological investigation project was conducted by an IGME/Hydrogeology Department team in the area of North Peloponnesus, funded by the 3rd EU Framework Directive budget. In 2008 using the results of this investigation and implementing article 5 of Water Framework Directive 60/2000/EU as well as articles of Ground Water Directive 2006/118/EU, eleven ground water bodies (management units) were able to be identified in this area. Using the DPSIR criteria six of them found to be needed further characterization and two out of these six were concluded not to be able to fulfil the required good (quantitative and chemical) groundwater status by 2015. All these results are presented here.

1 Introduction

In this paper the results of a hydrogeological investigation project conducted during the period 2004-2008 by the name "study of the water resources of North Peloponnesus with emphasis on quality characteristics and sea water intrusion" (Nikas and Antonakos 2010 b) are presented. The project was conducted by an IGME/Hydrogeology Department team and it was funded by the 3rd EU Framework Directive budget. The study area was the North Peloponnesus which constitutes the continental part of the country's Water Districts No 02 (W.D. 02). From the results a series of maps (47 maps) were able to be compiled and most of the conclusions drawn here are coming out of these maps but also from previous IGME studies (Nikas 2001), from previous studies (Nikas 2004) and from studies of other researchers (Voudouris et al. 2000); (Daskalaki et al. 1998) (Voudouris et al. 2004b), conducted in the area.

Generally, in North Peloponnesus, due to the prevailing geomorphology, the social and economic activity take place mostly in a narrow land strip adjacent to the sea. Ground water overexploitation has resulted in a sea water intrusion plume

N. Lambrakis et al. (Eds.), *Advances in the Research of Aquatic Environment, Vol. 2*
DOI 10.1007/978-3-642-24076-8,

in the coastal area and in quality degradation for the ground waters of the middle and upper zone and generally in the reduction of the potentially exploitable water resources. The aim of this project was to monitor these dynamic phenomena and to assess the water resources of the area in order to be able for the decision makers to establish a sustainable managing policy.

2 Geological and hydrogeological setting

For the understanding of the geology structure of the study area it is possible at first to distinguish two separate unities a) the bedrock formation unit and b) the cover formation unit.

The cover formations are younger post alpine sediments and their formation is attributed mostly to the neotectonic activity of the area. The neotectonic activity is also responsible for the creation of the Korinth - Patras rift. The bedrock formations are older (alpine) and constitute in the study area the following geotectonic zones (from west to east): Ionian, Gavrovo-Tripoli, Olonos-Pindos the Phillite-Quartzite series and the Subpelagonic or Eastern Greece zone.

The post alpine sediments (Pleio–Quaternary age) consist mostly from clay, clayey sand and sand intercalations, with a coarser conglomerate series appearing mainly in the perimeter of the plain coastal zone and in the semi- mountain area. Tectonics of the area is still active, playing a defining role in the shaping of today's relief, as well as in the development of the drainage network and in the formation of the local hydrogeological characteristics (Nikas and Antonakos 2005). Using International Association of Hydrogeologists (I.A.S.) proposals for the formation of an internationally accepted hydrogeological map legend (Nikas, et al 2010a), six hydro lithography units were able to be identified in the studied area. Their spatial distribution is shown in the map of Figure 1.

3 Main Groundwater Bodies (Management Units)

In 2008 using the results of the study and implementing article 5 of Water Framework Directive 60/2000/EU as well as articles of Directive 2006/118/EU, eleven ground water bodies (management units) were able to be identified in the area. Seven of them are porous and four karstic. This Main Ground Water Body Units (M.G.W.B.) is presented in the map of Figure 2 and in Table 1 with the following identity codes: GR204 Pinios System, GR206 N.W Achaia System, GR205 N.E. Achaia System, GR207 Panachaiko System, GR208 Erymanthos System, GR209 Kalavryta System, GR210 Mountainous Korinthia System, GR211 Ziria System, GR212 Kiato-Korinthos System, GR213 Nemea System (conglomerates), GR214 Nemea System (limestones).

The porous aquifers developed mostly in the plain and coastal areas and in some cases in inland sedimentary basins such as those of Kalavryta and Nemea. In the former case the groundwater system developed either in alluvium formation where water table horizons were created or in Pleio-Pleistocene formations where confined aquifers were created. In the latter case, of the inland basins, the groundwater system developed mostly in the Pleistocene conglomerate formations and, in the most cases, it is a water table type aquifer.

The karstic aquifer systems developed mostly in the mountainous zones of the Water District where the ground water system is located mainly in the Platy limestone's formation of Upper Cretaceous Olonos-Pindos zone and in some cases within the carbonate sequence formation of the Tripolis-Gavrovo zone. The details of each M.G.W.B can be seen in Table 1.

4 Pressures/Impact Assessment on the Ground Water Bodies

During the initial characterization of the water bodies it was made clear that certain ground water bodies needed further characterization regarding the pressures/impact assessment on them. In table 1 the water bodies as well as their pressures/impact data are shown. Using the DPSIR criteria (Water Framework Directive 60/2000/EU and European Commission booklet issue 2008) six of them found to be needed further characterization (classification data) and two out of those six (namely the GR206 and the GR212) were concluded not to be able to fulfill the required good (quantitative and chemical) ground water status by 2015. The DPSIR criteria applied to that M.G.W.B namely are: **D**riving forces, **P**ressure, **S**tate, **I**mpact and **R**esponse.

More specifically these pressures/impacts results are coming mostly from pumping (quantitative) and from pollution sources (qualitative). The major quantities of water demand is attributed to irrigation which for the total of the Water District is estimated to be about 485 million cubic meters annually. The demands for other uses (drinking, livestock farming, and industrial) are in total almost to the amount of 55 million cubic meters annually. A 53% percentage of those demands are covered from surface water bodies (Rivers, Stymphalia Lake and Pinios and Doxa artificial Lakes). The rest 47% that is about 255 million cubic meters annually is covered from the Water District's ground water bodies.

This amount is not equally spatially distributed since the biggest demands (either in irrigation or in drinking and industrial usage) are concentrated in the plain and coastal areas and in the inner land basins of Nemea and Kalavryta. The pollution sources can easily be distinguished, as they are coming out on one hand from natural sources and on the other from anthropogenic sources.

Fig. 1: Hydrogeological map of the study area showing the boundaries of major hydrogeological units as well as the boundaries of the Ground Water Bodies.

For instance the high concentration rates in Fe and Mn found either in the Olonos - Pindos sediments or in the Achaia and Ilia postalpine sediments can be easily attributed to the natural diffusive (non point) pollution sources.

The main anthropogenic diffusive (non point) pollution sources for the Water District are coming from the cultivations and the urban wastes disposal practices while the corresponding main point pollution sources from the industrial–handicraft small factory units, from areas of Uncontrolled Disposal of Urban Refuses and finally from the livestock farms which are dispersed into the major sub mountainous and mountainous zones of the Water District.

5 Conclusions and discussion

From the Chloride spatial distribution maps, sea water intrusion to the coastal areas of a) north east Korinthia (Almiri spring coastal area) b) north Korinthia (Kiato-Korinthos area) and c) north-west Achaia (Kato Achaia area) is observed. From the electrical conductivity spatial distribution maps high concentration rates in north east and north Korinthia and in North West Achaia are observed.

From the piezometric spatial distribution maps high negative inclinations (up to five metres below sea level) to the areas of NW Achaia and NE Achaia and to Kiato- Korinthos coastal area as well as in north Ilia coastal area are observed.

The biggest pressures are observed in the coastal porous aquifers. These pressures are mostly anthropogenic and they are attributed to the high population rate in the coastal area where almost all social activities are taking place. These areas can be defined from the high chloride and nitrate concentrations values which are also the main indicators for the quality degradation in the groundwater system. The groundwater overexploitation in these coastal areas has led to the groundwater level decline in negative levels and to the subsequently sea water intrusion regime. These phenomena are especially intense in NW Achaia where a large decline of ground water level is observed during the low water level season (September-October). The high sea water intrusion pressures in NW Achaia seems to be counteracted from the lagoon system of the area which led to the surface water infiltration into the coastal aquifers and that can be proven from the fact that there are no high chloride values corresponding to the groundwater level inclination in these areas. On the contrary in the Kiato-Korinthos coastal area the absence of such mechanism has led to high chloride concentrations rates and generally in an increase of the overall salinity of the groundwater. Parallel to that, almost in the same areas, the high intensive cultivation practices as well as the urban waste (liquid and solid wastes) disposal practices -and in some occasions industrial waste disposal practices- have led those areas in a nitrate pollution regime. The problem seems to be especially intense in the central and north Korinthia where the nitrate values exceed the limit of 50 mg/L set for drinkable waters.

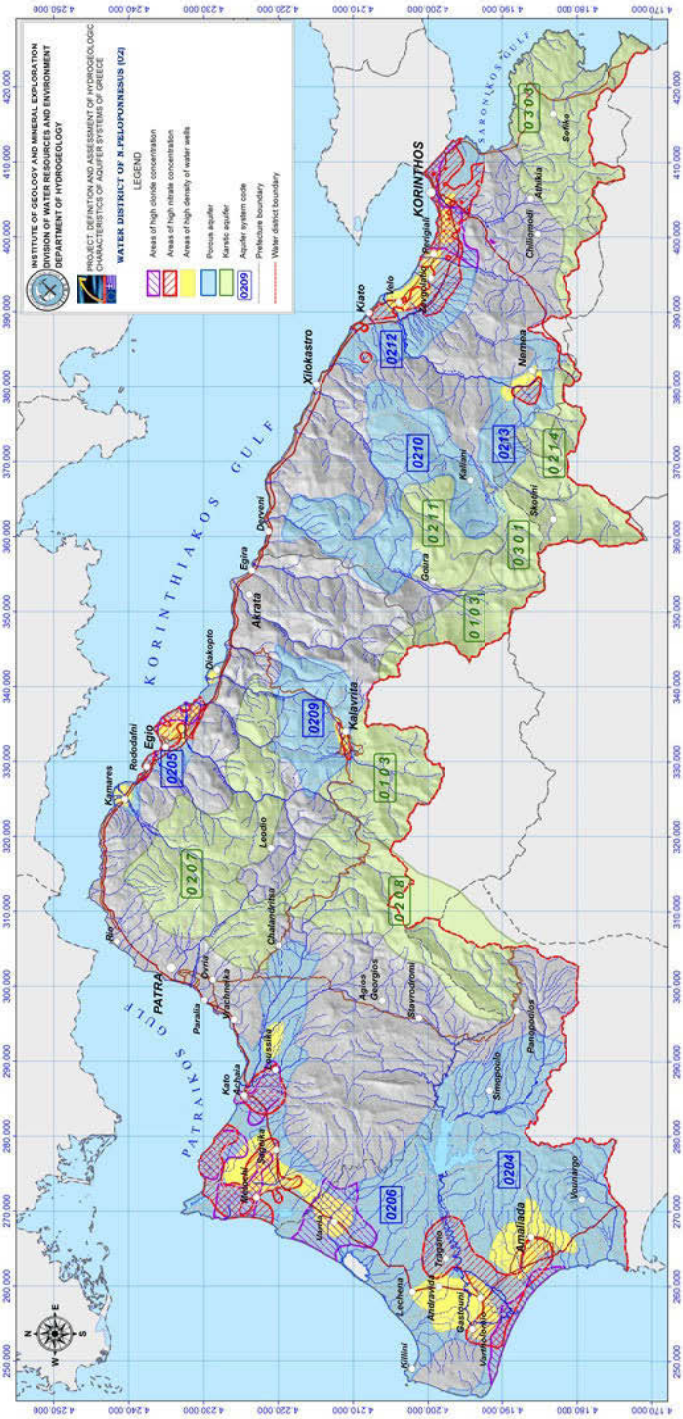

Fig. 2. Map of areas sensitive to groundwater quality degradation.

Table 1. Initial and Further characterization needed of the Main Ground Water Bodies (M.G.W.B).

Code	Name	Geology	Type of aquifer media	Sea water intrusion	Natural recharge ($10^6 m^3/y$)	Withdrawals ($10^6 m^3/y$)	Related surface water bodies - Ecosystems	Futher char-acterization needed
GR0204	Pinios	Tertiary and Neogene	Porous	YES	110	80	Pinios river and lake.	YES
GR0205	N.E.Achaia	Tertiary	Porous	YES	80	60	Selinous, Vouraikos,Foinikas, Kerynitis and Meganitis rivers	YES
GR0206	N.W.Achaia	Neogene and Tertiary	Porous	YES	70	70	Kotychi and Kalogria lagoons and Strofilia forest	YES
GR0207	Panachaiko	Pindos limestone	Karstic	NO	80	20	Selinous, Foinikas, Kerynitis and Meganitis rivers	NO
GR0208	Erymanthos	Pindos limestone	Karstic	NO	216	20	Pinios and Piros rivers	NO
GR0209	Kalavryta	Pleistocene	Porous	NO	60	40	Vouraikos river	YES
GR0210	Mountainous Korinthia	Pleistocene and Tertiary	Porous	NO	107	20	Dervenios and Sythas rivers, Stymfalia lake	NO
GR0211	Ziria	Pindos and Tripolis limestones	Karstic	NO		10	Stymfalia lake	NO
GR0212	Kiato-Korinthos	Tertiary	Porous	YES	72	65	Asopos, Rachiani and Zapanti rivers	YES
GR0213	Nemea	Pleistocene and Tertiary	Porous	NO	58	50	Asopos river	YES
GR0214	Nemea	Pindos and Tripolis limestones	Karstic	NO		10	Asopos river	NO

As it can be observed from the sensitive to groundwater quality degradation areas (Fig. 2) in most cases those areas coincide or are adjacent to areas of high concentration of productive water wells- a fact which contribute to the general idea that the intense anthropogenic activity is responsible for the groundwater quality degradation in the study area.

Apparently the whole concept of Ground Water Bodies (as they are expressed in the relative EC Frameworks Directives and in their Greek counterpart laws) and their interconnection with surface water and water basins is a matter of discussion. Another point of discussion is their applicability in the Greek Territory. The definition for example, of 45 water basins and 236 Ground Water bodies (the latter proposed by IGME in 2008) in the Greek Territory have not been fully understood, discussed, and accepted by the Greek scientific community. The authors of this paper took for granted the definition of 11 ground water bodies (as they were proposed by IGME in 2008) in the area of North Peloponnesus and carried on their research, presented here, although they are fully aware of the remain open questions.

References

Daskalaki, P, Voudouris, K, Diamantopoulou, P (1998) Hydrochemical study of North Peloponnesus quaternary and plio-pleistocene aquifers, Proc. Int. Con. Protection and restoration of the environment IV, Sani, Greece, Vol. I, 108-116

Ground Water Protection In Europe (2008) An EC booklet issue. http://bookshop.europa.eu

Ground Water Directive 2006/118/EU

Nikas, K, Antonakos, A, (2010) b. Study of the water resources of North Peloponnesus with emphasis on quality characteristics and sea water intrusion. Study in compliance to I.G.M.E - 3nd E.U. Framework project. 80 pp, 47 thematic maps in A3. Seven separate Annex issues. I.G.M.E. Library

Nikas, K, Antonakos, A, Kallergis, G, and Kounis, G (2010) a International Hydrogeological Map of Europe: Sheet D6 "Athina". Proceedings of the 12th International Congress, Patras, 2010 Bulletin of the Geological Society of Greece, Volume XLIII No 4, pages 1821-1830

Nikas, K., (2001) Research – Making useful Achaia Prefecture water resources (In Greek – English abstract and summary). Study in compliance to I.G.M.E -2nd E.U. Framework project. 199 pp, 63 thematic maps in A3. I.G.M.E. Library

Nikas, K., (2004). Hydrogeological conditions of the NE part of Achaia Prefecture (In Greek – English abstract and summary). Ph.D thesis. Patras University. Geology department. 392 pp.

Nikas, K, and Antonakos, A (2005) Influence of the active tectonics on the shaping of hydrogeological-hydraulic conditions and on the setting boundaries between the relevant units. The NE Achaia prefecture area example. 7th Hydrog. Conf., Athens. p.p. 383 -392

Voudouris K, Panagopoulos, A, Daniil, D (2000). Implications to surface water quality of Korinthos Prefecture from anthropogenic activities, Proc. Int. Conf. Protection and Restoration of the Environment V, Thassos, Greece, 2000

Voudouris K, Panagopoulos, A, Koumantakis, J (2004) b, Nitrate pollution in the coastal aquifer system of the Korinthos Prefecture (Greece). Global Nest: The International Journal, Vol. 6, No 1, 31-38, 2004

Water Framework Directive 60/2000/EU

Assessment of natural and human effect in the alluvial deposits aquifer of Sperchios' river plain

E. Psomiadis, G. Stamatis, K. Parpodis, A. Kontari

Agricultural University of Athens, Laboratory of Mineralogy-Geology, Iera Odos 75, GR-118 55 Athens, mpsomiadis@aua.gr.

Abstract Groundwater samples were collected from 43 wells of the alluvial deposits aquifer of Sperchios' river basin in 2007. The groundwater quality of the aquifer is influenced by various natural and anthropogenic factors. Evaluation of water quality for drinking and irrigation purposes is discussed. A comparison of these samples with the corresponding samples collected from IGME in 1971, for the same or nearby wells, was made. The spatial distribution of ions concentration was made using the inverse distance weighting (IDW) interpolation method of a Geographical Information System (GIS). The results showed an increase in most of the main chemical elements, such as Cl^-, NO_3^+ and SO_4^{2-}. Finally, increased concentrations of several heavy minerals were recorded having values that overcome the maximum allowable limits set by the EU.

1 Introduction

The Sperchios River flows through a valley, which is a graben-like asymmetrical depression with an E-W direction. The graben covers an area of 1.780 km^2 and is approximately 60-80 km long and 20-30 km wide. Flood events occur regularly exceeding the channel capacity. The Sperchios River forms an alluvial plain at the eastern part of its basin. The Gulf of Maliakos, together with the valley of the Sperchios River, form part of a tectonic trough which is controlled by major NW-SE and E-W trending faults parallel to the Atalanti normal fault zone (Psomiadis 2010). The study of the alluvial unconfined aquifer of Sperchios is aimed at the investigation of groundwater quality and the effects of natural and anthropogenic parameters during the last decades (Fig. 1). Human activities, such as the intense farming, the overexploitation of the aquifers, the uncontrolled disposal of urban waste water and industrial and agricultural facilities are the most important causes of the groundwater charge. The natural processes contributing to the degradation of the groundwater quality are the dissolution of minerals as well as the existence of thermometallic springs in the area. A significant number

N. Lambrakis et al. (Eds.), *Advances in the Research of Aquatic Environment, Vol. 2*
DOI 10.1007/978-3-642-24076-8,

of studies dealing with groundwater quality of Sperchios River basin have been made and taken under consideration (Stahl et al. 1975, Aust et. al 1980, Kakavas 1985).

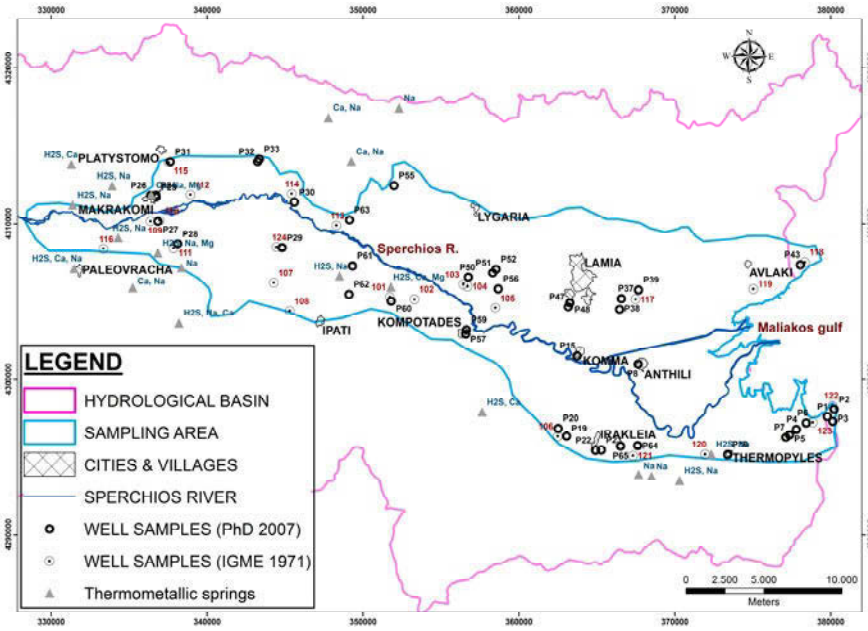

Fig. 1. The under study alluvial plain area of Sperchios' river basin, with the sampling points from 2007 and those selected (for comparison) from the IGME research in 1971.

The samples derived only from the wells of the basin delineate more precisely the charges of the aquifer. The results of the hydrochemical analyses were compared and evaluated based also on previous samplings in wells that had been held in the study area by the Institute of Geology and Mineral Exploration (IGME), on March 1971 (Kakavas 1978, Papadeas 1996). The comparison between the results was made for 24 wells out of the 43, that were either the same or very close to each other. However, no comparison for heavy metal concentrations has been made due to the lack of relevant hydrochemical analyses in the past. Nevertheless, there are several studies reporting data of hydrochemical analyses for heavy metals in the same area (Psyllidou-Giouranovits et al. 1997, Dassenakis et al. 2005), either for surface water or the Maliakos Gulf, and neither points out any high concentration values that exceed the upper permitted limits of the EU Council directive 98/83 for water.

2 Geological and hydrogeological setting

In the drainage basin of Sperchios river, there are three distinct lithological regions (Fig. 2) according to Ferrière (1977); these are: i) the western half which comprises the Paleocene-Eocene flysch of the East Pindus and Parnassos (Iti) geotectonic units; it is composed of alternating beds of argillite-siltstone-fine conglomerate and intercalations of shale. There is also a limited occurrence of pelagic and marly limestones of the Vardoussia unit in this area, ii) the south-eastern part of the basin is composed of M.Triassic-Jurassic massive dolomites and limestones of the Pelagonian unit, Upper.Cretaceous flysch of the Beotia unit consisting of coarse sandstone alternating with shale and sandy marl and U.Cretaceous thickly-bedded limestones and Eocene flysch of the Parnassos geotectonic unit composed of sandstone, clay and marl, iii) at the north and north-eastern part there is an ophiolithic complex in a shale-chert formation composed of shale, chert and limestone with ultra-basic and basic igneous rocks and metamorphosed green phyllite and schist; these belong to Maliakos (Subpelagonian) unit. In addition, Neogene and Quaternary unconsolidated deposits occupy the central and lower (elevations <500 m) part of the elongated drainage basin of Sperchios (Gartzos and Stamatis 1996). The hydrogeological formations that take part in the basin depends on the lithological composition, the porosity and the permeability and are categorized as: a) Permeable formations of carbonate rocks, lacustrine Pleistocene conglomerates, coarse material of talus cones and old and modern torrential deposits, b) semi-permeable to permeable formations of deep deltaic deposits and of areas of sands in alternation with clays. Also the ophiolithic formations of the area show significant permeability due to secondary porosity, c) Semi-permeable formations of the Quaternary deposits consisted of both coarse and fine material, showing limited and discontinuous aquifer and d) Impermeable formations of the flysch and the schist-chert complex formations, the silt-clayey deposits of the Sperchios as well as the limy tuffs of the warm springs' deposits. (Trippler 1979, Aust et al. 1980).

The Cretaceous limestones and the large limestone masses that overlay the schist-chert complex are of the greatest hydrogeological interest in the region. The same interest lies in the talus cones and fans that consist of both coarse and fine material, clays, sands, conglomerate-breccia and chippings. Within the coarse material areas the executed projects have high intake efficiency. The Oligocene-Miocene conglomerates show considerable importance as well as the lacustrine Pleistocene conglomerates especially when they extend beneath the modern sediments, where large quantities of groundwater are stored. The modern alluvial deposits of the river consisted of pebbles and sands show high permeability. The thickness of these formations rarely exceeds 30m, but the fact that they developed in the area crossing the main flow of the river makes them valuable as they can yield large quantities of water.

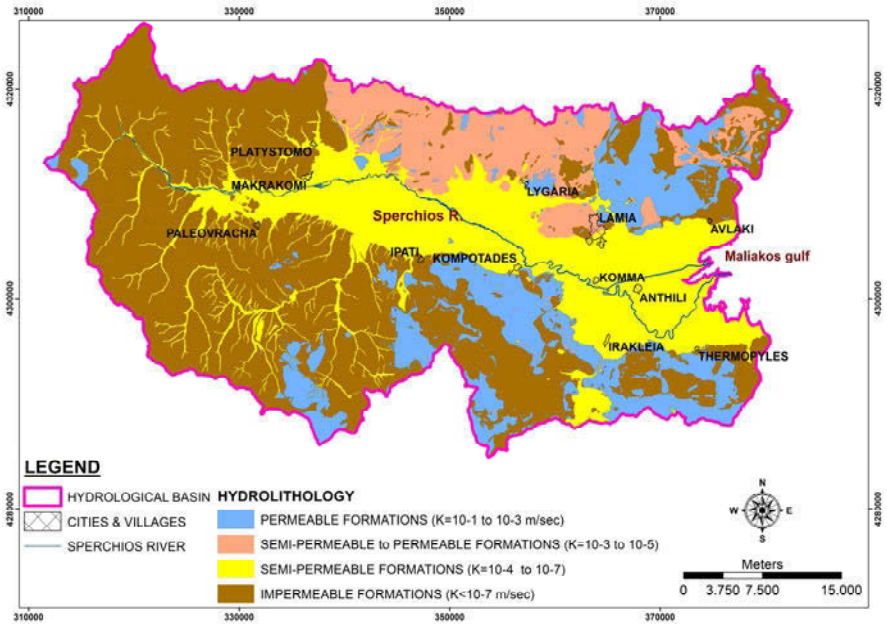

Fig. 2. The hydrolithological map of Sperchios' river basin.

The groundwater potential is based on productive aquifers primarily in unconsolidated sediments, mainly alluvial fans, river channels and delta deposits. The aquifers are unconfined or confined (artesian). The latter concerns aquifers in the delta and in parts of the Sperchios channel. The aquifers of the alluvial deposits appear both unconfined and confined at positions. The unconfined aquifer that is formed almost in the entire area of the alluvial deposits is characterized as heterogeneous while it shows moderate to good potentiality. The enrichment of the aquifers is ensured by the following: a) the direct infiltration of rainwater, b) the lateral and vertical racking and filtering of the groundwater from the big talus cones and c) the periodic lateral infiltration of the river water of Sperchios.

3 Groundwater quality

The hydrochemical analyses of 1971 and 2007 and the comparison of the results emerged some interesting issues. The Cl^- ions show a significant increase in 22 out of the 24 samples, with an average increase of 33.9 mg/L (Fig. 3). This increase, as been expected, shows the highest values in the southeastern region reaching 196.6 mg/L. In 14 of these samples, the Cl^- concentration exceeds the upper limited values of the EU Council directive 98/83 for drinking water (50 mg/L). The increasing concentrations, particularly in the southeast, are due to seawater intrusion

while the high concentrations inland are mainly geogenic. In 20 out of 22 samples the Na^+ ions appeared increased. However, in the southeastern part of the sampling area, the high Na^+ concentration values do not follow the proportional increase of chloride ions, as would be expected. This is probably due to the reverse cations exchange of groundwater and clay minerals. The groundwater concentration in NO^{3-} showed significant increase in 23 out of the 24 samples that were compared. Considerable increase was detected in almost the entire sampling area, with the highest values remarked in Irakleia and Damasta, east Makrakomi region, as well as in Ypati region where 191.5 mg/L of NO_{3-} were measured (Fig. 3).

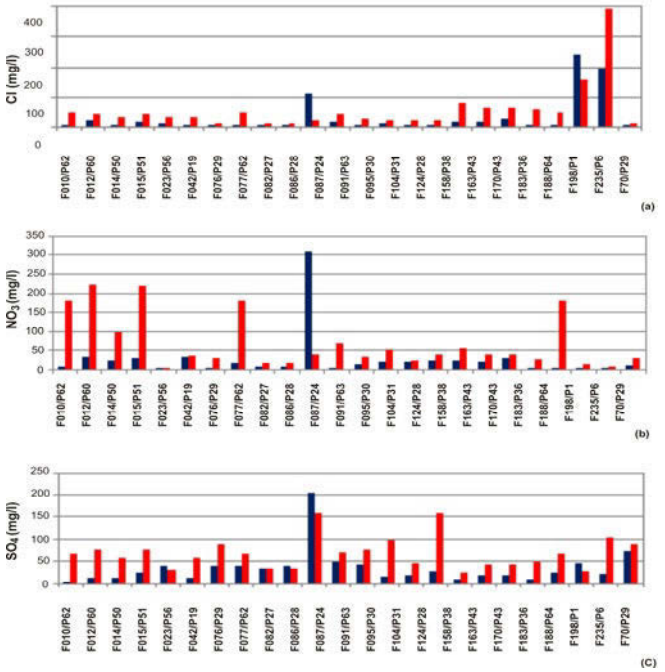

Fig. 3. The three diagrams a, b and c of the three main chemical elements Cl^-, NO_3^- and SO_4^{2-} accordingly. These diagrams show the concentration of these elements in the alluvial aquifer in 1971 (blue line) and 2007 (red line).

In 9 out of the 24 samples (37.5%) the NO_{3-} concentration sufficiently exceeds the upper permitted limits set by the EU for drinking water (50 mg/L). The increase in nitrates is mainly due to the intensification of agricultural production and the shift to more demanding crops in fertile soils which led to increased use of nitrogen fertilizers. Furthermore, livestock, which is highly developed in the area, plays an important role. The absence or non-functioning of biological stations, even in the big cities of Makrakomi and Sperchiada, septic tanks, industrial facilities, cemeteries and household waste are also some of the factors that make the nitrate problem even stronger (Fig. 4).

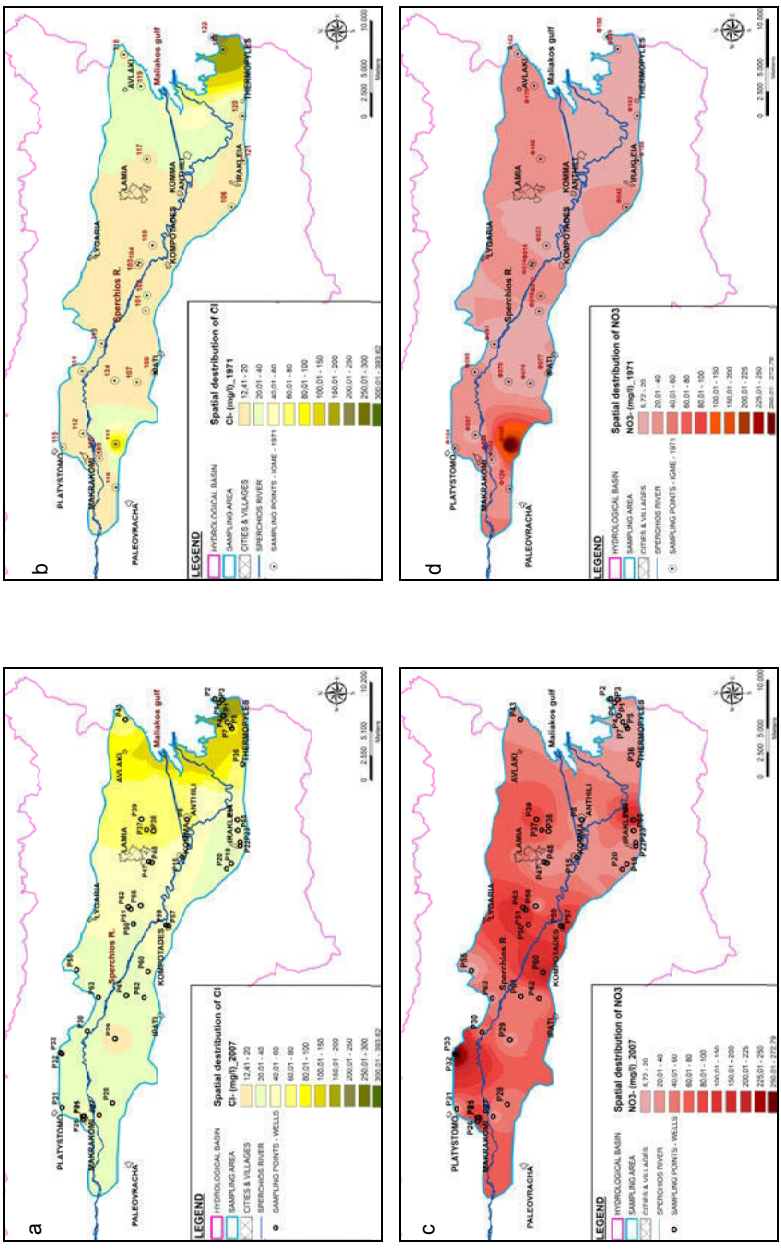

Fig. 4. The spatial distribution of a. Cl^-, b. NO_3^- concentration in the alluvial aquifer of Sperchios basin in 2007 and 1971 (b and d accordingly). The spatial distribution of ions concentration was made using the inverse distance weighting (IDW) interpolation method of a Geographical Information System (GIS).

On sulphate concentration in groundwater, again an important increase was detected in 19 out of the 24 samples (Fig. 3). Neither of them though exceeded the EU limits for drinking water (250 mg/L). The SO_4^{-2} concentration increase during the period 1971-2007 is associated with the intense use of organic fertilizers and the exploitation of the aquifers that are affected by the hot springs in Ypati, Platistomo and Paleovrahas in the central and western part of the area and the Damasta hot springs at the southeast. In coastal areas their appearance is associated with the seawater intrusion (Fig. 4).

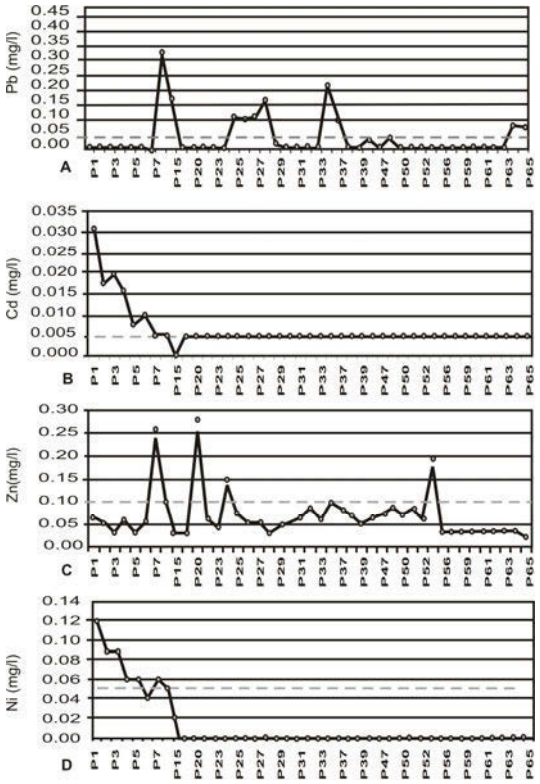

Fig. 5. Concentrations of Pb, Cd, Zn and Ni in the alluvial aquifer of Sperchios basin. The gray line shows the upper limit value of the EU Council directive 98/83 for drinking water.

According to the results of the heavy metals analyses, the concentrations of Cd, Pd, Zn and Ni have exceeded the upper permitted limits set by the EU Directive. Specifically, 11 samples, of the west and east part of the sampling area, show considerably higher Pb concentrations than the permitted (Fig. 5). The presence of Pb in this area is apparently related to the existence of the thermometallic springs but also to anthropogenic influences. Five samples of the east part of the study area revealed Cd concentrations above the permitted limits according to the EU Direc-

tive (0.05 mg/L) (Fig. 5). Its origin is attributed to anthropogenic influences as Cd is an essential trace element of phosphate fertilizers, but also to the uncontrolled waste dumps (batteries waste, plastic stabilizers and Cd-plated materials). The analysis of Zn in 5 samples of the southeastern part showed once more higher concentrations than the permitted limits of the EU (0.10 mg/L) and is concerned to relate to the hot springs of Damasta and Thermopyles (Fig. 5). Finally, the Ni shows equal or higher concentration than the one set by the EU (0.05 mg/L) (Fig. 5). These samples were collected by the east part of the area where industrial facilities are located. The bauxite horizons cited in the area may have a relation to the increased concentration values of Ni due to their dissolution.

Conclusions

The intensification of the anthropogenic intervention across the region, particularly in the east coastal part of the basin, from the 70's onwards, has negatively affected the groundwater of the area. The main anthropogenic interferences to the area concern: the intensification of farming through increased use of fertilizers which leads to the transfer of NH_4, NO_3 and NO_2 trace elements and of heavy metals (e.g. Cd, As) in the aquifer. Also, as been mentioned above, the growing demand for water for irrigation and water supply has led to the overexploitaton of surface water but mostly of the groundwater. As a result the east coastal part of the Sperchios basin has apparently undergone salinization and degradation of the groundwater quality. Agricultural products standardization and processing, several farms, stalls and cheese making industries of the region, some small industries as well as the uncontrolled disposal of urban and household waste water undoubtedly contribute to further pollution of the aquifer. All the above resulted in the degradation of the upper aquifer of the coastal area but also generally in an environmental degradation into a quite vulnerable region (Natura area) which requires strict protection measures. The results of the hydrochemical analyses displayed a large increase in the concentration of Cl^-, NO_3^- and SO_4^{-2} and high concentrations of heavy metals. In fact, they clearly demonstrated how necessary radical protection measures are, within the entire basin of the Sperchios river, against the careless anthropogenic intervention in the region, in order to enable a sustainable development before it is particularly late.

Acknowledgments The paper was financially supported by the Greek State Scholarships Foundation.

References

Aust H., Dounas A., Flathe H., Mühlfeld R., Kakavas N., Stahl W., Stavrou A., Tassios N., Trippler K., 1980. Groundwater in the Sperkhios basin, Central Greece. Geologisches Jahrbuch, C24, 3-24, Hannover

Dassenakis E., Kastritis A., Triantafyllaki S., Bourou P. and Paraskevopoulou V. 2005. Pollutants distribution in Sperchios basin and effects in the coastal zone. Proceedings of IWRM-WB / Global NEST, p. 209-214, Xanthi

E.U. Council, 1998. Council directive 98/83 about water quality intended for human consumption. Official paper of the European Communities, VL330, pp. 32-54

Ferrière J. 1977. Faits nouveaux concernant la zone isopique maliaque (Grèce continental orientale).-Proceed. VI Colloquium Geology of the Aegean region, 1977, I: 197-210

Gartzos E. and Stamatis G. 1996. Genesis of the thermal springs of the Sperchios graben, Greece. N.Jb.Geol.Paläont.Mh., 1996 (2): 91-115; Stuttgart

Kakavas N. 1978. Hydrogeological research of Sperchios' river basin. Institute of Geology & Mineral Exploration, Annex I: Inventory of water points, No. 26

Kakavas N. 1985. The condition of the underground water reservoir in Sperchios' river valley. Proposed ways to cover the deficit of water needs with the exploitation of underground water tanks. Institute of Geology & Mineral Exploration, No 44, p. 12, Athens

Papadeas D.G. 1996. Geological and Geothermal research in the Sperchios' river basin, Fthiotida. Institute of Geology & Mineral Exploration, No 3, p. 80 and Annex I & II, Athens

Psomiadis E. 2010. Geomorphologic and Environmental Changes Research in the Sperchios' River Basin Utilizing New Technologies. Doctorate Thesis elaborated at the Agricultural University of Athens, Laboratory of Mineralogy-Geology, p. 394

Psyllidou-Giouranovits R., Voutsinou-Taliadouri F., Nacopoulou C., Georgakopoulou-Gregoriadou E., 1997. River discharge effects on the distribution of nutrients and heavy metals of Maliakos Gulf, Hellas. Fresenius Environmental Bulletin, 6, pp. 72-77

Stahl W., Aust H., Dounas A., Kakavas A., 1975. Groundwater investigations, Sperchios basin/central Greece 1970-74. Internal. Report, IX: Stable isotope composition of different ground and surface waters from the Sperchios valley, p.40, Athens, I.G.M.E., (Unpubl)

Trippler K., Aust H., Tassios N., 1979. Interpretation of a large-area aquifer test by digital model simulation (Sperkhios valley, Central Greece). Geol. Jb., C23, 23-34

Groundwater contamination by nitrates and seawater intrusion in Atalanti basin (Fthiotida, Greece)

V. Tsioumas[1], V. Zorapas[1], E. Pavlidou[2], I. Lappas[1], K. Voudouris[3]

[1] Institute of Geology and Mineral Exploration, Sector of Water Resources and Environment, Department of Hydrogeology, 13677 Acharnai, Athens, Greece, zorapasv@igme.gr, ilappas@igme.gr
[2] Chemical Engineer, Environmental Consultant, pavlidou_eva@yahoo.gr
[3] Aristotle University of Thessaloniki, Laboratory of Engineering, Geology and Hydrogeology kvoudour@geo.auth.gr

Abstract The aim of the present essay is to evaluate the groundwater quality in the coastal alluvial aquifer of the Atalanti basin (Fthiotida, Greece). For this reason, data from the physical and chemical analyses of groundwater samples for eight sampling periods were collected and nitrate pollution was studied thoroughly. The period of June 2005 is the most appropriate and representative as far as dispersion and number of samples are concerned. The most dominant water type is Mg-(Ca)-HCO_3, due to the presence of dolomite and ultrabasic rocks. Moreover, the Na-Cl hydrochemical type is recorded near the coast line, due to seawater intrusion. Furthermore, it can be concluded that a) the high nitrates concentration values are related with the intensified agricultural production, the applied fertilizers and the absence of sewage systems, b) higher Mg concentration and Mg/Ca ratio values are observed near the coastline due to high Mg concentration in sediments and seawater intrusion, c) high Cl and Ca concentration in the southern area are connected with the discharge of the karst, saline spring in Tragana and seawater intrusion, d) according to factor analysis there are three main factors that are related with the aquifer salinization, the dolomite/ultrabasic rocks dissolution and the nitrate pollution with intense use of fertilizers, e) according to the cluster analysis, there are two clusters of water samples in Atalanti: the ones near the coastline with increased hardness, that are affected by salts and the ones in the central basin with reduced hardness, due to the short residence time in the ground Finally, some recommendations are proposed in order to protect and improve the groundwater quality in the study area.

1 Introduction

The groundwater degradation of coastal aquifers, observed in the last few years, is associated with seawater intrusion, industrial urbanization and intensive agriculture that require thoughtless use of chemical fertilizers and irrigation water.

N. Lambrakis et al. (Eds.), *Advances in the Research of Aquatic Environment, Vol. 2*
DOI 10.1007/978-3-642-24076-8,

The high values in NO_3^- are related with human activities, intensive agriculture, farms and uncontrolled urban waste disposal (due to septic cesspit). The agriculture constitutes the main source of nitrate pollution in surface and underground waters (Almasri 2007). Livestock production plays an important role in the aquifers' pollution by nitrates and phosphates. Increased nitrogen amounts are due to the high protein feed, which is greater than the animals' needs (Voudouris et al. 2004[a]).

The research program of 3rd Support Framework, which was successfully implemented by IGME, aims to monitor the qualitative and quantitative characteristics of aquifers across the country, including Atalanti basin. Part of the results of the above research program are presented in this essay and include an inventory of 650 sampling points, from which 100 were hydrogeologically selected for continuous monitoring of aquifers' qualitative and quantitative characteristics.

As found in the study area, the concentration of nitrates exceeded the thresholds that have been adopted by WHO (World Health Organization), ECE Directive 98/83 and Ministerial Decision Y2/2600/2001, according to which the maximum concentration is 50 mg/L for drinking purpose.

2 The Geomorphologic, geological and hydrogeological setting of the study area

The study area is located at Eastern Central Greece at Lokrida province of Fthiotida Prefecture. The complex geomorphology of Atalanti basin area (171 km^2 approximately) consists of areas with little or no slopes in valley where alluvial deposits are met and areas with very high and almost vertical slopes in rocky formations (Fig. 1).

The study area is open to the sea at Northeast and is surrounded by higher or lower mountains and hilly areas. Atalanti basin has a geomorphologic characteristic of diverged hydrographic network (streams, rivers), which has length of about several kilometers, converges to the east and reaches the sea. In any case there is no steady river flow but always seasonal, during winter and spring (Pavlidou 2010). The southern mountainous part of the above area has streams with very steep slopes and deep river bed, especially when passing through carbonate rocks.

One of the main causes for the geomorphologic setting of the study area is the water corrosion and its contribution to the weathering process. A very important factor in the above process is the intensive tectonic strain of rocks causing an extensive surface discontinuity, through which the erosion and weathering process begins (Palivos 2001).

The region's climate belongs to the Csa type (according to Koppen classification) which is representative of the Mediterranean climate with mild wet winters and mild hot and dry summers. The average annual precipitation is 555 mm. The

main features of climatic conditions in the region are the rotation period of a wet and cold season starting in October, according to precipitation and air temperatures and a dry and a hot one, starting in May. There is lack of uniformity in rainfall distribution between the lowlands and highlands with observed higher values in the mountains and lower ones in the valleys.

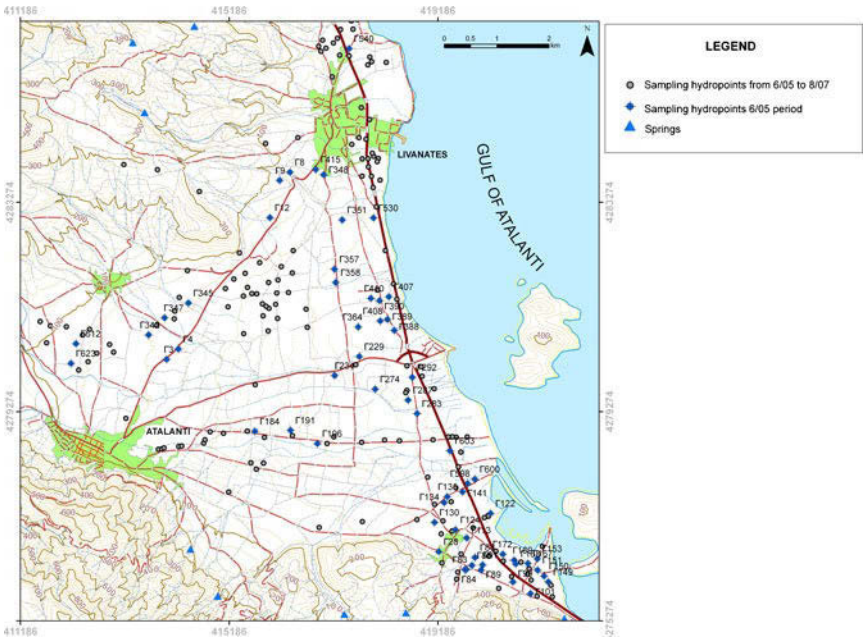

Fig. 1. The study's area topography with sampling points.

From a geological point of view, the study area belongs to the Subpelagonian geotectonic zone in a closed basin with post alpine deposits which has not been always communicating with the sea (Aggelidis 1992). The deposits have come from the surrounding mountain range rocks. Atalanti basin consists of formations which are as follows (Fig. 2):

- Paleozoic formations consisting of shales, sandstones and conglomerates. Triassic and Jurassic dolomites, limestones and ophiolitic rocks (gabbro, diabases, peridotites, serpentines), Creataceous limestones and flysch. Neogene sediments that were deposited after the closed basin formation consisting of marls, calcareous marls, marly limestones, clays, sandy loams, lignite and conglomerates.Quaternary formations have been deposited at the lower parts of the basin with materials derived from weathering of all previous formations, which come across at higher topographic positions. The main feature of the geological regime during Miocene is the large-scale faults in Atalanti basin which have created many faulting zones with West-Northwest and North-Northeast main directions.

The hydrogeological behaviour of geological formations depends on the lithological composition, degree of diagenesis and porosity. From the hydrogeological point of view, the study area is consisted of two main groups of rocks in which the groundwater flow mechanism and the storage capacity vary considerably. The first group consists of granular formations in which the hydraulic conductivity is based on the pores between the grains. The second group is composed by hard basement rocks which are limestones and igneous rocks, the hydraulic conductivity of which depends on fractures, cracks, karst pipes and other discontinuities that cross their mass. The main aquifer is developed in carbonate rocks; on the other hand aquifers of lower capacity are developed in the Quaternary-Neogene formations and igneous rocks. It is estimated that there is lateral communication between aquifers in carbonate rocks and the Neogene-Quaternary deposits, forming unconfined and semi-confined aquifers.

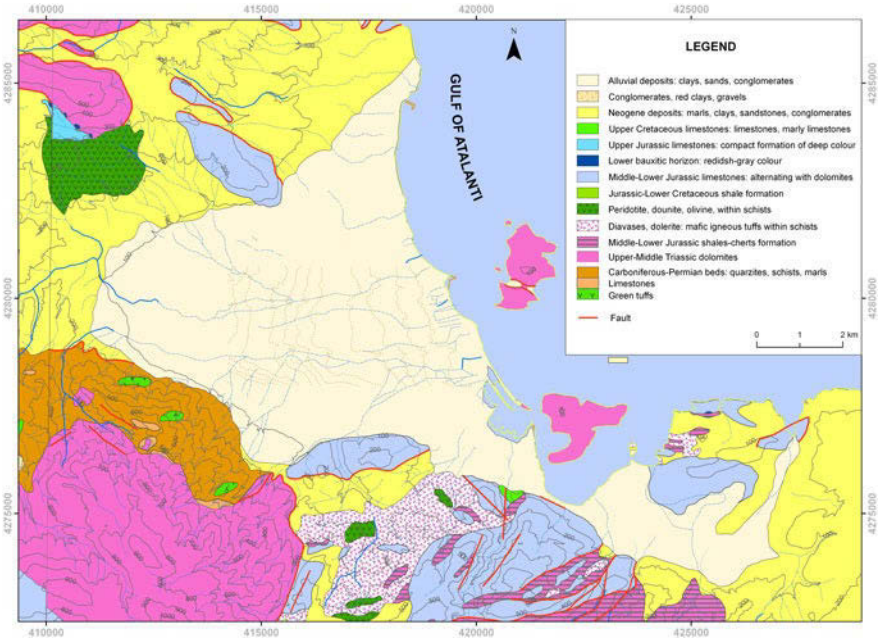

Fig. 2. The geological map of Atalanti area (Maratos 1965).

Unconfined aquifers are developed in carbonate rocks as well in granular formations with large effective porosity. On the other hand, the confined aquifers are developed within Neogene formations. The alluvial deposits due to their heterogeneity may be considered unconfined or semi-confined aquifers. The lowland aquifer, which is intensively exploited through boreholes (~ 650, mostly for irrigation use) is important for the economic development in the region. The depth to water table in the alluvial aquifer ranges from 1.5 to 86 m below surface ground or from 2.2 to 17.3 m above sea level. Groundwater flows are mainly from the West to-

ward East (Atalanti Gulf). This article is focused on the qualitative characteristics of the aquifer, which has already shown degradation problems.

3 Sampling data and evaluation of chemical analyses

Groundwater sampling took place along different periods so as to investigate the groundwater quality. During the period 2005-2007 and more specifically the months of June, July and August, 240 samples were taken. The results presented in this essay concern about 62 samples taken during the period June 2005.

Ca concentrations range from 30.5 to 179 mg/L, Mg from 1 to 149 mg/L and Na between 5.5 and 232.2 mg/L increasing linearly with salinity. Sulphate concentrations range from 6.2 to 195 mg/L and Cl between 3.5 to 691 mg/L (Fig. 3).

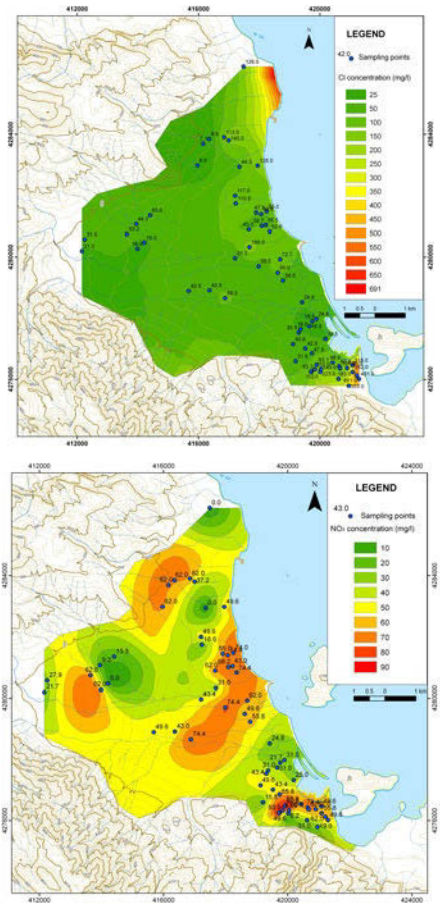

Fig. 3. Distribution map of a. Cl and b. NO_3 concentration in Atalanti basin.

Increase in electrical conductivity values is observed at the downstream area due to groundwater recharge with salts, but also because of seawater intrusion (Voudouris et al. 2004[b]). The highest values (2816 μS/cm) occur in the southern coastal part of the basin due to the aquifer's recharge with saline water from Tragana springs discharge. Furthermore, the over-exploitation of the coastal area's wells is observed which causes more rapid salinization. Finally, across Karagiozis stream, lower values of electrical conductivity and Cl concentration are met because of the upstream fresh water recharge (Pavlidou 2010).

According to Piper and Durov plots (Fig. 4) the majority of samples belong to Mg-HCO_3 water type (fresh water-recharge) associated with dolomitic limestones and ultrabasic rocks of bedrock, as well as sediments derived from erosion which have been deposited across the basin (Razack and Dazy 1990). Ca-HCO_3 water type is also met which indicates recharge waters from karst aquifers. Finally, Na-Cl water type is met at the coastal zone, where seawater intrusion takes place (Stamatis and Voudouris 2003).

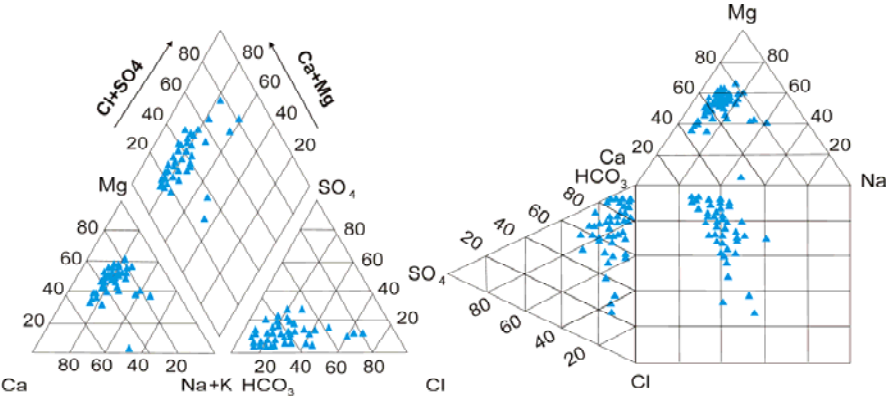

Fig. 4. a. Piper and **b.** Durov plots for Atalanti basin's groundwater.

Ion ratio of Mg/Ca from 0.5 to 0.7 is found at basin's margins where dolomitic limestones are met. Higher ion ratio at the coastal zone indicates Mg ions groundwater recharge because of the basin's sediments and seawater intrusion. Moreover, Na/K ion ratio points out that Karagiozis stream plays important role to groundwater movement. The Southwest basin's region is a recharge area due to the above stream control, on the contrary the central-north one is a discharge area. Finally, the low value of Na/Cl (0.3) during the period of June 2005 towards the coastal zone strongly indicates seawater intrusion (Hem 1985).

Nitrates concentration ranges from 0-93 mg/L with a mean value of 46.8 mg/L. Increased concentration of nitrates are generally presented in the plain and are attributed to agricultural sources of nitrate fertilizer (Antonakos and Lambrakis 2000, Tsioumas et al. 2008). Nitrate concentration is higher during dry periods and this is due to aquifer's infiltration of surface water rich in nitrates. In the western part of the area indicated high levels of nitrate concentration (over 70 mg/L)

are probably related to the existence of cemetery and livestock (Stigter et al. 1998). In the northern part, the high values (about 60 mg/L) are due to the existence of cropland and possibly of uncontrolled waste disposal. In the central coastal area nitrate pollution (60-75 mg/L) is associated with the wastewater disposal in septic tanks in settlements (Skala, Aghios Nikolaos). In the upstream area NO_3 concentration is also high due to intense agricultural activity. Finally, in the southern part values over 90 mg/L may be associated with industrial wastewater. It should be noted that the threshold of 50 mg/L set by the legislation has been exceeded by 27 samples (Fig. 3).

The applied multivariate statistical methods were conducted by means of SPSS. Factor analysis was applied to represent a large number of variables by a significant smaller number of variables, called "factors", each of which is a linear function of the original variables (R-factor analysis). The factor analysis is applied because of the limitations of trilinear diagramming (Piper), which utilizes relative percentages of ionic concentration rather than absolute values and further confining its analysis only to 6 variables (Voudouris et al. 1997, Razack and Dazy 1990, Briz-Kishore and Murali 1992, Antonakos and Lambrakis 2000). Factor analysis resulted in three main factors that interpret a great percentage of total variance: a) the aquifer salinization, b) the dolomite/ultrabasic rocks dissolution and c) the nitrate pollution due to the intense use of fertilizers.

Cluster analysis is a classification method of a large amount of data in groups with similar but distinctive characteristics (Ashley and Lloyd 1978). It resulted in two groups of samples: the first includes samples located in the coastal area rich in salts (hard water) and affected by salinization and the second contains samples belonging to the inner part of the study area with soft water due to the groundwater's short residence time.

4 Results – Conclusions – Proposals

The aim of this study was to determine the impacts of human activities on groundwater quality in alluvial aquifer of Atalanti basin. According to the results from hydrochemical investigation, using conventional methods and multivariate technique (factor and cluster analysis) two main groups of groundwater samples can be identified: Mg-(Ca)-HCO_3 (freshwater) and Na-Cl (water affected by seawater intrusion in coastal areas). Factor analysis resulted in 3 factors which are associated with: a) the aquifer salinization, b) the dolomite/ultrabasic rocks dissolution and c) the nitrate pollution due to the intense use of fertilizers.

The nitrate concentration in groundwater within Atalanti basin is increased with a maximum value of 93 mg/L. It should be pointed out that the majority of values is above the threshold of 50 ppm or very close to it. It is estimated that nitrate concentration will increase as intensive cultivation, use of fertilizers and uncontrolled sewage disposal continue, without protection measures and problem

awareness from the citizens and water users. Taking into account the chemical analyses, high nitrate concentrations are observed close to residential coastal areas. These cases are associated with the municipal wastewater disposal. In order to protect groundwater the following are proposed:

- Abide by the directives of the Ministry of Agriculture and agronomists to use the appropriate type and quantity of fertilizer per crop.
- Systematic monitoring of the evolution of nitrate pollution and seawater intrusion to ensure the future quality of groundwater.
- Direct application of project management of municipal wastewater and livestock so that they cannot enter to the hydrographical network or/and groundwater table by filtering. Thus, biological treatment for all settlements should be applied.
- Implementation of protection zones of water supply wells and springs to maintain the drinking water quality, taking into account the basin's hydrological and hydrogeological characteristics.
- Changes to the irrigation system (drops system, construction of irrigation network) and exploration of the possibility to use surface waters, artificial recharge using barriers along the streams in order to avoid overexploitation and seawater intrusion.

Finally, a monitoring program on groundwater quality should be established in selected sampling points, in order to improve the groundwater quality and avoid seawater intrusion phenomena and nitrate pollution on a large scale in the coastal aquifer system of Atalanti basin.

The authors would like to thank the Chemical Analytical Laboratory of the Institute of Geology and Mineral Exploration for the chemical analyses during the sampling period (2005-2007).

References

Aggelidis C (1992) Engineering and geologic conditions of Atalanti area (Fthiotida prefecture, Greece). Unpublished Technical report, IGME, Athens

Almasri M (2007) Nitrate contamination of groundwater: A conceptual management framework, Environmental Impact Assessment Review, 27: 3, 220-242

Antonakos A, Lambrakis N (2000) Hydrodynamic characteristics and nitrate propagation in Sparta aquifer, Water Research, 34: 16, 3977- 3986

Ashley R, Lloyd J (1978) An example of the use of factor analysis and cluster analysis in groundwater chemistry interpretation, Journal of Hydrology, 39: 3-4, 355-364

Briz - Kishore B, Murali G (1992) Factor analysis for revealing hydrochemical characteristics of a watershed, Environmental Geology – Water Science, 19: 1, 3-9

Hem J (1985) Study and interpretation of the Chemical characteristics of Natural Water, 3rd edition, United States Geological Survey Water – Supply Paper 2254

Maratos G (1965) Geological map of Atalanti sheet, scale 1:50.000, Institute of Subsurface Geological Research

Palivos N (2001) Geomorphologic study of Atalanti area of Fthiotida prefecture. PhD, Department of Geology, School of Sciences, Athens

Pavlidou E (2010) Impacts of human activities on groundwater quality in Atalanti region. MSc Thesis, Hellenic Open University

Razack M. and Dazy J (1990) Hydrochemical characterization of groundwater mixing in sedimentary and metamorphic reservoirs with combined use of Piper's principle and factor analysis, Journal of Hydrology, 114: 3-4, 371-393

Stamatis G, Voudouris K (2003) Marine and human activity influences on the groundwater quality of southern Korinthos area (Greece). Hydrological processes, 17, 2327-2345

Stigter T, Van Ooijen S, Post V, Appelo C, Carvalho A (1998) A hydrogeological and hydrochemical explanation of the groundwater composition under irrigated land in a Mediterranean environment, Algarve, Portugal, Journal of Hydrology, 208: 3-4, 262-279

Tsioumas V, Zorapas V, Manakos A, Stamatis G, Gioxas G (2008) Groundwater deterioration by nitrates in Xynias basin (Greece), 8th International Hydrogeological Congress, Athens.

Voudouris K, Lambrakis N, Papatheodorou G, Daskalaki P (1997) An application of factor analysis for the study of the Hydrogeological conditions in Plio-Pleistocene aquifers of NW Achaia (NW Peloponnesus, Greece). Mathematical Geology, 29: 1, 43-59

Voudouris K, Nikas K, Antonakos A (2004[a]) Study of the evolution of salinization in coastal aquifers. Case study of coastal NW Achaia, Bulletin of Greek Geological Survey, Proc. of the 10th International Congress, Thessaloniki, XXXVI/4, 1952-1961

Voudouris K, Panagopoulos A, Koumantakis I (2004[b]) Nitrate pollution in the coastal aquifer system of the Korinthos (Greece). Global Nest: the International Journal, 6:1, 11-18

Characterisation of water quality in the island of Zakynthos, Ionian Sea, Western Greece

G. Zacharioudakis, Ch. Smyrniotis

Institute of Geology and Mineral Exploration, Department of Hydrogeology, 1 Spirou Loui str, Acharnes, 13677. gzach@igme.gr

Abstract This paper summarises the hydrochemical characteristics of the main aquifers of the island of Zakynthos, in the Ionian Sea. A total of 677 groundwater samples were collected from 139 points between 2004 and 2008. The karstic limestone of the mount Vrachionas in the west comprises the major drinking water supply of the island. Increased water demand resulted in the overexploitation and the encroachment of saline water intrusion to the north and south of Vrachionas. Chloride concentrations exceed drinking water threshold in 40% of the samples. Simple groundwater-seawater mixing is the main process occurring within the limestone aquifer. In the east, the confined multilayered Neogene aquifer comprises the secondary drinking water supply of the island. Saline intrusion in this area is limited due to geological constraints and the water is of good quality. Groundwater is clustered in 4 different groups depending on the prevailing hydrochemical process. The alluvial deposits in the central part of the island comprise a shallow localised aquifer pumped mainly for irrigation. This minor aquifer provides good quality irrigation water with some exceedances in chloride and sulphide. Groundwater in this aquifer is a result of simple mixing between fresh and sea water. Trace elements were also analysed resulting in values within the drinking limits.

Introduction

This paper outlines the findings of the work that was undertaken by the Institute of Geology and Mineral Exploration (IGME) as part of the project "Groundwater resources' evaluation and development in the Ionian islands" which was funded by the 3rd Community Support Framework Programme "Competitiveness" and executed between 2004 and 2008 (Smyrniotis et al 2010). Part of the project objective was the assessment of the groundwater quality. At the island of Zakynthos 139 points (Fig. 1) were sampled and a total of 677 samples were analysed at the analytical laboratories of IGME (Zacharioudakis et al. 2010). Furthermore, selected samples were analysed for trace elements. Formations of the Paxoi and Ionian geotectonical zones comprise the geological setting. Triassic klastic sediments of

N. Lambrakis et al. (Eds.), *Advances in the Research of Aquatic Environment, Vol. 2*
DOI 10.1007/978-3-642-24076-8,

the Ionian Zone containing gypsum dominate the SE of the island underlying the Paxoi zone formations. A karstic Cretaceous to Eocene age limestone sequence, crop out on the mount Vrachionas, in the west. It is succeeded by a series of Neogene deposits. The above formations formulate Paxoi Zone on the island. Gypsum intrusions are present within the Miocene deposits of the Neogene. Recent alluvial deposits dominate the central part of the island.

Hydrogeological setting

The karstic limestone sequence at Mount Vrachionas in the west comprises the major drinking water supply aquifer of the island. There are about 40 groundwater abstractions exploiting the groundwater resource as drinking water supplies. The majority of the abstractions are located along the contact of the limestone sequence with the Neogene along the eastern foot of Vrachionas. In average, boreholes are extended deeper than the sea level and pumping rates are variable depending on the supply needs. The mount forms an anticline acting as a groundwater divide. Groundwater flows either to the east or to the west towards the Ionian sea (Fig. 1). The groundwater flow to the east is then divided into two flow components: one to the north and one to the south. The limestone aquifer is in direct contact with the sea in the west and in the north promoting naturally saline groundwater inflow in these areas. Evidence for this mechanism is given by borehole drilling findings in these areas (Skagias 1990) where natural groundwater Electrical Conductivity of 2000 μS/cm was measured, prior to borehole test pumping. Pumping tests (Zacharioudakis and Smyrniotis 2010, Diamantopoulou 2000) showed a transmissivity range between 250 m^2/day and 17000 m^2/day (average 3565 m^2/day) depending on the limestone type, age and degree of karstification. The Neogene sequence hosts a multilayered confined aquifer which is exploited by numerous boreholes for the supply of drinking and irrigation water. The multilayered nature and geometry of this aquifer, acts as a natural barrier preventing any potential saline water intrusion. It extends in the east of the island, to the NE of the city of Zakynthos, and also in the S-SE. During the aforementioned project execution, 53 groundwater abstractions were recorded in the area; however the presence of more abstractions is certain. The abstraction rates and overall productivity of the aquifer is limited due to the hydraulic properties of the neogene sequence. Diamantopoulou (2000) calculated transmissivity values between 60 m^2/day and 500 m^2/day (average 216 m^2/day). An unconfined shallow aquifer of localised interest is located within the alluvial deposits in central Zakynthos. Groundwater is used mainly for irrigation purposes through numerous wells. Fifty one wells were selected for monitoring purposes; the real number is estimated multifold.

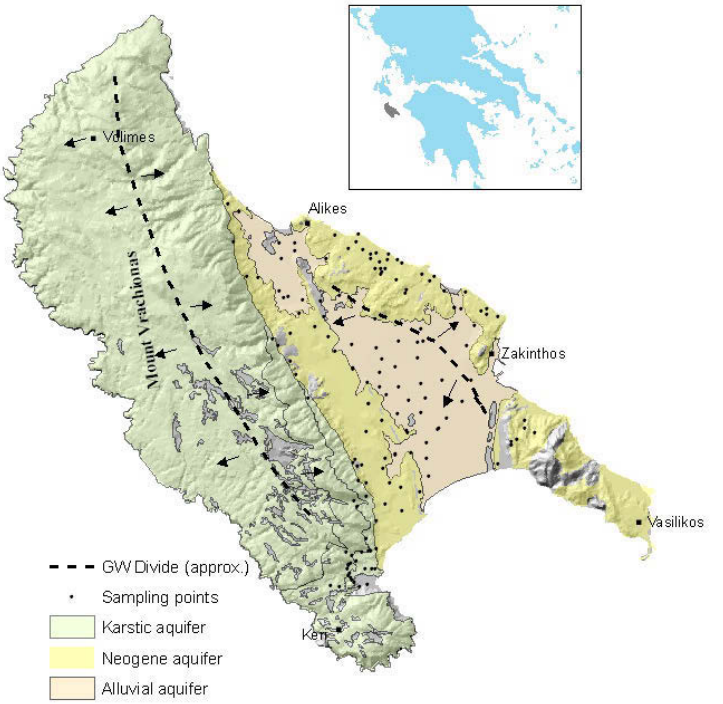

Fig. 1. Generalised hydrogeological setting of the study area.

Groundwater quality distributions

In total, 677 samples were collected from 139 sampling points and analysed for major ions. The majority of the sampling points were pumping boreholes and the rest were purged with a bailer. Groundwater samples were stored in plastic 1L bottles and analysed by the analytical laboratories of IGME. Electrical Conductivity, pH, and groundwater temperature were also measured on site. During the autumn 2007 sampling round Eh was also measured on site by means of an "ORP" electrode. During the autumn of 2007 and spring 2008, 76 samples collected from 50 (mainly drinking water supplies) points were also analysed for trace elements. The software HYDROCH (Giannoulopoulos, unpublished data) was used for the data processing and plotting. In total, 28 pumping, 3 non-pumping boreholes and one spring were sampled for the period between 2004 up to the end of 2008, collecting in total 202 samples from the karstic aquifer. The maximum measured values of chloride (2250 mg/L), sodium (1125 mg/L) and electrical conductivity (8100 μS/cm) indicate the influence of saline intrusion. The plot of Na versus Cl (in meq/L) shown on Figure 2, also indicates that the prevailing mechanism is

simple mixing between a fresh end-point water and saline end-point water (Richter et al. 1993). This mechanism is presented more clearly at the Piper (Appelo and Postma 1994) and expanded Durov plots (Fig. 3). The majority of the samples are clustered along the line joining fresh water and sea water at the Piper plot, whilst limited samples indicate that some ion exchange has taken place. This is also identified in the Expanded Durov plot where two distinct groundwater types can be grouped: One fresh water group (Type I - top left), and one more saline group (Type II - bottom right). The two water types are clustered along a line also indicating that simple dissolution or mixing is the prevailing process. Water type I comprises fresh recharging waters rich in HCO_3 and Ca (Lloyd 1986) sampled mainly inland at a distance from the sea. Water type II is present in the overexploited coastal areas in the S-SW and in the North. Chloride concentrations in Type II waters exceed the drinking water limit (250 mg/L) in 81 out of the 202 samples. The plot of Ca+Mg versus SO_4+HCO_3 (Fig. 2) shows that most of the groundwater samples are clustered around and above the 1:1 line. This plot will be close to the 1:1 line if the dissolutions of calcite, dolomite and gypsum are the dominant reactions in a system. Ion exchange tends to shift the points to the right due to an excess of SO_4+HCO_3. If reverse ion exchange is the dominant process, it will shift the points to the left due to a large excess of Ca+Mg over SO_4+HCO_3.

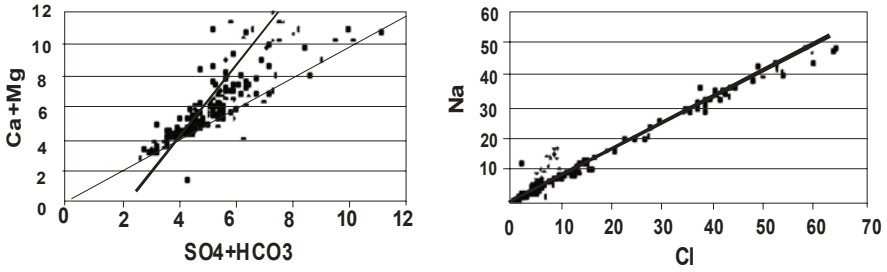

Fig. 2 a,b: Relation between Ca+Mg vs SO_4+HCO_3 and Sodium vs Chloride.

The overexploitation of the karstic aquifer which has activated and promoted the sea water intrusion is also demonstrated by the fact that chloride concentrations are over 1000 mg/L in 38 samples taken from 8 monitoring points in the S-SW coastal area. Similar is the exceedance in the electrical conductivity values. This is mainly due to uncontrolled pumping from numerous private groundwater abstractions for commercial purposes. No other major ion exceeds drinking water limits in the karstic aquifer. The nature of the salinisation is due to lateral sea water intrusion at least at the coastal areas. The Neogene aquifer is extended mainly in the E-NE areas of the island (Fig. 1). Groundwater is confined and occurs in multilayered sandy and sandstone aquifers which are naturally protected from sea water intrusion due to the presence of clayey and marly horizons.

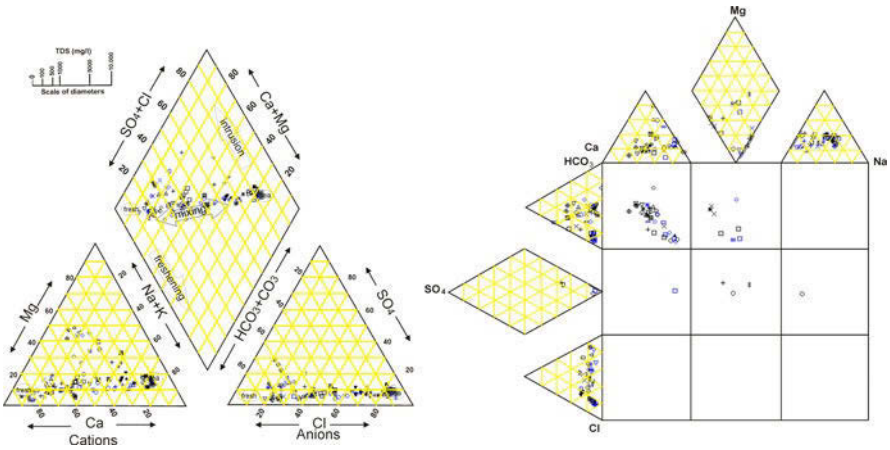

Fig. 3. a,b: Piper and expanded Durov Plots of the karstic aquifer samples.

In total, 222 samples were collected and analysed from 56 points. Groundwater demonstrates good quality with the exception of some localised hotspots of slightly elevated values of NO_2 (between 55 mg/L and 80 mg/L) and SO_4 (around 300 mg/L). Chloride concentrations exceed drinking water limit, in very few occasions. Trilinear plots (Fig. 4) show that most of the groundwater samples fall in the field of mixed Ca–Mg–Cl type of water. Expanded Durov plot separates groundwater samples in four distinct clusters: the majority of the samples represent fresh recharge waters while some of them have been undergone ion exchange, probably Na of the saline water with Ca from the rock matrix. The third group is related to SO_4 which occurs mainly in some shallow wells due to the recharge through the Miocene gyspiferous deposits. The fourth group represents samples that have been undergone simple mixing between a fresh water end point and a saline water end point. The majority of these samples also come from wells. Similar is the interpretation of the plot of Ca+Mg versus SO_4+HCO_3 where most of the samples are plot along the 1:1 line. Limited number of samples showing an excess of Ca+Mg perhaps due to some ion exchange processes and an excess SO_4+HCO_3 respectively, probably related to gypsum dissolution.

The Alluvium is present in the central part of the island to the west of the city of Zakynthos (Fig. 1). It is a shallow unconfined aquifer of small localised interest. Numerous wells abstract groundwater for irrigation of citros, olives and wine yards. During the project duration, 253 samples were collected from 50 sampling points. Trilinear plots indicate no distinct group of waters. Groundwater in the alluvium exhibits simple dissolution or mixing between fresh and sea water. A very limited number of sampling points demonstrate saline intrusion mainly in the north.

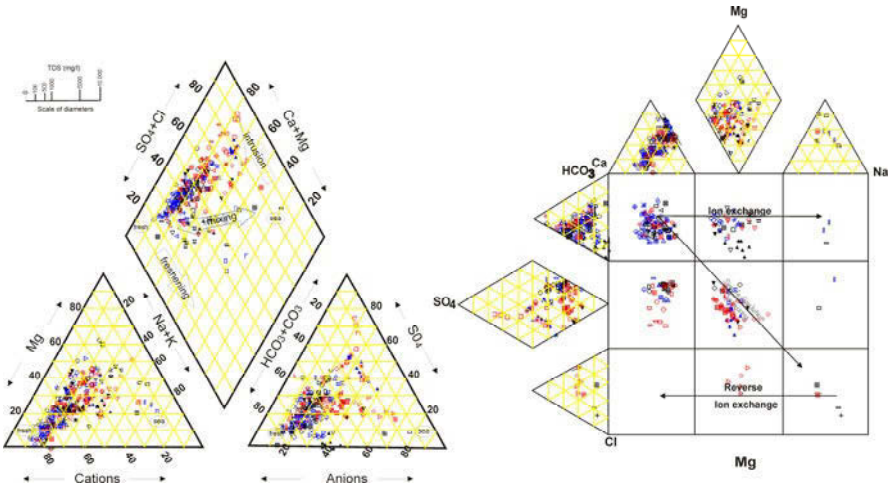

Fig. 4. a,b: Piper and expanded Durov Plots of the Neogene aquifer samples.

Groundwater is classified as brackish according to the average TDS values per sampling point which are between 1000 mg/L and 10000 mg/L. SO_4 is also present in some samples, probably due to the flushing and dissolution of gypsum through recharge. Electrical conductivity is a good measure of salinity hazard to crops as it reflects the TDS in groundwater (Richards 1954, Subramani 2005). According to this classification, 12 out of 50 monitoring points were proved Unsuitable (avg Ec>3000) for irrigation, 15 out of 50 were classified as Doubtful (2000-3000), 21 out of 50 were classified as Permissible (750-2000), one was classified as Good (250-750) and another one as Excellent (Ec<250). Sodium adsorption ratio (SAR) is an important parameter for determining the irrigation suitability of groundwater because it is a measure of alkali/sodium hazard to crops. Groundwater samples fall in the low sodium class (S1) except for 24 samples that are classified as S2 (Good water class). The sodium percentage (Na %) indicates that the groundwater is excellent (Na%<20) to good (40<Na%<20) for irrigation with the exception of 80 samples where groundwater has been classified as Permissible for irrigation (Subramani 2005). During 2007 and 2008, 76 samples were also analysed for trace elements. Forty one samples were collected from 25 sampling points of the karstic aquifer, 20 samples were collected from 14 points of the Neogene aquifer and 15 samples were collected from nine points of the alluvial aquifer. The determinants analysed were: SiO_2, Fe, Al, Cr, Mn, Ni, Cu, Zn, As, Cd, Ba, and Pb. The measured values do not exceed the drinking water limits (Council Directive 98/83/EC) except for iron. Iron concentrations from 4 sampling points of the karstic aquifer, from 5 points of the neogene aquifer and from 5 points of the alluvial aquifer exceed the Directive "parametric value" of 200μg/L. The majority of exceedances lie around 500 μg/L except for two samples where iron was measured around 6000 μg/L. Iron and manganese naturally occur in groundwater that has little or no oxygen, typically in deeper wells (but not always), in areas where

groundwater flow is slow, and in areas where groundwater flows through soils rich in organic matter. If the groundwater is oxygen poor, iron (and manganese) will dissolve more readily, particularly if the pH of the water is on the low side (slightly more acidic). It could also be attributed to the presence of iron pyrite, especially in the Neogene sediments, coupled with reducing conditions in the groundwater. Decomposition of the organic matter depletes the oxygen in the water and the iron dissolves as Fe^{2+} (Hem 1985). Zinc concentrations are slightly elevated in two sampling points of the karstic aquifer. Zinc could be related to the coating of the borehole casing.

Conclusions

Three main aquifers comprise the hydrogeological setting of the island of Zakynthos. The aquifer in the karstic limestone sequence in the west is the main drinking water supply of the island. Extensive saline intrusion occurs in the south and the north resulting in very high chloride concentrations and electrical conductivity. Simple mixing between the seawater and fresh water is the dominant process in the system. Overexploitation and uncontrolled private groundwater abstractions for commercial purposes are the main reasons for the ongoing saline water intrusion leading to the groundwater quality degradation. A regulated combined groundwater abstraction policy needs to be implemented so that the saline water propagation is retarded and gradually stabilized. The Neogene confined aquifer in the east provides good quality water as a secondary drinking water supply. Saline intrusion is limited in the aquifer. Groundwater is clustered in four distinct groups representing the nature of the prevailing geochemical processes: fresh water, ion exchange, simple mixing and sulfide reduction. The alluvial aquifer in the central part of the island provides good quality water for irrigation. Mixing between sea water and fresh water is the dominant process in the system. All the three aquifers demonstrated trace elements concentrations within the drinking water limits. Elevated iron concentrations may be related to the presence of organic matter in the water flowpaths which consumes oxygen from the groundwater promoting the iron dilution.

References

Appelo, C.A.J. Postma D. (1994). Geochemistry, Groundwater and Pollution. A.A. Balkema.

Diamantopoulou P. (2000) Hydrogeological conditions of the island of Zanynthos. Groundwater protection from contamination and pollution. Phd thesis. Department of Geology, University of Patras

Hem J. (1985) Study and interpretation of the chemical characteristics of natural water. USGS Water supply paper 2254

Giannoulopoulos P. “HYDROCH” Software for the processing and plotting of hydrochemical data. Unpublished
European Council (1998) Directive 98/83/EC of 3 November 1998 on the quality of water intended for human consumption L 330/32 Official Journal of the European Communities 5.12.98
Lloyd W.J., Heathcote A.J. (1985) Natural inorganic chemistry in relation to groundwater. Oxford: Claredon Press
Richards LA (1954) Diagnosis and improvement of saline alkali soils. US Department of Agriculture, Hand Book 60, pp 160
Richter B.C., Kreitler C.W., Bledsoe B.E. (1993) Geochemical techniques for identifying sources of ground water salinisation. C. K. Smoley
Skagias , D. (1990) Report on the 1989 drilling investigation findings, in the island of Zakynthos, Institute for Geology and Mineral Exploration, Report No: E6211
Smyrniotis Ch, Zacharioudakis G., Manakos K. (2010) “Groundwater resources’ evaluation and development in the Ionian islands”, Hydrogeology Report, 3rd Community Support Framework Programme “Competitiveness, IGME, Acharnai, Greece
Subramani T., Elango L., Damodarasamy S. R. (2005) Groundwater quality and its suitability for drinking and agricultural use in Chithar River Basin, Tamil . Environ Geol, 47, p.p. 1099-1110
Zacharioudakis G., Kouris Ch., Smyrniotis Ch. (2010) “Groundwater resources’ evaluation and development in the Ionian islands”, Groundwater chemical analyses report, 3rd Community Support Framework Programme “Competitiveness, IGME, Acharnai, Greece

Groundwater vulnerability assessment in the Loussi polje area, N Peloponessus: the PRESK method

R. Koutsi[2], G. Stournaras[1]

[1]Professor of Hydrogeology and Engineering Geology, Department of Geology and Geoenvironment, National and Kapodistrian University of Athens, GR 157 84, Panepistimioupolis Zografou, Athens, Greece, stournaras@geol.uoa.gr
[2]Dr Geologist, Athens, reginakoutsi@yahoo.gr

Abstract Loussi polje, located in North Peloponnesus on the SE of Kalavryta village is a very interesting but little studied karst area. Water from karst springs and boreholes that drain the local carbonate aquifers is exclusively used for water supply and irrigation purposes in this scarcely populated area. An attempt to delineate protection zones in karstic aquifers was made, by assessing the groundwater vulnerability to pollution. PRESK, an adaptation of the RISKE groundwater vulnerability method of carbonate aquifers was applied. Modifications were necessary in order to meet with the specificity of Loussi karst terrain. PRESK method takes into account the protective role of topography in combination with vegetation (P factor), the nature of geological formations (R), the presence of epikarst (E), the existence of an overlying soil cover above carbonate aquifers (S) and the degree of karstification of the carbonate formations themselves. Groundwater vulnerability was assessed for both Olonos - Pindos and Tripolis carbonate aquifers of the study area.

1 Introduction

Karstic aquifers are particularly vulnerable to contamination, due to their nature and heterogeneous structure showing either a dual or triple permeability, often with matrix or granular permeability and always with fractures and conduits (Daly et al. 2002). In karst aquifers, the residence time of contaminants is often short and natural attenuation processes do not occur effectively (Vias et al. 2006) since filtration and auto-purification phenomena are not enabled (Petelet - Giraud 2000). Several vulnerability methods especially for karstic environments have been developed during the last decade including EPIK (Doerfliger et al. 1998), PI (Goldscheider et al. 2000), RISKE (Petelet - Giraud 2000), COP (Vias et al. 2006) taking into account the peculiarities of karst. In Greece karst terrains occupy 35% of the land surface and a large proportion of the total drinking water supply is mainly contributed by karst groundwater. Therefore it is of vital importance for an opti-

N. Lambrakis et al. (Eds.), *Advances in the Research of Aquatic Environment, Vol. 2*
DOI 10.1007/978-3-642-24076-8, © Springer-Verlag Berlin Heidelberg 2011

mum quality and quantity preservation of these waters. The paper proposes PRESK method that takes its inspiration from RISKE. It is a modified approach which follows the accepted norm of an index-based mapping method with criteria weighting as well as the additional RISKE's aspect according to which it characterizes the vulnerability to infiltration and is a preliminary step of vulnerability characterization which does not lead to a determination of protection areas (Petelet-Giraud 2000). Since there was a lack of available data for Loussi polje study area, a necessary modification and simplification of the factors' values and categories was made according to the area's characteristics. The method follows five important steps (Petelet-Giraud 2000): mapping in a 1/20000 scale of each factor which is then subdivided in 4 indexes, discretization of each map, calculation of the Ig index and its subdivision in 4 vulnerability classes and finally the validation of the vulnerability map.

2 PRESK method and its characteristics

Five factors that control the groundwater pollution potential were defined, whose initials form the acronym PRESK: Protection, type of Rock, Epikarst, Soil Cover and Karstification degree. Every factor is divided into 4 categories from the less (index 0) to the most vulnerable (index 3), showing the degree of each one's impact, as far as pollution is concerned. The category index of each factor is multiplied by the factor's weight. The final Vulnerability Index (I_g) derives from the addition of all the obtained values.

The P Factor (Protection): The degree of a karst formation's vulnerability is determined by how easily or not a potential pollutant, mainly through water from precipitation, reaches the aquifer's saturated zone. The movement of water on the surface may be hindered and delayed by two key subfactors, which in turn play a protective role on karst aquifers. The slope (or inclination, I) and the vegetation (V) covering the surface are used for the assessment of P factor.

The topographic slope (I) deals with the inclination of the ground, the geomorphological characteristic that favors more or less the runoff at the expense of infiltration of water to greater depths (Petelet-Giraud 2000). Infiltration is directly linked to the topographic slope. The greater the slope, the more it encourages surface runoff away from the aquifer. Low topography promotes diffuse infiltration. Subfactor I is divided into four categories: I_0 Very steep slope >45^o, I_1 steep slope 25-45^o, I_2 moderate slope 5-25^o, I_4 low relief area 0-5^o.

Vegetation subfactor (V) takes into account the presence or absence of permanent vegetation and its density. Depending on the type of vegetation, the rate of average evaporotranspiration changes (Katzensteiner 1999). The four categories of V factor are: V_0 forests, V_1 sparse trees and dense shrubs, V_2 sparse shrubs and trees and cultivated fields and V_3 absence of vegetative cover.

Subfactors I and V, are weighted by 4/5 and 1/5 respectively. The sum of the combination of slope and vegetation with their weights provide the P factor: P=4/5I + 1/5V (Fig. 1).

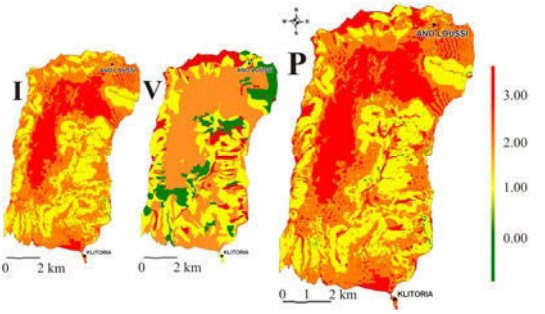

Fig. 1. Maps of Topographic slope (I-Inclination) and Vegetation of Loussi polje. The addition of the two to a 4/5 and 1/5 proportion respectively provides the Map of the P factor.

The R factor (Rock type): The R factor describes the type of lithology of the aquifer's formation in combination with tectonics which both control water's infiltration to a very large extent. All other formations are considered to play a protective role on karstic aquifers, by getting a zero value and therefore do not affect the final vulnerability index. R factor's categories are shown in Table 1.

Table 1. The four categories of the S factor and their characteristics.

Categories and characteristics of factor S	
Category	Characteristics
R0	Hard fissured rocks
R1	Alluviums, debris fall, conglomerates
R2	Thin bedded, slightly fractured limestones
R3	Massif, thick bedded, slightly fractured carbonate formations, thin bedded, heavily fractured limestones

The E factor (Epikarst): Epikarst is the uppermost weathered zone of carbonate rocks with substantially enhanced and more homogeneously distributed porosity and permeability than the bulk rock mass below it (Klimchouk 2003). Dissolution effectiveness and the secondary porosity are diminishing with depth, widened fissures taper downwards and become fewer (Williams 2003). The epikarst offers both a potential storage medium and potential pathways for contaminant migration into the aquifer (White 2003), however the recharge of the karst aquifer is partly delayed by a primary storage right below the ground surface (Bakalowicz et al. 1974). Recognition and mapping of different types of epikarst zones is difficult, especially where it is covered or where its lateral extention is discontinuous. However, the epikarst zone can be characterized indirectly, based on geomorphologic features which can easily be mapped (Doerfliger et al. 1998). The E factor is classi-

fied in four categories: E_0 highly developed epikarst >1 m of thickness, E_1 moderately developed epikarst of 50 cm to 1 m of thickness with temporary storage capacity of water near the surface, E_2 poorly developed epikarst with thickness <50 cm and E_3 absence of Epikarst. Storage capacity in Epikarst before it reaches the karst aquifer plays a significant role on the level of protection.

Pindos zone as Epikarst on Tripolis aquifer: Pindos zone is characterized by thrusts, where permeable formations (limestones) alternate with impermeable ones (e.g. flysch) resulting in the increase of the layers' thickness. Being overthrusted on Tripolis zone, with its more or less permeable formations lying directly above the Tripolis carbonate formations or flysch, Pindos zone can be considered to play the role of epikarst on Tripolis aquifer. Since tectonic stresses favor the good hydraulic communication between the two geological masses, a significant amount of water infiltrates from Pindos to the underlying Tripolis. Therefore, in this study, Pindos zone is regarded as the thick epikarstic zone of Tripolis aquifer with a very satisfactory protective capacity and is thus categorized as E0, with little or no impact on vulnerability.

The S factor (Soil cover): The soils create a protective cover above karstic aquifers which is very important for the final vulnerability index. The soil parameter that can be calculated relatively easily, if no other information is available, is thickness. Due to lack of data in the study area, the evaluation of S factor was based only on the soil thickness. Based on onsite investigations and mapping as well as on results from regional geophysical survey, four categories of the S factor were identified: thickness> 5 m, 1-5 m, < 1 m and poorly developed or total absence of soil cover.

The K factor (Karstification degree): The karst network development and its degree of organization plays an important role on water velocity flow and therefore on the vulnerability (Doerfliger et al. 1998). Calculating the K factor, especially when surface features are absent, is difficult and indirect methods are usually used. Here, the degree of karstification was assessed by (a) the presence of caves and avens (b) the results of recession curves analysis from springs' hydrographs proposed by Mangin (1975), (c) tracer tests on both polje's sinkholes. K factor categories are: K_0 aquifer with poorly developed network or absence of karstic fissures, K_1 fissured but not karstified aquifer, K_2 poorly karstified aquifer, K_3 well and very well developed karst network. Where the degree of karstification is low then the aquifer retains some natural protection.

3 Vulnerability index

The calculation of the final vulnerability index (Ig) was based on the following formula:

$$Ig = \beta P_i + \alpha R_j + \varepsilon E_n + \delta S_k + \gamma K_m$$

where Ig: the final vulnerability index, $\alpha, \beta, \gamma, \delta, \varepsilon$: weight of each factor, P_i, R_j, S_k, K_m, E_n: values of the factors for each category. The values of the Ig index are also grouped into four vulnerability categories (Very Low, Low, Moderate, High). The assessment of the weighting values was based on Analytical Hierarchy Process developed by Saaty (1977). A pairwise comparison matrix was formed (Table 2) in order to hierarchically organize the factors and to calculate their weights. According to their weights, the importance of each factor in PRESK method can be described as follows: S>P>E>R>K. Therefore the formula of the Final Vulnerability Index becomes:

$$Ig = 0.263P_i + 0.097R_j + 0.160E_n + 0.419S_k + 0.062K_m$$

Table 2. Hierarchical organization of the PRESK factors and their relative weights (left) and Definition of vulnerability categories according to the final vulnerability index (right).

	P	R	E	S	K	Weight
P	1	3	2	1/2	4	0.263
R		1	1/2	1/4	2	0.097
E			1	1/3	3	0.160
S				1	5	0.419
K					1	0.062

Ig categories	Vulnerability categories	
0 – 0.8	0	Very Low Vulnerability
0.8 – 1.6	1	Low Vulnerability
1.6 – 2.4	2	Moderate Vulnerability
2.4 – 3	3	High Vulnerability

4 Field Application: Loussi Polje

Vulnerability mapping using the PRESK method was carried out in N. Peloponnesus at Loussi Polje, an area of around 20 km^2 SW from Kalavryta with mean altitude from 940 to 1100 m. Manna River drains a part of the area into two sinkholes at an altitude of 967 m. Geotectonic zones of Olonos – Pindos and Tripolis are present with the first overthrusting the second. The appearing geological formations are: (1) recent alluvium and talus cones, which form the totality of the polje's surface sediments, and emanate mainly from Pindos formations (2) flysch of Eocene, (3) stratified limestones of Upper-Cretaceous, (4) radiolarites of Upper-Jurassic, (5) Upper-Triassic limestones of Pindos zone and from Tripolis zone Upper-Cretaceous carbonate series in the NE.

The two most important karstic aquifers of the region are Pindos Upper-Cretaceous limestones and Tripolis thick-bedded limestones. The first is a fissured karstic aquifer of small to moderate thickness, intensively tectonized and folded in alterations with the flysch and radiolarites of the same zone. Near the surface circulation of groundwater predominates and most of the aquifer's discharge is through springs around the polje at the contact with the more impermeable formations. On the other hand, Tripolis carbonate series is a karstic aquifer of consider-

able thickness (up to 1000 m), with a deep and large conduit flow system. The discharge from the aquifer is through springs with significantly great volume, at lower altitudes than in Pindos zone. Planitero spring in Tripolis zone at the SE outside the field area partly drains water from Loussi sinkholes (Koutsi and Stournaras 2005).

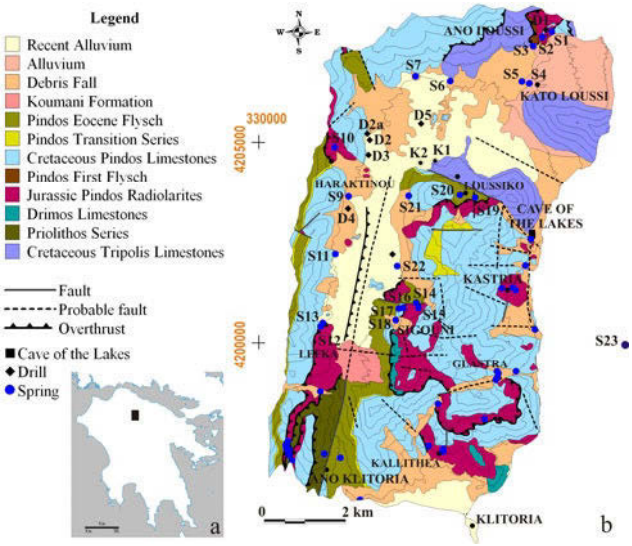

Fig. 2. a. Schematic map and **b.** geological map in the study area. **K1, K2:** the two Loussi polje sinkholes.

5 P, R, E, S and K factors and Final Vulnerability Map

Each factor of the PRESK method was mapped individually in the field at 1:20000 scale and then was digitized in MapInfo GIS. Vulnerability maps were constructed for every factor according to the given categories. The Final Vulnerability Map is the result of the multiplication of every map's category by the corresponding weight and their final addition. In PRESK map of Loussi polje (Fig. 3) all four vulnerability categories are represented, with moderate vulnerability being quite increased due to the presence of carbonate outcrops which in majority are poorly karstified.

Most of the High vulnerability areas are found on the top of carbonate formations where the karst landforms are not covered by soil, their degree of karstification moderate to high and the topography is low ($5^{o}<$) in combination with little or absence of vegetation.

The Manna River is drained into two sinkholes, and therefore its basin is classified as High vulnerability. It is considered as if there is not any soil cover protection and as if it is an area of a very high degree of karstification since water travels rapidly bypassing any protection.

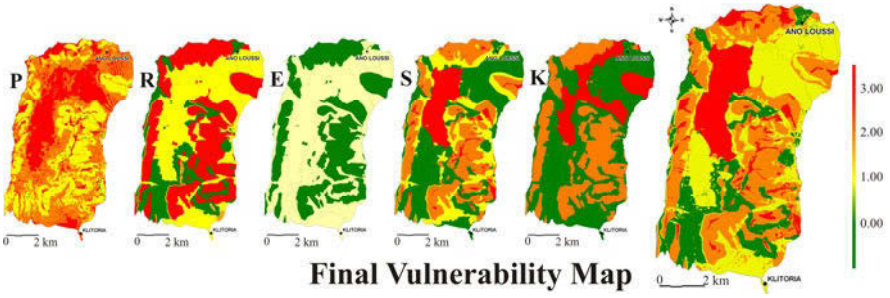

Fig. 3. Maps of the 5 vulnerability factors P, R, E, S, K and the Final Vulnerability Map of Loussi polje resulting from the Final Vulnerability Index $\mathbf{Ig} = 0.263\mathbf{P_i} + 0.097\mathbf{R_j} + 0.160\mathbf{E_n} + 0.419\mathbf{S_k} + 0.062\mathbf{K_m}$.

The areas of moderate vulnerability constitute over one third of the study area. The majority of Pindos limestones and Tripolis carbonate formations belong to this vulnerability category which indicates the primary role of factor R. These areas show a soil cover of thickness from less than 1m up to 5m and a moderate to high degree of karstification. The predominance of steep slopes and of the epikarst appearance lowers the vulnerability values to one category.

Scattered throughout the region, low vulnerability areas are characterized by: soil cover of thickness 1 - 5 m, absence or low topographical relief (from 0 to 45°), absence of karstification, sparse shrubs and trees and cultivated fields. The biggest areas of this category are situated in the NE and S part of the polje.

The lowest vulnerability category occurs where above the aquifer low permeability material (eg recent alluvium) and formations (eg radiolarites) are present. It covers approximately 20% of the region and reflects very high relief areas (> 45°), where infiltration is diminished and soil cover thickness exceeds 5m, there is a lack of karstification and usually a significant vegetative cover.

6 Conclusions

The PRESK method, an adaptation of RISKE method, was applied in Loussi polje. The specificity of the region, as well as the lack of necessary data led to a general modification upon the factors' categories and weightings. The five factors used are: Protection (P), Rock type (R), Epikarst (E), Soil Cover (S) and degree of Karstification (K), which were mapped and categorized according to the new categories. The Final Vulnerability Index and Map were obtained. All four vulnerability categories are represented with the Low and the Moderate being the most extended ones. The presence of the two sinkholes changed the way the factors S and K were categorized, taking high category values at the polje's area where Manna River flows until it reaches the sinkholes.

Acknowledgments The authors would like to especially thank Mrs. Valerie Plagnes, UPMC-Paris, for her kind and helpful scientific guidance and literature offer. The research was co-funded by the European Social Fund and National Resources in the framework of "HERACLEITOS" project.

References

Daly D, Dassargues A, Drew D, Dunne S, Goldscheider N, Neale S, Popescu C, Zwhalen F (2002) Main concepts of the "European Approach" for (karst) groundwater vulnerability assessment and mapping. Hydrogeol J 10(2):340-345

Bakalowicz M, Blavoux B, Mangin A (1974) Apports du traçage isotopique naturel à la connaissance du fonctionement d'un système karstique-teneurs en oxygène 18 de trois systèmes des Pyrénées, France: Journal of Hydrology 23, 141-158

Doerfliger N, Jeannin PY, Zeahlen F (1998) Water Vulnerability Assessment in karstic environments: a new method of defining protection areas using a multi-attribute approach and GIS tools (EPIK method). Environ Geol 39(2):165-176

Goldscheider N, Klute M, Sturm S, Hötzl H (2000) The PI method – a GIS-based approach to mapping groundwater vulnerability with special consideration of karst aquifers. Zeitschrift fur Angewandte Geologie 46(3):157-166

Katzensteiner K (1999) Die Einflüsse von Vegetation und Boden auf den Wasserhaushalt des Karstsystems. Final report NATIONALPARK KALKALPEN Karstprogramms von 1994 bis 1997, 72-97, Amt der oberösterreichischen Landesregierung, Linz

Klimchouk A (2003) Towards defining, delimiting and classifying epikarst: it's origin, processes and variants of geomorphic evolution. In: Jones, Culver, Herman/ Karst Waters Institute (ed) Epikarst – Proceedings of the symposium held October 1 through 4, 2003 Shepherdstown, West Virginia, USA, Special Publication 9

Koutsi R, Stournaras G (2005) Tracer test at Loussi polje karst system (Kalavryta – North Peloponnesus, Hellas), 7th Hellenic Hydrogeological Conference and 2nd MEM Workshop on fissured Rocks Hydrology, Conference proceedings, volume 2, 241-248

Mangin A (1975) Contribution a l'étude hydrodynamique des aquifères karstiques. Thèse de 3eme cycle, Université de Dijon, France

Petelet-Giraud E, Doerfliger N, Crochet P (2000) RISKE: méthode d'évaluation multicritère de la cartographie de la vulnérabilité des aquifères karstiques. Application aux syst èmes des Fontanilles et Cent-Fonts (Herault, Sud de la France) Hydrogeologie, N° 4, 2000,pp. 71-88

Saaty TL (1977) A scaling method for priorities in hierarchical structures. Journal of Mathematical Psychology, 15, 234-281

Vias JM, Andreo B, Perles MJ, Carrasco F, Vadillo I, Jimenez P (2006) Proposed method for groundwater vulnerability mapping in carbonate (karstic) aquifers: the COP method

White WB (2003) Contaminant storage and transport in the epikarst. In: Jones, Culver, Herman/ Karst Waters Institute (ed) Epikarst – Proceedings of the symposium held October 1 through 4, 2003 Shepherdstown, West Virginia, USA, Special Publication 9

Williams PW (2003) The epikarst: Evolution of understanding. In: Jones, Culver, Herman/ Karst Waters Institute (ed) Epikarst – Proceedings of the symposium held October 1 through 4, 2003 Shepherdstown, West Virginia, USA, Special Publication 9

Intrinsic vulnerability assessment using a modified version of the PI Method: A case study in the Boeotia region, Central Greece

E. Tziritis, N. Evelpidou

National & Kapodistrian University of Athens, Faculty of Geology and Geoenvironment

e-mail: evtziritis@geol.uoa.gr, Ilissia 157 84, Athens

Abstract The assessment of an aquifers' vulnerability to pollution is of great importance, and can be used as a tool to augment planning, effective protection and management of groundwater resources' quality, especially in the case of karstic aquifers. The present study aims to assess the intrinsic vulnerability of a karstic groundwater system, with the use of a modified version of the PI method. The assessments are functional to the effectiveness of the protective cover, as well as to the degree to which the protective cover is bypassed due to flow conditions. The used data was obtained by field work, empirical and semi-quantitative approaches regarding lithology, fissuring and karstification of bedrock, soil characteristics, hydrology, hydrogeology, topography and vegetation. The combinational effect of the above parameters, as processed with the aid of a GIS system, yielded the final calculation of the protection factor (π) and subsequently the vulnerability of the aquifer to pollution.

1 Introduction

Groundwater resources are often highly vulnerable to pollution from human activity, emerging the need for the appropriate protection measures, a point which is highlighted in the EU Water Framework Directive (2000). Karstic aquifers are well known for their particularly high vulnerability to pollution arising from their special characteristics, like thin soil covers, point recharge in dolines, shafts and shallow holes, as well as preferential flow paths in the epikarst and vadose zone. Such characteristics result in pollutants easily reaching groundwater, where they are transported rapidly in karstic conduits over large distances (Zwahlen 2003). Thus, defining integrated protection schemes for karstic groundwater systems is of vital importance, since they may be used to serve local communities and stakeholders for the definition and application of water management master plans, especially in environmental sensitive regions. The study area (Eastern Kopaida plain, Boeotia Greece) should be considered as such case, due to the specific geological characteristics and land use. Kopaida plain is a highly cultivated region over the last decades,

N. Lambrakis et al. (Eds.), *Advances in the Research of Aquatic Environment, Vol. 2*
DOI 10.1007/978-3-642-24076-8,

with a unique karstic environment which is characterized by extended superficial and underground karstification phenomena. These phenomena in general include a great number of katavothraes, which enhance the rate of infiltration and subsequent water recharge but simultaneously impose a significant potential threat to groundwater quality. The geological setting is characterized by karstic formations and a thick sequence of Quaternary deposits, of minor hydrogeological importance (Tziritis 2008). The hydrogeological setting of the area is thus dominated by the karstified rock units that define three individual aquifers with variable degrees of karstification and highly contrasting permeability values. These aquifers are practically interconnected on a regional scale and may be considered as a unified heterogeneous karstic system. General water flow direction is towards E and NE, with variable piezometric levels that range between 20 and 160 m (Tziritis 2008).

2 Methods and Materials

There are various methods to map intrinsic aquifer vulnerability, but in the case of study area the assessment was made using a modified version of the PI method (Goldscheider et al. 2000). Unlike the majority of the existing methods that cannot be applied in karstic areas, PI method is a GIS-based approach with special consideration of karstic aquifers. It is based on an origin-pathway-target model (Fig. 1), where the origin is supposed to be at the ground surface and the target is the uppermost aquifer. The pathway includes all the layers interfered between the extreme points of origin and target. The acronym stands for the two factors protective cover (P) and infiltration conditions (I). The P-factor describes the protective function of the layers (soil, subsoil, non karstic rock, and karstic rock) between the ground surface and the water table, and is calculated according to a slightly modified version of the German (GLA) method (Holting et al. 1995) which is divided into five classes from 1 (very low protection) to 5 (very high protection). The I-factor describes the infiltration conditions, and more specifically the bypass degree of protection cover, due to lateral and subsurface water flow in the catchment of karstic holes and sinking (blind) streams. If the protective cover is completely bypassed by a shallow hole through which surface water may pass directly into the karstic aquifer then I=0, while I=1 if the infiltration occurs diffusely (e.g. on a flat, highly permeable and free draining surface). The intermediate values occur in catchment areas of variable slopes, depending on the proportion of lateral flow components. The final protection factor "π" is extracted by the combination of P and I ($\pi = P \bullet I$) and subdivided into five classes, where $\pi \leq 1$ indicates very low degree of protection leading to extreme vulnerability, while $\pi=5$ indicates a very high protection with subsequent very low vulnerability (Vrba and Zaporozec 1994; Goldscheider et al. 2000). The spatial distribution of "π" factor with the use of a GIS system, defines the final outcome which is the assessment of the karstic aquifer's intrinsic vulnerability.

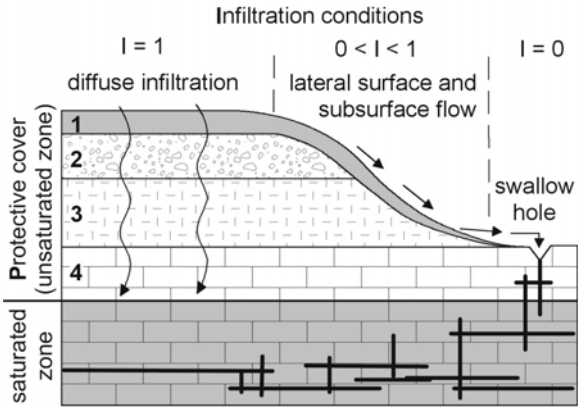

Fig. 1. Illustration of PI method concept (Goldscheider et al. 2000).

3 Results – Assessment of intrinsic vulnerability

The estimation of intrinsic vulnerability was conducted by using data from 72 boreholes of the karstic aquifer as well as from field work which included specific assessments of the geological setting (Tziritis 2008). The used data included the following parameters: vertical stratigraphy of the boreholes, piezometric level, aquifer's depth from the surface, fissuring and karstification degree of the substrate, topographic slope, lithology of the bedrock, type and origin of the Quaternary deposits, existence of katavothraes and sink holes, occurrence and route of blind river (a river sinking in a karstic form) which in our case is River Melas (Fig. 2), and finally spatial definition of the hydrological sub-basins. The modification of the original PI method included the addition of semi-quantitive assessments (soils thickness - depending on depth of substrate and topographic slope) to the final calculation of T-factor (Topsoil). This was considered as an essential modification in order to promote and assess in a better way the critical role of soil in the study area, regarding physical attenuation processes.

3.1 Estimation of P-factor (Protective cover)

The P-factor which expresses the impact of the protective cover was assessed on the basis of soils' effective field capacity (eFC), subsoil's grain size distribution, lithology, fissuring and karstification of the non-karstified and the karstified rock, thickness of all strata and mean annual recharge.

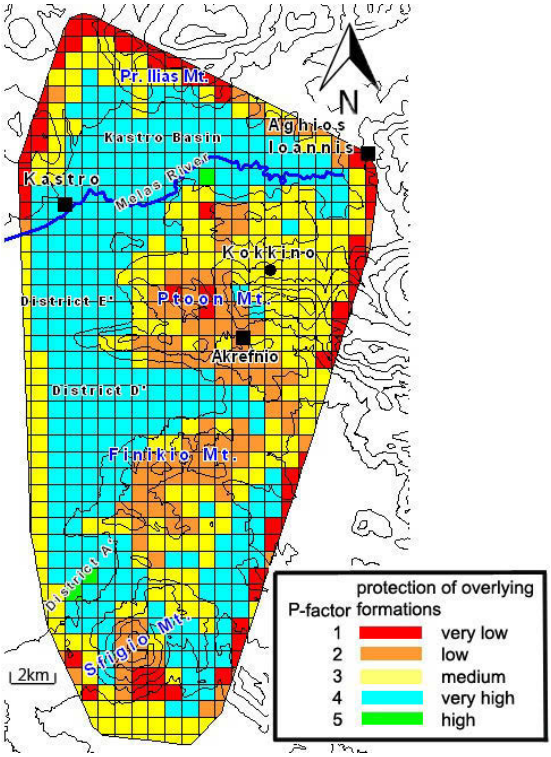

Fig. 2. Spatial distribution (P-map) of the P-factor (Protective cover) in the study area.

The above parameters were correlated with the "total protective function" (Goldscheider 2000) in order to define the degree of total protection (P_{TS}):

$$P_{TS} = \left[T + \left(\sum_{i=1}^{m} S_i \cdot M_i + \sum_{j=1}^{n} B_j \cdot M_j \right) \right] \cdot R + A \qquad \text{(Eq. 1)}$$

where: T is the T-factor that refers to topsoil, S is the S-factor that refers to subsoil, B is the B-factor that refers to bedrock, M is the thickness (m) in the unsaturated zone, R is the R-factor that refers to recharge in terms of precipitation height, and finally A is the A-factor that refers to artesian conditions, if present. The range of P_{TS} values corresponds to a P-factor value (Goldscheider 2000) which ranges from P=1 for an extremely low degree of protection to P=5 for very thick and protective overlying layers. Each one of the 72 data stations (boreholes) was assigned a value, and then with the use of spatial interpolation (natural neighbor method) the values of P-factor where simulated for the entire study area (Fig. 2).

3.2 Estimation of the I-factor (Infiltration)

The I-factor shows the degree to which the protective cover is bypassed by lateral surface and subsurface flow and subsequent concentrated recharge.

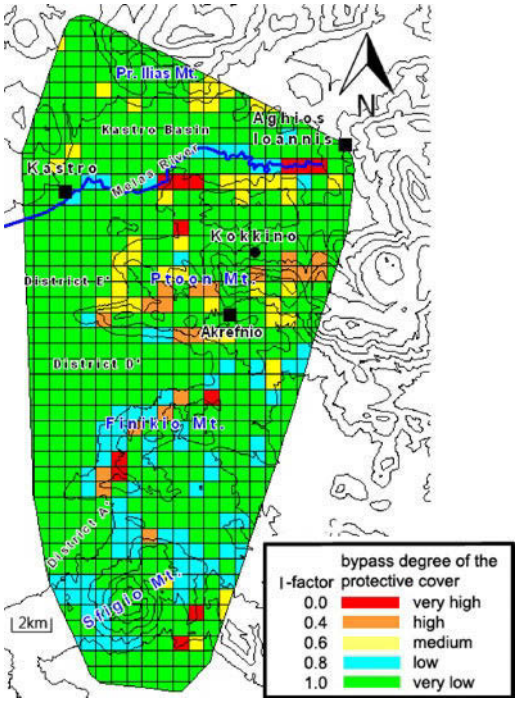

Fig. 3. Spatial distribution (I-map) of the I-factor (Infiltration conditions) in the study area.

In order to determine the I-factor, three consecutively steps were carried out:

- **Estimation of dominant flow process:** The estimation was based on the combination of i) topsoil's (or the uppermost layer) saturated hydraulic conductivity (m/s), and ii) the depth to low permeability layers inside or below the topsoil (or the uppermost layer). The combination of the above produced a map (GIS coverages) which determined the final result of dominant flow process.
- **Estimation of the I'-factor:** I'-factor depends on i) results from the previous step (dominant flow process), ii) topographic slope, and iii) vegetation. The combination of the above yielded for every single point of the study area a value ranging from 0.0 to 1.0. The result (GIS coverage) is called I'-map and shows the occurrence and intensity of lateral surface and subsurface flow.
- **Blind's river catchment map:** Lateral surface and subsurface flow may represent a risk to groundwater only if the water and possible pollutants enter the karst aquifer at another place in a concentrated way, e.g. via a sinking stream.

The above described sinking stream (also called Blind River) in the study area is River Melas (Fig. 3) which sinks in a karstic hole near Aghios Ioannis. According to the criteria imposed by the original PI method (Goldscheider 2000), River Melas catchment was distinguished in four buffer zones depending on relevant distances from the riverbed and the superficial occurrence of sinking holes and katavothraes. The obtained results included the construction of a relevant map (River Melas catchment map according to PI method criteria) with the aid of a GIS system.

The last step embraced the combination of the previous assessed data and the final construction of the I-map (Fig. 3) which shows the degree to which the protective cover is bypassed. The final I-map is obtained by the intersection of the I'-map (showing the occurrence and intensity of lateral flow) with the River Melas catchment map (showing the sinking streams and their catchments).

3.3 Estimation of the final Protective Factor (π)

The final Protective Factor (π) resulted from the combination of P and I factors (π=P•I) for every single point of the study area, with the use of the previous estimated data and spatial interpolation. The final outcome is the map of figure 4 which shows the intrinsic vulnerability of the karstic aquifer. Based on this map, the regions with very low vulnerability ($4<\pi<5$) are located in districts A', D' and E', as well as the larger part of Kastro basin. The above regions are dominated by thick series of Quaternary deposits and nearly zero topographic slopes. The regions with low vulnerability ($3<\pi<4$) appear in some minor parts of districts A' and D', in the southern and the eastern part of the study area, around Kokkino village, and north of Kastro. Low vulnerability conditions are related with the existence of Quaternary deposits as mentioned before, and also with the absence of katavothraes, karstic cavities and significant amount of bedrock fissuring. The regions of Sfigio, Finikio and Ptoon Mountains appear to have moderate vulnerability ($2<\pi<3$).

The same conditions characterize variable scattered regions in study area. On the contrary, the regions with high vulnerability ($1<\pi<2$) are located in small parts of Sfigio (NE part), Pr. Ilias and Finikio mountains, as well as eastern of Akrefnio city and north-west of Kastro. The major factors that confide the high vulnerability conditions should be related to the absence of protective cover and high water table. Finally, the regions which are characterized by very high ($0\leq\pi<1$) vulnerability are located only in few parts of the study area, mainly in parts of Finikio and Ptoon mountains, a small part of the southern extremities of Kastro basin, and around the region of Aghios Ioannis, where is the end (sinking point) of River Melas. The conditions which define the high vulnerability are attributed to the absence of Quaternary deposits, neighbouring with Melas riverbed, existence of karstic holes and cavities, as well as the small thickness of the unsaturated zone (high piezometric level).

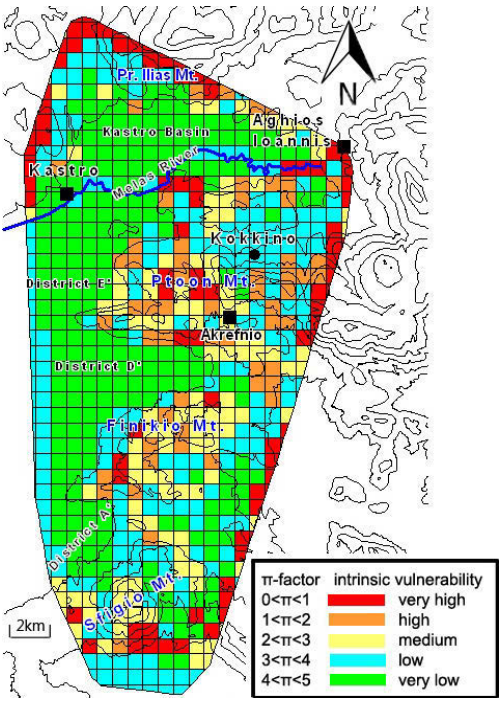

Fig. 4. Spatial distribution of karstic aquifers intrinsic vulnerability.

4 Conclusions

The intrinsic aquifer vulnerability was assessed with the use of geological data obtained from 72 borehole-stations and extensive field work. The assessment was based upon a modified version of the original PI method. Thus, the conceptual approach of the modified method included apart from the combination of the two main factors of the original version that describe the impact of the protective cover (P-factor) and the infiltration conditions (I-factor), also semi-quantitive estimations regarding topsoil thickness. The above was considered essential due to the significant role of topsoil in Kopaida plain, regarding physical attenuation processes. This innovative addition improved the quality of the results, and expanded the applicability of the method in areas with different geological characteristics. Thus, the final assessment embraced all the critical parameters that influence aquifer vulnerability in the study area, like thickness and nature of protective cover, occurrence of karstification phenomena and thickness of topsoil. As a result, a map of the total protective factor was finally produced with the aid of spatial interpolation through a GIS system, which presents aquifer vulnerability.

References

European Water Directive (2000) Directive 2000/60/EC of the European parliament and of the council of 23 October 2000 establishing a framework for community action in the field of water policy, European Commission, Brussels

Goldscheider N, Klute M, Sturm S, Hotzl H. (2000) The PI method – a GIS based approach to mapping groundwater vulnerability with special consideration of karst aquifers. Z.angew.Geol., 46(2000)3, p.157-166

Holting B, Haertle T, Hohberger K, Nachtigall K, Villinger E, Weinzierl W, Wrobel JP. (1995) Konzept zur ermittlung der Schutzfunktion der Grundwasseruberdeckung. Geol. Jb. C63, p.5-24

Tziritis E. (2008) Hydrogeochemical - Environmental study of east Kopaida – Yliki karstic system and assessment of vulnerability with the use of Geoinformatics. PhD thesis, University of Athens, Faculty of Geology & Geoenvironment

Vrba J, Zaporozec A. (1994) Guidebook on mapping groundwater vulnerability. International contributions to Hydrogeology (IAH), v.16, p.131

Zwahlen F. (2003) Vulnerability and risk mapping for the protection of carbonate (karst) aquifers, final report (COST action 620). European Commission, Directorate-General XII Science, Research and Development, Brussels, 297pp

Groundwater vulnerability assessment at SW Rhodope aquifer system in NE Greece

A. Kallioras[1], F. Pliakas[2], S. Skias[2], I. Gkiougkis[2]

[1] National Technical University of Athens, School of Mining and Metallurgical Engineering, Athens, Greece.

[2] Department of Civil Engineering, Democritus University of Thrace, Xanthi, GR 67100, Greece. fpliakas@civil.duth.gr

Abstract Proper management of coastal aquifers often demands the assessment of groundwater vulnerability achieved by the application of different vulnerability indexes, each one being developed for specific type of contamination. This paper presents the application of widely used vulnerability indexes such as DRASTIC, with respect to nitrate contamination, and GALDIT, regarding aquifers vulnerability to seawater intrusion, in order to assess the vulnerability of the coastal aquifer of the agricultural area of Xilagani, N. Greece. The results have been linked with GIS for the visualization of vulnerability, while they are also compared and hence evaluated and verified with field data of nitrates and Revelle values distribution.

1 Introduction

This paper refers to the assessment of groundwater vulnerability to seawater intrusion of the Xilagani - Imeros coastal aquifer system, at the SW part of Rhodope Prefecture, NE Greece. The research is based on the results of hydrogeological studies in the study area including: a) research activities for the period 20/2/1994–7/12/1997, during relevant research project carried out for the Greek Ministry of Agriculture, by the Laboratories of Engineering Geology and Hydraulics of the Department of Civil Engineering - Democritus University of Thrace, regarding the management of artificial recharge of aquifers in Xanthi and Rhodope (Pliakas et al. 2001; Sakkas et al. 1998), and b) relevant research activities of the Laboratory of Engineering Geology of the Department of Civil Engineering - Democritus University of Thrace during the period 17/12/2002–9/10/2006 (Pliakas et al. 2004, 2007).

The assessment of groundwater vulnerability to pollution has been subject to intensive research during the past years and a variety of methods have been developed (Panagopoulos et al. 2006). The DRASTIC method is a familiar method developed in the US Environmental Protection Agency (USEPA) by Aller et al.

N. Lambrakis et al. (Eds.), *Advances in the Research of Aquatic Environment, Vol. 2*
DOI 10.1007/978-3-642-24076-8,

(1987) and this method has been applied in several regions by different researchers (Sener et al. 2009). Groundwater vulnerability maps are designed to show areas of greatest potential for ground-water contamination on the basis of hydrogeologic and anthropogenic (human) factors. The maps are developed by using computer mapping hardware and software called a geographic information system (GIS) to combine data layers such as land use, soils, and depth to water (Rupert 1999).

Lobo Ferreira et al. (2005 a, b) have developed the GALDIT method believing that the most useful definition of vulnerability to seawater intrusion is one that refers to the intrinsic characteristics of the aquifer, which are relatively static and mostly beyond human control. It is, therefore, proposed that groundwater vulnerability to sea water intrusion to be defined as "the sensitivity of groundwater quality to an imposed groundwater pumpage or sea level rise or both in the coastal belt, which is determined by the intrinsic characteristics of the aquifer".

2 Description of the study area - geological and hydrogeological characteristics

The plain area of Xilagani – Imeros has mild morphologic characteristics with low elevation, extended between Lissos River and the western foot of Ismaros Mount, whereas Thracian Sea covers the southern boundaries of the area (Fig. 1). The geological environment of the study area includes recent sediments originated from Lissos River -and some other branches of the same river- overlying Neogene deposits or Paleogene deposits of Rhodope massif (Pliakas et al. 2004).

The main cultivation type of the area is cotton, while the southern part of the area of investigation is not arable due to groundwater salinization. There are 55 groundwater wells (about 10 of them abandoned), with mean depth of 70 m and mean pumping rate of approximately 40 m^3/h, while at the northern parts of the site the groundwater wells present pumping rates of approximately 60 to 70 m^3/h (Pliakas et al. 2004, 2007). The aquifer system of the study area contains clay materials and appears in the form of successive layers composed of clay-sands and sands with a width ranging from 1 to 10 m, with many interferences of clay layers. The relevant hydrogeological study of the semi-confined aquifer of the study area included the following research activities (Pliakas et al. 2001, 2004, 2007, Sakkas et al. 1998): (1) Drilling of 6 test wells at depths 45-70 m, performance of 20 geophysical (electrical sounding) measurements and grain size analyses of 25 soil samples (Fig. 1). The results showed 4 distinct main geoelectrical formations categorized according to the values of their specific electrical resistivity, as follows (ASCE 1987, Kallergis 2000): coarse grained sand (>40 Ohm×m), fine grained sand (25-40 Ohm×m), clay-sand materials (15-25 Ohm×m), clay (<15 Ohm×m), while the dominance of clay and clay-sand materials throughout the whole extent of the study site is very distinct. (2) Monitoring of groundwater

level fluctuation from 25 wells during the periods 20/2/1994–7/12/1997 and 17/12/2002–9/10/2006. The groundwater level gradually increases from October to March, due to natural recharge from direct infiltration from precipitation (at parts of the aquifer where it appears semi-confined or unconfined), percolation from Lissos River and lateral inflows from the NE part of the study area where there is a hydraulic connection with the mountainous zone. During the period between April and October the groundwater level appears below the mean sea level fact which is attributed to the overpumping conditions for irrigation purposes. (3) Design of potentiometric surface maps for the period 17/12/2002–9/10/2006 (Fig. 1), showing that the aquifer system is incapable to respond to the amounts of pumped groundwater during the irrigation period maintaining at the same time a potentiometric surface above sea level.

The evaluation and assessment of the qualitative characteristics of study aquifer involved the determination of certain chemical parameters, such as Na^+, K^+, Ca^{2+}, Mg^{2+}, Fe^{2+}, Zn^{2+}, Mn^{2+}, NH_4^+, Cl^-, HCO_3^-, SO_4^{2-}, PO_4^{3-}, NO_3^-, NO_2^-, and certain physicochemical parameters such as alkalinity P, alkalinity M, total hardness and pH (8/7/2003 and 20/7/2006). The majority of the groundwater samples of the investigated aquifer, according to specific standards and drinking water limits (Kallergis, 2000), are characterized as non-potable, as the concentrations of Cl^- (116-2,375 mg/L), Na^+ (58-726 mg/L), K^+ (3-86 mg/L), Ca^{2+} (37-497 mg/L), Mg^{2+} (16-207 mg/L) are above the quality standards (Pliakas et al. 2004, 2007). The values of electrical conductivity range between 800-12,380 μS/cm, where the higher values of electrical conductivity appear within the southern (coastal) part of the study site, fact which imposes the argument of seawater intrusion conditions.

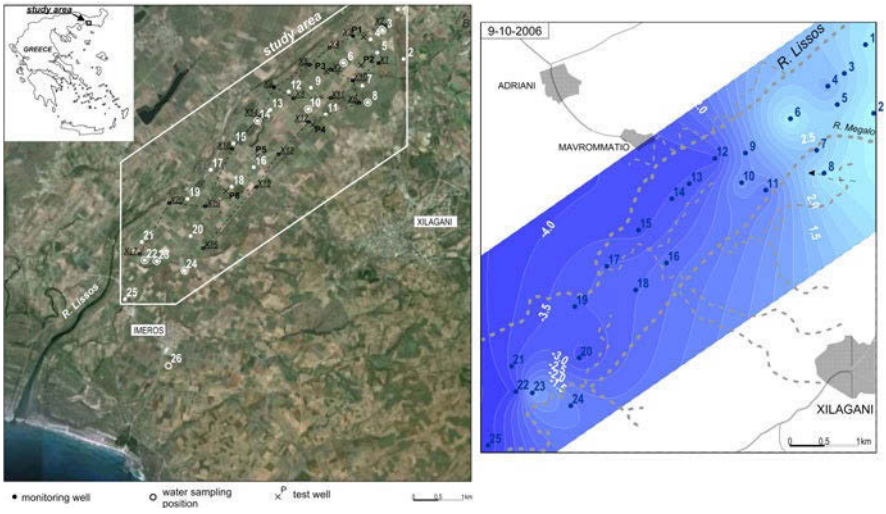

Fig. 1. (Left) Study area, positions of monitoring wells, test wells and geoelectric sounding measurements and their section axes, (Right) Potentiometric surface map (m a.s.l.) (Pliakas et al. 2004, 2007).

3 Application of DRASTIC and GALDIT methods

DRASTIC has been the most commonly used for mapping aquifer vulnerability in porous aquifers (Aller et al. 1987). The DRASTIC method considers seven parameters, which taken together, provide the acronym (Panagopoulos et al. 2006, Sener et al. 2009). These are depth to groundwater (D), net recharge ©, aquifer media (A), soil media (S), topography (T), influence of the vadose zone (I) and hydraulic conductivity (C). Each parameter is subdivided into ranges and is assigned different ratings in a scale of 1 (least contamination potential) to 10 (highest contamination potential). This rating is scaled by a pesticide and DRASTIC weighting factors ranging between 1 (least significant) and 5 (most significant). The linear additive combination of the above parameters with the ratings and weights was used to calculate the DRASTIC Vulnerability Index (DVI) as given below (Aller et al. 1987, Sener et al. 2009):

$$DVI = DrDw + RrRw + ArAw + SrSw + TrTw + IrIw + CrCw \quad (1)$$

where Dr: rating for the depth to water table, Dw: weight assigned to the depth to water table, Rr: rating for aquifer recharge, Rw: weight for aquifer recharge, Ar: rating assigned to aquifer media, Aw: weight assigned to aquifer media, Sr: rating for the soil media, Sw: weight for the soil media, Tr: rating for topography (slope), Tw: weight assigned to topography, Ir: rating assigned to impact of vadose zone, Iw: weight assigned to impact of vadose zone, Cr: rating for rates of hydraulic conductivity, Cw: weight given to hydraulic conductivity.

Table 1. DRASTIC Vulnerability Index (DVI) rating and weighting values for the various hydrogeological parameter settings.

2006 - Pesticide DVI: 119-183						
D (m) [1]	R (mm) [2]	A	S	T (%)	I	C (m/s)
1.85-8.97	44.4-55.5	clay -sandy deposits	clay -sandy material	0.1-1.2	clay -sandy deposits	1×10^{-6}-1×10^{-4}
Dr	Rr	Ar	Sr	Tr	Ir	Cr
1-10	1-3	6-9	4-8	9-10	4-9	2.5-7.5
Dw	Rw	Aw	Sw	Tw	Iw	Cw
5	4	3	5	3	3	2
	Vulnerability:	Very high	High	Moderate	Low	Very low
	DVI:	>160	140-160	100-140	80-100	<80

[1]: 9-10-2006, [2]: infiltration: 10% of mean annual rainfall (1954-2005): 555.3 mm (Kallioras et al. 2010)

The assessment of DVI included the values of all parameters (depth to water table, recharge, aquifer media, soil media, topographic relief, unsaturated zone in-

fluence, hydraulic conductivity) in every single investigated groundwater well (Table 1).

The topographic slope analysis has been made with the use of digitized basemap, while data from previous investigations have been used for the geological, hydrogeological and hydrological assessment of the study area (Pliakas 2004, 2007). The results from the application of DRASTIC vulnerability index have been linked with GIS, for the design of vulnerability maps in order to identify the parts where there is a serious potential for groundwater resources qualitative degradation (Fig. 2). Additionally, nitrate distribution map has been designed (nitrate ions in mg/L) as shown in Figure 3, where it is revealed that the NE part of the study area where increased nitrate concentrations are present coincides with the areas of high vulnerability based on the application of DVI (DVI >160).

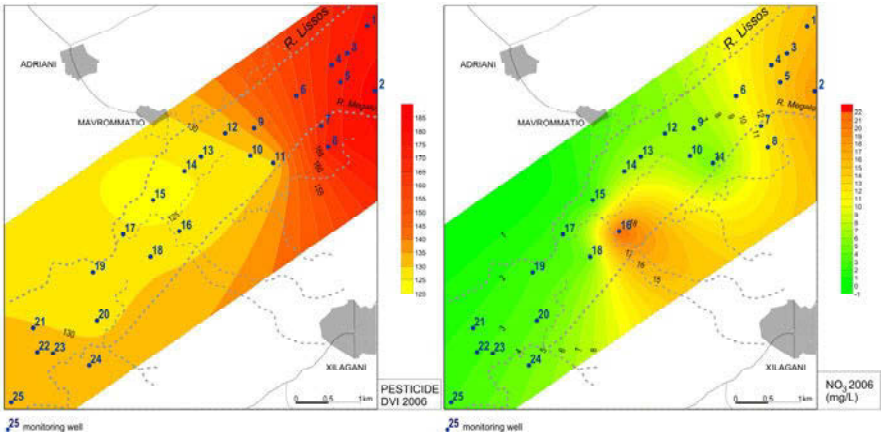

Fig. 2. Pesticide DRASTIC aquifer vulnerability map (DVI values) (2006) and distribution of nitrates (NO_3^-) concentrations map (2006).

The development of GALDIT index (GVI) is aiming the assessment of aquifer vulnerability to sea-water intrusion in coastal aquifers (Lobo Ferreira et al. 2005 a, b). The most important factors controlling seawater intrusion were found to be the following: Groundwater occurrence (aquifer type; unconfined, confined and leaky confined); Aquifer hydraulic conductivity; Depth to groundwater Level above the sea; Distance from the shore (distance inland perpendicular from shoreline); Impact of existing status of sea water intrusion in the area; and Thickness of the aquifer, which is being mapped. The acronym GALDIT is formed from the highlighted letters of the parameters for ease of reference. These factors, in combination, are determined to include the basic requirements needed to assess the general seawater intrusion potential of each hydrogeologic setting. GALDIT factors represent measurable parameters for which data are generally available from a variety of sources without detailed examination. A numerical ranking system to assess seawater intrusion potential

in hydrogeologic settings has been devised using GALDIT factors. The system contains three significant parts: weights, ranges, and ratings. Each GALDIT factor has been evaluated with respect to the other to determine the relative importance of each factor. Each of the six indicators has a pre-determined fixed weight that reflects its relative importance to seawater intrusion. The GALDIT Index is then obtained by computing the individual indicator scores and summing them as per the following expression:

$$GVI = \sum_{i=1}^{6} \{(W_i)R_i\} / \sum_{i=1}^{6} W_i \quad (2)$$

where Wi is the weight of the i^{th} indicator and Ri is the importance rating of the i^{th} indicator. Once the GALDIT-Index has been computed, it is therefore possible to classify the coastal areas into various categories of seawater intrusion vulnerability.

GALDIT Vulnerability Index, GVI, was calculated according to the values of each parameter in every single groundwater well which is influenced by seawater intrusion conditions such as: aquifer type, hydraulic conductivity, water table, distance from shoreline, seawater intrusion influence and thickness of saturated zone (Table 2).

Table 2. GALDIT Vulnerability Index (GVI) rating and weighting values for the various hydrogeological parameter settings.

		2006 – GVI: 4.5-8.5			
G	A (m/s)	L (m) [1]	D (m)	I (Revelle) [2]	T (m)
semi-confined aquifer	1×10^{-6}-1×10^{-4}	-3.7-4.4	3260-10790	0.3-25	7-27
R1	R2	R3	R4	R5	R6
10	2.5-7.5	2.5-10	2.5-10	2.5-10	7.5-10
W1	W2	W3	W4	W5	W6
1	3	4	4	1	2
		Vulnerability:	High	Moderate	Low
		GVI:	≥ 7.5	5 – 7.5	< 5

[1]: 9-10-2006, [2]: 20-7-2006

The results from the application of GALDIT vulnerability index were linked with GIS in order to design vulnerability maps for the study area with respect to the potential for aquifer contamination due to seawater intrusion (Fig. 3). Revelle coefficient was also calculated and distributed throughout the entire study area, so that the Revelle distribution map will be correlated against the vulnerability map from the application of GALDIT VI (Fig. 3). It was concluded that at the SW part of the study area (with a direction towards the shoreline) there is a coincidence between the zone of high vulnerability based of GALDIT VI (GVI > 7.5) and the high Revelle coefficient.

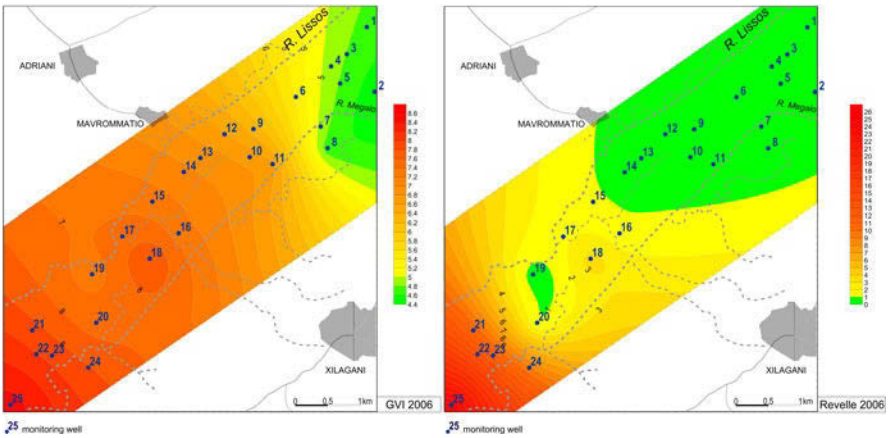

Fig. 3. GALDIT aquifer vulnerability map (2006) and distribution of Revelle values map (2006).

4 Conclusions

This paper included the analysis, interpretation of DRASTIC and GALDIT VI spatial distribution with respect to the spatial distribution of nitrate concentration and Revelle coefficient (respectively). The use of GIS for both vulnerability indexes was found effective for the evaluation of each method in comparison to real field data. An alternative approach could include the use of box plots for the analysis of statistical data of nitrates concentrations or Revelle values or chlorides concentrations mainly at the areas where high vulnerability is observed (by applying DRASTIC or GALDIT respectively).

The application of DRASTIC during this research regards the typical DRASTIC method, including the assignment of all related parameters. An alternative approach could include a modified DRASTIC index which does not take into account parameters such as influence of the unsaturated zone and aquifer type. An important modification could also include the land use (as an index for pollutant potential) which in turn may influence the aquifer recharge. Lastly a number of modifications for the improvement of the weighting factors could also be developed for both DRASTIC and GALDIT.

References

Aller L, Bennett T, Lehr JH, Petty RJ, Hackett G (1987) DRASTIC: a standardized system for evaluating ground water pollution potential using hydrogeologic settings. EPA-600/2-87-035, EPA, Washington, DC

ASCE (1987) Ground Water Management. 3rd Edition, ASCE Manuals and Reports on Engineering Practice No 40, New York

Kallergis G (2000) Applied – Environmental Hydrogeology. Volume B, published TCG, Athens, 345 p (in Greek)

Kallioras A, Pliakas F, Diamantis I (2010) Simulation of groundwater flow in a sedimentary aquifer system, subjected to overexploitation. Water, Air, & Soil Pollution, Springer, 211 [1-4], 177-201

Lobo Ferreira JP, Chachadi AG, Diamantino C, Henriques MJ (2005a) Assessing aquifer vulnerability to seawater intrusion using GALDIT method: Part 1 – Application to the Portuguese Aquifer of Monte Gordo. Proceedings of the 4th InterCeltic Colloquium on Hydrology and Management of Water "Water in Celtic Countries: Quantity, Quality and Climate Variability", eds. J.P. Lobo Ferreira and José M. P. Vieira, held at Universidade do Minho, Guimarães, Portugal, July 11- 13, 2005, http://www.iahs.info/, IAHS (International Association of Hydrological Sciences), (http://www.aprh.pt/celtico/PAPERS/25.PDF), Publication 310, pp. 161-171

Lobo Ferreira JP, Chachadi AG, Diamantino C, Henriques MJ (2005b) Assessing aquifer vulnerability to seawater intrusion using GALDIT method: Part 1 – Application to the Portuguese Aquifer of Monte Gordo. Proceedings of the 4th InterCeltic Colloquium on Hydrology and Management of Water "Water in Celtic Countries: Quantity, Quality and Climate Variability", eds. J.P. Lobo Ferreira and José M. P. Vieira, held at Universidade do Minho, Guimarães, Portugal, July 11- 13, 2005, http://www.iahs.info/, IAHS (International Association of Hydrological Sciences), (http://www.aprh.pt/celtico/PAPERS/25.PDF), Publication 310, pp. 161-171

Panagopoulos GP, Antonakos AK, Lambrakis NJ (2006) Optimization of the DRASTIC method for groundwater vulnerability assessment via the use of simple statistical methods and GIS. Hydrogeol J 14, 894-911

Pliakas F, Diamantis I, Petalas C, Panilas S (2001) Feasibility study of artificial recharge application to Rhodope plain areas aquifers in Thrace, Greece. A first approach. Proceedings of the 9th International Congress of the Geological Society of Greece, Athens, Greece, 26-28/9/2001, Vol. 5, pp. 1923-1932 (in Greek)

Pliakas F, Diamantis I, Kallioras A, Petalas C (2004) Study of the progress of seawater intrusion within a plain area of Rhodope Prefecture. Proceedings of the 10th International Congress of the Geological Society of Greece, Thessaloniki, Greece, 15-17/4/2004, pp. 2057-2066 (in Greek)

Pliakas F, Mouzaliotis A, Kallioras A, Diamantis I (2007) Hydrogeological assessment of the salinization problem of Xilagani – Imeros aquifer system in SW plain area of Rhodope Prefecture, Greece. Proceedings of the 11th International Conference of the Geological Society of Greece, Athens, Greece, 24-26/5/2007, Vol. 2, pp. 536-547

Rupert MG (1999) Improvements to the DRASTIC groundwater vulnerability mapping method. U.S. Geological Survey Fact Sheet FS-066-99, USGS, Reston, VA

Sakkas I, Diamantis I, Pliakas F et al. (1998) Groundwater artificial recharge study of Xanthi – Rhodope aquifers. Research Project for the Greek Ministry of Rural Development and Food. Sections of Hydraulics and Geotechnical Engineering, D.U.Th., Volume 3, Department of Civil Engineers D.U.Th., Xanthi. Greece

Sener E, Sener S, Davraz A (2009) Assessment of aquifer vulnerability based on GIS and DRASTIC methods: a case study of the Senirkent-Uluborlu Basin (Isparta, Turkey). Hydrogeology J. 17, 2023–2035

Comparison of three applied methods of groundwater vulnerability mapping: A case study from the Florina basin, Northern Greece

N. Kazakis, K. Voudouris

Aristotle University of Thessaloniki, Department of Geology, Laboratory of Engineering Geology and Hydrogeology, Greece. E-mail: kvoudour@geo.auth.gr

Abstract Three different methods of intrinsic groundwater vulnerability mapping were applied in the alluvial aquifer of Florina basin (NW Greece), covering an area of 180 km^2. Vulnerability maps were produced using the parametric methods DRASTIC, GOD, AVI and the results are compared and evaluated. The three methods use different number of parameters with different weight and produce relatively different results. The comparison between these methods shows that the GOD method has the stronger correlation with the other two methods and produces vulnerability maps comparable with DRASTIC and AVI method.

1 Introduction

Groundwater is under intense anthropogenic pressure in many countries, from sources such as changes in land use, urbanisation, lack of proper sewerage, intensive agriculture and a general increase in demand (Voudouris et al. 2007). These pressures can cause severe degradation of both the quality and quantity of groundwater resources (Polemio et al. 2009). Vulnerability evaluation is fundamental in order to define policies of groundwater resources protection and safeguard, especially for aquifers characterized by a high pollution risk due to intense human activities (Voudouris 2009). Vulnerability maps are a useful tool for groundwater protection and land use planning. Their reliability is depending on data availability, density and accuracy (Vrba and Zaporozec 1994).

In order to assess the groundwater vulnerability against pollution many methods have been developed. Each method uses different number of parameters ranging between 2 (e.g. AVI method–Van Stempvoort et al. 1992) and 7 (e.g. DRASTIC-Aller et al. 1987; SINTACS-Civita 1994). On the one hand, the use of large number of parameters allows one to simulate complex hydrogeological conditions (Gogu et al. 2003). On the other hand, the large number of parameters requires many data (meteorological, hydrogeological, soil data etc), their collection of which is difficult and time-consuming. Furthermore, the required data should be independent with high level of accuracy in order to be avoided inappropriate

N. Lambrakis et al. (Eds.), *Advances in the Research of Aquatic Environment, Vol. 2*
DOI 10.1007/978-3-642-24076-8,

protection zoning. The methods which involve fewer parameters are easily applicable, but they are generally difficult adaptable to specific geological conditions.

In this work, three different methods of intrinsic vulnerability mapping were applied in the alluvial aquifer of Florina basin, NW Greece: AVI (Van Stempvoort et al. 1992), DRASTIC (Aller et al. 1987) and GOD (Foster 1987). Vulnerability maps were illustrated from the aforementioned applied methods in GIS context (Arc/Info). The aim of this study was to compare the three methods and the producing vulnerability maps. Firstly, the hydrogeological study was carried out, in the frame of which the following data were collected: rainfall and temperature data, pumping test data, collection of 80 lithological profiles of drilled boreholes and water table measurements. Furthermore, many previous data concerning of geological conditions and soil texture data were performed. All existing geological, hydrogeological, and hydrochemical data were evaluated and reworked.

2 Description of the study area

Florina basin is located in the central part of Florina Prefecture, West Macedonia region, Greece, covering a total area about of 319 Km^2. The mean altitude of the basin is about 620 m (asl) and the mean slope 1.5%.

The land is used mainly for cultivation of cereals and cows and sheep graze the area. In a large part of the area irrigated agriculture is practiced. Lignite deposits have been occurred in the neogene sediments of the basin. The area is characterized by a semi-arid, Mediterranean climate, with an annual temperature of 12.6 °C and an annual rainfall of 472 mm. About 70-80% of annual rainfall occurs in wet period, while summers are usually dry.

3 Geological and Hydrogeological setting

From a geological point of view, the Florina basin is part of the Pelagonian geotectonic zone. The mountainous area of the basin is dominated by carbonate and crystalline rocks (Kazakis 2008). The lowlands of the study area consist of Neogene and Quaternary sediments. The Quaternary sediments are alluvial deposits and consist of alternations of sands, gravels, conglomerates and clays, while the Neogene sediments consist of marls, sandstone, sands and marly limestones.

In the study area two aquifer systems can be distinguished, one alluvial aquifer covering an area about 180 km^2 and the second one of low hydrogeological interest in Neogene deposits. The water needs of the basin, are predominantly being covered by the exploitation of the alluvial aquifer. The hydraulic conductivity (k) values of the alluvial aquifer range between $3x10^{-3}$ m/s and $4x10^{-6}$ m/s, as deduced from pumping tests. The depth of ground water ranges from less than 1 m to more than 45 m below ground surface.

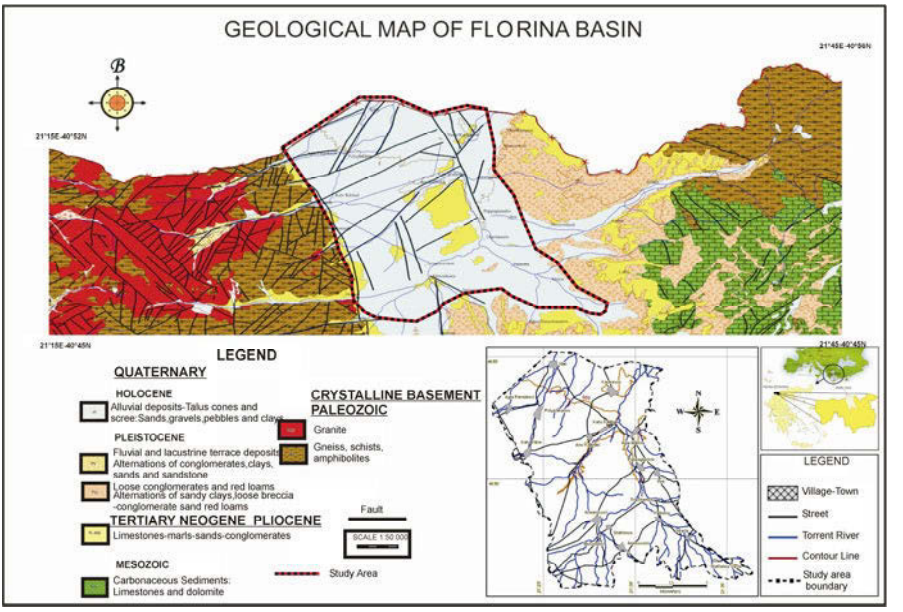

Fig. 1. Geological and topographic map of the study area (Modified from IGME Sheets Vevi and Florina, scale 1:50,000).

4 Applied methods

DRASTIC method (Aller et al. 1987) evaluates vertical vulnerability using seven parameters: Depth to groundwater, Aquifer media, net Recharge, Topography, Soil media, Impact of the vadose zone and Hydraulic Conductivity. Determination of the DRASTIC index involves multiplying each parameter weight by its site rating and summing the total. The equation for the DRASTIC Index (DI) is:

$$DI = \sum_{j=1}^{7} r_j . w_j$$

or DI=DrDw+RrRw+ArAw+SrSw+TrTw+IrIw+CrCw

where: D, R, A, S, T, I, C were defined earlier, r is the rating for the study area and w is the importance weight for the parameter. Each parameter including in the index must have a numeric value assigned between 1 and 10.

The higher the index, the greater is the groundwater pollution potential or greater aquifer vulnerability (Al-Zabet 2002). Parameters used by aforementioned method are derivable from monitoring gauges, hydrogeological field surveys in-

cluding water level measurements, pumping tests and soil analyses, as well as aero-photo and remote sensing studies (Al-Adamat 2003; Panagopoulos et al. 2005). Stigter et al. (2006) and Martinez-Bastida et al. (2010) highlight that none of the parameters used in the DRASTIC method account for the influence of groundwater flow direction, a property that greatly influences whether some parts of the aquifer receive groundwater from a larger area than others.

The **GOD** method (Foster 1987) is an empirical method for the assessment of aquifer pollution vulnerability. This method uses three parameters: (1) Groundwater occurrence, (2) Overlying Lithology, (3) Depth to groundwater. The second parameter is taken into account only in unconfined aquifers. The parameters assigned a value from 0 to 1. The equation for the GOD Index (I) is:

$$I = G \cdot O \cdot D$$

The *AVI* method proposed by Van Stempoort et al. (1992), computes the Aquifer Vulnerability Index (AVI) using two parameters: the thickness of each sedimentary unit above the uppermost aquifer (d), and the estimated hydraulic conductivity of each of these layers (k). The hydraulic resistance for layers 1 to i is:

$$c = \Sigma\, d_i/K_i$$

Table 1. Values of the respective classes for each method.

Classes	INDEX		
	GOD	AVI	DRASTIC
High	0.6-1	< 0	>140
Medium	0.3-0.6	0 - 4	100-140
Low	0-0.3	>4	<100

The c or logc value is a qualitative Aquifer Vulnerability Index by a relationship table. Three vulnerability maps were produced using the classification of Table 1. The vulnerability maps are presented in Figure 2.

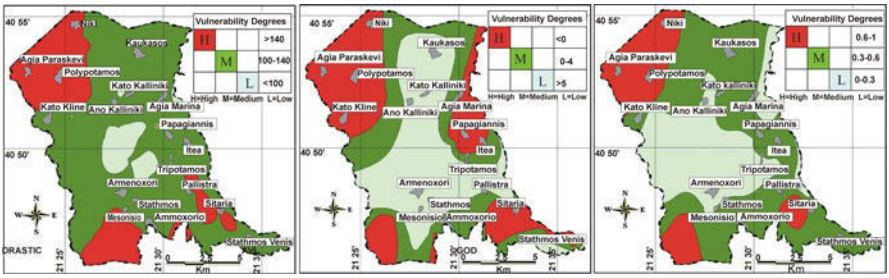

Fig. 2. Groundwater vulnerability maps with DRASTIC, AVI and GOD methods.

5 Comparison between the parametric methods

A quantitative comparison of vulnerability methods involves a normalization procedure to obtain comparable values. To make the normalization, many factors have to be considered such as the maximum and minimum values of each method and the procedure of stretching the vulnerability values between the maximum and minimum values (Corniello et al. 1997). For this reason three classes for the methods DRASTIC, AVI and GOD have been defined (Table 1). The areas representing the vulnerability classes obtained from the three methods in Km^2, as well as in percentages of the entire study area are shown in Table 2.

Table 2. Comparison between the areas representing the vulnerability classes.

Classes	DRASTIC		GOD		AVI	
	km^2	%	km^2	%	km^2	%
High	44.01	23.91	34.56	18.77	61.25	33.27
Medium	128.38	69.73	93.24	50.65	52.61	28.58
Low	11.71	6.36	56.3	30.58	70.24	38.15
total	184.1	100.0	184.1	100	184.1	100.0

According to Table 2, DRASTIC and GOD methods classify the largest area of the basin as medium vulnerability, while AVI method classifies it as high. Based on the DRASTIC method the smallest part of the area is low vulnerability.

Table 3. Correlation matrix between the maps computed using DRASTIC, AVI and GOD.

	GOD	AVI	DRASTIC
DRASTIC	0.76	0.27	1.00
AVI	0.46	1.00	
GOD	1.00		

The results of the correlation analysis between the three methods (linear regression analysis) are presented in Table 3. The highest correlation is shown between DRASTIC and GOD methods, while the lowest correlation between AVI and DRASTIC methods.

For better presentation of the differences between the three methods, the covering areas (Km^2) are presented in a histogram (Fig. 3). The graph shows that the distribution of the classes is uniform in AVI method and unimodal in medium class in DRASTIC and GOD method.

The differences between the three methods are associated with the fact that the calculation of each index takes into account different number of parameters with different weights. For the more integrated comparison, the created maps of common areas of the three methods (Fig. 4, 5) between DRASTIC-GOD, DRASTIC-AVI, GOD-AVI and DRASTIC-AVI-GOD were used.

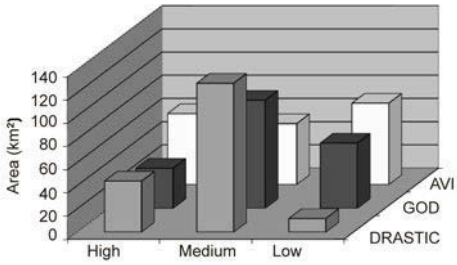

Fig. 3. Histogram showing the comparison of the areas between the vulnerability classes.

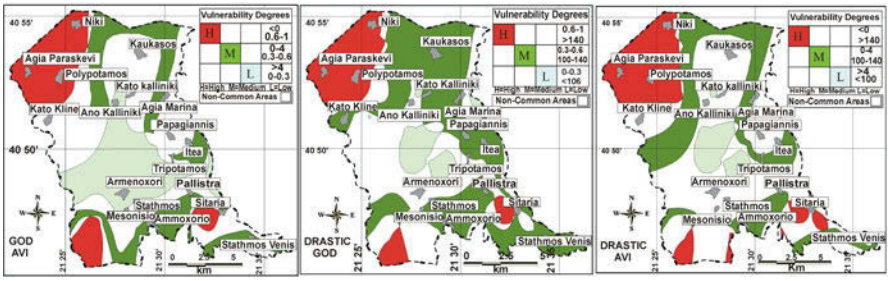

Fig. 4. Maps with common areas between the three methods.

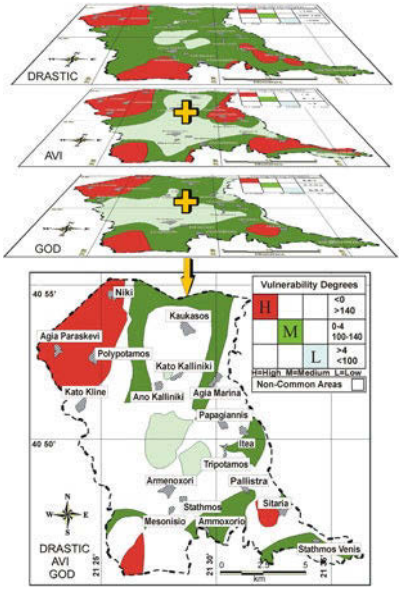

Fig. 5. Map of common areas between the three methods.

The results are shown in Table 4. Based on this Table it is concluded that, the classes of DRASTIC and GOD methods have the greater coincidence in percent 63.3%, while DRASTIC and AVI have the lower (48.4%). The three methods identify in 37.8%, while the area with high vulnerability covers 38.2%.

Table 4. Comparison of common areas between the three methods.

Classes	Drastic-GOD		Drastic-AVI		GOD-AVI		Drastic-AVI-GOD	
	km^2	%	km^2	%	km^2	%	km^2	%
High	28.42	24.37	32.30	36.26	31.8	30.23	26.64	38.23
Medium	77.26	66.27	45.94	51.56	37.76	35.89	32.82	47.10
Low	10.92	9.36	10.86	12.18	35.64	33.88	10.22	14.67
Total	116.6	63.33	89.1	48.39	105.2	57.14	69.68	37.85

According to the three applied methods, areas with high vulnerability are located in the northwestern and southwestern parts and in a small part between Sitaria and Pallistra village of the Florina basin. Low vulnerability values are recorded in the central part of the basin. The rest of the basin is characterized by medium vulnerability values with significant differences among the three methods.

Furthermore, it is concluded that the depth of groundwater table is very important parameter for the three methods, because the great depth is associated with low vulnerability values (Voudouris et al. 2010). Based on the results of chemical analyses (Gianneli et al. 2007) it is concluded that area of high vulnerability is related to high nitrate concentrations in groundwater.

6 Conclusions

Based on the comparison of the three applied methods DRASTIC, AVI and GOD the following considerations can be revealed:

1. According to DRASTIC and GOD methods, medium vulnerability zones cover the largest area in Florina basin, while using AVI method the largest part of the basin was estimated to be of low vulnerability.
2. The higher correlation and coincidence has been observed between the methods DRASTIC and GOD and the lower correlation between the methods DRASTIC and AVI.
3. The differences between the three methods are associated with the fact that the calculation of the indices of each method take into account different number of parameters with different weights.
4. The three methods identify in percent 38%, indicating that the methods produce different results.

The application of GOD method is more simple than the DRASTIC method. The GOD method should be applied before DRASTIC method in a region in order to make a rapid assessment of groundwater vulnerability of the region and guide the field research focusing on specific areas.

References

Al-Adamat RAN, Foster IDL, Baban SMJ (2003) Groundwater vulnerability and risk mapping for the basaltic aquifer of the Azraq basin of Jordan using GIS, Remote sensing and DRASTIC. Applied Geography 23, 303-324

Aller L, Bennett T, Lehr JH, Petty, RJ, Hackett G (1987) DRASTIC: A standardized system for evaluating ground water pollution potential using hydrogeologic settings. US Environmental Protection Agency, Report 600/2-85/018, Washington

Al-Zabet T (2002) Evaluation of aquifer vulnerability to contamination potential using the DRASTIC method. Environmental Geology 43, 203-208

Civita M (1994) Le carte della vulnerabilità degli acquiferi all' inquinamento. Teoria and practica. (Aquifer pollution vulnerability maps). Pitarora Ed., Bologna (in Italian)

Corniello A, Ducci D, Napolitano P (1997) Comparison between parametric methods to evaluate aquifer pollution vulnerability using a GIS: An example in the 'Piana Campana', southern Italy. In: Marinos P, Koukis G., Tsiambaos G., Stournaras G. (Eds) Engineering Geology and the Environment, Balkema, Rotterdam, 1721-1726

Foster SSD (1987) Fundamental concepts in aquifer vulnerability, pollution risk and protection strategy. In Van Duijvenbooden W, Waegeningh HG (eds) TNO Committee on Hydrological research, the Hague. Vulnerability of soil and groundwater to pollutants, Proc. Inf. 38, 69-86

Gianneli Ch, Stamos Al, Stamos Ap, Voudouris K (2007) Surface and groundwater quality in Florina prefecture. Proc. 1st Conf. on Environmental Management, Engineering, Planning and Economics (CEMEPE). Skiathos, June 24-28, 765-770

Gogu RC, Hallet V, Dassargues A (2003) Comparison of aquifer vulnerability assessment techniques. Application to the Néblon river basin (Belgium). Env. Geology 44, 881-892

Kazakis N (2008) Groundwater vulnerability assessment in Florina basin. MSc thesis, Dept. of Geology, Aristotle University of Thessaloniki, Greece (in Greek)

Martinez-Bastida JJ, Arauzp M, Valladolid M (2010) Intrinsic and specific vulnerability of groundwater in central Spain: the risk of nitrate pollution. Hydrogeology J. 18, 681-698

Panagopoulos G, Antonakos A, Lambrakis N (2005) Optimization of the DRASTIC method for groundwater vulnerability assessment via the use of simple statistical methods and GIS. Hydrogeology Journal 14, 894-911

Polemio M, Casarano D, Limoni PP (2009) Karstic aquifer vulnerability assessment methods and results at a test site (Apulia, southern Italy). Natural Hazards and Earth System Sciences 9(4), 1461-1470.

Stigter TY, Riberio L, Carvalho Dill, AMM (2006) Evaluation of an intrinsic and specific vulnerability assessment method in comparison with groundwater salinisation and nitrate contamination levels in two agricultural regions in the S. Portugal. Hydrogeology J. 14, 79-99

Van Stempoort D, Ewert L, Wassenaar L (1993) Aquifer vulnerability index (AVI): a GIS compatible method for groundwater vulnerability mapping. Can. Water Res. J. 18, 25-37

Voudouris K, Manos B et al. (2007) Development and utilization of vulnerability maps for the monitoring and management of groundwater resources in the ARCHIMED areas: Presentation of an INTERREG III B Project. Proc. of International Scientific Conference

"Modern Management of Mine Producing, Geology and Environmental Protection (SGEM 2007)". 11-15 June, Varna, Bulgaria

Voudouris K (2009) Assessing groundwater pollution risk in Sarigkiol basin, NW Greece. In: M. Gallo and M. Herrari (Eds) River Pollution Research Progress, Chapter 7, 265-281. Nova Science Publishers Inc

Voudouris K, Kazakis N, Polemio M, Kareklas K (2010) Assessment of intrinsic vulnerability using DRASTIC model and GIS in the Kiti aquifer, Cyprus. European Water 30, 13-24

Vrba J, Zaporozec A (1994) Guidebook on mapping groundwater vulnerability. Int. Association of Hydrogeologists. Int. Contributions to Hydrogeology; 16. Verlag Heinz Heise, Hannover

Degradation of groundwater quality in Stoupa-Ag.Nikolaos region (W.Mani Peninsula) due to seawater intrusion and anthropogenic effects

G. Stamatis, D. Gamvroula, E. Dikarou, A. Kontari

Agricultural University of Athens, Institute of Mineralogy-Geology, Iera Odos 75, GR-118 55 Athens, stamatis@aua.gr

Abstract The study of the hydrogeological conditions of the Stoupa-Ag. Nikolaos region (W. Mani) aimed the investigation of groundwater quality, analyzing the factors that caused its degradation due to seawater intrusion and anthropogenic effects. The study area is consisted of kastified carbonate rocks, flysch, Neogene sediments and Quaternary deposits. Two major aquifers are been distinguished, the karstic aquifer which is developed within the karstic carbonate formations and the shallow aquifer established within the Quaternary deposits and Neogene sediments of the plain area. Groundwater discharges through coastal and submarine springs into the Messinian gulf. The most dominant watertypes of the springs in mountainous and semi mountainous areas are Ca-HCO_3 and Ca-Mg-HCO_3, while no influence of surface pollutants is detected. On the other hand, in the plain area, the phreatic aquifer is characterized by Ca-Mg-Na-Cl-HCO_3 and Mg-Na-Cl-SO_4-HCO_3 watertypes, being influenced by the seawater intrusion -due to the overexploitation of the aquifer and the intense anthropogenic interference- is considered to be inappropriate for human consumption.

1 Introduction

The karst system of SW Taygetos develops at W. Mani region and is consisted of karstic carbonate Cretaceous and Triassic-Jurassic formations. The rich karstic aquifer discharges through coastal springs, but mainly through a great number of submarine springs in the gulf beween Kardamili, Stoupa and Ag. Nikolaos regions. The Karst system developed within the tectonic discontinuities in the area; contribute decisively to the evolution of the hydrogeological regime. The main issue of the Lefktron's Municipality is the inadequacy of water needs. The problem becomes even more pronounced during the dry period, when the water needs increase significantly. Actually, the municipality draws water from local dug wells and drilled wells partially covering the water needs. However, the overpumping of

N. Lambrakis et al. (Eds.), *Advances in the Research of Aquatic Environment, Vol. 2*
DOI 10.1007/978-3-642-24076-8, © Springer-Verlag Berlin Heidelberg 2011

the drilled wells causes severe salinity problems, especially during the dry period. The study aimed to the investigation of a) the hydrogeological regime prevailing in the region, b) the groundwater quality and the suitability for human consumption and c) the localization of new aquifers in order to partially alleviate the water shortage (Stamatis et al. 2009). The research was funded by the municipality of Lefktron and Messinia Prefecture.

2 Geological and hydrogeological setting

The study area is part of the Mani geotectonic unit, which appears as a tectonic window. Above the Mani unit there is a sequence of thrusts. Different nappes res on top including successively from the base to the top the Arna unit, the Tripolis unit and the Pindos unit (northwards) respectively. The geological setting of the region (Fig. 1) comprises i) Quaternary loose deposits (alluvial deposits, scree, old and recent fans, conglomerates of terraces), ii) Neogene sediments, which dominate in the coastal area and consisted of marine and partly lacustrine formations, iii) Flysch of the Mani unit, slightly metamorphic into shales with sandstone intercalations, with variable thickness 60-100m, iv) Limestones (Upper Cretaceous-Eocene), strongly folded, fractured and karstified, with up to 400m thickness, v) Multimix formations with alternations of marbles, dolomites, schists and phyllites of variable thickness (50-250m), vi) Crystalline limestones and dolomites (M. Triassic- L. Jurassic), medium-bedded, folded, fractured and karstified, more than 1000m thick., which overlie uncomformably the phyllite basement, vii) Calcite - quartzite phyllites and schists of the crystalline basement, more than 250m thick . The Alpine formations are strongly folded and thus long anticline and syncline structures have been formed with N-NNW axial direction. The faults are well developed, interrupting the continuity of the geological formations and are basically responsible for the coastal and semi-mountainous geomorphology development. Within the area older faults of N-S direction, as well as younger E-W transverse faults, had been identified. The geological formations of Mani unit are the main contributing factor to the configuration of the hydrogeological conditions in the region. More specific, the carbonate rocks prevailing in the region, the limited appearance of the crystalline phyllites' basement, the scalelike arrangement of the layers, the brittle tectonics and all kinds of discontinuities which subdivide the permeable rocks (Migiros et al., 2008, Papanikolaou D. and Skarpelis N., 1987).

Two major aquifers are been distinguished, the karstic aquifer which is developed within the karstic carbonate formations and the phreatic aquifer found within the Quaternary deposits and Neogene sediments of the plain area. In the mountainous area aquifers of low potential were identified which discharge through several contact springs of low discharge rates, such as the springs a) within the flysch, due to its lithologic heterogeneity, b) at the contact of the U. Cretaceous-

Eocene carbonate formations with the multimix formation of the L. Cretaceous-M. Jurassic. Smaller springs appear in the plain and semi-mountainous area mainly within the Plio-Pleistocene formation due to their multimix character. At the coastal and submarine area scattered springs of high discharge rates drain the karst aquifer. Both coastal and mountainous springs show strong seasonal discharge variations. The tectonic structures determine the groundwater flow direction within the plain area, the groundwater flows W-SW to the Stoupa bay and Ag. Nikolaos region (Fig. 2).

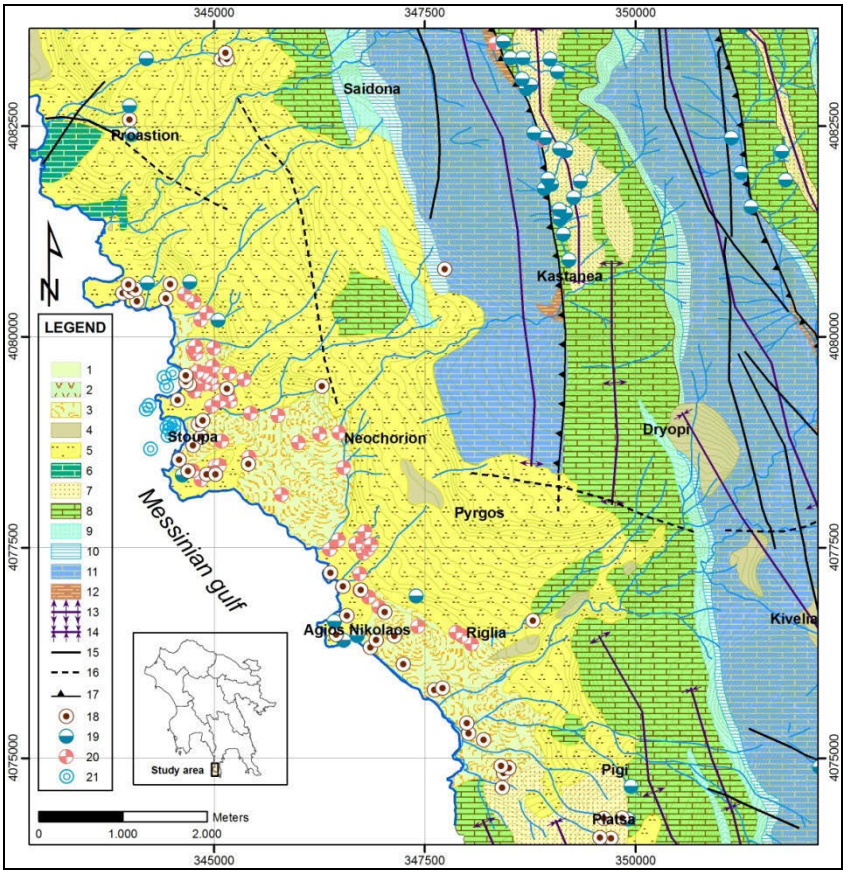

Fig. 1. A simplified geological map of the study area (Psonis K. et al., IGME, 1986): 1: Alluvial deposits (Holocene); 2: Scree (Holocene); 3: Old & recent fans (Holocene); 4: Terraces (Pleistocene); 5: Marine formations (Pliocene); 6: Limestones, dolomitic limestones (Cretaceous-U.Jurassic); 7: Flysch (U.Eocene-Oligocene); 8: Limestones (U.Senonian- U.Eocene); 9: Crystalline limestones (U.Jurassic-Cretaceous); 10: Sillicate schists (L.-M.Jurassic); 11: Dolomitic limestones- dolomites (M.-L. Triassic); 12: Phyllite-quartite series (Permian-L.Triassic); 13: Antcline; 14: Syncline; 15: Normal; 16: Probable; 17: Overthrust; 18: Well; 19: Coastal spring; 20: Borehole; 21: Submarine spring.

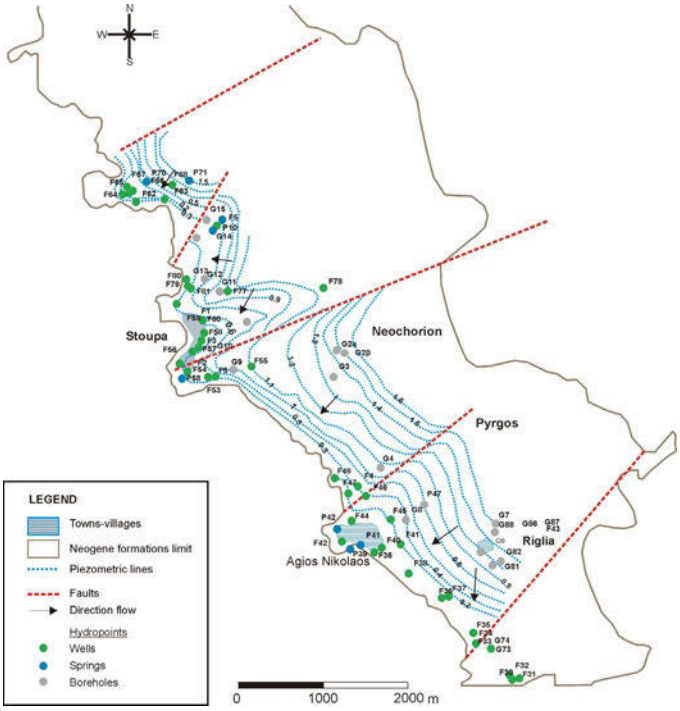

Fig. 2. Piezometric map of the plain area.

The piezometry in the area is characterized by low hydraulic gradients ranging from 1-2‰. The phreatic aquifer of the plain area is of intense exploitation from a large number of wells and boreholes for water needs. The discharge rate of drug wells is of the order of 10-15m^3/h while of the drilled wells is estimated at 30-40m^3/h.

3 Groundwater quality

Towards the end of the wet period (April 2010), water sampling of springs, dug wells and drilled wells took place in the area. Portable instruments were used in order to measure in situ the physicochemical parameters, such as temperature (ºC) and Electrical Conductivity EC (WTW/LF-330), pH, Eh (WTW/330i), dissolved Oxygen DO (mg/L) (WTW/OXI-96) values and discharge rates Q·l/s (Flow Probe FP101/Global Water). Additionally, in the laboratory of Mineralogy & Geology of the Agricultural University of Athens, with the implementation of titration methods, spectral photometer (HACH, DR /3000), flame photometer (INTECH /420) and atomic absorption spectrometer (GBC/908/AA), the following parameters were measured: Hardness, Ca^{2+}, Mg^{2+}, Na^{+}, K^{+}, HCO_3^{-}, Cl^{-}, SO_4^{2-}, NO_3^{-}, NH_4^{+}, PO_4^{3-}, Cd^{2+}, Pb^{2+}, Fe_{tot}, Cu^{2+}, Zn^{2+}. Table 1 presents the results of the analyses.

Table 1. Results of the chemical analyses.

Sampling ID	Springs		Boreholes		Wells	
	Min-Max	Aver.	Min-Max	Aver.	Min-Max	Aver.
Temperature °C	8.8-18.0	12.6	15.8-20.5	19.3	17.5-18.4	18.1
Ec (μS/cm)	65.0-795.0	311.8	539-1751	968.5	822.0-1888.0	1339
Ph	6.6-8.2	7.6	7.0-8.3	7.6	7.0-8.1	7.4
TDS (mg/L)	91- 749	328	450-1194	731	764-1437	1030
Hardness (°dH)						
Total	2.36-18.99	10.2	14.04-30.34	19.3	16.63-49.66	26.45
Temporal	2.24-19.88	9.36	9.52-15.68	12.26	10.92-22.96	16.08
Permanent	0.07-1.61	1.05	3.46-16.9	7.04	3.26-33.14	10.87
Elements (mg/L)						
Ca^{2+}	12.0-132.0	51.2	72.0-216.0	111.8	68.8-328.0	159.3
Mg^{2+}	2.2-32.4	13.2	0.4-37.3	15.8	1.4-31.6	20.2
Na^{+}	5.7-62.2	15	12.9-185.0	83.1	55.2-198.2	122.5
K^{+}	0.00-2.4	0.4	0.04-7.8	3	0.5-7.1	3.1
HCO_3^{-}	48.8-433.1	204	207.4-341.6	267.09	237.9-500.2	350.4
Cl^{-}	7.1-74.5	20.5	31.9-414.9	172.75	85.1-365.3	249.4
SO_4^{2-}	3.0-28.5	44.6	9.4-140.0	41.99	55.9-245.7	92.6
NO_3^{-}	7.0-13.6	9.3	12.8-58.1	32.59	11.0-50.2	30.8
NH_4^{+}	0.00-0.13	0.03	0.01-0.18	0.08	0.01-0.95	0.24
PO_4^{3-}	0.07-0.58	0.22	0.08-0.22	0.14	0.06-0.24	0.16
Cd^{2+}	0.01-0.06	0.04	0.01-0.07	0.04	0.03-0.09	0.05
Pb^{2+}	0.001-0.11	0.05	0.001-0.42	0.09	0.04-0.31	0.13
Fe_{tot}	0.001-0.04	0.03	0.001-0.08	0.04	0.001-0.03	<0.001
Cu^{2+}	0.04-0.09	0.07	0.07-0.09	0.08	0.07-0.09	0.08
Zn^{2+}	0.001-0.02	0.01	0.001-0.31	0.08	0.001-0.15	0.05

According to Table 1, water of springs within the flysch and metamorphic formations of the mountainous and semi-mountainous area, is characterized by low TDS concentration (TDS: 328 mg/L), low hardness values (°dH: 10.2 german degrees), slightly alkaline character (pH: 7.6), absence of anthropogenic pollutants, (NO_3^{-}: 9.3, NH_4^{+}: 0.03, PO_4^{3-}: 0.22 mg/L) and significantly low concentrations of heavy metals. In general, according to the Directive EU98/33, the parametric values of spring waters are low, they are of high quality and suitable for human consumption. On the other hand, water from wells and boreholes tapping the phreatic aquifers of the plain area, is characterized by high TDS concentration (TDS: 1030 mg/L), high values of hardness (°dH: 26.45 german degrees), significant local presence of anthropogenic pollutants (NO_3^{-}: 32.6, NH_4^{+}: 0.24, PO_4^{3-}: 0.16 mg/L), high seawater intrusion (Cl^{-}: 249.4 mg/L, Na^{+}:122.5 mg/L, SO_4^{2-}:92.6 mg/L), as well as high concentrations of heavy metals. Generally, waters of the plain area

undergo intense degradation, mainly due to overpumping, that leads to seawater intrusion and to surface pollutants' infiltration by the the agricultural activities. Most samples exceed the upper permitted limits of the Directive EU98/83 and therefore the water is unsuitable for human consumption.

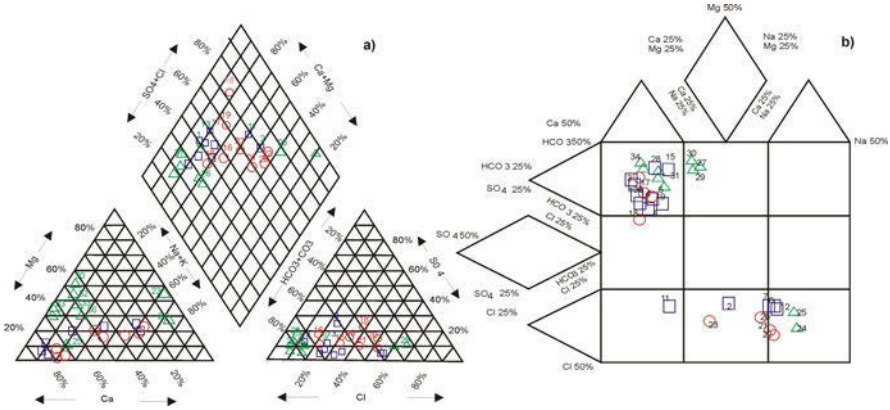

Fig. 3: Piper (a) and Durov (b) Plots, showing the composition of groundwater (Δ: Springs, □: Boreholes, ○: Wells).

According to the Piper diagram (Fig. 3a), groundwater is classified into the following categories, according to its hydrochemical composition: i) the geoalkaline springwater of the semi-mountainous and mountainous area, with Ca-HCO_3 and Ca-Mg-HCO_3 water type, it is fresh water and the presence of Ca^{2+} and Mg^{2+} is due to the dissolution of the calcite and the dolomite of the carbonate formations, ii) the brackish springwater of the coastal area with Na-Cl-HCO_3 water type, due to karstic water and seawater mixture and iii) the geoalkaline- with high concentration in alkalines- water of wells and boreholes of the plain area, with Ca-Mg-Na-HCO_3, Ca-Mg-Na-Cl-HCO_3 and Mg-Na-Cl-SO_4-HCO_3 water types, revealing the sea influence. Becoming the exception, a small number of boreholes, belong to Ca-HCO_3 and Ca-Mg-HCO_3 water types, showing the enrichment of their recharge area with fresh karstic water. As far as the Durov diagram is concerned (Fig. 3b), the majority of the study area (64 % of the boreholes, 44% of the wells and 87% of the springs), belongs to Ca-HCO_3 and Mg-HCO_3 water type and is characterized as enriched fresh water (Apelo and Postma 2005). A small number of boreholes, wells and springs, belong to the Na-Cl, Mg-Cl and Ca-Cl water type, revealing phenomena of reverse cations exchange, as well as brackish water of coastal springs, wells and boreholes that have been intensively intruded by the sea.

Figure 4 presents the spatial distribution of specific physicochemical parameters. EC's distribution reveals a couple of seawater intrusion fronts, as well as areas of high salinity values at the north and south part of the study area. The highest values are found at the south part, near Agios Nikoalos region. The seawater intrusion is influenced by the fault zones, the karstification of the Upper Creta-

ceous carbonate formations and by the overexploitation of the karstic aquifer. Ions of Cl^- indicate similar distribution as EC, while the distribution of NO_3^- and PO_4^{3-} ions reveal areas of intense human activity, such as the presence of septic tanks and farms.

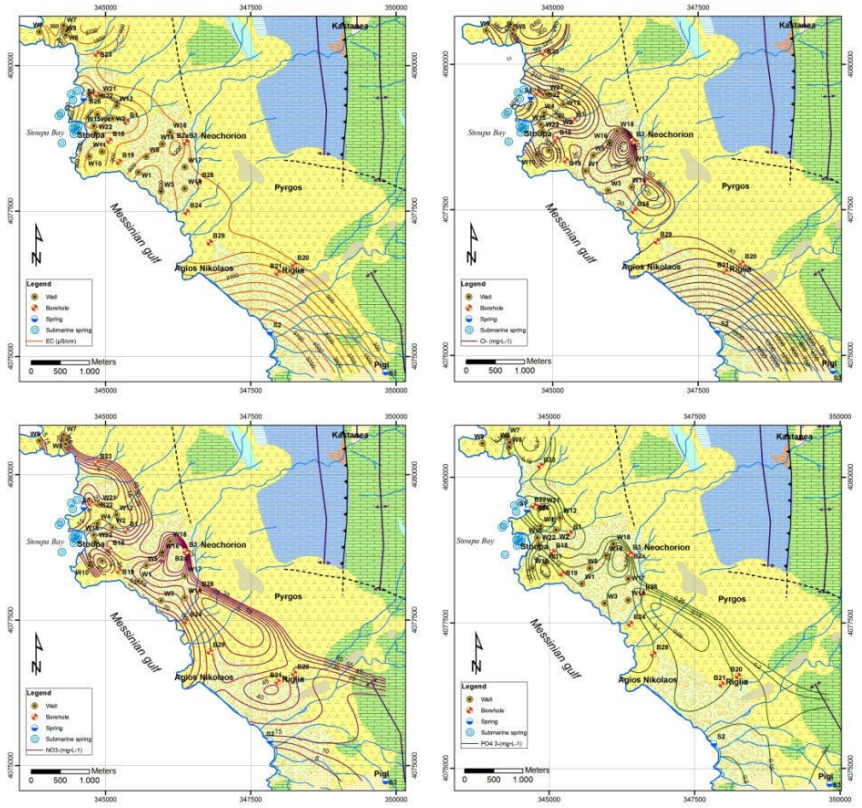

Fig. 4. Spatial distribution of the EC (μS/cm); Cl^- (mg/L); NO_3^-(mg/L) and PO_4^{3-}(mg/L).

Conclusions

The hydrogeological study of Stoupa- Ag. Nikolaos region yielded the following results: i) the orientation of the groundwater flow and the appearance of coastal and submarine karstic springs, are influenced by the intense karstification of the carbonate rocks of the Mani unit, the structure and the fracture zones of the area, ii) the springs of the mountainous area present low discharge rates, are characterized by low salt concentration, acidic to alcalic character, absence of anthropogenic effects and significantly low concentration of heavy metals. They are of

high quality and thus suitable for human consumption, iii) in the plain and coastal area, where the phreatic aquifer is developed, high salinization of the groundwater is observed, which is attributed to both natural factors and anthropogenic influences. Specifically, at the northwest and southern part distinct fronts of sea intrusion are observed, related to the fault zones and the overexploitation of water wells leading to chloride concentration to the order of 415mg/L, iv) in the residential areas and farmlands, high concentrations of Na^+, Cl^-, SO_4^{2-}, NO_3^-, NH_4^+ and PO_4^{3-} are observed, revealing the anthropogenic influence. Finally, water from dug wells are unsuitable for human consumption, while a small number of drilled wells, tapping the karst aquifer, is of high quality and suitable for human consumption.

References

Apelo, C. A. J. and Postma, D., (2005): Geochemistry, Groundwater and Pollution, A. A. Balkema, Rotterdam, Brookfield

Migiros G., Psomiadis E., Papanikolaou I., Karamousalis T., Stamatis G. (2008). Groundwater coastal discharge of the karstic system of Mani Peninsula, southern Peloponnesus- Greece, Proceedings of the 8th Int. Hydrogeological Congrss of Creece and 3rd MEMWorkshop on Fissured rocks Hydrology, Athens 2008, 1:317-326

Papanikolaou D. and Skarpelis N. 1987. The blueschists in the external metamorphic belt of the Hellenides: composition, structures and geotectonic significance of the Arna Unit. Geol Pays Hellen. 33:47-68

Psonis K., Tsapralis B., Skourtsi-Koronaiou B., Varti-Mataragka M. and Petridou B. (1986) : Geological map of Greece 1 :50.000, Xirokampion Sheet, IGME, Athens 1986

Stamatis G.(2009). Integrated marine and terrestrial study to the investigation of the quantity, quality and exploitation of the submarine spring (Anavalos), Stoupa, Messinia Prefecture. Progress report II. Unpublished report, pp 140. Agricultural University of Athens

Quality Characteristics of groundwater resources in Almyros Basin coastal area, Magnesia Prefecture Greece

Ch. Myriounis[1], G. Dimopoulos[2], A. Manakos[3]

[1]Dr. Geologist – Rural and Surveyor Engineer – Igoumenitsa P. Tsaldari 17 46100 cmyriounis@teemail.gr,

[2]School of Geology Aristotle University of Thessaloniki,

[3]I.G.M.E. Department of Central Macedonia

Abstract In this paper, groundwater quality characteristics of the coastal area of Almyros hydrological basin, which belongs in the Magnesia Prefecrure, Greece are analyzed. Geological, tectonic and stromatographic conditions of the coastal area, are described. Description and analysis of the hydrogeological conditions that dominate the region and the quality characteristics of groundwater resources of the area follows. Particular attention is given to the phenomena of seawater intrusion and nitrate pollution. The general conclusion is that groundwater resources of the study area are affected by the seawater intrusion phenomenon, mainly at the northern and the southern area of the coastal region, due to local geological and tectonic characteristics, refreshing conditions and overexploitation of the groundwater resources.

1 Introduction

Almyros basin is situated in Magnesia Prefecture in Thessaly Greece, south of the city of Volos, belongs to Almyros Municipality and covers an area of about 1000 km^2. The area of interest covers an area of 134.32 km^2 in the coastal part of Almyros basin and includes N.Anchialos, Mikrothives, Agia Triada, Sourpi and Drimonas settlements. To the north the area is bounded by the N.Anchialos fault zone, Drimonas village to the south and the limits of the coastal zone to the west (Fig.1).

The scope of the current study is the analysis of groundwater quality data for the coastal part of Almyros basin using geological, tectonic, hydrogeological and hydrochemical data. Particular attention is given to the phenomena of seawater intrusion and nitrate pollution.

N. Lambrakis et al. (Eds.), *Advances in the Research of Aquatic Environment, Vol. 2*
DOI 10.1007/978-3-642-24076-8, © Springer-Verlag Berlin Heidelberg 2011

2 Geologic and Tectonic setting

Alpine sediments of the Almyros basin belong to the Sub-Pelagonian and Pelagonian geotectonic units of the Hellenic Alpine System (Fig. 1).

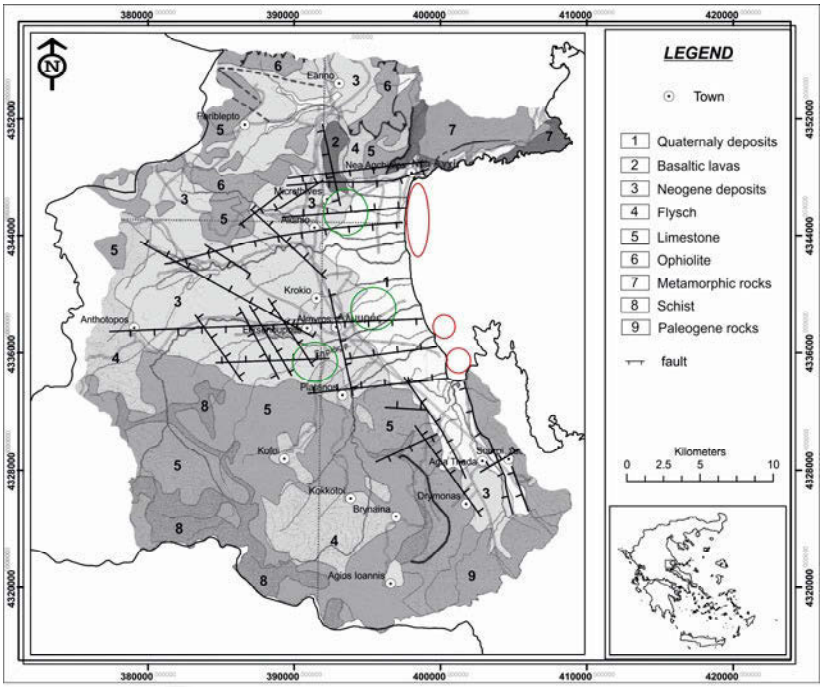

Fig. 1. General geologic map of Almyros basin. Submarine springs and outflows are marked with red color and artesian points with green color). From IGME and modified by Myrioynis (2008).

In brief, for the broad area Pelagonian formations include pre-alpine basement rocks, schists, carbonate schists and ultramafic rocks. Formations of Sub-pelagonian geotectonic unit that are found in the area are Paleozoic rocks (of Permian age), crystalline limestones of Triassic-Jurassic age, schist-chert unit along with ophiolites, limestones and flysch.

According to the stratigraphic setting of post-alpine sediments, Neogene sediments, fossiliferous and rich in lignite (marls), of lacustrine character and Early Pliocene age can be found there. In the Upper Pliocene, deposition of sub-yellow clayey marls take place, interrupted during short periods of semi-arid continental setting. Finally, during Pleistocene there is a dominant continental sedimentation, by coarse fluvioterrestrial deposits.

Almyros basin from a gemorphological point of view can be divided into two distinct watershed, Sourpi to the south, and Efxenoupoli in the northern part, fur-

ther divided into smaller watersheds. According to Galanakis (1997), relief in Almyros Basin is primarily controlled by tectonic activity in recent faults since Pliocene, many of whom are being re-activated during Quaternary period, and secondarily by climatic setting and differential erosion of rock formations. A distinct characteristic of Almyros Basin is its tilting towards east, along an north-south hypothetical axis crossing its central part.

3 Hydrogeological setting of coastal area

The hydrogeological conditions of the Almyros basin are affected by the karstic system of Northeastern Othris, in which the brackish water karstic spring of Kefalosi exists. The Kefalosi spring controls the hydrogeological conditions of the southern part of the study area and is characterized by high capacity. The Kefalosi spring is located at the karstic formation of Othris in the southern part of sub basin Efxenoupolis, eastly of the village Platanos. The spring is placed in an altitude 26.5 m above sea level and in a distance of 3250 m from the coast. According to Dimoloulos (1983, 1984), Myriounis (2008), the spring is characterized by brackish water which caused by mixing freshwater and seawater. The salinity of the spring is associated with the geological and tectonic conditions of the wider area.

In Sourpi area can be found the homonymous karst aquifer system, of dolomotic and carbonate composition. In this karst system, water drillings show better qualitative characteristic in contrast to the Othris aquifer system. This system consists of high capacity carbonate rocks and is marked by extensive seawater intrusion due to the hydraulic connection of carbonate aquifers with the seawater.

Neogene sediment aquifer system consist of alterations of coarse and fine grained material, creating free and under-pressure aquifers. Moving to the west, neogene sediment aquifers show lower capacity due to their lithological composition and their supply condition. Quaternary sediments cover the largest part of the area and are, in general, impermeable. Geophysical investigations in the area (Myriounis et al. 2006), have discovered the existence of a clay bed in the coastal part, which controls quality characteristics of groundwater in Neogene and Quaternary sediment aquifers.

Phenomena of artesian flow and submarine outflows can be found in the coastal part of the area (Fig. 1). Artesian phenomena exist in the central part of Efxenoupoli sub-basin and in the northern part, east of Aidini. It is attributed to the N-S aligned faults that submerge the eastern parts of the aquifers, leading to free aquifers transforming towards west into under-pressure aquifers revealing artesian phenomena.

Submarine outflows are situated in the northern coastal part of the area of interest, near Dimitriada and in the southern part of Almyros beach (Fig. 1). Position of the submarine outflows is connected to the W-E trending faults in the boundary of the area. In Dimitriada these outflows do not anymore exist, due to groundwater

level lowering. In contrast, in Almyros beach submarine outflows can be found even in 850m distance from the coast.

4 Quality characteristics of groundwater

For the investigation of groundwater data quality in the coastal part of Almyros basin, sampling operations took place during 2005, in May (104 samples) and September (90 samples), in a uniform aligned network of hydro-points (boreholes and springs) (Myriounis 2008). All field data were collected in a database system (MS Access) and where analyzed using Geographical Information Systems (ArcInfo).

Hydro-point network includes sampling points distributed not only to the Neogene and Quaternary sediments, but also in the karst aquifers of the area. Boreholes named NAGX, G302 and G305 to the west of N. Anchialos and boreholes S44 and S41 south of Sourpi are situated in carbonate karst rock formations.

Results of chemical analysis in karst aquifers show that groundwater is highly affected by seawater intrusion. Electrical conductivity values for Efxenoupoli area vary between 1050 and 2660 μS/cm, with higher values detected in the south part, in Kefalosi spring. For Sourpi area, values range between 600 and 672 μS/cm. Low values of Electrical Conductivity are attributed to the hydraulic sealing of the northern part of Sourpi sub-basin due to W-E trending faults. Specifically, Kefalosi spring shows salt water intrusion character, with electrical conductivity values higher than 1500 μS/cm. The main characteristic is the complex operating mechanism, leading to high Cl^- values even during winter months. This spring supplies the aquifers of Platanos coastal area from the west, so these aquifers are highly degraded.

In Figure 2 is presented the spatial distribution of electrical conductivity for Neogene and Quaternary sediment aquifers, for the period of September of 2005. Higher values are concentrated in the boundaries of Efxenoupoli sub-basin and in the coastal part of Sourpi sub-basin, in the contact between carbonate rocks and recent sediments. The same distribution is true for the Cl ions, with values ranging between 14 and 850 mg/L for Efxenoupoli sub-basin, and between 36 and 1092 mg/L for Sourpi sub-basin. From the spatial distribution of electrical conductivity it can be determined that in the central part of Efxenoupoli sub-basin and the southern part of Sourpi sub-basin, groundwater is barely affected by seawater intrusion.

This can be attributed to tectonic and hydrogeologic settings of the area. Tectonic activity (Fig. 1) leads to the appearance of artesian phenomena and submarine outflows. Submarine outflows are situated in the boundaries of Efxenoupoli sub-basin, following W-E trending faults and preventing the advance of the seawater intrusion from the strained boundaries to the central part of the area. Also, artesian phenomena in the central part of Efxenoupoli sub-basin show favorable supply conditions for the sediments. Correlation between geological cross-sections and geophysical profiles leads to the discovery of a clay bed, protecting seawater intrusion in the central part of the area.

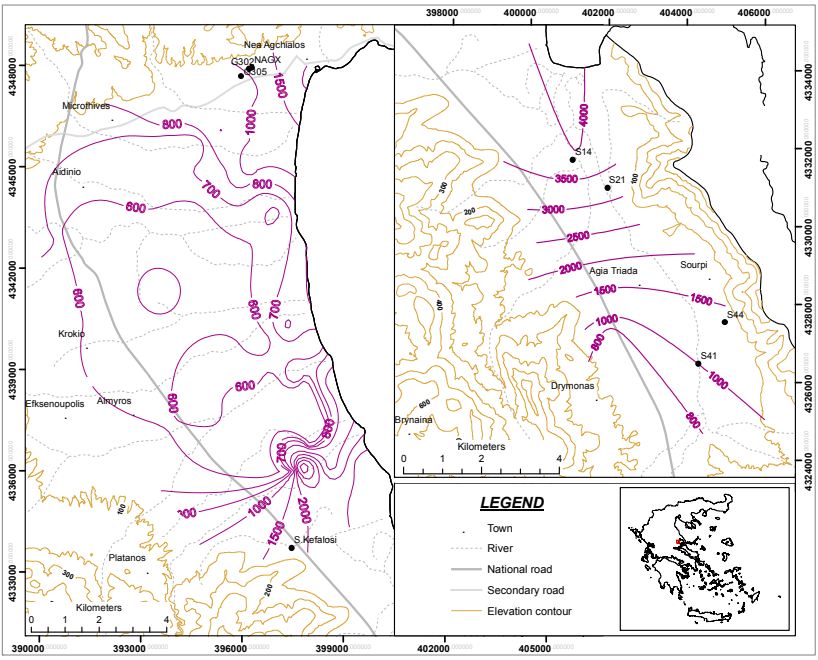

Fig. 2. Distribution of E.C. in Neogene and Quaternary sediments of the coastal area, period of Septembe (Myriounis 2008).

For the region of Sourpi it is found that groundwater shows better qualitative characteristics in the northern part, compared to the coastal part groundwater. This is attributed in contact and supply of loose sediments from high-altitude carbonate rocks, which are hydraulically differentiated in relation with the rest of the carbonate sediments of the area. This results in a clear differentiation of the chemical character of Sourpi area groundwater.

Regarding nitrate ion values (Fig. 3), they value between 8.5 and 133.3 mg/L, and 3.1 to 21.6 mg/L for loose sediments and carbonate rocks of Efxenoupoli. For Sourpi area, values range between 3.1 and 21.6 mg/L for loose sediments, and 37.2 to 45 mg/L for karst formations. Generally, in Sourpi area there are no nitrate contamination phenomena. In contrast, high concentration of nitrate ions can be found in the central part of Efxenoupoli area. High values of nitrate ions can be a result of the use of nitrogen fertilizers in agricultural lands, and also in the presence of a piggery, polluting downstream groundwater by its sewage. It is also worth noting that the areas showing seawater intrusion contamination, there can be found low values of nitrate ions, lower than 50 mg/L.

For the hydrochemical analysis of groundwater in the area, a number of hydrochemical ratios were calculated (Myriounis 2008, Myriounis and Theocharis 2010). The Mg/Ca ratio (Appelo and Postma 2007, Ghabayen et al. 2006) varies between 0.002 and 3.65 for month May, and between 0.022 and 4.1 for Septem-

ber, with higher values appearing in saltwater affected areas. This is attributed to Na ion adsorption by the aquifers.

The (Ca+Mg)/(Na+K), gives information about areas being enriched (Mandel and Shiftan 1981, Kallergis 2000). Higher values of this ratio are observed along the groundwater draining axis in Efxenoupoli sub-basin (in the traces of whom are localized the submarine outflows), and to the central part of the area. For Sourpi area, higher values are found in the south part, with values lower than unit in the coastal part.

From the ratio of Na/K (Kallergis 2000), ranging in the area between 10 and 70, it is shown that the largest values are observed in congested by the intrusion of seawater areas. This phenomenon is due to sodium adsorption, because of long residence time in the aquifer. Based on the above ratio it is shown that the brackish waters of the region have sufficient residence time in the aquifer in order to show effects of Na ions adsorption.

Also the ratio SO_4/Cl values (from 0.15 to 0.66), which gives information on the evolution of the salinity of aquifers (Gimenez and Morell, 1995), it is found that the margins of Efxenoupoli sub-basin groundwater is classified as of marine origin (SO_4/Cl <1), while moving to the central part it falls into sulphide character, showing a transition zone chloride groundwater. A similar situation prevails in the region of Sourpi, moving from north to south.

Finally, the ratio Na/Cl values (4 to 8) show that the lower values observed in congested areas due to the phenomena of ion exchange of Na with Ca, a phenomenon which occurs during the seawater intrusion to the land.

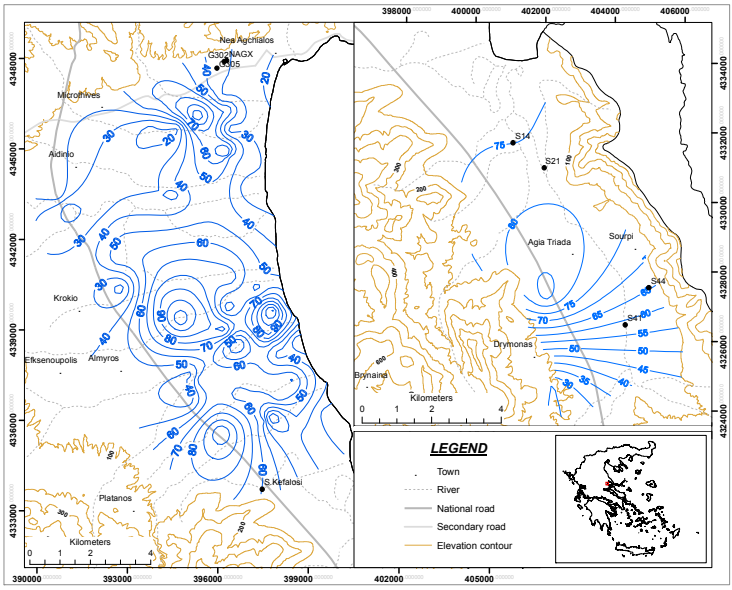

Fig. 3. Distribution of NO_3 ions in Neogene and Quaternary sediments of the coastal area period of September (Myriounis 2008).

5 Results

Main hydrochemical phases (Appelo and Postma 2007) of groundwater in the region for September of 2005 are shown in Figure 4.

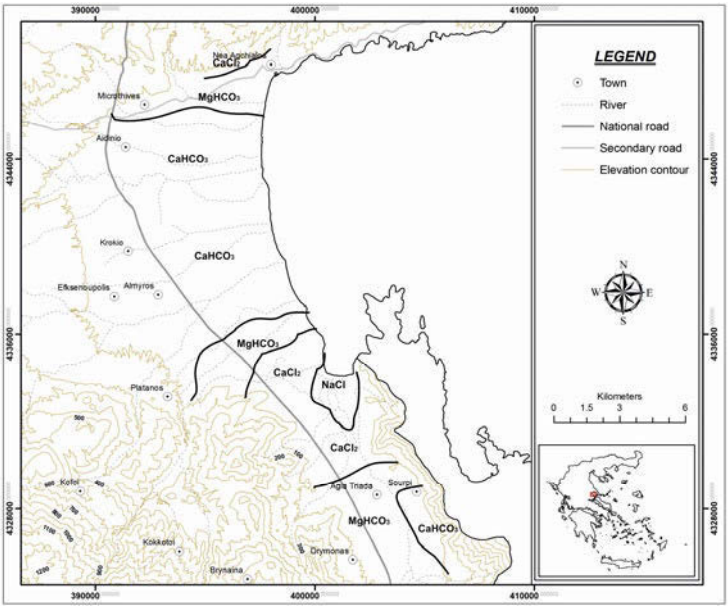

Fig. 4. Hydrochemical characters of groundwater resources of study area (Myriounis 2008).

In the margins of Efxenoupoli sub-basin and in the coastal part of Sourpi sub-basin, there is a clear separation of groundwater quality in relation to the rest of the coastal part of the Almiros basin.

Groundwater in impacted by seawater intrusion areas shows hydrochemical character NaCl and $CaCl_2$. The first hydrochemical type occurs in the area between the two sub-basins, and is configured by the intrusion of seawater into groundwater aquifers. The hydrochemical type $CaCl_2$, which occurs in brackish areas characterized by the phenomenon of cation-ion exchange between Na and Ca ions, at the intrusion of sea water on land (Martinez and Bocanegra 2002). In the central part of the area, groundwater resources are characterized by their hydrochemical types $MgHCO_3$ and $CaHCO_3$. The $MgHCO_3$ waters are adjacent to the $CaCl_2$ water, close to areas which are influenced by the presence of seawater intrusion. Unlike the central part of the Efxenoupoli sub-basin and the southern region of Sourpi sub-basin, where there is no brackish groundwater indication, is classified as $CaHCO_3$ type.

In conclusion seawater intrusion phenomena are presented on the edges of sub-basin Efxenoupolis and in the coastal and central area of sub-basin Sourpi, regions

what are in hydraulic connection with the brackish water of the karstic aquifers. The absence of seawater intrusion phenomena in the central area of sub-basin Efxenoupolis can be associated with the high hydraulic head in this area and with the local geological and tectonic conditions.

Acknowledgments The first author, Ch. Myriounis, would like to thank the State Scholarship Foundation for financial support under the 3998/2003-2004 program.

References

Appelo, C, Postma, D (2007) Geochemistry, Groundwater and Pollution, 2nd edition, A.A. Balkema Publishers, Rotterdam, pp. 650

Galanakis D (1997) Neotectonic structure and stratigraphy of Neogene-Quaternary sediments of the Almyros-Pagasitikos, Pilion, Oreon-Trikeri and Maliakos basins, PhD thesis, Thessaloniki pp. 258

Ghabayen, S, McKee, M, Kemblowski, M (2006) Ionic and isotopic ratios for identification of salinity sources and missing data in the Gaza aquifer, Journal of Hydrology, 318, pp. 360-373

Gimenez, E, Morell, I (1995) Hydrogeochemical analysis of salinization processes in the coastal aquifer of Oropesa (Castellon, Spain), Environmental Geology, 29 (1/2), pp. 118-131

Dimopoulos, G (1983) Salzwasserfuhrende Karstquellen oderhalb der Meeresoberflche, Zeitschrift fur angewandle Geologie, Bd. 29, pp. 565-568

Dimopoulos, G (1984) Geohydrologische und hydrochemische Probleme bei der Untersuchung von Salzkarstquellen, DGM, 28 H. 2, pp. 49-53

Kallergis G (2000) Applied - Environmantal Hydrogeology, 2nd edition, Volume B, published T.C.G., Athens, pp. 345. (in Greek)

Mandel, S and Shiftan, ZL (1981) Groundwater Resources Investigation and Development. Academic Press Inc., New York, 269 p; 1981

Martinez, DE, Bocanerga, EM (2002). Hydrochemistry and cation-exchange process in the coastal aquifer of Mar Del Plata, Argentina, Hydrogeology Journal, 10, pp. 393-408

Myriounis, C, Voudouris, K, Tsourlos, P, Soulios, G, Dimopoulos, G (2006). Hydrochemical and geophysical survey of the Almiros aquifer system, East Central Greece, 1st SWIM - SWICA, 19th Salt Water Intrusion Meeting, 3rd Salt Water Intrusion in Coastal Aquifers, Cagliari - Chia Launa, Italy, pp 221-227

Myriounis, Ch (2008) Hydrogeological and hydrochemical conditions of groundwater in the coastal part of the hydrological basin of Almyros prefecture Magnesia. Phd Thesis, School of Geology, Thessaloniki, pp. 397

Myriounis, Ch, Theocharis, M (2010) Quality characteristics of water resources, Environmental Impact assessment, Department of Crop Production, Technological Educational Institution of Epirus, pp. 333. (in Greek)

Quality regime of the water resources of Anthele Sperchios Delta area Fthiotida Prefecture

N. Stathopoulos, I. Koumantakis, E. Vasileiou, K. Markantonis

National Technical University of Athens, Mining and Metallurgical Engineering School, Sector of Geological Sciences, Laboratory of Engineering Geology and Hydrogeology, Hrwwn Polytexneiou 9, PC 15780, Athens, Greece, 15780, nstath@metal.ntua.gr, koumantakisioannis@gmail.com, elvas@metal.ntua.gr, markantonis@metal.ntua.gr

Abstract The studied area of Anthele, is located in the last part (delta) of Sperchios River (Fthiotida prefecture). The most significant problem that confronts, is the deterioration of surface water quality. At the eastern part of Sperchios River up to the coastline the water quality appears to be improper for irrigation. The water coming from the irrigation – drainage canals of the agricultural redistribution, in the east, south-southeastern part of the area is saline. Groundwater quality, in the west, between Anthele village and the national road appears to be good. At the eastern part of Anthele there are indications of degradation. The main sources of pollution are the agricultural activities, the deposition of solid and liquid wastes inside Sperchios River, the mineral - thermal waters in the south and southeast part and the intrusion of the sea in the low parts of Sperchios River and the coastal lowland zone. The region is declared as protected area (Natura), because of the appearance of specific environmental and ecological characteristics. The preservation and exploitation of the water resources is an important necessity for the improvement and further development of the area.

1 Introduction

The Basin of Sperchios River is located in the northern part of the water compartment in the east of Sterea Ellada and is delimited west from the mountain Timfristos, north from Orthri and south from Bardousia, Oiti and Kallidromo. The total river area comes up to 2116 km^2 and the average altitude 810 m (Kakavas 1984). The Sperchios valley develops steep slopes, that is the reason, which the river is characterized as mountainous – severe flood water supplies and very high sediment yield are measured during the time. The river's basin average annual surface overflow is 693 hm^3 (Koutsogiannis 2003). The flow path of Sperchios river is about 82.5 km, flows from the eastern sides of Timfristos mountain and discharges in Maliakos gulf. The average rainfall in the basin is estimated to 905 mm. (Kout-

N. Lambrakis et al. (Eds.), *Advances in the Research of Aquatic Environment, Vol. 2*
DOI 10.1007/978-3-642-24076-8, © Springer-Verlag Berlin Heidelberg 2011

sogiannis 2003). The deltaic alluvial part of the valley covers an area of almost 200 km^2 and is formed constantly with a unique rhythm in whole Greece (is estimated at about 130 acres per year). The river's embouchure, as well as the coastal area of Anthele, is ``Natura`` protected areas (Koutsogiannis 2003).

The area of the study is located at the eastern part of Sperchios River alluvial plain, is delimited from south and southwest by the old (natural) river's riverbed and in the north by the new riverbed which was created after the partial diversion of the river. From the east, part of the western coastline of Maliakos gulf constitutes the natural border of the area of interest. The area includes the village Anthele, the agricultural redistribution fields of Anthele community and is delimited from the west by the national road Athens – Lamia. The river Sperchios is also studied (old and new riverbed), from the point of the diversion up to the sea.

The aim of this study is the research mainly of the qualitative characteristics of water resources of the area (surface and groundwater).

2 Geology - Hydrogeology

The main formations which are deploited in the mountainous and semi - mountainous zone of the greater hydrological basin of the Sperchios river are limestones, schist -chert, ophiolite and flysch. The 450 km^2 of the low-land area of the river's basin is consisted of the most recent sedimentary deposits. The total thickness of these deposits, in the area of Sperchios delta exceeds the 1000 m.

Inside the basin there are 519 springs. The greater of those is the spring "Mauroneria", with average annual flow 13.6 x 10^{6}m^3 approximately, which is used partially for irrigation purposes (Kakavas 1984). The geologic formations are divided in four relevant categories due to the permeability of them (Kakavas 1984): a) permeable (carbonate rocks, conglomerates, coarse-grained materials, recent deposits of Sperchios riverbed, coarse-grained formations of alluvial, etc), b) medium permeable (deep deposits of Sperchios river, several petrologic types of the ophiolitic complex, etc), c) semi-permeable formations (weathered territorial mantle of flysch and of schist-chert, etc) and d) impermeable formations (formations of flysch, old deposits of Sperchios, the deposits of mineral-thermal springs, etc).

In the carbonate formations, karstic aquifers are deployed, while in the alluvial deposits there are unconfined and confined aquifers, with low or high hydrodynamic capacity.

The alluvial aquifers are pumped from the irrigation boreholes, with discharges that are fluctuated between 100 and 200 m^3/h (boreholes west of Anthele, TOEB archive, 2008) and some of them present during the period of high waters, artesian water flow to the surface up to 5 m^3/h (G23, G24). The main aquifers are deployed in the coarse-grained materials (pebbles, sands, gravels, etc) which are situated in alternations with clays and marls.

The values of transmissivity in several places of the aquifer, fluctuate from $2.54x10^{-3}$ m^2/sec up to $2.33x10^{-2}$ m^2/sec (TOEB Anthele – DEB Fthiotidos). More thoroughly (towards the sea), the coarse-grained aquifers are being reduced as wells as their discharges (e.g. Oruzwnes borehole 40 m^3/h, TOEB Anthele – DEB Fthiotidos).

3 Hydrochemistry

The sampling was done in two periods of 2008 and includes 71 in different sites, located in the entire studied area (Stathopoulos 2008). The first period of sampling took place shortly before the beginning of the irrigation period, while the second one, in the middle of summer and close to the irrigation period's end. The sampling consisted of a normal distributed drilling network, at the irrigation channels and Sperchios' riverbed and from many boreholes in different sites (Fig. 1).

Fig. 1. Locations of 2nd sampling for hydrochemical research (20/7/2008).

3.1 Chemical analysis of the waters in the irrigation channels

The moat waters of the agricultural redistribution come from a) Sperchios river b) drills c) the "Mauroneri" spring (small quantities) d) rain water and e) probably from the phreatic aquifer. Almost all samples have Ca-HCO_3 hydrochemical type

(it is mainly due to the waters' origin), except from one sample which is saline (Na-Cl), increased values Na^{+}, Mg^{+2} and Cl^{-} appeared from site to site (Table 1).

Table 1. Hydrochemical types of surface and underground waters (20/7/2008).

ID	Water type	ID	Water type	ID	Water type
N1	Ca-HCO_3	N10	Na-Ca-HCO_3-Cl	P3 new	Na-Ca-HCO_3-Cl
N2	Ca-Na-Mg-HCO_3	N11	Na-Ca-Cl-HCO_3	P4 new	Na-Ca-HCO_3-Cl
N3	Ca-Na-Mg-HCO_3	N12	Na-Cl-HCO_3	N17 Ekok	Na-Ca-Mg-HCO_3
N4	Ca-Mg-HCO_3	N13	Na-Mg-Cl-HCO_3	N18 Cem	Na-Ca-Mg-HCO_3
N5	Ca-Mg-HCO_3	N16 Pump	Ca-Na-Mg-HCO_3	G 23	Ca-HCO_3
N6	Na-Ca-HCO_3-Cl	N14 R	Na-Cl	G 24	Ca-HCO_3
N7	Ca-Na-HCO_3	N15 R	Na-Cl	G 27	Na-Ca-Mg-HCO_3
N8	Na-Ca-Mg-HCO_3-Cl-SO_4	N19 R	Na-Ca-HCO_3	S 30	Na-Ca-HCO_3
N9	Na-Cl	N20 R	Ca-HCO_3	G 26	Na-Ca-HCO_3

The collected samples from the west sector are of good up to medium quality (C2S1 according to Wilcox classification) for irrigation. In the east the waters are deteriorated and characterised as medium up to very medium for irrigation (C3S1). Near Maliakos gulf, the K-Na and chloride ions prevail and the waters are characterized as of very poor quality (C4S3). At the west borders of the area the surface waters are characterized as good quality water, to the south and to the east up to subsaline, while in the coastal areas are subsaline.

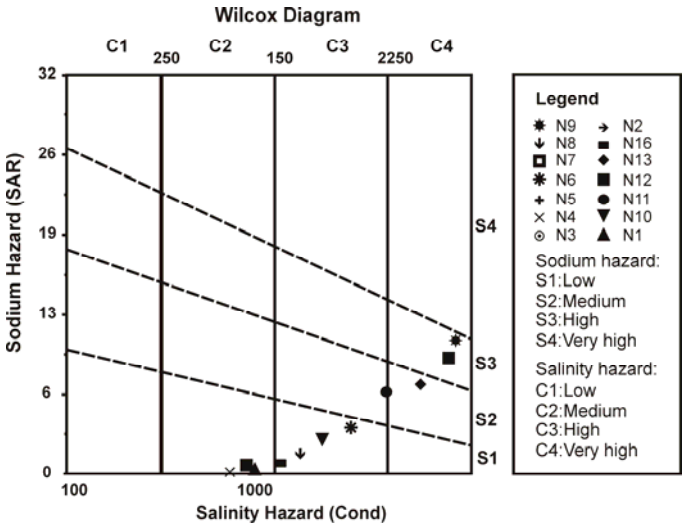

Fig. 2. Wilcox chart of surface waters (20/7/2008).

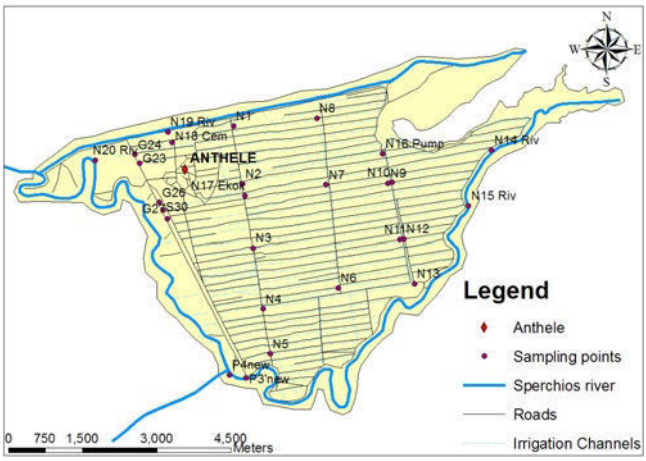

Fig. 3. E.C. distribution map of surface waters (20/7/2008).

At the second sampling period the Na-Cl type appears to be in larger parts of the area, with higher concetrations. In comparison with the 1st sampling period further quality deterioration of the ditch waters was observed, from the central parts to the area of the redistribution. The increase of E.C., is remarkable which is about double (from 2700 to 5600 μS/cm) in the second sampling period (Fig. 3). The waters, in the central and to the east part of the area, are up to improper for irrigation.

3.2 Chemical analysis of the waters in Sperchios River

The waters of Sperchios in the western part of the studied area have HCO_3-Ca type, which evolves in Na-HCO_3 at the south parts of the area. The concentrations of the ions Ca^{+2} and Mg^{+2} are high to the west and the concentrations Na^{+}, Cl^{-}, are increased from south up to east of the area (Table 1).

The quality of the river's waters, towards its delta deteriorates constantly and becomes up to unsuitable for use because of high salinity (Fig. 4). In the second sampling the domination of Na-Cl type becomes obvious, against the carbonic in regard to the 1st sampling.

It must be marked that from the south-southeast there is an important influence by the sector of the mineral thermal aquifers in Thermopulwn-Pswroneriwn.

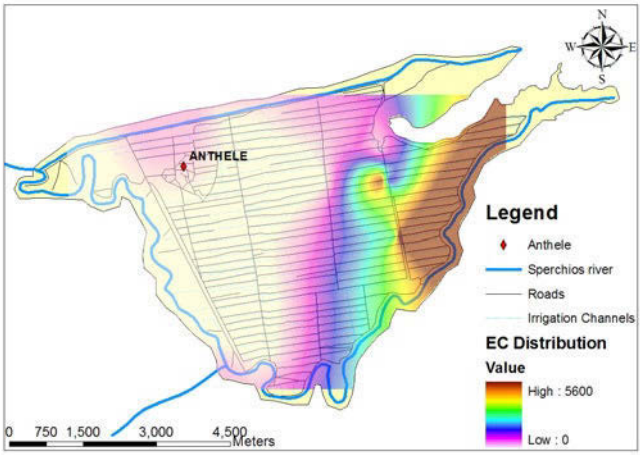

Fig. 4. Cl^- distribution map of surface waters (20/7/2008).

3.3 Chemical analysis of groundwater

The water from drills, show HCO_3 type because of the good recharge of them, increased concentrations of Na^+ were measured, in many areas, which are not saline. Fluctuation is noticed in the irrigative suitability, from good up to very medium, due to the ions Na^+ (Table 1). Generally the groundwater is of very good quality (with an exception in one site, 1km southeast of Anthele). A small deterioration in quality was observed in the phreatic aquifer (well in the village).

4 Conclusions – Suggestions

The most qualitative deterioration of the waters is noticed during the irrigation period (July - August), where the water needs are increased and there is not rich recharge. The low land elevations are vulnerable in the intrusion of sea, in the eastern part of the coastal zone with altitude that comes close to 0, as well as to the eastern part of Sperchios.

The irrigative suitability of the surface waters is decreased to the south and east of the area. In the south the waters are influenced by the thermal-mineral front Thermopulwn-Pswroneriwn. In many parts the waters are characterized as improper for irrigation and shouldn't be used.

The groundwaters are of good up to adequate quality and no salinity was detected. The high, in some locations, concentrations of ions Na^{+1}, downgrade their irrigative category. Through the high water period the confined aquifer presents artesianism, with automatic water flow in some places by the national road.

It is very encouraging the fact that the concentrations in NO_3^- are low, despite the extended agricultural activities, is positive. The high concentrations of HCO_3^- in various places mean adequate water renewal and good recharge, unable though to counterbalance the caused, general, qualitative deterioration of the surface waters to the east.

The area is characterized as "Natura", however the environmental pressures that take place are important. Pollution was ascertained in both riverbeds of the river and in the channels of the redistribution, from solid wastes (garbage, fertilizer packages, etc), liquid wastes, as well as the discard of polluted waters from the drainage after the irrigation, in Maliakos gulf.

It is estimated that the applied method till now, that uses the drained waters from the upstream agricultural areas, for the irrigation of the downstream areas, must be changed.

The change of the obsolete irrigation system is also advised, which consists of free, surficial, irrigation channels and works with flooding. This system has great water losses from leaks and even greater from the evaporation of the water flooded irrigation areas.

It is proposed, very good drainage, washout and ventilation of grounds, so that those will be capable of using medium quality waters, but also to avoid gathering salt that downgrade them in quality. The presence of salts was certified and visually in some areas of the eastern sector.

Finally, the use of the waters coming from the overflow from the artesian boreholes of the area during the periods of "high waters" (mainly in winter) is proposed, whether for "artificial recharge" or for creating water supplies, so that they will be used in the irrigation period. If this isn't possible, the boreholes should be sealed in order to stop the automatic water overflow.

Acknowledgments Special thanks to Colleague P. Tsaggarato for his help in using G.I.S.

References

D.E.B. Fthiotidas, Geological cross sections of boreholes

Kakavas NI (1984) Hydrological water balance of basin of Sperchios river, Phd Thesis, I.G.M.E., Athens

Koutsogiannis D (2003) (YP.AN., E.M.P., I.G.M.E., K.E.P.E.), Project plan of water resources management of the country, Ministry of Development – Directory of Water Dynamic and Natural Resources, Athens 2003

Stathopoulos, NI (2008) Research of the hydro-geological regime of Anthele area – Sperchios Delta of Fthiotida prefecture with emphasis at the quality of water resources, Master Diploma Thesis– DPMS Science and Technology of Water Resources, Athens

T.O.E.B. (1993) Anthele and D.E.B. Fthiotias, Technical report of the results of drilling 3 irrigative boreholes TOEB Anthele and 1 TOEB Fakitsas Fthiotidas, Protocol Number 9651, Lamia

Assessment of groundwater quality in the Megara basin, Attica, Greece

D. Gamvroula[1], D. Alexakis[2], G. Stamatis[1]

[1]Institute of Mineralogy-Geology, Agricultural University of Athens, Iera Odos 75, 118 55 Athens, Greece

[2]Centre for the Assessment of Natural Hazards and Proactive Planning and Laboratory of Reclamation Works and Water Resources Management, National Technical University of Athens, 9 Iroon Polytechniou, 157 73 Athens, Greece, E-mail: dial@survey.ntua.gr

Abstract Groundwater samples were collected from 58 sampling sites of the Megara basin aiming to describe the groundwater quality in relation to geology and anthropogenic activities. The methodology applied in this study includes chemical analysis, statistical analysis, GIS database and comparison of the groundwater contents with quality standards given by the Dir.98/83/EC. The elevated Cr_{total} (up to 70.3 μg/L), Ni (up to 25.39 μg/L) and Mn (up to 87.77 μg/L) groundwater concentrations of Megara basin constitute a natural case of contamination; while the high NO_3^- (up to 411 mg/L) and PO_4^{3-} (up to 4.74 mg/L) groundwater concentrations could be attributed to the application of fertilizers and leakage of domestic sewage. The elevated Cl^- (up to 3954.7 mg/L) and TDS (up to 8027 mg/L) groundwater contents recorded in coastal areas are attributed to the mixing of groundwater with seawater.

1 Introduction

The chemical composition and the quality of water are controlled by natural and anthropogenic factors that include geological structure, lithology and mineralogy of the aquifers, the reactions that take place within the aquifer as well as the type of land uses. The detailed knowledge of the water quality can promote effective management of groundwater resources. On this basis, a groundwater quality assessment was carried out in the Megara basin, Attica, Greece. In the present study, the objectives are: (a) to record the present quality status of the groundwater in the Megara basin, and (b) to aid the management and future development of water resources in the region.

N. Lambrakis et al. (Eds.), *Advances in the Research of Aquatic Environment, Vol. 2*

DOI 10.1007/978-3-642-24076-8,

2 Study area

The study area is situated within the western part of the Attica region, Greece. It is located about 41 km from Athens, the capital city of Greece and covers about 320 km^2.The area studied extends from the Korinthiakos Gulf coastline in the north to the Saronikos Gulf in the south, from the Geraneia Mountain in the west to the Pateras Mountain in the east (Fig. 1).

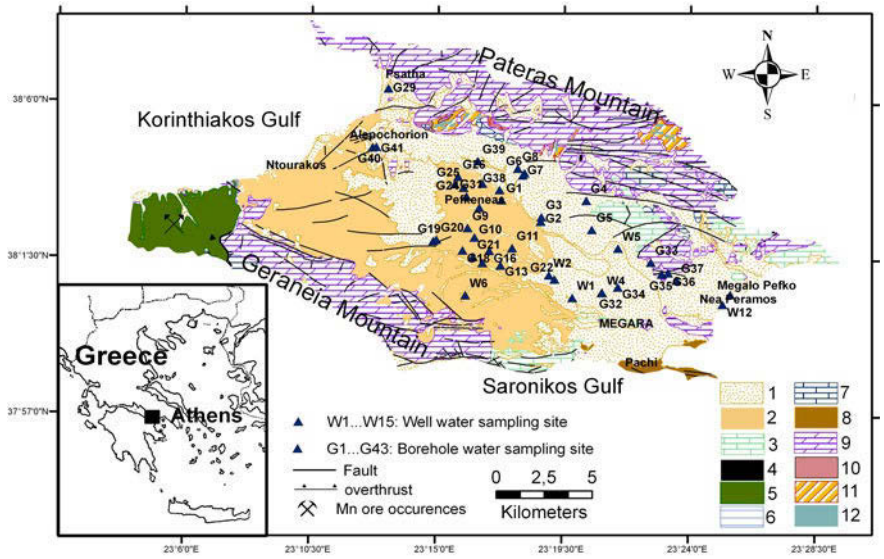

Fig. 1. Locality map of the study area showing groundwater sampling sites in comparison with geology. 1) Quaternary deposits, 2) Neogene deposits, 3) Limestones (U.Cretaceous), 4) Bauxites, 5) Ultrabasic rock masses, 6) Schist-chert formation (M.-U.Jurassic), 7) Limestones (L.-M.Jurassic), 8) Limestones-dolomites-marbles-cipolins (M.-U.Triassic), 9) Limestones-dolomites (M.-U.Triassic-L.Jurassic), 10) Complex of cherts, sandstones and schists (L.-M.Triassic), 11) Argilaceous shales and sandstones (Permian-U.Carboniferous), 12) Lenses of limestones.

The geological structure of the Megara basin, which is a part of the Sub-Pelagonian zone, is dominated by three main units (Fig. 1): (a) the crystalline basement rocks; (b) the alpine basement rocks; and (c) the post-alpine sediments. According to Dounas et al. (1971) the crystalline basement rocks are composed of metamorphic rocks (argillaceous shales including lenses of limestones, sandstones alternating with tuffites and bodies of basic igneous rocks) of Permian-U.Carboniferous age. The alpine basement rocks are composed of Complex of cherts-sandstones-schists (L.-M.Triassic age), carbonate rocks (karstified limestones-dolomites of M.-U.Triassic-L.Jurassic age, limestones-dolomites-marbles-cipolins of M.-U.Triassic age and limestones of L.-M.Jurassic age), Schist-Chert formation of M.-U.Jurassic age and Bauxites of pisolitic texture. Schist-Chert for-

mation consists of shales containing Mn-layers (Bornovas et al. 1984; Gaitanakis et al. 1984; Gaitanakis et al. 1985). Bodies of ultrabasic rocks are locally preserved over the carbonate platform (Bornovas et al. 1984; Gaitanakis et al. 1984; Gaitanakis et al. 1985). Limestones of U.Cretaceous age covering at places bauxite ores (Dounas et al. 1971). The post-alpine sediments consist mainly of Neogene and lignite bearing deposits, marls, lignite intercalations, marly limestones, sandy marls and other unconsolidated material (Bornovas et al. 1984, Gaitanakis et al. 1985). Aslam (1982) reported marly formations with manganese oxides and ultrabasic rock fragments within Neogene and Quaternary deposits. The Quaternary deposits consist of alterations of reddish brown clays, sandy clays, conglomerates and loams. The crystalline basement rocks are particularly impermeable rocks. The intensively karstified limestones- dolomites of M.-U.Triassic-L.Jurassic are permeable rocks that constitute the most important aquifer of the study area. The limestones-dolomites of M.-U.Triassic- L.Jurassic are thrusted at the impermeable crystalline basement rocks. The infiltration water of this karstic system moves laterally to the surrounding Neogene and Quaternary deposits. Small karst springs draining the karstic system outcrops at the north part of the study area. The Quaternary deposits form a poor aquifer possessing low hydraulic characteristics.

3 Materials and methods

A network of 58 sampling sites (15 wells and 43 boreholes; Fig. 1) was sampled during April 2009. Each water sample was then divided into two water subsamples. The first set of 58 subsamples was filtered with 0.22 μm disposable syringe filter, acidified to pH<2 with ultrapure HNO_3 and stored in 100 mL container for trace element analysis. The second set of 58 subsamples was stored in 1000 mL container and transferred to the laboratory where after filtration through 0.45 μm pore size membrane filters, major anions and cations were analyzed. The water temperature (T), dissolved oxygen (DO), conductivity (CND), total dissolved solids (TDS), salinity (Sal), pH and Eh were measured immediately after collection with YSI *Professional Plus* portable meter. Dissolved anions (Br, Cl^-, F, NO_2^-, NO_3^-, PO_4^{3-} and SO_4^{2-}) and cations (Ca^{2+}, K^+, Li^+, Mg^{2+}, Na^+ and NH_4^+) were measured on the non-acidified subsamples by ion chromatography (IC) using a Dionex ICS-3000 system at the Laboratory of Reclamation Works and Water Resources Management of the National Technical University of Athens (NTUA). Bicarbonate (HCO_3^-) was measured using a HACH digital titrator on the non acidified groundwater subsamples. Iodine (I) and SiO_2 were measured by spectral photometry using a HACH model DR/3000 at the Laboratory of Mineralogy and Geology of the Agricultural University of Athens. Trace elements were determined on the acidified subsamples including Cd, Co, Cr_{total}, Cu, Mn, Ni, Pb and Zn by inductively coupled plasma mass spectrometry (ICP-MS) using an Agilent model 7700 MassHunter at the Department of Chemical Sciences of the NTUA.

4 Results and discussion

Table 1 presents the summary statistics of groundwater physicochemical dataset of the Megara basin.

Table 1. Summary statistics of groundwater physicochemical dataset of the Megara basin.

			Wells (n=15)			Boreholes (n=43)			PV
	Units	DL	Min	Max	Mean	Min	Max	Mean	
Br	mg/L	5	<5	12.07	2.79	<5	2.96	0.70	-
Ca	mg/L	0.05	48.80	301.44	141.68	17.2	163.4	56.55	-
Cd	μg/L	0.05	<0.05	0.10	0.03	<0.05	0.34	0.03	5
Cl	mg/L	1	8.66	3954.7	1007.4	33.3	829.9	232.1	250
Co	μg/L	0.02	<0.02	0.97	0.18	<0.02	0.56	0.07	-
Cr_{total}	μg/L	0.5	<0.5	39.1	5.30	<0.5	70.3	25.24	50
Cu	μg/L	0.1	0.17	10.20	2.56	<0.1	8.06	1.26	2000
F	mg/L	0.05	<0.05	0.83	0.29	<0.05	0.54	0.24	-
HCO_3	mg/L	1	146	561	388	274	652.7	377.6	-
K	mg/L	0.05	0.79	91.60	19.55	0.49	32.08	3.97	-
Li	mg/L	0.1	<0.1	0.12	0.04	<0.1	0.08	0.02	-
Mg	mg/L	0.05	5.47	351.83	138.24	46.4	158.6	69.42	-
Mn	μg/L	0.05	<0.05	87.77	7.85	0.10	73.08	5.51	50
Na^+	mg/L	0.05	4.18	1789	475.94	22.7	504.7	125.4	200
NH_4^+	mg/L	0.01	<0.01	0.12	0.02	<0.01	0.71	0.05	0.5
Ni	μg/L	0.2	0.34	25.39	5.43	<0.2	11.13	1.35	20
NO_2^-	mg/L	0.01	<0.01	0.61	0.07	<0.01	0.52	0.02	0.5
NO_3^-	mg/L	1	<1	411	102.57	<1	197	19.27	50
DO	mg/L	0.1	3.95	10.96	7.83	3.45	16.6	9.44	-
Pb	μg/L	0.1	<0.1	1.24	0.20	<0.1	0.72	0.15	10
PO_4^{3-}	mg/L	0.10	<0.10	4.74	0.44	0.00	2.73	<0.10	-
SiO_2	mg/L	1	4.10	57.00	22.38	6.50	61.00	30.71	-
SO_4^{2-}	mg/L	1	20.75	867.12	168.35	6.69	441.8	55.21	250
T	°C	-	16.89	20.7	18.87	17.2	26.00	19.17	-
TDS	mg/L	2	212	8027	2779	403	2593	1029	-
Zn	μg/L	0.5	1.78	65.73	15.49	1.16	692.3	69.88	-
I	mg/L	0.02	0.02	0.21	0.12	0.03	0.52	0.12	-
H_{total}	mg/L	1	144.4	2170.5	921.00	243	1039	426	-
Eh	mV	-	-187	-63.5	-118	-186	214	-95.8	-
pH	-	-	6.81	8.20	7.60	7.08	8.73	7.86	6.5-9.5
Ec	μS cm^{-1}	1	326	12372	4245	624	3990	1562	2500
Sal	‰	-	0.16	7.12	2.91	0.33	2.10	0.82	-

DL: Detection Limit; PV: Parametric Value given by the Dir.98/83/EC; H_{total}:Total Hardness

The pH mean values of waters of wells and boreholes are 7.60 and 8.73, respectively, which indicates the alkaline nature of groundwater of Megara basin. There are no groundwater samples with pH values exceeding the Parametric Value (PV). The DO of the groundwater collected from the wells of Megara basin ranges from 3.95 to 10.96 mg/L; while the groundwater collected from the boreholes exhibit dissolved oxygen ranging between 3.45 and 16.6 mg/L. The mean concentrations of Cl^-, Na^+ and NO_3^- in water samples collected from the wells exceed the PVs given by the European Community (EC 1998). The percentage proportions of the water samples collected from wells with Cl^-, Mn, Na^+, Ni, NO_2^-, NO_3^- and SO_4^{2-} concentrations exceeding the PVs were 66.7 %, 6.7 %, 60 %, 6.7 %, 6.7 %, 53.3 % and 13.3 %, respectively. The percentage proportions of the water samples collected from boreholes with Cl^-, Cr_{total}, Mn, Na^+, NH_4^+, NO_2^-, NO_3^- and SO_4^{2-} concentrations exceeding the PVs were 25.6 %, 16.3 %, 2.3 %, 20.9 %, 2.32 %, 2.32 % , 6.9 % and 2.3 % , respectively. The elevated Cr_{total} (up to 70.3 μg/L) and Ni (up to 25.39 μg/L) groundwater concentrations of Megara basin can be attributed to natural sources, such as the weathering of ultrabasic rock fragments within Neogene deposits; while the elevated Mn (up to 87.77 μg/L) groundwater concentrations could be related to the following sources: (a) weathering of Mn-oxides occurrences; (b) presence of Mn-oxides within Neogene deposits; and (c) leaching of Mn from the lignite intercalations.

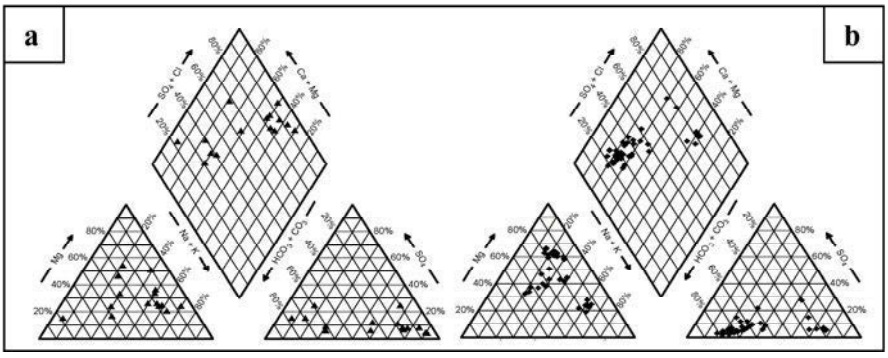

Fig. 2. Piper-tri-linear diagram depicting hydrochemical facies of the groundwater samples of Megara basin: (a) wells, (b) boreholes.

Various researchers (Ball and Izbicki 2004; Stamatis et al. 2011) have reported that elevated Cr_{total}, Mn and Ni concentrations in groundwater can result from these processes. Furthermore, according to Stamatis et al. (2011) naturally occurring Cr_{total} (up to 34.3 μg/L), Mn (up to 132.52 μg/L) and Ni (up to 83.5 μg/L) concentrations have been recorded in water bearing similar rock types. The percentage proportion of the water samples collected from wells with CND values exceeding the PV was 60 %; while the percentage proportion of the water samples collected from boreholes was 21 %. The concentrations of Cd and Pb in groundwater of Megara basin did not exceed the PVs. The Piper tri-linear diagram re-

veals three main water types in the Megara basin (Fig. 2 a, b). In the Ca-Mg-SO_4-Cl water type belong 33.3 % of the water samples of wells and 6.97 % of the water samples of boreholes. The second is Na-Cl-SO_4 water type corresponding to 33.3 % of the water samples of the wells and 18.60 % of the water samples of the boreholes. The third is Ca-Mg-HCO_3 water type which corresponds to 33.3 % of the water samples of wells and to the majority (74.4 %) of the water samples of the boreholes.

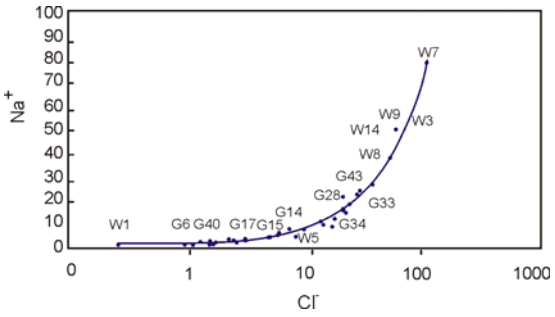

Fig. 3. Na-Cl scatter diagram for the groundwater of Megara basin (meq L^{-1}).

The majority of waters of wells (66.7 %) showed Ca-Mg-SO_4-Cl and Na-Cl-SO_4 types, which generally indicates a mixing process between two types of waters (seawater and fresh groundwater). The calculated Revelle values varied between 0.1 and 16.6; while according to Revelle values the 34.48% of the groundwater samples indicate mixing process between freshwater and seawater. Since the dissolution of carbonate minerals of Triassic limestones-dolomites is generally considered to be a primary source of Ca, Mg and HCO_3^-, the water samples belonging to the Ca-Mg-HCO_3^- type could be considered as infiltration water that moves laterally from the karstic limestones-dolomites to the Neogene sediments and Quaternary deposits. Figure 3 depicts the Na-Cl scatter diagram for the groundwater of Megara basin. In order to improve the visibility of low and moderate saline waters, a logarithmic scale is used for the Cl^- concentration. The curve connecting the end members W1 (minimum TDS concentration = 212 mg/L) and W7 (maximum TDS concentration = 8027 mg/L) represents mixing between fresh groundwater and seawater. It seems that in case of Na and Cl^- almost all the groundwater samples of the study area come from a mixture between end members (W1 and W7) and groundwater of similar chemical composition. The Cl^- concentrations of the groundwaters exceeding the PV in the wells of the coastal areas of Psatha, Ntourakos, Nea Peramos and Pachi could be attributed to the seawater intrusion (Fig. 4a). The lowest Cl^- concentration (8.7 mg/L) was observed at the sampling site W1 and the highest concentration (3954.7 mg/L) was recorded for sampling site W7. The elevated Cl^- groundwater concentrations recorded in an area close to the Megara city could be due to sewage effluents or other anthropogenic causes. Within the Megara basin, agricultural activities that involve the

application of commercial fertilizers are the main source of elevated NO_3^- (up to 411 mg/L) and PO_4^{3-} (up to 4.74 mg/L) concentrations in groundwater.

There is a wide spatial variation in nitrate contents in the groundwater of Megara basin (Fig. 4b). The lowest NO_3^- concentration (0.26 mg/L) was recorded for sampling site W1 and the highest concentration (411 mg/L) was found for sampling site W9. The elevated concentrations of NO_3^- indicate groundwater contamination due to application of fertilizers at the cultivated land and leakage of domestic sewage. Moreover, according to Vijay et al. (2010) the presence of NO_3^- in groundwater is an indicator of very recent sewage contamination.

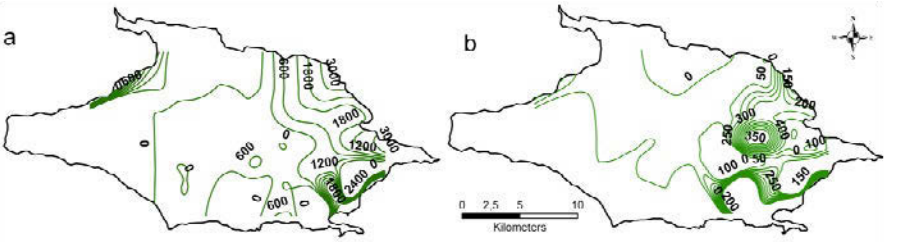

Fig. 4. Spatial variation of chloride (a) and nitrate (b) in groundwater of Megara basin (mg/L).

5 Conclusions

The elevated Cr_{total}, Mn and Ni contents in groundwater of the study area constitute a natural case of contamination where Cr_{total}, Mn and Ni concentrations exceed the PVs established by the European Community. Presence of Mn-oxides, ultrabasic rock fragments within Neogene-Quaternary deposits and bodies of ultrabasic rocks are the natural Cr_{total}, Mn and Ni contamination source for the groundwater of Megara basin. The Piper diagram reveals that the majority of waters of wells showed Ca-Mg-SO_4-Cl and Na-Cl-SO_4 types which generally indicates a mixing process between seawater and fresh. In addition, the calculated Revelle values indicate the mixing process between fresh water and sea water. The majority of waters of boreholes cluster in the Ca-Mg-HCO_3 type which indicates the laterally movement of the water from the karstic limestones-dolomites to the Neogene-Quaternary deposits. The major issues affecting the groundwater quality in the Megara basin are seawater intrusion, especially along coastal aquifers as a result of overexploitation of groundwater resources, nitrate and phosphate contamination in agricultural and urban areas as well as the weathering of ultrabasic rock fragments within Neogene and Quaternary deposits.

References

Aslam S (1982) Geomorphological study of Megara basin. Ph.D. Thesis, National and Kapodistrian University of Athens (in greek)

Bornovas J, Eleftheriou A, Gaitanakis P, Rondogianni Th, Simeakis C, Tsaila-Monopolis S (1984) Geological Map of Greece, scale 1:50000, Kaparellion Sheet.Inst Geol and Miner.Explor.,Athens

Ball J, Izbicki J (2004) Occurrence of hexavalent chromium in groundwater in the western Mojave Desert, California. Appl Geochem 19,1123–1135

Dounas A, Christodoulou G, Tsaila – Monopolis St (1971) Geological Map of Greece, scale 1:50.000, Erithrai Sheet. Inst Geol and Subsurface Research, Athens

EC (1998) Council Directive 98/83/EC Directive of the European Parliament on the quality of water intended for human consumption. The European Parliament and the Council of the European Union. Off J L 330

Gaitanakis P, Mettos A, Koutsouveli A, Rondogiani Th, Tsaila – Monopolis St, Tsapralis K, Chorianopoulou P (1984) Geological Map of Greece, scale 1:50.000, Megara Sheet. Inst Geol and Miner.Explor.,Athens

Gaitanakis P, Mettos A, Fytikas M, Tsaila – Monopolis St, Tsapralis V, Ioakim Ch (1985) Geological Map of Greece, scale 1:50.000, Sofikon Sheet. Inst Geol and Miner.Explor.,Athens

Stamatis G, Alexakis D, Gamvroula D, Migiros G (2011) Groundwater quality assessment in Oropos-Kalamos basin, Attica, Greece. Environ Earth Sci, doi 10.1007/s12665-011-0914-2

Vijay R, Khobragade P, Mohapatra P (2010) Assessment of groundwater quality in Puri City, India: an impact of anthropogenic activities. Environ Monit Assess, doi: 10.1007/s10661-010-1643-9

Environmental associations of heavy and trace elements concentrations in Sarigiol ground water coal basin area

K.I. Vatalis[1], K. Modis[2], F. Pavloudakis[1], Ch. Sachanidis[1]

[1]Technological Educational Institute of Western Macedonia, Kila, Kozani, GR 501 00
[2]National Technical University of Athens, 9 Zografou, Athens, GR 155 73
kvatalis@teikoz.gr

Abstract Ground water samples collected from 21 wells located in the hydrogeological, coal-bearing basin of Sarigiol, Western Macedonia, Greece have been analysed for determining trace elements concentrations. The water quality assessment reveals that the concentrations of heavy and toxic metals and trace elements are, for most of the samples; bellow the allowable limits specified by the existing regulatory framework. The trace elements As, Cd, Cu, Zn, V, Co, Be, B and Al are detected in very low concentrations, while Ti and Sn are detected in very low to negligible concentrations. The elements Pb, Hg, Ni, Mo, Cr_{tot} and Ba are present in low concentrations. This is also the case for Sr, Te and Bi. For these elements the legal framework does not specify allowable limits. Concentrations closed to or above the allowable limits have been determined for Sb and Tl. In addition, samples of water that have been collected from certain parts of Sarigiol basin show concentrations above the allowable limits for Al, Be, Ni, Cr, Sr and Se. However, the enrichment ratio, compared to the allowable limits determined by laws and regulations, is very low. Based on the results presented and evaluated in this contribution, it is concluded that adverse impacts to the human and natural environment are not probable. The water pumped from the wells of the area can be used safely for irrigation and water supply.

1 Introduction

The present study investigates the ground water quality characteristics of the hydrogeological basin of Sarigiol as far as the concentrations of 24 trace elements are of concern. The study examines trace and minor elements. For reasons of simplicity the term trace elements is used for both. The qualitative characteristics of the hydrogeological basin are determined from its sediments, the rocks of the surrounding mountains, the dynamic agricultural activities and the lignite mining activities of Public Power Corporation SA, which are divided into five open-pit mines with a total annual lignite production of 43Mt and total excavations of 280

N. Lambrakis et al. (Eds.), *Advances in the Research of Aquatic Environment, Vol. 2*
DOI 10.1007/978-3-642-24076-8,

Mm^3. According to the environmental permits of the lignite mining activities, the concentrations of the following trace elements and heavy metals must be determined on an annual basis: As, Pb, Cd, Hg, Ni, Cu, Cr, V and Zn. Further to these elements, in order to come to safer conclusions regarding the environmental impacts and ground water quality, in the frame of the present contribution the concentrations of the following trace elements are also determined: Al, Ba, Sr, Se, Sn, B, Be, Tl, Ag, Bi, Ti, Te, Sb, Co and Mo, as well as the concentrations of the main oxides of Fe and Mn and the pH value. Previous studies have shown that lignite mining does not affect the concentrations of heavy metals and trace elements and all the main physical and chemical characteristics of both surface water discharged from the mines (i.e. surface run-off collected in pumping stations that are usually constructed at the lowest points of mine pits) and ground water pumped from pit protection wells (i.e. wells bored for lowering water-table in order to reduce or even eliminate ground water inflow in the mine pit) (Sachanidis et al. 2001; Vatalis and Kaliampakos 2006). On the contrary, the quality of the water pumped from the wells is closely related to the sediments of Sarigiol basin and the rocks that surround the basin, which are mainly calcareous but also ultramafic and metamorphic (Figure 1). As far as the pH is concerned, it is alkaline both in surface and groundwater (Sachanidis and Pavloudakis 2001) and the soils of Sarigiol basin (IGME 1997). This fact, combined with the absence of acid mine drainages in the entire lignite mining area of Western Macedonia, does not favour the mobilization of trace elements.

2 Geological and hydrogeological conditions

The sedimentation basin of Sarigiol belongs to the Pelagon zone and is part of the tectonic trench of Bitola - Florina - Ptolemais - Kozani. The substrata and the rocks that surround the sedimentation basin consist of the crystallised schist of Pelagon zone. The Neogene sediments of the basin lie uncomformably on the crystallised schist. The quaternary sediments lie also uncomformably on the sediments of Pliocene (Anastopoulos and Koukouzas 1972). Karstified aquifers exist in the calcareous rocks that form the surrounding mountains (Vermio [East], Askion [West] and Skopos [South]) (Fig. 1). Bellow the sediments of the basin another deep karstified aquifer exists. In the quaternary sediment numerous aquifers exist, forming an upper system of aquifers with large ground water reserves and a lower system of aquifers of limited potential. The upper part of this polystromatic (multi-layered) aquifer is developed in the zone of overburden of the lignite-bearing strata, which consists from Quaternary sediments of maximum depth of 360m, while its lower part is developed below the lignite-bearing strata and consists of fine-particle materials of Pliocene and, in some parts of the basin, of Oligocene.

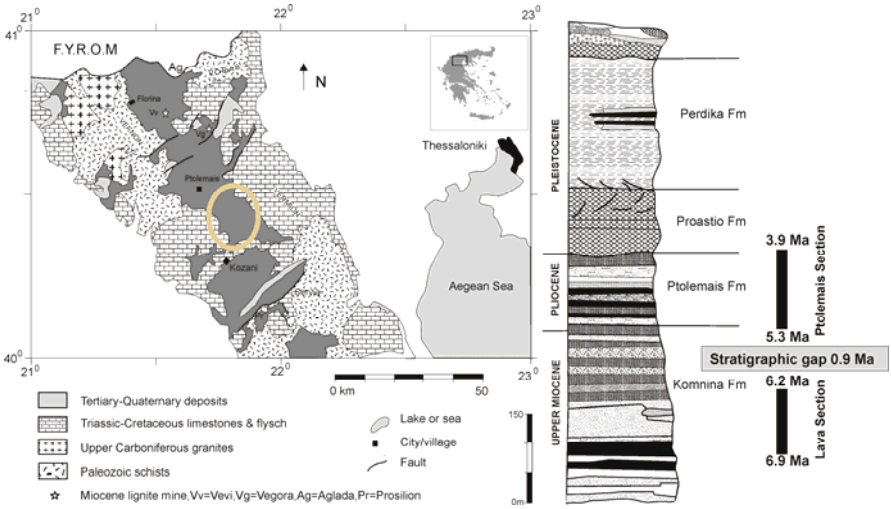

Fig. 1. Geological map of the study area and water sampling area. Source: GPPC 2010.

Practically impermeable formations are the folded metamorphic rocks, the flysch of upper Cretaceous, the lignite seams of Pliocene, while semi-permeable formations are considered the fractured ofiolite and the very fine clastics Quaternary and Neogene sediments. The maximum depth of Neogene sediments in the central part of the basin is 900m, while close to the margins of the basin the sediments have much less depth and are in contact with the calcareous rocks and karstified aquifers. The aquifers are unconfined, confined and aquiclude (leaky) and are characterized as anisotropic and inhomogeneous (Panilas and Koumantakis 2001).

3 Materials and methodology

Water samples were collected from both irrigation and water supply wells in a 9-years period (2000-2008). The number of samples collected from each one of the 21 wells varies from 8 to 12. The spatial distribution of the sampling points in the study area is presented in Figure 1. It is worth noticing that the physical and chemical parameters that were analysed were the same for all samples, no matter if they were collected from irrigation or water supply wells. Water samples were analyzed with atomic absorption analyzer, while for the determination of the heavy metals and trace elements concentrations ICP mass spectrometry was used.

4 Results

The results of chemical analyses were evaluated taking into consideration their spatial distribution in order to come to safer conclusions regarding the variations of trace elements concentrations in the ground water of Sarigiol basin. Based on the results presented in Table 1, there is evidence of water quality variations, in some cases significant, which can be related to (i) the depth of the Pliocene and Pleistocene sediments, (ii) the origin of water and the mechanism of water transport to the multilayered aquifer, (iii) the contact with rocks of the surrounding mountainous zone, and (iv) the stratigraphy of the Quaternary and Pliocene sediments (Panilas and Koumantakis 2001). The pH value varies slightly from neutral to alkaline, with an average value close to 7.5.

In seven wells located in the NE, SW and S parts of the basin, the total Iron and Manganese concentrations are high, with maximum values of 1,676 μg/L and 65 μg/L, respectively. Both values are above the allowable limits of 200 μg/L for Iron and 50 μg/L for Manganese. The explanation for these high concentrations can be related to one or more of the following facts:

- The presence of metamorphic rocks and clastic sediments in streams that were contemporary with the lake, which was filled with material originated from the metamorphic schist of the surrounding mountains.
- The presence of pyrite in high concentrations, in certain areas. Its dilution, under certain oxidation-reduction conditions favours the enrichment of groundwater in Iron and Manganese.
- The synclinal aspect of the layers, which allows, combined with the development of confined and aquiclude aquifers of short length, the development of reduction conditions, which in turn contribute to high concentrations of Iron and Manganese.
- The sulphates (SO_4), which are related to pyrite crystals that have been detected in the sediments and in the lignite deposit. Sulphates, after oxidation and biogenic processes, are a source of Sulphur and Iron (Lambrakis 2009).

It is worth noticing that the high concentrations of total Iron and Manganese in ground water pumped from these seven wells makes impossible its use for water supply without previous treatment.

As far as the trace elements concentration is of concern, the basic rule of nature that *everything contains a little of everything* is valid also in the examined case. All trace elements are present in various concentrations, which do not impact adversely the aquatic environment and do not deteriorate the water quality in a way that reduces the available water quantities for water supply, irrigation and industrial use. More specifically, based on their concentrations, trace elements have been divided into the following five groups:

Table 1. Concentrations in ppb of heavy metals and trace elements in Sarigiol basin (N=42).

	NE part of Sarigiol basin			SW part of Sarigiol basin			Permissible limits
	min	max	stdev	min	max	stdev	
As	0.49	1.53	0.33	0.50	0.58	0.04	10 μg/L*
Cd	<2.0	<2.0	0	<2	<2	0	5 μg/L*
Pb	<10	<10.0	0	<10	<10	0	20 μg/L*
Hg	<0.5	<0.5	0	<0.5	<0.5	0	1 μg/L*
Ni	<10	79	<6.9	<10	<10	0	20 μg/L*
Cr (tot)	<5	41.70	<12.39	<10	14.00	<1.22	50 μg/L*
Cu	<5	<5	0	4.60	7.00	0.79	2000 μg/L*
V	<5	<10	<2.47	<5.0	<5.0	0	200 μg/L*
Zn	2.20	194	61.47	8.30	16.00	2.00	5000 μg/L*
Al	20	856	292	21.6	23	0.67	200 μg/L*
Ba	17.6	67.2	17.8	34.7	35.00	0.14	100 μg/L*
Se	<10	<10	0	<10	<10	0	10 μg/L*
Sr	135	290	109	178	234	39.6	8000 μg/L2
Mo	<5	<10	<2.25	8.10	9.00	0.20	10 μg/L2
Co	<10	<10	0	<5	<5	0	10*
Sb	<10	<20	<4.94	<10	<10.0	0	10 μg/L*
Sn	<10	<10	0	<10	<10	0	5000 μg/L*
Tl	<10	<10	0	<10	<10	0	2 μg/L***
Te	<10	<20	<18.6	<10	<20	<3.5	
Ti	<2	<2	0	<2	<2	0	500 μg/L*
Bi	<10	<10	<10	<10	<10	0	
Be	<.02	<50	<13.9	<0.2	<0.2	0	500μg/L1
B	<.02	<50	<13.9	<50	<50	0	1000 μg/L*
Ag	<10	<10	<10	<10	<10	0	10 μg/L*
Fe	0.0	1.2	0.6	45	354	218.4	200 μg/L*
Mn	0.0	0.01	0.005	25	65	28.2	50 μg/L*
pH	7.4	7.8	7.6	7.33	7.61	0.20	6.5-9.5

*Common Ministerial Decision Y2/2600/2001, **European Community Directive, ***US-EPA
[1]USWA Sc.-USNA Eng. (1972). [2]Lambrakis, N. Introduction to Geochemistry Patras.

Concerning the trace elements Arsenic (As), Cadmium (Cd), Copper (Cu), Vanadium (V) and Boron (B) exhibit very low concentrations Moreover, Zinc (Zn) also displays low concentrations except from an analysis of a sample deriving from the SE part of the basin, Aluminum (Al) except for the SE part of the basin, where the maximum concentration that have been determined is 856 μg/L but also Cobalt (Co) and Beryllium (Be) with average concentrations less than 0,20 μg/L except from the samples coming from the NE part of the basin, where the concentration is higher but less than 50 μg/L. Additionally, Tin (Sn) displays average concentration

less than 10 μg/L when the allowable limit is 5,000 μg/L and Titanium (Ti) average concentration less than 2 μg/L when the allowable limit is 500 μg/L.

The trace elements that exhibit low concentrations are mainly Barium (Ba), and Lead (Pb). Mercury (Hg) also displays low concentrations except for samples coming from S and SE parts of the basin, where their concentrations varies between <5 μg/L and <10 μg/L. These higher concentrations are probably related to the formation of organic mercury compounds that are steady in aquatic systems (Kabata-Pendias 1992) or to the presence of HgS, metallic Hg and epigenetic pyrite (Finkelman 1998). Generally, Nickel (Ni) concentrations are low except for samples deriving from the SE part of the basin, where the maximum concentration is 79 μg/L. High Ni concentrations are probably related to: (i) the paleogeographic characteristics, especially the flow of Aliakmonas river through the study area during Villafrancian (Faugeres 1978) and the effects of sedimentation due to the transfer and sedimentation of Ni minerals from the ultramafic formations of the greater tectonic basin of Florina - Ptolemais - Kozani and (iii) the presence of millerite in the lignite deposit (Swaine 1990).

Mainly the total Cr (Cr_{tot}) concentrations are low except for the SE and E parts of the aquifer where higher concentrations have been determined. According to its geochemical character, the study area is affected from the presence of ultramafic rocks in the surrounding mountainous area (Vermion and Askion) (Faugeres 1978) and not from human activities.

There are also trace elements that they have not specified regulations, these are Tellurium (Te) and Bismuth (Bi).

Strontium (Sr) concentrations are relatively higher (maximum values 1,200 μg/L and 2,000 μg/L in samples collected from the NE and E parts of the basin) in relation to the other parts of the basin, where concentrations are very low. The value of 8,000 μg/L is referred as average concentration in sea water. Geochemically, Strontium is connected with sulphuric minerals contained in the sediments of the basin as easily diluted minerals, such as Gypsum and Anhydrite and less easily diluted minerals of Ba and Sr, such as Strontianite ($SrCO_3$) and Selenite ($SrSO_4$) (Lambrakis 2009).

Molybdenum (Mo) concentrations in natural water vary between 1-3 μg/L (Lambrakis 2009). The relatively higher concentrations in two wells located in W and SW part of the aquifer (with average concentrations of 8.5 μg/L and 7.74 μg/L, respectively, probably occur due to the presence of organic matter and iron oxides (Kabata-Pendias 1992).

According to the results there are also trace elements that present variable concentrations, always below the regulations, these are Selenium **(**Se) except for an analysis of a sample coming from the E part of the basin, with concentration of 21 μg/L (Selenium concentration in water usually does not exceed 1μg/L) and Silver (Ag) that its concentration is related to the presence of sulphuric minerals in sediments.

Finally, there are also trace elements with concentrations that are close to or above the regulations, these are Antimony **(**Sb) which in general, displays concen-

trations less than 10 μg/L, except for the SW and E parts of the basin, where the maximum concentration reaches <20 μg/L and Thallium (Tl) that its concentrations are constantly less than 10 μg/L when the allowable limit is 2 μg/L.

It is worth noticing that for the Antimony and Thallium the maximum allowable concentrations specified by the law are below the detection limit of the analyzer used in the frame of this study. Thus, for concluding that the concentrations of these elements are above the limits further sampling and analyses with more precise analytical techniques are required. In any case, the concentration of these two elements is related to presence of sulphur minerals in the sediments. Antimony concentrations are due to its organic affinity with the lignite deposit as well as due to volcanic activity (Swaine 1990).

5 Conclusions

From the evaluation of chemical analyses of water samples collected from 21 wells located in Sarigiol lignite-bearing basin and concern 24 trace-elements and two major elements the following conclusions have been reached:

- In general, the concentrations of the nine heavy-toxic metals, the fifteen trace elements - minor elements and two major elements (Iron and Manganese) in the groundwater of the sedimentary basin are low to very low and, in some instances, negligible. In certain parts of the basin, concentrations above the allowable limits have been determined in some of the water samples that were collected and analyzed during the 9-years period of this study.
- The concentrations of the trace elements, the two major elements and the pH value are closely related to the petrographic and stratigraphic characteristics of the sedimentary aquifer and the surrounding mountains. The relatively high concentrations of Ni and Cr_{tot} at the SE and E parts of the basin are connected directly to the presence of ultramafic rocks of the SW part of Vermion Mountain.
- There is no adverse impact in the quality of water of aquifers, which are currently used for meeting the demand of water supply, irrigation and industrial consumption. Water meets all the standards determined by the legal framework.
- Water with trace elements concentrations above the maximum allowable limits, which is pumped from certain wells, can be used for water supply after mixing with water pumped from neighboring wells that exhibit low trace elements concentrations.

References

Anastasopoulos, I and Koukouzas, K. (1972) Geology and economy geology in the south part of coal bearing basin of Ptolemais. pp 201, IGEY

Faugeres, L. (1978) Recherches geomorphologiques en Grece septentrionale. (Macedoine Centrale et Occidentale) Tome I, II. These Universite PARIS IV, Paris

Finkelman, R.B. (1998) The inorganic geochemistry in coal: a scanning electron microscopy view, Scanning Micros., 2(1), 97-105

IGME (1997) Chemical soils and soils study of the area Kozani-Ptolemais-Florina. Phani Gerouki Geologist-Geochemist. Second European Common Programme Support. Athens

Kabata, A. Pendias H. (1992) Trace elements in soils and plants. (2nd Edition). CRS Press, London

Lambrakis, N. (2009) Introduction to hydrogeochemistry. University of Patras / Department of Geology. Patras 2009

Panilas, S. Koumantakis, I. (2001) Ground water quality characteristics in South Field sub-basin of Ptolemais basin. 9th International Congress of the Geological Society of Greece. 3, 1893-1901. Athens

Sachanidis, C. Pavloudakis, F. and Charalambidis, G. (2001) Quality characteristic of soil waste dumps of the Ptolemais - Amyntaion Lignite Center. First Environmental Congress of Macedonia, Proceedings, pp 219-224, Thessaloniki

Sachanidis, C. Pavloudakis, F. (2001) Monitoring and control of the surface and ground water quality in the greater area of the mines of Ptolemais - Amynteon Center. Proceedings of Conference of The Geological Society of Greece. Vol XXXIV/5, 1941-1949, Sept. 2001

Swaine, D.J. (1990) Trace Elements in Coal. Butterworths London, Boston, Sydney, Toronto, Wellington

Vatalis, K.I. and Kaliampakos, D.C. (2006) An overall index of environmental quality in coal mining areas and energy facilities. Environmental Management, 38(6), 1031-1045

Marine and human activity effects on the groundwater quality of Thriassio Plain, Attica, Greece

V. Iliopoulos[1], G. Stamatis[2], G. Stournaras[1]

[1]Faculty of Geology and Geoenvironment, National & Kapodistrian University of Athens, Department of Dynamic Tectonics and Applied Geology, Panepistimioupolis Zografou,15784 Athens – Greece, viliopoulos@geol.uoa.gr,
[2] Division of Geological Science and Atmospheric Environment, Laboratory of Mineralogy and Geology, Agricultural University of Athens, Iera Odos 75, 11855 Athens, Greece

Abstract The Thriassio plain is located west of the city of Athens, in Attica prefecture, Greece, and is a favorable site for industrial development. The intense industrialization of the last few decades in the Thriassio plain has caused major pollution problems. Thus, several pollutants produced in this area are seriously polluting the air, soil and water. The present case study emphasizes on the hydrochemical conditions of Thriassio Plain's aquifers, including the study of the geological and hydrogeological factors. In order to determine the factors influencing water quality in the study area, groundwater samples from springs, wells and boreholes were analyzed. The graphical representations of the chemical analyses show that the main parameter controlling the chemical composition of groundwater is the human factor (industrial development, agricultural activities, groundwater over-exploitation). This results in serious degradation of groundwater quality in the study area due to seawater intrusion and heavy metals pollution.

1 Introduction

The Thriassio Plain is a well known industrial zone of Greece which is located in Attica. In this area during the last decades several changes of land use have been implemented focusing in industrialization. This transition was made without a decent environmental policy. The lack of a national water resources management strategy until very recently should be taken into consideration, in order to understand the extent of the problem related to the severe groundwater-quality deterioration in the Thriassion area. In addition, the presence, in the areas of Nea Liossia (east of the study area) and Aspropyrgos, of open dumps of disposing 1 million tn yr^{-1} of municipal wastes and 23,000 tn yr^{-1} of toxic wastes, generated in Metropolitan Athens, is an additional source of toxic leachates polluting the Thriassion Plain aquifers (Karavitis et al. 2001).

N. Lambrakis et al. (Eds.), *Advances in the Research of Aquatic Environment, Vol. 2*
DOI 10.1007/978-3-642-24076-8,

The study area mainly consists of alluvial deposits, Pleistocene torrential fan deposits, dilluvial conglomerate, Neogene flysch, Triassic and Cretaceous limestones and Paleozoic formations, parts of the sub-Pelagonian zone. Most of these formations are highly permeable (karstic limestones in the northern part of the region and clastic formations in the southern one). In the area two major aquifers are developed, one upper in the unconsolidated deposits and a deeper karstic one into the basement carbonate formations. The geological, hydrogeological and hydrochemical characteristics of the Thriassio Plain area are presented. A hydrochemical study was conducted in the Thriassio area, Attica, Greece (Fig. 1). This area was chosen for the following main reasons: (a) the continuous overexploitation of groundwater resources has caused groundwater table to decline as much as 3 to 7m in the last years (Karavitis et al. 2001), (b) the pollution of the groundwater as a result of various polluting activities (Kapniaris et al. 2005), and (c) the presence of saltwater intrusion into the coastal aquifer. This paper illustrates the distribution of the contaminants in the ground-water of the study area. The main target is to correlate the contamination with the environmental and human activity impact. The data of this paper are derived from the research that was conducted by Iliopoulos (2007) in the bachelor thesis.

2 Geological and hydrogeological setting of Study area

The Thriassio Plain geographically belongs to NW Attica. Its southern border is the Elefsis bay which has a coastline of approximately 15 km. This plain is situated between mount Egaleo, Patera and Parnitha at the SE, N and NE respectively. The Thriassio alluvial basin presents a smooth geomorphology and its flat part extends up to 100 km^2. This feature represents a prequaternary palaeokarstic graben that had been filled during the Quaternary with fluvial and lagunal deposits of 200 m thickness (Dounas 1971). The study area is mainly composed of carbonate formations and sedimentary deposits of Triassic to Paleocene age. They range in age from Triassic to Holocene Alluvial fans and older talus cones of Holocene age and dilluvial conglomerate are also present (Dounas 1971). The alpine formations include: a) flysch, b) Cretaceous Limestones, c) Thick karstified Triassic white dolomitic limestones. Alternations between carbonate Paleozoic formations, shales and sandstones are observed (Karabela 1997). Bauxite ores occur also in the west part of the Thriassio plain. A prequaternary palaeo-karstic graben is formed in this area which during the Quaternary period was filled by sediments deposited in lake and river environments. Permeable karstic and porous geological formations prevail in the study area. Cretaceous limestone layers are the principal geologic units in the karstic aquifer, the main aquifer in the Thriassio Plain, and crop out or underling much of the study area mainly in its NE part. The mean permeability is estimated about 10^{-3} m/s (Paraschoudis 2003).

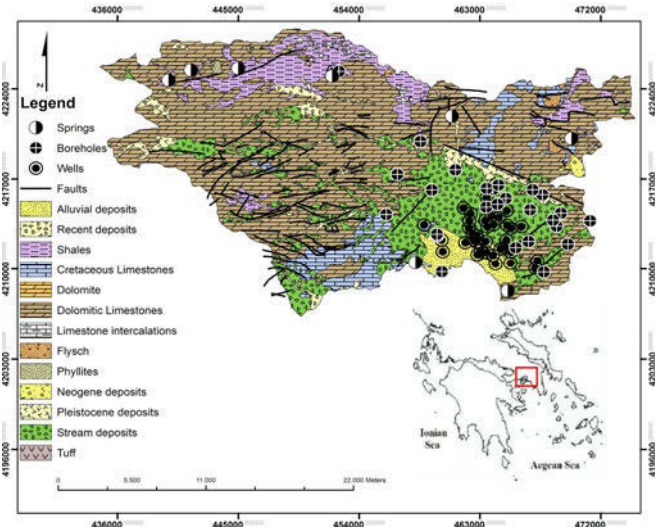

Fig. 1. Geological Map of the study area (Katsikatsos et al. 1986).

The boreholes that exploited the karstic aquifer have been characterized by the high values of water supply (100-200 m^3/h). A significant percentage of the karstic waters, which theoretically follow the slope of the sediments and the strike of the fault zones, has been discharged in the low topographic areas through the coastal (Koumoundouros Lake and Elefsis coastal springs) and the underwater springs which are located into and west of the Gulf of Elefsis. The clastic formations which consist of Pleistocene and Neogene deposits compose the upper aquifer. The number and spacing of fractures is very important in controlling both porosity and hydraulic conductivity of the unconfined aquifer. The hydraulic conductivity (K m/s) in the unconsolidated permeable formations is between 10^{-2} m/s and 10^{-4} m/s (Paraschoudis 2003). Development of groundwater supplies for agricultural and industrial purposes led to overexploitation of groundwater in the study area. This is justified by the great number of wells and boreholes in the present area of study.

3 Material and Methods

The Groundwater samples were collected March-April 2007. The samples were collected from 39 dug wells, 8 springs and 26 boreholes. Portable devices were used in order to measure the physicochemical parameters in situ, such as temperature (^oC) and Electrical Conductivity EC (WTW/LF-330), pH value (WTW/330i). Additionally, this research in the laboratories of the National and Kapodistrian University of Athens and the Agricultural University of Athens, using the titration

methods, spectralphotometric methods (HACH, DR/3000), flamephotometric methods (INTECH/420) and atomic absorption spectrometer (GBC/908/AA), detected the following parameters: hardness, Ca^{2+}, Mg^{2+}, Na^{+}, K^{+}, HCO_3^{-}, Cl^{-}, SO_4^{2-}, NO_3^{-}, NO_2^{-}, NH_4^{+}, PO_4^{3-} and heavy metals such as, Fe_{tot} and Cr_{tot}. Table 1 below shows the results the analyses.

4 Groundwater quality

Maximum, minimum and average concentrations of major ions present in groundwater (from dug wells, springs and boreholes) from the study area are presented in Table 1.

Table 1. Groundwater chemical analysis results.

Parameter		39 Dug Wells			8 Springs			26 Boreholes		
		min	max	Aver.	min	max	Aver.	min	max	Aver.
Temp.	(^{o}C)	16.0	36.00	20.9	12.5	20.0	16.6	18.0	31.0	21.4
pH		6.75	8.04	7.42	6.68	7.80	7.17	6.66	8.02	7.20
EC	(μS/cm)	316	6932.00	3624	313	15550	4173	335	4324	1558
TDS	(mg/L)	265	7347.00	2804	286	26953	5049	220	4244	1891
Hrd_{tot}	(^{o}dH)	10.1	194.60	102.3	10.6	31.6	19.4	8.4	77.4	42.9
Ca^{2+}	(mg/L)	41.6	801.60	190.9	43.2	297.6	133.5	43.2	296.8	121.9
Mg^{2+}	(mg/L)	7.8	492.30	128.1	3.4	611.9	171.7	6.3	155.8	55.3
Na^{+}	(mg/L)	1.0	1050.00	332.1	4.7	5520.0	1332.3	3.5	905.0	218.1
K^{+}	(mg/L)	0.2	34.00	5.3	0.1	76.7	12.1	0.6	39.2	8.8
NH_4^{+}	(mg/L)	0.15	6.80	1.24	0.15	5.23	1.34	0.17	7.15	0.82
HCO_3^{-}	(mg/L)	135.4	3506.50	546.4	189.3	563.2	344.9	112.3	509.2	304.3
Cl^{-}	(mg/L)	20.0	3385.00	760.5	10.0	9400.0	2313.1	5.0	1635.0	449.4
SO_4^{2-}	(mg/L)	5.0	440.00	165.9	10.0	1550.0	366.2	5.0	355.0	101.1
NO_3^{-}	(mg/L)	6.8	232.70	65.5	2.9	15.8	7.5	0.7	112.4	25.6
NO_2^{-}	(mg/L)	0.01	424.60	32.5	0.01	1.40	0.19	0.01	311.8	22.25
PO_4^{3-}	(mg/L)	0.05	1.72	0.25	0.07	1.80	0.32	0.05	0.37	0.13
Fe_{tot}	(ppm)	0.110	0.23	0.172	0.124	0.212	0.178	0.118	0.256	0.177
Cr_{tot}	(ppm)	0.001	0.10	0.040	0.001	0.035	0.012	0.001	0.051	0.016

The values of the physical and chemical parameters for all the samples were significant, especially for the samples obtained from the phreatic aquifer. Water samples that were collected from dug wells and boreholes located along the coastal area present higher content of chemical species. Water samples from the phreatic aquifer present (Table 1) the following range in the chemical composition of

the groundwater: EC: 316-6,932 μS/cm, TDS: 265-7,347 mg/L, Na^+: 0.1-1,050 mg/L, Cl^-: 20-3,385 mg/L, SO_4^{3-}: 5-440 mg/L, NO_3^-:6.8-232.8 mg/L, NO_2^-: 0.0026-424.0 mg/L, NH_4^+: 0.15-6.8 mg/L and PO_4^{3-}: 0.05-1.72 mg/L. These high concentrations in some dug wells and boreholes may be indicating the impacts of human activity such as septic tanks, livestock establishments and industrial waste that degrade the phreatic groundwater quality. High NO_3^- content in the study area is also mentioned in older studies (Stournaras 1994, 1998; Lioni et al. 2008). As a result the groundwater salinity values exceed the European standards which mean that is not suitable for any kind of use (EEC/80/778, 1980, 1999). Most of the spring water samples are characterized by low concentration values of the chemical species. All of these springs are located in metamorphic rocks in the north part of the area which is not affected by anthropogenic activities. The values of the chemical species range as follow: EC: 312-15550 μS/cm, TDS: 286-26.953 mg/L, Na^+: 4.7-5520 mg/L, Cl^-: 10-9400 mg/L, SO_4^{2-}:10-1550 mg/L, NO_3^-: 2.9-15.8 mg/L, NO_2^-: 0.012-1.4 mg/L, NH_4^+: 0.15-5,225 mg/L and PO_4^{3-}: 0.07-1.8 mg/L. The higher values of concentration of the ions of Na^+ (5,100-5,520 mg/L), Cl^- (8,900-9,400 mg/L) and SO_4^{2-} (1200-1550 mg/L) are observed in the springs of the coastal zone.

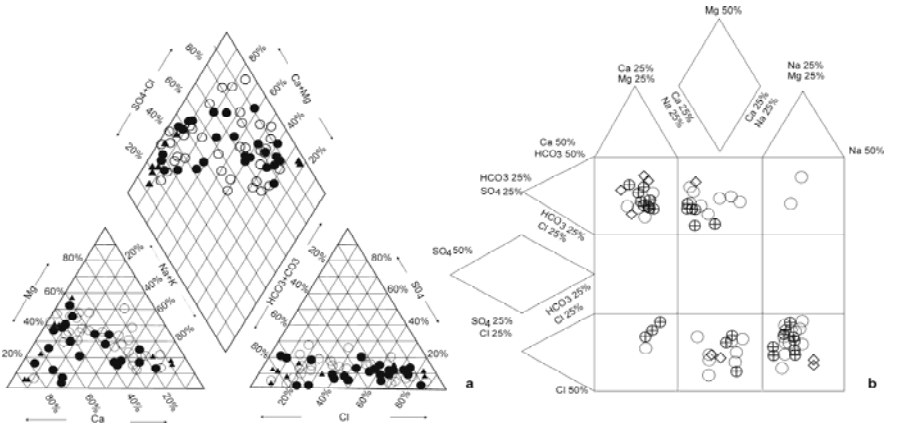

Fig. 2. Piper and Durov Diagrams for groundwater quality in the study area.

Obviously these high values are due to the sea water intrusion. Water classification based on the Piper (3a) and expanded Durov (3b) (Lambrakis 1991) diagrams are shown in Figure 3. The main hydrochemical types of the springs are Ca-HCO3 and Mg-HCO3, while the samples from the dug wells and boreholes are characterized by the presence of the following hydrochemical types: Na-Cl, Ca-Cl, Mg-Ca-Na-HCO_3-Cl-SO4 and Ca-Mg-Na-HCO_3-Cl.

In the Durov diagram six distinct groundwater quality types are discriminated by their plotting in certain subareas. In the first two fields fresh groundwaters are included which are enriched by Ca-HCO_3 and Mg-HCO_3. Groundwaters fall in the hydrochemical type Na-HCO_3 (third field), which results from cation exchange

processes. In the fields 7, 8 and 9 represent water samples with hydrochemical types of Ca-Cl, Mg-Cl and Na-Cl, which are respectively situated. The water samples in these fields have been hosted for a long period in the aquifer and through the cation exchange process (sea intrusion) the Na-Cl type is prevail.

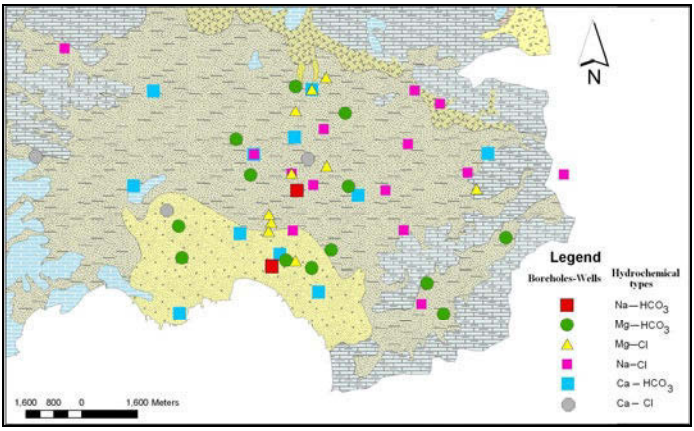

Fig. 3. Distribution of the various hydrochemical types of the groundwaters in the study area.

In Figure 3 is presented the distribution of the various hydrochemical types of the groundwaters. It is observed that the fresh water of enrichment, which have a hydrochemical type of Ca-HCO_3 type and Mg-HCO_3 type, are developed mainly to the northern and eastern parts of the Thriassion plain. These waters are coming from the carbonate consolidated formations that mainly from the north borders of the plain. The ground waters which belong to the hydrochemical types of Na-Cl, Mg-Cl and Ca-Cl types are located to the central part of the plain.

These specific waters are older and have been characterized of reverse cation exchange. The spatial distribution of Cl^-, $Cr_{tot,}$ Fe_{tot}, NO_3^-, Na^+, PO_4^{3-}, as well as the hydrochemical types of groundwaters are shown in Figure 4. According to the ions distribution of Cl^- and Na^+, is situated in a sea water intrusion interface west of the plain and is estimated up to 4-5 km to the mainland. The presence of high NO_3^- and PO_4^{3-} contents in groundwater from aquifers located in the urban and industrial area indicates serious deterioration of groundwater quality. Their presence is mainly attributed to the occurrence of septic tanks and the extensive use of fertilizers. The significant amount of the heavy metals Fe_{tot} and Cr_{tot} in the industrial zone as well as in the northern area can be related to geological and anthropogenic factors.

Severe pollution by heavy metals regarding the alluvial plain has been reported by Mavrakis et al. (2003). Coastal waters have been contaminated by Pb (Kersten M. et al 1997). Also the intense industrial activities and the observed soil contamination from industrial pollutants contributed to the aquifer quality deterioration.

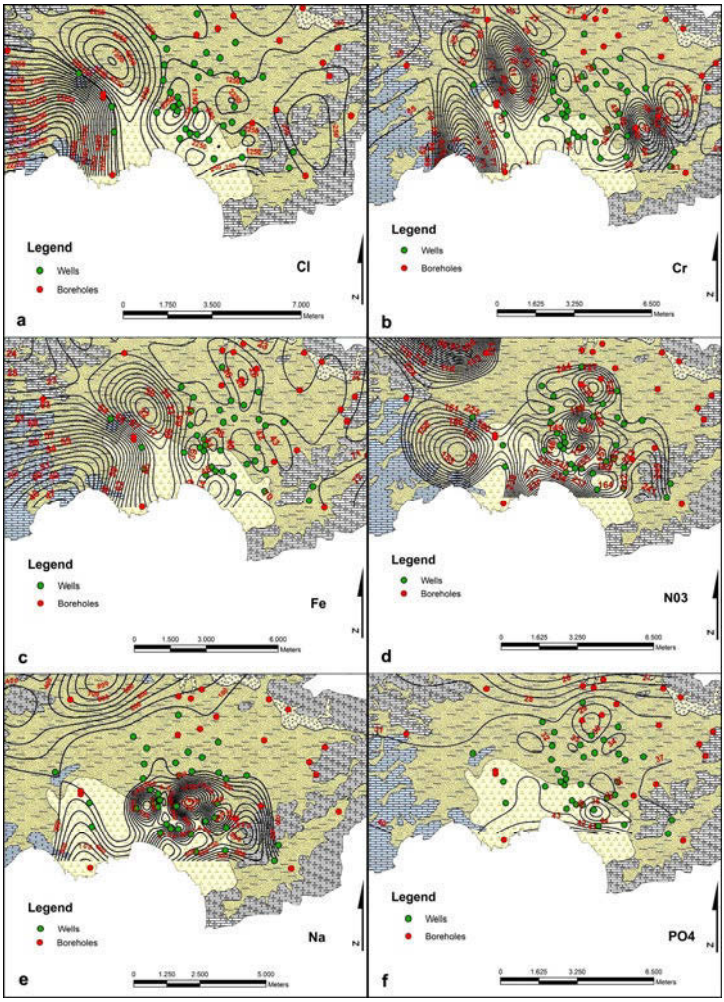

Fig. 4. Spatial distribution of (a) Cl^-, (b) Cr_{tot}, (c) Fe, (d) NO_3^-, (e) Na, (f) PO_4^{3-}.

Conclusions

The hydrochemical research that has been performed in the Thriassion plain has led to the following results: (a) In the area two aquifers have been developed, the karstic which is hosted in the intensively karstic carbonate formations, and the phreatic aquifer which is developed into the unconsolidated basin formations. (b)The quality of the mountain springs is characterized as alkaline with middle values of hardness and low concentration of total salts. Those waters belong to the hydrochemical type of Ca-HCO_3 and Mg-HCO_3. These waters are fresh, enriched

and are appropriate for any use.(c) On the contrary the water of the wells and boreholes coming from phreatic aquifer are degraded and present high concentrations in Na, Cl, SO_4, NO_3, NH_3 and PO_4 ions. These waters are characterized by degraded quality and are located mainly to urban and agricultural areas. Their overweighting is mainly due to the human activity (septic tanks, fertilizer usage, and industrial units) and the lack of environmental policy for the industrial and agricultural wastes. The hydrochemical types of Na-Cl, Mg-Cl and Ca- Cl which have been resulted through reverse cation-exchange processes are situated in the coastal zone. The greatest percentage of these groundwaters is being judged as improper for human usage.(d) By the shore, an area of sea-water intrusion has been located with concentrations of Cl and Na^+ ions that range from 1000 mg/L to 3385 mg/L and 0.5 mg/L to 1050 mg/L respectively. According to the spatial distribution maps of Cl and Na^+, the seawater intrudes for 4-5 km into the mainland.

Acknowledgments We would like to thank Professor Nikolaos Lamprakis, University of Patras, for the usage of the software (Lambrakis 1991) to project our data analysis in Durov expanded diagram.

References

Asimakopoulos D, Abatzoglou G (1989) Temporal and spatial distribution of pollution load in the Gulf of Eleusis, Proceedings of Congress of Env. Science and Technology, pp.355-370

Dounas A (1971) The geology between Megara and Erithres area, PhD University of Athens

Kapniaris S, Pantazidou M, Katsiri A and Christidis A (2005) Water and Sediment Pollutants in Elefsis Bay: Spatio-temporal trends and a risk-ranking approach, 9th GNEST (Global Network for Environmental Science and Technology) Conference of Environmental Science and Technology, Rhodes, Greece, Sept. 1-3

Karabela A (1997) Geomorphological and environmental evolution of Triassic field, PhD University of Athens

Karavitis CA, Bosdogianni A, Vlachos EC (2001) Environmental Management approaches and water resources in the stressed region of Thriassio, Greece, Global Nest: Int. J. 3(2), 131-144

Katsikatsos G. et al (1986) Geological Map Athens-Eleusis 1:50.000, I.G.M.E

Kersten M, Schonberg CDG, Thomsen S, Anagnostou C, Sioulas A (1997) Source apportionment of Pb pollution in the coastal waters of Elefsis bay, Greece

Lambrakis, N (1991) Elaboration of the hydrochemical data by PC. Mineral Wealth 74, 53-60 (In Greek)

Lioni A, Stournaras G, Stamatis G (2008) Degradation of Groundwater quality of Thriasio Plain through Natural Factors and human activity, Proceedings of the 8th Hydrogeoloical Congress of Greece, 2 577

Mavrakis A. Theocharatos G. Asimakopoulos D.N. Christides A. (2003) Distribution of trace metals in the sediments of Elefsis Gulf, Proceedings of 6th Hellenic Congress of Oceanography, I, 183-188, Chios

Paraschoudis V (2003) Hydrogeological study of Western Attica, Ministry of Agriculture (unpublished in Greek)

Stournaras G (1994) A trashyard to a graveyard, environmental aspects, J. Environ. Hydrol., 2(2)

Stournaras G (1998) Groundwater and Nitrates in Greece, an Overview, Journal of Environmental Hydrology 6

Transport of pathogens in water saturated sand columns

V.I. Syngouna, C.V. Chrysikopoulos

Department of Civil Engineering, Environmental Engineering Laboratory, University of Patras, Patras 26500, Greece.

Abstract Groundwater protection from microbial contamination necessitates a solid understanding of the factors controlling the migration and retention of pathogenic organisms (biocolloids) in the subsurface. Although coliform bacteria and coliphages are used worldwide to indicate fecal pollution of groundwater, their transport behavior is not fully understood. This study focuses on the transport behavior of three waterborne pathogens (*Escherichia coli*, MS2, and ΦX174) in laboratory-scale columns packed with clean quartz sand. Three different grain sizes and three pore water velocities were examined. The attachment behavior of *Escherichia coli*, MS2, and ΦX174 onto quartz sand was evaluated. The mass recoveries of the biocolloids examined were shown to be proportional to the sand size, and they were shown to be highest for *Escherichia coli* and lowest for MS2. The single collector removal and collision efficiencies were quantified using the classical colloid filtration theory.

1 Introduction

Groundwater may be accidentally contaminated with infective human enteric viruses from human and animal sewage through wastewater discharges, sanitary landfills, septic tanks, and agricultural practices or by artificial groundwater recharge, which is often used to reverse the rapid depletion of aquifers (Anders and Chrysikopoulos 2005; Masciopinto et al. 2008). To predict the presence of pathogens in water and wastewater, microorganisms known as indicator organisms (e.g. bacteria *Escherichia coli*, and coliphages MS2 and ΦX174), which are commonly associated with fecal contamination, are monitored.

Many studies examining the interaction of microorganisms with soil, sand, gravel or other model granular materials have been conducted using laboratory-scale columns under well-controlled environmental conditions. Theoretical and experimental studies have examined the effect of pore water solution chemistry (Bolster et al. 2001), fluid velocity (Chrysikopoulos and Sim 1996), matrix moisture content, temperature, grain size (Anders and Chrysikopoulos 2006, 2009) and presence of surface coatings (Bolster et al. 2001) on microbial transport and retention

N. Lambrakis et al. (Eds.), *Advances in the Research of Aquatic Environment, Vol. 2*
DOI 10.1007/978-3-642-24076-8,

in porous media. Quartz sand, either clean or coated, as well as glass beads have all been employed as model granular materials in such studies. Although a large number of studies on microbial transport have been published over the past two decades, our ability to predict the migration of bacteria, viruses or protozoa in natural subsurface environments remains limited.

The objectives of this study were to characterize the transport and attenuation of *E. coli*, MS2, and ΦX174 in 'clean' saturated quartz sand laboratory columns, and to examine the influence of grain size and pore water velocity on their transport and attenuation. The collision efficiencies of the three biocolloids examined were estimated and the factors that control biocolloid deposition were discussed.

2 Materials and methods

2.1 Bacterial and bacteriophage suspensions

The bacterial strain *Escherichia* (*E.*) *coli* (ATCC 13706-B1) is a well-characterized, Gram-negative, typical representative of the coliform bacteria. *E. coli* cells are motile rod shaped with approximate dimensions of 0.6 μm in width and 2 μm in length, or an equivalent spherical diameter of 1.21 μm. To provide a uniform inoculum for each experiment, a stock culture was cultivated in 50 mL of tryptic soy broth medium for 6 h to early stationary phase, harvested by centrifugation for 10 min at 5000×g and washed twice with sterile phosphate buffered saline (PBS) solution (1.2 mM NaCl, 0.027 mM KCl, and 0.10 mM Na_2HPO_4) to remove nutrients. Finally, the pellet was suspended in PBS solution and stored at 4 °C until application. Aliquots were taken to count the bacteria. Bacteria were suspended and diluted in PBS solution at pH=7 to concentrations of $1.94\pm0.06\times10^8$ colony-forming units per milliter (CFU/mL). The *E. coli* concentration was determined using optical density measurements (at 410 nm) with a UV-visible spectrophotometer (UV-1100, Hitachi). The bacterial cell concentrations (plate colonies) were determined using a standard spectrophotometer calibration curve.

The bacteriophage MS2 is a F-specific, single-stranded RNA phage with 31% nucleic acid content, whose host bacterium is *E. coli* (ATTC 15597-B1); whereas, the bacteriophage ΦX174 is an icosahedral, single-stranded DNA phage with 26% nucleic acid content, whose host bacterium is *E. coli* (ATTC 13706-B1). The MS2 particle diameter ranges from 24 to 26 nm; whereas, the ΦX174 particle diameter ranges from 25 to 27 nm. MS2 has hydrophobic protein coat; whereas, ΦX174 has hydrophilic protein coat. Both bacteriophage were assayed by the double-layer overlay method (Adams 1959), where 0.1 mL of the appropriate host bacterium and 0.1 mL of a diluted virus sample solution were mixed in a centrifuge tube. The mixture was combined with molten soft-agar medium (4.5 mL) maintained at

45 °C in a tube and poured onto a petri dish containing solid agar medium. The plates were solidified for 10 min and incubated overnight at 37 °C. Viable virus concentrations were determined by counting the number of plaques in each host lawn and reported as plaque-forming units per milliter (PFU/mL). Only dilutions that resulted in the range of 20-300 plaques per plate were accepted for quantification. All virus concentrations reported represent the average of two replicate plates. Bacteriophages, MS2 and ΦX174, were suspended and diluted in PBS solution at pH=7 to concentrations of 10^3-10^6 PFU/mL.

2.2 Chloride Analysis

Chloride, in the form of potassium chloride, was chosen as the nonreactive tracer for the transport column experiments. The nonreactive tracer solution was prepared with 0.01M KCl in PBS solution. It should be noted that alkali halides are the most commonly used salts for subsurface fluid tracing owing to a minimal effect on solution ionic strength (IS) (Chrysikopoulos 1993). Chloride concentrations were measured using ion chromatography (ICS-1500, Dionex Corp., Sunnyvale, CA).

2.3 Column packing material

Quartz sand of various sizes was used as packing material in the experimental columns. The sand was purchased directly from the manufacturer (Filcom Filterzand & Grind) and sieved into various size distributions. In this study three size distributions were used: (a) coarse (1.18-1.7 mm or sieve No 16), (b) medium (0.425-0.600 mm or sieve No 40), and (c) fine (0.150-0.212 mm or sieve No 100). The coefficient of uniformity, $C_u=d_{60}/d_{10}$, for each sand fraction were estimated to be C_u=1.19, 1.21, 1.2 for fine, medium, coarse sand, respectively. The chemical composition of the sand reported by the manufacturer was: 96.2% SiO_2, 0.15% Na_2O, 0.11% CaO, 0.02% MgO, 1.75% Al_2O_3, 0.78% K_2O, 0.06% SO_3 and 0.46% Fe_2O_3, 0.03% P_2O_5, 0.02% BaO, and 0.01% Mn_3O_4. The total organic carbon (% TOC) content, measured by the Walkley-Black method (i.e., chemical oxidation of the organic fraction) (Black, 1965), was found equal to 0.08±0.04% for the coarse, and 0.1±0.1% for both medium and fine sand fractions. Prior to the experiments, the sand fractions were cleaned with 0.1 M HNO_3 (70%) for a 3 h time period to remove surface impurities (e.g., iron hydroxide and organic coatings) that could promote physicochemical deposition of the biocolloids, rinsed with deionized water, then soaked in 0.1 M NaOH for a 3 h time period, and rinsed again with deionized water. After the cleaning steps, the sand was dried in an oven at 105 °C, and then stored in screw cap sterile beakers until use in the column experiments.

2.4 Column experiments (PBS experiments)

The glass columns (2.5 cm diameter and 30 cm length) were packed wet with sand under vibration to minimize any layering or air entrapment. The porosity of the sand column was determined by standard procedures and it was ranged from 0.36 to 0.43. The estimated bulk density was ranged from 1.65 to 1.72 g/cm^3. Prior to each experiment, the packed column was equilibrated by pumping 10 pore volumes of the background PBS solution through the column at a constant discharge rate of Q=2.5, 1.5 and 0.8 mL/min, corresponding to specific discharge or approach velocities of q=0.51, 0.31 and 0.16 cm/min, respectively. A suspension of each biocolloid of the same background PBS solution was pumped for 3 pore volumes at the same discharge rate followed by 5 pore volumes of biocolloid-free PBS solution. The apparatus used for the biocolloid transport experiments are shown in Figure 1.

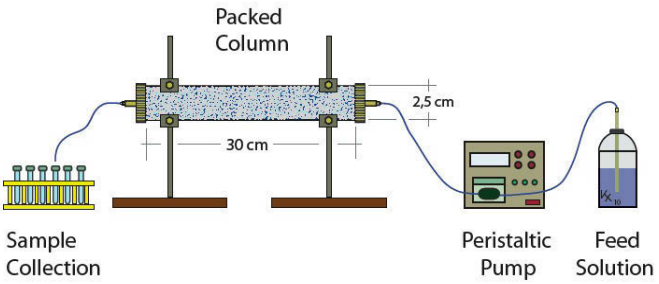

Fig. 1. Schematic illustration of the experimental apparatus.

3 Theoretical developments

3.1 Moments

The biocolloid concentration breakthrough data obtained at location x=L were analyzed by the absolute temporal moments:

$$m_n(x) = \int_0^\infty t^n C_i(x,t)\, dt \tag{1}$$

where the subscript n=0, 1, 2, ... indicates the order of the moment, and subscript i indicates *E.coli*, MS2, and ΦX174. The zeroth absolute temporal moment, m0,

quantifies the total mass in the concentration breakthrough curve; the first absolute moment, m1, describes the mean residence time; and second absolute temporal moment, m2, describes the degree of spreading of the concentration breakthrough curve. Also, the normalized temporal moments are defined as:

$$M_n(x) = \frac{m_n(x)}{m_0(x)} = \frac{\int_0^\infty t^n C_i(x,t)dt}{\int_0^\infty C_i(x,t)dt} \tag{2}$$

The first normalized temporal moment, M_1, characterizes the center of mass of the concentration breakthrough curve and defines the mean breakthrough time or average velocity. The second normalized temporal moment, M_2, characterizes the spreading of the breakthrough curve. Worthy to note is that that the ratio $M_{1(i)}/M_{1(t)}$ indicates the degree of velocity enhancement of biocolloid i relative to the conservative tracer. If this ratio is less than one, there exists velocity enhancement of biocolloid transport. If this ratio is greater than one there exists biocolloid retardation. Furthermore, the mass recovery, M_r, of the tracer or the suspended particles is quantified by the following expression:

$$M_r(L) = \frac{m_0(L)}{C_{i_0} t_p} = \frac{\int_0^\infty C_i(L,t)dt}{\int_0^{t_p} C_i(0,t)dt} \tag{3}$$

where L is the porous medium length.

3.2 Colloid filtration theory

Classical colloid filtration theory (CFT) was used to quantitatively compare the microbial and viral attachment onto quartz sand. CFT assumes that the removal of particles is described by first-order kinetics with a spatially and temporally constant rate of particle deposition, and the concentrations of suspended and retained particles decrease log-linearly with distance. However, recent studies (Tufenkji and Elimelech, 2004) have suggested that colloid retention decreased hyper-exponentially with distance, suggesting that the attachment rate coefficient is not constant. In the absence of straining, which is defined as the trapping of particles in pores that are too small to pass through, this hyper-exponential deviation from CFT could be attributed to the concurrent existence of both favorable and unfavorable colloidal interactions with collector surfaces (Tufenkji and Elimelech, 2004). The dimensionless collision efficiency, α (the ratio of the collisions resulting in attachment to the total number of collisions between particles and collector grains) and the dimensionless single-collector removal efficiency for favorable deposition, η_0 were calculated from each biocolloid breakthrough curve.

4 Results

The normalized chloride breakthrough data for the coarse sand and three different specific discharge velocities are presented in Figure 2. Similar results were observed (not shown) for the medium and fine sand. The normalized *E. coli* breakthrough data are presented in Figure 3 together with the fitted model predictions. For all cases considered the ratio $M_{1(i)}/M_{1(t)}$ was smaller than one, which indicated that the velocity of *E. coli* is enhanced by 7%–15%. The M_r values, ranged from 94.48 to 100%, indicate that there was no significant *E. coli* retention by the packed column. Slight attachment of *E. coli* onto the quartz sand was observed at the lowest q. However, no distinct relationships between M_r or $M_{1(i)}/M_{1(t)}$ and q or d_c could be established from the experimental results.

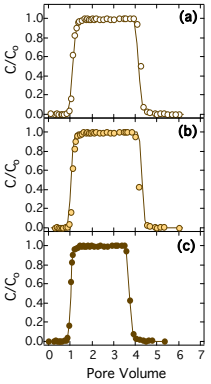

Fig. 2. Tracer breakthrough data (symbols) and fitted mathematical model predictions (solid curves) for specific discharge velocities of (a) 0.16, (b) 0.31, and (c) 0.51 cm/min in water-saturated columns packed with coarse sand.

Figure 4 presents the normalized MS2 breakthrough data together with the fitted model predictions. With the exception of the case of fine sand at q=0.51 cm/min, all estimated M_r values were quite low (ranged from 43.47 to 96.49%), suggesting that the MS2 particles retained in the packed column were either irreversibly attached onto the sand grains or inactivated. For the slowest specific discharge velocity (q=0.16 cm/min) M_r decreased with decreasing sand size; however, for the other two velocities employed there was no clear trend. Hence, MS2 attachment cannot be attributed to d_c variations, but to possible sand grain physicochemical heterogeneities. With the exception of the case of medium sand with q=0.31 cm/min, where slight retardation was observed ($M_{1(i)}/M_{1(t)}$=1.05>1), all calculated $M_{1(i)}/M_{1(t)}$ ratios were smaller than one, suggesting that the velocity of MS2 is enhanced by 2%–19% compared to the tracer.

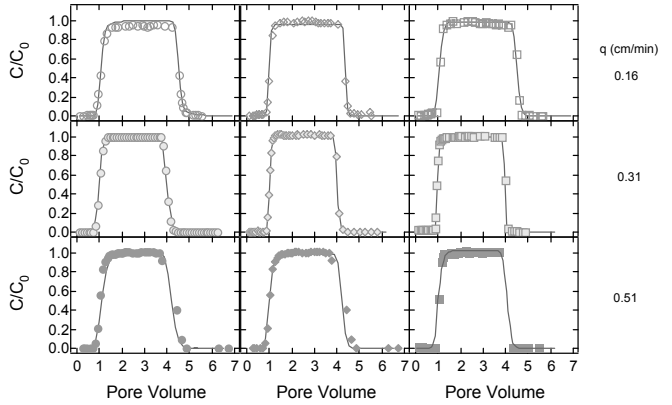

Fig. 3. Experimental *E. coli* CN13 breakthrough data (symbols) and fitted mathematical model predictions (solid curves) for volumetric flow rates of 0.16 cm/min (open symbols), 0.31 cm/min (filed symbols), and 0.51 cm/min (solid symbols) in water-saturated columns packed with coarse (circles), medium (diamonds) and fine (squares) sand.

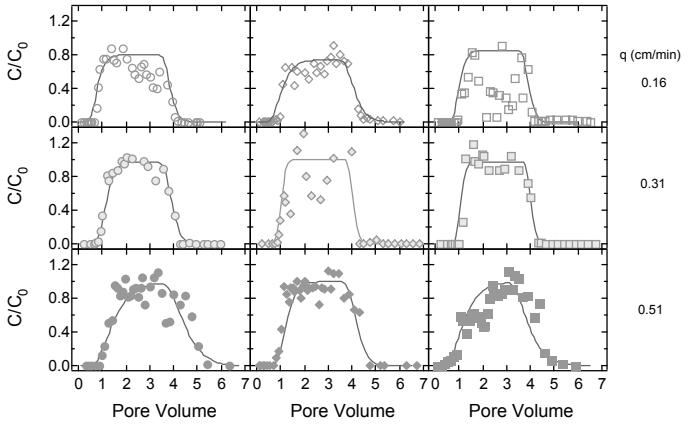

Fig. 4. Experimental MS2 breakthrough data (symbols) and fitted mathematical model predictions (solid curves) for volumetric flow rates of 0.16 cm/min (open symbols), 0.31 cm/min (filed symbols), and 0.51 cm/min (solid symbols) in water-saturated columns packed with coarse (circles), medium (diamonds) and fine (squares) sand.

Figure 5 shows the normalized ΦX174 breakthrough data together with the fitted model predictions. The calculated M_r values, ranged from 82.65 to 100%, indicated that there was no significant ΦX174 retention in the packed column. Furthermore, all calculated $M_{1(i)}/M_{1(t)}$ ratios were smaller than one, suggesting that the velocity of ΦX174 is enhanced by 4%–18% compared to the tracer. However, it should be noted that no clear trends between M_r or $M_{1(i)}/M_{1(t)}$ and q or d_c could be determined from the experimental results.

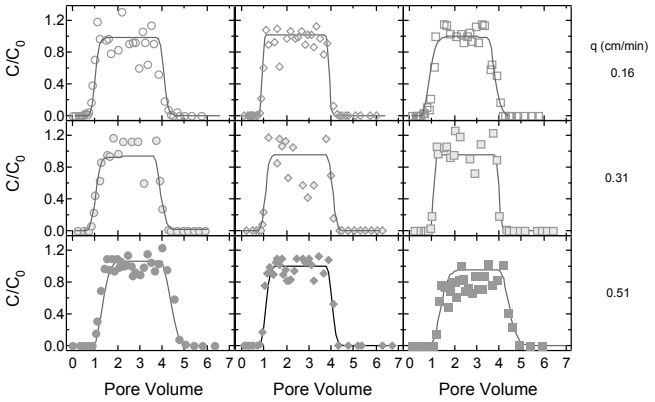

Fig. 5. Experimental ΦX174 breakthrough data (symbols) and fitted mathematical model predictions (solid curves) for volumetric flow rates of 0.16 cm/min (open symbols), 0.31 cm/min (filed symbols), and 0.51 cm/min (solid symbols) in water-saturated columns packed with coarse (circles), medium (diamonds) and fine (squares) sand.

The single collector removal efficiency under favorable deposition conditions, η_0, was calculated for MS2, ΦX174 and *E. coli*, three sand sizes (coarse, medium and fine), and three specific discharge velocities. Collision efficiencies, α, for MS2, ΦX174 and *E. coli* for the experimental conditions of this study, using the previously calculated η_0 values, are similar to values reported in the literature for MS2 (α=0.00045-0.0422 (Chu et al., 2003)), for ΦX174 (α=0.00077-0.0162 (Chu et al., 2003)), and for *E. coli* (α=0.008-0.875 (Foppen et al. 2007)).

5 Summary and Conclusions

The results of this study indicated that although the biocolloid mass recovery and degree of velocity enhancement were affected by the interstitial water velocity and sand grain size, no clear trends could be determined. Worthy to note is that the M_r of ΦX174 was higher than that of MS2 for all cases examined in this study. It was found that the dispersivity values for MS2 were higher than those obtained for ΦX174, which could be attributed to the higher charge repulsion between MS2 and sand grains and to the hydrophobic protein coat of MS2. Moreover, as it was expected, the dispersivity values for the smaller bacteriophages were found to be greater than that of the larger bacteria. The single collector removal efficiency was shown to be affected by the sand grain size and water velocity. The experimental collision efficiencies suggest more favorable attachment conditions for bacteriophage MS2 than for ΦX174. However no significant effect of sand grain size and interstitial velocity on the collision efficiency was observed. It is possible that factors as grain surface area, angularity and roughness may have contributed to physicochemical filtration and biocolloid retention.

References

Adams M.H. (1959). Bacteriophages, Interscience, New York, N.Y., pp 450-454

Anders R., Chrysikopoulos C.V. (2005). Virus fate and transport during artificial recharge with recycled water. Water Resour. Res. 41, W10415. doi: 10.1029/2004WR003419

Anders R., Chrysikopoulos C.V. (2006). Evaluation of the factors controlling the time-dependent inactivation rate coefficients of bacteriophage MS2 and PRD1. Environ. Sci. Technol. 40, 3237-3242

Anders R., Chrysikopoulos C.V. (2009). Transport of viruses through saturated and unsaturated columns packed with sand. Transp. Porous Media. 76, 121-138

Black C.A. (Eds.) (1965). Methods of Soil Analysis. Part 2. Chemical and Microbiological Properties. American Society of Agronomy, Madison

Bolster C.H., Mills A.L., Hornberger G.M., Herman J.S. (2001). Effect of surface coatings, grain size, and ionic strength on the maximum attainable coverage of bacteria on sand surfaces. J. Contam. Hydrol. 50, 287-305

Chrysikopoulos C.V. (1993). Artificial tracers for geothermal reservoir studies, Environ. Geol. 22, 60-70

Chrysikopoulos C.V., Sim Y. (1996). One-dimensional virus transport homogeneous porous media with time dependent distribution coefficient. J. Hydrol. 185, 199-219

ChuY., Jin Y., Baumann T., Yates M.V. (2003). Effect of soil properties on saturated and unsaturated virus transport through columns. J. Environ. Quality. 32, 2017–2025

Foppen J.W., van Herwerden M., Schijven J. (2007). Transport of *Escherichia coli* in saturated porous media: Dual mode deposition and intra-population heterogeneity. Water Res. 41, 1743–1753

Masciopinto C., La Mantia R., Chrysikopoulos C.V. (2008). Fate and transport of pathogens in a fractured aquifer in the Salento area, Italy. Water Resour. Res. 44, W01404. doi:10.1029/2006WR005643

Tufenkji N., Elimelech M. (2004). Correlation equation for predicting single-collector efficiency in physicochemical filtration in saturated porous media. Environ. Sci. Technol. 38, 529-536.

A preliminary study for metal determinations in Seawater and Natural Radionuclides in Sediments of Glafkos estuary in Patraikos Gulf (Greece)

K. Kousi, M. Soupioni, H. Papaeftymiou

Nuclear Chemistry Laboratory, Section of Physical, Inorganic and Nuclear Chemistry, Department of Chemistry, University of Patras, Rio-Patras, GR 26500, GREECE
m.soupioni@chemistry.upatras.gr

Abstract The Patraikos Gulf is situated in Western Greece between the mainland and the Peloponnese peninsula, opening into the Ionian Sea on the west. The Evinos, Glafkos and Pirros Rivers flow into the Gulf and the city of Patras, with its busy port, lies on the east side of the gulf. Glafkos is the largest river in Patras area and is considered to be a factor of pollution of the gulf, as it carries large amounts of water and sludge. Determination of metal concentrations (Fe, Mg, Ca, Ni, Zn) was attempted in sea water of Glafkos estuary on December 2009, February and March 2010. In addition, activity concentration values of the natural radionuclides ^{238}U, ^{232}Th, ^{226}Ra, ^{40}K and of the artificial ^{137}Cs were measured in sediments of the river and its estuary. In general, the results are close to the bibliographic ones, while in most of the cases there is statistically significant deviation between the metal concentrations in relation with the months.

1 Introduction

The Gulf of Patras (Patraikos Gulf) is situated in Western Greece between the mainland and the Peloponnese peninsula (Fig. 1). It is a marine embayment opening into the Ionian Sea on the west, and through the straits of Rio into the deep Gulf of Corinth, on the east, which communicates through the Corinth canal with the Aegean Sea. The Glafkos and Pirros Rivers drain into the south side of the gulf, while the Evinos River into the northwestern side of the gulf. The city of Patras, with a busy port and a population of about 200 000, is the largest urban area in the Patraikos Gulf, situated on the east side of the gulf. The industrial area of Patras is also along the southern coast of the Patraikos Gulf. The last seven years about 80% of the domestic effluents are biologically pre-treated and then discharged into the gulf. Glafkos is the largest river in Patras area, originating from Panaxaiko Mountain and is considered to be one of the main pollution

N. Lambrakis et al. (Eds.), *Advances in the Research of Aquatic Environment, Vol. 2*
DOI 10.1007/978-3-642-24076-8,

sources of the Gulf. Normally, Glafkos carries into the sea large amounts of water and sludge containing probably urban, industrial and agricultural wastes. So, the trend of marine pollution levels to increase continuously requires control strategies and routine monitoring of contaminants in the environment of Patraikos Gulf (Voutsinou-Talliadouri and Satsmadjis 1983; Friligos 1987).

It is well known that, metal and radioactive pollution can cause long-term effects on ecosystems. Radionuclides and metals can enter the organisms by the food chain or by the ingestion of polluted water. High metal concentrations may result in high risks for the environment and humans. Specifically, in aquatic environment, metals in high concentrations, especially the heavy ones, are considered the most important pollutants, because of their toxicity and accumulation by marine organisms consumed by people.

Although data for Patras Harbour presented by Papaefthymiou et al. (2007) and Papaefthymiou et al. (2010), serve as a useful background for many research purposes, there is a need for more detailed knowledge obtained through temporal surveys.

As this work is preliminary, the concentrations of Fe, Ca, Mg, Ni and Zn in seawater of Glafkos estuary in relation with the months are presented. Also, the activity concentration values of natural (^{238}U, ^{232}Th, ^{226}Ra, ^{40}K) and artificial (^{137}Cs) radionuclides were determined in sediments of sea and river at the same area.

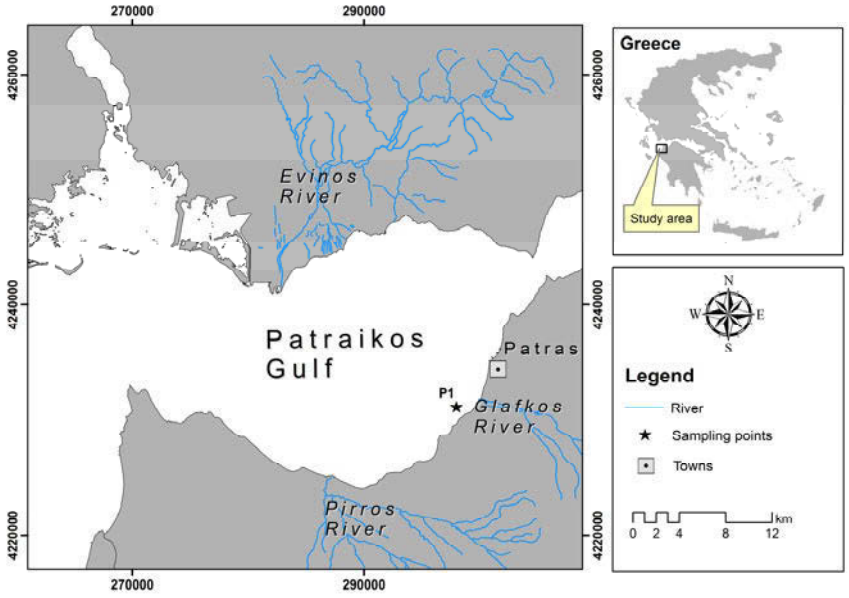

Fig. 1. Schematic map of the study area (Patraikos Gulf).

2 Methodology

All containers and laboratory materials that were used in this study, were made from polyethylene, PTFE or silica which had been washed with detergent, acid-soaked, and before use rinsed repeatedly with ultra pure water obtained by a Milli-Q water purifier system (resistivity 18.2 MΩ cm^{-1}).

2.1 Sampling

Three surface water samples per month were collected from the point P_1 (Fig. 1) on December 2009, February and March 2010 from the Glafkos estuary in Patraikos Gulf. The temperature of seawater was of 16-18 ^oC and the pH was slightly alkaline (pH=8). On November 2010 four surface nearshore sediments samples were also collected, two from the Glafkos estuary (S3, S4) at the location of P_1 point and two from the river [R1 (300 m from estuary), R2(600 m from estuary)]. The sampling area is located in the wide area of the outflow of the Glafkos River and consequently receives agricultural, domestic and industrial discharges carried on by the river. Also, this point is probably influenced by the Patras Harbour activities due to sea currents.

2.2 Metal Analyses

The collected seawater samples were acidified with a small quantity of HNO_3 (Suprapur 65%) and stored in polyethylene bottles at 4 ^0C until they were analysed. Before measuring, all the samples were filtered using cellulose membrane filters (0.45 μm). Finally, the concentrations of Fe, Ca and Mg were measured by Flame Atomic Absorption Spectrometry (FAAS) using a Shimadzu (AA-6500) spectrophotometer equipped with SR hollow cathode lamps for good background correction and a corrosion resistant nebulizer. Analytical precision was better than 10% on the basis of replicate analyses. The concentrations of Ni and Zn were tried to be determined in the graphite furnace of a Shimanzu (AA-6300) spectrophotometer (GAAS), because it provides much greater sensitivity than the flame in atomic absorption spectrometry. In that case, the proper method of internal standard sample was also used.

2.3 Natural Radioactivity and ^{137}Cs Analyses

The collected sediment samples were air dried, crushed to fine powder and homogenized. In order to perform the activity concentration measurements by γ-ray spectrometry, the homogenized samples were dried at 105 ^{o}C to constant weight, packed into cylindrical containers, weighted, sealed hermetically and stored for a minimum period of 3 weeks prior to counting to establish secular radioactive equilibrium between ^{226}Ra and its short-lived daughter products. Both energy and efficiency calibration procedures and activity concentration measurements are described in detail elsewhere (Papaefthymiou et al. 2010).

Briefly, all countings were performed using a Canberra HPGe detector with an energy resolution of 1.9 keV at the 1.33 MeV of ^{60}Co γ-ray and relative efficiency of 25%. The minimum counting time was 24 h. The spectra were analyzed using the GAMANAL routine, included in the GANAAS package, distributed by IAEA, while peak areas were determined using the Ganaas 3.1 computer program of IAEA. The accuracy was estimated against the IAEA-312 and IAEA-375 reference materials. The tests showed good correspondence with the certified/recommended values (<5%).

2.4 Statistical treatment

The statistical treatment of the data, including summary statistics and one-way analysis of variance (ANOVA) was performed using the SPSS v.15 software package.

3 Results and Discussion

In Table 1 the concentrations of Fe, Ca and Mg in seawater samples of the Glafkos estuary in Patraikos Gulf are presented.

Table 1. Average monthly (n=3) concentrations (in mg.kg^{-1} ± SD, except for Fe in μg.kg^{-1}± SD) of metals in seawater samples at Glafkos estuary in Patraikos Gulf.

Month	Fe	Ca	Mg	Ni	Zn
December 2009	6.6±1.7	202±6	937±22	UDL	UDL
February 2010	2.6±0.4	223±5	1080±10	UDL	UDL
March 2010	3.3±0.4	218±8	949±12	UDL	UDL
Average	4.2±2.1	214±11	989±80	UDL	UDL

UDL: Under detection limit
SD: standard deviation

As shown in this table, the concentrations of Zn and Ni were found to be under their detection limits (0.10 ppb and 0.41 ppb respectively).

The results showed that the determined Fe concentrations were very close to the bibliographic values (~3 ppb) during February and March 2010 (Mandilaras 2005). On the contrary, the Fe concentration was increased about 50% on December. The concentration of Mg was found to be higher during February 2010 compared to that on December 2009 and March 2010, while the values for Ca were more or less the same. The concentration of Mg, as well as Ca concentration, was lower than the expected one (1800 ppm and 350 ppm, respectively) from literature (Mandilaras 2005). These values could be considered as normal, since the seawater samples were collected from the mouth of the river.

The first results of the statistical treatment showed that, the differences in Ca and Mg concentrations in relation with the months were not statistically significant ($p=0.051$ and $p=0.065$, respectively). On the contrary, Fe concentration was significantly higher during December compared with that during February ($p=0.009$) and March ($p=0.021$), which could be attributed to the lower water discharge rate during December.

The results of ^{238}U, ^{226}Ra, ^{232}Th, ^{40}K and ^{137}Cs activity concentrations measured by direct γ-ray spectrometry (DS) in the nearshore surface sediment samples of Glafkos estuary in Patraikos Gulf are shown in Table 2.

Table 2. Activity concentrations of ^{238}U, ^{226}Ra, ^{232}Th, ^{40}K and ^{137}Cs in surface sediment samples of Glafkos estuary in Patraikos Gulf (units are in Bq kg^{-1} d.w. ± s_{tot}).

Sample	^{238}U	^{226}Ra	^{232}Th	^{40}K	^{137}Cs
R1	34.3±5.5	19.0±0.9	19.7±1.4	346±28	2.0±0.3
R2	20.3±3.4	16.1±0.6	21.7±0.5	308±25	1.7±0.3
S1	37.6±1.8	32.0±1.5	42.3±3.0	631±35	32.6±2.7
S2	36.4±3.5	28.3±2.3	32.5±0.9	524±29	23.7±2.0

s_{tot}: combined standard uncertainty.

Table 3 presents the average activity concentrations of the natural radionuclides mainly in nearshore sediments of different Greek areas, as well as the world and Greek average values for soil (UNSCEAR 2000). Generally speaking, the radionuclide concentrations in Glafkos estuary are lower than those measured in three coastal areas of Greece: Cyclades Islands (Florou et al. 1988), Milos Island (Florou and Kritidis 1991) and Gulf of Corinth (Papatheodorou et al. 2005). It should be mentioned that the elevated activities in these islands are due to the presence of volcanic rocks, while that of central Gulf of Corinth to the submarine bauxitic red mud deposits.

Table 3. The average activity concentrations of ^{238}U, ^{226}Ra, ^{232}Th and ^{40}K (in Bq kg^{-1}) in nearshore sediments of different Greek areas.

Greek area	^{238}U	^{226}Ra	^{232}Th	^{40}K	Sample type	Reference
Cyclades Islands	67 (29-110)	26 (7-159)	31 (4-106)	666 (189-1214)	Nearshore sediments	Florou et al. (1988)
Milos Island		70 (16-119)	75 (19-152)	890 (158-3893)	Nearshore sediments	Florou and Kritidis (1991)
Gulf of Corinth	79.5 (13.1-399.8)	48.7 (12.9-185.2)	85.5 (15.1-412.0)	318.8 (28.3-539.9)	Nearshore sediments	Papatheodorou et al. (2005)
Patras Harbour	21.8 (13.6-33.3)	24.5 (16.6-34.1)	24.5 (16.6-34.1)	497 (327-763)	Nearshore sediments	Papaefthymiou et al. (2007)
Greek average	25 (1-240)	25 (1-240)	21 (1-190)	360 (12-1570)	soil	UNSCEAR (2000)
World average	35 (16-110)	35 (17-60)	30 (11-64)	1700 (140-850)		UNSCEAR (2000)
Glafkos River	27	18	21	327	sediments	This study
Glafkos estuary (Patraikos Gulf)	37	30	37	578	sediments	This study

It is shown (Table 3) that the mean activity concentrations of all natural radionuclides in the Glafkos River sediments are close to Greek average ones for soil (UNSCEAR 2000). However, the mean activity concentrations of ^{238}U, ^{226}Ra and ^{232}Th in Glafkos estuary sediments are slightly higher compared to the Greek average for soil and Patras Harbour (Papaefthymiou et al. 2007) concentrations. It is also remarkable that the ^{40}K activity concentration in Glafkos estuary sediments is almost two fold higher compared to the Greek average for soil. This can be explained by the fact that seawater contains high concentrations of K and also the outflow of the Glafkos River receives many elements in agricultural, domestic and industrial discharges carried on by the river.

Finally, ^{137}Cs is an artificial radioactive nuclide, which can be found in the nature as a result of the fallout of atmospheric nuclear bomb tests in the early 1960s and also in 1986 following the Chernobyl reactor accident. Its half-life is approximately 30 years, so it is still detected.

As is apparent from Table 2, the ^{137}Cs activity concentrations were found to be higher in the sediment samples compared to those in the river ones. This could be due to the fact that ^{137}Cs is entering into the gulf via the water inputs from the river and also via the water inputs from inland.

4 Conclusions

The Fe, Ca and Mg concentrations in seawater at Glafkos estuary in Patraikos Gulf determined on December 2009, February and March 2010 are close to the bibliographic ones. Non significant variations in Ca and Mg concentrations were found between the different months, whereas the Fe concentration was found to be higher during December compared to that during February and March 2010. The activity concentrations of ^{238}U, ^{232}Th, ^{226}Ra and ^{137}Cs determined on November 2010 in river sediments and in Glafkos estuary sediments are close to the Greek average for soil. The ^{40}K activity concentration in sea sediments was fairly higher than the Greek average for soil, while the ^{137}Cs activity concentration was higher in the sea sediments compared to that in the river ones.

References

Florou, H, Kritidis, P (1991) Natural radioactivity in environmental samples from an island of volcanic origin (Milos, Aegean Sea). Marine Pollution Bulletin 22 (8), 417-419

Florou, H, Kritidis, P, Pavlakis, P, Veldeki, K (1988) Enhanced natural radioactivity in some areas of the Aegean Archipelagos. In: Proceedings of the International Conference on Environmental Radioactivity in the Mediterranean Area, Barcelona, 10-13 May

Friligos Nicholas (1987) Nutrient Conditions in the Patraikos Gulf. Marine Pollution Bulletin 18(10), 558-561

Papaefthymiou H, Papatheodorou G, Moustakli A, Christodoulou D, Geraga M (2007) Natural radionuclides and 137Cs distributions and their relationship with sedimentological processes in Patras Harbour, Greece. J. Environ. Radioactivity 94, 55-74

Papaefthymiou H, Papatheodorou G, Christodoulou D, Geraga M, Moustakli A, Kapolos J (2010) Elemental concentrations in sediments of the Patras Harbour, Greece, using INAA, ICP-MS and AAS. Microchemical Journal 96, 269–276

Mandilaras, D (2005) Environmental-Hydrogeological study of Glafkos River. PhD thesis, University of Patras. p. 332

Papatheodorou, G, Papaefthymiou, H, Maratou, A, Ferentinos, G (2005) Natural radionuclides in bauxitic tailings (red-mud) in the Gulf of Corinth, Greece. Radioprotection 40, 549-555

Voutsinou-Talliadouri Fanny, Satsmadjis John (1983) Distribution of Heavy Metals in Sediments of the Patraikos Gulf (Greece). Marine Pollution Bulletin 14(1), 33-35

UNSCEAR (2000) Sources and Effects of Ionizing radiation. United Nations Scientific Committee on the effects of atomic radiation. Report to General Assembly with Scientific Annexes. United Nations, New York

Purification of wastewater from Sindos industrial area of Thessaloniki (N. Greece) using Hellenic Natural Zeolite

A. Filippidis, A. Tsirambides, N. Kantiranis, E. Tzamos, D. Vogiatzis, G. Papastergios, A. Papadopoulos, S. Filippidis

School of Geology, Aristotle University, GR 541 24 Thessaloniki, Greece.
anestis@geo.auth.gr

Abstract The treatment of wastewater from Sindos industrial area of Thessaloniki, Greece (initial pH 7.8) with the Hellenic Natural Zeolite (HENAZE), resulted to clear water of pH 7.3, free of odours and improved by 93% in the colour, 69% in the chemical oxygen demand (COD), >97% in the P_2O_5 removal, 54% in the NO_3 removal and 77% in the Cr removal. The sorption and fixation of the different species from the wastewater by the micro- meso- and macroporous of HENAZE can be attributed to absorption (mainly ion exchange), adsorption and surface precipitation processes. Important role in these processes play the surface Broensted acidic and Lewis basic sites of the HEU-type zeolite. In addition the HENAZE treatment gave odourless and cohesive zeosludge, suitable for safe deposition since the fixation of dangerous components into the micro- meso- and macroporous of HENAZE, prevents the seepage of them by the rain water, protecting thus the quality of surface and underground waters. The used HENAZE sample, comes from Ntrista stream area of Petrota village (Evros Prefecture, Northeastern Greece) and contains 88 wt.% HEU-type zeolite, 4 wt.% mica + clays (92 wt.% microporous minerals), 5 wt.% feldspars and 3 wt.% SiO_2-phases (quartz + cristobalite). The mineralogical composition and the physico-chemical properties, make the HENAZE suitable material for numerous environmental, industrial, agricultural and aquacultural applications.

1 Introduction

Zeolite comprises a special solid crystalline microporous material, with open structure and void space. Some high quality HEU-type natural zeolites, display unique physical and chemical features and have a great variety of environmental, industrial, aquacultural and agricultural applications (e.g. Pond and Mumpton 1984, Tsitsishvili et al. 1992, Tserveni-Gousi et al. 1997, Colella and Mumpton 2000, Yannakopoulos et al. 2000, Kallo 2001, Panayotova 2001, Harben 2002, Armagan et al. 2004, Filippidis et al. 2005, 2009, 2010a, b, Oren et al. 2006, Fi-

N. Lambrakis et al. (Eds.), *Advances in the Research of Aquatic Environment, Vol. 2*
DOI 10.1007/978-3-642-24076-8, © Springer-Verlag Berlin Heidelberg 2011

lippidis and Kantiranis 2007, Filippidis 2010). Around the village of Petrota (Evros Prefecture, Northeastern Greece), eight different zeolitic occurrences show varying zeolite contents, by average 39-89 wt.% (e.g., Filippidis 2010). The Livadakia location on average, contains 39 wt.% HEU-type zeolite (range 35-43 wt.%), the Palestra location 47 wt.% HEU-type zeolite, the Petrota East location 53 wt.% HEU-type zeolite (range 42-62 wt.%), the Mavri Petra location 74 wt.% HEU-type zeolite (range 54-83 wt.%), the Fylakio Omega location 45 wt.% mordenite, the Gkazomylos location 59 wt.% HEU-type zeolite (range 41-75 wt.%), the Aloni-Kokkalo location 43 wt.% HEU-type zeolite and the Ntrista stream location 89 wt.% HEU-type zeolite (range 84-95 wt.%). In the Ntrista stream, a HEU-type zeolite deposit is located, the Hellenic Natural Zeolite (HENAZE) of GEO-VET N. Alexandridis & Co O.E. concession.

The purification of urban, dye-work and tanning-work wastewaters, as well as the production of odourless and cohesive zeo-sewage sludge, using 6.0-7.5 g of HENAZE and stirring time 5-60 min, has been investigated (e.g., Filippidis 2008, 2010, Filippidis et al. 2008a, 2009). The present study investigates the purification of wastewater from Sindos industrial area of Thessaloniki (N. Greece) using 0.1 g of Hellenic Natural Zeolite (HENAZE) and stirring time of 3 min.

2 Materials and methods

The Hellenic Natural Zeolite (HENAZE) sample used (collected from the Ntrista stream area of Petrota village) was supplied by the GEO-VET N. Alexandridis and Co O.E. A part of the rock-sample was ground in a mechanic tungsten mortar and the grain-size <0.5 mm (Fig. 1) was used for the butch-type experiments.

Fig. 1. The rock sample of HENAZE (left) and the grain-size <0.5 mm of HENAZE (right), used in the butch-type experiments.

Petrographic investigation of HENAZE was performed on thin sections. The morphology of the HEU-type zeolite was studied by Scanning Electron Microscopy (SEM). The mineralogical composition was determined by X-Ray

Powder Diffraction (XRPD). The XRPD analysis was performed using a philips diffractometer, Ni-filtered Cu_{Ka} radiation on randomly oriented sample. The sample was scanned from 3^o to 65^o 2θ at a scanning speed of 1.2^o/min. Semi-quantitative estimates were performed using external mixture standards of the identified mineral phases. The chemical formula of the HEU-type zeolite, determined by microprobe analyses, is $Ca_{1.5}K_{1.4}Mg_{0.6}Na_{0.5}Al_{6.2}Si_{29.8}O_{72}{\cdot}20H_2O$. The average chemical composition of HENAZE (whole rock samples), determined by Atomic Absorption Spectrometry (AAS), is 68.6 wt.% SiO_2, 11.8 wt.% Al_2O_3, 2.9 wt.% K_2O, 2.1 wt.% CaO, 1.1 wt.% Na_2O and 0.8 wt.% MgO. The average ammonia ion exchange capacity of HENAZE, determined by AMAS method, is 226 meq/100g (e,g., Filippidis and Kantiranis 2007, Filippidis 2010).

The wastewater from Sindos industrial area of Thessaloniki (Northern Greece), was treated at room temperature by HENAZE with grain-size of <0.5 mm, in butch-type experiment. In 300 ml of wastewater 0.1 g of HENAZE was added, the whole was stirred for 3 minutes and polyaluminium chloride as well as cationic polyelectrolyte was added. The overflowed clear water and the precipitated zeosludge were separated by filtering. The zeosludge was dried overnight at room temperature (RT). The starting wastewater and the overflowed clear water, were analyzed for (method): pH (electrometric), colour (photometric), COD (method of K_2CrO_6), P_2O_5 (molecular absorption spectrophotometry), NO_3, Cu, Zn and Cr (atomic absorption spectroscopy).

3 Results

Microscopic examination of thin sections reveals a fine-grained vitroclastic texture containing shards, angular to subangular quartz and feldspar crystals, as well as tabular mica crystals. The lath- or tabular shaped crystals of HEU-type zeolite are very abundant as interstitial cements or as polycrystallines in the shards. The peripheral zone of the shards is usually a rim composed of tiny clay mineral crystals (Fig. 2).

The HENAZE sample used contains 88 wt.% HEU-type zeolite (heulandite-clinoptilolite), 4 wt.% mica + clays (92 wt.% microporous minerals), 5 wt.% feldspars and 3 wt.% SiO_2-phases (quartz + cristobalite) (Table 1).

Table 1. Semi-quantitative mineralogical composition (wt.%) of HENAZE.

HEU-type zeolite (heulandite-clinoptilolite)	88	Feldspars	5
Mica + clay minerals	4	SiO_2-phases (quartz + cristobalite)	3
Subtotal (microporous minerals)	92	Subtotal	8

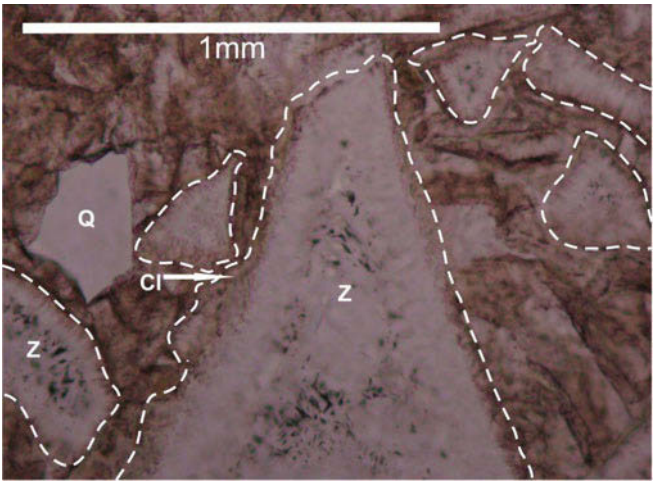

Fig. 2. Photomicrograph of thin section. Discontinuous line: Shards, Z: Lath-tabular shaped crystals of HEU-type zeolite, Q: Angular quartz crystal, Cl: Clay minerals in the peripheral rim-zone of the shards.

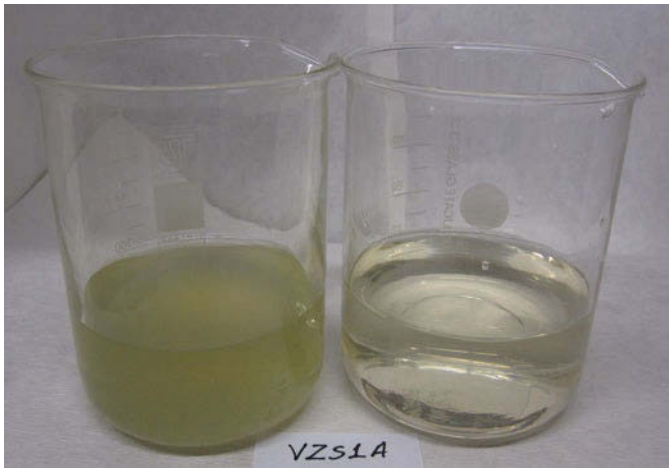

Fig. 3. Starting wastewater (left) and clear water (right) after the HENAZE treatment.

The wastewater from Sindos industrial area with an initial pH of 7.8, treated with the HENAZE gave clear water (Fig. 3) with pH of 7.3, free of odours and improved quality parameters by 93% in the colour, 69% in the chemical oxygen demand (COD), >97% in the P_2O_5 removal, 54% in the NO_3 removal and 77% in the Cr removal (Table 2).

Table 2. Chemistry of starting wastewater from Sindos industrial area (SWW) and clear water (CW) treated with 0.1 g of HENAZE at room temperature.

Quality parameters (detection limit)	SWW	CW	Improvement (%)
pH (0.1)	7.8	7.3	6
Colour, Pt-scale, mg/L (5)	929	65	93
COD: chemical oxygen demand, mg/L O_2 (15)	239	73	69
P_2O_5, mg/L (0.3)	9.1	<0.3	>97
NO_3, mg/L (2)	35	16	54
Cu, mg/L (0.1)	<0.1	<0.1	-
Zn, mg/L (0.1)	<0.1	<0.1	-
Cr, μg/L (5)	35	8	77

Simultaneously, the treatment gave as precipitate odourless and cohesive zeosludge, which was dried overnight at room temperature and had a weight of 0.173 g (0.1 g HENAZE and 0.073 g sludge) (Fig. 4).

Fig. 4. Odourless and cohesive zeosludge, dried overnight at room temperature.

4 Discussion and conclusions

The natural zeolites show a remarkable ability to remove inorganic, organic, organometallic compounds, gas species, metals and radionuclides from their aqueous solutions. The sorption of the different species from their solutions by the micromeso- and macroporous of natural zeolite can be attributed to absorption (mainly ion exchange), adsorption and surface precipitation processes (e.g. Tsitsishvili et

al. 1992, Misailides et al. 1995, Godelitsas et al. 1999, 2001, 2003, Collela and Mumpton 2000, Kallo 2001, Filippidis 2010). The sorption of gas phases results to oxygen enrichment of the air and to a remarkable decrease of the malodour. Also, they show an ability to neutralize the pH of acidic and basic waters, acting either as a proton acceptor or donor, exhibiting thus an amphoteric character (e.g. Filippidis et al. 1996, Charistos et al. 1997, Filippidis and Kantiranis 2007).

The Hellenic Natural Zeolite (HENAZE) is of very high quality (89 wt.% HEU-type zeolite), removes inorganic, organic, organometallic, cyanobacteria, gas species, metals, cations and anions from their aqueous solutions (e.g., Filippidis and Kantiranis 2007, Filippidis 2008, 2010, Filippidis et al. 2008a,b, 2009, 2010 a, b). The mineralogical composition and the unique physico-chemical properties, make the HENAZE suitable material for numerous environmental, industrial, agricultural and aquacultural applications, such as: Purification of industrial and urban wastewaters, production of odourless and cohesive zeosewagesludge, treatment of sewage and industrial sludge for safe deposition, purification and oxygen enrichment of aqua ecosystems, usage-reduction of irrigation water and fertilizers, sorption and removal of cyanobacteria, radionuclides and Cr^{6+}, constructed wetlands and wastewater treatment units, improvement of drinking water, fishery and fish breeding, odour control, conversion of manure to odourless fertilizer, gas purification and drying systems, animal nutrition, soil amendment for agriculture, conditioning of acid and basic soils, greenhouse and flowers substrates, food hygienic and safety, taste and quality improvement of foods, durability and health improvement of lawn, nutrition supplements (e.g., Misaelides et al. 1995, Godelitsas et al. 1999, 2001, 2003, Collela and Mumpton 2000, Kallo 2001, Harben 2002, Filippidis and Kantiranis 2007, Filippidis 2008, 2010, Filippidis et al. 2008a,b, 2009, 2010 a, b).

The treatment of 300 mL wastewater from Sindos industrial area of Thessaloniki (initial pH 7.8) with 0.1 g of HENAZE (grain-size <0.5 mm) and stirring time 3 min, gave overflowed clear water of pH 7.3, free of odours and improved by 93% in the colour, 69% in the chemical oxygen demand (COD), >97% in the P_2O_5 removal, 54% in the NO_3 removal and 77% in the Cr removal. The quality parameters, after repeated treatments, can easily reach values for the overflowed waters, fulfilling the requirements for disposition as downstream, irrigation, swimming and fish waters.

The sorption and fixation of the different species from the wastewater by the micro- meso- and macroporous of HENAZE can be attributed to absorption (mainly ion exchange), adsorption and surface precipitation processes. Important role in these processes play the surface Broensted acidic and Lewis basic sites of the HEU-type zeolite (e.g., Misaelides et al. 1995, Godelitsas et al. 1999, 2001, 2003, Kallo 2001). The HENAZE treatment gave also as precipitate, odourless and cohesive zeosludge of 0.173 g (0.1 g HENAZE and 0.073 g sludge), suitable for safe deposition since the fixation of dangerous components into the micro-meso- and macroporous of HENAZE, prevents the seepage of them by the rain water, protecting thus the quality of surface and underground waters (e.g. Filippidis 2010, Filippidis et al. 2008b).

Acknowledgments We express our gratitude to the GEO-VET N. Alexandridis and Co O.E., for the supply of the HENAZE.

References

Armagan B, Turan M, Ozdemir O, Celik M (2004) Color removal of reactive dyes from water by clinoptilolite. Journal of Environmental Science and Health, A39(5), 1251-1261

Charistos D, Godelitsas A, Tsipis C, Sofoniou M, Dwyer J, Manos G, Filippidis A, Triantafyllidis C (1997) Interaction of natrolite and thomsonite intergrowths with aqueous solutions of different initial pH values at 25^{o} C in the presence of KCl: Reaction mechanisms. Applied Geochemistry, 12, 693-703

Colella C, Mumpton FA (2000) Natural Zeolites for the Third Millennium. Napoli

Filippidis A (2008) Treatment and recycling of municipal and industrial waste waters using Hellenic Natural Zeolite: A Review. Proc. of AQUA, 3rd Intern. Conf. Water Science and Technology, 5p. Athens

Filippidis A (2010) Environmental, industrial and agricultural applications of Hellenic Natural Zeolite. Hellenic Journal of Geosciences, 45, 91-100

Filippidis A, Kantiranis N (2007) Experimental neutralization of lake and stream waters from N. Greece using domestic HEU-type rich natural zeolitic material. Desalination, 213, 47-55

Filippidis A, Godelitsas A, Charistos D, Misaelides P, Kassoli-Fournaraki A (1996) The chemical behavior of natural zeolites in aqueous environments: Interactions between low-silica zeolites and 1M NaCl solutions of different initial pH-values. Applied Clay Science, 11, 199-209

Filippidis A, Kantiranis N, Drakoulis A, Vogiatzis D (2005) Quality, pollution, treatment and management of drinking, waste, underground and surface waters, using analcime-rich zeolitic tuff from Samos island, Hellas. Proc. of 7th Hellenic Hydrogeological Conference, pp. 219-224. Athens

Filippidis A, Apostolidis N, Paragios I, Filippidis S (2008a) Zeolites clean up. Industrial Minerals, April, 68-71

Filippidis A, Apostolidis N, Paragios I, Filippidis S (2008b) Safe management of sewage sludge, produced by treatment of municipal sewage with Hellenic Natural Zeolite. Proc. AQUA, 3rd Intern. Conf. Water Science and Technology, 5p. Athens

Filippidis A, Papastergios G, Apostolidis N, Paragios I, Filippidis S, Sikalidis C (2009) Odorless and cohesive zeo-sewage sludge produced by Hellenic Natural Zeolite treatment. Proc. of 3rd AMIREG Intern. Conf. Resource Utilization and Hazardous Waste Management, pp. 96-100. Athens

Filippidis A, Moustaka-Gouni M, Papastergios G, Katsiapi M, Kantiranis N, Karamitsou V, Vogiatzis D, Filippidis S (2010a) Cyanobacteria removal by Hellenic Natural Zeolite. Proc. of Third Intern. Conf. Small Decentralized Water & Wastewater Treatment Plants, pp. 383-387. Skiathos

Filippidis A, Moustaka-Gouni M, Kantiranis N, Katsiapi M, Papastergios G, Karamitsou V, Vogiatzis D, Filippidis S (2010b) Chroococcus (cyanobacteria) removal by hellenic natural zeolite. Proc. of Zeolite 2010 – 8th Intern. Conf. Occurrence, Properties and Utilization of Natural Zeolites, pp. 91-92. Sofia

Godelitsas A, Charistos D, Dwyer J, Tsipis C, Filippidis A, Hatzidimitriou A, Pavlidou E (1999) Copper (II)-loaded HEU-type zeolite crystals: characterization and evidence of surface complexation with N,N-diethyldithiocarbamate anions. Microporous and Mesoporous Materials, 33, 77-87

Godelitsas A, Charistos D, Tsipis A, Tsipis C, Filippidis A, Triantafyllidis C, Manos G, Siapkas D (2001) Characterisation of zeolitic materials with a HEU-type structure modified by transi-

tion metal elements: Definition of acid sites in Nickel-loaded crystals in the light of experimental and quantum-chemical results. Chemistry European Journal, 7(17), 3705-3721
Godelitsas A, Charistos D, Tsipis C, Misaelides P, Filippidis A, Schindler M (2003) Heterostructures patterned on aluminosilicate microporous substrates: Crystallisation of cobalt (III) tris(N,N-diethyldithiocarbamato) on the surface of HEU-type zeolite. Microporous and Mesoporous Materials, 61, 69-77
Harben PW (2002) The Industrial Minerals HandyBook: A Guide to Markets, Specifications & Prieces. Blackwood, UK
Kallo D (2001) Applications of natural zeolites in water and wastewater treatment. In: Bish, D.L., Ming, D.W. (eds), Natural Zeolites: Occurrence, Properties, Applications. Reviews in Mineralogy and Geochemistry, Vol. 45, pp. 519-550. Mineralogical Society of America, Washington DC
Misaelides P, Godelitsas A, Filippidis A, Charistos D, Anousis I (1995) Thorium and uranium uptake by natural zeolitic materials. The Science of the Total Environment, 173/174, 237-246
Oren AH, Kaya A (2006) Factors affecting adsorption characteristics of Zn^{2+} on two natural zeolites. Journal of Hazardous Materials, B131, 59-65
Panayotova MI (2001) Kinetics and thermodynamics of copper ions removal from wastewater by use of zeolite. Waste Management, 21, 671-676
Pond WG, Mumpton FA (1984) Zeo-Agriculture: Use of Natural Zeolites in Agriculture and Aquaculture. International Committee on Natural Zeolites, Brockport, New York
Tserveni-Gousi AS, Yannakopoulos AL, Katsaounis NK, Filippidis A, Kassoli-Fournaraki A (1997) Some interior egg characteristics as influenced by addition of Greek clinoptilolitic rock material in the hen diet. Archiv fur Geflugelkunde, 61(6), 291-296
Tsitsishvili GV, Andronikashvili TG, Kirov GN, Filizova LD (1992) Natural Zeolites. New York
Yannakopoulos A, Tserveni-Gousi A, Kassoli-Fournaraki A, Tsirambides A, Michailidis K, Filippidis A, Lutat U (2000). Effects of dietary clinoptilolite-rich tuff on the performance of growing-finishing pigs. In: Colella, C. Mumpton, F.A. (eds), Natural Zeolites for the Third Millennium, pp. 471-481. De Frede, Napoli

Geothermics and thermal waters

Monitoring heat transfer from a groundwater heat exchanger in a large tank model

B.M.S. Giambastiani, M. Mastrocicco[1], N. Colombani

Department of Earth Sciences, University of Ferrara, 44100 Ferrara, Italy

[1]corresponding author: mtm@unife.it

Abstract A large tank (4x8x1.4 m), equipped with 26 standard piezometers and six temperature loggers with four channels each installed at different depth, is used to carry out thermal monitoring test and investigate environmental impact of heat borehole exchange. Loamy sediments (35 m^3), used to fill the tank, were excavated from an unconfined alluvial aquifer near Ferrara (Northern Italy). To evaluate spatial heterogeneity, the tank's filling material was characterized via slug tests and grain size distribution analysis. Constant heat input rate test was conducted by originating a heat plume using a groundwater heat exchanger (GHE). Temperature was monitored in continuous via data loggers. The effect of heat borehole exchange was small compared with the temperature applied. Results show a heat flux dominated by temperature gradient and thermal conduction. The effect of hydraulic conductivity heterogeneity on heat plume development is discussed. Tank model presented in this research looks to be suitable for heat transport modeling. Recommendations for future development of the research and future groundwater and heat transport modeling are also reported.

1 Introduction

Changes in groundwater temperature distribution can affect groundwater quality (Prommer and Stuyzand 2005) and can also interfere with aquifers usages (Massmann et al. 2006) and surface water systems (Engeler et al. 2011). Understanding groundwater heat transport is essential for the impact assessment of thermal devices such as groundwater heat pumps (Nam and Ooka 2010). Thermal response tests are becoming increasingly more popular for measuring in situ thermal conductivity and thermal properties of the subsurface geologic units (Signorelli et al. 2007; Fujii et al. 2002). Recently, analytical solutions and numerical modeling (Hidalgo et al. 2009; Ruhaak et al. 2008, Fujii et al. 2005) have been employed to quantify the impact of GHE on aquifers.

In this paper, a physical model representing an unconfined shallow aquifer was utilized to avoid uncertainties on boundary conditions such as groundwater flow

N. Lambrakis et al. (Eds.), *Advances in the Research of Aquatic Environment, Vol. 2*
DOI 10.1007/978-3-642-24076-8,

magnitude and direction. A large tank was filled with aquifer materials, whose grain size distribution and hydraulic conductivity (k) were intensively characterized to obtain an accurate estimate of sediment heterogeneities. Multi level slug tests were used to estimate k values along piezometers depth (Rus et al. 2001). To assess the impact of borehole heat exchange, the temperature distribution, induced by a groundwater heat exchanger (GHE), was monitored through temperature data loggers installed at different locations and depths in the tank. The effects of sediment heterogeneity on the development of a heat plume generated from the GHE are discussed. Recommendations for future improvement on groundwater and heat transport modeling are also reported.

2 Materials and methods

The experiment was performed in a large tank (4 m wide by 8 m long and 1.4 m deep) located in the Hydrogeology Laboratory at the Scientific and Technological Pole of the University of Ferrara (Fig. 1). The tank was assembled with an internal structure of armed PVC fastened on an external wooden structure. The tank was filled with 42 m^3 of unconsolidated material (35 m^3 of natural sediments and 7 m^3 of gravel). Natural sediments were excavated from a sand pit located along a paleo-meander bend of the Po River (Italy) (Mastrocicco et al. 2009). The principal Quaternary lithofacies of the area include coarse-grained facies associations (fluvial-channel and crevasse sands) and fine grained ones (floodplain, prodelta and marsh deposits) (Amorosi et al. 2003). An external reservoir (constant head) was connected to the tank via three inflow pipes (Fig. 1). The constant head was introduced to create a steady state flux. In order to maintain uniformity of the potentiometric surface, two gravel walls were built, one at the inflow and the other at the outflow of the tank. Twenty-six piezometers were installed on the base of a semi-regular monitoring grid (Fig. 1). Seventy-eight undisturbed 1 inch cores were collected every 0.3 m for grain size analyses. Particle size curves were obtained using a sedimentation balance for the coarse fraction and an X-ray diffraction sedigraph 5100 Micromeritics for the finer fraction. To estimate the k variability 130 multi level slug tests were performed every 0.15 m within the saturated zone using small inflatable straddle packers. All the acquired slug test responses were analyzed using the Bouwer and Rice method (Bouwer and Rice 1976). An accurate description of methods employed to characterize the permeability field within the tank is given in Mastrocicco et al. 2010. Steady state flow was inferred as heads variation was null or within the measurement error (±2 mm).

In order to run experiments to quantify the heat borehole exchange, a groundwater heat exchanger was positioned within a PVC tube (5 cm i.d.) in the upper side of the tank (GHE in Fig. 1). µloggers Model-4R (Zeta-tec, UK) were employed to record temperature every 10 minutes in each channel, cou-

pled with stainless steel cylindrical thermistors (4 mm diameter and 10 cm length) able to record temperature shifts of 0.01 °C, with an accuracy of ±0.2 °C and range of -40+85 °C. Six temperature loggers (B2, B3, C2, C3, D2, and D3 in Fig. 1) with four channels each located at different depths were installed along the supposed heat plume direction in order to monitor temperature changes. The thermistors were directly inserted into the ground 10 cm upgradient each piezometer, to minimize the distortion of groundwater flow induced by piezometers (Ma et al. 2011). The water was heated by the GHE which acted as a point-like source, the GHE consisted of a heater probe equipped with an anti-Joule effect resistor and a controller for temperature tuning with an accuracy of ±0.3 °C. The heater was switched on to provide a constant source of heat (32±0.3 °C) within the open well for three weeks. The tests started with the tank at uniform temperature of 23±0.5 °C.

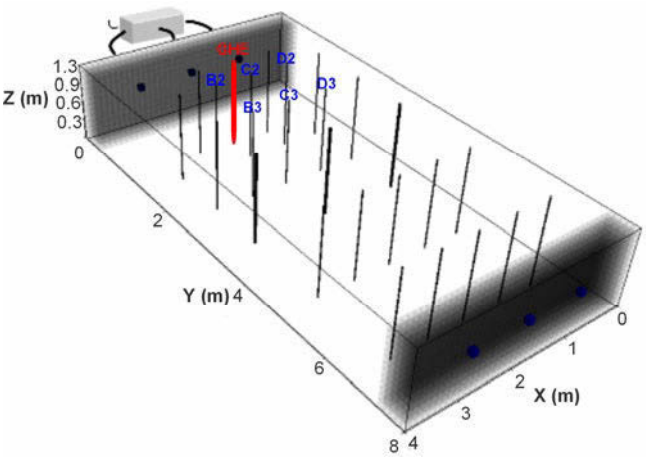

Fig. 1. Three-dimensional view (scale in m above datum) of the tank with the constant head reservoir (left hand side) which creates a flux towards the outflow pipes (right hand side, blue cubes); gravel walls are depicted near the inflow and ouflow walls (shaded areas); 2.5 cm and 5.0 cm i. d. piezometers are plotted with black lines; groundwater heat exchanger (GHE) is shown with a red cilinder encircled by temperature loggers (B2, B3, C2, C3, D2, D3).

3 Results and discussion

The grain size analysis of the 78 samples confirms that sediments come from the same depositional environment, identified as a crevasse splay.

Because this depositional environment is characterized by a broad range of textures, due to traction and traction plus fall-out processes, a considerable variability in the grain size distribution is registered (Amorosi and Marchi 1999).The median of the average grain radius varies from 0.043 to 0.107 mm, which is typi-

cal of very fine sands; the uniformity coefficient (U) varies from 1.65 to 3.12 depicting different sorting of the samples; the skewness coefficient (S) remains within 0.40 to 0.84, indicating a quasi-normal distribution with small tailing towards the large grain size. Following the Wentworth classification these sediments can be defined as silty-sands. The k values measured in the tank range from $3.2e^{-7}$ m/s to $1.7e^{-5}$ m/s, spreading over two orders of magnitude, with an average k of $3.1e^{-6}$ m/s. In order to understand if there is a preferential distribution in hydraulic conductivity, a three-dimensional plot depicting isosurfaces of k is created with the inverse distance interpolator. Two different isosurfaces of k are generated; the first is equal to $6e^{-6}$ m/s and represents the zones with a hydraulic conductivity above the average permeability, while the second envelope is set equal to $3e^{-6}$ m/s, equivalent to the average permeability. The $6e^{-6}$ m/s isosurface demarcates a large zone extending from the centre to the right side of the outflow wall where groundwater migrates faster than in other zones (Fig. 2). Figure 3 shows the temperature curves registered at different depths for the six loggers. The monitoring reveals that the temperature plume created by the constant heat input rate test is quite small with temperature variations of maximum 3 °C measured after 20 days in logger C2, set at 0.5 m to the GHE. The GHE was started at day 0 from the beginning of the experiment and temperature increased in all loggers simultaneously after approximately 1 hour. Considering the slow groundwater flow in the tank (average velocity 2.6 cm/day, up to 15 cm/day in more permeable zones), this simultaneous thermal response in all loggers is thought to be due to thermal conduction and not to convection. In fact, in the tank the convective component is quite slow as explained above and in addition is affected by retardation with respect to groundwater flow (Markle and Schincariol 2007). If the heat flux was dominated by convection, temperature would breakthrough at successive times along a flow path down gradient to the GHE. In the shallowest part of the tank (1.0 m above datum) temperature data are affected by daily temperature oscillations that occurred in the room during the test. This effect is evident in all loggers and can affect the interpretation of the thermal response data (Signorelli et al. 2007). In the deepest portion of the tank (0.1 above datum) the temperature appears to enter a quasi-steady regime by reaching a plateau after approximately 15 days. The further the logger is from the GHE, the smaller the temperature variation is; temperature in C2, that is located 0.5 m far from GHE, registers the largest temperature variation amongst all loggers located in the tank. Figure 3 shows that heat conduction is not uniform through the sediment. For instance logger D3 registers the smallest variations in temperatures at all depths except at 0.6 m above the datum, where logger C3 shows minimum variations. This is probably due to the heterogeneity of the system. In fact, three thermistors (1.0, 0.3, and 0.1 m above the datum) in D3 are located in a low permeability area characterized by silty-clay sediments (dark red color in Fig. 2), and thus with smaller thermal conductivity with respect to silty-sand sediments (Markle and Schincariol 2007).

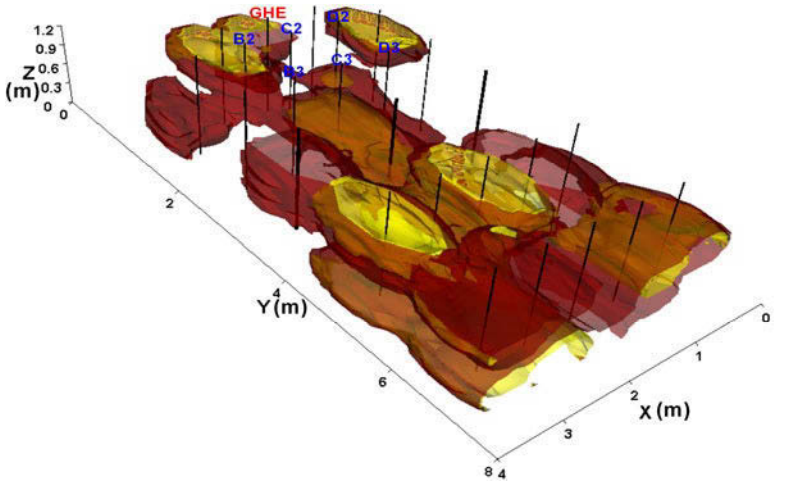

Fig. 2. Three-dimensional representation (scale in m above datum) of hydraulic conductivity isosurfaces equal to $6e^{-6}$ m/s (yellow) and to $3e^{-6}$ (dark red). Temperature loggers are shown in blue color.

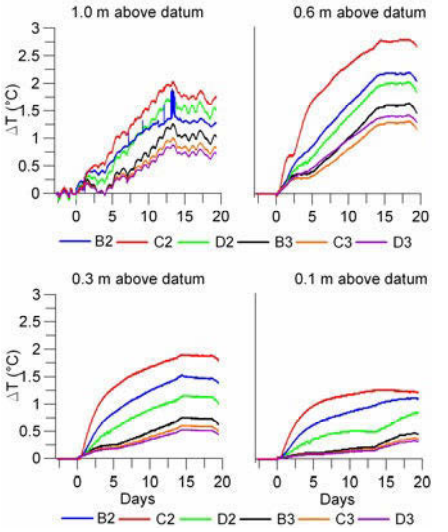

Fig. 3. Temperature curves monitored at different depths (0.1, 0.3, 0.6 and 1.0 m above datum) in the six µloggers (B2, B3, C2, C3, D2, D3) during the constant heat input rate test. (Note: for datum it is considered the bottom of the tank model).

It is evident how the heterogeneity of the system can influence the temperature distribution (Hidalgo et al. 2009). However in order to quantify the influence of hydraulic conductivity and thermal conductivity distribution on heat propagation within the tank a numerical flow and transport model needs to be implemented. Finally, it should be noted that the thermistors register an integrated temperature

along 10 cm depth and not a punctual value, thus advective transport could still occur at the centimetric scale but will be masked by the measuring set up.

4 Conclusions

A large tank experiment was implemented to evaluate the environmental impact of heat borehole exchange on low permeability sediments, typical of lowland alluvial plains. An accurate three-dimensional reconstruction of the k field and local heterogeneity within the tank was achieved through 130 multi level slug tests and grain size analysis. Thermal monitoring test was performed in the boreholes. During the test the heat input rate was held constant at a temperature of 32°C. Temperature data indicate that the impact of heat borehole exchange is small. The amount of heat flowing between the GHE and the surrounding ground is determined by temperature gradients and thermal conductivities and the convection component is not significant due to the slow groundwater flow maintained in the system during the test. The heat flow varies due to the heterogeneity in the sediments and the corresponding thermal conductivities values. The tank model presented in this research shows evidence of being suitable for future heat transport modeling, to define the effect of heterogeneity on thermal response data and thermal conductivity. A methodological implication of this study is that laboratory experiments can provide robust results. Since data are sensitive to small temperature disturbance, daily temperature fluctuations in the laboratory needs to be controlled during the experiment in order to avoid temperature oscillation that can affect data interpretation.

Acknowledgments We gratefully acknowledge the funding by the GEO. POWER project ('Geothermal energy to address energy performance strategies in residential and industrial buildings'), which is part of the INTERREG IVC Operational Programme.

References

Amorosi A, Centineo MC, Colalongo ML, Pasini G, Sarti G, Vaiani SC (2003) Facies architecture and latest Pleistocene-Holocene depositional history of the Po Delta (Comacchio area), Italy. J. Geol. 111, 39-56

Amorosi A, Marchi N (1999) High-resolution sequence stratigraphy from piezocone tests: an example from the late quaternary deposits of the SE Po Plain. Sediment. Geol., 128, 69-83

Bouwer H, Rice RC (1976) A slug test for determining hydraulic conductivity of unconfined aquifers with completely or partially penetrating wells. Water Resour. Res., 12(3), 423-428

Engeler I, Franssen HJH, Muller R, Stauffer F (2011) The importance of coupled modelling of variably saturated groundwater flow-heat transport for assessing river-aquifer interactions. J.Hydrol. 397(3-4), 295-305

Fujii H, Akibayashi S, Ohshima K (2002) Interpretation of thermal response tests in shallow deposits. Geotherm. Resour. Council Trans. 26, 143-148

Fujii H, Itoi R, Fujii J, UchidaY (2005) Optimizing the design of large-scale ground-coupled heat pump systems using groundwater and heat transport modelling. Geothermics. 34(3), 347-364

Hidalgo JJ, Carrera J, Dentz M (2009) Steady state heat transport in 3D heterogeneous porous media. Adv. Water Resour. 32, 1206-1212

Ma R, Zheng CM, Tonkin M, Zachara JM (2011) Importance of considering intraborehole flow in solute transport modeling under highly dynamic flow conditions. J. Cont. Hydrol. 123(1-2) 11-19

Markle J. M. and Schincariol R. A. (2007) Thermal plume transport from sand and gravel pits - Potential thermal impacts on cool water streams. J. Hydrol. 338, 174-195

Massmann G, Greskowiak J, Dünnbier U, Zuehlke S, Knappe A, Pekdeger A (2006) The impact of variable temperatures on the redox conditions and the behaviour of pharmaceutical residues during artificial recharge. J.Hydrol. 328, 141-156

Mastrocicco M., Colombani N., Palpacelli S (2009) Fertilizers mobilization in alluvial aquifer: laboratory experiments. Env Geol 56, 1371-1381

Mastrocicco M., Colombani N., Palpacelli S., Castaldelli G. (2010) Large tank experiment on nitrate fate and transport: the role of permeability distribution. Environ. Earth Sci. doi:10.1007/s12665-010-0759-0

Nam Y, Ooka R (2010) Numerical simulation of ground heat and water transfer for groundwater pump system based on real-scale experiment. Energ. Buildings. 42, 69-75

Prommer H, Stuyfand PJ (2005) Identification of temperature-dependent water quality changes during a deep well injection experiment in a pyritic aquifer. Environ. Sci.Technol. 39, 2200-2209

Ruhaak W, Rath V, Wolf A, Clauser C (2008) 3D finite volume groundwater and heat transport modeling with non-orthogonal grids, using a coordinate transformation method, Adv. Water Resour. 31(3), 513-524

Rus DL, McGuire VL, Zurbuchen BR, Zlotnik VA (2001) Vertical profiles of streambed hydraulic conductivity determined using slug tests in central and western Nebraska. U.S. Geol. Surv. Water Resour. Invest. Rep. 01-4212, 32 pp

Signorelli S, Bassetti S, Pahud D, Kohl T (2007) Numerical evaluation of thermal response tests. Geothermics 36, 141-166

Origin of thermal waters of Nisyros volcano: an isotopic and geothermometric survey

D. Zouzias, K.St. Seymour

Department of Geology, University of Patras, Rio-Patras, GR 26 504, Greece.

dizouzias@upatras.gr; kstseymr@upatras.gr

Abstract Nisyros is characterised by a high enthalpy geothermal system. Numerous thermal springs are concentrated near the coastline with temperatures of 27°-43°C. Isotopic composition of Nisyros thermal water samples reveals mixing between *seawater* with *magmatic water* and *geothermal steam* and the possible involvement of *groundwater* and/or *meteoric water*. Combined silica and K^2/Mg geothermometry indicates temperatures of 90°-140°C while deep geothermal fluids display temperatures of 245°C and steam heated samples approximately 210°C. We have calculated the initial temperature of the hot component of mixing using the diagram of dissolved SiO_2 versus enthalpy. We propose that the geothermal system of Nisyros consists of two major reservoirs. A deeper one (1400-1800 m) with temperatures greater than 245°C which is the result of mixing between *seawater* and *primary geothermal fluid* and hosts hot waters of high enthalpy which cool adiabatically and ascend, due to separation of vapours, to the shallow reservoir (0-500m) of lower enthalpy. In this mixing occurs mixing between *seawater* and *geothermal vapours* and/or *underground water* or *meteoric water* with a *hot water component* of approximately 180°-220°C. The latter is derived from the ascent of the high enthalpy waters into the shallow reservoir which represents the mixing zone of the geothermal system and is characterised by lower enthalpy compared to the deeper reservoir displaying temperatures of 90°-140°C whilst the temperature of the separated vapours are approximately 225°C.

1 Introduction

Nisyros is a complex volcano in the easternmost part of the Aegean volcanic arc with an active geothermal system of high enthalpy and reservoir temperatures above 300°C (Geotermica Italiana 1984). Two deep exploratory boreholes (NIS-1 at 1800m and NIS-2 at 1550m) have been sunk on the caldera floor by Public Power Corporation (P.P.C.) to evaluate the geothermal potential of Nisyros.

N. Lambrakis et al. (Eds.), *Advances in the Research of Aquatic Environment, Vol. 2*
DOI 10.1007/978-3-642-24076-8,

We present isotopic and geothermometric data of the thermal waters of Nisyros in order to investigate their origin and to obtain information about the temperatures of the geothermal aquifers and of the physicochemical processes that take place in the geothermal system of Nisyros. Finally, we developed a hydrological model of the thermal-fluid subsurface flow at Nisyros volcano.

2 Geological setting

Nisyros is a calcalkaline stratovolcano, the result of the subduction of the African plate under Aegean microplate. Historic phreatic activity has been reported on Nisyros from 1422 to 1888 A.D. (Vougioukalakis 1993). Seismic studies suggest a magma chamber at a depth 2 km (Papadopoulos et al. 1998). The volcanic evolution of Nisyros can be divided in two cycles: one stratovolcano-building and a second which was explosive and resulted in the formation of a caldera. Major faultsystems trending NE-SW and NW-SE are related to surface geothermal manifestations such as fumarolic activity and thermal springs (Vougioukalakis 1993).

3. Sampling and analytical methods

Water samples were collected from thermal springs, boreholes and from the sea for chemical analysis during 2006-2008. Samples were subsequently filtered, acidified with ultrapure nitric acid and stored in polyethylene vials. Temperature, pH and alkalinity were measured in the field. Chemical analyses were performed using ICP/MS and ICP/EOS for major elements. Ion chromatography has been used for the determination of ions. Eight samples were collected for stable isotope analyses of $\delta^{18}O$ and δD (Table 1). Stable isotope analyses of $\delta^{18}O$ and δD were performed with precision and sensitivity of 1‰ (natural abundance) and 3‰ (enriched) for ™D and 0.15‰ (natural abundance) 0.4‰ (enriched) for $\delta^{18}O$, performing repeated analyses to minimize ambiguity. No admixture of Mercuric Chloride was used when collecting samples for stable isotope analyses. Additional, isotopic data from the literature were used such as the geothermal fluids of the NIS-2 geothermal borehole (Dotsika et al 2009), the sea and the thermal springs Thermiani, Pali and Loutra (Kavouridis et al. 1999; Brombach et al. 2003 and Dotsika et al. 2009), the Primary Geothermal Liquid (PGL) (Brombach et al. 2003) and the “andesitic water” of (Giggenbach 1992).

Table 1. Representative chemical and isotopic analyses of the waters of Nisyros volcano. Concentrations are in mg/l and δ values are in per mil V-SMOW. Samples NIS-1 and NIS-2 are from Dotsika et al 2009. Star indicates borehole sampling points.

Analyte Symbol	T°C	pH	Na	Mg	K	Ca	SiO_2	NO_3	HCO_3	SO_4	Cl	δD	$\delta^{18}O$
EL-5*	35.9	6.5	129	4.45	15.3	12.3	17.3	0.03	24.4	17.6	237	-19.9	-4.92
KAS-1*	35.7	8.79	833	132	77.2	599	88.3	0.49	61	553	2220	-16.3	-4.20
MAN-41*	33.7	5.74	11800	1090	610	1050	105.8	3.3	280.6	2330	21000	6.9	0.64
PALI	27.3	6.94	5970	635	371	1220	74.4	3.3	244	1340	14000	0.6	-0.05
THERMIANI	27.4	7.57	9070	722	503	1410	104	3.3	183	1620	18400	7.3	1.52
LOUTRA	43.5	6.78	10400	637	759	1660	133.8	3.3	25.6	1600	21800	2.7	-0.02
STEF	86.7	2.28	269	34.1	55.1	62	470	2.2	335.5	155	302	17.2	10.73
Sea	22.5	7.88	13100	1400	465	470	-	3.3	176.9	2840	21500	10.9	1.41
NIS-2	290	-	21610	78	2870	7340	693	-	20	25	50390	-2.1	4.1
NIS-1	100	6.8	25290	1950	4300	17640	13	-	134	149	81500	-	-

4 Stable isotope composition of water

By plotting stable isotope composition $\delta^{18}O$ and δD of water samples from Nisyros we derive information about their origin (Fig. 1a, Table 1). The correlation function relating δD with $\delta^{18}O$ for Nisyros samples with a correlation factor r=0.98 is: $\delta D = 4.9\delta^{18}O + 2.8$.

Water samples EL-5 and KAS-1 (plot between the Global and Mediterranean Meteoric Lines, indicating a *meteoric origin* for these samples (Fig. 1a). The isotopic compositions of water samples from Loutra, Pali, Thermiani and MAN-41 plot along a curved mixing line (Fig. 1a) defined by the samples of meteoric origin (EL-5 and KAS-1), the Standard Mean Ocean Water (SMOW) and the Primary Geothermal Liquid (PGL) which represent the three end-members of this curved mixing line. Consequently, samples that plot between SMOW and PGL reveal mixing between these two end-members and enrichment in magmatic components while samples that plot between SMOW and the Global Meteoric Line are characterized by the contribution of seawater. Therefore, samples from Pali which plot between SMOW and the Global Meteoric line reveal a *marine origin* or waters that resulted from *mixing with seawater*. Samples from Loutra, Thermiani, MAN-41 and NIS-2 plot between SMOW and PGL and are classified as *magmatic* and/or *marine origin* waters according to the percentage of enrichment in the magmatic component (PGL) (Fig. 1a). Geothermal fluids of the NIS-2 borehole are relatively enriched in the *magmatic component* relatively to the geothermal vapors, since they plot closer to PGL revealing *magmatic origin* whilst geothermal vapors display a *magmatic-marine origin* (Fig. 1a). The thermal waters of Nisyros are the result of mixing between meteoric water, seawater and deep hot steam

suggesting seawater as the major component involved, which is consistent with their Na-Cl dominated chemistry (Table 1). Therefore, the geothermal vapors of the NIS-2 geothermal borehole participate in the mixing process of Nisyros waters coupled with transfer of heat, chemical and isotopic components. Taking this into account, Loutra samples that plot close to SMOW are of *marine origin* while samples MAN-41 that plot between SMOW and the geothermal vapors of NIS-2 represent mixtures of seawater and geothermal vapors. They display positive shifts of $\delta^{18}O$ in relation to SMOW due to enrichment in the magmatic component revealing a *marine-magmatic origin* (Fig. 1a). Thermal water samples from Thermiani spring display greater positive shifts of $\delta^{18}O$ in relation to SMOW than MAN-41 and enrichment in the magmatic component. They plot between SMOW and the geothermal vapors of NIS-2 borehole revealing a *magmatic-marine origin* (Fig. 1a). Water samples from the boiling mud-pots of the hydrothermal crater Stefanos (STEF) are the result of mixing of soil moisture with droplets of oxidized fumarolic steam precipitate. They are strongly enriched in the magmatic component and carry the isotopic identity of *Mediterranean Magmatic Waters* of Giggenbach (1997) revealing a *magmatic origin* (Fig. 1a).

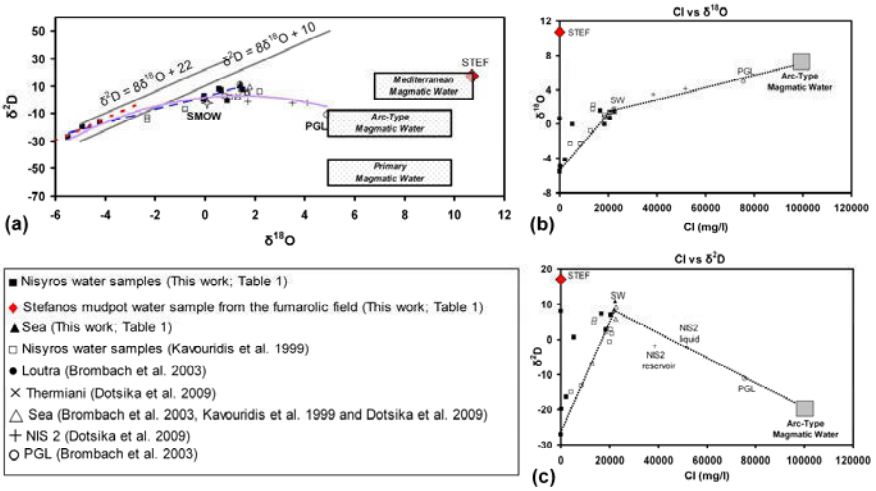

Fig. 1. (a) $\delta^{18}O$ versus $\delta^{2}D$ isotopic composition for Nisyros water samples. Red line indicates the correlation function of meteoric origin waters. Blue line indicates the correlation function of all Nisyros water samples. Mixing processes between three components (meteoric water, seawater, primary geothermal liquid) are indicated by a purple curved line. **(b, c)** $\delta^{18}O$ and $\delta^{2}D$ isotopic composition versus Cl concentrations for all Nisyros water samples.

The origin of the Primary Geothermal Fluid (PGL) is attributed to mixing between the Arc-Type Magmatic Water of Giggenbach (1992) and the local seawater (Brombach et al. 2003; Marini and Fiebig 2005; Dotsika et al. 2009). In view of the participation of magmatic water in the Nisyros geothermal system, a plot of Cl versus $\delta^{18}O$ and δD (Fig. 1b and 1c) indicates that the geothermal fluid

of NIS-2 can be considered as a mixture of approximately 40% of the primary geothermal liquid (PGL) and 60% of the local seawater, in agreement with Dotsika et al. (2009). Taking into account the isotopic composition of fumaroles form Stefanos and Polyvotis hydrothermal craters (Kavouridis et al. 1999) which plot close to PGL, we conclude that mixing in the Nisyros geothermal system involvees local seawater, magmatic water, geothermal steam and the possible involvement of local groundwater and/or meteoric water.

5 Geothermometry

Surface temperatures of the thermal waters samples from Nisyros range from 27^{o} to 43^{o}C (Table 1). Since these water samples are characterized by mixing and water-rock interactions, we consider the cation geothermometry as unreliable.

Quartz and quartz steam loss geothermometers (Fournier, 1977) of these waters indicate a temperature range from 115^{o} to 140^{o}C for the Nisyros samples (Table 2). However, since the quartz geothermometer probably works best in the temperature range 150-225^{o}C, for temperatures below 150^{o}C the solubility of silica is controlled by chalcedony or cristoballite (Fournier 1977).

Table 2. Calculated subsurface reservoir temperatures from the thermal waters using quartz, quartz steam loss geothermometers (Fournier 1977) and dissolved silica versus enthalpy calculations for the initial temperature of hot component of mixed waters (Truesdell and Fournier 1977).

	Quartz	Quartz steam loss	SiO_2 vs. enthalpy		Quartz	Quartz steam loss	SiO_2 vs. enthalpy
EL-5	49	56	112.95	Loutra	139	134	218.82
KAS-1	117	115	180.66	Thermiani	125	122	220.98
Pali	108	108	206.12	STEF	224	204	227.32
MAN-41	126	123	191.28	NIS2	258	230	233.7

Chemical systems based on dissolved SiO_2 and the water component of K and Mg provide evidence of the water-rock interaction temperatures just before water discharge (Fig. 2). Nisyros samples plot along the conductive cooling line after fully equilibrating with chalcedony at temperatures of 90^{o}-140^{o}C (Fig. 2). This agrees with the temperatures calculated by silica geothermometry, where the solubility of silica is controlled by chalcedony (Table 2). Sample EL-5 differs from the others probably due to dilution with meteoric water (Fig. 2). Sample NIS-2 plots along the equilibrium line of quartz corresponding to adiabatic cooling and displays temperatures of 245^{o}C (Fig. 2) relatively close to the temperatures of 290^{o}C (>350^{o}C) measured in geothermal drilling. Sample STEF displays high silica content and temperatures of approximately 210^{o}C (Fig. 2) in agreement with the temperatures calculated by silica geothermometry (Table 2).

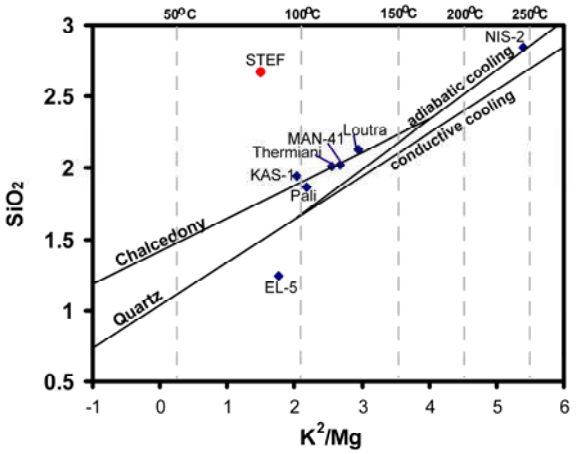

Fig. 2. Log of silica concentrations (Log SiO2) versus (Log K^2/Mg) of Nisyros thermal waters comparing silica (Fournier 1977) and K-Mg-based (Giggenbach et al. 1983) geothermometers.

We testify also here the existence of two major reservoirs which are located at depths of 0-500 m for the shallow one and 1400-1800 m for the deeper one (Geotermica Italiana 1984). These two reservoirs are characterized by temperatures of 90°-140°C and over 245°C respectively. The geothermal reservoirs of Nisyros are at higher than boiling surface temperatures; therefore, the hot fluid is cooled adiabatically and ascends to the surface separated from steam (Fournier 1977). Since mixing in the Nisyros geothermal system takes place between hot and cold waters it is necessary mixing to be taken into consideration in the calculations of reservoir temperatures. Truesdell and Fournier (1977) proposed a simplified procedure of calculating the initial temperature of the hot component of mixing using the diagram of dissolved SiO_2 versus enthalpy. We have calculated the reservoir temperatures of the mixing zone applying the methodology as described by Fournier (1977) for waters subjected to mixing where enthalpy of the hot water in the mixing zone is less than the enthalpy of the hot water in the depth due to separation of steam during ascent (Table 2). Samples KAS-1, MAN-41, Loutra, Pali and Thermiani display temperatures of 180° to 220°C, which are much lower than the temperatures of 290°C measured in the NIS-2 at depth 1550m (Geotermica Italiana 1984). This occurs since the enthalpy of hot water in the shallow reservoir (0-500m) in the mixing zone is less than the enthalpy of hot water in the deeper reservoir (1400-1800m) due to separation of steam during ascend of the thermal fluid. Sample STEF is heated by the fumarolic activity and display temperature of approximately 225°C which corresponds to the temperature of the separated vapours from the adiabatically cooled hot water that ascends to the mixing zone. Sample EL-5 has lower temperatures (~113°C) and probably is governed by leaching and dissolution of minerals.

6 Discussion and Conclusions

Surface temperature of the thermal water samples from Nisyros range from 27° to 43°C and are the result of mixing between seawater, meteoric water and deep hot steam. Seawater is the major component involved, consistent with their chemistry which is dominated by Na and Cl (Table 1). Isotopic compositions of Nisyros thermal waters plot along a curved mixing line (Fig. 1a) where samples that plot between SMOW and Primary Geothermal Liquid (PGL) reveal mixing between these two end-members and enrichment in a magmatic component. Samples between SMOW and the Global Meteoric Line are characterized by seawater contribution. Samples from Pali reveal a *marine origin* and samples from Loutra, Thermiani, MAN-41 and NIS-2 a *magmatic* and/or *marine origin* according to the percentage of enrichment in the magmatic component (Fig. 1a). The geothermal fluid of NIS-2 borehole can be considered as a mixture of approximately 40% of PGL and 60% of local seawater (Fig. 1b and 1c) in agreement with Dotsika et al. (2009). Taking into account the isotopic composition of fumaroles from Stefanos and Polyvotis hydrothermal craters from Kavouridis et al. (1999) which plot close to PGL we conclude that mixing in the Nisyros geothermal system takes place between *local seawater* with *magmatic water* and *geothermal steam* and the possible involvement of *local groundwater* and/or *meteoric water*.

Quartz and quartz steam loss geothermometers (Fournier 1977) indicate a temperature range from 115° to 140°C for the Nisyros samples (Table 2). However, since the temperatures are below 150°C the results should be treated carefully. In the chemical system based on dissolved SiO_2 and the water component in K and Mg, Nisyros samples display temperatures ranging from 90° to 140°C (Fig. 2) which agree with temperatures calculated by silica geothermometry (Table 2). Sample NIS-2 displays a temperature of 245°C relatively close to the temperature of 290°C measured in the geothermal drilling (Geotermica Italiana 1984). Sample STEF displays a temperature of approximately 210°C (Fig. 2) in agreement with the temperatures calculated by silica geothermometry (Table 2).

Since mixing in the Nisyros geothermal system takes place between hot and cold waters we have calculated the initial temperature of the hot component of mixing using the diagram of dissolved SiO_2 versus enthalpy. The initial temperature of the hot component calculated for the Nisyros waters display temperatures of 180° to 220°C, much lower than the temperature of 290°C (>350°C) measured in the NIS-2 geothermal borehole at depth 1550 m (Geotermica Italiana 1984). This occurs since the enthalpy of hot water in the shallow reservoir (0-500; Kavouridis et al. 1999) in the mixing zone is less than the enthalpy of hot water in the deeper reservoir (1400-1800 m; Geotermica Italiana 1984) due to separation of steam during geothermal fluid ascent. Temperatures of approximately 225°C for sample STEF correspond to the temperature of the separated vapours of the adiabatically cooled hot water that ascends to the mixing zone. Sample EL-5 has lower temperatures (approximately 113°C) and probably is governed by leaching and dissolution of minerals.

We propose that the geothermal system of Nisyros consists of two major reservoirs. The deeper one (1400-1800 m) with temperatures greater of 245°C (Fig. 2) is the result of mixing between *local seawater* and *primary geothermal fluid* (PGL) (Fig. 2) and hosts hot waters of high enthalpy which cool adiabatically and ascend due to separation of vapours to the shallow reservoir of lower enthalpy. The shallow reservoir (0-500 m) is the result of mixing between *local seawater* and *geothermal vapours* and/or *underground water* or *meteoric water* (Fig. 1a) with a *hot water component* of approximately 180° to 220°C temperatures derived from the ascent of the high enthalpy waters due to separation of vapours and represents the mixing zone of the geothermal system which is characterised by lower enthalpy in relation to the deeper reservoir with temperatures ranging ranges from 90° to 140°C while the temperature of the separated vapours are approximately 225°C.

Acknowledgments The authors wishes to thank Mr. Ioannis Leontiadis and Mr. Michael Fytikas for reviewing this manuscript; the Laboratory of Hydrogeology, Department of Geology, University of Patras, Greece for supplying lab facilities and field equipment; the Municipality and the inhabitants of Nisyros for their kind co-operation during field surveying.

References

Brombach T, Caliro S, Chiodini G, Fiebig J, Hunziker JC and Raco (2003) Geochemical evidence for mixing of magmatic fluids with seawater, Nisyros hydrothermal system, Greece Bulletin of Volcanology Volume 65, Number 7, 505-516

Dotsika E, Poutoukis D, Michelot JL, Raco B (2009) Natural tracers for identifying the origin of the thermal fluids emerging along the Aegean Volcanic arc (Greece): Evidence of Arc-Type Magmatic Water (ATMW) participation Journal of Volcanology and Geothermal Research 179 (2009) 19-32

Fournier RO (1977) Chemical geothermometers and mixing models for geothermal systems Geothermics, Vol. 5, pp. 41-50. Pergamon Press, 1977

Geotermica Italiana, (1984) Nisyros 1 and 2Geothermal Well, Athens, PCC-EEC Report

Giggenbach WF (1997) The origin and evolution of fluids in magmatic-hydrothermal systems, In: Barnes, H.L. (Ed.), Geochemistry of hydrothermal ore deposits,3d Edition. Wiley, pp. 737–796

GiggenbachWF (1992) Isotopic shifts in waters from geothermal and volcanic systems along convergent plate boundaries and their origin. Earth Planet. Sci. Lett. 113,495–510

Giggenbach WF, Gonfiantini R, Panichi C (1983) Geothermal systems. Guidebook on nuclear techniques in hydrology. Techn. Reports Series 91, 359–379 A.I.E.A., Vienne

Kavouridis T, Kuris D, Leonis C, Liberopoulou V, Leontiadis J, Panichi C, La Ruffa G and Caprai A (1999) Isotope and chemical studies for a geothermal assessment of the island of Nisyros (Greece). Geothermics 28, 219-239

Marini L and Fiebig J (2005) Fluid geochemistry of the magmatic-hydrothermal system of Nisyros (Greece). Mém. Géol. 44, 192

Papadopoulos GA, Sachpazi M, Panopoulou G and Stavrakakis G (1998) The volcano-seismic crisi of 1996-97 in Nisyros, SE Aegean Sea, Greece. Terra Nova, 10, 151-154

Truesdell, A. H. and Fournier, R. O. (1977) Procedure for estimating the temperature of a hot water component in a mixed water using a plot of dissolved silica vs enthalpy. (1977) U.S. Geol Survey J. Res. 5, 49-52

Vougioukalakis G (1993) Volcanic stratigraphy and evolution of Nisyros island. Bull. of Geol. Soc. Greece, XXVIII/2: 239-258, Athens, 1993

Hydrogeochemical characteristics and the geothermal model of the Altinoluk-Narli area, in the Gulf of Edremit, Aegean Sea

N. Talay[1], A.M. Gözübol[2], F.I. Barut[3]

1Department of Geology, University of Istanbul, Avcılar, Turkey, nstlay@gmail.com

2 Department of Geology, University of Istanbul, Avcılar, Turkey. alimalikgozubol@gmail.com

3 Istanbul University, Institute of Marine Sciences and Management, Vefa-Fatih/Istanbul/Turkey barutif@istanbul.edu.tr

Abstract The Altınoluk-Gure region is at the foot of Mount Kazdag. There are many thermal springs to the east of the area (Gure ande Kucukcetmi). Because of the geologic and tectonic settings, it is considered that the Altınoluk-Gure-Narlı area may have a geothermal potential as well. In this study the hydrochemical data were mapped out by sampling from the existing springs and, in order to determine the geothermal potentiality of the region, the relationship between volcanism, tectonics and springs were investigated.

1 Introduction

The Altınoluk-Gure region is an area that potentially has geothermal energy at foot of Mount Kazdag (Ida Mountain). There are many thermal springs to the east of the area (Gure and west Kucukcetmi). Due to its the geologic and tectonic settings, it is thought that the Altınoluk-Gure-Narlı area may also have a geothermal potential. This study is aimed at mapping out the hydrochemical data by sampling from the existing springs and, in order to determine the geothermal potentiality of the region, an investigation was performed into the relationship between volcanism, tectonics and springs. The results of chemical and isotopic analyses were used to correlate the relation between thermal and cold waters and establish a geothermal model.

N. Lambrakis et al. (Eds.), *Advances in the Research of Aquatic Environment, Vol. 2*
DOI 10.1007/978-3-642-24076-8,

2 Geologic and Tectonic Outline

In the area Kazdag the metamorphic massif of Paleozoic age occurs and it is overlain by the Lower Triassic Karakaya formation and Upper Jurassic-Lowe Cretaceous (sandy or chert nodules bearing) limestones rest upon the Karakaya Formation (Fig. 1 a, b). Products of volcanic activity that has been effective from Upper Oligocene to Lower Miocene and granodiorites coeval to these volcanites are observed at the area**.** Sedimentary rocks representing the Middle-Upper Miocene time period were deposited in the lacustrine environment. The Pliocene aged volcanites are overlain by basaltic rocks developed by fissure volcanism and, in turn, these are capped by cemented pebblestones, sandstones and claystones of the same age. It is concluded that the important tectonic lines that provide the geothermal discharge are NE-SW trending dextral strike-slipe faults, NW-SE oriented sinistral faults and normal faults running in E-W direction. The rock units in the region are porous and permeable; thus, they can store groundwater that percolated into the depths.

3 Material And Method

Geological maps, cross sections, reports and geochemical data, which were presented by previous researchers, were investigated and made necessary arrangements. During the field survey general geological features of the region (formation boundaries, hydrogical settings, fracture, fault and fissure systems, etc.) and hot/cold source points were determined. All the samples collected in-situ in polyethylene vessels were washed by source water three times. The pH, EC and temperature were measured by means of a multiparameter device of ELMETRON CPC 401. For each source three sets of samples were taken (Table 1). Finally the radioactivity was measured for both water and soil samples and the results are shown in Table 2.

The first set, which was put under protection by adding 5 ml concentrated HCl for 500 ml, is for cation analysis. The second set is for anion and third one is for isotope and heavy metal analysis. Water samples were sent to the I.S.K.I (Istanbul Water and Canalisation Authority) laboratory for major anion and cation analyses and also Agency of T.U.B.I.T.A.K M.A.M. for the isotope analysis. Using oxygen 18 and deuterium values East Mediterranean Sea meteoric water line was drawn, data were transferred to the SMOW graph and an attempt was made to find out a the recharge paths. Hot and cold water sources were correlated by using the Piper and Schoeller diagrams (Fig. 2 a, b).

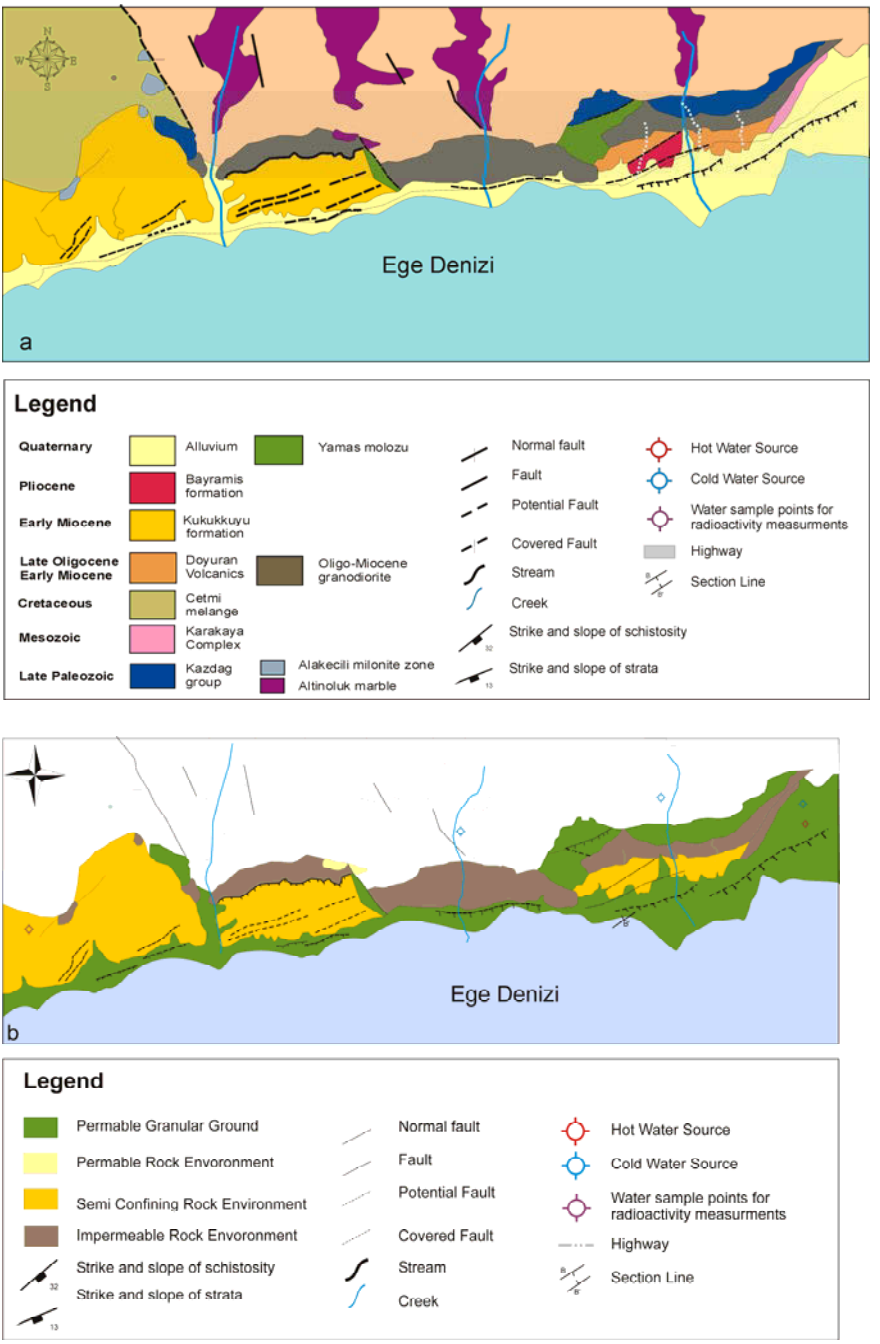

Fig. 1. a Geology map of the Gure-Altınoluk-Kucukcetmi area (Talay 2010), **b** Hydrogeology map of the Gure-Altınoluk-Kucukcetmi area (Talay 2010).

In order to calculate reservoir temperature a chalcedony geothermometer was used as the temperature range was under 180 Celsius degree. In addition, geothermal waters were classified based on TSE (Turkish Standards Institute), W.H.O and A.B.D. Corel-Draw, Aquachem, Rockware, Surfer and Didger softwares were used to establish.

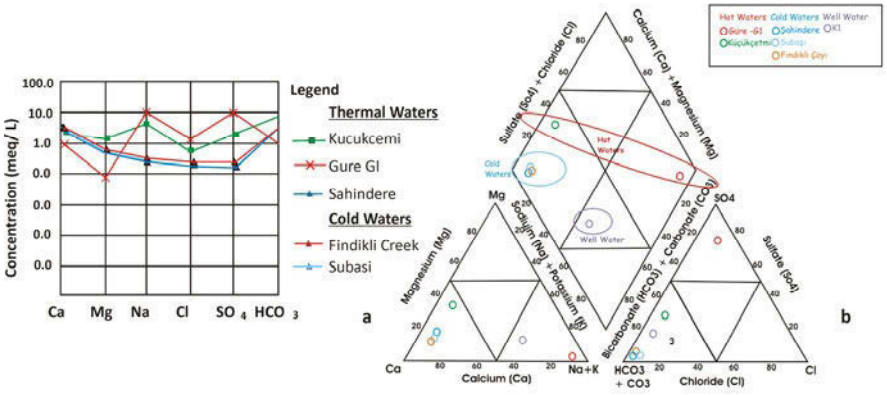

Fig. 2. a. Schoeller diagram for thermal waters and cold surface waters **b.** Piper diagram for thermal waters.

Table 1. Chemical composition of the samples.

Sample Id	Gure G1	Kucukcetmi	Subası	Sahindere	Fındıklı Creek	K1
Date	10/2009	10/2009	10/2009	10/2009	10/2009	10/2009
Coordinate (UTM)	X:0490081 Y:4382362	X:0465598 Y:4380180	X:0479204 Y:4381235	X:0479204 Y:4381730	X:0485501 Y:4382224	X:0482836 Y:4380665
Elevation (m)	10	131	122	110	105	40
Temp. (T°C)	51	41.6	15.2	17.8	18	21.3
EC (µs/cm)	1050	750	580	670	870	1570
pH	6.65	7.24	7.49	8.36	6.65	7.15
Ca^{+2}	17.8	51	51.8	53.4	67.2	114.2
K^{+}	6.08	8.89	0.96	1.05	1.8	3.42
Mg^{+2}	1	16.5	8.3	6.8	7.3	46.2
Na^{+}	238	118	6.2	6.6	8.4	17.8
Cl^{-}	50	22.6	7.56	8.84	29.7	29.7
$HCO3^{-}$	156.6	463.6	229.36	204.96	253.76	390.4
SO_4^{-}	411.8	92.6	8.52	8.1	12.7	158.1
SiO_2	59	49	-	-	-	25

Table 2. Radioactivity levels of water and soil samples.

Features Sample	Location	Total alfa (Bq/L)	Total beta (Bq/L)
	Adatepe	0.113 ± 0.024	0.263 ± 0.029
	Avcılar	0.040 ± 0.012	0.122 ± 0.016
	Camlıbel	0.050 ± 0.017	0.184 ± 0.025
Water	Gure	0.019 ± 0.005	0.040 ± 0.012
Samples	Kucukcetmi	0.070 ± 0.019	0.365 ± 0.030
	Subası	0.036 ± 0.011	0.070 ± 0.014
	K1	0.025 ± 0.016	0.218 ± 0.041
	Tahtakuslar	0.068 ± 0.014	0.098 ± 0.015
	Avcılar	584 ± 59	1257 ± 64
	Camlıbel	569 ± 59	772 ± 50
Soil	Gure	1154 ± 81	1874 ± 76
Samples	Kucukcetmi	433 ± 51	1009 ± 57
	Narlı	590 ± 60	810 ± 53
	Tahtakuslar	975 ± 75	1677 ± 73

4 Discussion

Although the formation is a little bit different in Gure and Kucukcetmi thermal fields, the system basically is the same. Meteoric waters percolate into the depths, gets hot depending on geothermal gradient in fault zones, come up to the surface, mix with cold water around the surface in porous and permeable units and finally outcrop at the surface as a hot spring like Gure and Kucukcetmi. Even though the cap rock is thick in Gure, as water circulation is long and flow yield is low the temperature is low as well. Usually, if any geothermal system takes place nearby the seaside, it is thinkable that the hot liquid consists of sea and meteoric water. But, in this case, Cl level must show an increaseas opposed to a decrease in Mg-SO_4 and HCO_3 level. In spite of the fact that Gure is located at the seaside, (Cl level is low, but SO_4 and HCO_3 level is high (Table 1). According to the isotope rates which were sampled before rainfalls in the region only Kucukcetmi hot spring takes place between East Mediterranean Meteoric Water Line. So it is understood that all the water sources are of meteoric origin and recharge from local rainfalls. As volcanic rocks outcrop in wide areas, there comes a question to the mind. Is the origin of the hot liquid volcanics or not? But the low level of Cl, Br, B, As, and Li provide an answer for it.

5 Conclusions

Based on the lithology and structural features, the units were divided into different hydrogeological environments. According to this Triassic aged limestones in the Cetmi melange and marbles in the Kazdag massive are permeable rock units, the Fındıklı formation and silicified volcanites are semi-permeable rock units, the Pliocene aged Bayramic formation and Quaternary aged alluvium and talus are granular permeable units. Neogene aged lacustrine sediments and tuffs at Gure and Kucukcetmi are cap rocks. Fault zones, fractures, fissures were mapped out. In addition, NE-SW trending dextral strike slip faults NW-SE oriented snistral faults and normal faults were observed. Some of the rock units in the region are porous and permeable; thus they can store groundwater that percolated into the depths and some of them have a secondary porosity as a result of tectonic activities, like Kazdag metamorphics. Annual precipitation of the area is 679.50 mm. 52% of the rainfall evaporates and 42% of it is discharged. For the calculation of reservoir temperature using a silica geothermometer, as the temperature range is under 180 degree a chalcedony geothermometer was preferred. Thus, approximate temperature was calculated to be between 60-80 degree.

References

Bingöl E (1968) Contribution a L' e' tude ge'ologiue de la Partir Centrale et sud-est du Massif de Kazdag (Turquei), Doktora Tezi, Nancy Univ. Fransa, (yayınlanmamış), 190p

Bingöl E (1969) Kazdag Masifinin Merkezi ve Güneydoğu Kesiminin Jeolojisi, Maden Tetkik ve Arama Enstitüsü Dergisi, 72, 110-123

Bingöl E Akyürek B Korkmazer B (1973) Biga Yarımadasının Jeolojisi Ve Karakaya Formasyonun Bazı Özellikleri, Cumhuriyetin 50. Yılı Yerbilimleri Kongresi, Ankara, 1973, 70-76

Bingöl E (1978) Batı Anadolu'nun Jeotektonik Evrimi, MTA Dergisi No: 86, 14-34

Craig H (1961) Isotopic Variations in Meteoric Waters, Science, 133, 10702-10703

Ercan T, Satir M, Steinitz G, Dora A, Sarifakioğlu E, Adis C, Walter HJ, Yildirim T (1995) Biga Yarımadası İle Gökçeada, Bozcaada ve Tavşan Adalarındaki (KB Anadolu) Tersiyer Volkanizmasının Özellikleri, MTA Dergisi No:117, 55-56

Diller JS (1883) Notes on the Geology of the Troad. Quarterly Journal Geological Society of London, XXXIX, 627-639

Duru M (2004) Türkiye Jeoloji Haritaları İ17 Paftası, 1:100000, M.T.A, Ankara Er Z, Tuğrul AB (1995) Çeşitli Madensuyu ve Sodaların Radyoaktivite

Seviyelerinin Tayini, V.Ulusal Medikal Fizik Kongresi, Istanbul, 11-15 Eylül 1995

Eyidoğan H (1988) Rates Of Crustal Deformation In Western Turkey As Deduced From Major Earthquakes. Tectonophysics, 148, 83-92

Fournier RO (1977) Chemical Geothermometers and Mixing Models For Geothermal Systems. Geothermics. 5, 41-50

Fournier RO And Truesdell AH (1973) An emprical Na-K-Ca geothermometer for natural waters, Geochimica et Cosm. Acta. 37, 1255-1275

Gat JR (1980) The Isotopes of Hydrogen and Oxygen In Precipitation, In Handbook of Environmental Isotope Geochemistry, P. Fritz and J.C. Fontes, (Eds.), Vol 1, 21-48

Gat JR (1981) Isotopic Fractination, In Stable Isotope Hydrology, Deuterium and Oxygen-18 in Water Cycle, Technical Report Series 210, IAEA, Vienna, 21-34, Comments on the Stable Isotope Method in Regional Groundwater Investigations, Water Resources Research, 7:980-993

Giggenbach W F (1988), Geotermal Solute Eguilibria. Derivation of Na-K-Mg Ca Geoindicators. Geochim. Et Cosmochim. Acta, 52:2749-2765

Giggenbach WF (1991) Collection and Analysis of Geothermal and Volcanic Water and Gas Discharge, Application of Geochemistry in Geothermal Reservoir Development (Edited by F. D'amore) Unitar, Rome, 119-144

Hochstein MP (1990) Classification And Assessment Of Geothermal Resources, In Small Geothermal Resorces, A Guide To Devolpoment And Utilization, Unıtar/Undp Cenntre Of Small Energy Resources, 31-60, Rome, Italy

Mckenzie DP And Yilmaz Y (1991) Deformation And Volcanism In Western Turkey And The Agean, Bull. Tech. Univ. İstanbul, 44, 345-373

Piper AM (1944) A Graphiv Procedure In The Geochemical Interpretetion Of Water Analysis, Trans. Amer. Geophys. Union, Vol. 25, p 914-923

Saka K (1979) Edremit Körfezi Ve Civarı Neojen'inin Jeolojisi Ve Hidrokarbon Olanakları: TPAO Arama Grubu Raporu No:1341, 17p

Şimsek S (1986) Geotermal Activity in Turkey. United Nations Workshop on the Development and Explotation of geotermal Energy in Devoloping Countries, Iceland, DTCD/NRED/CTB/2p 1-4

Şimsek S, Doğdu MS, Akan B (1997) HID 645 Hidrojeotermometreler Ders

Notları, H.Ü. Mühendislik Fakültesi Jeoloji (Hidrojeoloji) Mühendisliği Bölümü, Ankara

Sheppard S.Mjf, and Taylor HP (1981) Hydrogen and oxygen isotope evidence: For the origins of water in the Boulder batàolith, Geology, 69, 926-946

Taylor HP (1974) The Application of Oxygen and Hydrogen Isotope Studies to Problems of Hydrothermal Alteration and Ore Deposition: Economic Geology, 69, 843-883

Yilmaz Y, Karacik Z (2001) Geology of the northern side of the Gulf of Edremit and its tectonic significance for the development of the Aegean grabens. Geodinamica Acta, 14, 31-43

Groundwater hydrochemistry of the volcanic aquifers of Limnos Island, Greece

G. Panagopoulos[1], P. Giannoulopoulos[2], D. Panagiotaras[3]

[1]Department of Mechanical and Water Resources Engineering, Technological Educational Institute (T.E.I.) of Messolonghi, Nea Ktiria, 30 200, Messolonghi, Greece. gpanagopoulos@teimes.gr
[2]Institute of Geology and Mineral Exploration, Division of Hydrogeology, Sp. Loui 1, Olympic Village, Acharnai, 13 677, Athens, Greece
[3]Department of Mechanical Engineering, Technological Educational Institute (T.E.I.) of Patras, 26 334, Patras, Greece

Abstract The hydrogeological research conducted in the Limnos Island showed the existence of three confined volcanic aquifers overlying the impermeable flysch. The limited natural recharge induced by the low annual areal precipitation and the overexploitation of the aquifers for irrigation and drinking water supply lead to groundwater salinization due to seawater intrusion. The wider Romanou area has been affected in a higher grade because bears the greatest number of agricultural activities. The extensive application of nitrogenous fertilizers results in nitrates contamination deteriorating thus the groundwater quality. Ion exchange is the dominant hydrochemical process; however, the enrichment of groundwater in various metals, especially in potassium and magnesium, is attributed to rock and mineral weathering and dissolution.

1 Introduction

Limnos is the eighth largest island of Greece, covering a total area of 478 km^2 and lies in the North Aegean Sea. Myrina is the capital and major port of the island. The major occupation of the inhabitants is fishery and farming, especially the cultivation of cereals and vineyards. In the last decade, tourism plays an important role in the local economy. The total population of the island (2001 census) is approximately 18,000 inhabitants.

Based on the Limnos meteorological station (Hellenic National Meteorological Service), the climate of the island can be considered as semi-arid. The mean annual rainfall is only 478.7 mm, namely 228.8×10^6 m^3 and varies from 7.5 mm in September to 78.6 mm in November. The mean monthly temperature ranges from 7.4 ^oC in January to 26.0 ^oC in August with an average annual value of 16.0 ^oC, while the mean annual relative humidity is 70.3%. The water balance parameters have been computed based on the procedures described by Thornthwaite and Mather (1955). 76.9% of the annual precipitation, namely 176.0×10^6 m^3, is lost

N. Lambrakis et al. (Eds.), *Advances in the Research of Aquatic Environment, Vol. 2*
DOI 10.1007/978-3-642-24076-8, © Springer-Verlag Berlin Heidelberg 2011

via evapotranspiration, while the remaining 23.1%, namely 52.8 x 10^6 m^3, supply the surface and groundwater runoff. The very low percentage of surface and groundwater runoff leads to a limited recharge of the local aquifers and to a considerable imbalance of the groundwater budget.

2 Geological setting

During the Miocene, the island of Limnos was the site of volcanic activity, thus magmatic rocks overlay the shelf deposits (Pe-Piper and Piper 2001). Magmatic rocks consist of both plutonic and volcanic rocks, and cover a large part of the studied region. The end of the Miocene is characterized by the limited sedimentation of conglomerates, marls and calcareous sandstones. Local Pleistocene porous calcareous and locally oolithic limestones, and Holocene alluvial coastal deposits and dunes were also found (Maravelis and Zelilidis 2010).

The magmatic rocks of the island consist of hypabyssal intrusions, lava domes, flows, and pyroclastic deposits. They are andesites, trachyandesites, trachytes and dacites, with porphyritic texture and microlithic groundmass, consisting mainly of plagioclase, alkali feldspars and quartz (Roussos et al. 1993). The radiometric ages of these rocks range from 21-18.2 Ma (Innocenti et al. 1994; Fytikas et al. 1984). Hydrothermal alteration of these rocks produces kaolin deposits in the western and southern part of the studied area (Papoulis and Tsolis-Katagas 2008).

The Lower Miocene intrusive and volcanic rocks are divided by Innocenti et al. (1994) into three units (Fig. 1). The Katalakon Unit, consisting principally of subvolcanic stocks, dikes, and sills of porphyritic trachyandesite and dacite that include the Fakos quartz monzonite. The Romanou Unit consists of stratified pyroclastic and volcaniclastic deposits up to 160 m thick. Volcaniclastic breccias and conglomerates with clasts up to boulder size occur near the base, and these are overlain by several welded ignimbrite horizons interbedded with flow tuffs that interfinger with five chert beds containing plant fossils. The cherts thicken toward meter-scale circular masses that appear to mark the sites of hot springs. Locally, domes and mono mictic breccias are present. Rocks of the Romanou Unit range from trachyandesite to rhyolite; this unit includes the most potassium-rich rocks of the island, occurring as glassy trachyandesite lavas and as blocks within conglomerate.

The Therma Unit of Innocenti et al. (1994) resembles parts of the Romanou Unit and consists of interbedded marl and volcanic tuff with early Miocene plant fossils in tectonic contact with the apparently overlying Myrina Unit. The Myrina Unit consists of domes and monomictic breccias (Innocenti et al. 1994). The rocks are all strongly porphyritic and mainly dacite with subordinate trachydacite (Pe-Piper et al. 2009).

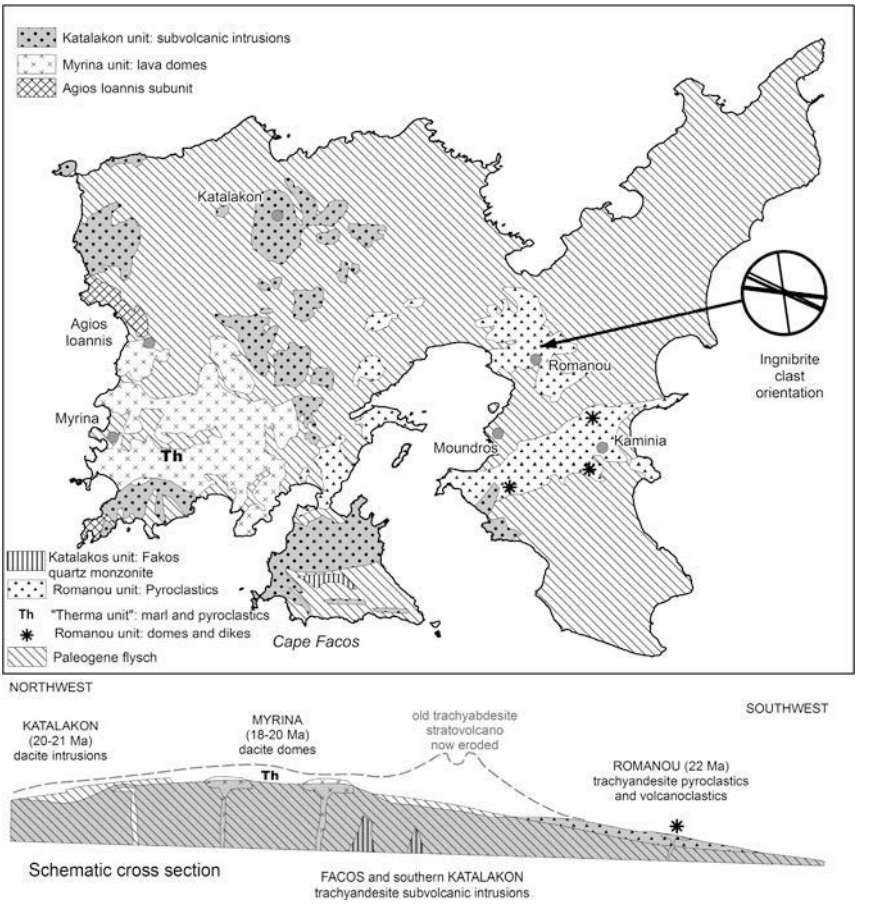

Fig. 1. Geological map of Limnos (Piper et al. 2009).

3 Hydrogeological regime

In general, Limnos presents a hydrogeological regime that is common to many other volcanic regions: fissured and highly permeable lavas are interbedded with discontinuous layers of low permeability pyroclastics, forming thus confined aquifers. The underlying impermeable flysch forms the substratum of the main Limnos aquifers as well as the lower confining unit of them. Outcrops of fractured volcanic rocks and pyroclastics facilitate the direct infiltration of rainwater.

Based on structural, geological, and geochemical data obtained, three main hydrogeological basins have been identified, corresponding to the three major volcanic units of Limnos, namely Katalakon, Romanou and Myrina (Fig. 1). Highly weathered and fractured andesites and trachytes, fractured tuff, volcaniclastic

breccias and conglomerates, ignimbrites and other pyroclastics could be highly productive aquifers of secondary porosity and permeability. However, in the case of Limnos, due to the low annual precipitation height, the natural replenishment of the aquifers is very limited, leading thus to restricted groundwater reserves. As a result, the yields of the water wells screened within these aquifers range between 5 and 20 m^3/h.

The presence of an impermeable sedimentary basement beneath Limnos volcanics and the limited thickness of the latter prevent groundwaters from reaching considerable depths and thus limit their thermalization. The temperatures measured in groundwaters of Limnos are generally lower than 23 ^oC. The only thermal manifestation (spring) occurs in the Therma region, near the village of Kornos, with temperature up to 42.5 ^oC.

4 Hydro-geochemistry

The chemical composition of the groundwater in the Limnos aquifers is the product of complex, interdependent hydrogeochemical processes which are related with effects of mixing water quantities of dissimilar chemical composition and source, with water-rock interactions and man - made interventions.

Table 1. Average values of major elements (in mg/L) and physicochemical parameters of the Limnos volcanic aquifers (March 2005 period).

Aquifer	Katalakon (n=9 samples)	Myrina (n=9 samples)	Romanou (n=17 samples)
Temperature (^oC)	18.6	23.9	18.5
pH	7.8	7.7	7.6
EC (μS/cm)	972	1107	1341
TDS	689.7	748.2	899.4
Ca	59.8	74.5	52.0
Mg	34.9	31.8	34.2
Na	94.9	112.4	170.6
K	2.2	4.5	8.7
HCO_3	269	195	204
Cl	127.1	191.5	273.4
SO_4	80.7	127.2	75.1
NO_3	21.0	11.4	23.2

Based on water samples taken by I.G.M.E. during the period 2004 – 2007, a network of 35 productive wells, boreholes and springs (Fig. 2), screened within the volcanic aquifers, was selected for the interpretation of the dominant hydrogeochemical processes occurring in the groundwaters of Limnos.

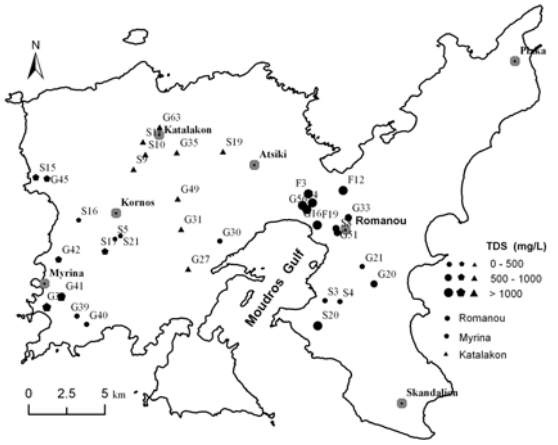

Fig. 2. Distribution map of TDS of the Limnos volcanic aquifers.

The sampling campaign was performed in March 2005. Chemical analyses were conducted in the Laboratory of I.G.M.E. and summary statistics concerning each aquifer system is presented in Table 1. Figures 2 and 3 depict distribution maps of TDS and nitrates in each aquifer, while the ionic concentrations are plotted in the Piper diagram of Figure 4.

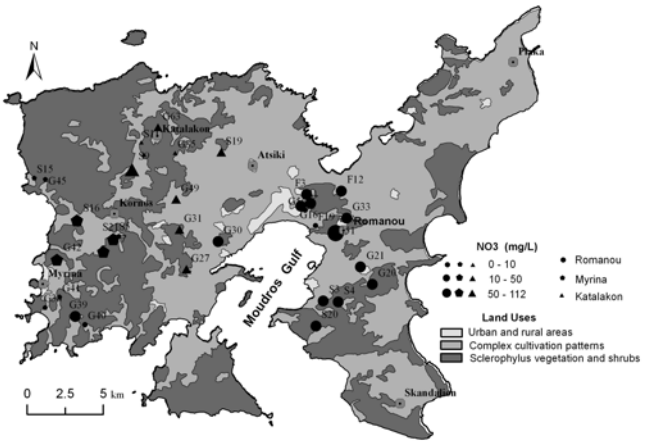

Fig. 3: Distribution map of NO_3^- of the Limnos volcanic aquifers.

Seawater intrusion constitutes a major problem concerning the groundwater quality of Limnos and it is caused from overpumpings in order to cover the increased drinking and irrigation water demands. Consequently, the hydrochemical composition of the volcanic aquifers is characterized by the dominance of Na^+ and Cl^- ions originated from mixing of fresh with seawater. Groundwater salinization is more intensive in the Romanou and Myrina aquifer systems (Fig. 2) with a

mean concentration of TDS of 899.4 and 748.2 mg/L respectively and the hydrochemical type of the groundwater is Na-Cl. On the other hand, the salinization of Katalakon aquifer is lower, because the formation is often confined by the impermeable flysch, and water-rock interactions define the hydrochemical character of groundwater, inducing mixed $Cl+SO_4$ - HCO_3 water types (Fig. 4).

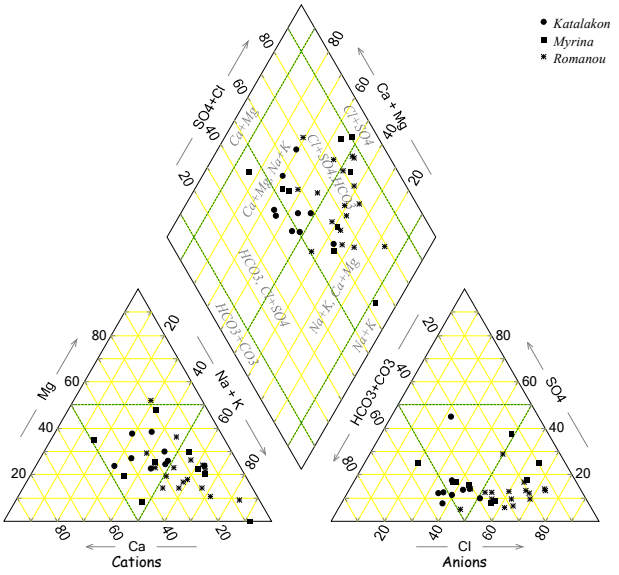

Fig. 4. Piper plot showing the chemical composition of the three volcanic aquifers.

The dominance of conservative mixing mechanisms in the volcanic aquifers of Limnos is clearly displayed in the cross-plots of Figure 5. The common origin of Na^+ and Cl^- from seawater is verified by the coincidence of the ions's trend line with the conservative mixing line of fresh and seawater (Fig. 5). Disposition of the samples below the FW-SW line indicates ion-exchange phenomena between Na^+ from seawater and Ca^{2+} or Mg^{2+} from the aquifer's material, while the reverse is happened in samples plotted above this line. The shoshonites of Limnos are potassium-rich (Pe-Piper et al. 2009), thus, rock weathering explains the remarkable abundance of K^+ with respect to seawater (Fig. 5). Dissolution of calcite is the major source of Ca^{2+} and HCO_3^- in the groundwaters. Consequently, the samples are plotted above the FW-SW line in Figure 5. From the same plot, an almost clear relationship between Ca^{2+} and Cl^- ions is defined, showing that the exchange of Na^+ from seawater with the aquifer's material releases Ca^{2+} ions to groundwater. Similar exchange can be considered for Mg^{2+} and Cl^-, but in this case, Mg^{2+} is released to groundwater from magnesium-bearing minerals, such as pyroxenes and amphiboles, which are present in the shoshonites of Limnos (Pi-Piper et al. 2009). The enrichment observed for SO_4^{2-} (Fig. 5), may be related to an additional source of sulfates, except seawater mixing, coming from sulphides oxidation process. Thus, production of

SO_4^{2-} ions, could also derived from H_2S oxidation explained by the hydrothermally altered zones in Romanou and Katalakon units (Pe-Piper et al. 2009).

Nitrates show maximum values (up to 112 mg/L) in the wider Romanou area (Fig. 4), and are associated with agricultural practices such as overfertilization. Areas covered by complex cultivation patterns, mainly cereals and vineyards, have increased content of nitrates (Fig. 4), as the mean concentrations in the three aquifers range between 11.4 and 23.2 mg/L (Table 1).

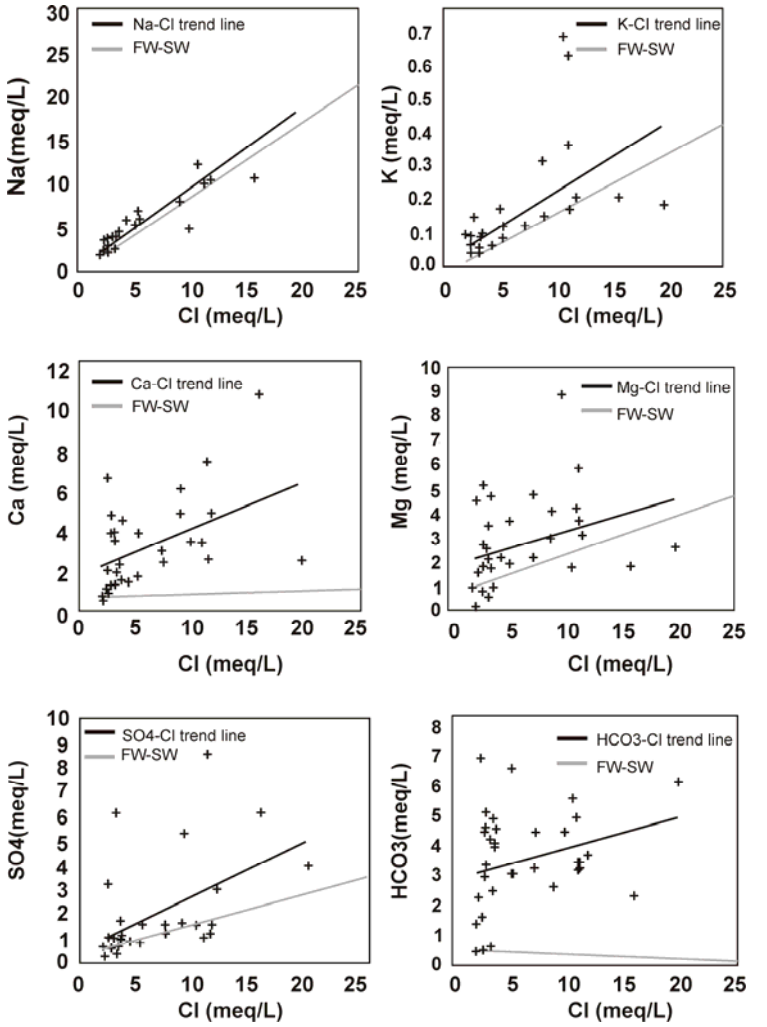

Fig. 5. Cross-plots of Cl^- vs Na^+, K^+, Ca^{2+}, Mg^{2+}, SO_4^{2-} and HCO_3^- of the Limnos volcanic aquifers.

5 Conclusions

The hydrogeological research conducted in the Limnos Island showed the existence of three confined volcanic aquifers overlying the impermeable flysch. The limited natural recharge induced by the low annual areal precipitation and the overexploitation of the aquifers for irrigation and drinking water supply lead to groundwater salinization due to seawater intrusion. The wider Romanou area has been affected in a higher grade because bears the greatest number of agricultural activities. The extensive application of nitrogenous fertilizers results in nitrates contamination deteriorating thus the groundwater quality. Ion exchange is the dominant hydrochemical process, however, rock and mineral weathering contributes as an additional source of K^+ and Mg^{2+} ions. Excess of Ca^{2+} and HCO_3^- is related to dissolution of calcite, while the enrichment observed for SO_4^{2-} attributes to seawater mixing, and sulphides and H_2S oxidation processes.

References

Fytikas M, Innocenti F, Manetti P, Mazzuoli R, Peccerillo A, Villari L (1984) Tertiary to Quaternary evolution of volcanism in the Aegean region. In: Dixon, J.E., Robertson, A.H.F. (eds.). The Geological evolution of the Eastern Mediterranian. Geol. Soc. London, Spec. Publ. 17, 687-699

Innocenti F, Manetti P, Mazzuoli R, Pertusati P, Fytikas M, Kolios N (1994) The geology and geodynamic significance of the island of Limnos, North Aegean sea, Greece. N. Jb. Geol. Palaont . Mh. 11, 661-691

Maravelis A, Zelilidis A (2010) Organic geochemical characteristics of the late Eocene–early Oligocene submarine fans and shelf deposits on Lemnos Island, NE Greece. Journal of Petroleum Science and Engineering 71, 160–168

Papoulis D, Tsolis-Katagas P (2008) Formation of alteration zones and kaolin genesis, Limnos Island, northeast Aegean sea, Greece. Clay Minerals 43, 631-646

Pe-Piper G, Piper DJW (2001) Late Cenozoic, postcollisional Aegean igneous rocks: Nd, Pb and Sr isotopic constraints on petrogenetic and tectonic models: Geological Magazine 138, 653–668

Pe-Piper G, Piper DJW, Koukouvelas I, Dolansky LM, and Kokkalas S (2009) Postorogenic shoshonitic rocks and their origin by melting underplated basalts: The Miocene of Limnos, Greece. Geological Society of America Bulletin, 121 (1-2), 39-54 doi: 10.1130/B26317.1

Roussos N, Katsaounis A, Tsaila-Monopoli S, Ioakeim X, Karadasi S, Davi E (1993) Geological Map of Limnos Island. IGME

Thornthwaite CW, Mather JR (1955) The water balance. Climatology 8, 1-37

Geothermal exploration in the Antirrio area (Western Greece)

T. Efthimiopoulos[1], E. Fanara[1], G. Vrellis[1], E. Spyridonos[2], A. Arvanitis[1]

[1] Institute of Geology and Mineral Exploration (I.G.M.E.), Entrance C, Olympic Village, Acharnae, Attica, GR 136 77, Greece. arvanitis@igme.gr

[2] PPC Renewables, 3 Kapodistriou str., Ag. Paraskevi, Attica, GR 153 43, Greece.

Abstract The Riza - Antirrio area constitutes a new low enthalpy geothermal field located on the northern side of the Corinthian Gulf in Western Greece. After a detailed and systematic reconnaissance study including evaluation of geological and tectonic setting of the area, geophysical surveys, water temperature measurements at the heads of the existing irrigation and water supply wells, sampling and hydrochemical study, 4 geothermal wells were drilled. The first geothermal exploration borehole was drilled to a depth of 402 m during 1998-99. Two more wells were drilled in the period 2005-2006. Exploration borehole GL-1 was drilled down to 275.5 m and the temperature of 38°C was recorded at 270 m. Production well GLP-1 has a depth of 229 m and it yields 25 kg/s water of 36°C and Na-CI type with TDS content of 45.7 g/L. The geothermal reservoir of this low enthalpy field composed of Eocene limestones is located at depths of about 110-250 m.

1 Introduction

The Riza - Antirrio area constitutes a new low enthalpy geothermal field located on the northern side of the Corinthian Gulf (Fig. 1). The exploration in the area began in the framework of the I.G.M.E. project entitled "Identification and estimation of geothermal potential in Western Greece" (1995-2000). After the first stages of reconnaissance investigation including evaluation of geological and tectonic setting of the area, geoelectrical surveys, water temperature measurements at the heads of the existing irrigation and water supply wells, water sampling, chemical analyses and hydrochemical study, the first geothermal exploration borehole was drilled down to 402 m during 1998-1999. Due to positive drilling results, a new large diameter well, 80 m deep, was constructed later (Traganos et al. 2000). The exploration of the Antirrio area continued in the period 2003-2006 and it was supported financially by the 3rd European Community Support Framework 2000-2006 (Operational Programme "Competitiveness"). New geological and tectonic data were collected and studied, additional water temperature measurements were performed, geophysical methods (geoelectrical surveys and gravimetric method) were

N. Lambrakis et al. (Eds.), *Advances in the Research of Aquatic Environment, Vol. 2*
DOI 10.1007/978-3-642-24076-8, © Springer-Verlag Berlin Heidelberg 2011

applied, new water samples were taken from springs and wells, 2 new geothermal wells (1 exploration and 1 production) were drilled, pumping tests were performed at the production well and finally a preliminary conceptual model of the field was compiled (Efthimiopoulos et al. 2009). The results of the above-mentioned exploration works carried out by I.G.M.E. resulted in the official characterization of the area as "proven low temperature geothermal field of Riza - Antirrio" by a Ministerial Decision (Official Gazette, 1058/B´/2 June 2009).

2 Geological and tectonic setting

Geologically, the area belongs to the Gavrovo - Tripolis Zone. It is made up of Cretaceous and Eocene limestones and Eocene flysch (Fig. 1). The Neogene and Quaternary sediments consist of marine, brackish, lacustrine, torrential and terrestrial deposits (Loftus and Tsoflias 1971, Mettos and Karfakis 1991). They are composed of Pleistocene conglomerates and alternations of clayey-loamy marls, sandstones and conglomerates of the same age. Older and younger talus cones, scree and alluvial sediments have also been deposited. In the lowland area (plain), the Neogene and Quaternary sediments consist of consolidated conglomerates, clayey sands, loams and yellow-brown clays and their total thickness does not exceed 700 m.

The fault pattern of the wider Antirrio area is dominated by NW-SE and NE-SW faults. Vertical intersection between these two fault systems is observed in the area and a high fault density is caused. The present-day stress field is extensional characterized by a $\sigma 3$ axis in a NNE-SSW direction. The intense tectonic activity resulting in the intense fracturing of the basement rocks (Cretaceous and Paleocene - Eocene limestones) as well as the present-day extensional tectonic regime create favorable conditions for deep water circulation. The waters are heated at great depths and then rise toward the surface.

Geoelectrical surveys carried out by I.G.M.E. and their interpretation detected the existence of 3 normal faults. The Eocene limestones have relatively low resistivities (25 Ωm). A geoelectric layer overlying these limestones has higher resistivities ranging from 30 to 200 Ωm. This layer corresponds to the Eocene flysch. Except the geoelectrical surveys, the gravimetric method is also used and a W-E-trending gravimetric profile, totaling 3.9 km in length, was interpreted. Both geophysical methods (geoelectrics and gravimetry) have provided good information about the depths of the Eocene limestones in the study area. This carbonate basement is located at a depth of 40 m in the Riza area, then deepens eastwards and reaches > 600 m deep in the area of the Loggies stream ("Loggies Rema") (Angelopoulos 2000, Lachanas 2005).

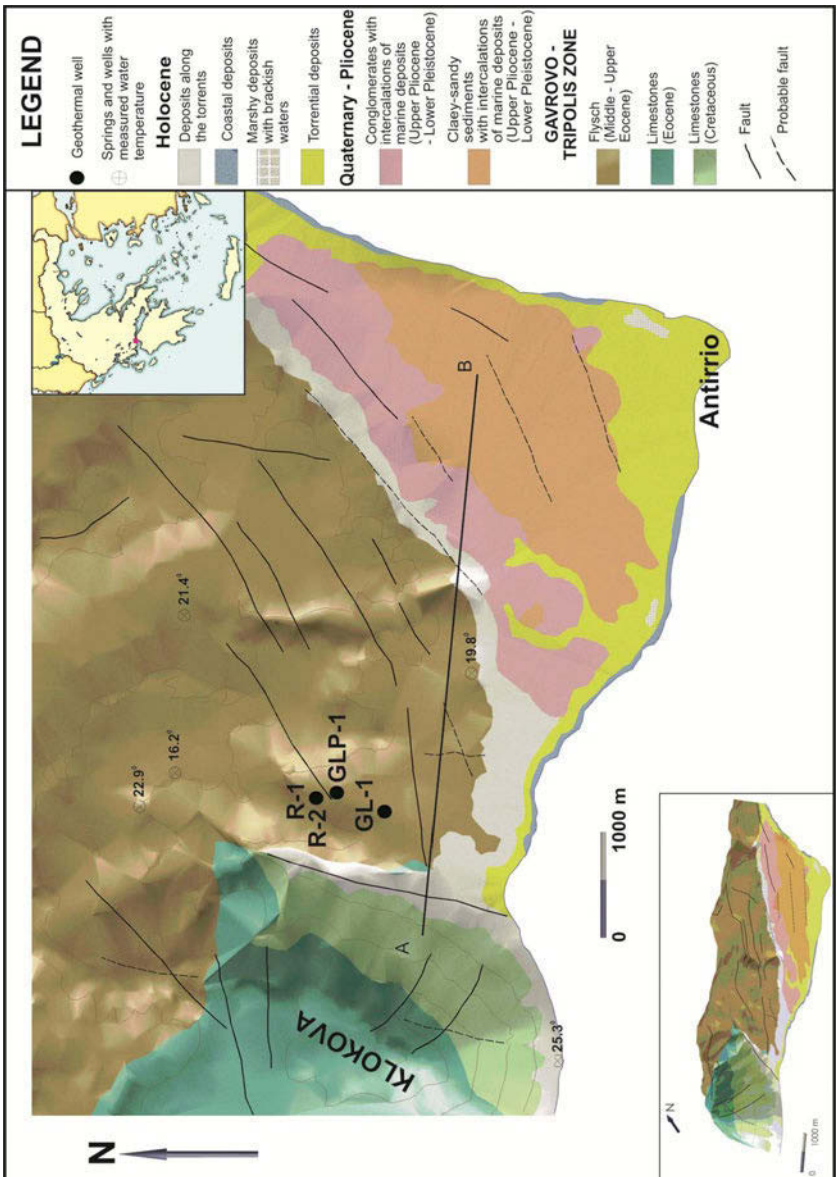

Fig. 1. Location and geological map of the study area (after Loftus and Tsoflias (1971), Mettos and Karfakis (1991), modified).

3 Geothermal wells

After a reconnaissance investigation, four (4) wells were drilled in the Riza - Antirrio area. These wells were drilled between 1998 and 2006 in two periods (1998-1999 and 2005-2006).

The first geothermal exploration borehole (R-1) was drilled during 1998-1999. The total drilled depth was 402 m and the borehole was cased down to 150 m. The casing has a diameter of 4´´ at 0-36 m and 2´´ at 0-150 m. The temperature values of 36 and 31°C were recorded at depths of 143 and 402 m respectively (Traganos et al. 2000). Due to positive drilling results, a new large diameter well (R-2), 80 m deep, was constructed later. The presence of large karstic cavities, the gravel falling down and the existence of a large aquifer system prevented the continuity of drilling. The borehole was cased down to 80 m and 13½´´, 8 $^{5}/_{8}$´´ and 4´´ casings were set at depths of 0-10.5, 0-71 and 70-80 m correspondingly. The temperature of 31.9°C was measured at 72 m.

Geothermal exploration well GL-1 was drilled during October 2, 2005-January 27, 2006. The coordinates of the drilling site are X: 299939 and Y: 4247664 (Greek Grid, GGRS1987) and its elevation is 75 m above sea level. The total drilled depth was 275.5 m. A sedimentary sequence composed of alternations of sandstones and intensely fractured shales overlies the Eocene limestones. These limestones were located at a depth of 245.5 m and they are karstified and more or less fractured. The borehole was cased down to 152 m. The temperature of 38°C was measured at a depth of 273 m.

Geothermal production well GLP-1 was placed at a small distance NNE of the well GL-1 site at an altitude of 100 m above sea level. It was drilled during April 10 - June 27, 2006. The coordinates of the drilling site are X: 300031 and Y: 4247854 (Greek Grid, GGRS1987). The total drilled depth was 229 m. Well GLP-1 was cased down to 229 m and the casing has a diameter of 14´´ at 0-6 m, 8 $^{5}/_{8}$´´ at 0-179 m and 4´´ at 179-229 m. Screens were placed below 201.5 m depth. Temperature, water conductivity and gamma ray logs were performed in the borehole. The temperature of 35.7°C was recorded at the final depth of 229 m. The maximum value of water conductivity was 47300 μS/cm and it was measured at 220 m.

Two pumping tests were performed on production well GLP-1, as follows: (a) a short duration (4 ½-hours) pumping test at pumping rates of 22.5 to 58 m^3/h and 13-hour recovery, and (b) a long-term test (25 hours) at pumping rates of 64 m^3/h for 11 hours and 93 m^3/h for 14 hours followed by 13-hour recovery. The hydraulic conductivity K was estimated at 5 x 10^{-4} m/sec, an expected value for fractured karstified aquifers. During the pumping tests the water temperature was measured at 36°C at the well head. The presence of dissolved gases (CO_2 and H_2S) caused some instabilities on the water level measurements.

4 Hydrochemistry

Water samples were collected from various cold and sub-thermal springs and wells existing in the area (water temperature: 16.6 - 22.2°C) during February 2004 - June 2005. Water sampling from geothermal production well GLP-1 was performed during pumping tests on November 9-10, 2006. Additionally, sea water sample was taken near the coast on October 29, 2007. The results of chemical analyses are plotted on a trilinear diagram (Fig. 2) according to Piper (1949).

The water samples from geothermal well GPL-1 with TDS values of 43.6-45.7 g/L and a pH of 7.0-7.1 belong to the Na-Cl type. The chemical composition of water from this well remains nearly constant during pumping tests. The sample taken at the end of 14-hour constant-rate (Q=93 m^3/h) pumping test is considered to be the most representative sample. Its TDS value is 45.66 g/L and its chemical composition is as follows: Na^+ 13922 mg/L, K^+ 413 mg/L, Ca^{2+} 1244 mg/L, Mg^{2+} 1342 mg/L, Cl^- 26060 mg/L, HCO_3^- 458 mg/L, CO_3^{2-} 0 mg/L, SO_4^{2-} 2405 mg/L, NO_3^- 0 mg/L, Li^+ 0.49 mg/L, Sr^{2+} 32 mg/L, Ba^{2+} 0.043 mg/L, Mn^{2+} 0.022 mg/L, Al^{3+} 0.15 mg/L, Cu^{2+} 0.37 mg/L, SiO_2 11.6 mg/L, B 1,23 mg/L, Fe (total) 0.65 mg/L, Hg<1 µg/L and U<5 µg/L.

The cold and sub-thermal waters having temperature values of 16.6-22.2°C and TDS contents of 0.26-1.3 g/L are classified into various types namely Ca,Mg,Na-HCO_3SO_4, Ca,Mg,Na-HCO_3SO_4Cl, Ca,Mg,Na-HCO_3Cl, Ca,Na-HCO_3Cl, Ca,Na-HCO_3, Ca,Mg,Na-HCO_3, Ca,Mg-HCO_3, Mg,Ca-HCO_3SO_4Cl, Ca-HCO_3SO_4Cl and Ca-HCO_3 (Fig. 2). Their chemical composition depends on the lithology of the aquifers (limestones, sands, sediments with calcareous matrix or calcitic grains etc) and a small, probable influence of sea water on such aquifers.

The geothermal water from well GLP-1 is plotted near the sea water samples. Additionally, its chemical composition is very close to that of sea water and therefore a strong influence of sea water can be considered. The positive correlation between Cl^- and Na^+ indicates that the high Cl^- content of thermal water arises from the contribution of sea water. However, the geothermal water has higher Ca^{2+} and HCO_3^- concentrations compared to those in sea water indicating probable circulation of fluids in limestones and $CaCO_3$ dissolution. Moreover, the geothermal aquifer penetrated by this well is composed of Eocene limestones and the geothermal water is saturated with respect to calcite, dolomite and aragonite (carbonate minerals). The thermodynamic model Wateq-f (Truesdell and Jones 1974) that was used has shown that the calculated value of pCO_2 for the geothermal water is $10^{-1.6602}$ (=2.187 x 10^{-2}) atm. This value is similar to those of local cold and sub-thermal waters ranging from $10^{-2.5085}$ to $10^{-1.5763}$ atm. The tendency of the geothermal water for $CaCO_3$ scaling can be estimated using the Langelier Index and the Ryznar Index. The Langelier Index has a value of +1.22 (positive value). The Ryznar Index has been calculated to be 4.66 (<7.0). Based on the values of these indexes, geothermal water from well GLP-1 may theoretically form scales. General comments on the corrosivity of geothermal waters can be made with regards

to the classification system of geothermal water corrosivity suggested by Ellis (1981). The Total Key Species (TKS) value of the water from well GLP-1 has been estimated at 28923 mg/L. In this case, the pH value is 7.1 while the Cl^- concentration corresponds to the 90.1% of the TKS. The parameters of TKS, CI fraction in TKS, total alkalinity, pH and water temperature are taken into account in the design of the geothermal system and the selection of suitable materials.

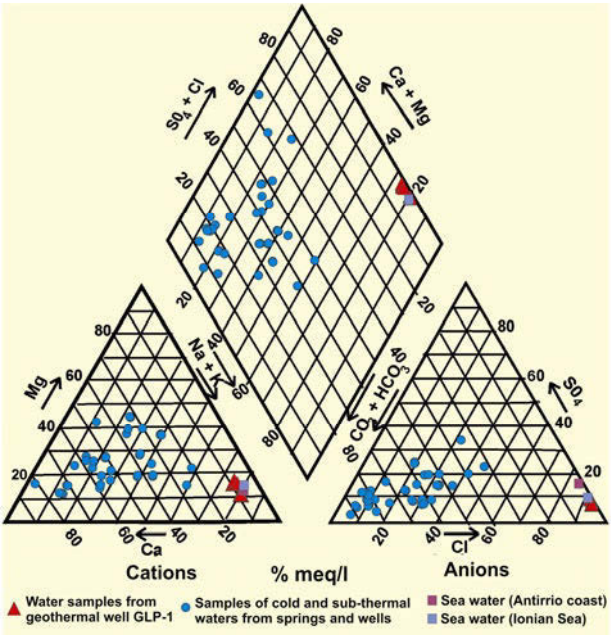

Fig. 2. Plotting the results of chemical analyses of waters from the Riza - Antirrio area on a trilinear diagram according to Piper (1949).

The SiO_2 (Fournier 1981), Na-K (Arnorsson et al. 1983), Na-K-Ca (Fournier and Truesdell 1973) and Na-Li (Fouillac and Michard 1981) chemical geothermometers has been applied to the representative geothermal water sample giving temperatures of 44.1, 97, 158.1 and 41°C respectively. The contribution of marine solutions to the geothermal water is one of the main causes for the disturbance of the chemical geothermometers. The geothermal water is modified sea water and therefore direct application of geothermometers to this sample and seawater provides very similar results (the major difference is observed for the quartz geothermometer as sea water is almost silica-free and silica is rapidly acquired through water-rock interaction). Additionally, the geothermal water is plotted very close to the sea water within the same area of the partial equilibrium waters on the triangular Na-K-Mg diagram according to Giggenbach (1988). Consequently, this sample cannot be used for application of geothermometers, since it is not representative of water-rock equilibrium.

5 Conclusions

The Antirrio area is a continuation of the Corinthian Gulf graben structure. The region consists of limestones of Cretaceous and Eocene age, Eocene flysch, Pleistocene lacustrine, brackish and marine formations, scree and alluvial deposits. The hydrogeological conditions are controlled by the permeable limestones, the impermeable clays and semi-permeable conglomerates. The geothermal reservoir is made up of limestones, a secondary reservoir is hosted by the conglomerates while the overlying clays in the flysch act as a cap rock formation. Two main fault systems trending NW-SE and NE-SW are observed. The present-day stress field is extensional with σ3 axis in a NNE-SSW direction. Extensional tectonics creates favorable conditions for deep water circulation. The water is heated at great depths and then rises toward the surface through the faults (Fig. 3).

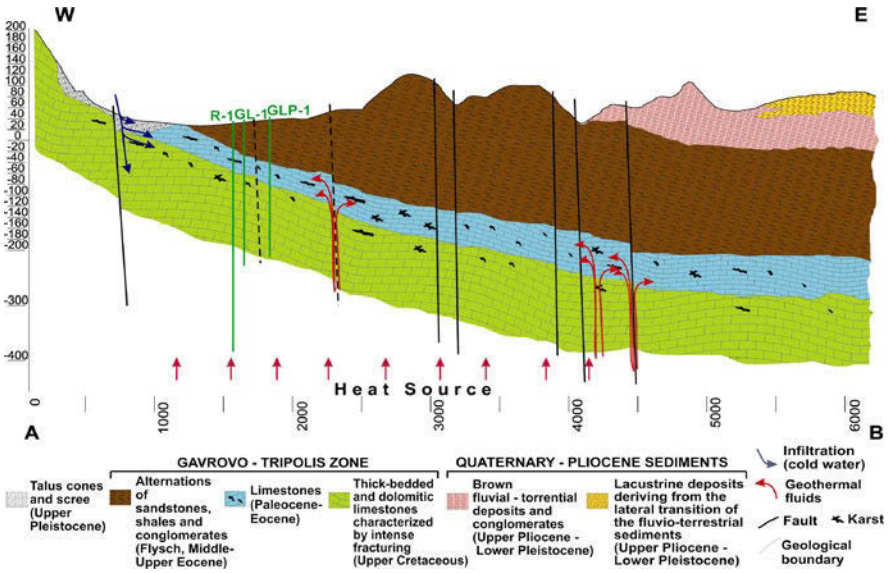

Fig. 3. Geological section and conceptual model of the Riza - Antirrio low enthalpy geothermal field.

Combining the borehole data, the results of the geophysical survey and the tectonic analysis, the morphology of the top of the limestones underlain by the flysch formations can be reproduced. The limestones are located at depths of 40 m west of Riza and the top of this formation dips eastwards. At the Loggies stream ("Loggies Rema"), 3 km east of Riza, the limestones are expected at a depth of about 600 m.

The geothermal exploration carried out by I.G.M.E. has proven the existence of a low enthalpy field in the Riza - Antirrio region covering a very limited area of 1.5 km^2. The Na-Cl geothermal waters of the Riza - Antirrio field having a tem-

perature of 36°C and a high TDS content (45.7 g/L) can be used for direct uses such as greenhouse heating, fish farming, anti-frost protection and balneology.

References

Angelopoulos A (2000) Geothermal investigation in the Riza Antirrio area. Inst. Geol. and Miner. Explor. Athens (in Greek)

Arnorrson S, Gunnlaugsson E, Svararsson H (1983) The chemistry of geothermal waters in Iceland: III. Chemical geothermometry in geothermal investigations. Geochim. Cosmochim. Acta 47, 567-577

Efthimiopoulos T, Fanara E, Vrellis G, Spyridonos E, Arvanitis A (2009) Final report on the study of the Riza - Antirrio geothermal field. Inst. Geol. and Miner. Explor. Athens (in Greek)

Ellis PF (1981) A geothermal corrosivity classification system. Geoth. Res. Council Trans. 5, 463-469

Fouillac C, Michard G (1981) Sodium lithium ratio in water applied to geothermometry of geothermal reservoirs. Geothermics 10, 55-70

Fournier RO (1981) Application of water geochemistry to geothermal exploration and reservoir engineering. In: Rybach, L., Muffer, L.J.P. (eds.) Geothermal Systems: Principles and Case Histories. J. Wiley, pp. 109-143. New York

Fournier RO, Truesdell AH (1973) An empirical Na-K-Ca geothermometer for natural waters. Geochim. Cosmochim. Acta 37, 1255-1275

Giggenbach WF (1988) Geothermal solute equilibria. Derivation of Na-K-Mg-Ca geoindicators. Geochim. Cosmochim. Acta 52, 2749-2765

Lachanas G. (2005) Geophysical investigation in the Riza - Antirrio area in the prefecture of Aitoloakarnania. Inst. Geol. and Miner. Explor. Athens (in Greek)

Loftus DL, Tsoflias P. (1971) Geological Map of Greece, scale 1:50000, Nafpaktos Sheet. Inst. Geol. and Miner. Explor. Athens

Mettos A, Karfakis J. (1991) Geological Map of Greece, scale 1:50000, Evinokhorio Sheet. Inst. Geol. and Miner. Explor. Athens

Piper AM (1944) A graphic procedure in the geochemical interpretation of water-analyses. Trans. Amer. Geophysical Union 25, 914-928

Traganos G, Simeakis K, Vrellis G, Efthimiopoulos T, Mpimpou A (2000) Identification and estimation of geothermal potential in Western Greece. Inst. Geol. and Miner. Explor. Athens (in Greek)

Truesdell AH, Jones BF (1974) WATEQ-F a computed program for calculating chemical equilibria of natural waters. U.S. Geol. Surv. Journ. Res. 2, 233-248

The role of water in constructions projects

Sedimentary media analysis platform for groundwater modeling in urban areas

R. Gogu[1,2], V. Velasco[3], E. Vázquez - Suñe[4], D. Gaitanaru[1], Z. Chitu[1], I. Bica[1]

[1] Technical University of Civil Engineering, Bucharest, Romania, radu.gogu@utcb.ro

[2] Romanian Academy Center for Artificial Intelligence Bucharest, Romania

[3] Department of Geotechnical engineering and Geosciences Technical University of Catalonia, Barcelona, Spain

[4] Institute of Environmental Analysis and Water Studies, CSIC Barcelona, Spain

Abstract In Europe numerous urban areas are located in the flood plains of the rivers. Sedimentary media (alluvial sediments, deltas, etc.) form particular frequently occurring environments within these valley fills. However, sedimentary media are normally significant aquifers due to their high permeability, storage capacity, interaction with surface water, etc. A reliable management of the hydraulic resources in urban areas can be performed only by using modeling. The models can provide accurate results if they correctly reproduce the hydrogeological processes. Tools and methodologies should allow the representation in three dimensions of the geological record heterogeneity and of its spatial distribution as well as the interaction of the groundwater with the urban infrastructure. The paper will focus on the main aspects of these instruments, which are currently developed within a national research project, that have to support 3D hydrogeological modeling. Within this project a software platform has been developed containing methodologies and tools that facilitate the integration of the 3D geological models in sedimentary media into the hydrogeological modeling of flow and contaminant transport. This is composed by a geospatial database and a set of tools allowing accurate stratigraphical analysis. An application of this platform is currently developed for the Moesic aquifer system (Bucharest city Region).

1 Introduction

In Europe numerous urban areas are located in the flood plains of the rivers. Sedimentary media form particular frequently occurring environments within these valley fills. However, sedimentary media are normally significant aquifers due to their high permeability, storage and management ability, interaction with surface water, etc. A reliable water management can be obtained by groundwater modeling. The models allow conceptualizing and quantifying the hydrogeological processes and simulate various scenarios as droughts, water resource exploitation, wa-

N. Lambrakis et al. (Eds.), *Advances in the Research of Aquatic Environment, Vol. 2*
DOI 10.1007/978-3-642-24076-8, © Springer-Verlag Berlin Heidelberg 2011

ter quality evolution and contamination aspects, interaction with civil works in terms of hydraulical and geomechanical ground behavior.

These models can provide accurate results if they correctly reproduce the hydrogeological processes. Nevertheless, it is well-known that sedimentary media are normally extraordinarily heterogeneous, which is a paradox as it leads to simplified models based on the homogeneity of large zones characterizing the medium. The paper presents a software platform containing methodologies and tools that facilitate the integration of the 3D geological models in sedimentary media into the hydrogeological modeling of flow and contaminant transport. This is composed by a geospatial database and a set of tools allowing accurate stratigraphical analysis. The geospatial database is used for the management of a large amount of different data types coming from different sources (geophysical, geological, hydraulic, and others). Its structure allows storing accurate and very detailed geological core description that can be straightforwardly generalized and further upscaled.

The obtained methods and tools are used for spatial data manipulation, which support understanding the detailed geology of the sedimentary media and the integration of the geological processes that controlled their formation. From the existing data and the developed methods, the petrophysical characteristics could be extrapolated to the entire sedimentary volume considered at a local level, by using various techniques such as the deterministic or stochastic methods.

The described platform has been initially designed starting from the existing hydrogeological model of Barcelona region (Vázquez-Suñé et al. 2006). Currently an application of this platform is developed for the Moesic aquifer system of Bucharest city area. This involves: (1) 3D geological characterization - application of the methodologies and developments suggested, (2) 3D parameterization of the Moesic aquifer system (Fratesti strata, Mostistea, and Colentina), (3) Management of the hydrogeological data base (tests and hydraulic parameters, level data, hydrochemical data, etc.), (4) Hydraulic definition/parameterization of facies and other geological concepts and, (5) Interaction between underground infrastructure and groundwater.

2 Study case geological and hydrogeological conditions

In the Bucharest city region, the Moesic platform shows two main aquifer types (Fig. 1). One is a regional high depth fissured-karstic carbonate aquifer of the Superior Jurassic – Inferior Cretaceous and the other one is located in the Pliocene and Pleistocene raw deposits.

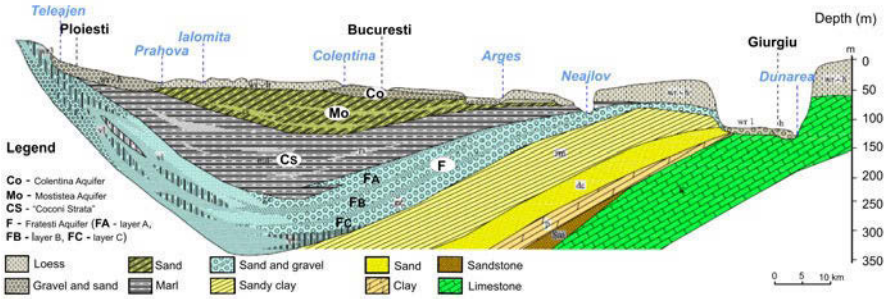

Fig. 1. Hydrogeological cross-section of the study area.

The second aquifer system called "Fratesti strata" (Liteanu 1953) is placed in the Tertiary deposits of the Upper Pleistocene and of Lower Pleistocene. This represents the main hydrogeological formation used for water supply of the South-Eastern Romania. It behaves as a confined multilayered aquifer. On the Northern side, the Fratesti strata aquifer system is made of three main layers indexed as A, B, C. These layers are regrouped in the Southern part forming a single aquifer layer. The thickness of the three layers shows a spatial variability. The mean thickness of the A aquifer layer is between 25 and 60 m. Its hydraulic conductivity takes values between 12 -24 m/day and 4-12 m/day in Northern Bucharest. The B aquifer layer is located at a higher depth and its mean thickness is between 5 and 50 m. The mean thickness of the deepest aquifer layer (C) is between 25 and 30 m. Between the three aquifer layers (A, B, and C) sandy-clayey strata with a thickness variation of 40 m to 5 m can be found (Pascu 1983). A sequence of marl and clay layers with slim sandy intercalations overlay the "Fratesti strata". In the Bucharest area its thickness decreases from north to south from about 150m to 40m. The marl sequence is covered by a permeable raw rocks layer made of fine and medium sands with gravel intercalations. This is called "Mostistea sands" aquifer and is located at depths between 25 m and 70 m. It is a confined aquifer and its hydraulic head takes values similar to another upper aquifer layer. The upper aquifer stratum of these quaternary formations called "Colentina gravels" is made of gravels and sands. This unconfined aquifer can be found mainly in the Bucharest city region at depths between 15 m and 20 m. However the water quality is quite low, the groundwater level can be found at 5 to 10 m depth. The aquifer thickness is between 3 to 5 m showings a variation of the particle size distribution. The hydraulic conductivity varies between 10 m/day and 70 m/day, sometimes being higher than 100 m/day. A clayey-marl layer is located between the "Mostistea sands" and the "Colentina gravels".

3 The analysis software platform

The 3D analysis platform for groundwater modeling is composed by a hydrogeological geospatial database and several sets of instruments facilitating the development of the geological model and allowing hydrogeological analysis. One set of instruments using the database spatial information is dedicated to stratigraphical analysis. It has been developed on the ArcMap software, part of the ArcGIS (ESRI) package. This considerably extends the functionalities of ArcMap. Another set of instruments allows borehole local estimation of hydraulic conductivity for lithological strata and for stratigraphical units.

The Hydrogeological Geospatial Database

The design of geospatial database has an Object-Oriented approach and is easily extensible. A large spectrum of data was identified, as many related domains are concerned: geography, geology, hydrology, hydrogeology, meteorology, water engineering, land management and others. The architecture of the hydrogeological database (Figure 2) follows international standards for geospatial data encoding. This is reflected in its object-oriented approach supported by the Open Geospatial Consortium (OGC) and the International Organization for Standardization (ISO).

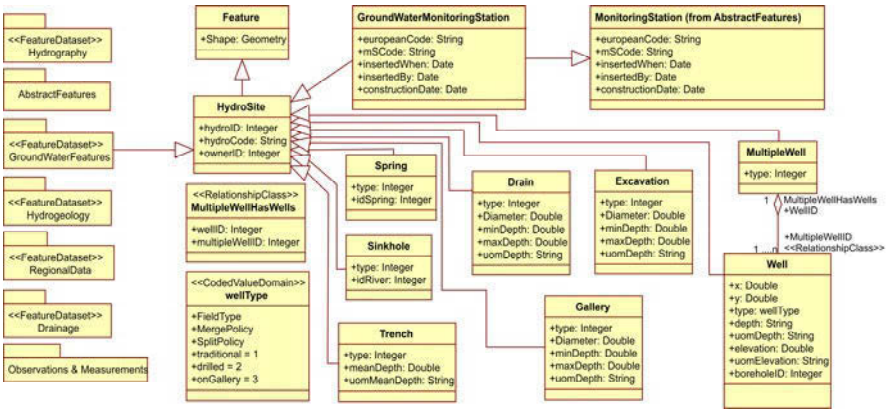

Fig. 2. Overview of the hydrogeological database scheme.

The database structure allows storing an accurate and very detailed geological core description that can be straightforwardly generalized and further upscaled. It serves to improve the quantification of the hydrogeological parameters. Relationships between the petrological, paleontological, chronological data could be established. Petrological characteristics are described for clastic and carbonated sediments in terms of textural (sediment size, sorting, roundness, matrix support),

lithological, colour, and others. The sedimentary structures, the geological layers boundaries, the geological units chronology or facies assignment, the paleontological content, and some complementary information are represented.

Lithological and stratigraphical analysis tool

The design of the lithological and stratigraphical analysis instruments has been set up to facilitate firstly the hydrogeological data interpretation. This subset of tools is made of several subcomponents. One of them allows the visualization of the borehole core lithological and stratigraphical information. Another one allows generating the geological profiles by query and visualization of the lithological and stratigraphical information. By using the third set of instruments, the user is able to identify stratigraphic units, analyze their characteristics, and export them in a 3D environment.

Borehole diagram instruments

This tool has been developed in order to facilitate the visualization and the analysis of the borehole detailed geological core description. To ease the analysis, the data visualization was designed following the classical geologist working bearings. By selecting a point representing a borehole on the map, the user has the possibility of querying the attached lithological and stratigraphical information. For each lithological stratum can be visualized the petrological characteristics in terms of texture (sediment size, sorting, roundness, matrix support), lithology, and colour.

Stratigraphic cross-sections correlation tool

The basic idea of this instrument is to facilitate the process of stratigraphic well correlation to the geologist. This kind of perception pulls on the understanding of geological processes, examination of exposures, and theoretical knowledge gathered by the modeler. This set of tools starts from the creation of a geological profile by querying a buffer zone line on a map, the user is drawing on screen. The profile is generated automatically by displaying the boreholes lithological columns together with the defined stratigraphical units/subunits. Complementary information is shown like the surface terrain profile extracted from the DEM, the distance between the boreholes, and the depth of each stratum. On this basis, an interactive analysis environment is created for a subsequent set of instruments. The user is

able to analyze and to vectorize on screen the identified existing stratigraphical elements by using lines, polygons, or points. For each feature a set of attributes like the type of the contact surface, the position between the hydrogeological units or subunits as well as different hydraulic parameters or other observations can be stored. Possible existing faults and fractures can be identified and drawn on screen within the same environment. The obtained information, represented by the user identified geological features, can be then converted within a 3D environment. The export procedure provides spatial features as points, lines, or polygons with their attached attributes. The resulted 3D features could be then used within the same GIS environment or by external software packages for further stochastic analysis or to build-up the geological 3D model.

Tool for the hydraulic conductivity initial estimation

Several steps have been made in quantifying hydraulic conductivity hydrogeological strata in boreholes, on the basis of the grain size distribution. For each lithological stratum or for the user defined hydrogeologic units, the hydraulic conductivity can be computed by using empiric formulas on the basis of the existing lithological description. This procedure could provide for the hydrogeologic models, hydraulic conductivity values closer to the reality.

4 Results and Discussions

Bucharest city area represents the first target for the software platform application on an alluvial environment. This is developed on the city region for the Moesic aquifer system. After analyzing large sets of data, the geological model is currently developed. Using the presented tools, several geological cross-sections are compiled. Figure 3 shows a cross-section located in the north-eastern part of the city.

The final target for the performed work focuses especially the characterization of groundwater, as well as the dynamics of water systems and their standard distribution in space. In this sense, the presented set of instruments represents a working environment for integrating the 3D sedimentary media spatial distribution standards of the different hydraulic parameters, in the regular hydrogeology modeling methodologies. The final goal is to explain the relationship between the computed hydraulic conductivity values and the effective-type values, which are the ones that in reality define the dynamics of the aquifers. This improves the conceptual model to build-up a hydrogeological model. The developed database structure allows storing data for most of the hydrogeological studies.

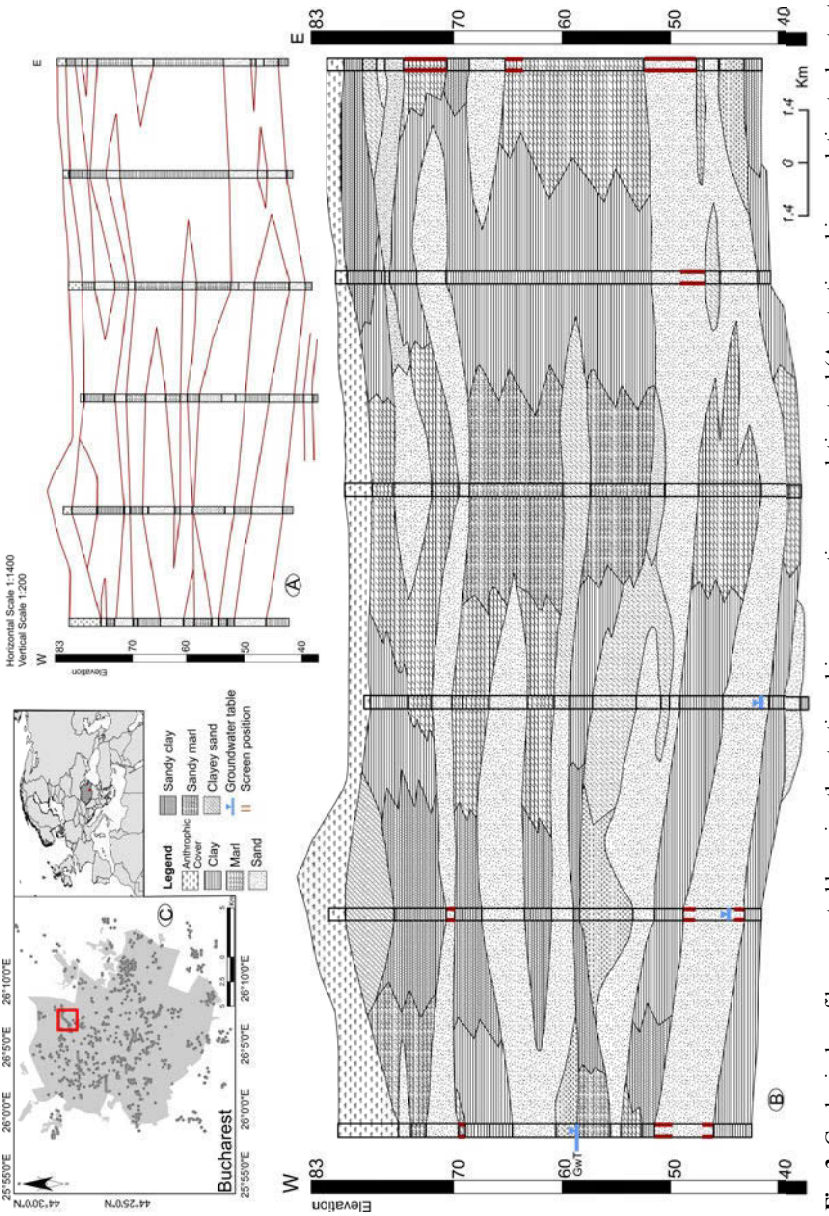

Fig. 3. Geological profile generated by using the stratigraphic cross-sections correlation tool (A - stratigraphic correlation tool output, B - geological cross-section interpretation, C - location of the geological profile on the map of Bucharest city).

The integration of detailed core stratigraphical and lithological description with hydrogeological local and regional parameters, hydrogeological tests as pumping and tracer tests, surface hydrology features, information related to different observations and measurements, give the user a consistent image on the studied aquifer behavior. As the described software allows performing detailed geological analysis, it also represents an excellent tool for managing and obtaining geotechnical information. This will help in studying the current geotechnical conditions and in recommending infrastructure development methods taking into account the environmental requirements. To date the presented software platform offers tools and methodologies that allow the representation in three dimensions of the geological record heterogeneity and its spatial distribution. The current research work focuses on the interaction of the groundwater with the urban infrastructure in terms of water supply and sewer systems, drainage systems of basements, subway network, and others.

5 Conclusions

The design of the described instruments is following the geologist classical way of working when they characterize geologically a study area. The instruments have been thought to be applied for hydrogeological analysis but they could be applied to other kinds of geological, geotechnical, or environmental studies. The presented work support the development of 3D geological characterization methods in sedimentary media, to carry out the development of hydraulic parametrization techniques for hydrogeological modeling. This represents the base for developing a reliable groundwater model facing urban aspects. The analysis of the geotechnical aspects in relationship to different ground and underground infrastructure elements as well as their interaction with groundwater will represent the next step of using the 3D geological software platform.

Acknowledgments This work is supported by the National Authority for Scientific Research of Romania, in the frame of the project "Sedimentary media modeling platform for groundwater management in urban areas (SIMPA)", no. 660.

References

Liteanu E (1952) The geology of the Bucharest city region. Geological Committee for Research and Exploration of the Underground Treasures. Bucharest

Pascu M (1983) Apele Subterane din Romania. Ed. Tehnica Bucuresti, Bucuresti

Vázquez-Suñé E, Abarca E, Carrera J, Capino B, Pool M, Gámez D, Simó T, Batlle F, Niñerola J.M, Ibáñez X. (2006) Groundwater modelling as a tool for the European Water Framework Directive (WFD) application: The Llobregat case, Physics and Chemistry of the Earth 31, 1015-1029

Seasonal ground deformation monitoring over Southern Larissa Plain (Central Greece) by SAR interferometry

I. Parcharidis, M. Foumelis, P. Katsafados

Department of Geography, Harokopio University of Athens, Athens, GR 176 71, Greece, parchar@hua.gr, mfoumelis@hua.gr, pkatsaf@hua.gr

Abstract Increase of water demand in Larissa Plain due to extensive cultivation, fulfilled by the over-exploitation of ground-water resource, lead to an intensive subsidence phenomenon causing in turns considerable damages to many buildings. DInSAR technique was proven to be a useful tool to measure ground deformation despite the unfavorable conditions inducing decorrelation. By exploiting differential interferometric pairs of short temporal separation and perpendicular baselines, it was possible to identify the area affected by ground deformation. Seasonal deformation signals were recognized at the southwestern part of the basin, reaching several centimeters during summer period.

1 Introduction

Land subsidence is a gradual settling or sudden sinking of the Earth's surface owing to subsurface movement of earth materials. The compaction of unconsolidated aquifer systems that can accompany excessive ground-water pumping is by far the single largest cause of subsidence. Land subsidence due to large amount of water withdrawal from an aquifer occurred in numerous regions throughout the world and is characterized, as a potential risk especially in the case the overlapping surface is a build up area. Subsidence is directly resulted from lowering of the piezometric surface due to fluid extraction. Poland and Davis (1996) demonstrated that the centers of subsidence coincided with the centers of major pumping. The magnitude and spatial extend of such vertical displacements are not easily detectable with conventional geological and geotechnical methods, which are additionally expensive and time consuming.

Interferometric Synthetic Aperture Radar (InSAR) technique has a great potential to detect and quantify ground subsidence caused by aquifer system compaction. A great number of researchers demonstrated the capability of Differential InSAR (DInSAR) to detect and measure ground subsidence, caused by the removal of subsurface groundwater (Galloway et al. 1998, Amelung et al. 1999, Fruneau et al. 2005, Parcharidis et al. 2006).

N. Lambrakis et al. (Eds.), *Advances in the Research of Aquatic Environment, Vol. 2*
DOI 10.1007/978-3-642-24076-8,

The aim of this study is to investigate surface deformation signals associated with annual precipitations and groundwater withdrawal, demonstrating the suitability of DInSAR for examining dewatering induced subsidence. Specifically, we attempt to measure seasonal deformation and its spatial distribution. Displacement maps of high spatial resolution were generated for the broader Larissa Plain using SAR acquisitions from ERS and ENVISAT satellites.

2 Larissa Plain

The present study is focused on the Southern part of Larissa plain, within the Thessaly basin, located in Central Greece (Fig. 1). Physiographically the area represents a typical plain of about 13700 km^2, surrounded by mountain ranges and traversed by Pinios River. The elevation ranges from sea level at the eastern coastal region to more than 2800 m at the eastern and western mountain areas, with mean elevation at nearly 500 m.

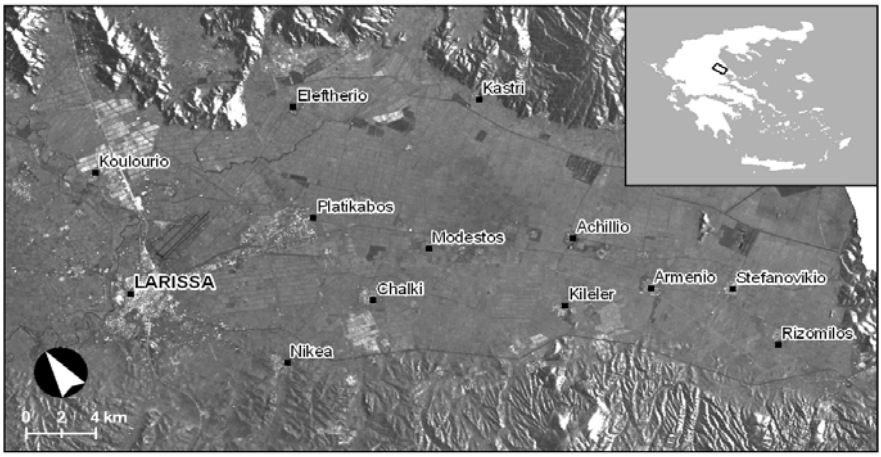

Fig. 1. Average intensity SAR image of Southern Larissa Plain.

During summer season in Thessaly is usually very hot and dry and in July and August temperatures can exceed 40°C. Mean annual accumulated precipitation varies from 400 mm at the plain area to more than 1850 mm at the western mountain ranges (Loukas and Vasiliades 2004). More specifically, the mean annual accumulated precipitation of the meteorological station at the airport of Larissa (22° 25′, 39° 38′) and it is operated from the Hellenic National Meteorological Service is 423,2 mm for a 43 year period (1955-1997). During this period the meteorological station which is located southeasterly of Larissa, near the city of Volos (22° 48′, 39° 13′), is recorded a slightly increased mean annual precipitation up to 500 mm.

The geomorphology of Thessaly is controlled by two orientations of normal faults. The main NW-SE trending basins of Karditsa and Larissa and their separating range are controlled by NW-SE trending normal faults (Caputo and Pavlides 1993). The younger normal faults strike E-W forming graben that cross-cut the older structures, uplifting and offsetting Late Quaternary deposits (Caputo 1993) and are concentrated in a northern and a southern zone. The northern zone at the north of Larissa basin comprises the Rodia, Tyrnavos and Larissa-Omolio faults (Caputo 1993). It is less active seismically in modern and historical times with just one earthquake of Ms 6.1 in 1941.

The bedrock geology consists of gneiss, schists, marbles, quartzites, serpentinites, flysch and carbonate formations (Paleozoic to Upper Cretaceous). The Quaternary sediments covering the basin consist of lacustrine and fluvial deposits poorly consolidated, with predominance of the fine grain size (Kaplanides and Fountoulis 1997). Very rich aquifers are observed in the poorly consolidated Quaternary formations and in the karstified carbonate rocks of the basin bedrock. The depth of water table varies considerably within the area.

Larissa Plain is characterized as the most cultivated and productive agricultural region in Greece. The extensive cultivation has lead to a remarkable increase of water demand, which is usually fulfilled by the over-exploitation of ground-water resources. Only a small part of this demand is covered by the Pinios River, its tributaries as well as a few small reservoirs and lagoons adjacent of Pinios River (Loukas and Mylopoulos 2004).

The above increased water demand has been associated with severe extreme and persistent droughts during the period from mid to late 1970s and the period from late 1980s to mid 1990s, interrupted by the wet 1990-1991, which mostly affected the northern part of Thessaly Basin (Loukas and Vasiliades 2004). These dry conditions result in irrigation cutbacks, overexploitation of groundwater and significant losses of crop yields. The subsidence phenomenon caused considerable damages to buildings in the area. Field observations made by the authors' indentified subsidence induced ground fissures in locations like Larissa-Airport, Kambos, Nikea and Melia villages.

3 SAR interferometric processing

The broader study area was repeatedly imaged by the European Space Agency satellites. For the purposes of this study, 48 ERS-1 and ERS-2 SAR scenes (Track 279 – Frame 2812 in descending mode) and 39 ENVISAT ASAR scenes (Track 279 – Frame 2807 in descending and Track 143 – Frame 783 in ascending modes) were acquired covering the periods 1992-2001 and 2001-2010 respectively. For the selection of the interferometric pairs (Table 1), we adopted two main criteria. First, a perpendicular baseline (Bp) component of up to 150 m was considered, although few pairs with slightly higher values were to be useful. Second, we dealt

on orbit pairs of different time spans and epochs in order to capture short and long term deformation signals.

Table 1. Interferometric parameters of the DInSAR pairs.

Sensor	Track	Dates	Total months	Bp (m)	Orbit
ERS	279	31/12/1995 – 14/04/1996	3.5	11.1	descending
ERS	279	02/08/1998 – 06/09/1998	1.2	-1.4	descending
ENVISAT	143	05/08/2004 – 09/09/2004	1.2	-23.3	ascending
ENVISAT	279	11/01/2009 – 15/02/2009	1.2	330.9	descending

The meteorological station at the airport of the city of Larissa accumulated 205.6 and 14.7 mm during the winter periods (31/12/1995 – 14/04/1996 and 11/01/2009 – 15/02/2009) and 0.4 and 18.5 mm during the summer periods referenced in the Figure 2.

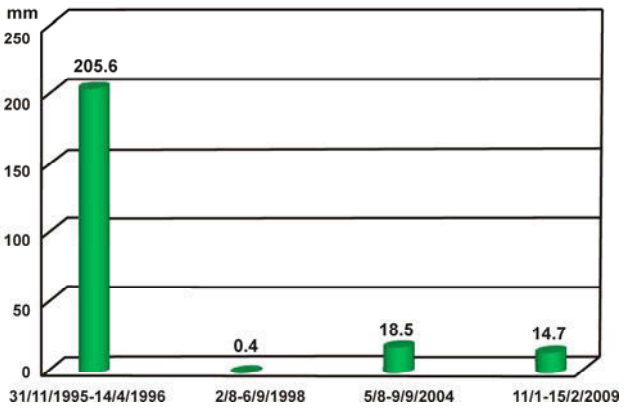

Fig. 2. Accumulated precipitation recorded by the Larissa meteorological station.

Interferometric processing was performed using GAMMA s/w packages (Wegmüller et al. 1998). Initial estimates of the interferometric baselines were calculated from available DORIS and DELFT precise orbit state vectors. A default number of 9 state vectors are initially given on 60s intervals. Due to the insufficient number of state vectors provided, in terms of cover of the area of interest, additional state vectors with an interval of 5.0s were introduced by respectively interpolation of the available state vectors and orbit propagation.

Precision co-registration based on the intensity cross correlation technique was implemented, achieving accuracies of sub-pixel level (~0.3 pixels). After removal of flat-Earth phases using the estimated interferometric geometry parameter values and refinement of the baselines, no phase ramps (orbital fringes) were recognized in the differential interferograms.

Topography related phases were simulated based on SRTM V3 DEM of approximate 90 m spatial resolution, oversampled to 20 m to fit with that of SAR data. Although the area exhibit rugged terrain, small perpendicular baselines ensures the minimization of possible topographic residuals. An adaptive filtering of the differential interferograms based on the local fringe spectrum was considered to assist and reduce possible residues during the unwrapping procedure. Unwrapping of differential phases was performed by applying a Minimum Cost Flow (MCF) algorithm (Costantini 1998).

Finally, accurate geocoding of interferometric results enables not only precise overlays with other data sources in a common map geometry, but also normalization for the systematic influence of terrain on image radiometry during image co-registration step. Finally a large number of interferograms were obtained, specifically 65 ERS pairs (Bp ≤50 m) and 48 ENVISAT pairs (Bp ≤150 m) in descending mode as well as 23 ERS pairs (Bp ≤100 m) and 43 ENVISAT pairs (Bp ≤400 m) in ascending mode.

4 Results and discussion

Interferometric pairs of short temporal separation and baselines were mainly utilized for the needs of the study, due to intensive decorrelation phenomena observed. Coherence levels are dramatically reduced within few months, narrowing the time span for robust observations.

It was possible however, to obtain an almost continuous displacement field and to delineate the area affected by ground deformation. Deformation patterns corresponding to ground subsidence are evident in interferograms covering the period between May and October. The deformed area (about 180 km^2) retains an elongated shape with NW-SE orientation (major axes almost 25 km), while covering only the southeastern part of the plain. The area of maximum deformation is located to the North of Kileler village, reaching -17.5 cm along the line of site in the summer of 1998 (from August to September), whereas for the same period in 2004 lower but also significant magnitudes of -12.7 cm are observed (Fig. 3). During winter seasons deformation is considerably reduced to -0.5 cm and -0.1 cm for 3.5 months (Dec.1995 – April 1996) and 1.2 months (Jan. – Feb. 2009) period respectively (Fig. 4). Rebound phenomena with significantly lower values were observed during high precipitation periods mainly at the NE of the basin (Fig. 3).

Larger subsidence should be expected when considering the entire summer season, where most of the irrigation and over-exploitation of ground-water are taking place. Accurate estimation of the deformation with conventional DInSAR techniques is however, not easily archived for larger time spans, due to extend of decorrelation phenomena in the region. Alternatively, it is questionable whether the implementation of advance processing techniques, such as Interferometric Stacking and PSInSAR, would offer better results. The magnitude and the pronounced

seasonal character of the deformation signal could not easily described adopting linear time-dependent models.

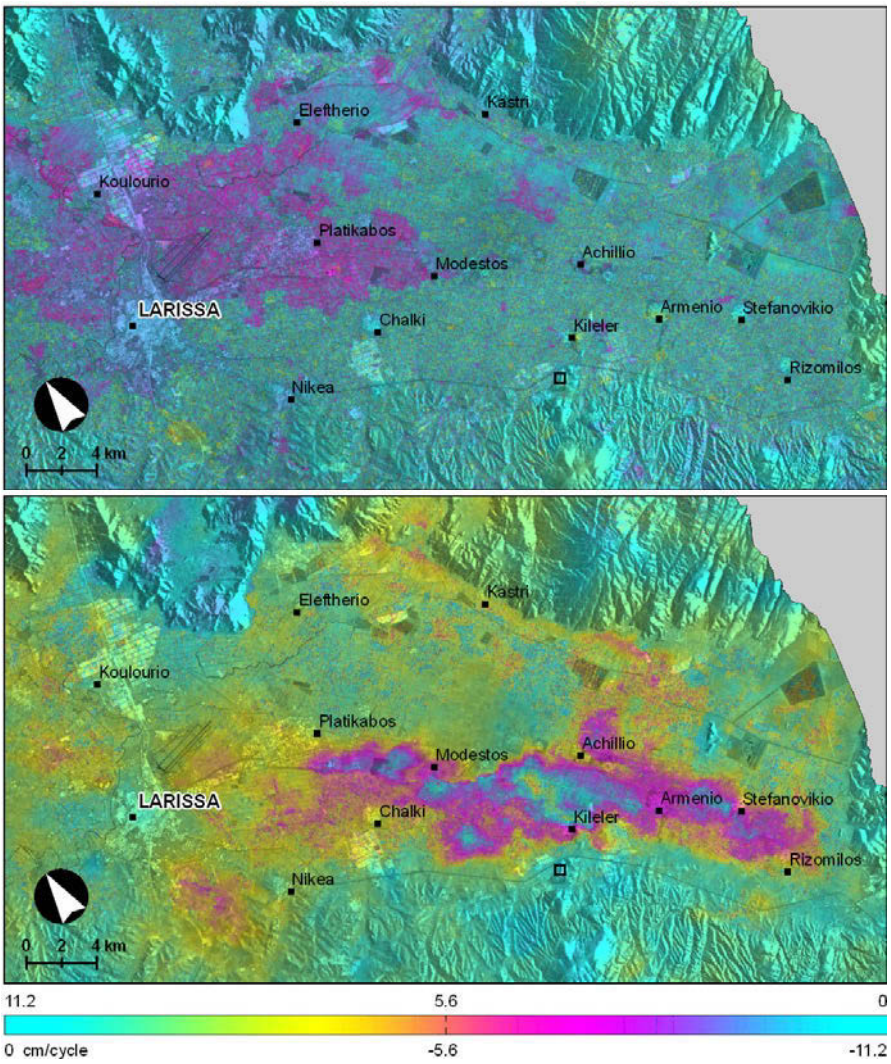

Fig. 3. Differential SAR interferograms between winter scenes 31/12/1995 – 14/04/1996 (up) and summer scenes 02/08/1998 – 06/09/1998 (down). Square corresponds to the reference point.

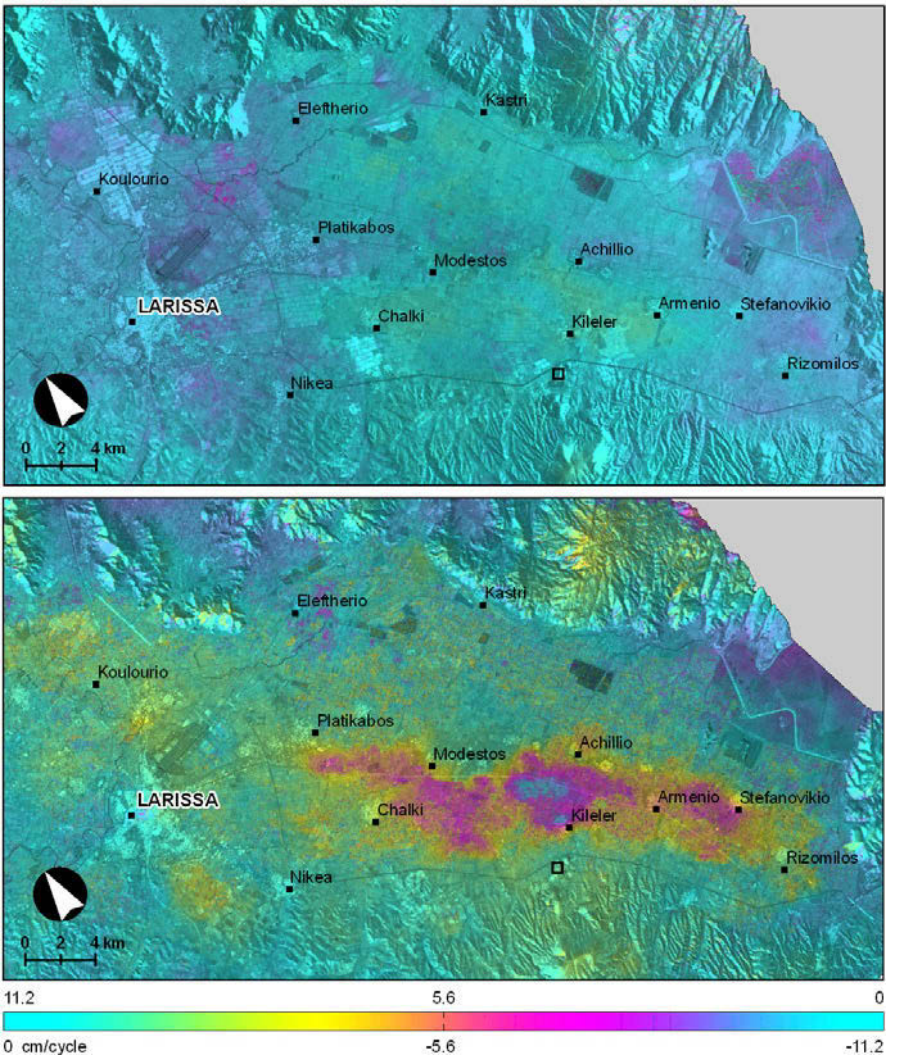

Fig. 4. Differential SAR interferograms between winter scenes 11/01/2009 – 15/02/2009 (up) and summer scenes 05/08/2004 – 09/09/2004 (down). Square corresponds to the reference point.

Acknowledgments The present study is part of TERRAFIRMA_X project supported by ESA's GMES Service Element Program. ERS SAR and ENVISAT ASAR scenes were provided by ESA within the frame of the project.

References

Amelung F, Galloway DL, Bell JW, Zebker HA, Laczniak RJ (1999) Sensing the ups and downs of Las Vegas: InSAR reveals structural control of land subsidence and aquifer-system deformation. Geology 27, 483–486

Caputo R, Pavlides S (1993) Late Cenozoic geodynamic evolution of Thessaly and surroundings (central-northern Greece). Tectonophysics 223 (3-4), 339-362

Caputo R (1993) Morphotectonics and kinematics of the Tyrnavos fault, northern Larissa Plain. Zeitschrift fur Geomorphologie 94, 167-185

Costantini M (1998) A novel phase unwrapping method based on network programming. IEEE Transactions on Geoscience and Remote Sensing 36 (3), 813-821

Fruneau B, Deffontaines B, Prunier-Leparmentier A.-M, Arnaud, A (2005) Reflexions and insights from Urban SAR interferometry for monitoring vertical deformation due to water pumping: The Haussmann-St-lazare case example (Paris, France). European Space Agency, (Special Publication) ESA SP (572), art. no. 575, 947-951

Galloway DL, Hudnut KW, Ingebritsen SE, Phillips SP, Peltzer G, Rogez F, Rosen P (1998) Detection of aquifer system compaction and land subsidence using interferometric synthetic aperture radar, Antelope Valley, Mojave Desert, California. Water Resources 34, 2573–2585

Kaplanidis A, Fountoulis D (1997) Subsidence phenomena and ground fissures in Larissa, Karla Basin, Greece: Their results in urban and rural environment. In: Proc. of the International Symposium “Engineering Geology and the Environment” v.1, 729-735

Loucas A, Mylopoulos M (2004) Effects of hydrotechnical works development and water resources management on the availability of water resources of Pinios river basin. In: Proc. of the 7th International Conference of Protection and Restoration of the Environment. Mykonos

Loukas A, Vasiliades L (2004) Probabilistic analysis of drought spatiotemporal characteristics in Tessaly region, Greece. Natural hazards and Earth System Sciences 4 (5-6), 719-731

Parcharidis I, Lagios E, Sakkas V, Raucoules D, Feurer D, Le Mouelic S, King C, Carnec C, Novali F, Ferretti A, Capes R, Cooksley G (2006) Subsidence monitoring within the Athens basin (Greece) using space radar interferometric techniques. Earth Planets and Space 58, 505-513

Poland JF, Davis GH (1996) Land subsidence due to withdrawal of fluids. In: Varnes DJ (ed) Reviews in engineering geology v.II, 187-268. Geological Society of America, Boulder Colorado

Wegmüller U, Werner C, Strozzi T (1998) SAR interferometric and SAR differential interferometric processing chain. In: Proc. of IGARSS v.2 pp. 1106-1008

Ruptures on surface and buildings due to land subsidence in Anargyri village (Florina Prefecture, Macedonia)

G. Soulios, Th. Tsapanos, K. Voudouris, T. Kaklis, Ch. Mattas, M. Sotiriadis

Aristotle University of Thessaloniki, Department of Geology gsoulios@geo.auth.gr

Abstract This paper deals with the land subsidence due to groundwater overexploitation in Anargyri village (Florina prefecture, West Macedonia). The decline of groundwater table is necessary for lignite exploitation by the Public Power Corporation (PPC). The lignite deposits are occurred in Neogene sediments, consisting of alternations of clayey and marly layers. In these deposits are developed successive confined aquifers. The overexploitation of these aquifers had led in a decline of groundwater table, ranging between 30-40 m during the last years. Land subsidence phenomena resulted in ruptures on surface and buildings, rendering most of the houses uninhabitable. The ruptures on surface were examined in relation to geological and hydrogeological conditions and conclusions are drawn.

1 Introduction

In 1982 the Public Power Corporation (PPC) started the construction of thermal power plant of Amyntaio, which operated in 1987 using the lignite deposits of both mines Amyntaio and Anargyri. The excavations at the Anargyri mine started in 1984 and the first amounts of lignite produced in 1986. The excavations at the large Amyntaio mine started in 1989 and the first amounts of lignite produced in 1990.

Today, the excavations at the Amyntaio mine are from a depth ranging between 140 m and 170 m below ground surface. Before the excavation, groundwater table was at a depth of 2-5 m below ground surface. The exploitation of lignite deposits from PPC requires the drawdown of water table. For this reason extraction of groundwater began in this period with an annual amount of water equal to 2.4×10^6 m^3, which increased continuously with the expansion of the mine. Thus, the annual abstracted amounts of water during the period 2007-2009 were estimated to be approximately $6\text{-}7 \times 10^6$ m^3.

N. Lambrakis et al. (Eds.), *Advances in the Research of Aquatic Environment, Vol. 2*
DOI 10.1007/978-3-642-24076-8, © Springer-Verlag Berlin Heidelberg 2011

The excavations started from East toward West, near the thermal power plant, about 2 Km from the village Anargyri. Nowadays the front of excavations is only 300 m from the first houses of the village. Ruptures on surface and buildings in the village Anargyri are first observed in the end of 1998 and mainly in 1999, when the front of excavations was 750 m from the village and the depth was 100 m. Since then, the ruptures have been increasing and enlarging continuously, so many buildings in the village were damaged and many houses are uninhabitable.

This paper examines the land subsidence phenomena in relation to hydrogeological conditions of the study area. This scientific work was carried out by the Aristotle University of Thessaloniki (Dept. of Geology), in the framework of a research project funded by Municipality of Aetos (Soulios et al. 2010).

2 Geological setting

From a geological point of view, the study area is part of the Pelagonian geotectonic zone. The crystalline bedrock (schists, gneisses, marbles, limestones) occurs at great depth from the ground surface in the study area. Neogene and Quaternary deposits overlay the aforementioned bedrock.

According to the geological map of I.G.M.E. (Ptolemaida sheet, scale 1:50,000, Koukouzas, Ioakeim 1997) and the field investigation, the Neogene and Quaternary sediments consist of the following geological formations, as illustrated in geological map (Fig. 1) and geological section (Fig. 2):

- **Soil cover** (Fig. 2, layer Z) with a thickness of 0.20-0.50 m, consisting of sapropel (swamp facies) and calcitic- clayey materials (lacustrine facies) of Holocene age.
- **Alternate layers** (Fig. 2, layer E) of fined size sand with layers consisting of clayey-sandy-loamy and marly materials. Their depth is 10 m increasing toward West. The thickness of sand layers is about one meter each. It is one lacustrine formation of Upper Pleistocene-Holocene age.
- **Loam-clay-clayey marls** (Fig. 2, layer D) with intercalations of fined size sand or sandy-clayey materials. The thickness of aforementioned deposits ranges between 10 and 15 m increasing toward West and North. This formation can be considered as an aquifuge bed of Upper Pleistocene age.
- **Sand** with interlayered fine size materials (Fig. 2, layer C) consisting of clayey marls with a thickness of 20-30 m. These deposits are mainly of medium grain size sand or cross-bedding of sand. The intermediate layers of clayey marls are thin with a thickness of 0.5 m. This formation is terrestrial and fluvial of Middle-Upper Pleistocene age and it can be considered as permeable layer.
- **Clays** (Fig. 2, layer B) of red color with intercalations at places of gravels and pebbles. This terrestrial formation is of Middle Pleistocene age with a thickness of 15-30 m and it can be considered as aquifuge bed.

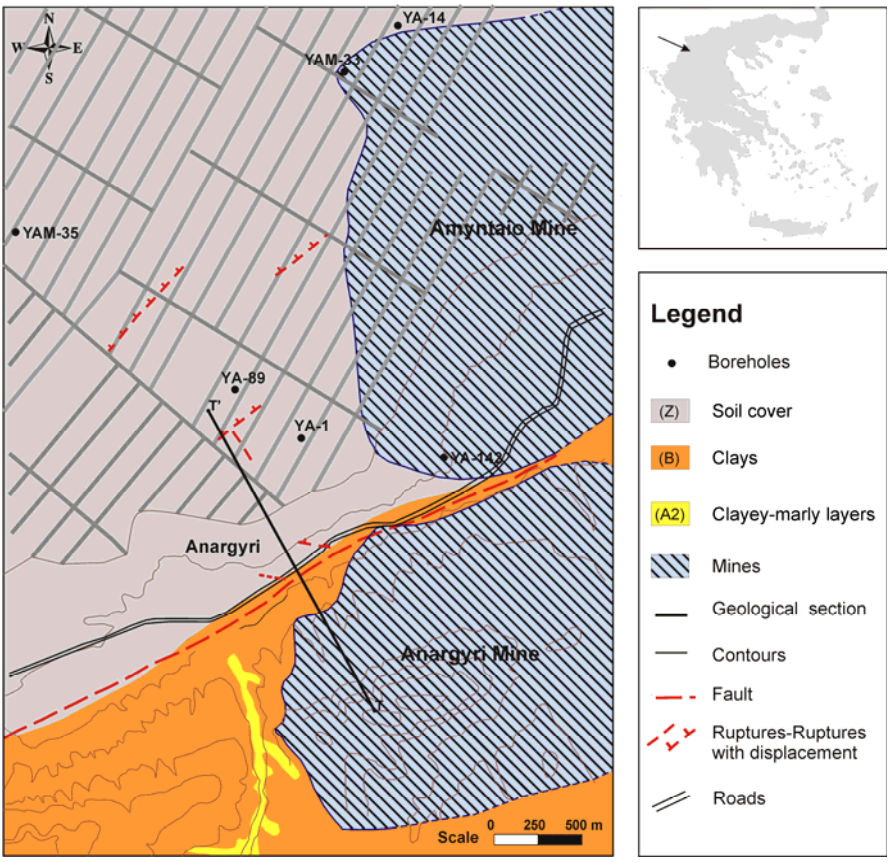

Fig. 1. Geological map of the study area (see text).

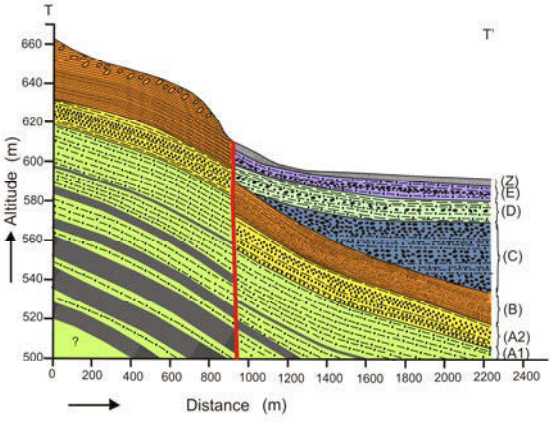

Fig.2. Geological section (see text). Direction T-T' is shown in Figure 1.

- **Clayey-marly layers** (Fig. 2, layer A2) of gray-yellow color with a thickness of 15-20 m, passing progressively to the following deposits. They are lacustrine deposits of Upper Pleistocene age and are characterized as aquifuge beds.
- **Marls** (Fig. 2, layer A1) of yellow-green to gray-green color with lignite intercalations. Lignite deposits in the upper part have a thickness of 0.10-0.20 m, while in the deep layers have a thickness of 0.5-2 m with intermediate thin marly intercalations. The whole sequence is lacustrine to lacustrine-marsh with a thickness of 50 m of Upper Miocene age. It is characterized as aquifuge bed.

3 Land subsidence phenomena

Land subsidence phenomena are caused by the overexploitation of the aquifers, and the consequent significant groundwater level drawdown. These phenomena have been recorded in many different places on earth and have been referenced by many researchers: in San Francisco and Texas of U.S.A. (Jumikis 1963), in Japan (Akagi 1979), in Bangok of Thailand (Premchitt 1979), in China (Chen et al. 2003), in Bordaux of France (Schneebeli 1991), in different places of Italy (Astori and Bezoari 1991), etc.

In Greece these phenomena have been observed in many regions, such as:

- Kalabaka area (Kallergis 1971)
- Karla, Thessaly area (Kaplanidis and Fountoulis 1997, Soulios 1997)
- Kalochori, Thessaloniki area (Andronopoulos et al. 1983, Soulios 1980, Loupasakis and Rozos 2010)
- Megalopoli, Arkadia area (Dimitrakopoulos and Koumantakis 1995)
- Stavros, Farsala, Thessaly area (Rozos et al. 2010) etc.

The main reason for the creation of these phenomena is the significant long term (over 1 year) groundwater level drawdown (usually over 10 m). The water level drops causes a reduction to the upward pressure born by the fluid and causes an increase of the effective stress ($\Delta\sigma$) born by the aquifer: $\Delta\sigma=\Delta h.\gamma$ (where Δh=change in water level, γ=specific weight of water). In the case of alluvial aquifer, recently formatted and unconsolidated with great compressibility, land subsidence is caused, that means reduction of the thickness and therefore withdrawal of its surface. As a result, ruptures are appeared due to the heterogeneity which implies differential land subsidence (Schmeebeli 1966).

Consequently, the progress of the piezometric surface and the geological composition of an area is the main reason that causes land subsidence and ruptures manifestation.

4 Monitoring of the piezometric surface in the area

It is important to examine the progression of the piezometric surface starting before the beginning of the excavation and water pumping until the manifestation of the ruptures and cracks on the buildings.

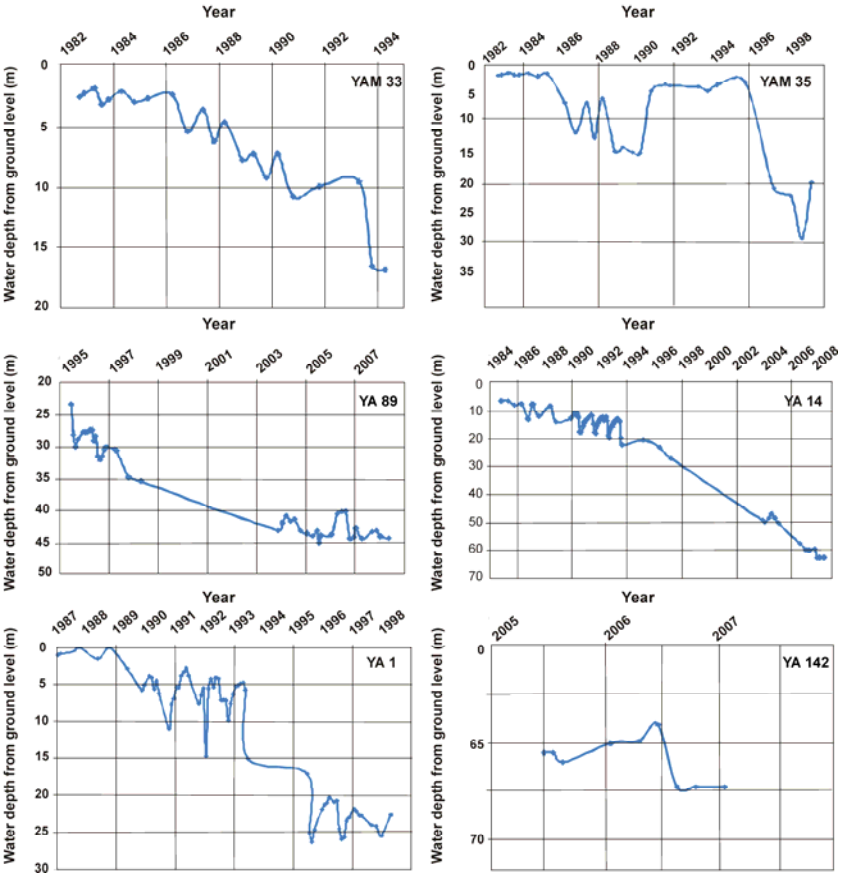

Fig. 3. Water level drawdown (see text).

There are totally nine (9) piezometric boreholes in the study area drilled by P.P.C. and seven (7) by Institute of Geology and Mineral Exploitation (I.G.M.E.). There are no continuous measurements for all these boreholes, because some of them were destroyed during the advance of the excavation front and also because the piezometric programs were not continuous. There are six (6) boreholes with the most complete data records the locations of which are shown in the map of Figure 1. For these boreholes the following comments are given:

- Borehole YAM33. Given that the period 1989-1990 was particularly dry, it seems that the water level continued to decline with a very intense rate during the following years, due to the mining excavation (Fig. 3). In 1994 the water level drawdown was 15 m. Apparently, in 1998, when the fissures got visible, the drawdown was greater.
- Borehole YAM35. It is located far from the mine and in even longer distance. For this reason the water level cone of depression reached this borehole in a later time. Therefore, the rapid water level drawdown began in 1995 and in the years 1998-1999 was about 25 m (Fig. 3).
- Borehole YA1. It is located very close to the Anargyri village at a distance of 2.0-2.5 Km away from the place where the water-pumping began. The rapid water level drawdown started in 1993 and in the year 1998 it was about 25 m (Fig. 3).
- Borehole YA89. It is located very close to the Anargyri village, at a distance of about 2.5 Km from the place that the excavation works began. The borehole was drilled in 1995, by the time that other boreholes had already been destroyed due to the mining excavation. At that time, the water level drawdown was over 20 m. During the years 1998-1999, the total water level drawdown was more than 30m (Fig. 3).
- Borehole YA14. It is located close to the Anargyri village, 2.0-2.5 Km away from the place that water pumping began. The water level started to drawdown rapidly since 1993. In the years 1998-1999 a water table drop of more than 20 m was recorded, while in 2008 the water decline was 50 m (Fig. 3).
- Borehole YA142. It was drilled in 2005 inside the mine area. Since then, the groundwater level was at depth of 65 m below ground surface approximately depth, which means that the water level drawdown is about 60 m (Fig. 3).

Conclusively, already since 1993 the groundwater level decline was more than 20 m around the village Anargyri. Consequently, according to the widening and deepening of the depression cone it is concluded that, the water level drawdown around the village area should be more than 10-15 m in 1998, and already over 20-25 m nowadays (2011).

5 Surface ruptures and cracks on the buildings

As it has been mentioned, the ruptures were first observed in 1998-1999 and since then their number and size were constantly increasing until 2008. On the ground surface they follow two dominant directions:

- One almost E-W direction with displacements towards the north, i.e. to the center of the plain, where the thickness of the Quaternary sediments increases.
- Another one of circular shape, almost parallel to the advance of the mine excavation front, with a displacement towards the front, i.e. to the direction of the greater water level drawdown.

The cracks and fractures on the buildings are more dense and intense to those that are closer to the mine, as well as to those buildings located in the recent Quaternary formations. On the contrary, they are smaller to negligible or almost nonexistent to the buildings that are distant from the mine and especially to those located in the Lower-Upper Pleistocene red beds.

6 Discussion-Conclusions

The ground ruptures and the building cracks observed in the Anargyri village could theoretically be attributed to:

- Earthquake: There is no earthquake of magnitude $M \geq 5R$ recorded in the broader area since 1998. Furthermore, in case of an earthquake all fissures should had been developed simultaneously and not in a continuous manner for more than a decade (1998-2008).
- Landslide: Not even a single horizontal dislocation was observed, neither superficial nor underground, as deduced from inclinometer measurements in selected boreholes.
- Land subsidence: In fact, the space-time progression of the phenomenon coincides with the groundwater level drawdown, which is greater than 10-15 m and maybe exceeds 20 m and lasted for many years. In addition, the geologic layers are very recent with high compressibility. Finally, it is concluded that the excessive extraction of groundwater has caused the ground ruptures in the study area.

References

Akagi T (1979) Some land subsidence experiences in Japan and their relevance to subsidence in Bangkok, Thailand. Geotech. Engin. Bangkok, 10:1, 37-48

Andronopoulos B, Roizos D, Chatzinakos I (1990) Geotechnical study of the surface subsidence in Kalohori area, Municipality of Thessaloniki. I.G.M.E. Internal technical report, p. 45

Astori B, Bezoari G (1991) Experiences of land subsidence measurements in Italy and related problems. International Symposium on “Land subsidence”, Dhanbad, India.

Chen C, Pei S, Jiao J (2003) Land subsidence caused by groundwater exploitation in Suzhou, China. Hydrogeology Journal 11, 275-287

Dimitrakopoulos D, Koumantakis I (1995) Big troughs creation on the surface from covered karst activation due to drawdown caused by overpumping for mine protection and in dry periods. Proceedings of 3rd Hydrogeological Congress, Herakleion, 393-407

Jumikis A (1963) Soil Mechanics. D. van Nostrand Company, Inc. London, 299-305

Kallergis G (1971) Land subsidence during overpumping of artesian aquifers due to their limited elasticity. Technical Chronicles, 599-602

Kaplanides A, Fountoulis D (1997) Subsidence phenomena and ground fissures in Larissa, Karla basin, Greece: Their results in urban and rural environment. Proc. Symposium "Engineering Geology and the Environment", Vol. 1, 729-735

Koukouzas K, Ioakeim C (1997) Geologic map of Greece, scale 1:50,000, Ptolemaida sheet, IGME

Loupasakis K, Rozos D (2010) Land subsidence induced by the overexploitation of the aquifers in Kalochori village-New approach by means of the computational geotechnical engineering. Proceedings of the 12th International Congress, Patras, May, 2010. Bulletin of the Geological Society of Greece, Vol. XLIII, No 3, 1230-1237

Premchitt J (1979) Land subsidence in Bangkok, Thailand: results of initial investigation. Geotech. Engin. Bangkok, 10: 1, 72-76

Rozos D, Sideri D, Loupasakis K, Apostolidis E (2010) Land subsidence due to excessive groundwater withdrawal. A case study from Stavros-Farsala site, West Thessaly Greece. Proceedings of the 12th International Congress, Patras, May, 2010. Bulletin of the Geological Society of Greece, XLIII: 4, 1850-1857

Schmeebeli G (1966) Hydraulique souterraine Eyroles, 111-113, Paris

Soulios G (1980) Allouvial soils land subsidence due to the pumping of the underlying aquifers. Examples from Greece. Technical Chronicles, 4, 205-210

Soulios G (1997) Subsidence de terrains alluviaux dans le sud-est de la plaine de Thessalie Proc. Symp. International, "Engineering Geology and the Environment", 1, 1067-1072

Soulios G, Tsapanos Th, Voudouris K, Kaklis T, Mattas Ch, Sotiriadis M. (2010) Investigation of the causes of ruptures on surface and buildings in Anargyri area, Prefecture of Florina. Technical report of research project. Department of Geology, Aristotle University of Thessaloniki (in Greek)